NATIONAL BUREAU OF STANDARDS
MICROCOPY RESOLUTION TEST CHART

ADA050968

REPORT DOCUMENTATION PAGE	READ INSTRUCTIONS BEFORE COMPLETING FORM

1. REPORT NUMBER	2. GOVT ACCESSION NO	3. RECIPIENT'S CATALOG NUMBER
AFOSR-TR-78-0247		

4. TITLE (and Subtitle)	5. TYPE OF REPORT & PERIOD COVERED
THEORIES OF ENERGY DISPOSAL IN CHEMICAL REACTIONS.	Final rept. 1 Jun 73 - 30 Jun 77,
	6. PERFORMING ORG. REPORT NUMBER

7. AUTHOR(s)	8. CONTRACT OR GRANT NUMBER(s)
Aron Kuppermann	AFOSR-73-2539

9. PERFORMING ORGANIZATION NAME AND ADDRESS	10. PROGRAM ELEMENT. PROJECT, TASK AREA & WORK UNIT NUMBERS
California Institute of Technology Division of Chemistry and Chemical Engineering Pasadena, CA 91125	61102F 2303/B1 B1

11. CONTROLLING OFFICE NAME AND ADDRESS	12. REPORT DATE
Air Force Office of Scientific Research/NC Bolling AFB DC 20332	February 1978
	13. NUMBER OF PAGES
	250 192 p.

14. MONITORING AGENCY NAME & ADDRESS(if different from Controlling Office)	15. SECURITY CLASS. (of this report)
	UNCLASSIFIED
	15a. DECLASSIFICATION/DOWNGRADING SCHEDULE

16. DISTRIBUTION STATEMENT (of this Report)

Approved for public release; distribution unlimited.

17. DISTRIBUTION STATEMENT (of the abstract entered in Block 20, if different from Report)

DDC
RECEIVED
MAR 8 1978
F

18. SUPPLEMENTARY NOTES

19. KEY WORDS (Continue on reverse side if necessary and identify by block number)

20. ABSTRACT (Continue on reverse side if necessary and identify by block number)

Accurate and approximate quantum dynamical calculations on elementary chemical reactions of importance for the fundamental aspects of chemical dynamics and for advanced technologies of interest to the US Air Force, such as high energy chemical lasers, plume technology, and the chemical effects of high energy radiation, were performed. These included calculations of three-atom exchange reactions, breakup collisions, three-body recombinations, vibrational quenching by reaction resonances, and electronic branching ratios. The aim of these calculations was to develop an understanding of these processes and to develop benchmark data against which approximate methods could be tested.

FINAL REPORT ON A RESEARCH GRANT FROM THE

UNITED STATES AIR FORCE OFFICE OF SCIENTIFIC RESEARCH

Institution: Division of Chemistry and Chemical Engineering
California Institute of Technology
Pasadena, California 91125

Title of Project: Theories of Energy Disposal in Chemical Reactions

Grant Number: AFOSR-73-2539

Time Period Covered by
the Grant and the Report: 1 June 1973 through 30 June 1977

Principal Investigator:

Aron Kuppermann
Professor of Chemical Physics

TABLE OF CONTENTS

1. PROJECT ABSTRACT

The purpose of this project was to perform accurate and approximate quantum dynamical calculations on elementary chemical reactions of importance for the fundamental aspects of chemical dynamics and for advanced technologies of interest to the United States Air Force, such as high energy chemical lasers, plume technology, and the chemical effects of high energy radiation. These included calculations of three-atom exchange reactions, breakup collisions, three-body recombinations, vibrational quenching by reaction, resonances, and electronic branching ratios. The aim of these calculations was to develop an understanding of these processes and to develop benchmark data against which approximate methods could be tested.

2. SCIENTIFIC BACKGROUND AND SUMMARY OF WORK PERFORMED

The prediction and interpretation of the details of chemical reactions from first principles has been a goal of chemistry since the advent of wave mechanics, 50 years ago. However, methodological and computational difficulties have prevented the achievement of this goal until very recently. In 1929, Dirac[1] made his famous statement concerning this matter: "The underlying physical laws necessary for the mathematical theory of a large part of physics and the whole of chemistry are thus completely known, and the difficulty is only that the exact application of these laws leads to equations much too complicated to be soluble." Insofar as chemical reactions are concerned, this statement was completely accurate at the inception of this grant (1 June 1973). Only in late 1975 was this state of affairs changed, with the publication of the first accurate three-dimensional (3D) quantum dynamical calculations on realistic potential energy surfaces for the H_3 system.[2,3] A significant fraction of this progress was due to the work supported by the present grant.[4] This development opened up the possibility of applying the methods developed for these calculations to other systems, and has permitted a test of the validity of some approximate methods. The usefulness of good approximations is that they can be applied to more complex systems for which accurate ab initio calculations cannot presently be performed. This kind of approach to the testing of approximate theories has advantages over the one based on a comparison between theory and experiment. The reason is that potential energy surfaces are not at present experimentally known. Therefore, it is necessary to make assumptions concerning such surfaces which usually involve some calibration to yield appropriate dynamical behavior. This biases the test of the dynamical model. However, if such a model is used and an accurate quantum dynamical calculation is performed on the same assumed (but fairly realistic) potential

energy surface (for electronically adiabatic processes), this logical difficulty disappears and the approximate dynamical model is indeed given a very good test.

The development of the accurate 3D quantum dynamical computational methods has been the result of a long evolutionary process, a summary of which has been published.[5] Most of this work has been done during the last ten years, and a large fraction of it over the last five years. Our laboratory has been very active in this field, having published 27 papers in it since 1973. Much of this work was done under an AFOSR grant which started in June 1973. The field of quantum reaction dynamics, as pointed out in Section 3 below, is important for the development of modern technologies of interest to the Air Force. We now summarize the contributions of our laboratory to the development of this area of chemistry.

Our first involvement in this field was to modify the boundary value finite difference method[6] so as to be able to use it on realistic potential energy surfaces and to apply it to the collinear H_3 system[7] and its isotopic counterparts.[8] These calculations were the first ones done on a realistic potential energy surface at high enough collision energies to show quantum oscillations. A lifetime and scattering matrix analysis later showed these oscillations to be due to interferences between direct and resonant (i.e., compound state) reaction mechanisms.[9] We also compared the accurate collinear H_3 quantum results with approximate ones obtained from the same potential energy surface using quasi-classical trajectory and semi-classical methods.[10] These showed that quantum effects were very large for this system and that quasi-classical and semi-classical reaction probabilities and rate constants could differ significantly from the accurate quantum ones. A streamline analysis of the scattering wavefunction[11] showed that tunneling proceeded by cutting the activation barrier

corner and contributed significantly to the rate constant even for temperatures
high enough for the Arrhenius plot not to show curvature. Even at 1000°K,
tunneling was responsible for about 25% of the collinear rate constant. We also
made an analysis of the scattering wavefunction in terms of the vibrationally
adiabatic theory of chemical reactions[12] and concluded that it is approximately
valid only over a relatively narrow range of collision energies, breaking down
both at low energies (due to tunneling) and at high energies.

The boundary value finite difference method used to calculate the collinear
H_3 scattering wavefunction consumed large amounts of computer time.[7] For
this reason we developed a significantly more effective coupled-channel tech-
nique in which coordinates and basis sets are chosen differently in different
regions of configuration space to take into account the shape of the potential
energy surface and to minimize the number of basis functions required for a
good local representation of the wavefunction.[13] This method was two to three
orders of magnitude more efficient than the finite difference one. It was used
to extend the collinear H_3 calculations to higher energies[9] while maintaining
a high computational accuracy (1% or better). This permitted the detailed
characterization of two resonances and the discovery of a third one. We then
used this method in a detailed study of the collinear $F + H_2 \rightarrow FH + H$ reaction
and of its isotopic counterparts.[14] We also performed quasi-classical trajectory
and semi-classical calculations on the same surface, and found large quantum
effects on this system also, which led to very erroneous quasi-classical product
vibrational population ratios.[14] Interestingly, the results of the "reverse"
quasi-classical calculations are much better than those of the "forward" ones.[14bc]
We also applied this coupled-channel method to study the collinear deactivation
of vibrationally excited HF by exchange collisions with H atoms on a LEPS
surface[15] having a barrier of only 1 kcal/mole. It was found that this is a

very efficient process.[16] Recent <u>ab initio</u> calculations of this surface[17] show that the correct value of this barrier is probably much higher, of the order of 30 or 40 kcal/mole. As a result, we have made an extensive series of calculations on the exchange reaction $H + FH(v) \rightarrow HF(v') + H$ and of its isotopic counterparts for six different barrier heights ranging from 1 to 40 kcal/mole. This work is being written up for publication. The results indicate that this exchange reaction cannot fully explain the preferential deactivation of $HF(v)$ for $v = 4, 5, 6$ compared with $v = 1, 2, 3$.

The experience gained in the development and application of the coupled-channel method for collinear reactive systems permitted us to extend it to coplanar systems. A serious conceptual difficulty appeared in connection with the bifurcation of the wavefunction into the two-reaction product arrangement channels. It was overcome with the help of a new representation[18] of the potential energy function in terms of symmetrized hyperspherical coordinates. We were than able to obtain accurate solutions for coplanar H_3[19] without major difficulty. These showed that, as for the collinear system, three or more closed vibrational quantum states had to be used in the coupled-channel expansion for convergence to be achieved. Neglect of such closed channels leads to large errors in the cross sections.

The next step was to extend the method to the full three-dimensional system. This was achieved fairly rapidly in view of the experience with the coplanar problem, and fully-converged calculations for the H_3 system were obtained.[2,5,20] These calculations indicated that the resonances found in the collinear system continued to appear in 3D. The 3D resonance energy[5,20a] was shifted upwards with respect to the 1D one by about twice the zero-point energy of the bending mode of the saddle-point configuration, indicating that it is related to the properties of the surface in the neighborhood of that point.

The exchange rate constant was computed using the quantum cross sections. At 200°K, it was 18 times greater than the corresponding quasi-classical one, indicating the importance of tunneling in this system. A polarization quasi-selection rule was discovered, according to which the dominant reactive channel is the $m_j = m'_{j'} = 0$ one where $m_j(m'_{j'})$ is the component of the angular momentum of the reagent (product) molecule along the initial (final) relative velocity vector. This rule is interpreted as being due to the fact that the H_3 system is collinearly dominated,[5, 20c] and may in the future be used as an experimental test of the collinear nature of a reactive system. For nonreactive collisions, the cross sections from a given m_j to all final $m'_{j'}$ (for given initial j and final j' diatom angular momentum quantum numbers) are of the same order of magnitude, indicating that the m_j conservation principle is not valid for such collisions. The accurate 3D calculations were performed to high enough energies for the first resonance to develop.[20a] These are the only such calculations ever done and have predicted the existence of Feshbach resonances in chemical reactions in the real 3D world. These calculations are the only ones available which are sufficiently accurate to give reliable angular distributions. To obtain such distributions, enough partial waves must be used and each one of them must be converged with respect to closed vibrational channels, since otherwise spurious oscillations can appear in the differential cross section.[21] We have found three of four closed vibrational channels to be necessary to achieve such a convergence.[2, 20bc] In the only other 3D accurate quantum dynamical calculation,[3] only two closed vibrational channels were used throughout without attempting to test for vibrational channel convergence, and differential cross sections were not calculated. It is possible to obtain reliable integral cross sections without achieving such complete convergence,

if the absolute values of the elements of the partial wave scattering matrices have approximately converged. Convergence of their phase is more difficult to achieve, and it is the lack of convergence in them which produces the spurious differential cross section oscillations just mentioned. We were also able to see oscillations in the para-to-para differential cross sections associated with inter-ference between the direct and exchange scattering amplitude. We performed, in addition, calculations using angular momentum decoupling schemes[22] (see Section 3.3 below) and found that they furnish accurate $m_j = m'_{j'} = 0$ integral reaction cross sections but inaccurate ones for other reactive and all nonreactive state-to-state cross sections. However, when calculating nonreactive cross sections summed over $m'_{j'}$ and averaged over m_j, good agreement was again found between the decoupled and accurate results, indicating that this approxi-mation transfers all nonreactive flux into the $m'_{j'} = 0$ product state.

Computer programs needed for the computation of accurate quantum mechanical cross sections of reactions of the type $A + B_2 \rightarrow AB + B$ and $A + BC \rightarrow AB + C$, $AC + B$ have been written and are presently being tested.

We have also used hyperspherical coordinates to develop a rigorous method for the calculation of exchange reactions, breakup collisions, and of termolecular recombinations. The accuracy of this method is being tested, and the preliminary results are encouraging.

The problem of the electronic branching ratio for the products of a chemi-luminescent chemical reaction is a very important one for the development of electronic chemical lasers. Such reactions are electronically nonadiabatic, and in their simplest form involve two electronic potential energy surfaces and an interactive one. We have investigated such electronically nonadiabatic processes in a collinear model for the important chemiluminescent reaction, $Ba + ON_2 \rightarrow BaO^* + N_2$. A comparison[23] of accurate quantum calculations and

surface-hopping[24] ones indicated that the latter were unreliable due to the presence of large quantum effects. A de Broglie wavelength analysis at thermal energies indicates that this system, although quite heavy, has nevertheless a strongly quantum character, i.e., the potential energy surface varies appreciably over a distance of one wavelength.

In the process of trying to experiment with different potential energy surfaces for studying collinear reactions, we have developed a useful semi-numerical representation of such surfaces[25] which permits one to change independently each of their different topological characteristics. We have generalized this representation to noncollinear systems and a paper describing such a generalization is in preparation.

In summary, the progress achieved in the solution of important quantum dynamical problems in our laboratory over the four-year period covered by this report was substantial.

3. OVERVIEW OF THE WORK PERFORMED AND OF ITS RELEVANCE TO THE AIR FORCE

The research performed under the present grant involved a set of theoretical investigations which were aimed at the understanding of elementary processes in bimolecular or termolecular collisions of reactive atoms or molecules. The central unifying theme in this research was the nature of the energy flow in chemical reactions and the magnitude of quantum effects in determining such flow. Examples of questions we investigated were: For a given shape of a potential energy surface, how does the height of the activation barrier affect the reaction cross section and the distribution of energy among the vibrational levels of the products? How valid are classical and semi-classical approximations to the accurate quantum dynamics describing such reactive systems? How valid are angular momentum decoupling schemes? What are the characteristics of avoided crossings of potential energy surfaces which are effective in producing electronically excited reaction products? How significant are Feshbach resonances in chemical reactions? Can the cross sections for breakup collisions be efficiently calculated by quantum methods? The answers to questions of this type were provided by obtaining accurate or approximate solutions to the quantum dynamical equations of motion describing such systems. To obtain these answers, accurate potential energy surfaces were not required. It was sufficient to do accurate and approximate quantum dynamical calculations on the same reasonably realistic surface. This approach permits the exploration of the relation between the nature of such surfaces and the outcome of the chemical reactions occurring on it. In cases in which the prediction of quantitative reaction cross sections is required, accurate potential energy surfaces are needed, and in this case it is useful to know, ahead of time, what regions of the surfaces most influence the dynamical

know, ahead of time, what regions of the surfaces most influence the dynamical results. Calculations with approximate surfaces provide an answer to this question.

In many chemical systems of interest, one can, on the basis of a de Broglie wavelength analysis, expect the presence of significant quantum effects. This is the case not only for hydrogen-atom containing systems, such as H_3, H_2F, and H_2Cl, but also for those involving fairly heavy atoms, such as $BaON_2$, as described in Section 2. An analysis of a model of this system[23] indicated that at thermal energies and higher, the value of the potential energy along the reaction coordinate changes appreciably over one de Broglie wavelength, and dynamical calculations show the presence of significant quantum effects in this heavy system. It was therefore most important to use quantum dynamics in studying such systems to determine the regions of the surface to which the reaction is sensitive and to establish the degree to which classical and semi-classical approaches may give reliable results.

The answers to the questions mentioned above are useful not only for the basic understanding of reactive processes but also for the application of this knowledge to advanced technologies such as high energy chemical lasers, plume technology, and the chemical effects of high energy radiation, which are of interest to the United States Air Force. Specific examples are the transfer of energy in collisions involving F atoms, H_2 molecules, and FH molecules and their isotopic counterparts, which are important in connection with the fluorine-hydrogen chemical laser, and the calculation of electronic branching ratios, of importance for the development of electronic inversion chemical lasers. These technologies and their applications are closely coupled to the current status of scientific development, and the latter must advance very rapidly if it is not to be an absolute barrier to the progress of the former. It is hoped that the research reported here has contributed towards the achievement of this goal.

4.   REFERENCES

1.   P. A. M. Dirac, Proc. Roy. Soc. (London), A123, 714 (1929).

2.   Aron Kuppermann and G. C. Schatz, J. Chem. Phys. 62, 2502 (1975).

3.   A. B. Elkowitz and R. E. Wyatt, J. Chem. Phys. 62, 2504 (1974);
       ibid. 63, 702 (1975).

4.   A. L. Robinson, "Chemical Dynamics: Accurate Quantum Calculations
       at Last," Science, 19, 275 (1976).

5.   Aron Kuppermann, "Progress in the Quantum Dynamics of Reactive
       Molecular Collisions," in The Physics of Electronic and Atomic Collisions,
       edited by J. S. Risley and R. Geballe (University of Washington Press,
       Seattle, 1976), pp. 259-274.

6.   D. J. Diestler and V. McKoy, J. Chem. Phys. 48, 2951 (1968).

7.   D. G. Truhlar and Aron Kuppermann, (a) J. Chem. Phys. 52, 3841 (1970);
       (b) ibid. 56, 2232 (1972); (c) D. J. Diestler, D. G. Truhlar and Aron
       Kuppermann, Chem. Phys. Lett. 13, 1 (1972).

8.   D. G. Truhlar, Aron Kuppermann, and J. T. Adams, J. Chem. Phys.
       59, 395 (1973).

9.   G. C. Schatz and Aron Kuppermann, J. Chem. Phys. 59, 964 (1973).

10.   J. M. Bowman and Aron Kuppermann, (a) Chem. Phys. Lett. 12, 1
       (1971); (b) ibid. 19, 166 (1973); (c) Chem. Phys. 2, 158 (1973); (d) J.
       Chem. Phys. 59, 6524 (1973).

11.   Aron Kuppermann, J. T. Adams, and D. G. Truhlar, Abstracts of
       Papers, Eighth International Conference on the Physics of Electronic
       and Atomic Collisions, edited by B. C. Cobic and M. V. Kurepa
       (Institute of Physics, Belgrade, Yugoslavia, 1973), p. 149.

12.   J. M. Bowman, Aron Kuppermann, J. T. Adams, and D. G. Truhlar,
       Chem. Phys. Lett. 20, 229 (1973).

13. Aron Kuppermann, (a) <u>Proceedings of the Conference on Potential Energy Surfaces in Chemistry</u>, University of California, Santa Cruz, California, 10-13 August 1970 (IBM Research Laboratory, San Jose, California, 1971), pp. 121-134; (b) <u>Abstracts of Papers, Seventh International Conference on the Physics of Electronic and Atomic Collisions,</u> edited by L. Branscomb (North-Holland Publishing Co., Amsterdam, 1971), p. 3.

14. G. C. Schatz, J. M. Bowman, and Aron Kuppermann, (a) J. Chem. Phys. 58, 4023 (1973); (b) Chem. Phys. Lett. 24, 378 (1974); (c) J. Chem. Phys. 63, 674 (1975); (d) <u>ibid.</u> 63, 685 (1975).

15. (a) P. A. Whitlock and J. T. Muckerman, J. Chem. Phys. 61, 4618 (1975); (b) J. T. Muckerman, personal communication (surface 5).

16. G. C. Schatz and Aron Kuppermann, "An Exact Quantum Study of Vibrational Deactivation by Reactive and Nonreactive Collisions in the Collinear Isotopic H + FH Systems," <u>Proceedings of the Army Symposium on High Energy Lasers</u>, Redstone Arsenal, Alabama, 3-4 November 1975, in press.

17. C. F. Bender, B. J. Garrison, and H. F. Schaefer III, J. Chem. Phys. 62, 1188 (1975).

18. Aron Kuppermann, Chem. Phys. Lett. 32, 374 (1975).

19. Aron Kuppermann, G. C. Schatz, and M. Baer, (a) J. Chem. Phys. 61, 4362 (1974); (b) <u>ibid.</u> 65, 4596 (1976); (c) G. C. Schatz and Aron Kuppermann, <u>ibid.</u> 65, 4624 (1976).

20. G. C. Schatz and Aron Kuppermann, (a) Phys. Rev. Lett. 35, 1266 (1975); (b) J. Chem. Phys. 65, 4642 (1976); (c) <u>ibid.</u> 65, 4668 (1976).

21. G. Wolken and M. Karplus, J. Chem. Phys. 60, 351 (1974).

22. Aron Kuppermann, G. C. Schatz, and J. P. Dwyer, Chem. Phys. Lett. 45, 71 (1977).

23. J. M. Bowman, S. C. Leasure, and Aron Kuppermann, Chem. Phys. Lett. 43, 374 (1976).

24. (a) R. K. Preston and J. C. Tully, J. Chem. Phys. 54, 4297 (1971); (b) J. C. Tully and R. K. Preston, ibid. 55, 562 (1971); (c) J. R. Krenos, R. K. Preston, R. Wolfgang, and J. C. Tully, ibid. 60, 1634 (1974).

25. J. M. Bowman and Aron Kuppermann, Chem. Phys. Lett. 34, 523 (1975).

5.   LIST OF PUBLICATIONS AND REPRINTS

The following is a list of publications which have resulted so far from the work of this grant.

Coplanar and Collinear Quantum Mechanical Reactive Scattering: The Importance of Virtual Vibrational Channels in the $H + H_2$ Exchange Reaction.
Aron Kuppermann, G. C. Schatz, and M. Baer.
J. Chem. Phys. 61, 4362 (1974).

Quantum Mechanical Reactive Scattering: An Accurate Three-Dimensional Calculation.
Aron Kuppermann and G. C. Schatz.
J. Chem. Phys. 62, 2502 (1975).

A Useful Mapping of Triatomic Potential Energy Surfaces.
Aron Kuppermann.
Chem. Phys. Lett. 32, 374 (1975).

Exact Quantum, Quasiclassical, and Semiclassical Reaction Probabilities for the Collinear $F + H_2 - FH + H$ Reaction.
G. C. Schatz, J. M. Bowman, and Aron Kuppermann.
J. Chem. Phys. 63, 674 (1975).

Exact Quantum, Quasiclassical, and Semiclassical Reaction Probabilities for the Collinear $F + D_2 - FD + D$ Reaction.
G. C. Schatz, J. M. Bowman, and Aron Kuppermann.
J. Chem. Phys. 63, 685 (1975).

A Semi-Numerical Approach to the Construction and Fitting of Triatomic Potential Energy Surfaces.
J. M. Bowman and Aron Kuppermann.
Chem. Phys. Lett. 34, 523 (1975).

Progress in the Quantum Dynamics of Reactive Molecular Collisions.
Aron Kuppermann.
In the Physics of Electronic and Atomic Collisions (Invited Lectures, Review Papers, and Progress Reports of the IXth International Conference on the Physics of Electronic and Atomic Collisions, Seattle, Washington, 24-30 July 1975), edited by J. S. Risley and R. Geballe (University of Washington Press, Seattle, 1976), pp. 259-274.

An Exact Quantum Study of Vibrational Deactivation by Reactive and Nonreactive Collisions in the Collinear Isotopic $H + FH$ Systems.
G. C. Schatz and Aron Kuppermann.
In the Proceedings of the Symposium on High Energy Transfer Lasers, Redstone Arsenal, Alabama, 3-4 November 1975 (U.S. Army Missile Command, Redstone Arsenal, August, 1976), Special Report RH-7T-1, pp. 132-142.

Dynamical Resonances in Collinear, Coplanar, and Three-Dimensional Quantum Mechanical Reactive Scattering.
G. C. Schatz and Aron Kuppermann.
Phys. Rev. Lett. 35, 1266 (1975).

Quantum Mechanical Reactive Scattering for Planar Atom Plus Diatom Systems. I. Theory
A. Kuppermann, G. C. Schatz, and M. Baer.
J. Chem. Phys. 65, 4596 (1976).

Quantum Mechanical Reactive Scattering for Planar Atom Plus Diatom Systems. II. Accurate Cross Sections for $H + H_2$.
G. C. Schatz and A. Kuppermann.
J. Chem. Phys. 65, 4624 (1976).

Quantum Mechanical Reactive Scattering for Three-Dimensional Atom Plus Diatom Systems. I. Theory.
G. C. Schatz and A. Kuppermann.
J. Chem. Phys. 65, 4642 (1976).

Quantum Mechanical Reactive Scattering for Three-Dimensional Atom Plus Diatom Systems. II. Accurate Cross Sections for $H + H_2$.
G. C. Schatz and A. Kuppermann.
J. Chem. Phys. 65, 4668 (1976).

Large Quantum Effects in a Model Electronically Nonadiabatic Reaction: $Ba + N_2O \rightarrow BaO^* + N_2$.
J. M. Bowman, S. C. Leasure, and A. Kuppermann.
Chem. Phys. Lett. 43, 374 (1976).

Validity of the Adiabatic Approximation for Vibrational Energy Transfer in Collisions Between Diatomic Molecules.
J. P. Dwyer and A. Kuppermann.
Chem. Phys. Lett. 44, 499 (1976).

Angular Momentum Decoupling Approximations in the Quantum Dynamics of Reactive Systems.
A. Kuppermann, G. C. Schatz, and J. P. Dwyer.
Chem. Phys. Lett. 45, 71 (1977).

PhD Theses

Joel Mark Bowman, Theoretical Studies of Electronically Adiabatic and Non-Adiabatic Chemical Reaction Dynamics, California Institute of Technology, 1975.

George Chappell Schatz, The Quantum Dynamics of Atom Plus Diatom Chemical Reactions, California Institute of Technology, 1976.

John Patrick Dwyer, Quantum Mechanical Studies of Molecular Scattering, California Institute of Technology, 1978.

Reprints of these publications are attached, except for the three PhD theses, which are very bulky. They are available upon request.

Coplanar and collinear quantum mechanical reactive scattering: The importance of virtual vibrational channels in the H + H₂ exchange reaction·

Aron Kuppermann, George C. Schatz[*], and Michael Baer[‡]

Arthur Amos Noyes Laboratory of Chemical Physics,[§] California Institute of Technology, Pasadena, California 91109
(Received 22 August 1974)

We have performed accurate quantum mechanical calculations for the coplanar H + H₂ exchange reaction, using sufficient rotational and vibrational basis functions in the close-coupling expansion to ensure convergence. We repeated these calculations with a converged rotational basis set but with only one vibrational basis function, in analogy to what Saxon and Light[1] and Wolken and Karplus,[2] respectively, did for the similar coplanar and three dimensional reaction. The vibrationally converged and one-vibration results differ substantially for the coplanar as well as the collinear reaction, indicating the crucial role played by virtual vibrational channels.

To solve the Schrödinger equation for the coplanar reaction, we first integrated the appropriate coupled equations into the interaction region from each of the three arrangement channel regions, using an extension of the method developed by Kuppermann.[3] The resulting solutions were then smoothly matched on three conveniently chosen surfaces in configuration space. The R matrix and other asymptotic quantities were then obtained.

Calculations for the Porter–Karplus surface[4] using 4 or 5 vibrations and 10 or 12 rotations per vibration for a total of 40 to 60 channels yielded reaction probabilities that change by less than 2%–5% as additional vibrational or rotational basis functions are added, over the total energy range 0.30–0.60 eV. Without forcing orthogonalization at any time, the results satisfy conservation of flux to 0.5% or better and time reversal invariance to 6% or better. The calculations were repeated using the same number of rotations but only one vibration, and introducing an appropriate vibrational orthogonalization.

The resulting total reaction cross sections σ_0^R are plotted in Figs. 1(a) and 1(b) and show differences between the vibrationally converged and one-vibration results greater than 3 orders of magnitude at low energies. The ratio of the one-vibration to vibrationally converged ortho–para rate constants is 3.15 at 300 °K and 532 at 100 °K.

Using the method developed previously,[3] we calculated the collinear converged[5] and one-vibration reaction probabilities for the same potential energy surface. The ratios of the coplanar to collinear cross sections are plotted in Fig. 1(c). Although these cross sections vary individually by about 12 orders of magnitude over the energy range considered, their ratios vary by less than 2 orders of magnitude, indicating a remarkably similar energy dependence. Virtual vibrational channels are

furthermore about equally important in the collinear[6] and coplanar H + H₂ reaction. This will probably still be the case for this system in three dimensions as well as for other reactions.

We have also calculated the reactive, inelastic, and antisymmetrized differential cross sections for coplanar
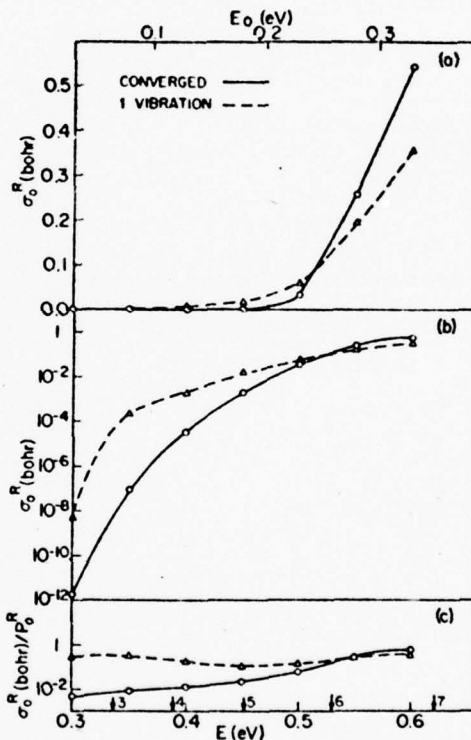
FIG. 1. Total reactive cross section σ_0^R versus the total energy E and translational energy E_0 for the coplanar exchange reaction H + H₂ ($v = 0, j = 0$) → H₂ ($v = 0, j'$) + H (summed over all j') where the atoms are considered distinguishable. Arrows in abscissa indicate energies at which the vibration–rotation states ($v = 0, j'$) of H₂ become accessible. (a) Linear plot; (b) semilogarithmic plot. In (c) we plot the ratio σ_0^R/P_0^R versus energy, where P_0^R is the collinear total reaction probability (the collinear total reaction cross section) for reagents H₂ in $v = 0$ initially. In all cases, a solid line indicates vibrationally converged results, while a dashed line indicates one-vibration results as defined in text.

$H + H_2$. Contrary to the results of Saxon and Light[1] our reactive differential cross sections show only backward peaking in both the one-vibration and vibrationally converged results. In addition, we find no evidence for a quasiselection rule governing the reaction probabilities similar to the ortho–ortho and para–para nonreactive selection rule. We were able to artificially produce such a reactive quasiselection rule using matching procedures in which incorrect symmetry restrictions were placed on the matched wavefunctions.[7]

The inelastic cross sections are generally backward or sideward peaked and exhibit no fine oscillatory structure. Quantum symmetry oscillations resulting from interference between the direct and exchange amplitudes characterize some ortho–ortho and para–para antisymmetrized differential cross sections at total energies greater than 0.5eV.

In conclusion, virtual vibrational channels play a central role in the collinear and coplanar $H + H_2$ reaction, and probably in the three dimensional one and in many other reactions. Therefore, the results of calculations using only open vibrational channels must be used with great caution. Once those virtual channels are included in a close-coupling reactive scattering calculation and convergence ascertained, a wealth of detailed physically meaningful information is obtained against which a variety of dynamical models can be tested. Work along these lines is proceeding in this laboratory.

We thank Ambassador College for the use of their

computational facilities in most of the calculations reported here.

[1]R. P. Saxon and J. C. Light, J. Chem. Phys. **56**, 3874 (1972); **56**, 3885 (1972).
[2]G. Wolken and M. Karplus, J. Chem. Phys. **60**, 351 (1974).
[3]A. Kuppermann, *Potential Energy Surfaces in Chemistry*, edited by W. Lester (University of California at Santa Cruz, Santa Cruz, 1970), pp. 121–129; *VII International Conference on the Physics of Electronic and Atomic Collisions, Abstracts of Papers* (North-Holland, Amsterdam, 1971), p. 3; G. C. Schatz, J. M. Bowman, and A. Kuppermann, J. Chem. Phys. **56**, 4023 (1973); G. C. Schatz and A. Kuppermann, *ibid.* **59**, 964 (1973); J. M. Bowman, G. C. Schatz, and A. Kuppermann, Chem. Phys. Lett. **24**, 378 (1974).
[4]R. N. Porter and M. Karplus, J. Chem. Phys. **40**, 1105 (1964).
[5]These results are identical to those of D. J. Diestler, J. Chem. Phys. **54**, 4547 (1971).
[6]Virtual channels have been found to be important in many collinear collisions, such as in M. E. Riley and A. Kuppermann, Chem. Phys. Lett. **1**, 537 (1968); D. G. Truhlar and A. Kuppermann, J. Chem. Phys. **52**, 3841 (1970); **56**, 2232 (1972); S. F. Wu and R. D. Levine, Mol. Phys. **22**, 881 (1971); and Ref. 3 above.
[7]Recently J. C. Light has obtained similar results in a modified version of his one-vibration method (private communication).

Quantum mechanical reactive scattering: An accurate three-dimensional calculation*

Aron Kuppermann and George C. Schatz[†]

A. A. Noyes Laboratory of Chemical Physics, Division of Chemistry and Chemical Engineering,[‡] California Institute of Technology, Pasadena, California 91125
(Received 16 December 1974)

We have performed accurate three-dimensional (3-D) quantum-mechanical calculations of differential and total cross sections for the $H + H_2$ exchange reaction on the Porter–Karplus[1] potential energy surface. These are the first such calculations that are vibrationally and rotationally converged, and the results are believed to be accurate to 5% or better. They can serve as a comparison standard against which approximate methods can be tested.

To solve the body-fixed 3-D Schrödinger equation for the nuclear motion we perform a partial wave expansion, followed by a close-coupling expansion. For the latter we use variables and basis functions which vary from region to region of configuration space so as to optimize the representation of the wavefunction. This approach, developed previously,[2] has been successfully applied to collinear[3] and coplanar[4] reactions also. The coupled equations are integrated into the interaction region from each of the three arrangement channel regions, using the use of the Gordon method.[5] The solutions are smoothly matched on three appropriately chosen surfaces in internal configuration space by employing the convenient system of coordinates described elsewhere.[6] The full three-body Hamiltonian was used in these calculations, and no approximations were introduced other than those inherent in the numerical methods.

We have performed extensive calculations in the range of total energy $E = 0.40-0.70$ eV and have found that up to 30 rotational, 4 vibrational, and 100 total basis functions are necessary for convergence of the reaction probabilities to within 5%. The converged results usually satisfy conservation of flux to 1% or better and time reversal invariance to about 6% or better. We found however that, as for the coplanar reaction,[4] results satisfying flux conservation and time reversal invariance could be obtained before satisfactory convergence was achieved. One cannot, therefore, rely on flux conservation and time reversal invariance as sufficient conditions for convergence. All values of the total angular momentum J from 0 to about 12 are needed for convergence of the reactive differential cross sections. The angular dependence of the differential cross sections are very sensitive to the magnitudes and phases of the scattering matrix elements. It is of crucial importance to establish the vibrational and rotational convergence of the results for each J, since otherwise spurious oscillations in the differential cross sections can result. The integral reaction cross sections are much less susceptible to these effects. Computation times on an IBM 370-158 for each E were 13, 33, 62, and 64 minutes for $J = 0$, 1, 2, and 3, respectively, and approximately 75 min for $J \geqslant 4$ and 100 basis functions.

The following conclusions can be inferred from the results obtained:

(1) Inclusion of closed vibrational channels in the close-coupling expansion is essential, in spite of the fact that this increases the computational time by factors of 10–30. For example, at 0.50 eV the $J = 0$ distinguishable-atom reaction probability for the $v = 0$, $j = 0$ reagent to the $v' = 0$, $j' = 1$ product[7] is 0.71×10^{-3} for the vibrationally converged results and 1.87×10^{-3} when using only ground vibrational state basis functions, a difference of a factor of 2.6. Also, at $E = 0.55$ eV the vibrationally converged, orientation-averaged (i.e., summed over m'_j and averaged over m_j), para–ortho reaction cross section for the same process, is 0.040 bohr².
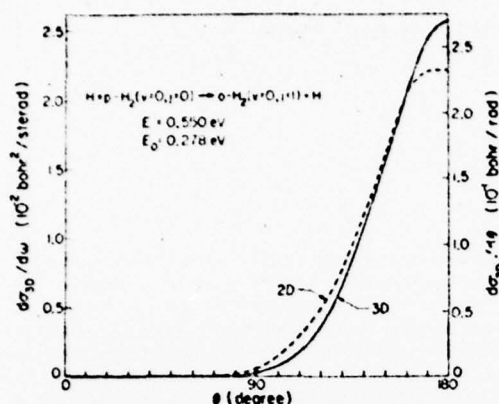
FIG. 1. Three-dimensional $(d\sigma_{3-D}/d\omega)$ and coplanar $(d\sigma_{2-D}/d\theta)$ para → ortho differential reactive cross section as a function the scattering angle θ for the $H + H_2 \rightarrow H_2 + H$ exchange reaction on the Porter–Karplus[1] potential energy surface at a total energy $E = 0.550$ eV and relative reagent translational energy $E_0 = 0.278$ eV. The corresponding wave functions have been antisymmetrized with respect to hydrogen atom exchange. The para-H_2 reagent is in its ground $v = 0$, $j = 0$ vibrational–rotational state. The ortho-H_2 product is in its ground $v' = 0$ vibrational and $j' = 1$ rotational state, the lowest permitted by the Pauli principle. Contributions from all mj' values of the component of the angular momentum of the diatom product have been included in the cross sections. The solid line represents the three-dimensional results, for which the ordinate scale is at the left of the figure, and the dashed line depicts the coplanar results, for which the ordinate scale is at its right. The corresponding integral reaction cross sections are $\sigma_{3D} = 0.040$ bohr^2 and $\sigma_{2-D} = 0.36$ bohr, respectively.

Wolken and Karplus,[8] in their pioneering work in which similarly only ground vibrational state basis functions were employed, obtained a value of about 0.43 bohr^2. This difference of a full order of magnitude between these last two results must be due at least in part to their neglect of closed vibrational channels. Their phenomenological energy threshold is approximately 0.05 eV below our vibrationally converged one.

(2) Because of the much smaller times involved in the $J = 0$ calculations, it would be very helpful if computations of this type, such as those performed by Elkowitz and Wyatt,[9] were representative of the over-all reaction. We do find that at each energy E, the ratio of two orientation-averaged integral reaction cross sections from the same state of the reagents to different states of the products, usually agrees to within 20% with the corresponding $J = 0$ reaction probability ratio. However, the value of J which most contributes to the integral reaction cross sections is 2 at 0.40 eV increasing to 4 at 0.70 eV. As a result, the $J = 0$ calculations do not furnish accurate predictions for other appropriate quantities. For example, if we compare the ratio of two orientation-averaged integral reaction cross sections from different states of reagents to the same state of the products, at the same total energy, with the corresponding $J = 0$ reaction probability ratio, these quantities can

differ by a factor of 2 or greater.

(3) Let Ω be the angular momentum associated with the tumbling of the triatomic plane around the position vector of the atom with respect to the diatom.[10] For small J, we observe in each arrangement channel only a weak dynamic coupling between states having different values of Ω. This agrees with previous observations by Pack[10] and McGuire and Kouri[11] for nonreactive rotationally inelastic scattering. In addition, for J less than about 5 or 6, the $\Omega = 0$ reaction probabilities are usually significantly larger, by factors of 2–20, than the others. Neglect of Ω-coupling and of unimportant Ω contributions can shorten the computation time by one or two orders of magnitude. Preliminary calculations of this type indicate that these approximations can yield results which are quite accurate.

(4) The distribution of products among the several orientation-averaged rotational energy levels is very similar for the 3-D and coplanar reactions. In addition, the angular dependence of the corresponding differential cross sections is also very similar, as shown in Fig. 1.

(5) Over the range of total energies 0.60–0.70 eV, our distinguishable-atom reaction cross section from $v = j = 0$ reagent, summed over all final states of the products, agrees with the quasiclassical trajectory results of Karplus, Porter, and Sharma,[12] within the accuracy of the calculations.

Although Conclusions (1) and (2) indicate that accurate calculations are quite lengthy and can only be done for a small number of benchmark systems, conclusions (3)–(5) indicate that approximate methods that are still very realistic but much faster, might be developed and usefully applied to a significantly larger number of reactions.

We thank Ambassador College for generous use of their computational facilities.

[1] R. N. Porter and M. Karplus, J. Chem. Phys. 40, 1105 (1964).
[2] A. Kuppermann, Potential Energy Surfaces in Chemistry, edited by W. Lester (University of California at Santa Cruz, Santa Cruz, 1970) pp. 121–129; VII International Conference on the Physics of Electronic and Atomic Collisions, Abstracts of Papers (North-Holland, Amsterdam, 1971), p. 3.
[3] G. C. Schatz and A. Kuppermann, J. Chem. Phys. 59, 964 (1973); G. C. Schatz, J. M. Bowman, and A. Kuppermann, J. Chem. Phys. 58, 4023 (1973).
[4] A. Kuppermann, G. C. Schatz, and M. Baer, J. Chem. Phys. 61, 4362 (1974).
[5] R. G. Gordon, J. Chem. Phys. 51, 14 (1969).
[6] A. Kuppermann, "A Useful Mapping of Triatomic Potential Energy Surfaces," Chem. Phys. Lett. (in press).
[7] The unprimed v, j, and m_j are the vibrational, rotational and magnetic quantum numbers of the reagent molecule, whereas

the corresponding primed quantities refer to the product molecule.

[8]G. Wolken and M. Karplus, J. Chem. Phys. 60, 351 (1974).

[9]A. B. Elkowitz and R. E. Wyatt, "Three-dimensional natural coordinate asymmetric top theory of reactions: Application to $H + H_2$," J. Chem. Phys. (in press).

[10]R. T. Pack, J. Chem. Phys. 60, 633 (1974).

[11]P. McGuire and D. J. Kouri, J. Chem. Phys. 60, 2488 (1974).

[12]M. Karplus, R. N. Porter, and R. D. Sharma, J. Chem. Phys. 43, 3259 (1965).

A USEFUL MAPPING OF TRIATOMIC POTENTIAL ENERGY SURFACES *

Aron KUPPERMANN

*Arthur Amos Noyes Laboratory of Chemical Physics **, Division of Chemistry and Chemical Engineering,
California Institute of Technology, Pasadena, California 91125, USA*

We present in this paper a mapping of triatomic three-dimensional Born–Oppenheimer potential energy surfaces V for which all arrangement channels are represented evenhandedly. This representation is very useful for visualizing the geometrical and dynamical properties of such surfaces.

Consider the system of atoms A_α, A_β, A_γ and let $\lambda\nu\kappa$ be a cyclic permutation of $\alpha\beta\gamma$. Let r_λ' and R_λ' be respectively the vector from A_ν to A_κ and from the center of mass of $A_\nu A_\kappa$ to A_λ. We define [1–3] two scaled vectors r_λ and R_λ as $a_\lambda^{-1} r_\lambda'$ and $a_\lambda R_\lambda'$, respectively, where a_λ is the dimensionless scale factor $(\mu_{\lambda,\nu\kappa}/\mu_{\nu\kappa})^{1/4}$, $\mu_{\nu\kappa}$ being the reduced mass of $A_\nu A_\kappa$, and $\mu_{\lambda,\nu\kappa}$ that of the $A_\lambda + A_\nu A_\kappa$ pair. The $r_\lambda, R_\lambda \rightarrow r_\nu, R_\nu$ transformation is a rotation in configuration hyper-space [3].

V depends only on three scalar internal configuration coordinates. These can be chosen as r_λ, R_λ and the angle γ_λ (in the 0, π range) between r_λ and R_λ. In order to map $V(r_\lambda, R_\lambda; \gamma_\lambda)$, we must establish a correspondence between r_λ, R_λ, γ_λ and points P_λ of a three-dimensional internal arrangement configuration space $OX_\lambda Y_\lambda Z_\lambda$. One such correspondence is to assign to P_λ spherical polar coordinates r, η_λ, γ_λ where r is $(r_\lambda^2 + R_\lambda^2)^{1/2}$ and is independent [1] of the choice of λ, and η_λ is $\cos^{-1}(R_\lambda/r)$ in the range 0, $\pi/2$. For collinear configurations ($\gamma_\lambda = \pi$) this correspondence becomes one of the standard representations of V †. It suffers, however, from three serious disadvantages. One is that to each configuration in which A_λ coin-

cides with the center of mass of $A_\nu A_\kappa$ (i.e., $R_\lambda = 0$) there corresponds an infinity of points P_λ (forming a circle on the $OX_\lambda Y_\lambda$ plane centered on O and having radius r_λ). The second is that equivalent arrangement channels are not represented equivalently. The third is that an r, η_λ, $\gamma_\lambda \rightarrow r$, η_ν, γ_ν transformation does not preserve distances and distorts equipotential surfaces. These disadvantages make it difficult to obtain an unbiased vizualization of V in all regions of internal configuration space. A similar difficulty is present in the ingenious related representation proposed by Smith (see ref. [3], eqs. (24)).

A second mapping of $V(r_\lambda, R_\lambda, \gamma_\lambda)$ is to assign to P_λ spherical polar coordinates r, $\theta_\lambda = 2\eta_\lambda$ and γ_λ. The factor 2 by which θ_λ and η_λ differ is of central importance, in that it eliminates the difficulties described above by bringing about the validity of three very significant properties: to every internal configuration there corresponds only one point P_λ; undistinguishable arrangement channels are represented undistinguishably; and an r, θ_λ, $\gamma_\lambda \rightarrow r$, θ_ν, γ_ν transformation simply rotates equipotential surfaces around the OY_λ axis without distorting them. This produces a representation of the entire internal configuration space unbiased by the particular choice of λ used to define it.

In fig. 1 we depict intersections of the equipotential surfaces with the $OX_\alpha Z_\alpha$ and $OY_\alpha Z_\alpha$ planes for the notorious Karplus and Porter [5] potential function for the H_3 system. The OY_α axis, perpendicular

---

† Like that adopted by Tang et al. [4] after a rescaling of the distances by the a_λ factor as described in the present paper.
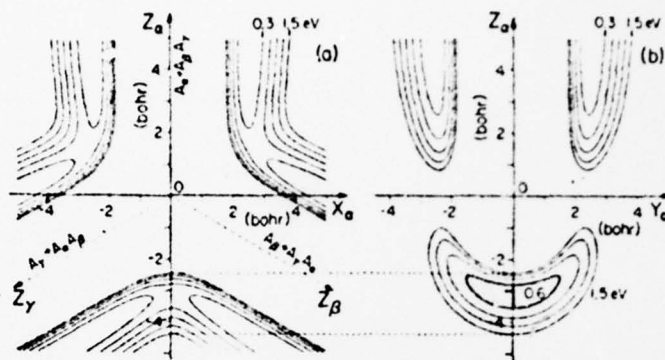
Fig. 1. Equipotential surfaces for H_3. The cartesian coordinates X_α, Y_α, Z_α are $r \sin\theta_\alpha \cos\gamma_\alpha$, $r \sin\theta_\alpha \sin\gamma_\alpha$ and $r \cos\theta_\alpha$, respectively, with r, θ_α and γ_α defined in the text. The range of γ_α was extended from $(0, \pi)$ to $(-\pi, \pi)$ by setting, for $\gamma_\alpha < 0$, $V(r, \theta_\alpha, -\gamma_\alpha) = V(r, \theta_\alpha, \gamma_\alpha)$. The curves are intersections of $V(r, \theta_\alpha, \gamma_\alpha) = E$ surfaces with the perpendicular planes $OX_\alpha Z_\alpha$ (fig. 1a) and $OY_\alpha Z_\alpha$ (fig. 1b). The origin of measurement of E is the minimum of the H_2 diatomic potential energy curve with the third atom removed. The values of E range from 0.3 eV to 1.5 eV in steps of 0.3 eV, as indicated on top of figure. All points on fig. 1a and those on the OZ_α axis of fig. 1b correspond to collinear configurations. Points on fig. 1b off that axis represent non-collinear configurations. Those on the OY_α axis (except for O) correspond to perpendicular configurations. The horizontal dashed lines interconnect the fig. 1a and fig. 1b intersections of the $E = 1.5$ eV equipotential with OZ_α. The OZ_λ axes ($\lambda = \alpha, \beta, \gamma$) in fig. 1a, as $r \to \infty$, correspond to the three separated atom–diatom arrangements. The fact that the angle between them is 120° rather than the usual [6] 60° is of central importance in permitting the three arrangement channels to be represented equivalently and in making the $r, \theta_\alpha, \gamma_\alpha \to r, \theta_\beta, \gamma_\beta$ transformation correspond to a rotation (without distortion) around the OY_α axis, which itself is invariant under this transformation. The bottom part of fig. 1b corresponds to the region halfway between configurations $A_\gamma + A_\alpha A_\beta$ and $A_\gamma A_\alpha + A_\beta$. All classically allowed pathways leading from one to the other of these configurations, at total energies not exceeding 0.6 eV, must pass through the hatched area enclosed by the corresponding equipotential.

to the plane of fig. 1a, is a threefold axis of symmetry of V, due to the equivalence of the three H atoms and of the corresponding arrangement channels. The lower part of fig. 1b depicts in detail the "transition state" region of configuration space halfway between the $A_\gamma + A_\alpha A_\beta$ reactant and $A_\gamma A_\alpha + A_\beta$ product configurations. At any energy E, all classically allowed pathways leading from such reagents to such products must pass through the region enclosed by the corresponding equipotential. The smaller E, the more confined is this region and the less can the intermediate reactive configurations deviate from collinearity. The characteristics of these "passages" between reagents and products influence significantly the dynamical properties of V.

We have constructed three-dimensional models of such equipotential surfaces, for the H_3 and FH_2 systems. The general properties of the $r, \theta_\lambda, \gamma_\lambda$ mapping will be published in detail separately, together with pictures of those models. The present paper should

suffice, however, to indicate that this mapping provides a very powerful means for visualizing the properties of triatomic potential energy surfaces and for developing exact and approximate reactive scattering theories.

References

[1] L.M. Delves, Nucl. Phys. 9 (1959) 391; 20 (1960) 275.
[2] D. Jepsen and J.O. Hirschfelder, Proc. Natl. Acad. Sci. US 45 (1959) 249.
[3] F.T. Smith, J. Math. Phys. 3 (1962) 735.
[4] K.T. Tang, B. Kleinman and M. Karplus, J. Chem. Phys. 50 (1969) 1119.
[5] R.N. Porter and M. Karplus, J. Chem. Phys. 40 (1964) 1105.
[6] S. Glasstone, K.J. Laidler and H. Eyring, The theory of rate processes (McGraw-Hill, New York, 1941) ch. 3.

Exact quantum, quasiclassical, and semiclassical reaction probabilities for the collinear F+H₂ → FH+H reaction*

George C. Schatz,† Joel M. Bowman,‡ and Aron Kuppermann

Arthur Amos Noyes Laboratory of Chemical Physics,§ California Institute of Technology, Pasadena, California 91125
(Received 22 October 1974)

Exact quantum, quasiclassical, and semiclassical reaction probabilities and rate constants for the collinear reaction F + H₂ → FH + H are presented and compared. The exact quantum results indicate a large degree of population inversion of the FH product with P_{02}^A and P_{03}^A being the dominant reaction probabilities. The energy dependence of these two probabilities at low translational energies are quite different. P_{02}^A shows an effective threshold of 0.005 eV which can largely be interpreted as resulting from tunneling through a vibrationally adiabatic barrier. P_{03}^A has a much larger effective threshold (0.045 eV) apparently resulting from dynamical effects. Quasiclassical probabilities for the collinear F + H₂ reaction were calculated by both the forward (initial conditions chosen for reagent F + H₂) and reverse (initial conditions for product H + FH) trajectory methods. The results of both calculations correctly indicate that P_{02}^A and P_{03}^A should be the dominant reaction probabilities. However, the threshold behavior of the quasiclassical forward P_{03}^A disagrees strongly with the corresponding exact quantum threshold energy dependence. By contrast, there is good agreement between the reversed trajectory results and the exact quantum ones. The uniform semiclassical results also agree well with the corresponding exact quantum ones indicating that the quasiclassical reverse and the semiclassical methods are preferable to the quasiclassical forward method for this reaction. The important differences between the threshold behavior of the exact quantum and quasiclassical forward reaction probabilities are manifested in the corresponding rate constants primarily as large differences in their activation energies. Additional exact quantum results at higher total energies indicate that threshold effects are no longer important for reactions with vibrationally excited H₂. Resonances play an important role in certain reaction probabilities primarily at higher relative translational energies.

I. INTRODUCTION

The reactions F + H₂(D₂, DH) → FH (FD) + H (D) have recently been the subject of several experimental studies in which very detailed rate constants and cross sections for these reactions have been measured. Relative rate constants into specific vibrational (and sometimes vibrational–rotational) states of the products have been measured by both infrared chemiluminescence[1] and chemical laser[2] techniques and, quite recently, both methods have been used to study the temperature dependences of these relative rates.[1c,3a] Angular distributions for specific product vibrational states of the F + D₂ reaction have been studied at several incident energies by a crossed molecular beam apparatus.[3] In addition, there exist several (usually indirect) determinations of the over-all bulk rate constants for the F + H₂ reaction[4] and, more recently, studies of isotope effects for the F + H₂, F + D₂, F + HD, and F + DH series.[5] A very important application of these reactions has been to the fluorine-hydrogen chemical lasers,[5a,6] where F + H₂ → FH + H serves as the main pumping reaction.

Complementing these experimental studies have been several quasiclassical trajectory studies on F + H₂[7,8,9] F + D₂[7,10,11] and F + DH(HD),[7,9] and one recent semiclassical study on collinear F + D₂.[12] The results of the quasiclassical studies have generally been in reasonably good agreement with the detailed rate constants obtained by infrared chemiluminescence and chemical laser experiments but in much poorer agreement with the angular distributions obtained by the molecular beam experiments. There also exists some disagreement between experiment and the classical calculations on the rotational distribution of the detailed rate constants,[7b] and on isotope effects.[5] Additional theoretical developments have been

the characterization of the product state distributions by temperaturelike parameters,[13] and the establishment of a relationship between these parameters and certain details of the potential energy surface.[14] All of the classical theoretical studies have employed semiempirical potential energy surfaces.[7–11] An *ab initio* potential energy surface has also been calculated,[15] and the semiempirical surfaces are in reasonable agreement with it.

Aside from possible defects in the potential energy surface used, the most important sources of disagreement between the quasiclassical trajectory calculations and experiment are (a) electronically nonadiabatic effects, and (b) quantum dynamical effects. The first problem has been discussed by various investigators,[19–48] but its importance is not completely understood at present and we shall not consider it here.

In this paper, we study the importance of quantum dynamical effects in the F + H₂ → FH + H reaction by comparing the results of accurate quantum mechanical solutions to the Schrödinger equation for the collinear collisions to the results of the corresponding quasiclassical and semiclassical calculations. In the following paper (hereafter referred to as II), we make the analogous study for the F + D₂ reaction and also examine exact quantum results for F + HD(DH). Results of our preliminary studies[19,20] indicated that quantum effects were quite important in the collinear F + H₂ reaction[19] and, in fact, the disagreement between the quasiclassical and exact quantum reaction probabilities at low reagent relative translational energies was quite large. In the present paper, we give a more detailed analysis of the reaction probabilities for F + H₂ as calculated by four different methods: an exact quantum mechanical solution, the quasiclassical forward and quasiclassical re-

verse trajectory methods, and the uniform semiclassical method. We also present and compare the corresponding rate constants obtained from the results of these four methods. In addition, we examine resonances, tunneling, and energy partitioning in this reaction, and examine the results of exact quantum calculations at total energies for which two vibrational states of the reagent H_2 are accessible.

In all cases, we restrict our considerations to collinear collisions of a fluorine atom with a hydrogen molecule where the two hydrogen atoms are considered to be distinguishable. The resulting cross sections are in the form of dimensionless probabilities of reaction between specific vibrational states of the reagents to form products in specific states and are not directly comparable with experiment (although certain other quantities such as final state distributions can, with caution, be subject to such a comparison). Our justification for studying collinear dynamics lies mainly in its use as a predictive model for the energy release behavior in actual three-dimensional collisions[31] and as a testing ground for approximate theories of chemical dynamics.[32] Exact quantum dynamics is currently feasible for many types of collinear reactions, and thus the importance of quantum effects in chemical reactions can readily be established within the collinear restriction. How these quantum effects will be modified in two- or three-dimensional systems has not yet been fully established, but some progress has been made towards obtaining exact quantum solutions to these problems,[33] and quite recently accurate converged results have been obtained for the $H + H_2$ coplanar and 3-D exchange reaction.[34]

In Sec. II, the potential energy surface used in our calculations is described. In Sec. III we compare the quantum, quasiclassical, and semiclassical reaction probabilities for $F + H_2$, and in Sec. IV we compare the corresponding rate constants. Reaction probabilities for $F + H_2$ in the higher total energy range where two reagent vibrational states are open are discussed in Sec. V, and in Sec. VI is a short summary.

II. POTENTIAL ENERGY SURFACE

We used the semiempirical LEPS potential energy surface of Muckerman[12,25] (his surface 5). This surface is intermediate in character between his surfaces 2 and 3 of Ref. 7b and was chosen to optimize agreement between his three-dimensional trajectory results and experiment.[7b,12] Using Muckerman's notation, the parameters describing the extended LEPS surface are D_e (HF) = 6.1229 eV, β_e(HF) = 2.2187 Å⁻¹, R_e(HF) = 0.9170 Å, Δ(HF) = 0.167, $D_e(H_2)$ = 4.7462 eV, $\beta_e(H_2)$ = 1.9420 Å⁻¹, $R_e(H_2)$ = 0.7149 Å, and $\Delta(H_2)$ = 0.106. The exothermicity is 1.3767 eV (31.76 kcal/mole) and the barrier height 0.0461 eV (1.06 kcal/mole). Figure 1 shows an equipotential contour plot of the collinear surface along with the minimum energy path. The coordinate system for the plot (and for all calculations) is chosen to diagonalize the kinetic energy with a single reduced mass and is defined by[26]

$$x_1' = \left(\frac{\mu_{F,HH}}{\mu_{HH}}\right)^{1/4} \left(r_{HF} + \frac{\mu_{HH}}{m_H} r_{HH}\right),$$
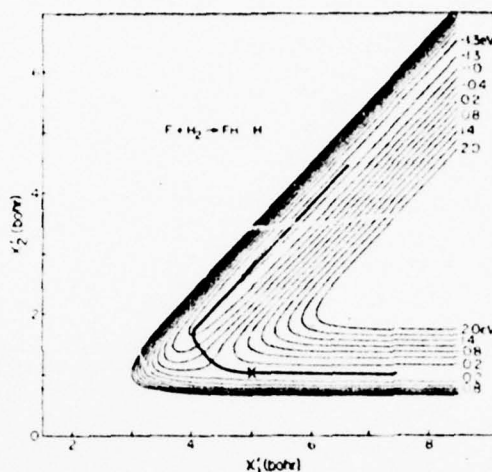
FIG. 1. Equipotential contour plot of the FH_2 collinear potential energy surface used in all calculations reported here. Energies given are relative to the minimum in the H_2 diatomic potential curve. Coordinate system is defined in text. Heavy line denotes the minimum energy path with saddle point indicated by a cross.

$$x_2' = \left(\frac{\mu_{HH}}{\mu_{F,HH}}\right)^{1/4} (r_{HH}),$$

where r_{HF} is the shorter of the two HF bond distances in the H–H–F linear geometry. The analogous coordinate system appropriate for the product arrangement channel (FH + H) is

$$z_1' = \left(\frac{\mu_{H,FH}}{\mu_{FH}}\right)^{1/4} \left(r_{HH} + \frac{\mu_{FH}}{m_H} r_{HF}\right),$$

$$z_2' = \left(\frac{\mu_{HF}}{\mu_{H,FH}}\right)^{1/4} (r_{HF}).$$

These coordinate systems have the advantage over others[27] in that the transformation between the (x_1', x_2') coordinate system appropriate for reagents and the (z_1', z_2') system appropriate for the products is orthogonal.

Since the vibrational spacing in H_2 is about 12 kcal/mole and that in HF is 11 kcal/mole, four vibrational states of HF are normally accessible for thermal distributions of reagent H_2 due to the exothermicity of the reaction.

III. QUANTUM, QUASICLASSICAL, AND SEMICLASSICAL REACTION PROBABILITIES FOR COLLINEAR $F + H_2 \rightarrow FH + H$

A. Exact quantum reaction probabilities

1. Numerical method

We used the close coupling propagation method of Kuppermann[28] to solve the Schrödinger equation for the collinear system $F + H_2$. The method involves dividing the configuration space depicted in Fig. 1 into different regions and then propagating though a given region in a

coordinate system appropriate to that region. In partic-
ular, rectangular coordinates were used in the near
asymptotic regions appropriate to reagents and products
and polar coordinates in the strong interaction region
with the origin of the coordinate system chosen in the
classically inaccessible plateau area corresponding to
dissociation. A basis set of pseudovibrational eigenfunc-
tions describing motion transverse to the direction of
propagation was used for expanding the wavefunctions.
These eigenfunctions were calculated by a finite differ-
ence procedure,[29] and the basis set was changed often
during the propagation to insure an efficient representa-
tion of the wavefunction. Contributions from continuum
vibrational channels are not included in this method. The
integration of the coupled Schrödinger equation was done
with an Adams—Moulton 4th order predictor—4th order
corrector method (with a 4th order Runge–Kutta–Gill
initiator). The procedure for extracting the probability
matrices from the asymptotic solutions is similar to
that used by Truhlar and Kuppermann.[23] Convergence
of the final reaction probabilities was carefully checked
by observing the effect of varying the location of the
origin of the polar coordinate system, location of the
end point of the integration,[30] number of closed vibra-
tional channels, number of integration steps, and number
of grid points in the finite difference eigenfunction deter-
mination. Using 12 to 15 vibrational channels through-
out the integration, we obtained a scattering matrix for
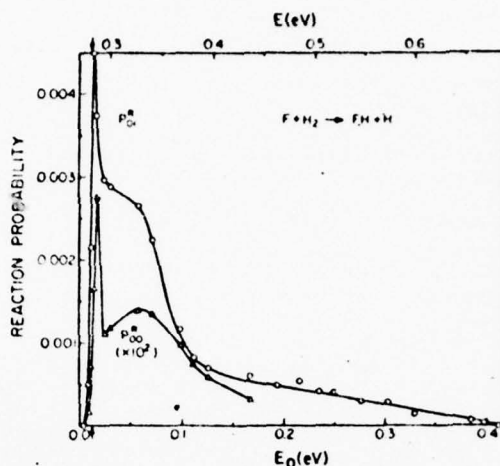
FIG. 3. Exact quantum reaction probabilities P_{01}^R and P_{00}^R (sim-
ilar to Fig. 2).

which unitarity and symmetry were deemed adequate
(flux conservation to 0.5% and symmetry to 5% or better)
in the reagent translational energy range (relative to ν
= 0) E_0 = 0.0 to 1.10 eV. The computation time for a 13
channel calculation on an IBM 370-158 computer was
approximately 32 min for the initial calculation in which
a large amount of energy independent information was
stored on disk for subsequent use and 5 min per energy
thereafter.

2. Results

We define the probability of reaction from an initial
state ν (of the reagent H₂) to a final state ν' (of the prod-
uct HF) by the symbol $P_{\nu\nu'}^R$. (This symbol will also be
used as a shorthand notation for the phase "$\nu \to \nu'$ reac-
tive collision.") The total reaction probability P_ν^R from
a given incident state ν is the sum of $P_{\nu\nu'}^R$ over all acces-
sible ν'. The exact quantum (EQ) reaction probabilities
P_{02}^R, P_{03}^R, and P_0^R for F + H₂ in the translational energy range
E_0 = 0.0–0.4 eV are presented in Fig. 2. The reaction
probabilities for the transitions P_{00}^R and P_{01}^R, which are also
allowed in this E_0 range, are plotted in Fig. 3. We see that
P_{00}^R and P_{01}^R have an energy dependence very similar to P_{02}^R,
but with much smaller values ($P_{00}^R \simeq 6 \times 10^{-3} P_{02}^R$, P_{01}^R, $\simeq 1$
$\times 10^{-4} P_{02}^R$). As a result, only P_{02}^R and P_{03}^R contribute ap-
preciably to P_0^R in the energy range considered. As was
pointed out previously,[19] P_{02}^R and P_{03}^R have remarkably
different threshold behaviors. We shall define the effec-
tive threshold energy E_T for the $\nu \to \nu'$ transition as the
difference between the (lowest) energy for which the cor-
responding $P_{\nu\nu'}^R$ is equal to, say, 1% of the maximum
value attained by this quantity and the energy at which
the $\nu \to \nu'$ process becomes energetically possible. With
this definition, P_{02}^R has an effective threshold of 0.005
eV, while for P_{03}^R (which is energetically forbidden until
E_0 = 0.013 eV), E_T is 0.045. Note that while the barrier
height is 0.0461 eV, the zero point energy of H₂ is 0.268
eV, so the transition P_{02}^R is energetically allowed even at

FIG. 2. Exact quantum reaction probabilities for collinear
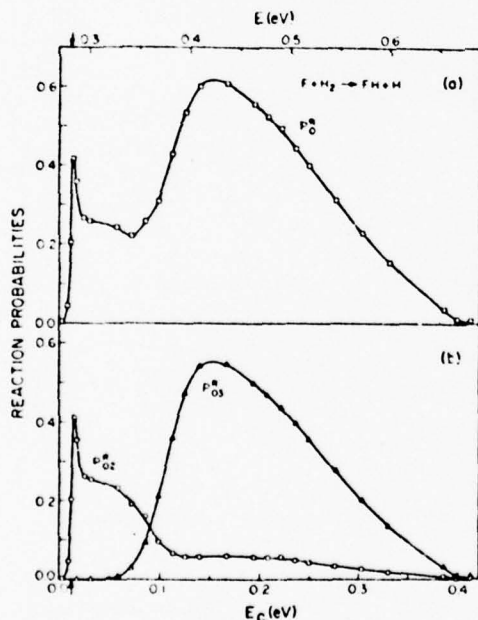F + H₂ as a function of relative translational energy E_0 and total
energy E (relative to minimum in H₂ diatomic potential energy
curve). (a) Total reaction probability P_0^R from ν = 0 of H₂; (b)
reaction probabilities P_{02}^R and P_{03}^R (defined in text). Vertical
arrow in abscissa indicates the energy at which ν = 3 of HF be-
comes accessible.

zero translational energy. Likewise the 0–3 reactive transition is energetically allowed as the HF(3) channel opens up at $E_0 = 0.013$ eV. One possible explanation for why the effective threshold of P_{03}^R is greater than zero is that the exchange of energy between motion transverse to the reaction coordinate and that along the reaction coordinate is not efficient (at least in the entrance channel region of configuration space where the saddle point lies). Truhlar and Kuppermann have shown[22] that a more realistic estimate of the effective barrier height in H + H$_2$ is obtained from vibrationally adiabatic theory. The vibrationally adiabatic barrier (for zero curvature and using the harmonic approximation) for F + H$_2$ is 0.026 eV, which is still appreciably larger than the effective quantum threshold energy for P_{03}^R (0.005 eV), although it is quite close to the P_{03}^K quasiclassical threshold energy (0.025 eV) (see Sec. III. B. 2). This difference between the quantum and quasiclassical threshold energies could in part be due to tunneling through the one-dimensional adiabatic barrier, within the framework of an adiabatic description of the quantum dynamics in the neighborhood of the saddle point. In Paper II we shall see that the results for F + D$_2$, F + HD, and F + DH support this conclusion. The high threshold energy for P_{03}^R is not easily explained as resulting from one-dimensional adiabatic barrier tunneling and is probably due to a dynamical effect, as will be discussed in Sec. III. B. 2.

The sharp spike in the P_{03}^R curve at energies slightly above threshold is reminiscent of the Feshbach type internal excitation resonances observed in the collinear H + H$_2$ reaction.[31] A discussion of other resonances in the F + H$_2$ reaction is presented in Sec. V.

Simultaneously with the reactive transition probabilities, we have calculated the nonreactive ones corresponding to the collisions F + H$_2$(0) → F + H$_2$(0) and FH(ν) + H → FH(ν') + H. The probabilities for the first of these nonreactive processes are simply the difference between unity and the total reaction probability P_0^R (as long as ν = 1 of H$_2$ is closed). The transition probabilities for the H + HF(ν') inelastic ($\nu' \neq \nu$) processes are all quite small (generally less than 0.01) up to $E_0 = 0.4$ eV and vary relatively slowly with energy. Unitarity of the scattering matrix then forces the elastic probabilities for H + HF(ν) collisions to be roughly equal to the difference between unity and the probability for the F + H$_2$(0) → FH(ν) + H reactive process. The behavior of the inelastic transition probabilities for nonreactive H + HF collisions contrasts strongly with the corresponding inelastic transition probabilities for collinear H + FH collisions.[32] In the latter case we find that the probability of an inelastic collision is comparable in magnitude to the elastic transition probabilities and, in addition, the probabilities of multiquantum jump transitions are often greater than the probabilities of single quantum jump transitions. A more complete discussion of the results for collinear H + FH will be given in Ref. 32.

B. Quasiclassical reaction probabilities

1. Method

The classical trajectory calculations were carried out in the same way as in a previous H + H$_2$ study.[33,34] The

initial phase angle variable for the vibration of the ground state of H$_2$ was varied uniformly over a grid of typically 100 points in the interval 0 to 2π. The final action number of the product HF was computed for each reactive trajectory and assigned a quantum number by rounding off the action number to the nearest integer. Thus, the transition probability $P_{0\nu'}^R$ was defined as the fraction of reactive trajectories with final quantum number ν'.

When this procedure is carried out in the direction F + H$_2$(ν = 0) → FH(ν') + H, we term the quasiclassical transition probabilities "quasiclassical forward" (QCF). For the reverse reaction, the quasiclassical transition probabilities are termed "quasiclassical reverse" (QCR). Quantum mechanically, the forward and reverse probabilities are rigorously equal at the same total energy, but quasiclassically they are not.[20] Therefore, either of the two quasiclassical results, QCF or QCR, could be used to represent the probabilities for the (forward) reactive collisions. Since there is presently no *a priori* way of deciding which of these two procedures will give results closer to the EQ ones, we have used them both, and corresponding results are presented below.

2. Results

In Fig. 4 we plot the QCF and EQ reaction probabilities P_{03}^R, P_{03}^R, and P_0^R vs the translational energy E_0, as

FIG. 4. Quasiclassical forward and exact quantum reaction probabilities for F + H$_2$: (a) P_0^R, (b) P_{02}^R and P_{03}^R. Dashed line indicates QCF results with their associated statistical errors indicated by vertical bars. Solid line indicates EQ results (as in Fig. 2).
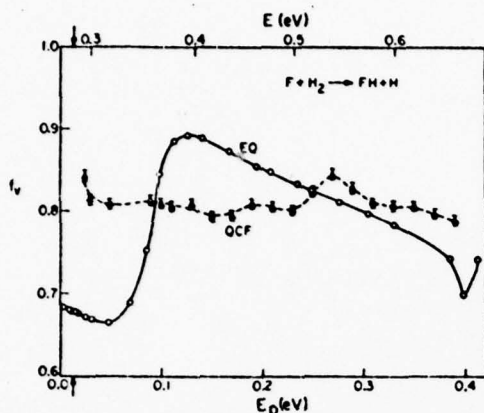
FIG. 5. Fraction (f_v) of the total reagent energy (in excess of product zero point energy) which ends up as vibrational energy in the product HF as a function of the reagent translational energy E_0 and total energy E. Solid line indicates EQ results and dashed line QCF results. Other notation analogous to Fig. 2.

well as the corresponding exact quantum ones given in Fig. 2. Out of the 100 trajectories, none yielded HF with $v = 0$ or 1 (i. e., $P_{01}^R = P_{00}^R = 0$ probably to within 0.01 or less). There are two important points to be noted in comparing the EQ and QCF results. First, both the exact quantum and the quasiclassical results predict roughly the same amount of vibrational excitation in the HF product on *the average*. Indeed, if we define f_v as the fraction of the total energy which ends up as vibrational energy in the product HF, then in Fig. 5 we see that f_v is roughly 0.81 and nearly independent of E_0 in the QCF results, and fluctuates between 0.66 and 0.89 with an average value of 0.79 in the EQ results. From this, we conclude that the quantum and quasiclassical dynamics agree (on the average) with respect to partitioning of product energy between translational and vibrational degrees of freedom. Second, despite this average agreement, there are very significant differences between the EQ and QCF reaction probabilities, particularly with respect to the P_{03}^R threshold and the P_{03}^R/P_{02}^R ratio. In Fig. 6 this ratio is displayed as a function of E_0 for both the EQ and QCF results. As has been pointed out previously, [19] the lack of agreement between the individual transition probabilities P_{02}^R and P_{03}^R can be partially explained as arising from the reasonable but nevertheless arbitrary way of assigning a discrete quantum number to a continuous product vibrational energy. However, the large differences in the energy dependence of the EQ and QCF P_{0v}^R ($v = 2, 3$) suggests that this is probably not the whole explanation and that other significant differences exist between the classical and quantum dynamics in this system. In addition, this arbitrariness in the definition of a product quantum number is not present in the total reaction probabilities P_0^R, yet the differences in magnitude and energy dependence of the EQ and QCF results are still very significant.

It is also of interest to analyze the EQ and QCF reaction probabilities by an information theoretic approach. [13]

In order to include a study of isotope effects in this analysis, we defer a discussion of this to Paper II.

In Fig. 7 are plotted the QCR and EQ reaction probabilities P_{02}^R, P_{03}^R, and P_0^R, vs E_0. The transition probability P_{02}^R is nonzero at zero reagent translational energies. This can occur because of the convention of rounding classical vibrational quantum numbers to the nearest integer. [20,33,34]

The QCR results in Fig. 7 are in much better agreement with the quantum probabilities than are the QCF results in Fig. 4. This is true not only of the total reaction probabilities P_0^R but also of the individual transition probabilities, especially P_{03}^R. The fact that the threshold behavior of the P_{03}^R transition can be described correctly by a quasiclassical method suggests that the 0.045 eV effective threshold energy in P_{03}^R(EQ) is a dynamical effect related to motion through classically accessible regions of configuration space. The fact that the reverse rather than the forward trajectory method produces the best agreement with the exact quantum results must be regarded as an empirical observation at present. It would be interesting to further analyze the quasiclassical results from the viewpoint of what regions of configuration space are being sampled by the QCR and QCF trajectories and with what velocities, and how well the current density fields derived from these trajectories agree with the corresponding exact quantum current densities. [35] The good agreement between the QCR and EQ results suggests that the QCR procedure should be applied to a three-dimensional trajectory calculation. If the differences between the one-dimensional QCR and QCF results are also found in three-dimensional calculations, this could be indicative of the presence of important quantum dynamical effects in the three-dimensional reaction.

FIG. 6. Ratio of reaction probabilities P_{03}^R/P_{02}^R vs translational energy E_0 and total energy E. Solid line indicates EQ results and dashed line QCF results. Other notation analogous to Fig. 2.
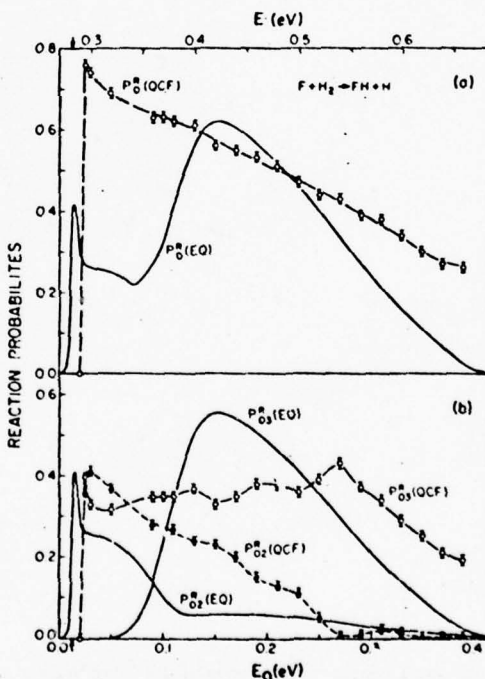
FIG. 7. Quasiclassical reverse and exact quantum reaction probabilities for $F + H_2$: (a) P_0^R, (b) P_{02}^R and P_{03}^R. Dashed line indicates QCR results with their associated statistical errors indicated by vertical bars. Solid line indicates EQ results (as in Fig. 2).
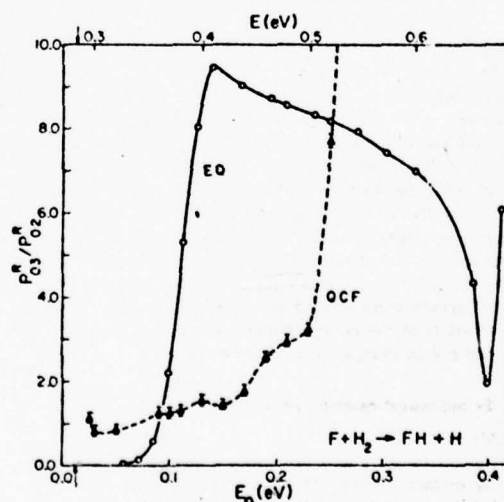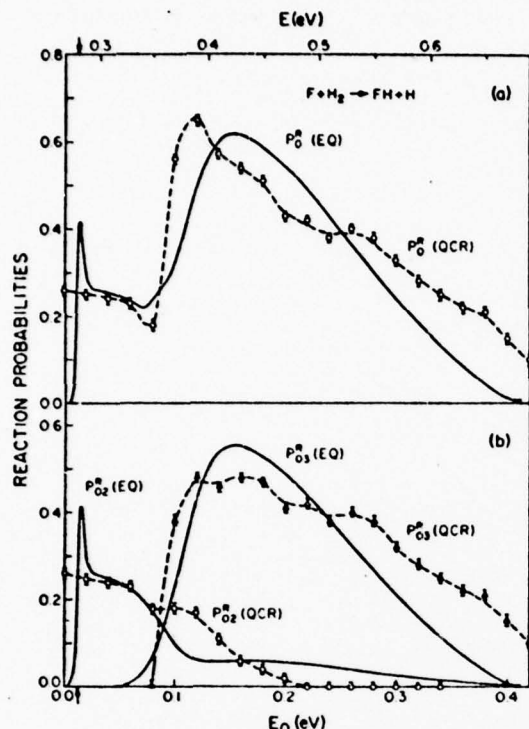
Wilkins[36] has completed a three-dimensional QCF study of the reaction $FH(\nu) + H \rightarrow H_2(\nu') + F$ (ν varying from 1 through 6). His results can be considered to be QCR calculations for the reaction $F + H_2(\nu') \rightarrow FH(\nu) + H$. He has also published QCF rate constant calculations[9a] for the latter reaction with $\nu' = 0$. It would be very interesting to compare the corresponding (QCR and QCF) cross sections. Perry et al.[37] have recently published a three-dimensional comparison of the QCR and QCF cross sections for the endothermic $I + H_2 \rightarrow HI + I$ reaction at one total energy. They found that microscopic reversibility was approximately obeyed at this energy but made no detailed study of the energy dependence of the cross sections and did not investigate threshold effects.

C. Semiclassical reaction probabilities

1. Method

For most energies, uniform semiclassical reaction probabilities were calculated according to the procedure described in Ref. 34. However, for translational energies E_0 greater than 0.10 eV, the transition P_{03}^R was computed by a simple analytical continuation technique,[38] similar in spirit to that of Miller.[30] This was necessary

in order to obtain a nonvanishing value of this transition probability, since in the above energy range, although energetically allowed, it is dynamically forbidden.[34,39] In addition, it was found that P_{03}^R was illdetermined near threshold in that a plot of final FH vibrational action number m_f vs initial H_2 vibrational phase angle (q_0) revealed "raggedness" (i.e., very rapid variation of m_f with q_0) for m_f near the value 3.[40] Raggedness was also observed over a range of energies for the $F + D_2(\nu = 0) \rightarrow FD(\nu' = 4) + D$ reaction by us (see following Paper II) and by Whitlock and Muckerman.[12] We managed to overcome this difficulty at several energies by doing the semiclassical analysis for the reverse reaction, i.e., $H + HF(\nu = 3) \rightarrow H_2(\nu = 0) + F$.[41] For this reaction, the results were considerably less ragged for m_f approximately equal to 0 than they were for the forward reaction around $m_f = 3$. A more complete discussion of this procedure is given in Paper II for the $F + D_2$ reaction.

2. Results

The semiclassical reaction probabilities P_{02}^R and P_{03}^R for $F + H_2$ are presented in Fig. 8 along with the corresponding exact quantum probabilities. In the absence of considering complex-valued trajectories (in complex phase space at complex times), vanishing quasiclassical reaction probabilities implies that the corresponding semiclassical ones also vanish. Therefore, $P_{01}^R(USC) = P_{00}^R(USC) = 0$. From the appearance of the reaction probabilities in Fig. 8, we see that the qualitative agreement between the EQ and USC results is quite good. There are large differences between the magnitudes of the USC and EQ probabilities at certain energies, but such differences are not usually too important for the resulting collinear rate constants (see Sec. IV). Of more serious consequence for such rate constants is the small difference between the threshold energies of the P_{02}^R curves. As pointed out in Sec. III. B. 1., this threshold difference of about 0.020 eV could be partly due to an adiabatic tunneling effect, and it may be possible to improve the agreement between the EQ and USC results by using complex trajectories.[42,43]

D. Comparison of EQ, QCF, QCR, and USC reaction probabilities

In Figs. 9 and 10 we compare the exact quantum, quasiclassical forward, quasiclassical reverse, and semiclassical reaction probabilities P_{02}^R, P_{03}^R, and P_0^F for $F + H_2$ as a function of the reagent translational energy. Note that the QCR results resemble the USC ones much more than the QCF results do. Obviously, the USC threshold energy must be larger than or equal to both the QCF and QCR threshold energies. However, we cannot presently put forward an a priori reason that would have permitted us to predict which of the latter two energies is greater nor which of the quasiclassical reaction probabilities should be closer to the USC ones. It is also very interesting to note that the QCR results resemble the EQ ones more than the USC ones do. One should, however, be cautious not to generalize this observation. As shown in Paper II, the reverse behavior is found for the $F + D_2$ reaction.

IV. EQ, QCF, QCR, AND USC RATE CONSTANTS FOR F + H₂

The detailed $\nu \to \nu'$ rate constant for a one-dimensional bimolecular reaction such as $F + H_2(\nu) \to FH(\nu') + H$ is defined as

$$k^R_{\nu\nu'}(T) = \langle V_\nu P^R_{\nu\nu'}(V_\nu)\rangle_T$$

$$= \int_0^\infty f_T(V_\nu) V_\nu P^R_{\nu\nu'}(V_\nu) dV_\nu \, ,$$

where V_ν is the initial relative velocity of the reagents $F + H_2(\nu)$ and $f_T(V_\nu)$ is the one-dimensional Boltzmann relative velocity distribution function. Changing the integration variable from V_ν to the initial relative reagent translational energy E_ν, this expression becomes[22]

$$k^R_{\nu\nu'}(T) = \frac{1}{(2\pi\mu_{F,HH} kT)^{1/2}} \int_0^\infty P^R_{\nu\nu'}(E_\nu) e^{-E_\nu/kT} dE_\nu \, .$$

Note that for one-dimensional systems, number densities are expressed in molecule/cm, so that a bimolec-
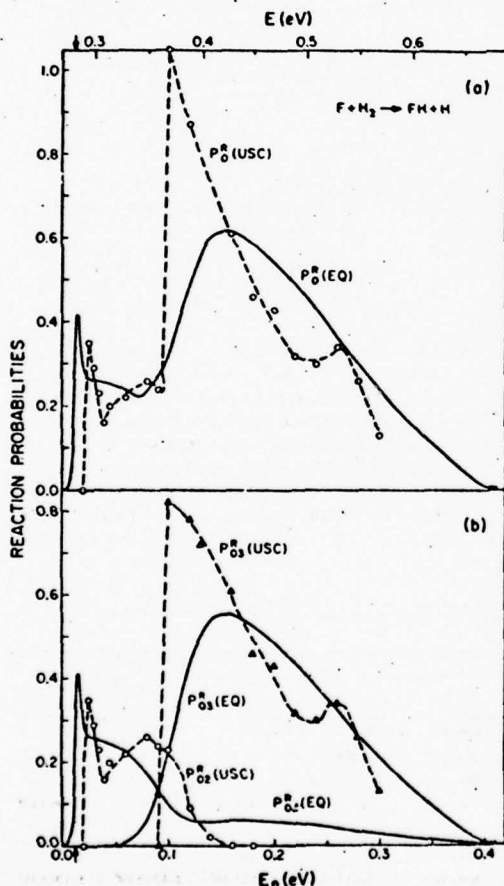
FIG. 8. Uniform semiclassical and exact quantum reaction probabilities for F + H₂: (a) P^R_0, (b) P^R_{02} and P^R_{03}. Dashed line indicates USC results, solid line EQ results as in Fig. 2.
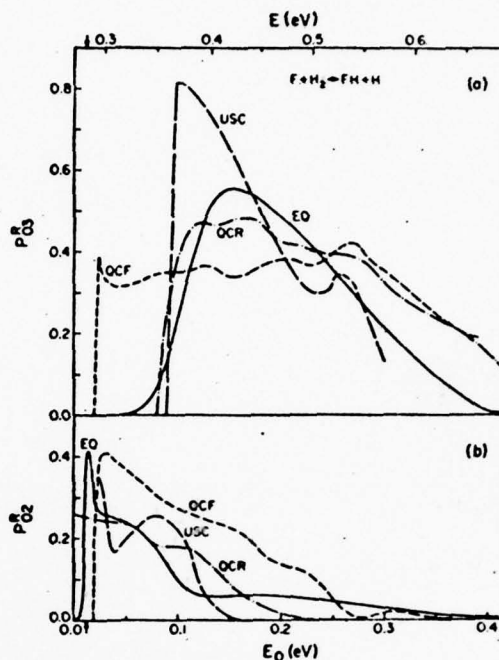
FIG. 9. EQ (solid), QCF (short dash), QCR (dash–dot), and USC (long dash) reaction probabilities P^R_{02} (a) and P^R_{01} (b) for F + H₂ (from Figs. 2, 4, 7, 8).

ular rate constant has the units cm/(molecule·sec).

Using the reaction probabilities presented in Fig. 7, we have calculated the rate constants k^R_{02} and k^R_{03} from the EQ, QCF, QCR, and USC reaction probabilities. Arrhenius plots of these rate constants are presented in Fig. 11. We see that for k^R_{03} all plots are nearly linear at high temperatures. Because of the extremely small effective threshold energies of P^R_{02}, the Arrhenius plots of k^R_{02} are only linear at low temperature (< 500 K). At high temperature, the temperature dependence of k^R_{02} approaches $T^{1/2}$, which is characteristic of a reaction with zero activation energy. Arrhenius activation energies E^{02}_a and E^{03}_a and preexponential factors A_{02} and A_{03}, which were determined by a least squares fit to the 200–400 K results and to the 900–1200 K results, are given in Table I. It is clear from Fig. 11 and Table I that k^R_{03}(QCF) has an activation energy which is significantly lower than the activation energies of k^R_{03}(EQ, QCR, or USC). This is an obvious consequence of the different effective threshold energies of the reaction probabilities (Fig. 9) and illustrates how these threshold differences can affect the detailed rate constants. As might be expected from Fig. 9, k^R_{03} (QCR) and k^R_{03}(USC) are in quite good agreement with k^R_{03}(EQ).

The relative agreement among the corresponding three k^R_{02} rate constants is much less satisfactory at low temperatures, the difference between k^R_{02}(EQ) and k^R_{02}(USC) is mainly determined by the 0.02 eV difference in the threshold energies of the P^R_{02} reaction probabilities.
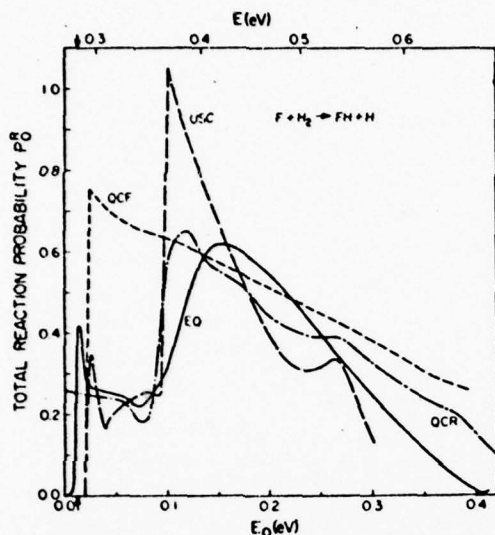
FIG. 10. EQ (solid), QCF (short dash), QCR (dash-dot), and USC (long dash) total reaction probability P_0^R for F + H₂ (from Figs. 2, 4, 7, 8).

FIG. 11. Arrhenius plot of EQ (solid), QCF (short dash), QCR (dash-dot), and USC (long dash) rate constants for F + H₂: (a) k_{02}^R, (b) k_{03}^R.

Since P_{03}^R(QCR) has its effective threshold at zero translational energy, k_{03}^R(QCR) has a smaller activation energy than k_{03}^R(EQ), which in turn has a smaller activation energy than k_{03}^R(QCF or USC). The total rate constant k_0^R which is essentially due to the contributions of k_{03}^R and k_{02}^R does not exhibit simple Arrhenius behavior because it is the sum of two Arrhenius expressions which are of equal magnitude near $T = 1000$ K, but which have quite different activation energies. Note that the experimental activation energy (which is 1.71 kcal/mole)[44] seems to represent an average of the present EQ values of E_0^{02} and E_0^{03}.

In Fig. 12 we plot the ratio k_{03}^R/k_{02}^R as a function of temperature. The large difference between the temperature variation of the QCF ratio and that of the EQ, QCR, or USC ratios is again a consequence of the difference in the reaction probabilities in Fig. 9. It is interesting to note that the three-dimensional quasiclassical forward trajectory method yields a rate constant ratio which is nearly independent of temperature,[9a] in agreement with the one-dimensional QCF results presented here. An experimental measurement of the temperature dependence of k_{03}^R/k_{02}^R[2d] seems to agree reasonably well with the three-dimensional QCF result[9a] and consequently disagrees with our EQ result. This may indicate that the strong difference between the activation energies of k_{03}^R and k_{02}^R observed here is largely averaged out in three dimensions. On the other hand, for the F + D₂ reaction, the agreement between experiment and the quasiclassical results is not as consistent as it is for F + H₂ (to be discussed in Paper II), so it is possible that the averaging process in three dimensions does not completely destroy the important differences between the results of quantum and classical mechanics as reported
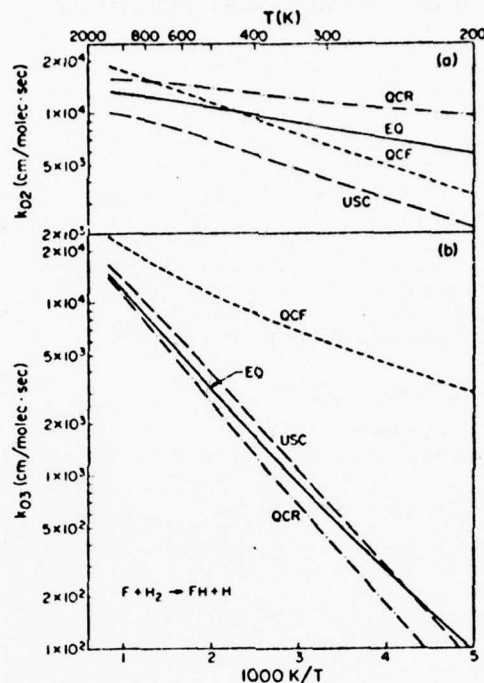
in this paper.

In contrast to the k_{03}^R/k_{02}^R ratio, k_{02}^R(EQ)/k_{01}^R(EQ) is nearly constant in the temperature range considered here. This agrees with the temperature variations of both the experimental[2d] and three-dimensional QCF[9a] results, although the absolute magnitudes of the ratios are quite different (~ 90 for 1-D vs ~ 3 for 3-D). We also found that k_{01}^R(EQ)/k_{00}^R(EQ) is nearly independent of temperature with a value of roughly 210. Therefore k_{01}^R(EQ) and k_{00}^R(EQ) are, respectively, about 2 and 4

TABLE I. Arrhenius rate constant parameters for F + H₂ → FH + H.[a]

	Temperature range (°K)	EQ	QCF	QCR	USC
E_0^{02}	200–400	0.411	0.791	0.230	0.766
E_0^{03}	200–400	2.279	0.853	2.596	2.495
A_{02}	200–400	1.620×10^4	2.424×10^4	1.669×10^4	1.486×10^4
A_{03}	200–400	2.667×10^4	2.492×10^4	3.377×10^4	4.621×10^4
E_0^{02}	900–1200	0.223	0.750	0.086	0.390
E_0^{03}	900–1200	2.628	1.444	2.869	2.348
A_{02}	900–1200	1.459×10^4	2.558×10^4	1.628×10^4	1.182×10^4
A_{03}	900–1200	4.433×10^4	4.464×10^4	4.659×10^4	4.499×10^4

[a]$k_{0j}(T) = A_{0j} \exp(-E_0^{0j}/RT)$, where E_0^{0j} is in kcal/mole and A_{0j} is in cm/(molecule·sec).
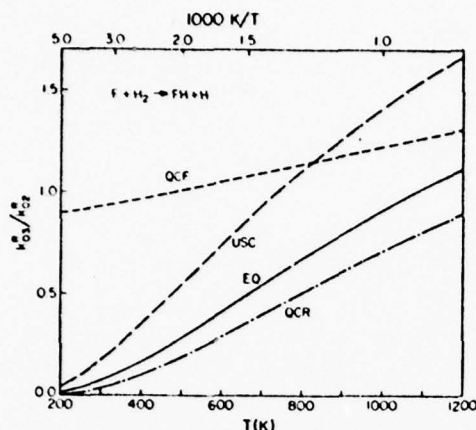
FIG. 12. Ratios of rate constants k_{03}^R/k_{02}^R for $F + H_2$ as a function of temperature. EQ (solid), QCF (short dash), QCR (dash-dot), and USC (long dash).

orders of magnitude smaller than k_{02}^R(EQ).

V. EXACT QUANTUM REACTION PROBABILITIES FOR VIBRATIONALLY EXCITED REAGENTS

In order to observe the effect of vibrational excitation of the reagent H_2 on the resulting reaction probabilities, we extended the range of our exact quantum calculations to total energies of 1.4 eV. In Fig. 13 we plot P_{02}^R, P_{03}^R, and P_{14}^R, the three largest reaction probabilities for $F + H_2$ in this energy range, as a function of energy. There are several important points to note about this figure.

First, the transition P_{14}^R has virtually zero effective threshold energy but otherwise has a similar translational energy dependence to that of P_{03}^R(which has the same $\nu' - \nu$ value as P_{14}^R). The absence of a significant threshold energy in P_{14}^R indicates that the dynamical effects responsible for the appearance of a significant effective energy threshold in P_{03}^R are no longer significant in P_{14}^R. This will lead to lower activation energies and higher rates of reaction for reagents which are initially vibrationally excited. The similarity between P_{14}^R and P_{03}^R implies that for the most significant reaction probabilities, an increase in the vibrational energy of the reagent results in a corresponding increase in the vibrational energy of the product. This agrees with experimental observations for $F + D_2$. [1f]

Second, the reaction probabilities P_{03}^R and P_{14}^R have sharp peaks at $E_0 = 0.425$ eV and 0.823 eV, respectively. An analysis of the energy dependence of the scattering matrix elements corresponding to similarly shaped reaction probability curves in the $H + H_2$ collinear reaction[31,45] and in several other model reactions[46] showed that narrow peaks (or dips) in the reaction probabilities were the result of the presence of internal excitation (Feshbach) resonances. These resonances are associated with excitations of virtual states of the intermediate triatomic complex (FHH in the present case). From Fig.

13 we see that the contributions of the direct processes seem to be rather small in regions of energy where the resonance processes are important. This results in only small interference effects between direct and compound state contributions to the scattering amplitude, and the resulting reaction probabilities have nearly symmetrical peaks as a function of energy near the resonance energies. The resonance widths are about 0.01 eV, and only one nonnegligible reaction probability seems to show resonant behavior at either of the two resonance energies. There seems to be a correlation between the appearance of an internal excitation resonance and the opening of a specific vibrational state of the product (as in the resonance at 0.823 eV, which is close to the opening of the $\nu = 5$ channel in HF at 0.839 eV). This indicates a correlation of the resonance state with the reaction products rather than with the reagents or with the transition state. We shall analyze this phenomenon further in Paper II when we examine the high energy $F + D_2$ reaction probabilities.

Although the total E in Fig. 13 extends to 1.16 eV only, we have done calculations up to $E = 1.4$ eV but found all reaction probabilities in this higher energy range to be less than 0.01. This behavior seems to be related to "centrifugal" effects associated to the angle between the x_i' and z_i' axes (i.e., the skew angle between the asymptotic portions of the minimum energy path for the potential of Fig. 1) and will be further discussed in Paper II.

VI. SUMMARY

Many of the dynamical effects presented in this paper will be further examined in Paper II, to where we will relegate a more extensive summary of quantum effects in the $F + H_2$ reaction. In this paper we have seen that there are very serious differences between the results

FIG. 13. Exact quantum reaction probabilities P_{02}^R, P_{03}^R, and P_{14}^R for $F + H_2$ at translational energies higher than those in Fig. 2. Arrows near $E_0 = 0.44$ eV and 0.84 eV indicate the opening of $\nu = 4$ and 5, respectively, of HF, while that at 0.51 eV indicates the energy E_0 at which $\nu = 1$ of H_2 becomes accessible.

of quantum and standard quasiclassical mechanics for collinear $F + H_2$, most notably in the energy dependence of the reaction probability P_{03}^R near threshold. These differences in the behavior of the reaction probabil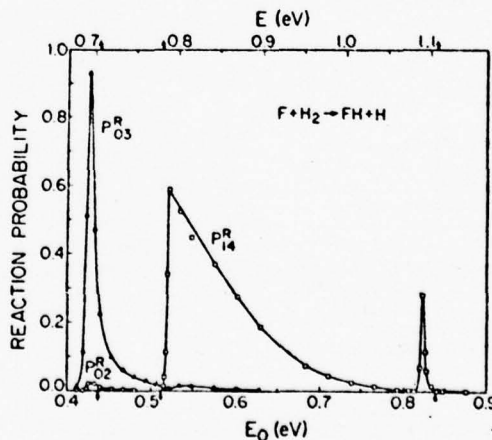ities result in important differences in the detailed thermal rate constants. The fact that the quasiclassical forward reaction probabilities and rate constants disagree quite strongly with the exact quantum results is of great significance, since nearly all the trajectory studies done to date on this reaction have been of the quasiclassical forward type. For the present reaction, both the quasiclassical reverse and uniform semiclassical methods provide us with more accurate ways of approximating the exact quantum results. This suggests that it might be of interest to use these methods in three dimensions. Indeed, it may be possible to use the results of collinear calculations such as the ones presented here as a guideline when choosing an approximate method for doing three-dimensional calculations.

Additional exact quantum results for $F + H_2$ show that threshold effects are no longer important when the reagent H_2 is initially vibrationally excited. The dominant transitions appear to be those which channel additional vibrational energy in the reagents into additional vibrational energy in the products. Internal excitation resonances are found to play an important role in the reaction probabilities at certain translational energies. There seems to be a one-to-one correspondence between the energy at which a resonance occurs and the energy at which a related product vibrational channel opens.

ACKNOWLEDGMENT

*Work supported in part by the United States Air Force Office of Scientific Research.
†Work performed in partial fulfillment of the requirements for the Ph. D. degree in Chemistry at the California Institute of Technology.
‡Present address: Department of Chemistry, Illinois Institute of Technology, Chicago, IL 60616.
§Contribution No. 4988.
[1](a) J. C. Polanyi and D. C. Tardy, J. Chem. Phys. 51, 5717 (1969); (b) K. G. Anlauf, P. E. Charters, D. S. Horne, R. G. MacDonald, D. H. Maylotte, J. Polanyi, W. J. Skrlac, D. C. Tardy, and K. B. Woodall, J. Chem. Phys. 53, 4091 (1970); (c) N. Jonathan, C. M. Melliar-Smith, and D. H. Slater, Mol. Phys. 20, 93 (1971); (d) N. Jonathan, C. M. Melliar-Smith, D. Timlin, and D. H. Slater, Appl. Opt. 10, 1821 (1971); (e) N. Jonathan, C. M. Melliar-Smith, S. Okuda, D. H. Slater, and D. Timlin, Mol. Phys. 22, 561 (1971); (f) J. C. Polanyi and K. B. Woodall, J. Chem. Phys. 57, 1574 (1972); (g) H. W. Chang and D. W. Setser, J. Chem. Phys. 58, 2298 (1973).
[2](a) K. L. Kompa and G. C. Pimentel, J. Chem. Phys. 47, 857 (1967); (b) K. L. Kompa, J. H. Parker, and G. C. Pimentel, J. Chem. Phys. 51, 91 (1969); (c) O. D. Krogh and G. C. Pimentel, J. Chem. Phys. 51, 5717 (1969); (d) R. D. Coombe and G. C. Pimentel, J. Chem. Phys. 59, 251 (1973); (e) W. H. Green and M. C. Lin, J. Chem. Phys. 54, 3222 (1971); (f) M. J. Berry, J. Chem. Phys. 59, 6229 (2973).
[3](a) T. P. Schaefer, P. E. Siska, J. M. Parson, F. P. Tully,

Y. C. Wong, and Y. T. Lee, J. Chem. Phys. 53, 3385 (1970); (b) Y. T. Lee (VII ICPEAC), The Physics of Electronic and Atomic Collisions, edited by T. R. Govers and F. J. de Heer (North-Holland, Amsterdam, 1971), p. 357.
[4]See compilations by N. Cohen, Report No. TR-0073(3430)-9, The Aerospace Corporation, El Segundo, CA, 1972 and Report No. TR-0074(4530)-9, The Aerospace Corporation, El Segundo, CA, 1974.
[5]A. Persky, J. Chem. Phys. 59, 5578 (1973).
[6](a) D. J. Spencer, T. A. Jacobs, H. Mirels, and R. W. F. Gross, Int. J. Chem. Kinet. 1, 493 (1969); (b) T. F. Deutsch, Appl. Phys. Lett. 10, 234 (1967); (c) S. N. Suchard, R. L. Kerber, G. Emanuel, and J. S. Whittier, J. Chem. Phys. 57, 5065 (1972) and references therein.
[7](a) J. T. Muckerman, J. Chem. Phys. 54, 1155 (1971); (b) 56, 2997 (1972).
[8](a) R. L. Jaffe and J. B. Anderson, J. Chem. Phys. 54, 2224 (1971); (b) 56, 682 (1972); (c) R. L. Jaffe, J. M. Henry, and J. B. Anderson, J. Chem. Phys. 59, 1128 (1973).
[9](a) R. L. Wilkins, J. Chem. Phys. 56, 912 (1972); (b) R. L. Wilkins, J. Phys. Chem. 77, 3081 (1973).
[10]N. C. Blais and D. G. Truhlar, J. Chem. Phys. 58, 1090 (1973).
[11]A. Ding, L. Kirsch, D. Perry, J. Polanyi, and J. Schreiber, Discuss. Faraday Soc. 55, 252 (1973).
[12]P. A. Whitlock and J. T. Muckerman, J. Chem. Phys. 61, 4618 (1975).
[13](a) A. Ben-Shaul, R. D. Levine, and R. B. Bernstein, Chem. Phys. Lett. 15, 160 (1972); (b) A. Ben-Shaul, R. D. Levine, and R. B. Bernstein, J. Chem. Phys. 57, 5427 (1972); (c) A. Ben-Shaul, G. L. Hofacker, and K. L. Kompa, J. Chem. Phys. 59, 4664 (1973).
[14]G. L. Hofacker and R. D. Levine, Chem. Phys. Lett. 15, 165 (1972), also unpublished results.
[15](a) C. F. Bender, S. V. O'Neil, P. K. Pearson, and H. F. Schaefer, III, Science 176, 1412 (1972); (b) C. F. Bender, P. K. Pearson, S. V. O'Neil, and H. F. Schaefer, III, J. Chem. Phys. 56, 4626 (1972).
[16]D. G. Truhlar, J. Chem. Phys. 56, 3189 (1972).
[17]J. T. Muckerman and M. D. Newton, J. Chem. Phys. 56, 3191 (1972).
[18]J. C. Tully, J. Chem. Phys. 60, 3042 (1974).
[19]G. C. Schatz, J. M. Bowman, and A. Kuppermann, J. Chem. Phys. 58, 4023 (1973).
[20]J. M. Bowman, G. C. Schatz, and A. Kuppermann, Chem. Phys. Lett. 24, 378 (1974).
[21](a) P. J. Kuntz, E. M. Nemeth, J. C. Polanyi, S. D. Rosner, and C. E. Young, J. Chem. Phys. 44, 1168 (1966); (b) J. C. Polanyi and W. H. Wong, J. Chem. Phys. 51, 1439 (1969).
[22]D. Truhlar and A. Kuppermann, J. Chem. Phys. 56, 2232 (1972).
[23](a) R. Saxon and J. Light, J. Chem. Phys. 56, 3874 (1972); (b) 56, 3885 (1972); (c) G. Wolken and M. Karplus, J. Chem. Phys. 60, 351 (1974); (d) A. B. Elkowitz and R. E. Wyatt, J. Chem. Phys. 62, 2504 (1975).
[24](a) A. Kuppermann, G. C. Schatz, and M. Baer, J. Chem. Phys. 61, 4362 (1974); (b) A. Kuppermann and G. C. Schatz, J. Chem. Phys. 62, 2502 (1975).
[25]J. T. Muckerman (private communication).
[26]L. M. Delves, Nucl. Phys. 20, 275 (1960).
[27]G. Glasstone, K. Laidler, and H. Eyring, Theory of Reaction Rates (McGraw Hill, New York, 1941), p. 101; M. Karplus and K. Tang, J. Chem. Phys. 50, 1119 (1970).
[28](a) A. Kuppermann, Potential Energy Surfaces in Chemistry, edited by W. A. Lester (University of California at Santa Cruz, 1970), pp. 121–129; (b) Abstracts of papers, (VII ICPEAC), Electronic and Atomic Collisions, edited by L. Branscomb (North-Holland, Amsterdam, 1971), p. 3.
[29]D. G. Truhlar, J. Comput. Phys. 10, 123 (1972).
[30]The reaction probabilities were found to be independent of the location of the endpoints of the integrations in each arrange-

ment channel before the potential had completely reached its asymptotic value. However, the translational energies computed at the points of termination of the integrations were slightly smaller than their correct asymptotic values. The results reported here have been corrected by the difference (less than 0.0002 eV).

[31]G. C. Schatz and A. Kuppermann, J. Chem. Phys. 59, 964 (1973).

[32]G. C. Schatz and A. Kuppermann (to be published).

[33]J. M. Bowman and Aron Kuppermann, Chem. Phys. Lett. 12, 1 (1972).

[34]J. M. Bowman and Aron Kuppermann, J. Chem. Phys. 59, 6524 (1973).

[35]A. Kuppermann, J. T. Adams, and D. G. Truhlar, *Abstracts of Papers, Eighth International Conference on the Physics of Electronic and Atomic Collisions*, edited by B. C. Cobic and M. V. Kurepa (Institute of Physics, Belgrade, 1973), p. 149.

[36]R. L. Wilkins, J. Chem. Phys. 58, 3038 (1973).

[37]D. S. Perry, J. C. Polanyi, and C. W. Wilson, Chem. Phys. Lett. 24, 484 (1974).

[38]J. M. Bowman, Ph.D. thesis, California Institute of Technology, 1974.

[39]W. H. Miller, Chem. Phys. Lett. 4, 431 (1970); J. Chem. Phys. 53, 3578 (1970).

[40]C. C. Rankin and W. H. Miller, J. Chem. Phys. 55, 3150 (1971).

[41]This procedure is obviously valid if the function $m_f(q_0)$ is "smooth" (i.e., nonragged) for both the forward and reverse trajectories, since under these conditions, semiclassical reaction probabilities (contrarily to quasiclassical ones) rigorously obey microscopic reversibility. [34] As a result, when one of these $m_f(q_0)$ is smooth and the other not, it is reasonable to associate the semiclassical reaction probability of both the forward and reverse reactions to the smooth $m_f(q_0)$.

[42]W. H. Miller and T. F. George, J. Chem. Phys. 56, 5668 (1972); J. Chem. Phys. 57, 2458 (1972).

[43]For the $H + H_2$ reaction, the complex trajectory method yields reaction probabilities differing by less than 30% from the exact quantum results for energies less than the barrier (Ref. 32).

[44]G. C. Fettis, J. H. Knox, and A. F. Trotman-Dickenson, J. Chem. Soc. 1960, 1064.

[45]R. D. Levine and S. F. Wu, Chem. Phys. Lett. 11, 557 (1971).

[46]S. F. Wu, B. R. Johnson, and R. D. Levine, Mol. Phys. 25, 839 (1973).

Exact quantum, quasiclassical, and semiclassical reaction probabilities for the collinear F+D$_2$ → FD+D reaction*

George C. Schatz,† Joel M. Bowman,‡ and Aron Kuppermann

Arthur Amos Noyes Laboratory of Chemical Physics,§ California Institute of Technology, Pasadena, California 91125
(Received 22 October 1974)

Exact quantum, quasiclassical, and semiclassical reaction probabilities and rate constants for the collinear reaction F + D₂ → FD + D are presented. In all calculations, a high degree of population inversion is predicted with P_{03}^R and P_{04}^R being the dominant reaction probabilities. In analogy with the F + H₂ reaction (preceding paper), the exact quantum 0→3 and 0→4 probabilities show markedly different energy dependence with P_{03}^R having a much smaller effective threshold energy ($E_T = 0.014$ eV) than P_{04}^R (0.055 eV). The corresponding quasiclassical forward probabilities P_{03}^R and P_{04}^R are in poor agreement with the exact quantum ones, while their quasiclassical reverse and semiclassical counterparts provide much better approximations to the exact results. Similar comparisons are also made in the analysis of the corresponding EQ, QCF, QCR, and USC rate constants. An information theoretic analysis of the EQ and QCF reaction probabilities indicates nonlinear surprisal behavior as well as a significant isotope dependence. Additional quantum results at higher energies are presented and discussed in terms of threshold behavior and resonances. Exact quantum reaction probabilities for the related F + HD → FH + D and F + DH → FD + H reactions are given and an attempt to explain the observed isotope effects is made.

I. INTRODUCTION

In the preceding paper[1] (hereafter referred to as I), we compared the exact quantum (EQ), quasiclassical forward (QCF), quasiclassical reverse (QCR), and uniform semiclassical (USC) reaction probabilities for the collinear F + H₂ →FH + H reaction. The results of all four methods agreed in their prediction of a high degree of population inversion in the products of this exothermic reaction. However, the QCF probabilities were found to differ substantially from the corresponding EQ results in threshold behavior and energy dependence. This could have important consequences regarding the validity of the standard three-dimensional quasiclassical method which has been used on F + H₂ (D₂) and which is the three dimensional version of the QCF method. We found much better agreement between the exact quantum probabilities and both the quasiclassical reverse and the uniform semiclassical results, thus indicating that either of the last two methods might be preferred to the quasiclassical forward one in three-dimensional calculations.

In this paper we present the analogous EQ, QCF, QCR, and USC results for the collinear F + D₂ reaction over roughly the same range of translational energies as was used in I. We shall also make an analysis of the surprisal function for the EQ and QCF results for F + D₂ (and F + H₂) to determine if an information theoretic description of the product state distributions can be useful. In addition, exact quantum probabilities for the reactions F + HD (DH) → FH(FD) + H(D) are given. We also study the importance of tunnelling and resonances in F + D₂, F + HD, and F + DH. These calculations were done in order to assess the effect of isotopic substitution on the magnitude of the quantum effects and on the validity of the approximate methods.

The potential energy surface used in these calculations is identical to that described in I.[2] In addition, most of the numerical techniques are the same as was used in I and will not be described again here except to note changes made.

In Sec. II we discuss the EQ, QCF, QCR, and USC reaction probabilities for F + D₂, and the corresponding collinear rate constants are presented in Sec. III. Section IV contains a study of the behavior of the reaction probabilities at energies sufficiently high to excite the first two vibrational states of reagent D₂. In addition, we discuss resonances in this reaction, giving specific comparisons between the results of the exact quantum, and approximate methods in the vicinity of these resonances. Section V contains a description of the EQ reaction probabilities for F + HD (DH), and in Sec. VI we present a summary of conclusions.

II. QUANTUM, QUASICLASSICAL, AND SEMICLASSICAL REACTION PROBABILITIES FOR COLLINEAR F + D₂ → FD + D

A. Exact quantum reaction probabilities

Since the vibrational spacing in D₂ is roughly 9 kcal/mole and that in FD is about 8 kcal/mole, and the reaction is exothermic by 32 kcal/mole approximately, at least five vibrational levels of DF are accessible when D₂ has an initial quantum number $\nu = 0$. By coincidence, the $\nu = 3$ and 4 vibrational levels of DF have nearly the same total energies as the $\nu = 2$ and 3 vibrational levels of HF, respectively. This results in remarkable similarities between these two reactions despite the significant difference in the corresponding reduced masses ($\mu_{F,H_2}/\mu_{F,D_2} = 0.548$). As in I, we will designate by $P_{\nu\nu'}^R$ the reaction probability for a reagent initially in state ν to form product in state ν', and by P_ν^R the total reaction probability from initial state ν (i.e., $\sum_{\nu'} P_{\nu\nu'}^R$). In Fig. 1 we present the exact quantum reaction probabilities P_{04}^R, P_{03}^R, and P_0^R for F + D₂ at relative translational energies (E_0) in the range 0.0–0.25 eV. The corresponding probabilities P_{02}^R, P_{01}^R, and P_{00}^R are plotted in Fig. 2. It is apparent from these figures that P_{04}^R and P_{03}^R are the most significant contributors to P_0^R in this E_0 range. The P_{02}^R, P_{01}^R, and P_{00}^R curves are all very similar in appearance to the P_{03}^R one, but with greatly

reduced magnitudes ($P_{03}^R \sim 6.8 \times 10^{-2}\ P_{03}^R$, $P_{01}^R \sim 5 \times 10^{-4}\ P_{03}^R$, $P_{00}^R \sim 6 \times 10^{-6}\ P_{03}^R$). There is a very significant difference between the threshold behavior of P_{03}^R and that of P_{04}^R quite analogous to what was observed in I for the reaction probabilities P_{02}^R and P_{03}^R of $F + H_2$. As in I, it is convenient to define an effective threshold energy E_T for the $\nu \rightarrow \nu'$ reaction as the difference between the (lowest) energy for which the corresponding $P_{\nu \nu'}^R$ is equal, say, to 1% of the maximum value attained by this quantity and the energy at which the $\nu \rightarrow \nu'$ process becomes energetically possible. Table I contains the values of E_T for several important reaction probabilities for the reactions of F with H_2, D_2, HD, and DH as well as the corresponding vibrationally adiabatic zero curvature barrier heights E_{VAZC} (described in I). From it we see that for $F + D_2$ the value of E_T for P_{03}^R (EQ), 0.014 eV, is appreciably lower than the E_{VAZC} value of 0.032 eV. This can be interpreted as an indication of the extent of vibrationally adiabatic one-dimensional tunnelling (see paper I) in this system. The value of E_T for P_{03}^R (QCF) of 0.030 eV is very close to E_{VAZC}. This suggests that the chemical motion for this system is nearly vibrationally adiabatic in the approach coordinate in the sense that the local action number for the motion transverse to the reaction coordinate should vary relatively little between the separated reagent region and the saddle point region. The corresponding values of E_T and E_{VAZC} for P_{03}^R (EQ) of $F + H_2$ are 0.005 eV and 0.026 eV,

indicating somewhat more tunnelling in this system than in $F + D_2$, as expected. The effective threshold energy of P_{04}^R ($F + H_2$) ($E_T = 0.055$ eV) is similar to that of P_{03}^R ($F + H_2$) (0.045 eV). The near coincidence in energy between the $\nu = 3$ and 4 vibrational levels of FD and $\nu = 2$ and 3 of FH is probably responsible for the very similar appearance of the corresponding EQ reaction probabilities. (Compare Fig. 2 of I with Fig. 1 of the present paper.) There are, however, differences in the maximum values of certain analogous reaction probabilities, especially P_{03}^R ($F + D_2$) and P_{02}^R ($F + H_2$) (which have maximum values of 0.66 and 0.44, respectively). We shall see in Sec. IV that the differences between analogous reaction probabilities for the two reactions become even more important for $E_0 > 0.25$ eV.

B. Quasiclassical reaction probabilities

In Fig. 3 are plotted the QCF and EQ reaction probabilities P_{03}^R, P_{04}^R, and P_0^R for $F + D_2$. No reactive trajectories yield DF with $\nu' = 0$ or 1, but there is a small probability of reaction to $\nu' = 2$ (always < 0.1 and vanishing for $E_0 > 0.12$ eV). The corresponding QCR reaction

FIG. 2. Exact quantum reaction probabilities P_{02}^R, P_{01}^R, and P_{00}^R for $F + D_2$ (similar to Fig. 1).

FIG. 1. Exact quantum reaction probabilities for $F + D_2$ as a function of relative translational energy E_0 and total energy E (relative to minimum in D_2 diatomic potential curve). (a) Total reaction probability P_0^R. (b) Reaction probabilities P_{03}^R and P_{04}^R.

TABLE I. Effective threshold energies (E_T) for the most significant reaction probabilities in the $F + H_2$, $F + D_2$, $F + DH$, and $F + HD$ reactions.[a]

	$F + H_2$	$F + HD$
$E_T[P_{02}^R(\text{EQ})]$	0.005	0.010
$E_T[P_{02}^R(\text{QCF})]$	0.025	N.C.[b]
$E_T[P_{03}^R(\text{EQ})]$	0.045	0.071
$E_T[P_{03}^R(\text{QCF})]$	0.012	N.C.[b]
E_{VAZC}	0.026	0.02
	$F + D_2$	$F + DH$
$E_T[P_{03}^R(\text{EQ})]$	0.014	0.011
$E_T[P_{03}^R(\text{QCF})]$	0.030	N.C.[b]
$E_T[P_{04}^R(\text{EQ})]$	0.055	0.022
$E_T[P_{04}^R(\text{QCF})]$	0.030	N.C.[b]
E_{VAZC}	0.032	0.028

[a] All energies are in eV.
[b] No QCF calculations were done for this transition.

FIG. 3. Quasiclassical forward (dashed curve) and exact quantum (solid curve) reaction probabilities for $F + D_2$: (a) P_0^R. (b) P_{03}^R and P_{04}^R.

what higher than the experimental result (0.66).[4] This general average agreement between the EQ and QCF f_v vs E_0 curves indicates that the dynamic processes governing the *average* energy disposal between vibrational and translational degrees of freedom of the products can be well approximated by the classical trajectory method. However, one should keep in mind that this is not so for the distribution of this vibrational energy among the available vibrational states, i.e., that large differences between product state population ratios obtained from the EQ and QCF methods do exist, as indicated in Fig. 6.

C. Semiclassical reaction probabilities

Figure 7 shows the uniform semiclassical reaction probabilities P_{23}^R and P_{04}^R along with the corresponding EQ results. The USC results are similar to the ones obtained independently by Whitlock and Muckerman in an analogous calculation.[2] It was noted in Paper I (Sec. III C) that "raggedness" (i.e., very rapid variation of m_f with q_0) in the final action number $m_f(q_0; \nu, E)$ as a function of initial vibrational phase q_0 caused difficulties in calculating USC transition probabilities at the threshold of the $F + H_2(0) \to FH(3) + (H)$ reaction. The same problem occurred for the $0 \to 4$ transition in the $F + D_2$ reaction, and was also encountered by Whitlock and Muckerman. We were able to overcome this difficulty by using the reverse final action number function, $n(q_0; m, E)$, which was found to be smooth for $m = 4$ and s around 0. The justification for using this procedure was given in I.

probabilities for the same energy range ($0.0 < E_0 < 0.12$ eV) are plotted in Fig. 4. In Fig. 3 we see that there is a very large difference between the threshold behavior of P_{04}^R (EQ) and P_{04}^R(QCF). In analogy with the $F + H_2$ P_{03}^R behavior,[1] we find that the quasiclassical reverse P_{04}^R of $F + D_2$ (Fig. 4) has a threshold behavior which is much closer to the exact quantum one than is the QCF threshold. Unlike P_{03}^R ($F + H_2$), the energy dependence of P_{03}^R ($F + D_2$) is predicted somewhat more accurately by the QCF method than by the QCR method. The EQ and QCF total reaction probabilities P_0^R (Fig. 3) are in somewhat better average agreement than are the EQ and QCF total reaction probabilities in $F + H_2$ (Fig. 4 of Paper I). This seems to indicate that the differences between quantum and classical dynamics are less severe for $F + D_2$ than for $F + H_2$. However, at least for collinear reactions, these differences are still quite significant.

In Fig. 5 we plot as a function of E, the fraction f_v of the total energy which appears as vibrational energy of the DF product for the EQ and QCF calculations. It can be seen that f_v (QCF) is nearly independent of E_0 and has an average value of 0.79. The corresponding EQ curve has a more pronounced E_0 dependence but about the same average value over the E_0 range considered. We find that the average value of f_v is almost the same for both $F + H_2$ and $F + D_2$. This independence of isotopic substitution agrees with the corresponding experimental result[8] and with the predictions of three-dimensional trajectory calculations,[9] although our value of f_v(0.79) which ignores rotational degrees of freedom is some-

FIG. 4. Quasiclassical reverse (dashed curve) and exact quantum (solid curve) reaction probabilities for $F + D_2$: (a) P_0^R, (b) P_{03}^R and P_{04}^R.
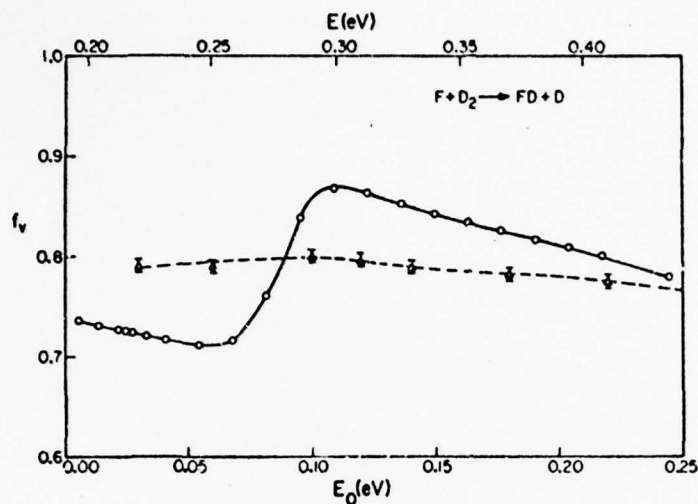
FIG. 5. Fraction (f_v) of the total reagent energy (exclusive of product zero point energy) which ends up as vibrational energy in the product DF plotted as a function of the reagent translational energy E, and total energy E. Solid line indicates EQ results and dashed line QCF ones. Other notation analogous to Fig. 1.

The curves for the forward and reverse values of m_f for this 0−4 transition at an energy $E = 0.3107$ eV ($E_0 = 0.12$ eV) are given in Fig. 8. When all the relevant semiclassical quantities are well-behaved ("nonragged") functions of q_0, the USC transition probabilities obey microscopic reversibility,[5] and it is not necessary to calculate both the forward and reverse results. However, as the example above demonstrates, when raggedness exists, it is advisable to consider the forward and the reverse results. In our example, the reverse results are the preferred ones, since there is no raggedness in the region corresponding to D + DF(4) → D₂(0) + F. These were the ones used in calculating P_{04}^R (and P_{03}^R for the F + H₂ reaction) in its threshold region. The USC

P_{04}^R transition probabilities at $E_0 = 0.08$ eV and 0.085 eV were calculated in the statistical approximation.[6] At these energies the reverse reaction showed that the 4 − 0 transition was dynamically forbidden. However, since statistical (i.e., ragged) behavior was evident in the forward reaction, we did calculate a nonzero value for P_{04}^R at the two energies just mentioned.

The USC probabilities in Fig. 7 are in much better agreement with the corresponding EQ results than are the quasiclassical ones. As was the case with the QCF P_{03}^R threshold, there is a small difference between the P_{03}^R (USC) and P_{03}^R (EQ) threshold energies, but the USC result may be improved by using complex trajectories.[7]
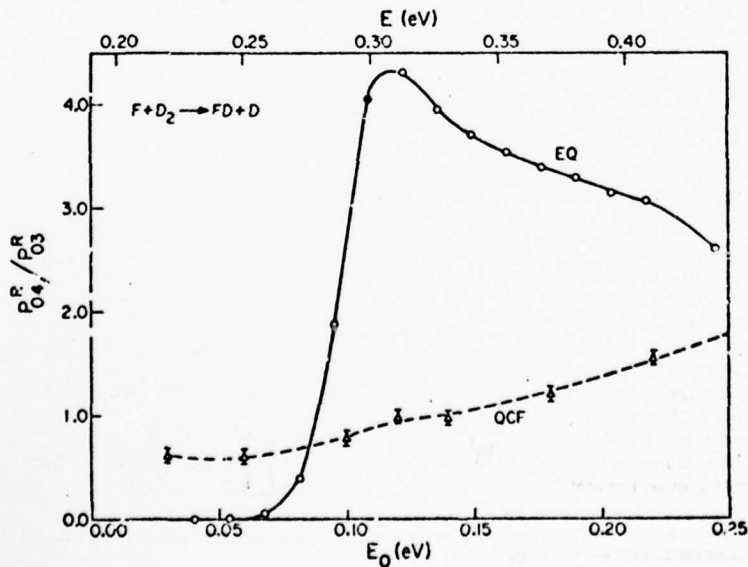
FIG. 6. Ratio of reaction probabilities P_{04}^R/P_{03}^R vs translational energy E_0 and total energy E. Solid line indicates EQ results and dashed line QCF ones. Other notation analogous to Fig. 1.
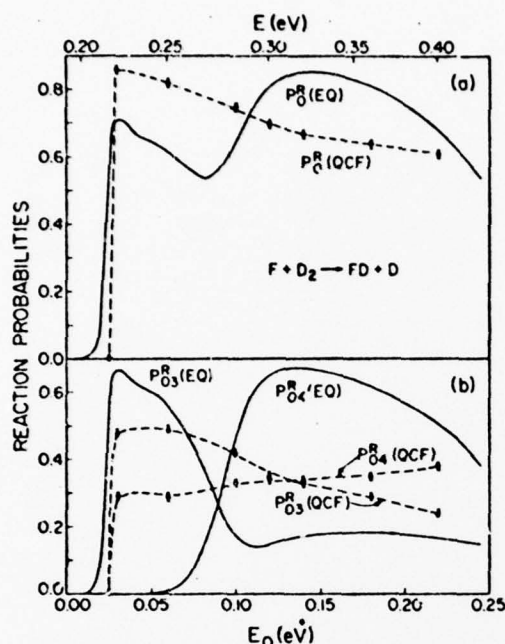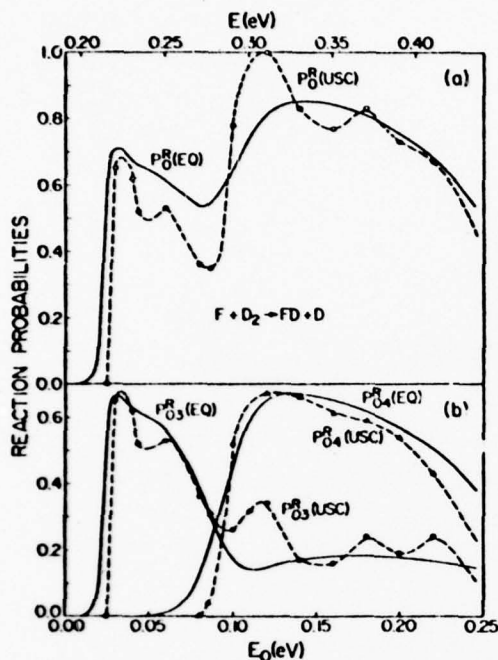
FIG. 7. Uniform semiclassical (dashed curve) and exact quantum (solid curve) reaction probabilities for $F + D_2$: (a) P_0^R, (b) P_{03}^R and P_{04}^R.

The oscillations in P_{03}^R (USC) in the E_0 range 0.10 eV–0.25 eV do not have any analog in the quantum results. These oscillations are due to phase interferences arising from a relatively rapid variation with energy of the differences in phases associated with the two contributing trajectories. One might expect that the raggedness in the plot of final action vs initial phase [see Fig. 8(a)] could be an indication of resonant behavior in this energy range, but the quantum results of Fig. 1 do not substantiate this. In Sec. IV we discuss the possible relationship between resonances in the EQ results and raggedness in the USC ones.

One significant aspect of the comparison between the USC and EQ results in Fig. 7 is that the maximum values of the EQ and USC reaction probabilities P_{03}^R and P_{04}^R are nearly identical. This contrasts with the results of both the QCF and QCR calculations which generally tend to underestimate the maximum values of the probabilities (Figs. 3 and 4). The significant improvement in the quality of the results obtained in going from the quasiclassical to the semiclassical approximation suggests that an equivalent improvement may occur for the three-dimensional $F + D_2$ reaction and that the semiclassical results may be quite reliable for this case. However, we must stress that the utilization of uniform rather than primitive semiclassical techniques is essential to the success of this method for the collinear reaction, and thus it seems likely that an analogous uniform pro-

cedure will be required in the three-dimensional problem.[9]

D. Comparison of EQ, QCF, QCR, and USC reaction probabilities

In Fig. 9 we compare the reaction probabilities P_{03}^R and P_{04}^R of $F + D_2$ as calculated by all four methods EQ, QCF, QCR, and USC. Figure 10 presents the analogous comparison for the total reaction probability P_0^R. It is apparent from both figures that the USC method gives the best agreement with the EQ reaction probabilities for this reaction.
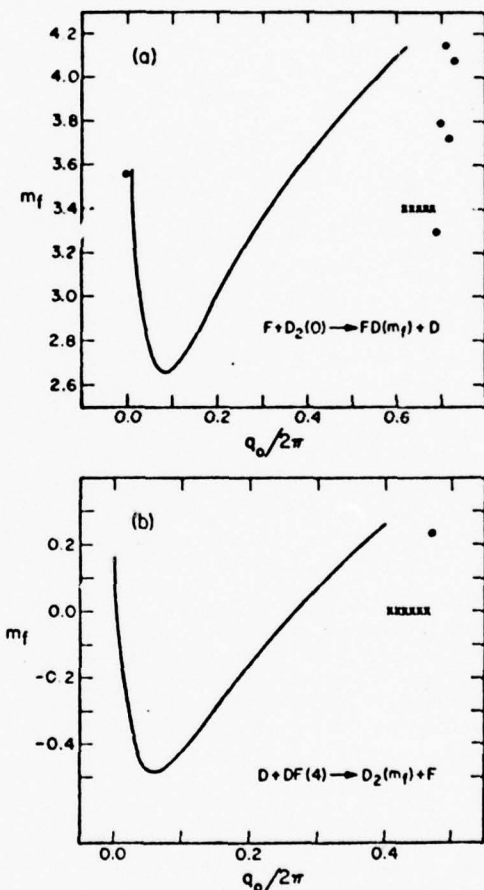
FIG. 8. (a) m_f vs q_0 for the forward $F + D_2 (0) \rightarrow FD(m_f) + D$, at a total energy E of 0.3107 eV; (b) m_f vs q_0 for the reverse reaction $D + DF(4) \rightarrow D_2(m_f) + F$, at the same total energy E. The solid curves represent the majority of the reactive trajectories computed. The dots and crosses represent, respectively, reactive and nonreactive trajectories in regions of raggedness, for which m_f varies very rapidly with q_0. Since the values of m_f for nonreactive trajectories correspond to a different range of variation than the reactive ones, the crosses were placed at an arbitrary ordinate and are only meant to indicate the values of q_0 for which such trajectories occur.
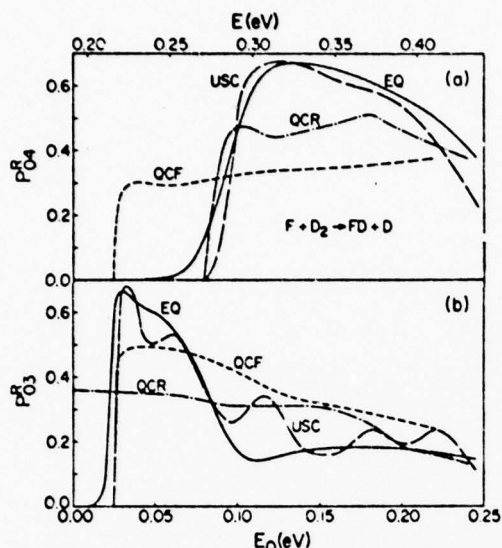
FIG. 9. EQ (solid), QCF (short dash), QCR (dash—dot), and USC (long dash) reaction probabilities P_{04}^R (a) and P_{03}^R(b). (From Figs. 1, 3-4, 7.)

E. Information-theoretic analysis of EQ and QCF reaction probabilities

It is also of interest to perform an information—theoretic analysis of the EQ and QCF results. In this section, we shall consider both the $F + D_2$ reaction probabilities discussed above and the $F + H_2$ probabilities described in Paper I.

In analogy with the equations used in three-dimensional studies,[9] we have used a one-dimensional form of the surprisal for a vibrational distribution given by

$$I(f_{v'}) = - \ln[P(f_{v'})/P^0(f_{v'})].$$

$P(f_{v'})$ is the normalized reaction probability to product vibrational state v' expressed as a function of the fraction of the total energy which becomes vibrational energy in the product DF or HF (exclusive of product zero point energy). $P^0(f_{v'})$ is the statistical reaction probability to state v' and is given by

$$P^0(f_{v'}) = \frac{(1 - f_{v'})^{-1/2}}{\sum_{v'=0}^{v'}(1 - f_{v'})^{-1/2}} ,$$

where the sum is over all accessible product vibrational states. Note that this expression for $P^0(f_{v'})$ predicts inverted statistical vibrational population distributions. This rather surprising result for such a distribution is a straightforward consequence of the use of a one-dimensional density of states function [which varies as $(E_{v'})^{-1/2}$, where $E_{v'}$ is the translational energy relative to vibrational state v'] rather than the corresponding three-dimensional density (which varies as $E_{v'}^{1/2}$).

Figure 11 depicts the EQ and QCF surprisal functions $I(f_{v'})$ vs $f_{v'}$ for $F + D_2$ and $F + H_2$ at three different relative translational energies. We see that none of the EQ or QCF plots has the straight line dependence on $f_{v'}$ re-

quired if the distribution is to be characterized by a single information—theoretic temperature parameter. The most severe deviations of the EQ results from linearity occur at the lowest energies and are a direct consequence of the unusual threshold behavior of P_{04}^R in F + D₂ and P_{03}^R in F + H₂. This threshold effect is not present in the QCF results, and yet the surprisal functions associated with these probabilities show strong deviations from linearity. The curves in Fig. 11 indicate that at least in this case, the information—theoretic analysis has limited usefulness as a predictive tool for estimating unknown reaction probabilities from known ones. For example, if we assumed a linear surprisal function and used the results of the two largest EQ probabilities to predict the third largest by linear extrapolation, we would be in error by at least 1 order of magnitude in most of the examples depicted in Fig. 11.

Figure 11 also indicates that in many situations, the surprisal function is not independent of isotopic substitution. This is especially true of the EQ results with $v' = 0, 1$, where the differences between the surprisal functions for $F + D_2$ and $F + H_2$ are quite large. However, at higher energies [Fig. 11(a), especially] and for higher vibrational quantum numbers ($v' = 2-4$), the EQ points for both $F + D_2$ and $F + H_2$ fall on essentially the same curve. In addition, the QCF results for $F + D_2$ and $F + H_2$ in both Figs. 11(a) and 11(b) seem to form a single curve, and for this reason, only one dashed line was drawn through the points. This indicates that at certain energies and for certain ranges of $f_{v'}$, the surprisal function is independent of isotopic substitution, but this property is not generally valid.

The behavior of the surprisal functions (nonlinearity and dependence on isotopic substitution) observed in these collinear results contrasts strongly with the shape of the corresponding surprisal functions obtained from three-dimensional trajectory calculations and experiments on the same reactions.[9] In the three-dimensional case, linear surprisal functions which are nearly inde-
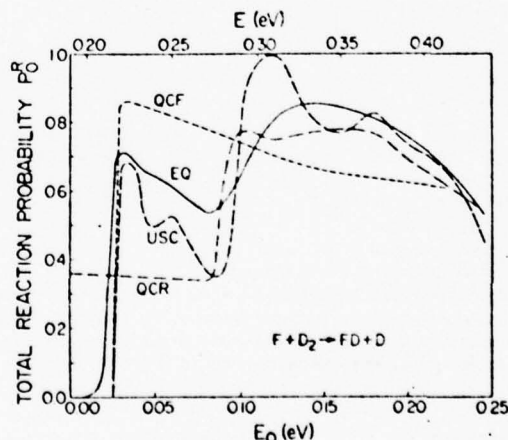
FIG. 10. EQ (solid), QCF (short dash), QCR (dash—dot), and USC (long dash) total reaction probabilities P_0^R for F + D₂. (From Figs. 1, 3-4, 7.)
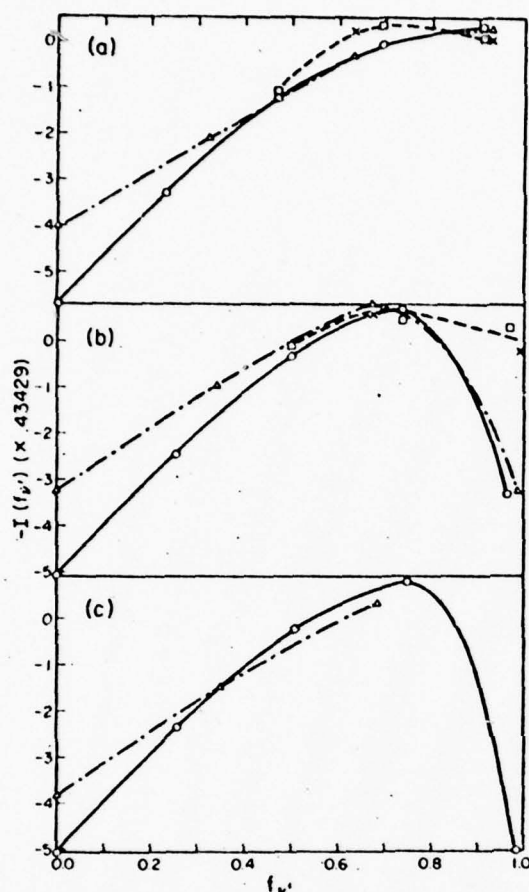
FIG. 11. Surprisal function $I(f_{\nu'})$ vs fraction $f_{\nu'}$ of the total product energy which is in product vibrational state ν' (exclusive of zero point energy). Symbols plotted have the following meanings: circles—EQ results for F + D₂; triangles—EQ results for F + H₂; squares—QCF results for F + D₂; and crosses—QCF results for F + H₂. (a) $E_0 = 0.12$ eV, (b) $E_0 = 0.03$ eV, (c) $E_0 = 0.005$ eV. The F + D₂ (EQ) results are connected by a solid line, while a dashed–dotted line connects the F + H₂ (EQ) results. A dashed line approximately connects both F + H₂ and F + D₂ (QCF) results. Note that at the lowest energy considered [Fig. 10(c)], only $\nu' = 0-2$ of HF are energetically accessible, and all QCF reaction probabilities are zero.

pendent of isotopic substitution were obtained in an analysis of the detailed rate constants (rather than reaction probabilities) from both quasiclassical trajectory calculations and from infrared chemiluminescence experiments (which are, of course, quantum mechanical). We have analyzed the surprisal functions for our collinear EQ rate constants for both F + H₂ and F + D₂ (Sec. III) and find no marked change from the results depicted in Fig. 11, the nonlinearity and dependence on isotopic substitution being essentially as pronounced as for the reaction probabilities.

Recently, the relationship between the one- and three-

dimensional classical surprisal functions was computationally investigated, [10a] and it was proposed [10b] that the surprisal function should be approximately dimensionally invariant. Our comparison of the one- and three-dimensional surprisal functions for F + H₂ and F + D₂ indicates that this dimensional invariance does not hold for these reactions. Although the validity of our conclusion depends in part on the accuracy of the potential energy surface used in our calculations, we would not expect it to be qualitatively changed if a more accurate potential energy surface were used. In addition, we note that three-dimensional quasiclassical results for F + H₂ and F + D₂ on similar approximate surfaces[3] agree with experiment in their prediction of a linear surprisal function.[9] The computational comparison of one- and three-dimensional surprisal functions of Ref. 10a involved several model potential energy surfaces, but none of these simulated the attractive nature of the F + H₂ interaction. We conclude that the invariance of the surprisal function with respect to the dimensionality of the collision may depend significantly on the characteristics of the potential energy surface being considered. Therefore, caution must be exercised in attempting to obtain 3-D reaction cross sections from collinear reaction probabilities.[10c]

III. EQ, QCF, QCR, AND USC RATE CONSTANTS FOR F + D₂

The rate constants k_{03}^R and k_{04}^R obtained from the EQ, QCF, QCR, and USC reaction probabilities P_{03}^R and P_{04}^R for F + D₂ are plotted in Fig. 12. The expression for these rate constants is the same as the one given in Paper I.[1] The corresponding Arrhenius parameters obtained from fits to the rate constants in the 200–400 K and 900–1200 K temperature ranges are listed in Table II. The difference between k_{04}^R (QCF) and k_{04}^R (EQ) (which results from the different threshold properties of the P_{04}^R's in Fig. 9) is quite noticeable and leads to a 0.8 kcal difference between the corresponding high temperature activation energies in Table II. In analogy with our F + H₂ study,[1] the QCR and USC rate constants $k_{04}^{\sim}$ and corresponding activation energies E_{04}^a agree with the EQ ones better than do the QCF quantities. The similar comparison for the rate constants k_{03}^R is much less satisfactory. The low temperature differences between various k_{03}^R's are determined to a large extent by the different threshold energies of the corresponding reaction probabilities P_{03}^R. The transition probability P_{03}^R (QCR) has zero threshold energy and thus the largest rate constant at low temperatures, while the EQ, USC, and QCF P_{03}^R's have successively higher threshold energies and therefore successively lower rate constants. [See Fig. 9(b).] This illustrates that the low energy (< 0.03 eV) behavior of the reaction probabilities (or cross sections) can be exceedingly important in determining the low temperature (< 300 K) behavior of the corresponding rate constants for these reactions.

The ratios k_{04}^R/k_{03}^R are plotted as a function of temperature in Fig. 13. We see that the QCF ratio is nearly temperature independent while the EQ, QCR, and USC ratios increase monotonically with increasing temperature, approaching the QCF ratio at high temperatures.
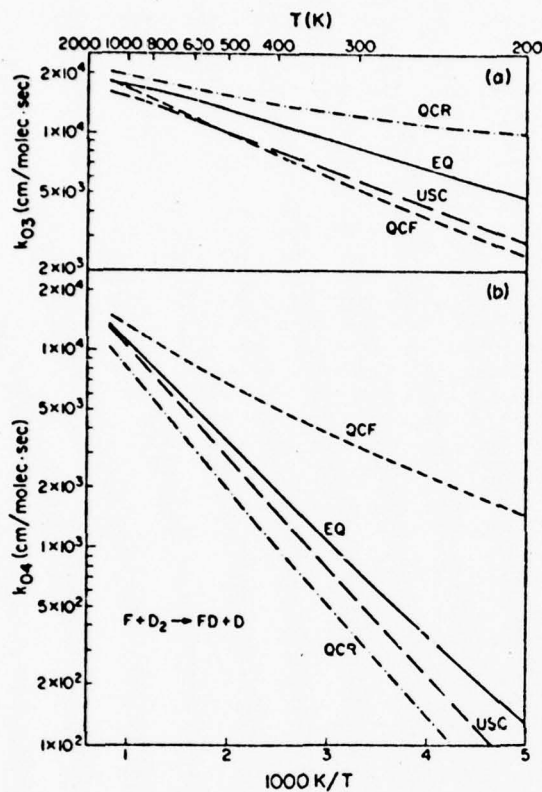
FIG. 12. Arrhenius plot of EQ (solid), QCF (short dash), QCR (dash-dot), and USC (long dash) rate constants for $F + D_2$: (a) k_{03}^R. (b) k_{04}^R.

FIG. 13. Ratios of rate constants k_{04}^R / k_{03}^R for $F + D_2$; EQ (solid), QCF (short dash), QCR (dash-dot), USC (long dash).

These k_{04}^R / k_{03}^R ratios are quite similar in appearance to the k_{03}^R / k_{02}^R ratios for the $F + H_2$ reaction given in Fig. 12 of Paper I, but the $F + D_2$ ratios actually increase somewhat more slowly with temperature than do the $F + H_2$ ones.

The QCF ratio k_{04}^R / k_{03}^R is 0.63 at 300 K, in approximate agreement with the experimental value[11] of 0.66. The results of three-dimensional classical trajectory calculations indicate that this ratio is not strongly tempera-

ture dependent.[12] If this is also true experimentally then, in analogy with $F + H_2$, we would have evidence that the collinear model overestimates the effects of threshold differences on reaction rates to different product vibrational states. We might note, however, that Lee and co-workers[12,13] have measured the ratio of cross sections σ_{04}/σ_{03} at three different energies, and they find that it increases rapidly with increasing energy from 0.75 at $E_0 = 0.034$ eV to 3.5 at $E_0 = 0.11$ eV. If we consider the analogous collinear ratio P_{04}^R / P_{03}^R (Fig. 6), we find that it also increases rapidly with increasing energy (much more rapidly than Lee's cross section ratio) from near zero at zero translational energy to roughly a value of 4.3 for $E_0 \sim 0.12$ eV. The ratios of cross sections from three-dimensional QCF trajectory calculations over a family of several potential energy surfaces do not reproduce this energy dependence (Ref. 12, Table VI). This may indicate that the differences between quantum and quasiclassical results are still significant in three dimensions and, indeed, are observable in experiments which are at least partially state selected such as cross section measurements.

TABLE II. Arrhenius rate constant parameters for $F + D_2 \rightarrow FD + D$.[a]

	Temperature range (K)	EQ	QCF	QCR	USC
E_a^{03}	200–400	0.676	0.935	0.266	0.852
E_a^{04}	200–400	2.167	0.990	2.576	2.471
A_{03}	200–400	2.531×10^4	2.443×10^4	1.884×10^4	2.340×10^4
A_{04}	200–400	2.775×10^4	1.686×10^4	2.502×10^4	3.269×10^4
E_a^{03}	900–1200	0.361	0.912	0.416	0.611
E_a^{04}	900–1200	2.108	1.343	2.742	2.344
A_{03}	900–1200	2.104×10^4	2.674×10^4	2.402×10^4	2.082×10^4
A_{04}	900–1200	3.240×10^4	2.604×10^4	3.261×10^4	3.365×10^4

[a]E_a^{04} is in kcal/mole and A_{04} is in cm/(molecule·sec).

IV. HIGHER ENERGY REACTION PROBABILITIES FOR F + D$_2$

Figure 14 shows the higher energy exact quantum reaction probabilities P_{03}^R, P_{04}^R, P_{05}^R, P_{14}^R, and P_{15}^R for F + D$_2$ in the translational energy range E_0 = 0.25-0.70 eV. Those transition probabilities not plotted are all small (usually < 0.02). P_{04}^R (QCR) is also plotted in Fig. 14 in the energy range 0.25-0.42 eV for reasons to be discussed in detail below. This figure is analogous in many ways to Fig. 13 of I, although the close correlation between the reaction probabilities of F + H$_2$ and the related F + D$_2$ ones (see end of Sec. II A) becomes less important as the energy is increased. Nevertheless, many of our remarks concerning the F + H$_2$ reaction probabilities described in I are also applicable here. We note that the transition probabilities P_{15}^R in Fig. 14 and P_{04}^R in Fig. 1 have similar translational energy dependences except near threshold. This confirms our statement in I that reaction probabilities for reagents initially in $\nu = 1$ are virtually insensitive to the presence of a barrier in the F + H$_2$ (D$_2$) reagent channel. In addition, P_{15}^R is significantly larger than the other $P_{1\nu'}^R$ with $\nu' < 5$ over the energy range considered. This implies that the additional vibrational energy in the reagents is being predominantly channelled into additional vibrational energy in the products.[14]

The transition probability P_{05}^R exhibits a rather unusual energy dependence. As shown in Fig. 14, it remains quite small (< 0.01), even though energetically allowed, until the total energy becomes high enough to excite $\nu = 1$ of D$_2$, at which point it rises suddenly to a peak value of 0.34 before finally levelling off at about 0.13. It is not obvious how simple resonance or threshold theories can explain this unusual behavior, since the effective threshold is apparently related to the opening of a vibrational state not involved in the transition asymptotically. One possible explanation for the influence of the $\nu = 1$ state of D$_2$ on this transition probability can be formulated by observing that the inelastic 0→1 transition probability for F + D$_2$ is quite appreciable[15] (0.10-0.25) and, as noted above, P_{15}^R is quite large. This suggests that the 0→5 reactive transition occurs almost exclusively with $\nu = 1$ as an intermediate state. It is also significant that it is not sufficient for this state to be accessible via virtual transitions, rather, it must be open asymptotically. This seems to indicate that a high degree of vibrational excitation must be maintained over a considerable region in configuration space. This would only be possible if the $\nu = 1$ vibrational state is open, and hence there is no enhancement of P_{05}^R when the state is closed.

For the transitions P_{04}^R at E_0 = 0.327 eV and P_{15}^R at E_0 = 0.599 eV, we see peaks in the reaction probabilities suggestive of internal excitation resonances.[16] In contrast to the resonances observed in Paper I in F + H$_2$, the direct processes in F + D$_2$ still seem to be quite important in the vicinity of the resonances. The resultant interference between the direct and resonant contributions to the scattering amplitude leads to characteristic oscillations in the reaction probabilities in the vicinities of the resonance energies quite similar to what was observed in the H + H$_2$ reaction.[16,17] As in the F + H$_2$ reac-

tion, we see an approximate correspondence between the appearance of a resonance and the opening of a specific vibrational state of the product DF ($\nu = 5$ at E_0 = 0.29 eV and $\nu = 6$ at E_0 = 0.59 eV). This implies that the virtual states of the triatomic complex may have energy levels resembling product states more than reagent states. The relation is probably complicated, however, since the correspondence between the resonance energy and the energy of the associated product vibrational level is not always in the same direction (i.e., the resonance energy is sometimes greater and sometimes smaller than the corresponding vibrational energy, as can be seen in Fig. 13 of Paper I and Fig. 14 in the present paper).

It is interesting to note that the QCR reaction probability P_{04}^R depicted in Fig. 14 seems to "average out" the quantum oscillations in P_{04}^R (EQ) in the vicinity of the E_0 = 0.327 eV resonance. It is also of interest to examine the semiclassical results at this energy. Rankin and Miller have reported extensive statistical behavior in
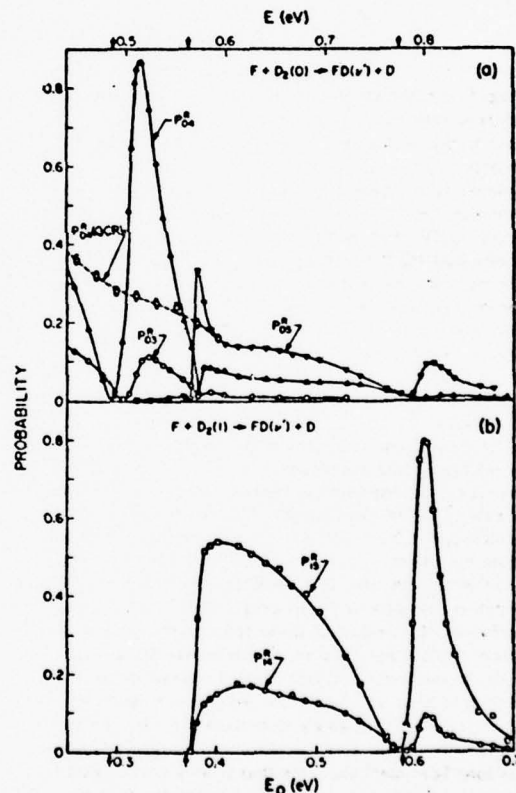
FIG. 14. Exact quantum reaction probabilities at translational energies higher than those in Fig. 1. (a) P_{03}^R, P_{04}^R, and P_{05}^R. (b) P_{14}^R and P_{15}^R. Also shown in (a) is the QCR P_{04}^R curve (dashed). Arrows near E_0 = 0.29 eV and 0.59 eV indicate the opening of $\nu = 5$ and 6, respectively, of DF, while that at 0.37 eV indicates the energy E_0 at which $\nu = 1$ of D$_2$ becomes accessible.
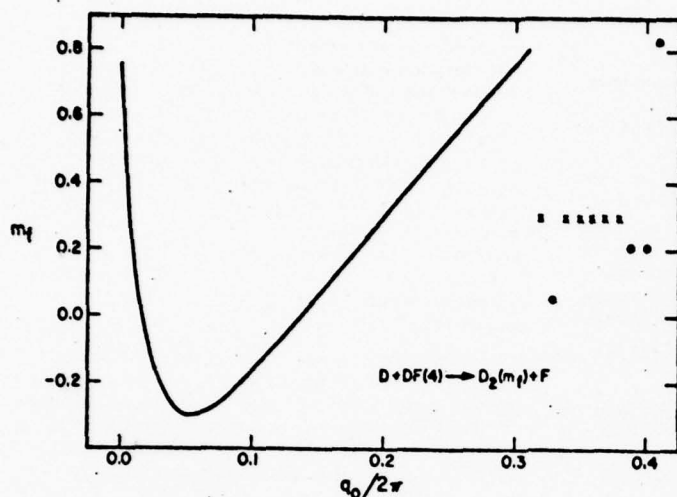
FIG. 15. m_f vs q_0 for the reverse reaction D + DF (4) → D$_2$(m_f) + F at the resonance nergy 0.5107 eV (corresponding to E_0 = 0.32 eV). See Fig. 8 for explanation of dots and crosses.

the final action number function, m_f, for the H + Cl$_2$ collision.[6] From this behavior, they inferred that a converged quantum treatment of that reaction would yield internal excitation resonances. However, as Fig. 15 shows, m_f, at the resonance energy, is a reasonably smooth function of q_0 with about the same degree of raggedness (i.e., very rapid variation of m_f with q_0) as seen previously away from resonance in Fig. 8(b). An accurate EQ study of the collinear H + H$_2$ reaction has shown that P_{00}^R has a broad resonance at 0.90 eV total energy and a narrow one at 1.28 eV, and that both are due to interference effects between direct and compound-state mechanisms.[16] Recently, Stine and Marcus[16] searched for and found snarled (i.e., multiple collision) trajectories in the narrow region of q_0 between the reactive and nonreactive branches of the $m_f(q_0: \nu, E)$ curve. They showed that the broad resonance at 0.90 eV could be generated semiclassically if interference effects between direct and snarled trajectories are included, a result consistent with the lifetime analysis of the accurate quantum calculations.[16] Were it not for the knowledge of the existence of this resonance derived from the EQ calculations, it would be easy to miss such snarled trajectories in a semiclassical calculation in which the density of the q_0 grid was not high enough.[5,19] Inclusion of a search of these trajectories and of their effects on the reaction probabilities significantly increases the computational effort involved in the semiclassical approach. Narrow resonances, such as the one occurring at 1.28 eV in collinear H + H$_2$, may be even more difficult to calculate semiclassically, since its long lifetime[16] suggests that it may correspond to extremely snarled trajectories, requiring inclusion of multiple collisions of high order[16] and use of an extremely high density q_0 grid. In the present paper, we have only included the effect of direct (i.e., nonsnarled) trajectories in the semiclassical calculations. It would be interesting to add the effect of snarled ones, in order to verify whether they could reproduce the resonant be-

havior of P_{04}^R at E_0 = 0.327 eV.

We conclude that raggedness in the $m_f(q_0; \nu, E)$ curves could perhaps be a necessary condition for the existence of quantum mechanical internal excitation resonances, but it is certainly not a sufficient one, as shown by the presence of raggedness in Fig. 8(b), calculated at a non-resonant energy.

V. EXACT QUANTUM REACTION PROBABILITIES FOR THE REACTIONS F + HD → FH + D AND F + DH → FD + H

We have also calculated the exact quantum reaction probabilities for F + HD → FH + D and F + DH → FD + H, hereafter designated F + HD and F + DH, respectively. In three dimensions, these two reactions represent different product arrangement channels of the same collision system. In collinear collisions, however, they must be considered entirely separately. This implies that coupling between these two product arrangement channels is ignored in our collinear calculations.

The largest reaction probabilities for the two reactions are plotted in Fig. 16[20] as a function of the reagent translational energy E_0 (relative to ν = 0 of HD) in the range 0–0.25 eV. For F + HD, the only reaction probability greater than 0.025 in the energy range studied is P_{02}^R, while P_{04}^R, P_{03}^R, and P_{02}^R are the major contributors to the total reaction probability in F + DH (P_{02}^R is always less than 0.10). From Fig. 16 it is apparent that the reaction probabilities P_{04}^R and P_{03}^R of F + DH are very similar in shape to the corresponding probabilities P_{04}^R and P_{03}^R of F + D$_2$ (Fig. 10), although the sharp differences between the threshold energies of P_{04}^R and P_{03}^R (F + D$_2$) are reduced considerably for P_{04}^R and P_{03}^R (F + DH). In contrast, the results for F + HD do not show a strong resemblance to those for F + H$_2$ (Fig. 2 of Paper I). Instead, we see that P_{02}^R (Fig. 16) consists of one very sharp (width ~0.0005 eV) spike near 0.012 eV and then
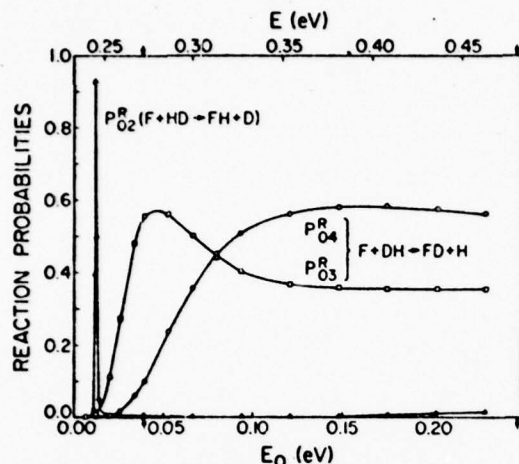
FIG. 16. Exact quantum reaction probabilities P_{02}^R for F + HD, and P_{03}^R and P_{04}^R for F + DH as a function of relative translational energy E_0 and total energy E (relative to minimum in HD diatomic potential curve). Arrow near 0.04 eV indicates the energy at which $\nu = 3$ of HF becomes accessible.

remains quite small (< 0.02) for the remainder of the energy range studied. P_{03}^R, which is energetically forbidden until $E_0 = 0.039$ eV, is quite small throughout the energy range considered here. The rather dramatic differences between the results for F + HD and F + DH can probably be explained as resulting from the difference in the mass of the atom being exchanged in the collinear triatomic collision system. The small mass of the H atom in F + HD in comparison with that of the D atom in F + DH results in much more important pseudocentrifugal barriers in "turning the corner" in the former reaction than in the latter. That this should be the case is apparent from a comparison of the skew angles (defined in Paper I) for these two systems. For F + HD this angle is 37.3°, while for F + DH it is 56.7°, thus indicating that the curvature along the reaction path should be much larger for F + HD than for F + DH. Only at low translational energies do the centrifugal effects become small enough to render F + HD dynamically allowed. For F + DH, on the other hand, the centrifugal effects are not important in the energy range studied, and thus we observed very large reaction probabilities throughout that energy range.

From Fig. 16, we can also conclude that the rate constant for formation of DF is predicted to be greater than that for formation of HF [except at very low temperatures ($< 150°$), where the slightly smaller effective threshold of F + HD becomes important]. This disagrees with the experimental result[21] that the rate of H atom transfer is a factor of 1.45 faster than that for D atom transfer at 298 K. The disagreement can probably be explained by noting that the distance of the H atom from the center of mass of HD is about twice that of the D atom from the same center of mass. This means that H sweeps through a larger volume of space than D when HD rotates and thus is more "visible" to the attacking

F atom. Since the barrier height is quite low (except near the "perpendicular" orientation[12]), one would expect that H should be preferentially abstracted. For collinear reactions, this three-dimensional effect is ignored and we find, instead, that dynamical effects such as pseudocentrifugal barriers are important in the reaction. These centrifugal effects favor reaction with the D atom and thus explain why the collinear results differ from the experimental ones. A similar argument has been used to explain the J dependence of three-dimensional quasiclassical cross sections for the same reactions.[34] One might add that for a reaction with a high barrier, which simultaneously favors reaction through collinear geometries, the three-dimensional effect should be less important and the collinear results should be more representative of the experimental results. This has indeed been observed for the Cl + HD (DH) reactions.[22]

VI. DISCUSSION

We shall now summarize the differences between the results of the exact quantum, quasiclassical, and semiclassical methods for studying the F + H₂ (Paper I) and F + D₂ reactions. The most important of these differences may be categorized into three divisions: vibrationally adiabatic tunnelling, resonances, and threshold dynamical effects. These effects may, however, be coupled to one another to a lesser or greater extent.

Vibrationally adiabatic tunnelling seems to be most significant at very low energies, especially for F + H₂ and for those transitions for which at threshold there are no strongly restrictive dynamical effects (of the type occurring in P_{03}^R for F + H₂). Such tunnelling appears to be responsible for important differences between EQ and QCF rate constants at low temperatures [Figs. 11(a) in I and also 12(a) in this paper]. The semiclassical complex trajectory method (which was not studied here) may be able to describe tunnelling quantitatively.[5,7] Internal excitation resonances seem to be very important at higher translational energies and will therefore not be significant in thermal experiments. They may be important in beam and hot atom experiments if these resonance effects carry over without strong attenuation into three dimensions.[23] The current semiclassical theories do not seem to furnish a computationally practical description of the interference effects associated with these resonances.[20] Threshold dynamical effects are very significant for collinear F + H₂ and F + D₂, and this leads to important differences between exact quantum and quasiclassical reaction probabilities and rate constants for thermal distributions of reagents. These threshold effects are partially classical in nature, since we found that the QCR method was capable of describing roughly the proper threshold behavior within a completely classical framework. An important result of this paper was the demonstration that the uniform semiclassical method provides a greatly improved description of threshold behavior of the quantum results in comparison with the QCF method. How important these threshold effects will be in three dimensions is not entirely clear from an analysis of existing experimental and theoretical studies, but it appears that the effects

are at least partially attenuated by the averaging that inevitably occurs in experimental measurements. They may, however, still be important for experiments which are sufficiently state selected.

ACKNOWLEDGMENTS

We thank J. T. Muckerman, with whom we have exchanged results on the USC calculations, for useful discussions. We also thank Ambassador College for the use of their computational facilities in most of the work reported here.

[1]G. C. Schatz, J. M. Bowman, and A. Kuppermann, J. Chem. Phys. 63, 674 (1975), preceding paper.
[2](a) J. T. Muckerman (private communication); (b) P. A. Whitlock and J. T. Muckerman, J. Chem. Phys. 61, 4618 (1974).
[3](a) J. T. Muckerman, J. Chem. Phys. 54, 1155 (1971); (b) *ibid.* 56, 2997 (1972).
[4]J. C. Polanyi and K. B. Woodall, J. Chem. Phys. 57, 1574 (1972).
[5]J. M. Bowman and A. Kuppermann, J. Chem. Phys. 59, 6524 (1973).
[6]C. C. Rankin and W. H. Miller, J. Chem. Phys. 55, 3150 (1971).
[7]W. H. Miller and T. F. George, J. Chem. Phys. 56, 5668 (1972); J. D. Doll, T. F. George, and W. H. Miller, J. Chem. Phys. 58, 1343 (1973); J. Stine and R. A. Marcus, Chem. Phys. Lett. 15, 536 (1972).
[8]W. H. Miller, J. Chem. Phys. 54, 5386 (1971); R. A. Marcus, J. Chem. Phys. 57, 4903 (1972); J. D. Doll and W. H. Miller, J. Chem. Phys. 57, 5019 (1972); J. N. L. Connor, Mol. Phys. 25, 181 (1973).
[9](a) A. Ben-Shaul, R. D. Levine, and R. B. Bernstein, Chem. Phys. Lett. 15, 160 (1972); (b) A. Ben-Shaul and R. D. Levine, J. Chem. Phys. 57, 5427 (1972).
[10](a) C. Rebick, R. D. Levine, and R. B. Bernstein, J. Chem. Phys. 60, 4977 (1974); (b) R. B. Bernstein and R. D. Levine, preprint.
[11]M. J. Berry, J. Chem. Phys. 59, 6229 (1973).
[12]N. C. Blais and D. G. Truhlar, J. Chem. Phys. 58, 1090 (1973).
[13]T. P. Schaefer, P. E. Siska, J. M. Parson, F. P. Tully, Y. C. Wong, and Y. T. Lee, J. Chem. Phys. 53, 3385 (1970). See also Ref. 10.
[14]A. Ding, L. Kirsch, D Perry, J. Polanyi, and J. Schreiber, Discuss. Faraday Soc. 55, 252 (1973).
[15]G. C. Schatz and A. Kuppermann (unpublished calculations).
[16]G. C. Schatz and A. Kuppermann, J. Chem. Phys. 59, 964 (1973).
[17]R. D. Levine and S.-F. Wu, Chem. Phys. Lett. 11, 557 (1971).
[18]J. R. Stine and R. A. Marcus, Chem. Phys. Lett. 29, 575 (1974). This work appeared in print after the present paper was submitted for publication. All references to it were incorporated subsequently, at the time some revisions suggested by the referee were made.
[19]J. D. Duff and D. G. Truhlar, Chem. Phys. 4, 1 (1974).
[20]Note that for these calculations, a slightly different value of β(HF) was used (2.2087 Å⁻¹) than in Paper I (2.2187 Å⁻¹).
[21]A. Persky, J. Chem. Phys. 59, 5578 (1973).
[22]M. Baer, U. Halavee, and A. Persky, J. Chem. Phys. 61, 4362 (1974).
[23]Recent three dimensional calculations on the H + H₂ reaction indicate that the attenuation of resonance effects in going from 1D to 3D is not severe [G. C. Schatz and Aron Kuppermann (to be published)].

A SEMI-NUMERICAL APPROACH TO THE CONSTRUCTION AND FITTING
OF TRIATOMIC POTENTIAL ENERGY SURFACES*

Joel M. BOWMAN

Department of Chemistry, Illinois Institute of Technology, Chicago, Illinois 60616, USA

and

Aron KUPPERMANN

*Arthur Amos Noyes Laboratory of Chemical Physics **, California Institute of Technology.
Pasadena, California 91125, USA*

The Wall–Porter method of rotating a Morse function to construct potential energy surfaces for collinear atom–diatom chemical reactions is modified by using a numerical spline interpolation technique. This procedure is shown to have great flexibility in giving a potential surface desired characteristics, such as the saddle-point location and the barrier height and curvature at this point, for either symmetrical or unsymmetrical reactions. Extensions of the method to non-reactive and non-collinear potential surfaces are also discussed.

The great difficulty in calculating potential energy surfaces by accurate ab initio techniques has necessitated the use of phenomenological approaches of a semi-empirical nature to generate approximate surfaces with reasonably realistic topographies for use in atom–molecule dynamics calculations. The LEPS method [1] is used extensively for this purpose since it provides the means for smoothly and conveniently interpolating the potential surface between the various separated atom–diatom arrangement channels. It suffers from several well-known shortcomings, however, due to the simplicity of the mathematical form of the LEPS function.

Let us consider as an example a linear triatomic system. First, after specifying the potential function parameters of the diatomic reagent and product and the classical barrier height there is only one degree of freedom left in the LEPS function to determine the two position coordinates of the saddle point and the curva-

tures of the surface along and transverse to the minimum energy path at that point, which are important features of the surface. Thus, the specification of these important properties of a potential surface creates a highly overdetermined problem for the LEPS function. Second, this function may develop spurious "hollows" if it is forced to have approximately the desired barrier height and saddle point location. Third, it is not possible to make a change in a localized region of the potential surface without significantly affecting the entire surface. This aspect of the LEPS function makes it less than ideal for calculations which explore the relationship between potential surface characteristics and its reaction-dynamical properties (reaction cross sections, internal energy distributions, etc.). Fourth, for reactions in three dimensions the problem of overdetermination of the LEPS function is compounded greatly so that it is difficult for the important features considered above, in each of the three regions connecting the three separated arrangement channels, to be specified even approximately. Clearly, this lack of flexibility of the LEPS function makes it in general unsuitable for fitting available ab initio data points of a

523
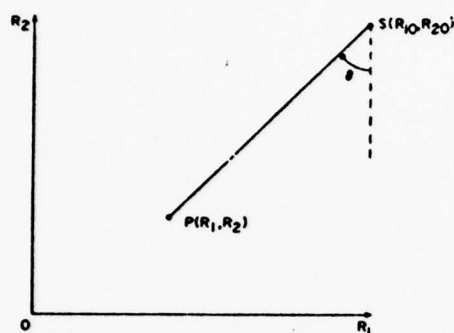
Fig. 1. Swing coordinates l, θ of Mo.$\cdot\cdot$ function about the point $S(R_{10}, R_{20})$.

given potential energy surface.

The Wall–Porter function [2] cleverly overcomes several of these shortcomings for collinear collisions. Let us consider the configuration space spanned by the two internuclear distances R_1 and R_2 to the central atom. In the Wall–Porter approach a Morse function is rotated from the reagent region to the product region of this space around an adequately chosen point in the high plateau region of the surface. The Morse function parameters are chosen to be simple and similar analytical functions of the rotation angle, θ. Although features such as saddle-point location and barrier height can be specified, the simple nature of the θ-dependence of the Morse parameters and their interrelation reduces the usefulness of the method, since these characteristics preclude making localized changes in the potential. Furthermore, the resulting potential surface is not as smooth as the corresponding LEPS surface. This lack of flexibility and smoothness of the Wall–Porter function is largely overcome by the HMF (hyperbolic map function) method of Bunker and co-workers [3], in which the Morse function parameters are given by flexible analytical functions (e.g., Eckart functions) of the distance along a hyperbolic reaction path. An alternative to the HMF extension of the Wall–Porter approach is explored in the present paper. A similar approach has recently been used by Conner et al. [4].

In the spirit of the Wall–Porter method let us construct a collinear potential energy surface by rotation of a Morse function. Specifically, the potential as a

function of R_1 and R_2 is given by

$$V(R_1, R_2) = D(\theta)\{\{1 - \exp[\beta(\theta)(l_{eq}(\theta) - l)]\}^2 - 1\}$$

$$+ D(\theta = 0),$$

where

$$\tan \theta = (R_1 - R_{10})/(R_2 - R_{20})$$

and

$$l = [(R_1 - R_{10})^2 + (R_2 - R_{20})^2]^{1/2}$$

are the circular polar coordinates of the point $P(R_1, R_2)$ with respect to a system whose origin is the swing point $S(R_{10}, R_{20})$ and whose reference axis is antiparallel to OR_2, as indicated in fig. 1. We determine the θ-dependence of the Morse parameters $D(\theta)$, $\beta(\theta)$, and $l_{eq}(\theta)$ by assigning their values at a finite number of
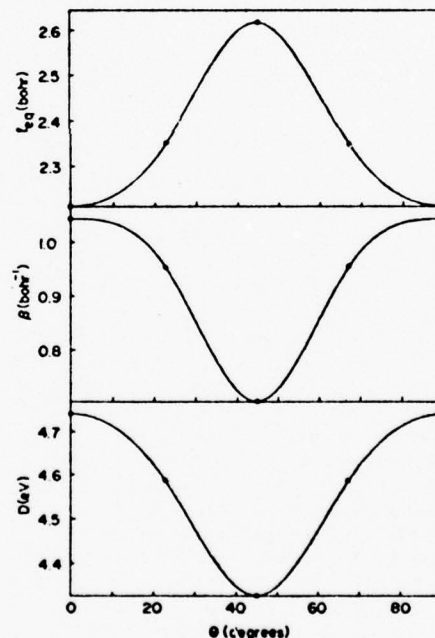
Fig. 2. Morse parameters D, β, and l_{eq} as a function of swing angle, θ, for the scaled SSMK H_3 potential surface. The points indicated correspond to specified values of the parameters and the lines are obtained by a cubic spline interpolation procedure.
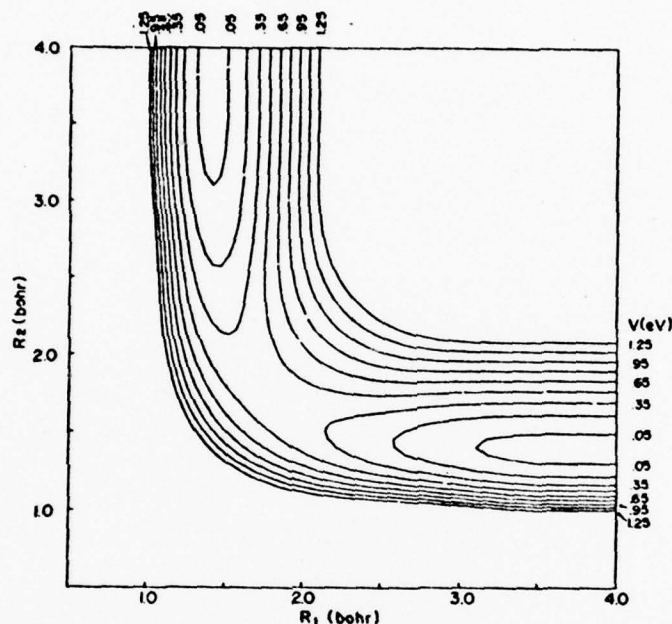
Fig. 3. Equipotential contour plot of the spline-generated H_3 potential energy surface of fig. 2.

values of θ and then performing a cubic spline interpolation [5] between the resulting points. This method of specifying the Morse parameters serves a dual purpose. First, it allows us to require that the potential energy surface have important desired characteristics. Thus, the saddle-point location, the barrier height, the curvature of the reaction path, etc., can be directly specified. Second, this fitting procedure can aid in the ab initio mapping of a potential energy surface. A spline-generated potential made to fit a small number of ab initio points could suggest the locations of additionally needed ab initio points.

As an example of application of this spline technique, consider the collinear $H + H_2 \rightarrow H_2 + H$ reaction. Truhlar and Kuppermann [6] have generated a Wall–Porter fit to the SSMK surface [7] for this reaction, with a corrected barrier height of 9.8 kcal/mole, which has been used for extensive quantum mechanical [6], classical [8] and semi-classical [9] calculations. The Morse parameters D, β, and l_{eq} for this surface are

plotted in fig. 2 as a function of θ. The five indicated points for each parameter are for θ equal to $0°$, $45°$, and $90°$ corresponding to reagents, transition state, and products, respectively, and also for θ equal to $22.7°$ and $67.3°$. The interpolation between these points was made using a cubic spline [5]. The resulting potential energy surface is displayed in fig. 3 in the form of an equipotential energy plot. The smoothness of this plot points out one desirable aspect of the spline method.

As another example consider a potential surface in which the Morse parameters of the reactant BC molecule are, $D = 3.64$ eV, $R_e = 2.68$ bohr and $\beta = 1.0$ bohr^{-1} and of the product AB molecule are, $D = 3.84$ eV, $R_e = 4.46$ bohr, and $\beta = 0.71$ bohr^{-1}, with a barrier height of 1.5 kcal/mole and for which the saddle point location is given by $R_1 = 5.2$ bohr and $R_2 = 2.7$ bohr*. It was found that the LEPS function could not

* These parameters were chosen for a ground state surface in a study of an electronically non-adiabatic chemical reaction [10].
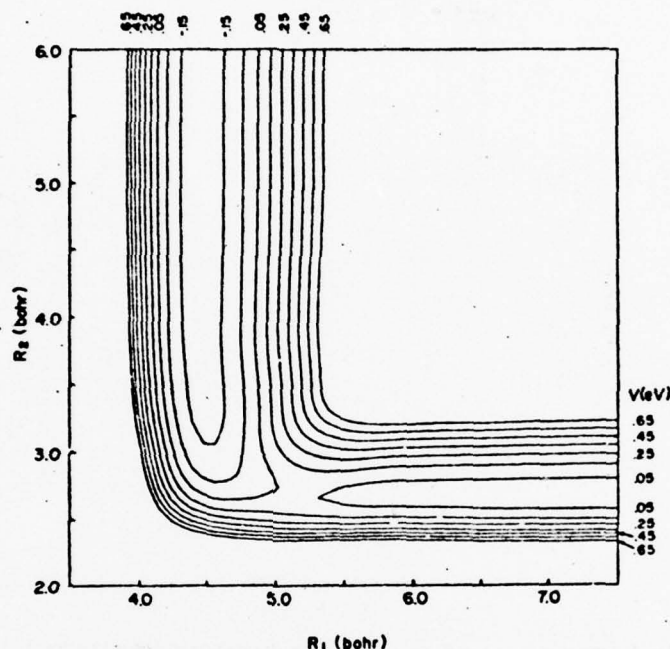
Fig. 4. Equipotential contour plot of the spline-generated potential surface described in the text, corresponding to the Morse parameters of fig. 5.

satisfy these specifications without also introducing spurious "hollows" in the reactant entrance channel. The cubic spline approach can produce the desired surface as seen in fig. 4. The θ-dependence of the corresponding Morse parameters is given in fig. 5. Twelve values of each parameter are specified. This was done because the potential of interest is somewhat long-ranged and requires "anchoring" in the asymptotic regions of space. A shorter range potential could have been constructed with the above specifications and fewer points would have been required as input.

There are two directions of interest in which to extend the spline approach given above. The first is to non-reactive potential surfaces and to surfaces with cusps, such as the one corresponding to the first excited singlet state of H_3^+ [11]. A rotating Morse function cannot represent such potential surfaces accurately. A

possible extension of the spline method is to consider a linear combination of a Morse function V_M and an "anti-Morse" function V_{aM}. For non-reactive surfaces this linear combination could be of the form

$$V(R_1, R_2) = \alpha(\theta)V_M(\theta) + [1 - \alpha(\theta)]V_{aM}(\theta),$$

where $0 \leq \alpha \leq 1$. This function contains three Morse parameters, three anti-Morse parameters, and the "switching" parameter α all of which are functions of θ. As previously, these parameters would be spline-fitted to give the desired potential surface. The second extension of interest is to allow V to be a function of the bond angle γ (as well as of R_1 and R_2). This extension is necessary to describe reactions in three dimensions. A straightforward way of doing this would be to multiply the function $V(R_1, R_2, \gamma = 0)$ by a function of γ as done by Bunker and co-workers [3].

526
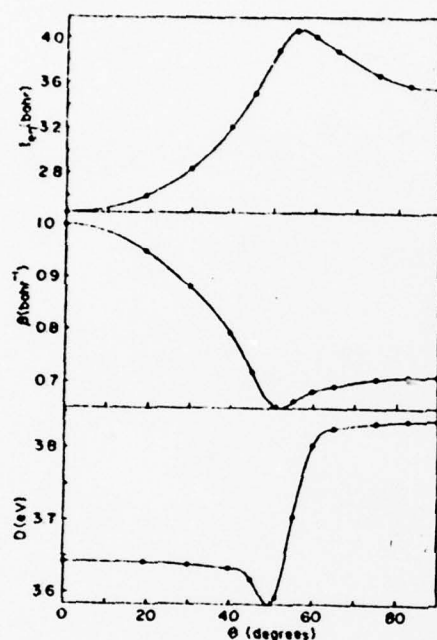
Fig. 5. Morse parameters D, β, and l_{eq} as a function of swing angle, θ, corresponding to the potential surface shown in fig. 4.

This, however, would restrict the flexibility of the fit and would introduce undesired restrictions on the shape of the function. Instead, it would be better to consider the swing point coordinates and the θ-dependent Morse parameters as functions of γ, to be deter-

mined by spline interpolations. Thus, a two-dimensional spline routine would be required to generate a potential surface for three-dimensional reactive scattering calculations. Both of the above extensions are currently under study.

References

[1] F. London, Z. Flektrochem. 35 (1929) 552;
S. Sato, J. Chem. Phys. 23 (1955) 2465;
P.J. Kuntz, E.M. Nemeth, J.C. Planyi, S.D. Rosner and
C.E. Young, J. Chem. Phys. 44 (1966) 1168.

[2] F.T. Wall and R.N. Porter, J. Chem. Phys. 36 (1962) 3256.

[3] D.L. Bunker and N.C. Blais, J. Chem. Phys. 41 (1964) 2377;
D.L. Bunker and C.A. Parr, J. Chem. Phys. 52 (1970) 5700;
D.L. Bunker, Methods Comp. Phys. 10 (1971) 287.

[4] J.N.L. Connor, W. Jakubetz and J. Manz, Mol. Phys. 29 (1975) 347.

[5] R.W. Hamming, Numerical methods for scientists and engineers, 2nd Ed. (McGraw-Hill, New York, 1973) pp. 49–356.

[6] D.G. Truhlar and A. Kuppermann, J. Chem. Phys. 56 (1972) 2232.

[7] I. Shavitt, R.M. Stevens, F.L. Minn and M. Karplus, J. Chem. Phys. 48 (1968) 2700.

[8] J.M. Bowman and A. Kuppermann, Chem. Phys. Letters 12 (1972) 1.

[9] J.M. Bowman and A. Kuppermann, Chem. Phys. Letters 19 (1973) 166; J. Chem. Phys. 59 (1973) 6524.

[10] J.M. Bowman and A. Kuppermann, unpublished results.

[11] R.K. Preston and J.C. Tully, J. Chem. Phys. 54 (1971) 4297.

PROGRESS IN THE QUANTUM DYNAMICS OF REACTIVE MOLECULAR COLLISIONS[†]

Aron Kuppermann

Arthur Amos Noyes Laboratory of Chemical
Physics,[‡] California Institute of Technology,
Pasadena, California 91125

ABSTRACT

Progress in accurate quantum mechanical calculations
of reactive collisions is reviewed. The results of three-
dimensional calculations are described and compared
with those of approximate methods. Resonances in reactive
scattering are discussed as well as electronically nonadiabatic
chemical reactions.

I. HISTORICAL INTRODUCTION

Given an electronically adiabatic potential energy
surface for a triatomic system, it is possible in principle to
solve the Schrödinger equation describing the motion of the
nuclei on that surface and to obtain, from such solutions,
state-to-state differential and integral reaction cross sections.
These cross sections furnish very detailed information about
the dynamics of the reaction and can also be used to calculate
rate constants for bulk reactions. This problem is, however,
computationally formidable, and as a result the first attempts to
solve it were limited to collinear reactions in which the three

atoms were constrained to lie on a straight line. This reduces
the number of independent variables on which the wavefunction
depends from six to two, greatly simplifying the problem.
The first solution of this collinear problem for a realistic
potential energy surface was obtained by Mortensen and
Pitzer (1) for the H + H$_2$ exchange reaction and extended
later (2) to some of its isotopic counterparts. The method
used was a finite difference numerical solution of the two-
variable time-independent Schrödinger partial differential
equation coupled with an iterative procedure for imposing the
appropriate reactive-scattering boundary conditions. A
variation of the finite difference method in which the boundary
conditions were imposed by a noniterative approach involving
a sufficiently large number of linearly independent solutions
of the Schrödinger equation was developed by Diestler and
McKoy (3) and applied by Truhlar and Kuppermann (4) to
H + H$_2$ and by Truhlar, Kuppermann, and Adams (5) to some
of its isotopic counterparts. An interesting variation of the
finite difference method was introduced by McCollough and
Wyatt (6) who used it to solve the time-dependent Schrödinger
equation for the H + H$_2$ exchange reaction, replacing thereby
a boundary value problem by an initial value one.

The finite-difference approach in any of the variations
mentioned above is computationally very inefficient and inappro-
priate for extension to a wide energy range or to problems of
higher dimensionality. As a result, several other methods
have been developed and used recently. These include the
variational approach used by Mortensen and Gucwa (7) for
collinear H + H$_2$, and the integral equation method developed
by Sams and Kouri (8) and applied to several collinear systems
by Adams, Smith, and Hayes (9). However, the most widely
used approach for collinear collisions is the coupled-
equation (i.e., close-coupling) method, in one of its several
forms. The basic method consists in choosing a set of two
convenient variables, x and y, to describe the internal config-
uration of the system. These variables may be different in
different regions of configuration space but satisfy the central
property that for x equal to a constant $\bar{x}$ the potential energy
function $V(\bar{x}, y)$ is bound. The wavefunction $\psi(x, y)$ is expanded
in eigenfunctions of $V(\bar{x}, y)$, (which are called the vibrational
basis set) and the resulting coupled ordinary differential
equations in the x-dependent coefficients of this expansion are
solved. Variations of this approach have been developed by
Light (10), Kuppermann (11), Diestler (12), and Johnson (13)
and applied to a variety of collinear systems (10-18). As a
result, a significant amount of knowledge has accumulated
about the reactive scattering properties of collinear reactive
systems.

When the constraint of collinearity is
relaxed, the problem becomes significantly more difficult.
For coplanar triatomic reactions, the wavefunction depends
now on four variables (after the motion of the center of mass
is removed) and the potential energy function V on three. A
partial wave expansion reduces the problem to a set of
uncoupled partial wave Schrödinger equations depending on the
same three variables as V (19, 20). One of these is usually an
angle, and expansion of the wavefunction in terms of a complete
set of basis functions of that angle (the rotational basis set)
yields a set of coupled two-variable partial differential equa-
tions. For triatomic reactions in three-dimensional space,
the wavefunction depends on six variables, three of which can
be chosen to be the ones on which V depends (21, 22). It is
possible to eliminate the other three variables by a partial
wave expansion in terms of Wigner rotation functions, leading
to a set of coupled partial wave Schrödinger equations depend-
ing on the same three variables as V. A further expansion in
terms of the angular variable usually appearing in V leads
again to a set of coupled two-variable partial differential
equations, the number of which is usually appreciably larger
than for the coplanar case. There have been relatively few
studies of such noncollinear reactions. The coplanar $H + H_2$
system was investigated by coupled-equation techniques by
Light and co-workers (19), using a single vibrational basis
function, and by Kuppermann and co-workers (20), in a con-
verged vibrational-rotational expansion approach. Baer and
Kouri (23) developed a coupled T-operator integral equation
technique and applied it to a simple three-dimensional model
atom plus diatom system in which reaction with only one end
is permitted. Wolken and Karplus (24) applied an integro-
differential equation method proposed by Miller (25) to the
three-dimensional $H + H_2$ reactive system using a one-
vibrational basis function approximation. Very recently,
Kuppermann and Schatz (21) have achieved accurate vibration-
ally and rotationally converged results by an extension of the
coupled-equation techniques previously used for collinear and
coplanar systems (11, 20), and Elkowitz and Wyatt (22) have
applied a different version of the coupled-equation method
using hindred rotor basis functions in the expansion (22, 26).
In a somewhat different vein, Micha (27) has developed a
Fadeev-equation approach to the problem of reactive scattering.

In this paper we focus attention on the accurate 3-D
results (21, 22) all of which have appeared since the previous
ICPEAC meeting was held in Belgrade in July of 1973. Co-
planar and collinear results as well as other approximate
methods will be invoked mainly for comparison purposes.
However, some recent accurate collinear studies of reactive
scattering resonances and of electronically-nonadiabatic

chemical reactions will also be discussed.

II. POTENTIAL ENERGY SURFACES IN
SYMMETRIZED HYPERSPERICAL COORDINATES

In order to summarize the characteristics of the reactive scattering problem and the approaches used to solve it, it is useful to describe the nature of the interaction potentials under consideration. For electronically adiabatic chemical reactions the Born-Oppenheimer separation approximation permits us to describe the motion of the nuclei during a chemical reaction as that due to a potential energy function V which depends on the relative positions of the nuclei but not on the electronic coordinates. V is obtainable by assuming these nuclei to be fixed and solving the electronic motion problem. The resulting electronic wavefunction and energy depend parametrically on the nuclear geometry. Let us consider a system of three atoms $A_\alpha (\equiv A)$, $A_\beta (\equiv B)$, and $A_\gamma (\equiv C)$. For notational purposes, let $\lambda \nu \kappa$ be any cyclic permutation of $\alpha\beta\gamma$, meaning that $A_\lambda + A_\nu A_\kappa$ represents any of the channels $A + BC$, $B + CA$, or $C + AB$. Let r'_λ and R'_λ be respectively the vector from A_ν to A_κ and from the center of mass of $A_\nu A_\kappa$ to A_λ. For example, for $\lambda\nu\kappa \equiv \alpha\beta\gamma$ r'_α is the vector from B to C and R'_α the vector from the center of mass of BC to A. The potential energy function can be considered to depend on any of the sets of variables $(r'_\alpha, R'_\alpha, \gamma_\alpha)$, $(r'_\beta, R'_\beta, \gamma_\beta)$, or $(r'_\gamma, R'_\gamma, \gamma_\gamma)$ where γ_λ $(\lambda = \alpha, \beta, \gamma)$ is the angle in the $(0, \pi)$ range between r'_λ and R'_λ.

It has recently been shown that a very convenient set of coordinates exists for mapping V (28). These are the symmetrized hyperspherical coordinates $r = (r_\lambda^2 + R_\lambda^2)^{1/2}$, $\theta_\lambda = 2 \cos^{-1}(R_\lambda /r)$ and γ_λ, where $r_\lambda = (\mu_{\nu\kappa}/\mu_{\lambda, \nu\kappa})^{1/4} r'_\lambda$, and $R_\lambda = (\mu_{\lambda, \nu\kappa}/\mu_{\nu\kappa})^{1/4} R'_\lambda$ are scaled (29-31) distances. The masses $\mu_{\nu\kappa}$ and $\mu_{\lambda, \nu\kappa}$ are respectively the reduced mass of $A_{\nu\kappa}$ and of the $A_\lambda + A_\nu A_\kappa$ pair, the angle θ_λ is in the $(0, \pi)$ range and r is independent of λ (30, 31). The factor 2 in the expression for θ_λ is crucial and makes the present hyperspherical coordinates differ from those suggested previously (30-32). We now consider r, θ_λ, γ_λ to be the spherical polar coordinates of a point P_λ in a three-dimensional internal arrangement

configuration space $OX_\lambda Y_\lambda Z_\lambda$. In order for this space to be completely scanned by those variables, we extend the range of γ_λ from $(0,\pi)$ to $(-\pi,\pi)$ by setting, for $\gamma_\lambda < 0$, $V(r,\theta_\lambda,-\gamma_\lambda) = V(r,\theta_\lambda,\gamma_\lambda)$. The mapping of V in this space (but not in the space in which the factor of 2 just mentioned is omitted) has two very important properties: (a) an $r,\theta_\lambda,\gamma_\lambda \to r,\theta_\nu,\gamma_\nu$ transformation rotates equipotential surfaces around OY_λ without distorting them and (b) the symmetry properties of the map are the same as those of the reaction. For example, the mapping for the H_3 system has the symmetry properties of an equilateral triangle and that for the FH_2 those of an isosceles triangle. These symmetry properties do not depend on the choice of the arrangement channel λ and permit us to visualize the characteristics of V for all configurations in one single representation, the α one for example.
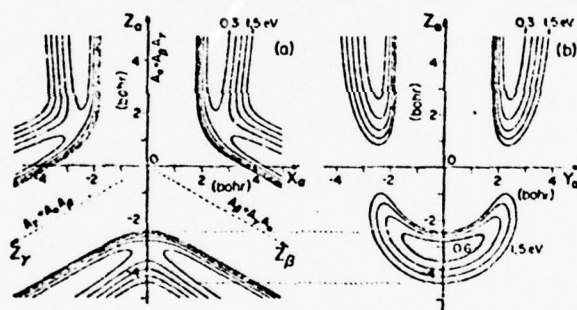
Figure 1. Equipotential surfaces for H_3. The cartesian coordinates $X_\alpha, Y_\alpha, Z_\alpha$ are $r \sin\theta_\alpha \cos\gamma_\alpha$, $r \sin\theta_\alpha \sin\gamma_\alpha$, and $r \cos\theta_\alpha$, respectively, with r, θ_α defined in the text. The curves are intersections of $V(r,\theta_\alpha,\gamma_\alpha) = E$ surfaces with the planes $OX_\alpha Z_\alpha$ (Fig. 1a) and $OY_\alpha Z_\alpha$ (Fig. 1b). The origin of measurement of E is the minimum of the H_2 diatomic potential energy curve with the third atom removed to infinity. The values of E range from 0.3 eV to 1.5 eV in steps of 0.3 eV, as indicated on top of figure. All points on Fig. 1a and those on the OZ_α axis of Fig. 1b correspond to linear configurations. Those off the OZ_α axis on Fig. 1b correspond to perpendicular (i.e., isosceles triangle) configurations in which A_α is the odd atom.

In Fig. 1 we depict intersections of the equipotential surfaces with the $OX_\alpha Z_\alpha$ and $OY_\alpha Z_\alpha$ planes for the Porter and Karplus (30) potential function describing the H_3 system. The OY_α axis, perpendicular to the plane of Fig. 1a, is a three-fold axis of symmetry of V, due to the equivalence of the three H atoms and of the corresponding arrangement channels. The angle between any of the three axes OZ_α, OZ_β, and OZ_γ is 120°, rather than the usual 60° (34), due to the factor 2 in the definition of θ_λ. It is this factor which permits the three arrangement channels $A_\lambda + A_{\nu\kappa}$ ($\lambda = \alpha, \beta, \gamma$) to be represented equivalently. The lower part of Fig. 1b, in the negative Z_α half-plane, depicts in detail the "transition state" region of configuration space halfway between the $A_\gamma + A_\alpha A_\beta$ reactant and $A_\gamma A_\alpha + A_\beta$ product configurations. At any energy E, all classically allowed pathways leading from such reagents to such products must pass through the region enclosed by the corresponding equipotential. The hatched area on the bottom of Fig. 1b s enclosed by the E = 0.6 eV equipotential. The smaller E, the more confined is this region and the less can the intermediate reactive configurations deviate from collinearity. The characteristics of these "passages" between reagents and products influence significantly the dynamical properties of V. For example, if they are narrow, the reaction is collinearly dominated.

With the help of these symmetrized coordinates we can describe graphically the nature of the atom-diatom reactive scattering problem and of the methods used for solving it. Collisions of A_α with $A_\beta A_\gamma$ correspond to configurations in Fig. 1 initially with X_α and Y_α of the order of the $A_\beta A_\gamma$ equilibrium internuclear distance and Z_α large with respect to that distance. After the collision has occurred, the system rebounds into that region for nonreactive collisions, or moves to regions in the vicinity of the Z_β axis with large Z_β for reactive collisions resulting in $A_\beta + A_\gamma A_\alpha$ products or the Z_γ axis for $A_\gamma + A_\alpha A_\beta$ products. One must obtain scattering wavefunctions which behave accordingly in these different regions of configuration space. Using a time-dependent language, a wave packet approaching the origin O from the large Z_α direction is partially reflected and partially bifurcates into the OZ_β and OZ_γ directions due to reaction of A_α with

either Λ_β or Λ_γ respectively. This bifurcation problem, which encompasses the competition between these two reactions, is conceptually a rather difficult one and has been at least partially responsible for the slowness of the progress in the reaction dynamics of noncollinear systems.

III. COUPLED-EQUATION METHOD FOR 3-D REACTIVE SCATTERING

An approach we recently used in obtaining accurate solutions for the 3-D H + H$_2$ system (21) is summarized below. The Schrödinger equation for the triatomic system can be considered to be a function of the six variables $R_\lambda, r_\lambda, \gamma_\lambda, \theta_\lambda, \phi_\lambda, \psi_\lambda$. The first three have been defined in the previous section, θ_λ and ϕ_λ are the polar angles of R_λ in a laboratory-fixed system of reference, and ψ_λ is the "tumbling" angle between the instantaneous triatom plane and a fixed reference plane containing R_λ. We consider wavefunctions Ψ_{JM}^λ of these six variables which are simultaneously solutions of the Schrödinger equation and eigenfunctions of the square of the total angular momentum and its component along a laboratory-fixed Oz axis. We expand Ψ_{JM}^λ in terms of the Wigner rotation functions (35) $D_{M\Omega_\lambda}^J (\phi_\lambda, \theta_\lambda, 0)$ and the spherical harmonics $Y_{j_\lambda \Omega_\lambda} (\gamma_\lambda, \psi_\lambda)$. The resulting coefficients are functions of the two distances R_λ, r_λ and satisfy a set of coupled differential equations. A final expansion is made in terms of local vibrational wavefunctions, which are cuts of the rotationally averaged potential along directions transverse to an appropriately chosen propagation coordinate, which varies from region to region of the R_λ, r_λ configuration space. The resulting coupled ordinary differential equations are integrated into the interaction region from each of the three λ arrangement channel regions, using the Gordon method (36). These solutions are then smoothly matched along three half-planes of the configuration space of Fig. 1, all limited by the $0Y_\alpha$ axis of that figure and containing the negative half of the $0Z_\alpha$, $0Z_\beta$, and $0Z_\gamma$ axes, respectively. This matching procedure contains built into it the solution to the bifurcation problem mentioned in the previous section. It involves using basis functions for the matching which are localized on those half-planes but

when taken together are complete ov r the entire γ_α, γ_β, or γ_γ angular range. Finally, linear combinations of the smoothly matched solutions are used to obta' the reactance and scattering matrices for each value of J from which the differential and integral cross sections for re tive and nonreactive processes are calculated.

IV. RESULTS AND DISCUSSION OF 3-D CALCULATIONS

The coupled-equation method described above was applied to the H + H_2 system (21) using the Porter and Karplus potential energy surface (33) depicted in Fig. 1. In addition to distinguishable atom reactive and nonreactive cross sections, calculations were made of antisymmetrized cross sections corresponding to scattering amplitudes which are the appropriate linear combinations of the direct and exchange contributions necessary to make the scattering wavefunction antisymmetric with respect to the exchange of any two hydrogen atoms. In the 0.40 to 0.70 eV range of total energy E, up to 30 rotational, 4 vibrational, and 100 total basis functions were found necessary for convergence of the results for each J to within 5%. Convergence of the reactive differential cross sections required all values of J from 0 to about 12.

The J = 0 reactive probabilities have a dependence on energy very similar to that of the corresponding coplanar and collinear ones, over several orders of magnitude of the probabilities. These curves are shifted towards higher energies by about 0.05 eV in going from 1-D to 2-D and from 2-D to 3-D probabilities, probably due to the zero point energy stored in the bending mode of the transition state. This behavior suggests how 3-D probabilities can be obtained approximately from 1-D ones for this collinearly dominated reaction (21).

In Fig. 2 we present the distinguishable atom integral reaction cross sections Q_{0j}^R from the ground vibrational state and initial rotational state j (j = 0, 1, 2) of the reagent, as a function of E, for several calculations: the converged (21) (SK), the hindred rotor (22) (EW) and the quasi-classical (37) (KPS) ones. The latter agree quite well with the SK cross sections for j = 0 and 1, at energies above the effective quasi-classical threshold. This agreement was to be expected, since it had already been observed for the collinear reaction (38). As a consequence one obtains near equality in the SK quantum and KPS quasi-classical thermal rate constants at 600°K. At lower temperatures the effects of tunneling become very important, and the SK rate constants are larger than the KPS
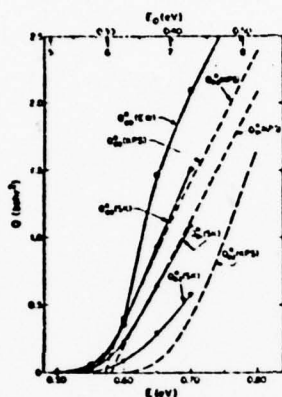
Figure 2. Comparison of integral reactive cross sections from several H + H_2 calculations.
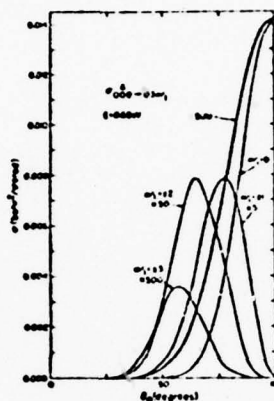
Figure 3. Antisymmetrized differential cross sections and their sum in the helicity representation.

ones by factors of 3.2 and 18 at 300°K and 200°K respectively (21). The EW Q_{00}^R results have been recently decreased, bringing them to within approximately 15% of the SK ones (39). The one vibrational basis function integro-differential equation results of Wolken and Karplus for the antisymmetrized Q_{00-01}^A cross section have an effective threshold about 0.05 eV lower than the SK ones and rise much more rapidly with energy. This is probably due to the severely truncated nature of their vibrational-rotational basis set. The Choi and Tang distorted wave calculation (40), done at a higher energy, seems to fall on an extrapolation of the SK Q_{00-01}^A curve.

In Fig. 3 we plot the antisymmetrized $\sigma_{000-03m_j'}^A$ para-ortho differential cross sections as well as their sum, as a function of the scattering angle θ_R, for $|m_j'| = 0$ through 3. We see that the $m_j' = 0$ cross section is backward peaked and that it dominates over the others. This highly nonstatistical behavior of the polarization of the products is the manifesta-

tion of an $m_j = 0$ to $m'_j = 0$ quasi-selection rule for low j which has been proposed (21) for collinearly dominated reactions, due to maximum atom-diatom collinear overlap for those values of m_j and m'_j. In contrast, the degeneracy-averaged (i.e., summed over m'_j and averaged over m_j) product rotational distributions can be fitted to temperature-like distributions to a high degree of accuracy, indicating a statistical-type behavior. The corresponding rotational temperature parameters increase nearly linearly with energy from 228°K at E = 0.45 eV to 446°K at 0.70 eV.

The degeneracy-averaged antisymmetrized para – para differential cross sections σ^A_{00-01}, to which only exchange collisions contribute, are smooth backward peaked functions of the scattering angle. In contrast, the σ^A_{00-02} para – ortho cross sections are peaked sideways, due to the large contribution from direct processes, and display an oscillatory behavior as a function of the scattering angle, due to the interference between the direct and exchange scattering amplitudes, both of which contribute to this cross section. The backward-peaked shape of the σ^A_{00-01} differential cross section for the coplanar reaction at an energy E is essentially identical to the one for the 3-D reaction at an energy E + 0.05 eV over the entire energy range considered. The energy shift again suggests an effect of the bending energy of the transition state. The agreement in these angular distributions is not unexpected, since the same potential is sampled in both cases and the primary difference between the two calculations is the additional centrifugal coupling resulting from the tumbling of the three-atom plane. The existence of the strong product polarization effect mentioned above indicates that such coupling is weak compared with the potential coupling responsible for the linear geometry requirement. This suggests a close similarity between the 2-D and 3-D dynamics and conversion of 2-D results to 3-D ones promises to be an accurate approximate technique. Another promising approximation is the neglect of the weak coupling between different tumbling angular momenta, which reduces the numerical effort in a 3-D reactive scattering calculation to that of a 2-D one.

V. RESONANCES IN REACTIVE SCATTERING

For the H + H$_2$ system, reactive scattering resonances have been observed in collinear (10), coplanar, and 3-D collisions (41). In Fig. 4 we depict the reaction probabilities for

these three kinds of collisions. As can be seen, a dip appears
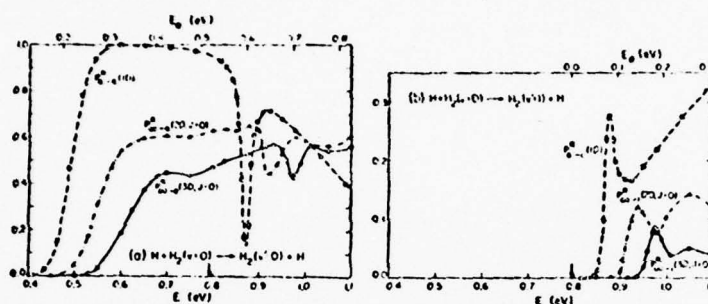
Figure 4. Collinear (1-D), coplanar (2-D), and three-dimensional reaction (3-D) reaction probabilities as a function of total energy E and translational energy E_0. The noncollinear results have been summed over all product rotational states within the product vibrational manifold indicated.

in the vibrationally elastic reaction probability curves (left side panel) and a peak in the vibrationally inelastic ones (right side panel). For the 1-D case, a time-delay analysis indicates (16) that this structure is due to interference between a direct mechanism and a compound state one associated with an internal excitation dynamical (Feshbach) resonance. A vibrationally adiabatic analysis (42) of the collinear resonance indicates that in the region of the potential energy function saddle point and at the resonance energy the system has a 90% probability of being found in the first vibrationally excited state of the transverse (symmetric stretch) internally excited mode of motion. This indicates that trapping of the energy in this mode is responsible for the resonance. Estimates of the energy dependence of the integral cross section for the reaction from the ground vibrational-rotational state of the reagent to the first vibrationally excited state of the product, for 3-D collisions, is similar to that of the corresponding J = 0 reaction probability, depicted in the right panel of Fig. 4, and has a peak value of 0.05 bohr^2.   Therefore the partial wave and product rotational state sums involved in the calculation of this cross section do not wash out the resonances observed in collinear collisions, at least for the present collinearly dominated reaction. This is the first time that a resonance has been predicted for a 3-D reaction whose potential energy function does not have an attractive well. Since Feshbach resonances have also been detected in collinear calculations for the collinearly dominated F + H_2 (D_2, HD) (17) and Cl + H_2

(last of Ref. 18 papers) reactions (using potential energy surfaces devoid of wells), it is quite possible that such resonances may exist for these reactions in the real world as well. The shift in the position of the 1-D, 2-D, and 3-D resonances of Fig. 4 is approximately equal, once more, to the zero-point energy of the bending mode of the transition state. This suggests how the position of 1-D resonances could be used to predict where the 3-D ones should lie for collinearly dominated reactions. In going from the SSMK potential energy surface used in the study of Ref. 16 to the Porter and Karplus one used in Ref. 41, the width of the 1-D $H + H_2$ resonance being considered decreases from about 0.05 eV to 0.022 eV, indicating a great sensitivity of the properties of the resonance to the shape of the potential energy surface. As a result, resonances may prove a sensitive probe for the experimental characterization of potential energy surfaces and for the development and testing of approximate reaction-dynamic theories.

VI. ELECTRONICALLY NONADIABATIC CHEMICAL REACTIONS

Partly as a result of the possibility of developing chemical lasers involving electronic state population inversions, interest in the theoretical understanding of electronically chemiluminescent reactions has recently increased. A particular example is the $Ba + N_2O \rightarrow BaO + N_2$ reaction, in which the BaO may be formed in an electronically excited state (43-45). No accurate theoretical calculations for such electronically nonadiabatic reactive processes have yet been attempted. A classical trajectory-hopping scheme has been developed and applied to the $H^+ + D_2 \rightarrow HD^+ + D$ reaction (46). In addition, a semi-classical description of such reactions based on the Feynman propagator has been formulated and applied to this same reaction (47). As a means of assessing the validity of these approximate schemes, an accurate two-potential energy surface collinear reactive scattering calculation method was developed and applied to a simplified model of the $Ba + N_2O \rightarrow BaO + N_2$ reaction (48). These calculations indicate that a substantial fraction of the BaO product can indeed, for this model, be produced in an electronically excited state. These accurate collinear calculations can now be used to test the validity of approximate ones for the same potential energy surfaces.

VII. SUMMARY

Substantial progress has occurred over the last few years in the development of accurate 3-D quantum mechanical methods for calculating cross sections of electronically adiabatic reactions. Out of such calculations have emerged predictions of a product polarization quasi-selection rule and of the existence of Feshbach resonances for collinearly dominated reactions. Such predictive ability is indicative of the vigor of the field. Progress has also been made in the calculation of electronically nonadiabatic reaction cross sections.

ACKNOWLEDGMENTS

REFERENCES

1.   E. M. Mortensen and K. S. Pitzer, J. Chem. Soc. (London) Spec. Publ. 16, 57 (1962).

2.   E. M. Mortensen, J. Chem. Phys. 48, 4029 (1968).

3.   D. J. Diestler and V. McKoy, J. Chem. Phys. 48, 2951 (1968).

4.   D. G. Truhlar and A. Kuppermann, J. Chem. Phys. 52, 3841 (1970); ibid. 56, 2232 (1972).

5.   D. G. Truhlar, A. Kuppermann, and J. T. Adams, J. Chem. Phys. 59, 395 (1973).

6.   E. A. McCullough, Jr., and R. E. Wyatt, J. Chem. Phys. 51, 1253 (1969); ibid. 54, 3578, 3592 (1971).

7.   E. M. Mortensen and L. D. Gucwa, J. Chem. Phys. 51, 5695 (1969).

8.   W. M. Sams and D. J. Kouri, J. Chem. Phys. 51, 4809 (1969).

272   ARON KUPPERMANN

9.   J. T. Adams, R. L. Smith, and E. F. Hayes, J. Chem. Phys. 61, 2193 (1974).

10. C. C. Rankin and J. C. Light, J. Chem. Phys. 51, 1701 (1969); G. Miller and J. C. Light, ibid. 54, 1635, 1643 (1971).

11. A. Kuppermann, Proceedings of the Conference on Potential Energy Surfaces in Chemistry, University of California, Santa Cruz, W. A. Lester, Ed. (August 1970), p. 121; Electronic and Atomic Collisions, Proceedings of VII ICPEAC (North-Holland, Amsterdam, 1971), p. 3.

12. D. J. Diestler, J. Chem. Phys. 54, 4547 (1971).

13. B. R. Johnson, Chem. Phys. Letts. 13, 172 (1972).

14. S. F. Wu and R. D. Levine, Mol. Phys. 22, 881 (1971).

15. E. J. Shipsey, J. Chem. Phys. 58, 232 (1973).

16. G. C. Schatz and A. Kuppermann, J. Chem. Phys. 59, 964 (1973).

17. G. C. Schatz, J. M. Bowman, and A. Kuppermann, J. Chem. Phys. 58, 4023 (1973); 63, 674, 685 (1975).

18. M. Baer and D. J. Kouri, Chem. Phys. Letts. 24, 37 (1974); M. Baer, J. Chem. Phys. 60, 1057 (1974); A. Persky and M. Baer, ibid. 60, 133 (1974); M. Baer, V. Halavee and A. Persky, ibid. 61, 5122 (1974); M. Baer, Mol. Phys. 27, 1429 (1974).

19. R. P. Saxon and J. C. Light, J. Chem. Phys. 56, 3874, 3885 (1972); A. Altenberger-Siczek and J. C. Light, J. Chem. Phys. 61, 4373 (1974).

20. A. Kuppermann, G. C. Schatz, and M. Baer, J. Chem. Phys. 61, 4362 (1974); J. Chem. Phys., forthcoming; G. C. Schatz and A. Kuppermann, J. Chem. Phys., forthcoming

21. A. Kuppermann and G. C. Schatz, J. Chem. Phys. 62, 2502 (1975); G. C. Schatz and A. Kuppermann, J. Chem. Phys., forthcoming.

22. A. B. Elkowitz and R. E. Wyatt, J. Chem. Phys. 62, 2504, 3683 (1975).

23. M. Baer and D. J. Kouri, Chem. Phys. Letts. 11, 238 (1971); J. Chem. Phys. 56, 1758 (1972); 57, 3991 (1972).

24. G. Wolken and M. Karplus, J. Chem. Phys. 60, 351 (1974).

25. W. H. Miller, J. Chem. Phys. 50, 407 (1969).

26. S. A. Harms and R. E. Wyatt, J. C. Phys. 62, 3162, 3173 (1975).

27. D. A. Micha, J. Chem. Phys. 57, 2184 (1972); D. A. Micha and J.-M. Yuan, forthcoming.

28. A. Kuppermann, Chem. Phys. Letts. 32, 374 (1975).

29. D. Jepsen and J.O. Hirschfelder, Proc. Natl. Acad. Sci. U.S. 45, 249 (1959).

30. L. M. Delves, Nucl. Phys. 9, 391 (1959); 20, 275 (1960).

31. F. T. Smith, J. Math. Phys. 3, 735 (1962).

32. P. M. Morse and H. Feshbach, Methods of Theoretical Physics (McGraw-Hill, New York, 1953), p. 1729.

33. R. N. Porter and M. Karplus, J. Chem. Phys. 40, 1105 (1964).

34. S. Glasstone, K. J. Laidler, and H. Eyring, The Theory of Rate Processes (McGraw-Hill, New York, 1941), Chap. 3.

35. A. S. Davydov, Quantum Mechanics (NEO Press, Ann Arbor, 1966), Chap. VI.

36. R. G. Gordon, J. Chem. Phys. 51, 14 (1969).

37. M. Karplus, R. N. Porter, and R. D. Sharma, J. Chem. Phys. 43, 3259 (1965).

38. J. M. Bowman and A. Kuppermann, Chem. Phys. Letts. 12, 1 (1971).

39. R. E. Wyatt, personal communication.

40. B. H. Choi and K. T. Tang, J. Chem. Phys. 61, 2462, 5147 (1974).

274 ARON KUPPERMANN

41. G. C. Schatz and A. Kuppermann, Phys. Rev. Letts. in press.

42. J. M. Bowman, A. Kuppermann, J. T. Adams, and D. G. Truhlar, Chem. Phys. Letts. 20, 229 (1973).

43. Ch. Ottinger and R. N. Zare, Chem. Phys. Letts. 5, 243 (1970); C. D. Jonah, R. N. Zare, and Ch. Ottinger, J. Chem. Phys. 60, 4369 (1974); A. Schultz and R. N. Zare, ibid. 60, 5120 (1974).

44. R. W. Field, C. R. Jones, and H. P. Broida, J. Chem. Phys. 60, 4377 (1974).

45. C. J. Hsu, W. D. Krugh, and H. B. Palmer, J. Chem. Phys. 60, 5118 (1974).

46. R. K. Preston and J. C. Tully, J. Chem. Phys. 54, 4297 (1971); J. C. Tully and R. K. Preston, ibid. 55, 562 (1971); J. R. Krenos, R. K. Preston, R. Wolfgang, and J. C. Tully, ibid. 60, 1634 (1974).

47. W. H. Miller and T. F. George, J. Chem. Phys. 56, 5637 (1972); T. F. George and T.-W. Lin, J. Chem. Phys. 60, 2340 (1974); T.-W. Lin, T. F. George, and K. Morokuma, Chem. Phys. Letts. 22, 547 (1973); J. Chem. Phys. 60, 4311 (1974).

48. J. W. Bowman, Theoretical Studies of Electronically Adiabatic and Nonadiabatic Chemical Reaction Dynamics, Ph. D. Thesis, California Institute of Technology, Pasadena, CA, 1975; J. W. Bowman and A. Kuppermann, forthcoming.

AN EXACT QUANTUM STUDY OF VIBRATIONAL DEACTIVATION
BY REACTIVE AND NONREACTIVE COLLISIONS
IN THE COLLINEAR ISOTOPIC H + FH SYSTEMS*

George C. Schatz and Aron Kuppermann
Arthur Amos Noyes Laboratory of Chemical Physics†
California Institute of Technology
Pasadena, California 91125

The success of the HF chemical laser depends to a large extent on the relative rates of: (1) the $F + H_2$ pumping reaction which produces vibrationally excited HF(v), and (2) the deactivation of HF(v) by collisions with H_2, F, H, buffer gas, and HF itself. Although the deactivation of HF by H_2,[1] F,[2] and HF[3] has been both experimentally and theoretically well-characterized with generally good agreement between experiment and theory, the situation is far less satisfactory for H + FH and its isotopic counterparts, D + FD, H + FD, and D + FH. The three experimental determinations of the H + FH (v = 1) deactivation rate [2,4,5] give rate constants at 300°K of $< (7 \pm 4) \times 10^{11}$,[4] $\leq 9 \times 10^9$,[2] and $(1.4 + 0.4) \times 10^{11}$ cm^3/mole-sec,[5] thus disagreeing with one another by amounts well outside their respective error limits. Agreement with the results of a theoretical (classical trajectory) calculation of this rate constant is no better with a predicted value of 2.2×10^{12} cm^3/mole-sec at 300°K. Similar experimental and theoretical comparisons of the rate constants for the deactivation of D + FD (v = 1), D + FH (v = 1), and H + FD (v = 1) are also poor.[5]

The approximation of classical dynamics has been analyzed in detail for the $F + H_2$[7] and $F + D_2$[8] reactions, and its most important consequences for reactive collisions were found to be an inadequate description of resonances, neglect of tunneling, and dynamical threshold effects. In considering vibrational deactivation processes, we must also examine the validity of the quasi-classical prediction[6] that multi-quantum jump transitions are extremely important in deactivating collisions (both nonreactive and reactive) for H + FH. If true, it could be important, for it would mean that H atoms can be very efficient deactivators of HF. In addition, much of the theoretical analysis is predicated on the assumption of the dominance of single quantum jump transitions.[9]

In this paper we examine the dynamics of reactive and nonreactive H + FH and its isotopic counterparts using accurate quantum mechanical methods. In all calculations we restrict our considerations to collinear collisions, an approximation which renders the quantum mechanical problem tractable while still retaining many of the important dynamical features of the three-dimensional (3-D) world.[10,11]

The potential energy surface used was Muckerman's Surface Five[12,13] whose LEPS parameters are given by Schatz et al.[7] This surface has a barrier height of 1.23 kcal/mole for the collinear F + FH → HF + H exchange reaction. Recently, Bender et al.[14] have shown that this barrier is seriously in error, the correct value being estimated at about 40 kcal/mole. The present results may nevertheless be qualitatively correct if the quantum number of the initial vibrational states considered are increased so as to place these states above the correct barrier. Those features of the results depending on the atomic masses (such as the skew angle between the coordinate axis in terms of which the kinetic energy operator is diagonal) should be correct. Calculations of the effect of barrier height on these results are in progress and will be presented elsewhere.

The method used in the calculation was a coupled-channel propagation technique[15] previously applied to H + H$_2$,[16] F + H$_2$[7,17] and F + D$_2$.[8] Convergence, conservation of flux, and microscopic reversibility indicate that the results are accurate to 1% or better.

The transition probability from vibrational state v of the reagent to state v' of the product is denoted by the symbol $P^R_{vv'}$ for reactive collisions and by $P^V_{vv'}$ for nonreactive ones. Figures 1 through 3 display the reactive and nonreactive probabilities $P_{3v'}$ (v' = 0,1,2) as a function of the relative kinetic energy E$_3$ of the reagents. In all these figures, reactive probabilities exceed the nonreactive ones in the low kinetic energy region important for thermal rate constants. Furthermore, the multiquantum jump probabilities are of the same magnitude as the single quantum jump ones. Similar results are obtained for v = 2.

Figures 4 and 5 depict several of the $k^R_{vv'}$ and $K^V_{vv'}$ collinear rate constants for H + FH. They indicate that the reactive rate constants are in general significantly larger than the nonreactive ones. Figure 6 shows the total deactivation rate constants k^R_v and k^V_v. At 300°K, the ratio k^R_v/k^V_v is 8.3 for v = 1, 8.5 for v = 2, and 3.5 for v = 3. Figure 7 contains Arrhenius plots of k^R_{10} and k^V_{10} for H + FH, D + FD, H + FD, and D + FH, which indicate that substitution of H by D does not qualitatively affect these results, except for the H + FD system.

In summary, for all transition probabilities and rate constants the reactive mechanism dominates over the nonreactive one in producing vibrational deactivation. This result is apparently of general validity over a wide range of impact parameters since the same conclusions (even the same ratios of rate constants) were obtained by Wilkins[6] in his 3-D

133

classical calculations. Secondly, multiquantum jump transition proba-
bilities are comparable in magnitude to single quantum jump transition
probabilities. This is clearly a consequence of the use of a reactive
potential energy surface since the analogous H + HF results (for a
surface which is nonreactive at the energies considered) indicate that
single quantum jump transition probabilities are orders of magnitude
larger than all others. Finally, we should reiterate that the potential
energy surface used is of questionable validity because of its low
barrier height, but that similar results may still be obtained for
higher barriers for those reagent vibrational states which lie above
the barrier.
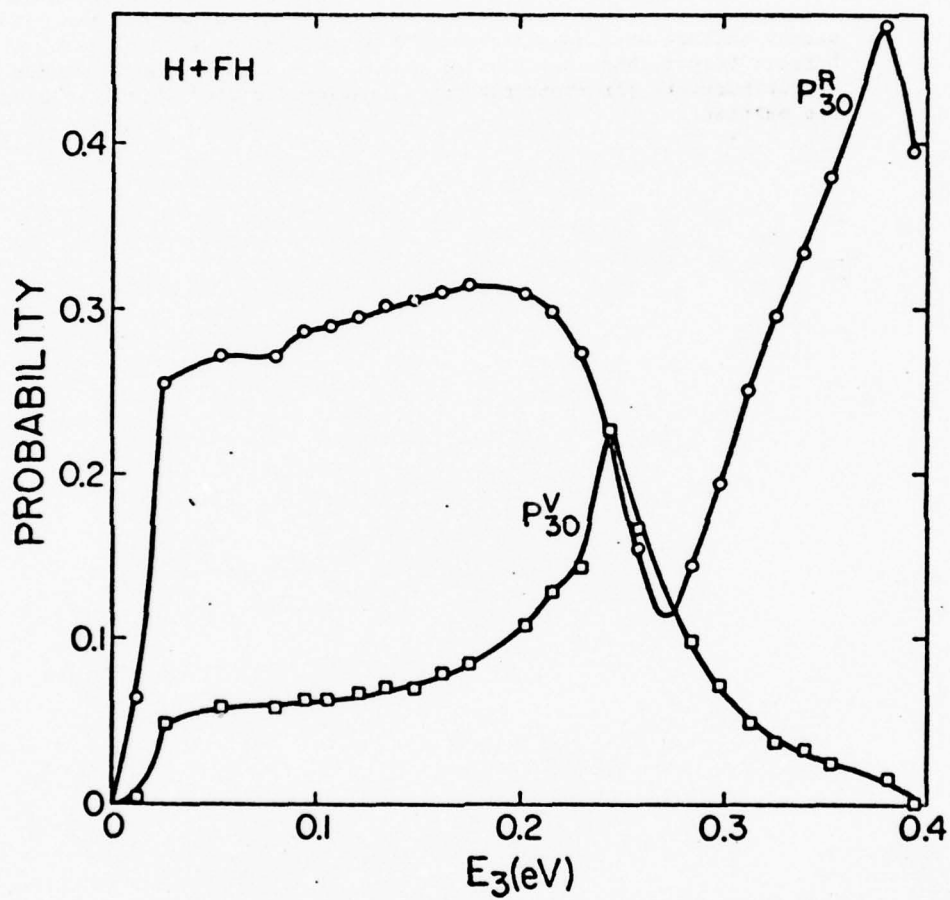
Figure 1. Transition probabilities P_{30}^R and P_{30}^V for H + FH as a function of the reagent relative translational energy E_3.
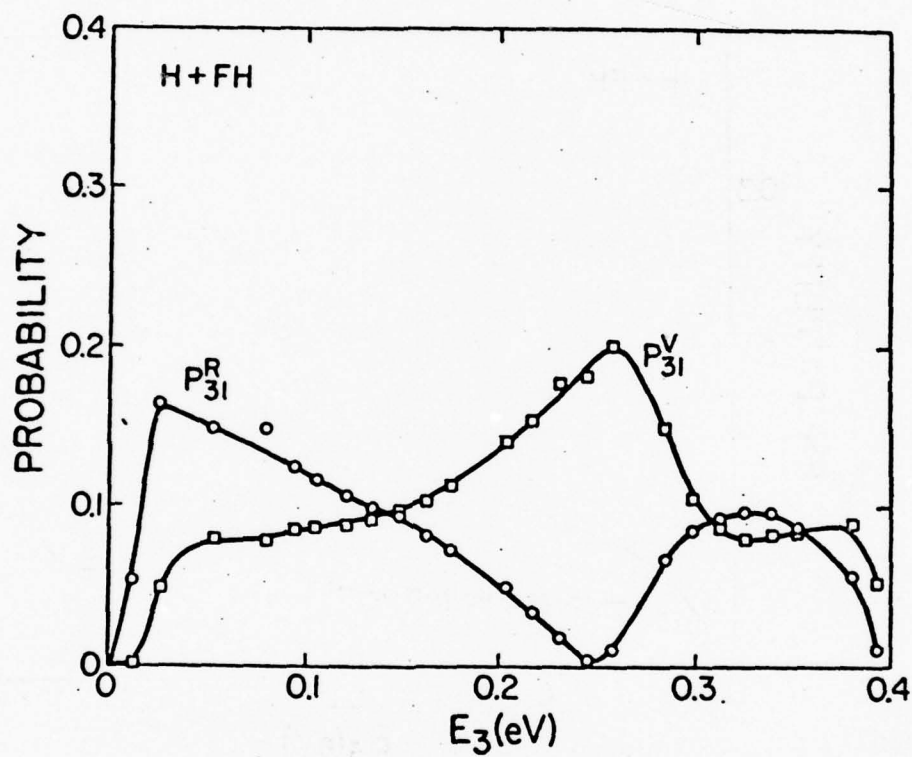
Figure 2. Transition probabilities P_{31}^R and P_{31}^V for H + FH analogous to Figure 1.

136
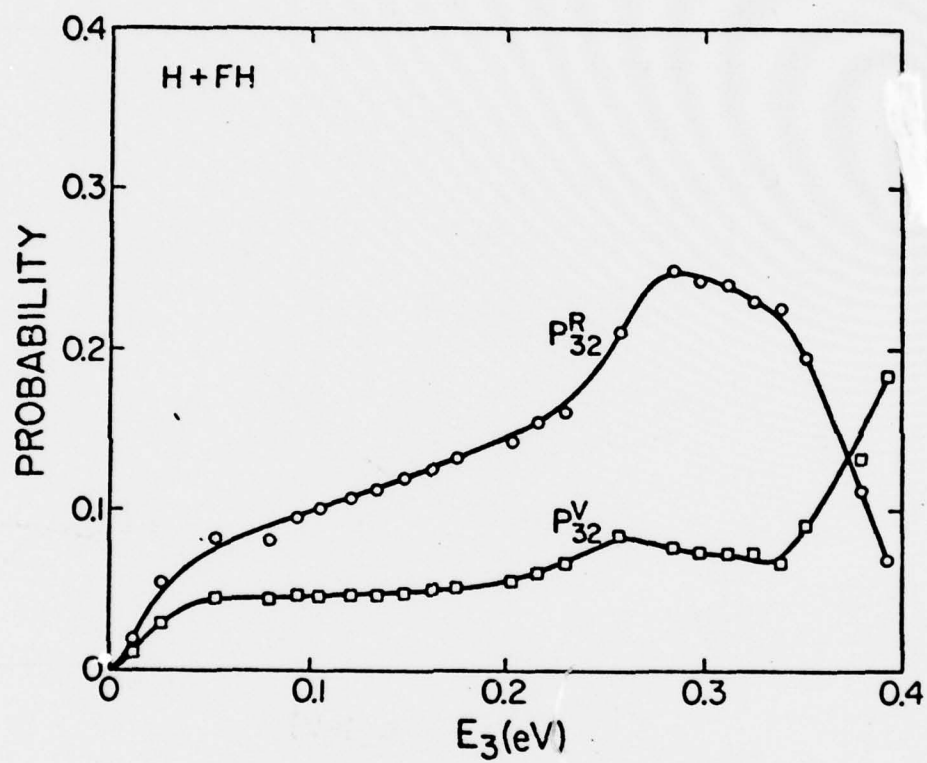
Figure 3. Transition probabilities P_{32}^R and P_{32}^V for H + FH analogous to Figure 1.
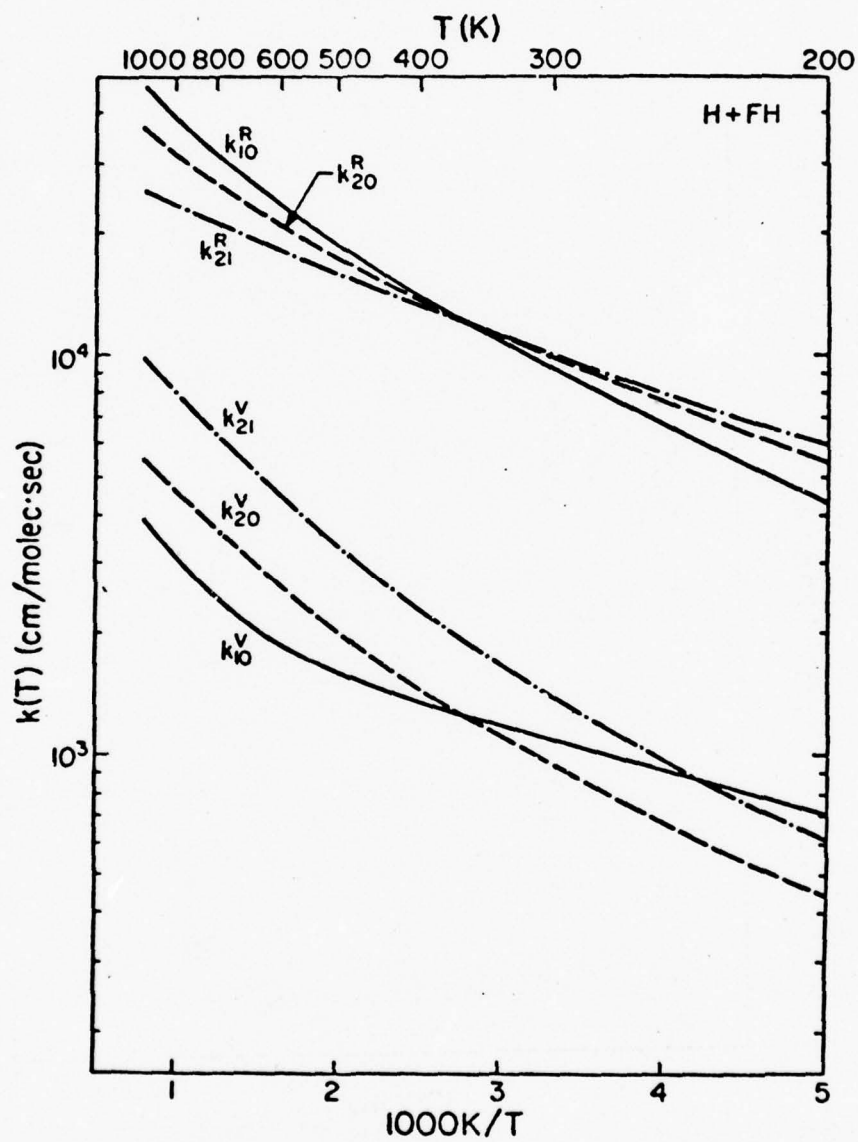
Figure 4. Arrhenius plot of the rate constants k_{10}^R, k_{10}^V, k_{20}^R, k_{20}^V, k_{21}^R, and k_{21}^V.

138
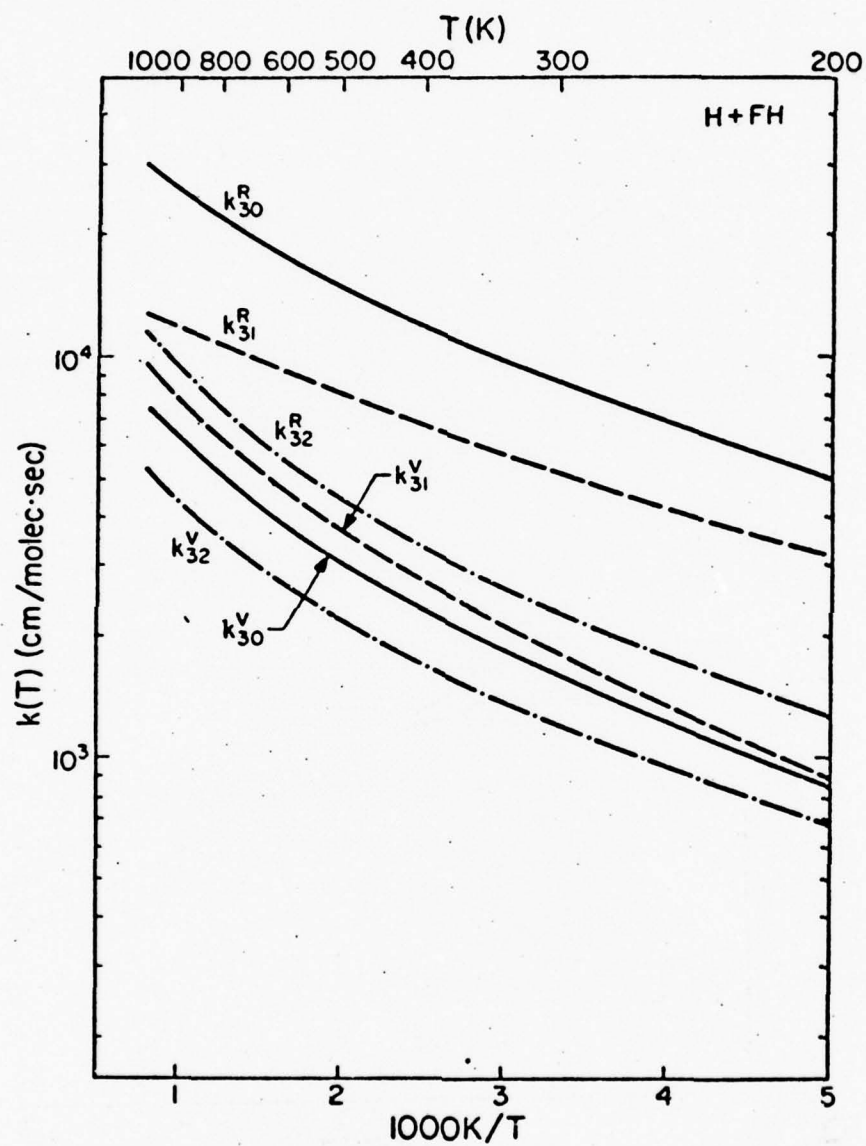
Figure 5. Arrhenius plot of the rate constants k_{30}^R, k_{30}^V, k_{31}^R, k_{31}^V, k_{32}^V, k_{32}^R, and k_{32}^V.

139
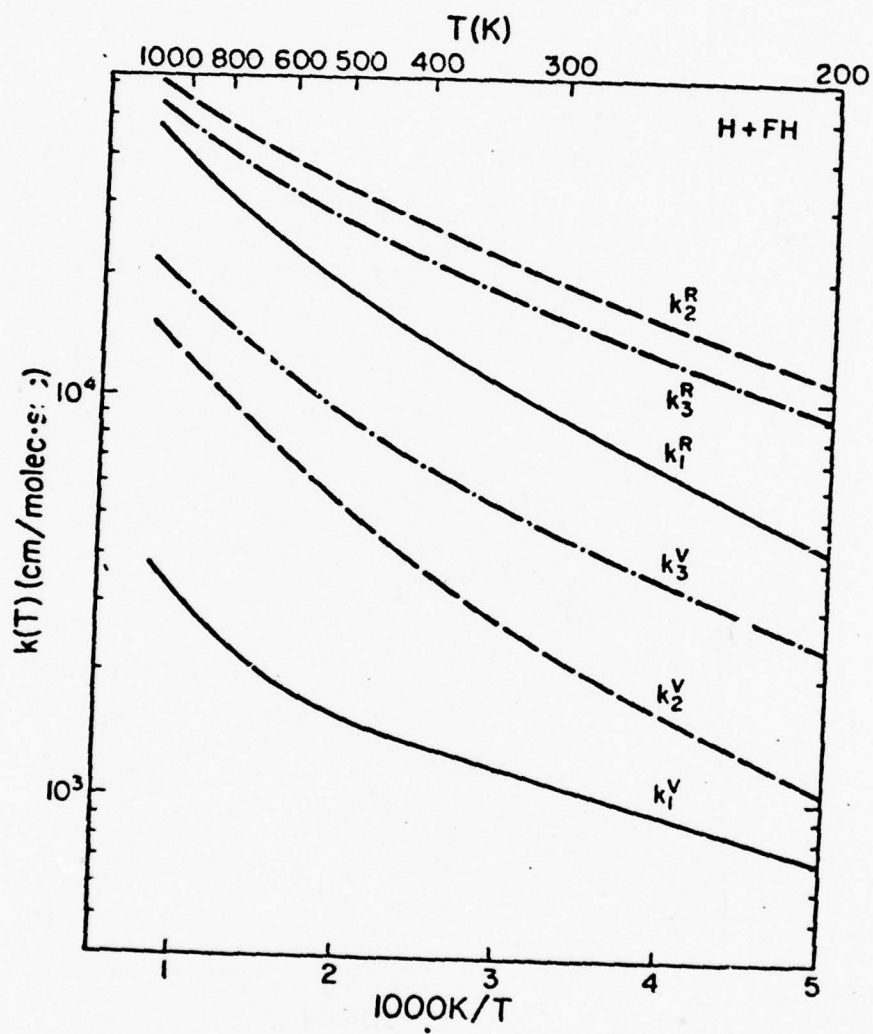
Figure 6. Arrhenius plot of the total inelastic rate constants k_1^R, k_1^V, k_2^R, k_2^V, k_3^R, and k_3^V.
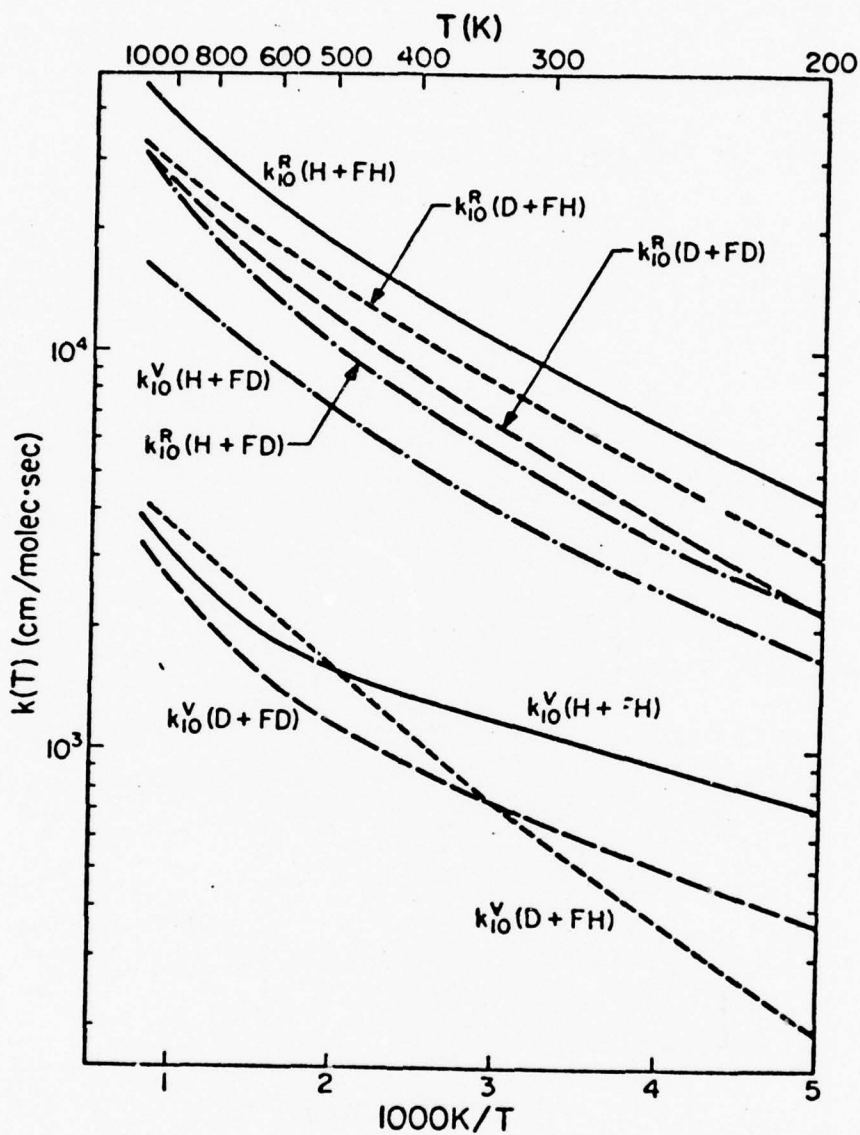
Figure 7. Arrhenius plot of the rate constants k_{10}^R and k_{10}^V for H + FH, k_{10}^R and k_{10}^V for D + FD, k_{10}^R and k_{10}^V for D + FH, and k_{10}^R and k_{10}^V for H + FD.

141

REFERENCES

1. J. F. Hancock and W. H. Green, J. Chem. Phys. 56, 2474 (1972); 57, 4515 (1972).

2. G. P. Quigley and G. J. Wolga, Chem. Phys. Letters 27, 276 (1974); R. L. Wilkins, J. Chem. Phys. 59, 698 (1973).

3. J. F. Bott, J. Chem. Phys. 61, 3414 (1974).

4. M. A. Kwok and R. L. Wilkins, J. Chem. Phys. 60, 2199 (1974).

5. R. F. Heidner and J. F. Bott, J. Chem. Phys. 63, 1810 (1975).

6. R. L. Wilkins, J. Chem. Phys. 58, 3038 (1973).

7. G. C. Schatz, J. M. Bowman, and A. Kuppermann, J. Chem. Phys. 63, 674 (1975).

8. G. C. Schatz, J. M. Bowman, and A. Kuppermann, J. Chem. Phys. 63, 685 (1975).

9. D. L. Thompson, J. Chem. Phys. 56, 3570 (1972).

10. G. C. Schatz and A. Kuppermann, Phys. Rev. Letters 35, 1266 (1975).

11. G. C. Schatz and A. Kuppermann, J. Chem. Phys., submitted.

12. J. T. Muckerman, J. Chem. Phys. 54, 1155 (1971); 56, 2997 (1972).

13. J. T. Muckerman, private communication.

14. C. F. Bender, B. J. Garrison, and H. F. Schaefer, J. Chem. Phys. 62, 1188 (1975).

15. A. Kuppermann, Proceedings of the Conference on Potential Energy Surfaces in Chemistry, W. A. Lester, Ed. (held at the University of California, Santa Cruz, August 10-13, 1970) (IBM Research Laboratory, San Jose, California, 1971), pp. 121-134; A. Kuppermann, Abstracts of Papers of the VIIth International Conference on the Physics of Electronic and Atomic Collisions, Amsterdam, The Netherlands, 26-30 July 1971, Edited by L. M. Branscomb et al. (North-Holland Publishing Co., Amsterdam, 1971), pp. 1-5.

16. G. C. Schatz and A. Kuppermann, J. Chem. Phys. 59, 964 (1973).

17. G. C. Schatz, J. M. Bowman, and A. Kuppermann, J. Chem. Phys. 58, 4023 (1973).

Dynamical Resonances in Collinear, Coplanar, and Three-Dimensional Quantum Mechanical Reactive Scattering*

George C. Schatz† and Aron Kuppermann
Arthur Amos Noyes Laboratory of Chemical Physics, California Institute of Technology, Pasadena, California 91125
(Received 27 May 1975)

We present results of one-, two-, and three-dimensional calculations for the H + H₂ exchange reaction which provide the first evidence for dynamical internal excitation (Feshbach) resonances in chemical reactions using noncollinear calculations. The change of the resonance energy and width with collision dimensionality and with total angular momentum is analyzed and indicates the existence of observable effects on certain reactive cross sections.

Internal excitation resonances have been observed in a large number of diverse collision phenomena including π-p scattering,[1] electron-atom and electron-molecule scattering,[2] and (theoretically) rotationally inelastic atom-molecule scattering,[3] but they have yet to be detected in atom-diatom reactive scattering experiments. Their existence has previously been established theoretically only in collinear models of these simple chemical reactions.[4-8] The results of those collinear calculations indicate that these resonances are responsible for oscillations in the reaction probabilities near the resonance energies through their interference[8] with the direct mechanisms. However, because of partial-wave averaging, it was not known whether such resonances would exist in the three-dimensional (3-D) world. We present here the results of accurate quantum mechanical calculations for 1-D, 2-D, and 3-D collisions for the historically important H + H₂ exchange reaction which provide the first evidence for dynamical resonances in chemical reactions for noncollinear systems. An understanding of the relation between the characteristics of such resonances and the nature of the potential surfaces which give rise to

them may prove a sensitive probe in the experimental characterization of these surfaces and in the development and testing of approximate reaction-dynamic theories.

The methods used for solving the Schrödinger equation for the collinear, coplanar, and three-dimensional H + H₂ collisions are the same as those we developed and used previously.[8-11] In order to obtain accurate results in the 2-D and 3-D calculations at the relatively high energies at which the resonances were found, quite large vibration-rotation basis sets were required, involving five or six vibrations and rotational quantum numbers $j = 0$–6 to $j = 0$–9 for each vibration for a total of sixty coplanar channels (for all values of total angular momentum quantum number J), and 40 to 90 ($J = 0, 1$) 3-D channels. For most of these noncollinear calculations, tests of conservation of flux, microscopic reversibility, and invariance with respect to number and choice of expansion functions indicated convergence of 5 to 10% although a few poorer results (20%) were included. The collinear results, for which ten vibrational basis functions were used, are accurate to 0.5% or better. The Porter-Karplus[12] potential energy surface was used for all calcula-

tions.

The resulting 1-D,[13] 2-D, and 3-D reaction probabilities P^R, defined in the figure caption, are plotted as a function of the total energy E in Fig. 1. It can be seen that all vibrationally elastic probabilities in Fig. 1(a) show a similar behavior, rising from an effective threshold energy E_{thres} (the value of E for which $P^R = 0.01$) to a relatively flat plateau, and dipping later to a
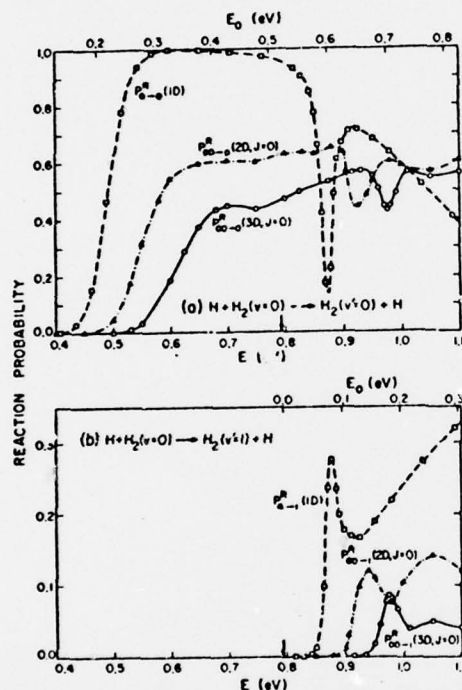
FIG. 1. Collinear (1-D), coplanar (2-D), and three-dimensional (3-D) reaction probabilities for the H + H$_2$ exchange reaction as a function of the total energy E and relative translational energy E_0. $P_{0 \to 0}^R$ and $P_{0 \to 1}^R$ are the collinear reaction probabilities from $v = 0$ of the reagent H$_2$ to $v' = 0$ and $v' = 1$, respectively, of the product H$_2$. $P_{\infty \to 0}^R$ and $P_{\infty \to 1}^R$ are the 2-D or 3-D (as specified) reaction probabilities for the total angular momentum $J = 0$ partial wave from $v = 0$, $j = 0$ of the reagent H$_2$ to $v' = 0$ and $v' = 1$, respectively, of the product H$_2$ summed over all product rotational states within a given vibrational manifold. (a) The vibrationally elastic reation probabilities, (b) the vibrationally inelastic ones. The points actually computed are indicated by geometrical symbols. Arrow in abscissa indicates the energy at which the $v = 1$ state of H$_2$ becomes accessible.

minimum at an energy E_r. The values of E_{thres} are 0.420, 0.470, and 0.525 eV and of E_r are 0.873, 0.922, and 0.975 eV for the 1-D, 2-D, and 3-D systems, respectively. The vibrationally inelastic P^R of Fig. 1(b) are also analogous to one another and display maxima at the same energies E_r for which the vibrationally elastic ones show minima. In a previous study,[8] we used a delay-time analysis (for a slightly different H + H$_2$ potential energy surface[4]) to show that the minima and maxima in the 1-D $P_{0 \to 0}^R$ curves are the result of resonances. Since there are no attractive wells in the H + H$_2$ potential surface, it is inferred that these are internal excitation (Feschbach) resonances. This inference is confirmed for the 1-D case by a vibrationally adiabatic analysis[14] in which the scattering wave function from the $v = 0$ reagent state is expanded in terms of the bound-state eigenfunctions of cuts of the potential surface transverse to the reaction coordinate. In the region of the saddle point this analysis indicates that at the resonance energy the system has a 90% probability of being found in the $v = 1$ state of this transverse (symmetric stretch) internally excited mode of motion (i.e., that the energy is "trapped" in this mode). The physical situation in the 2-D and 3-D systems is analogous to the 1-D one, and since the reaction probabilities in Fig. 1 for all these systems show similar dips and peaks, we conclude that all three correspond to a Feshbach resonance centered at the values of E_r given above, and with approximate widths of 0.022, 0.045, and 0.035 eV for the 1-D, 2-D, and 3-D cases, respectively. The $P_{\infty \to 1}^R(3\text{-D}, J = 0)$ reaction probability is dominated by this resonance at energies within 0.1 eV of the effective threshold, in spite of the sum over all product rotational states.

The change in resonance energy with dimensionality is almost identical to the corresponding change in the effective threshold energies and is in the range 0.050 to 0.055 eV for both the 1-D to 2-D and 2-D to 3-D shifts. These shifts agree with previous estimates[15] of the additional zero-point "bending" energy which must be put into the triatomic motions of the coplanar and 3-D transition states. This indicates that these resonances are influenced by the potential energy surface in the strong interaction region. Both coplanar and 3-D calculations indicate that the resonance has a significant effect only on the $J = 0$–7 partial waves (which appears to coincide with the range of J for which $P_{\infty \to 1}^R$ is significant), whereas nonnegligible reaction probabilities $P_{\infty \to 0}^R$ are

1207

found for the wider J range 0–17. *No significant change of either resonance energy or width with the quantum number J was detected for the 2-D system.*[16] This very important result is probably due to the dominant character of potential (rather than angular momentum) coupling in the region of strong interaction, and suggests that the partial-wave sum present in the expressions for the reaction cross sections will not eliminate the effect of the individual partial-wave resonances. From the width of the 3-D resonance we estimate a lifetime of 3.8×10^{-14} sec (corresponding approximately to 2–3 transition-state symmetric stretch vibrations), about $\frac{2}{3}$ of the 1-D lifetime. A crude estimate of the effect of the resonance on the integral cross section $\sigma_{00 \to 1}{}^R$ for the reaction between distinguishable atoms in three dimensions can readily be obtained by a simple interpolation procedure. The shape of the coplanar $P_{00 \to 1}{}^R(J)$ curve both on and off resonance as a function of J has a very simple monotonically decreasing form which is quite similar in appearance to the shape of $P_{00 \to 0}{}^R(J)$ at lower collision energies. Incomplete 3-D calculations for the 3-D $P_{00 \to 1}{}^R(J)$ curve indicate that an analogous comparison with the lower energy $P_{00 \to 0}{}^R$ curves is valid. We have therefore used these 3-D $P_{00 \to 0}{}^R(J)$ curves along with the accurately known $J = 0, 1$ values of $P_{00 \to 1}{}^R(J)$ and its $J = 7$ cutoff to interpolate the remaining $P_{00 \to 1}{}^R(J)$ needed for a cross-section calculation. The reactive cross section obtained in this manner shows an energy dependence similar to that of $P_{00 \to 1}{}^R(J = 0)$ of Fig. 1(b), with a peak value of 0.014 Å^2 at the resonance energy.[17,18] To estimate the effect of the resonance on the angular dependence of the differential reactive cross sections ($\sigma_{00 \to 0}{}^R$ and $\sigma_{00 \to 1}{}^R$), we note that below the resonance energy, this dependence shows no oscillations and is backward peaked.[11] At the resonance energy, one should expect oscillations to develop as a result of the interference between direct and resonance mechanisms.[19,20]

We conclude, in summary, that dynamical resonances do indeed exist in noncollinear $H + H_2$ and can cause nonnegligible effects on observable reaction cross sections. Such resonances are bound to exist in other reactions also, as they have already been detected in collinear calculations for $F + H_2$ (D_2, HD)[21] and $Cl + H_2$,[22] whose potential energy surfaces also do not have attractive wells. An understanding of the circumstances that give rise to Feshbach resonances can play an important role in the improvement of our

knowledge of reactive collision dynamics. Since classical trajectory methods do not include the interference effects associated with the resonances, nor do most semiclassical[21,23] and approximate quantum methods,[24] a theoretical 3-D treatment of resonances for most other chemical reactions will require the development of better approximate techniques, and the results presented here should be valuable in this endeavor. In addition, accurate quantum mechanical results (be they 1-D, 2-D, or 3-D) can serve as a useful predictive guide in the experimental search for dynamical resonances, and it is hoped that the present paper will stimulate such a search.

We thank Ambassador College for generous use of their computational facilities.

[1]R. Cool, O. Piccioni, and D. Clark, Phys. Rev. 103, 1082 (1956); R. K. Adair, Phys. Rev. 113, 338 (1959); R. G. Moorhouse, Annu. Rev Nucl. Sci. 19, 301 (1969).

[2]G. J. Schultz, Phys. Rev. Lett. 10, 104 (1963); P. G. Burke, Adv. At. Mol. Phys. 4, 173 (1968), and references therein.

[3]D. A. Micha, Phys. Rev. 162, 88 (1967); R. D. Levine, B. R. Johnson, J. T. Muckerman, and R. B. Bernstein, J. Chem. Phys. 49, 56 (1968).

[4]D. G. Truhlar and A. Kuppermann, J. Chem. Phys. 52, 3841 (1970), and 56, 2232 (1972).

[5]R. D. Levine and S. F. Wu, Chem. Phys. Lett. 11, 557 (1971); S. F. Wu and R. D. Levine, Mol. Phys. 22, 881 (1971).

[6a]D. J. Diestler, J. Chem. Phys. 54, 4547 (1971).

[6b]D. J. Diestler, D. G. Truhlar, and A. Kuppermann, Chem. Phys. Lett. 13, 1 (1972).

[7]B. R. Johnson, Chem. Phys. Lett. 13, 172 (1972).

[8]G. C. Schatz and A. Kuppermann, J. Chem. Phys. 59, 964 (1973).

[9]A. Kuppermann, in *Potential Energy Surfaces in Chemistry*, edited by W. Lester (University of California at Santa Cruz, Santa Cruz, Calif., 1970), pp. 121–129, and in *Proceedings of the Seventh International Conference on the Physics of Electronic and Atomic Collisions, Amsterdam, 26–30 July 1971, Abstracts of Papers*, edited by L. M. Branscomb et al. (North-Holland, Amsterdam, 1971), p. 3.

[10]A. Kuppermann, G. C. Schatz, and M. Baer, J. Chem. Phys. 61, 4362 (1974).

[11]A. Kuppermann and G. C. Schatz, J. Chem. Phys. 62, 2502 (1975).

[12]R. N. Porter and M. Karplus, J. Chem. Phys. $\underline{40}$, 1105 (1964).

[13]The present results are essentially identical to those of Ref. 6a.

[14]J. M. Bowman, A. Kuppermann, J. T. Adams, and D. G. Truhlar, Chem. Phys. Lett. $\underline{20}$, 229 (1973).

[15]A. B. Elkowitz and R. E. Wyatt, J. Chem. Phys. $\underline{62}$, 3683 (1975).

[16]Accurate 3-D calculations for $J > 0$ in the neighborhood of the resonance are very difficult to perform because of the large number of basis functions required in the close-coupling expansion. We do however have some preliminary 3-D $J > 0$ results which are in agreement with the italicized statement about the 2-D system.

[17]Since the distinguishable-atom nonreactive probability $P_{00\to1}{}^N(J)$ is very similar in both energy and J dependence to $P_{00\to1}{}^R(J)$, we expect that the nonreactive integral cross section $\sigma_{00\to1}{}^N$ should also have a peak at the resonance energy. This implies that the effect of atom indistinguishability should not appreciably alter the conclusions of this analysis.

[18]The smallness of this cross section may lead to experimental detection difficulties, and other reactive systems may be more favorable candidates for experimental investigation. The point we are making is nevertheless of significant conceptual importance, namely that resonances can exist and play an important role in chemically reactive collisions for which the corresponding potential energy surface does not have an attractive well.

[19]The individual partial-wave contributions to the differential cross sections are highly oscillatory in nature, and fairly slight calculational inaccuracies in the elements of the scattering matrix element for one partial wave are usually enough to upset the delicate balance between partial waves which leads to nonoscillatory differential cross sections, thereby resulting in strong spurious oscillations. It is reasonable to expect that the presence of resonances in some of the partial waves which contribute significantly to the cross sections should have a similar effect, as is experimentally observed for inelastic electron scattering. (See H. Ehrhardt, in *Physics of the One and Two Electron Atoms*, edited by F. Bopp and H. Kleinpoppen (North-Holland, Amsterdam, 1969), p. 598.

[20]This argument, developed for the distinguishable-atom cross sections, retains its validity for indistinguishable-atom para → ortho channels.

[21]G. C. Schatz, J. M. Bowman, and A. Kuppermann, J. Chem. Phys. $\underline{63}$, 674, 685 (1975).

[22]M. Baer, Mol. Phys. $\underline{27}$, 1429 (1974).

[23]J. M. Bowman and A. Kuppermann, J. Chem. Phys. $\underline{59}$, 6524 (1973); for a counter-example, see J. R. Stine and R. A. Marcus, Chem. Phys. Lett. $\underline{29}$, 575 (1974).

[24]For example, the distorted-wave method [K. T. Tang and M. Karplus, Phys. Rev. A $\underline{4}$, 1844 (1971)] and the one-vibrational-basis-function method [G. Wolken and M. Karplus, J. Chem. Phys. $\underline{60}$, 351 (1974)].

Quantum mechanical reactive scattering for planar atom plus diatom systems. I. Theory*

Aron Kuppermann, George C. Schatz,[†] and M. Baer[‡]

Arthur Amos Noyes Laboratory of Chemical Physics,[§] California Institute of Technology, Pasadena, California 91125
(Received 22 December 1975)

A method is presented for accurately solving the Schrödinger equation for the reactive collision of an atom with a diatomic molecule on a space-fixed plane. The procedure consists primarily of two steps. First, the Schrödinger equation in each of the three arrangement channel regions is transformed into a set of coupled differential equations and numerically integrated in each of these regions to generate primitive solutions. The rotational part of the vibration-rotation basis functions involved is not changed from its asymptotic form during this propagation, but the vibrational eigenfunctions as well as the integration variable are changed periodically so as to follow the vibrational motions in a nearly adiabatic manner. In the second step, the primitive solutions generated in each of the three arrangement channels are smoothly matched to each other on a set of appropriately chosen matching surfaces. The resulting solutions are then linearly combined to satisfy the proper asymptotic boundary conditions, and the scattering matrix, scattering amplitudes, and cross sections are determined. Application of this procedure to the special case of the $H + H_2$ reaction is discussed in detail including simplifications arising from the additional symmetries involved, and the inclusion of effects resulting from indistinguishability of identical particles.

I. INTRODUCTION

In recent years, much interest has developed in the *ab initio* calculation of bimolecular reaction cross sections on realistic potential energy surfaces by accurate quantum mechanical techniques. The motivation for such calculations has been to interpret the results of crossed molecular beam experiments, to understand the effect of the relative translational energy of the reactants and of their internal state on such cross sections and on the disposal of energy among the reaction products, to elucidate the role of direct and compound state dynamical mechanisms, to test the range and degree of validity of approximate reaction models (such as the adiabatic and statistical ones), to develop new physical models of known reliability, to examine the correctness of the dynamical assumptions of transition state theory, to establish the conditions of applicability of the quasiclassical trajectory calculations and of semiclassical improvements thereof, and last, but not least, to make detailed qualitative and quantitative predictions from first principles about reactions difficult to investigate experimentally.

Owing in part to the lack of appropriate numerical techniques and to limitations of the memory size and computational speed and cost of present-day large computers, most of these quantum calculations so far have been performed for collinear atom—diatom reactions.[1-13] In recent years, several attempts have been made to do calculations for nonlinear triatomic systems. Saxon and Light[14] and Altenberger-Siczek and Light[15] have investigated the coplanar $H + H_2$ exchange reaction by a coupled-channel technique which excluded closed vibrational channels. Wolken and Karplus[16] have made a study of this same reaction in three dimensions, also ignoring closed vibrational channels. Wyatt and co-workers[17] have developed techniques which include closed vibrations in calculations on one and two reaction path atom plus diatom reactions, and Elkowitz and Wyatt[17a] have applied these methods to the three-dimensional $H + H_2$ reaction. Baer and Kouri[18] have done fully

converged calculations in three dimensions on a model (one reaction path) triatomic system in which one of the atoms was assumed infinitely heavy and in which the simple potential used allowed a partially analytic treatment.

In an earlier communication,[19] we presented preliminary results of the first fully converged quantum mechanical calculation for a coplanar reaction on a realistic electronically adiabatic potential energy surface, that for $H + H_2$. These results indicated that the quantitative differences between calculations in which closed vibrations are included and those for which they are not can be quite serious. In this paper, we will present a detailed description of the method used to perform such calculations. We will formulate the method for a general atom plus diatomic molecule collision on a single reactive potential energy surface using $H + H_2$ as a specific example. A detailed description of the results of our extensive calculations on coplanar $H + H_2$ will be given elsewhere.[20]

The method is based on an earlier coupled-channel (i.e., close-coupling) propagation technique[9] which has been extensively applied to the collinear $H + H_2$ and $F + H_2$ reactions.[10] The spirit of the collinear method is to choose different variables and different pseudovibrational basis functions for expansion of the solutions of the Schrödinger equation in different local regions of the (collinear) configuration space so as to minimize the number of terms needed for accurate convergence of the expansions. This concept is retained for the vibrational motion in our application of the method to coplanar collisions. However, the variables and basis functions describing rotational motion are not changed (and hence retain their asymptotic meanings) during the integration into the interaction region from each of the three separated arrangement channel regions of internal configuration space. As a result, an additional step is required at the completion of the integration in which the primitive solutions in each of the three arrangement channel regions are smoothly matched to each other on a set of

three appropriately chosen surfaces which separ. ' these three regions.[21] The restriction that the th. ee atoms should be confined to a space-fixed plane was introduced for computational convenience to test out the effectiveness of the method without excessive expenditure of compution time. Extension to reactions in three-dimensional space is reasonably straightforward and has recently been implemented by Kuppermann and Schatz[22] for 3D H + H₂ in the first fully converged quantum mechanical treatment of a chemical reaction on a realistic potential energy surface.

In Sec. II of this paper we formulate the Schrödinger equation for the problem and describe the partial wave expansion used to obtain the partial differential equations, in internal configuration coordinates, which must be solved. The method used to integrate these equations in the different regions of configuration space is described in Sec. III, and in Sec. IV we describe how we smoothly match the solutions obtained from these integrations. The asymptotic analysis is developed in Sec. V, including the methods of calculating the reactance and scattering matrices, the scattering amplitudes, and the cross sections. Finally, in Sec. VI we describe the simplifications and changes involved in an application of the method to the H + H₂ exchange reaction due to the identicity of the three atoms, including a discussion of the technique of antisymmetrizing the scattering wavefunction (post antisymmetrization) in a way which is applicable to the three-dimensional case also.

II. FORMULATION OF THE PROBLEM

A. General considerations

We are interested in calculating cross sections for the exchange reaction A + BC → AB + C, AC + B in which the three atoms A, B, and C are confined to remain on a space-fixed plane. We assume that the Born–Oppenheimer separation approximation between the electron and nuclear motions is valid and that the resulting ground electronic state potential energy surface V is known. We further assume that all higher potential energy surfaces are sufficiently greater than the total energy E of the system everywhere in configuration space for us to be able to neglect their influence on the cross sections. This "single potential energy surface" model is applicable to a high degree of accuracy to many triatomic reactions. We also assume that E is sufficiently low for the existence and effect of break-up collisions of the type A + BC → A + B + C to be negligible. Finally, we assume that the interactions between the nuclear spin and nuclear orbital angular momenta are negligible.

Let r_A, r_B, and r_C be the position vectors of nuclei A, B, and C, respectively, with respect to their center of mass. We wish to obtain a solution to the time-independent Schrödinger equation for the motion of the nuclei which satisfies the following three conditions:

(a) In configuration space r_A, r_B, r_C it is everywhere single valued and continuous and has gradients which are everywhere continuous (except at points in that space for which two of the three atoms coincide).

(b) It is antisymmetric (symmetric) with respect to

exchange of the space and spin coordinates of any two identical nuclei of half odd-integral (integral) nuclear spin.

(c) It satisfies the asymptotic conditions describing the collision phenomenon under consideration, i.e., the collision of A and BC with a given relative kinetic energy and a given initial internal quantum state of BC, to produce receding products A + BC, AB + C, or AC + B in all possible internal states of the diatom compatible with the total energy of the system.

If we can find a sufficient number of independent solutions satisfying Condition (a), it is possible to obtain linear combinations of them which, in addition, satisfy Conditions (b) (by postantisymmetrization methods[23]) and (c) (by reactance or scattering matrix analysis techniques[24]).

B. The Schrödinger equation

Let $\bar{R}_\alpha$ be the position vector of A with respect to the center of mass of BC and $\bar{r}_\alpha$ the position vector of C with respect to B, as indicated in Fig. 1. As $\bar{R}_\alpha \to \infty$ with $\bar{r}_\alpha$ remaining finite, we denote the corresponding configuration as arrangement channel $\alpha \equiv (A, BC)$. Let $(\bar{r}_\alpha, \theta_{r_\alpha})$ and $(\bar{R}_\alpha, \theta_\alpha)$ be, respectively, the planar polar coordinates of $\bar{r}_\alpha$ and $\bar{R}_\alpha$ with respect to a fixed system of reference attached to the plane (all angles being measured from the Ox axis of Fig. 1). The reduced mass associated to the motion of C with respect to B is denoted by $\mu_{\beta\gamma}$ and that associated to atom A with respect to molecule BC is $\mu_{\alpha,\beta\gamma}$. We define analogous vectors $\bar{r}_\beta$, $\bar{R}_\beta$ and $\bar{r}_\gamma$, $\bar{R}_\gamma$ (Fig. 1) and associated coordinates and reduced masses so that as $\bar{R}_\beta \to \infty$ or $\bar{R}_\gamma \to \infty$ with $\bar{r}_\beta$ or $\bar{r}_\gamma$ finite, we obtain the arrangement channels $\beta \equiv (B, CA)$ and $\gamma \equiv (C, AB)$, respectively. Note that the directions of the vectors in Fig. 1 are defined in a cyclic manner in the indices $\alpha\beta\gamma$. Finally, let $\lambda\nu\kappa$ represent any one of the three possible cyclic permutations $\alpha\beta\gamma$, $\beta\gamma\alpha$, and $\gamma\alpha\beta$.
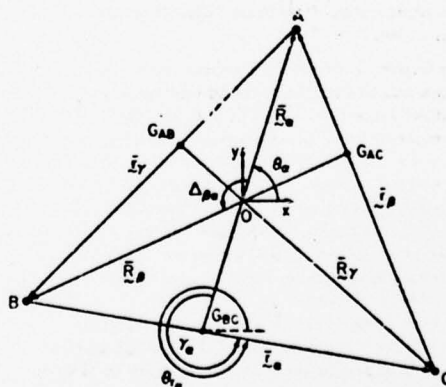
FIG. 1. Vectors used to specify the location of three atoms in the A, B, C collision system relative to the center of mass O. G_{BC}, G_{AC}, and G_{AB} denote the locations of the centers of mass of the diatomic, BC, AC, and AB, respectively. $\bar{R}_\alpha$, $\bar{r}_\alpha$, $\bar{R}_\beta$, $\bar{r}_\beta$, $\bar{R}_\gamma$, $\bar{r}_\gamma$ are defined in text.

In the system of coordinates characterized by index λ (= α, β or γ), the Schrödinger equation describing the internal motion of the three-particle system is

$$\left[-\frac{\hbar^2}{2\mu_{r\lambda}}\left(\frac{1}{\bar{r}_\lambda}\frac{\partial}{\partial\bar{r}_\lambda}\bar{r}_\lambda\frac{\partial}{\partial\bar{r}_\lambda}+\frac{1}{\bar{r}_\lambda^2}\frac{\partial^2}{\partial\theta_{r\lambda}^2}\right)\right.$$
$$-\frac{\hbar^2}{2\mu_{\lambda,r\lambda}}\left(\frac{1}{\bar{R}_\lambda}\frac{\partial}{\partial\bar{R}_\lambda}\bar{R}_\lambda\frac{\partial}{\partial\bar{R}_\lambda}+\frac{1}{\bar{R}_\lambda^2}\frac{\partial^2}{\partial\theta_\lambda^2}\right)$$
$$\left.+V^\lambda(\bar{r}_\lambda,\bar{R}_\lambda,\gamma_\lambda)-E\right]\Psi^\lambda(\bar{r}_\lambda,\bar{R}_\lambda,\theta_{r\lambda},\theta_\lambda)=0 , \quad (2.1)$$

where V^λ is the potential energy function of the system expressed in λ coordinates, and E is its total energy. γ_λ is by definition the counterclockwise angle from $\bar{R}_\lambda$ to $\bar{r}_\lambda$. It lies in the 0 to 2π range and is equal to $\theta_{r\lambda}-\theta_\lambda$ modulo 2π. In the absence of external fields, the potential function depends only on the internal variables $\bar{R}_\lambda$, $\bar{r}_\lambda$, γ_λ and satisfies the relation $V^\lambda(\bar{R}_\lambda,\bar{r}_\lambda,\gamma_\lambda)=V^\lambda(\bar{R}_\lambda,\bar{r}_\lambda,2\pi-\gamma_\lambda)$.

Let us now introduce a set of coordinates used previously by Delves,[25] Jepsen and Hirschfelder,[26] and Smith.[27] They have the advantage of leading to an equation containing a single effective mass μ which is independent of the arrangement channel λ; this simplifies many of the equations presented below. These coordinates are

$$r_\lambda=a_\lambda^{-1}\bar{r}_\lambda , \quad (2.2a)$$
$$R_\lambda=a_\lambda\bar{R}_\lambda , \quad (2.2b)$$

where a_λ is a dimensionless scaling constant defined by

$$a_\lambda=(\mu_{\lambda,r\lambda}/\mu_{r\lambda})^{1/4} . \quad (2.3)$$

Substitution into Eq. (2.1) leads to

$$\left[-\frac{\hbar^2}{2\mu}\left(\frac{1}{r_\lambda}\frac{\partial}{\partial r_\lambda}r_\lambda\frac{\partial}{\partial r_\lambda}+\frac{1}{r_\lambda^2}\frac{\partial^2}{\partial\theta_{r\lambda}^2}+\frac{1}{R_\lambda}\frac{\partial}{\partial R_\lambda}R_\lambda\frac{\partial}{\partial R_\lambda}+\frac{1}{R_\lambda^2}\frac{\partial^2}{\partial\theta_\lambda^2}\right)\right.$$
$$\left.+V^\lambda(r_\lambda,R_\lambda,\gamma_\lambda)-E\right]\Psi^\lambda(r_\lambda,R_\lambda,\theta_{r\lambda},\theta_\lambda)=0 , \quad (2.4)$$

where the circular polar angles of R_λ, r_λ are the same as those of $\bar{R}_\lambda$, $\bar{r}_\lambda$, and μ is the effective mass alluded to above and defined by

$$\mu=(\mu_{r\lambda}\mu_{\lambda,r\lambda})^{1/2}=(m_\alpha m_\beta m_\gamma/M)^{1/2} , \quad (2.5)$$

where

$$M=m_\alpha+m_\beta+m_\gamma$$

is the total mass of the system, and m_α, m_β, and m_γ are the masses of atoms A, B, and C, respectively. We now change from the angular variables $\theta_{r\lambda}$, θ_λ to γ_λ, θ_λ, obtaining the following expression from Eq. (2.4):

$$\left\{-\frac{\hbar^2}{2\mu}\left[\frac{1}{r_\lambda}\frac{\partial}{\partial r_\lambda}r_\lambda\frac{\partial}{\partial r_\lambda}+\frac{1}{r_\lambda^2}\frac{\partial^2}{\partial\gamma_\lambda^2}+\frac{1}{R_\lambda}\frac{\partial}{\partial R_\lambda}R_\lambda\frac{\partial}{\partial R_\lambda}\right.\right.$$
$$\left.+\frac{1}{R_\lambda^2}\left(\frac{\partial^2}{\partial\theta_\lambda^2}-2\frac{\partial^2}{\partial\theta_\lambda\partial\gamma_\lambda}+\frac{\partial^2}{\partial\gamma_\lambda^2}\right)\right]+V^\lambda(r_\lambda,R_\lambda,\gamma_\lambda)$$
$$\left.-E\right\}\Psi^\lambda(r_\lambda,R_\lambda,\gamma_\lambda,\theta_\lambda)=0 . \quad (2.6)$$

This is called the body-fixed Schrödinger equation, because γ_λ is the angle of r_λ with respect to the body-fixed

R_λ direction rather than the laboratory-fixed Ox axis. Similarly, R_λ, θ_λ, r_λ, γ_λ are called the body-fixed λ coordinates. The independence of V^λ on θ_λ in the above equation introduces very convenient simplifications, as is shown in the next section.

C. Partial wave expansion

The total angular momentum J of the triatomic system (with respect to its center of mass) is a constant of the motion which commutes with the Hamiltonian H. The solution of the Schrödinger equation we are seeking, satisfying Conditions (a), (b), and (c) of Sec. II.A, is not an eigenfunction of J.[28] It is, however, convenient to perform the coplanar analog of partial wave analysis by expanding Ψ^λ in terms of the simultaneous eigenfunctions Ψ_J^λ of H and J.

In the system of coordinates r_λ, R_λ, $\theta_{r\lambda}$, θ_λ the operator J is given by

$$J=\left[\frac{\hbar}{i}\left(\frac{\partial}{\partial\theta_\lambda}\right)_{\theta_{r\lambda}}+\frac{\hbar}{i}\left(\frac{\partial}{\partial\theta_{r\lambda}}\right)_{\theta_\lambda}\right]\hat{z} \quad \lambda=\alpha,\beta,\gamma , \quad (2.7)$$

where $\hat{z}$ is the unit vector perpendicular to the fixed plane of motion of the three particles. We recognize from Eq. (2.7) that J is the *algebraic* sum of the rotational angular momentum $j_\lambda=(\hbar/i)(\partial/\partial\theta_{r\lambda})_{\theta_\lambda}\hat{z}$ and the orbital angular momentum $l_\lambda=(\hbar/i)(\partial/\partial\theta_\lambda)_{\theta_{r\lambda}}\hat{z}$. Transforming J to the angular variables θ_λ, γ_λ, we get

$$J=\frac{\hbar}{i}\left(\frac{\partial}{\partial\theta_\lambda}\right)_{\gamma_\lambda}\hat{z} \quad \lambda=\alpha,\beta,\gamma , \quad (2.8)$$

which may be physically interpreted as indicating that if γ_λ is maintained constant, a variation of the angular coordinate θ_λ of R_λ produces a rotation of the entire triatomic system.

The orthonormal eigenfunctions of J are given by[30]

$$\varphi_J(\theta_\lambda)=(2\pi)^{-1/2}\exp(iJ\theta_\lambda) \quad J=0,\pm1,\pm2,\dots \quad (2.9)$$

The simultaneous eigenfunctions of H with energy E and of J with total angular momentum $J\hbar$ are of the form

$$\Psi_J^\lambda(r_\lambda,R_\lambda,\gamma_\lambda,\theta_\lambda)=\varphi_J(\theta_\lambda)\chi_J^\lambda(r_\lambda,R_\lambda,\gamma_\lambda) , \quad (2.10)$$

where

$$\left\{-\frac{\hbar^2}{2\mu}\left[\frac{1}{r_\lambda}\frac{\partial}{\partial r_\lambda}r_\lambda\frac{\partial}{\partial r_\lambda}+\frac{1}{r_\lambda^2}\frac{\partial^2}{\partial\gamma_\lambda^2}+\frac{1}{R_\lambda}\frac{\partial}{\partial R_\lambda}R_\lambda\frac{\partial}{\partial R_\lambda}\right.\right.$$
$$\left.+\frac{1}{R_\lambda^2}\left(-J^2-2iJ\frac{\partial}{\partial\gamma_\lambda}+\frac{\partial^2}{\partial\gamma_\lambda^2}\right)\right]+V^\lambda(r_\lambda,R_\lambda,\gamma_\lambda)$$
$$\left.-E\right\}\chi_J^\lambda(r_\lambda,R_\lambda,\gamma_\lambda)=0 . \quad (2.11)$$

Any solution Ψ^λ of the Schrödinger equation which is not necessarily an eigenfunction of J can be written as

$$\Psi^\lambda(r_\lambda,R_\lambda,\gamma_\lambda,\theta_\lambda)=\sum_{J=-\infty}^\infty C_J^\lambda\Psi_J^\lambda(r_\lambda,R_\lambda,\gamma_\lambda,\theta_\lambda) . \quad (2.12)$$

The constant coefficients C_J^λ appropriate for the problem being considered will be determined by the asymptotic conditions specified in Requirement (c) of Sec. II.A and will be discussed in Sec. V.B.

We now simplify Eq. (2.11) by defining a new function $\tilde{\chi}_J^\lambda$ by

$$\psi_J^\lambda(r_\lambda, R_\lambda, \gamma_\lambda) = (r_\lambda R_\lambda)^{1/2} \chi_J^\lambda(r_\lambda, R_\lambda, \gamma_\lambda) . \tag{2.13}$$

Substituting this into Eq. (2.11), we obtain

$$\left\{-\frac{\hbar^2}{2\mu}\left[\frac{\partial^2}{\partial r_\lambda^2} + \frac{\partial^2}{\partial R_\lambda^2} + \frac{1}{r_\lambda^2}\frac{\partial^2}{\partial \gamma_\lambda^2} + \frac{1}{R_\lambda^2}\left(-J^2 - 2iJ\frac{\partial}{\partial \gamma_\lambda} + \frac{\partial^2}{\partial \gamma_\lambda^2}\right)\right]\right.$$
$$\left. + V^\lambda - E\right\}\psi_J^\lambda(r_\lambda, R_\lambda, \gamma_\lambda) = 0 . \tag{2.14}$$

This equation is solved numerically by the method described in Secs. III and IV.

III. INTEGRATION OF THE SCHRÖDINGER EQUATION

A. The partitioning of configuration space into arrangement channel regions

We now wish to expand $\psi_J^\lambda(r_\lambda, R_\lambda, \gamma_\lambda)$ in terms of sets of two-variable internal state basis functions in order to reduce the partial differential equation (2.14) to a system of coupled ordinary differential equations. Our choice for the internal state basis functions and the corresponding variables will be different in different regions of the three-dimensional internal configuration space $r_\lambda, R_\lambda, \gamma_\lambda$ and will be largely determined by the local shape of the potential energy function $V^\lambda(r_\lambda, R_\lambda, \gamma_\lambda)$. This is done in order to represent solutions of the full Schrödinger equation in an efficient manner in all regions of configuration space so as to reduce computation time as much as possible. A useful conceptualization of the nature of the problem can be gained by noting the appearance of the potential energy function $V^\lambda(r_\lambda, R_\lambda, \gamma_\lambda)$. This function is most conveniently displayed with the aid of a mapping procedure previously developed for this purpose.[30] In this mapping we consider a space $OX_\lambda Y_\lambda Z_\lambda$ in which a point P has spherical polar coordinates $\zeta, \omega_\lambda, \gamma_\lambda$ where the radial variable ζ is defined by

$$\zeta = (r_\lambda^2 + R_\lambda^2)^{1/2} \tag{3.1a}$$

and is independent of λ as shown in Eq. (A6) of Appendix A, and the polar angle ω_λ is defined by

$$\omega_\lambda = 2\tan^{-1}(r_\lambda/R_\lambda), \quad 0 \le \omega_\lambda \le \pi . \tag{3.1b}$$

The azimuthal angle γ_λ has been defined after Eq. (2.1). Using the example of the $H + H_2$ reaction, the resulting contour plot of the Porter–Karplus[31] potential for six different values of γ_λ is depicted in Fig. 2 This representation has the advantage of treating all three arrangement channels equivalently in that a change from coordinates λ to coordinates ν produces a clockwise rotation without distortion of Fig. 2 around the OY_λ axis by an angle of 120°.[30] We see from the figure that the accessible areas of configuration space are in the form of three tubelike regions whose mutual intersection defines the three-particle interaction region. For less symmetric potentials Fig. 2 would be less symmetric, but the considerations below have general validity.

Our approach for solving the Schrödinger equation consists of dividing the configuration space depicted in Fig. 2 into three subspaces called *arrangement channel regions* and labeled by the indices λ, ν, κ. Each of these three arrangement channel regions includes one

of the three tubes corresponding to a separated atom plus diatom, along with that part of the interaction region which retains the "general appearance" of that particular tube. For the $H + H_2$ system, a very natural separation of the three arrangement channel regions is obtained by the use of the three half-planes $\pi_{\nu\lambda}$, $\pi_{\kappa\nu}$, and $\pi_{\lambda\kappa}$ whose common edge is the OY_λ axis and which intersect the $OX_\lambda Z_\lambda$ plane in the symmetrical positions depicted in Fig. 2(a). A general definition of these three half-planes which is also applicable to reactions other than $H + H_2$ is

$$\pi_{\nu\lambda}: \quad r_\lambda = r_\nu \quad 0 \le \gamma_\lambda \le \pi/2 \text{ and } 3\pi/2 \le \gamma_\lambda < 2\pi , \tag{3.2a}$$

$$\pi_{\kappa\nu}: \quad r_\nu = r_\kappa \quad 0 \le \gamma_\nu \le \pi/2 \text{ and } 3\pi/2 \le \gamma_\nu < 2\pi , \tag{3.2b}$$

$$\pi_{\lambda\kappa}: \quad r_\kappa = r_\lambda \quad 0 \le \gamma_\kappa \le \pi/2 \text{ and } 3\pi/2 \le \gamma_\kappa < 2\pi . \tag{3.2c}$$

A proof that these equations do indeed define half-planes whose edge is the OY_λ axis, as graphically indicated in Fig. 2(a), is given in Appendix A along with the equations describing the λ to ν coordinate transformation. For some reactions, the half-planes defined above may be inadequate as they may not separate the three arrangement channel regions into physically intuitive ones as determined by the shape of the potential functions. In these cases, alternative surfaces may be chosen and treated by a straightforward extension of the theory presented in this paper. For the reactions $H + H_2$, $D + H_2$, $H + D_2$, etc., the half-planes of Eqs. (3.1) are quite satisfactory, so we shall proceed to formulate our theory using the arrangement channel regions into which they divide internal configuration space.

With the arrangement channel regions thus defined, we organize the work involved in solving Eq. (2.14) into two steps. First, within each of the three arrangement channel regions, we integrate the Schrödinger equation using rotational coordinates and basis functions appropriate to the asymptotic part of that arrangement channel but changing vibrational coordinates and basis functions in a way which transforms "smoothly" from one arrangement channel to another. Then, we match the resulting three sets of solutions to one another on the three half-planes $\pi_{\nu\lambda}$, $\pi_{\kappa\nu}$, $\pi_{\lambda\kappa}$ described above (and hereafter called the *matching surfaces*). Since the vibrational coordinates are designed to transform smoothly from one arrangement channel to the others, it is primarily the rotational parts of the wavefunctions which must be considered in the matching procedure. Our rotational expansion is similar to that of Saxon and Light,[14] but not to that of Wyatt and co-workers,[17] who allow both their vibrational and rotational coordinates to transform smoothly in going from one arrangement channel to the next.

In the remainder of this section, we will detail the method used for integrating the Schrödinger equation in each of the arrangement channel regions. The crucial smooth matching procedure is outlined in Sec. IV.

B. The rotationally coupled Schrödinger equations

We now consider the solution of Eq. (2.14) in each of the three arrangement channel regions $\lambda = \alpha, \beta, \gamma$.

The body-fixed rotational angular momentum operator
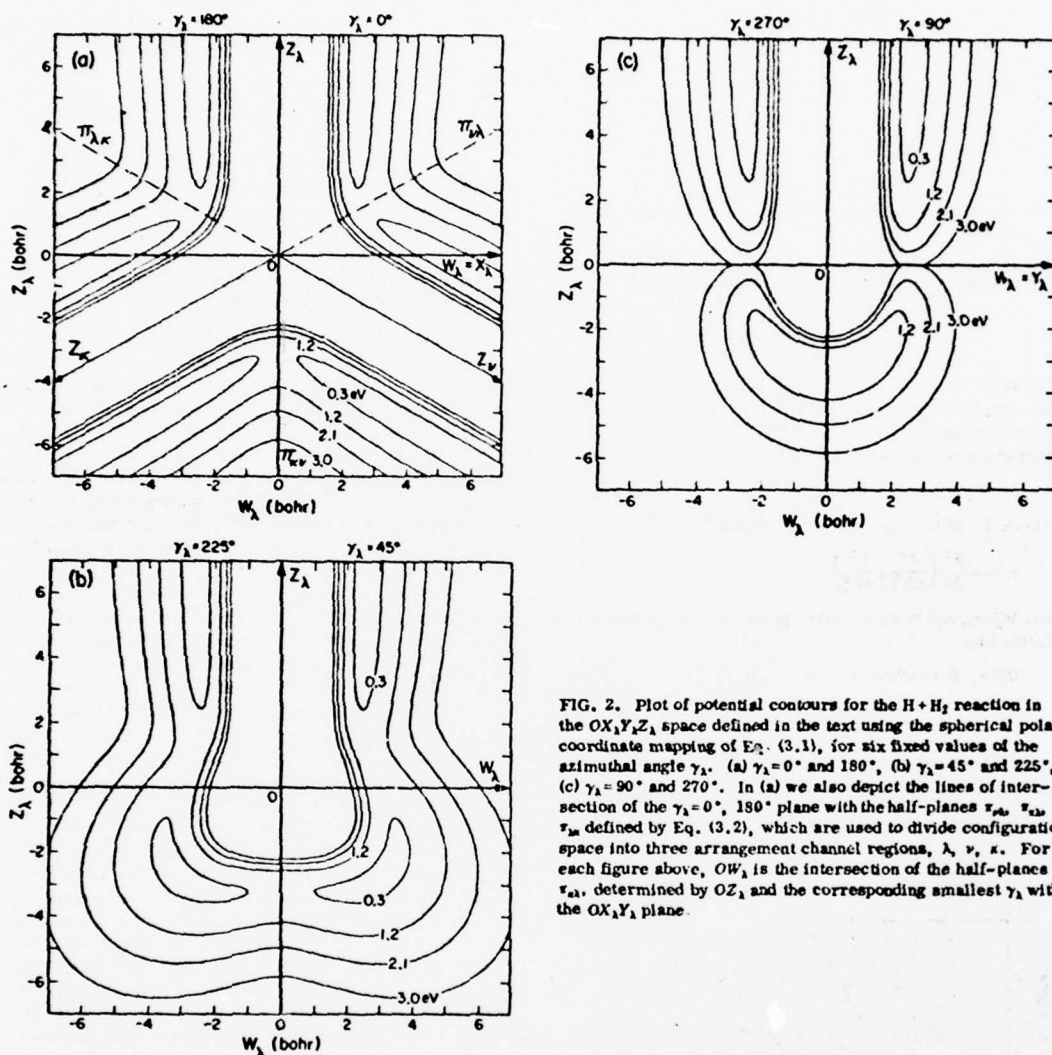
FIG. 2. Plot of potential contours for the $H + H_2$ reaction in the $OX_\lambda Y_\lambda Z_\lambda$ space defined in the text using the spherical polar coordinate mapping of Eq. (3.1), for six fixed values of the azimuthal angle γ_λ. (a) $\gamma_\lambda = 0°$ and $180°$, (b) $\gamma_\lambda = 45°$ and $225°$, (c) $\gamma_\lambda = 90°$ and $270°$. In (a) we also depict the lines of intersection of the $\gamma_\lambda = 0°$, $180°$ plane with the half-planes $\pi_{\nu\lambda}$, $\pi_{\kappa\lambda}$, $\pi_{\lambda\lambda}$ defined by Eq. (3.2), which are used to divide configuration space into three arrangement channel regions, λ, ν, κ. For each figure above, OW_λ is the intersection of the half-planes $\pi_{\nu\lambda}$, $\pi_{\kappa\lambda}$, determined by OZ_λ and the corresponding smallest γ_λ with the $OX_\lambda Y_\lambda$ plane.

j_λ associated with r_λ is defined as

$$\mathbf{j}_\lambda = \frac{\hbar}{i}\left(\frac{\partial}{\partial \gamma_\lambda}\right)_{\theta_\lambda, R_\lambda, r_\lambda} \hat{z} , \tag{3.3}$$

and its eigenfunctions are

$$\varphi_{j_\lambda}(\gamma_\lambda) = (2\pi)^{-1/2} \exp(ij_\lambda \gamma_\lambda) \quad j_\lambda = 0, \pm 1, \pm 2, \ldots \tag{3.4}$$

The expansion of ψ_λ^λ, defined by Eq. (2.13), in terms of these eigenfunctions is

$$\psi_\lambda^\lambda(r_\lambda, R_\lambda, \gamma_\lambda) = \sum_{j_\lambda} \varphi_{j_\lambda}(\gamma_\lambda) F_{j_\lambda}^\lambda(r_\lambda, R_\lambda) . \tag{3.5}$$

Substituting this into Eq. (2.14), taking the scalar product of both sides by $\varphi_{j'}$ and interchanging the primed and unprimed quantum numbers, we obtain the following set of coupled partial differential equations in the two

scaled distances r_λ, R_λ:

$$-\frac{\hbar^2}{2\mu}\left(\frac{\partial^2}{\partial r_\lambda^2} + \frac{\partial^2}{\partial R_\lambda^2} - \frac{j_\lambda^2 - \frac{1}{4}}{r_\lambda^2} - \frac{(J-j_\lambda)^2 - \frac{1}{4}}{R_\lambda^2}\right) F_{j_\lambda}^\lambda(r_\lambda, R_\lambda)$$

$$+ \sum_{j'_\lambda} V_{j_\lambda j'_\lambda}^\lambda(r_\lambda, R_\lambda) F_{j'_\lambda}^\lambda(r_\lambda, R_\lambda)$$

$$= E F_{j_\lambda}^\lambda(r_\lambda, R_\lambda) \quad J, j_\lambda = 0, \pm 1, \pm 2, \ldots , \tag{3.6}$$

where

$$V_{j_\lambda j'_\lambda}^\lambda(r_\lambda, R_\lambda) = \langle j_\lambda | V^\lambda | j'_\lambda \rangle$$

$$= \int_0^{2\pi} \varphi_{j_\lambda}^*(\gamma_\lambda) V^\lambda(r_\lambda, R_\lambda, \gamma_\lambda) \varphi_{j'_\lambda}(\gamma_\lambda) d\gamma_\lambda . \tag{3.7}$$

Since $V^\lambda = V(r_\lambda, R_\lambda) = V(r_\lambda, R_\lambda, E_\lambda, 2\pi - \gamma_\lambda)$, we can expand the potential in terms of a cosine Fourier series

$$V^\lambda(r_\lambda, R_\lambda, \gamma_\lambda) = \sum_{k=0}^{\infty} V_k^\lambda(r_\lambda, R_\lambda) \cos(k\gamma_\lambda) , \qquad (3.8a)$$

where

$$V_k^\lambda(r_\lambda, R_\lambda) = \frac{2}{(1 + \delta_{k0})\pi} \int_0^\pi \cos(k\gamma_\lambda) V^\lambda(r_\lambda, R_\lambda, \gamma_\lambda) d\gamma_\lambda .$$

$$(3.8b)$$

Substituting Eq. (3.8) into (3.7) and integrating, we find that

$$V_{j_\lambda j_\lambda'}^\lambda(r_\lambda, R_\lambda) = \frac{1}{2 - \delta_{|j_\lambda - j_\lambda'|, 0}} V_{|j_\lambda - j_\lambda'|}^\lambda(r_\lambda, R_\lambda)$$

$$= \frac{1}{\pi} \int_0^\pi \cos(|j_\lambda - j_\lambda'| \gamma_\lambda) V^\lambda(r_\lambda, R_\lambda, \gamma_\lambda) d\gamma_\lambda .$$

$$(3.9)$$

Equation (3.9) shows that $V_{j_\lambda j_\lambda'}^\lambda$ depends on j_λ and j_λ' only through $|j_\lambda - j_\lambda'|$. We can write Eq. (3.6) in a condensed matrix notation by regarding $\mathbf{F}_J^\lambda(r_\lambda, R_\lambda)$ as a column vector whose elements are the $F_{J j_\lambda}^\lambda(r_\lambda, R_\lambda)$. We get

$$T^\lambda \mathbf{F}_J^\lambda + \mathbf{V}_J^{\lambda e} \mathbf{F}_J^\lambda = E \mathbf{F}_J^\lambda , \qquad (3.10)$$

where T^λ is the kinetic energy operator

$$T^\lambda = -\frac{\hbar^2}{2\mu} \left(\frac{\partial^2}{\partial R_\lambda^2} + \frac{\partial^2}{\partial r_\lambda^2} \right) \qquad (3.11)$$

and $\mathbf{V}_J^{\lambda e}(r_\lambda, R_\lambda)$ is an effective potential energy matrix defined by

$$\mathbf{V}_J^{\lambda e}(r_\lambda, R_\lambda) = \mathbf{V}^\lambda(r_\lambda, R_\lambda) + \mathbf{V}_J^{\lambda c}(r_\lambda, R_\lambda) . \qquad (3.12)$$

$\mathbf{V}^\lambda$ is the J-independent interaction potential matrix

FIG. 3. Division of the R_λ, r_λ space into four regions, I, II, III, and IV. The contours are equipotentials of the matrix element $V_0^\lambda(r_\lambda, R_\lambda)$ [see Eq. (3.9)] is ek for the Porter-Karplus H + H₂ potential energy function. The dashed line L is the line of steepest ascents and descents [see (?)]. The procedures of the points P_0', P_0, and P_1 are discussed in text. [all of the text is too rough to make clearer.]

whose elements are the $V_{j_\lambda j_\lambda'}^\lambda$ defined by Eq. (3.9) while $\mathbf{V}_J^{\lambda c}$ is the diagonal centrifugal potential matrix defined by

$$[\mathbf{V}_J^{\lambda c}(r_\lambda, R_\lambda)]_{j_\lambda j_\lambda'} = \frac{\hbar^2}{2\mu} \left(\frac{j_\lambda^2 - \frac{1}{4}}{r_\lambda^2} + \frac{(J - j_\lambda)^2 - \frac{1}{4}}{R_\lambda^2} \right) \delta_{j_\lambda j_\lambda'} . \quad (3.13)$$

From Eqs. (3.6) and (3.9) we conclude that the $F_{J j_\lambda}^\lambda$ for different j_λ are coupled through the $V_k^\lambda(r_\lambda, R_\lambda)$ functions with $k > 0$, V_0^λ representing a noncoupling potential.

C. The division of r_λ, R_λ space into regions and the choice of variables in each region

We now consider the expansion of the function $F_{J j_\lambda}^\lambda(r_\lambda, R_\lambda)$ in terms of a set of single-variable functions which describe a vibrationlike motion. To pick this vibration variable and the corresponding vibrational basis set, it is convenient to examine the behavior of $V_0^\lambda(r_\lambda, R_\lambda)$ since, as one can conclude from the remark at the end of Sec. III.B, this function together with the centrifugal potential $(\hbar^2/2\mu)(j_\lambda^2 - \frac{1}{4})/r_\lambda^2$ determines the r_λ dependence of $F_{J j_\lambda}^\lambda$ in the absence of j_λ (i.e., rotational) coupling. For the H + H₂ reaction, equipotentials of $V_0^\lambda(r_\lambda, R_\lambda)$ are represented in Fig. 3, together with the corresponding line L of steepest ascents and descents. Cuts of V_0^λ normal to L look like diatomic internuclear potential energy functions, displaying a minimum on L, a dissociation plateau in the direction away from the coordinate axes, and a steep repulsive point in the opposite direction. These characteristics are analogous to those presented by collinear triatomic potential energy functions and suggest that we divide the r_λ, R_λ space in regions in a manner analogous to that employed for collinear reactions, [5,10] using different coordinates and/or vibration basis functions in each region. The corresponding vibration coordinates will be a distance along appropriately chosen lines transverse (but not necessarily orthogonal) to L. In each region, in addition to such vibration coordinates, there will be a "propagation" coordinate in terms of which Eq. (3.6) will be expressed as a system of coupled ordinary differential equations. For H + H₂ we indicate a convenient choice for these regions in Fig. 3. They are denoted as follows: I—the asymptotic region; II—the weak interaction region; III—the strong interaction region; and IV—the matching region. The boundary points P_0', P_0, and P_1 in Fig. 3 are chosen as follows. The abscissa r_{λ_0} of P_0' and P_0 is chosen so that these points lie in the classically forbidden plateau area where the wavefunction may be assumed to vanish. The ordinate P_0' of P_0' is picked large enough so that the potential $V_0(r_\lambda, R_\lambda)$ is independent of R_λ for $R_\lambda \geq R_{\lambda_0}'$. R_{λ_0} is determined by setting η_{λ_0} of Fig. 3 equal to $\pi/2 - \alpha_{\nu\lambda}/2$, from which we get

$$R_{\lambda_0} = r_{\lambda_0} \tan(\alpha_{\nu\lambda}/2) . \qquad (3.14)$$

The reason for this choice is that in order to perform the matching of the different arrangement channel solutions, as described in Sec. III.A, we need the $F_{J j_\lambda}^\lambda$ defined by Eq. (3.5) for a range of values of r_λ. As justified after Eq. (3.14), the lower limit of this range is the r_{λ_0} just chosen. The upper matching limit is at r_λ
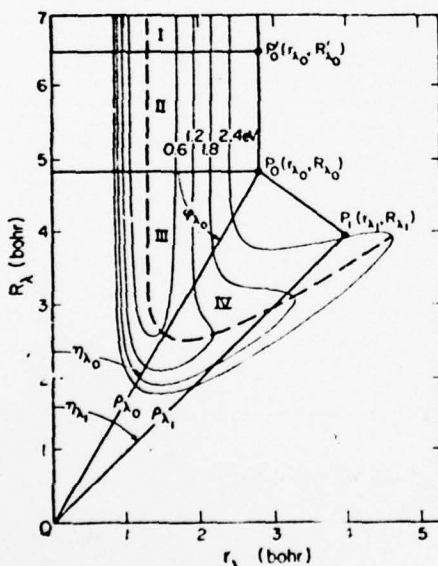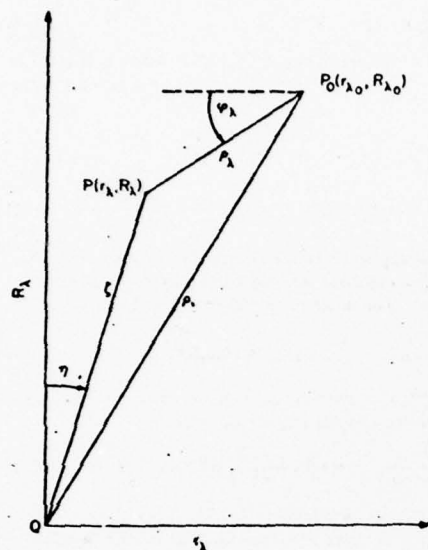
FIG. 4. The polar coordinates ρ_λ, φ_λ and ζ, η_λ and their interrelationships in R_λ, r_λ space.

$= \pi/4$, from which we get (see Fig. 3)

$$R_{\lambda_1} = r_{\lambda_1} . \qquad (3.15)$$

This common value of R_{λ_1} and r_{λ_1} is chosen so that $P_1(r_{\lambda_1}, R_{\lambda_1})$ also lies in the plateau region.

The coordinate systems used in each of these four regions are as follows. In the asymptotic region (I) and in the weak interaction region (II), we use the Cartesian coordinates r_λ, R_λ as vibration and propagation coordinates, respectively. In the strong interaction region (III) we switch to the polar coordinates ρ_λ, φ_λ (as depicted in Fig. 4) with $P_0(r_{\lambda_0}, R_{\lambda_0})$ as origin and related to r_λ, R_λ by

$$r_\lambda = r_{\lambda_0} - \rho_\lambda \cos\varphi_\lambda , \qquad (3.16a)$$

$$R_\lambda = R_{\lambda_0} - \rho_\lambda \sin\varphi_\lambda . \qquad (3.16b)$$

ρ_λ is the vibration and φ_λ the propagation coordinate for this region. In the matching region (IV), we use another set of polar coordinates (ζ, η_λ) which have their origin at Q (Fig. 4) and which are related to r_λ, R_λ by

$$r_\lambda = \zeta \sin\eta_\lambda , \qquad (3.17a)$$

$$R_\lambda = \zeta \cos\zeta_\lambda . \qquad (3.17b)$$

ζ ($\geqslant 0$) and η_λ (in range $0-\pi/2$) are, respectively, the vibration and propagation variables for Region IV. We note that the ζ defined here is identical to that given by Eq. (3.1a), while the angles ω_λ and η_λ are related, as can be seen from Eqs. (3.17) and (3.1b), by

$$\omega_\lambda = 2\eta_\lambda . \qquad (3.18)$$

Once we know the $F_{f/\lambda}^{\lambda}$ functions for a fixed r_λ and variable ζ, Eq. 3.5 furnishes the wavefunction ψ_λ^λ on a cone of constant $\omega_\lambda = 2\eta_\lambda$ in the $OX_\lambda Y_\lambda Z_\lambda$ coordinate system. As pictured in Fig. 5(a). We actually want to

determine this wavefunction on the matching surfaces $\pi_{\nu\lambda}$ and $\pi_{\lambda\mu}$ rather than on the ω_λ = constant cones since it is on these surfaces that we will smoothly match the solutions obtained from the integration of the Schrödinger equation in the three arrangements channels $\lambda = \alpha$, β, γ. However, for a given ω_λ (within a certain range) we do have the wavefunctions on the lines of intersection of the constant ω_λ cone with the half-planes $\pi_{\nu\lambda}$ and $\pi_{\lambda\mu}$ (see Fig. 5(a)). The relation between ω_λ and γ_λ at the lines of intersection with $\pi_{\nu\lambda}$ is given by Eq. (A14) of Appendix A. As ω_λ is scanned from $\omega_{\lambda_0} = 2\eta_0$ to $\omega_{\lambda_1} = 2\eta_{\lambda_1}$ (Figs. 3 and 5), these intersection lines scan the entire $\pi_{\nu\lambda}$ matching half-plane and thus we can obtain the desired wavefunction ψ_λ^λ on it from a knowledge of the $F_{f/\lambda}^\lambda(\zeta, \eta_\lambda)$ for η_λ in the range η_{λ_0} to η_{λ_1}. The angles ω_{λ_0} and ω_{λ_1} correspond to the intersection of $\pi_{\nu\lambda}$ with the $\gamma_\lambda = 0$ and $\gamma_\lambda = \pi/2$ half-plane, respectively (in $OX_\lambda Y_\lambda Z_\lambda$ internal configuration space). From Eq. (A14) we find that $\omega_{\lambda_0} = \pi - \alpha_{\nu\lambda}$ and $\omega_{\lambda_1} = \pi/2$. These values determine the values of η_{λ_0} and η_{λ_1} of Fig. 3 through Eq.
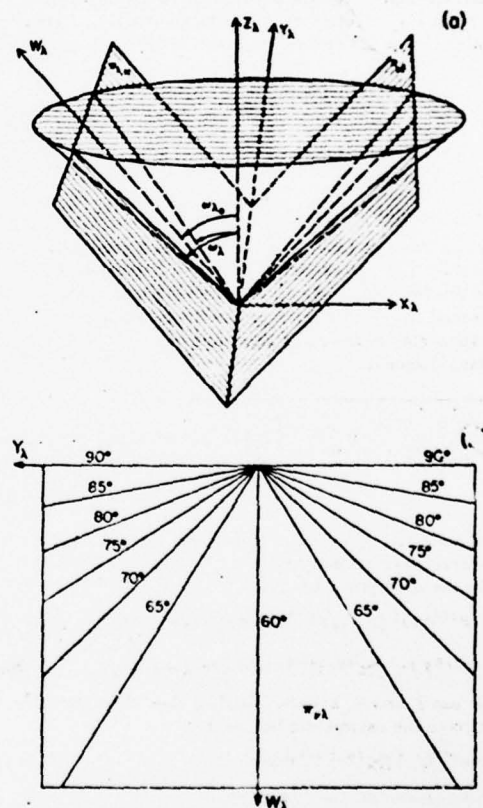
FIG. 5. (a) Plot of the matching half-planes $\pi_{\nu\lambda}$ and $\pi_{\lambda\mu}$ and their intersection with a cone of constant ω_λ ($3 \pi_\lambda \leqslant \omega_\lambda$) showing the straight lines of intersection which occur at two angles along the which cone $\ldots$ start, and are more $\ldots$

(3.18), and consequently the positions of P_0 and P_1. Indeed, by using Eqs. (3.17) and (3.18) together with the values of ω_{λ_0} and ω_{λ_1} given above, we obtain the equations (3.14) and (3.15) that were previously used in locating P_0 and P_1.[28] One additional complication in this procedure arises when $m_\nu \neq m_\kappa$ (for the integration in arrangement channel λ). In that case, the angles $\alpha_{\nu\lambda}$ and $\alpha_{\kappa\lambda}$ are different [see Eq. (A3)] so that the value of ω_{λ_0} for $\pi_{\nu\lambda}$ (i.e., $\omega_{\lambda_0} = \pi - \alpha_{\nu\lambda}$) is different from ω'_{λ_0} for $\pi_{\kappa\lambda}$ ($\omega'_{\lambda_0} = \pi - \alpha_{\kappa\lambda}$). In order to obtain the wavefunction on both of the matching surfaces $\pi_{\nu\lambda}$ and $\pi_{\kappa\lambda}$, we modify our definition of ω_{λ_0} to

$$\omega_{\lambda_0} = \min(\pi - \alpha_{\nu\lambda}, \pi - \alpha_{\kappa\lambda}) . \qquad (3.19)$$

ω_{λ_1}, on the other hand, is mass independent and always equal to $\pi/2$ for the choice of matching surfaces given by Eq. (3.2).

Having defined the four regions of each r_λ, R_λ space ($\lambda = \alpha, \beta, \gamma$) and their associated vibration–propagation coordinate systems, we are ready to introduce a vibrational expansion into the Schrödinger equations Eq. (3.6) [or their matrix counterpart Eq. (3.10)], thus obtaining the actual ordinary coupled differential equations to be integrated. We shall do this for each region separately, starting with the asymptotic region.

D. The coupled Schrödinger equations in the propagation variable

1. The asymptotic region

As mentioned above, the vibration and propagation variables for this region are r_λ and R_λ, respectively. The function $V^\lambda(r_\lambda, R_\lambda, \gamma_\lambda)$ becomes the isolated diatomic potential $v^\lambda(r_\lambda)$ for $R_\lambda \geq R'_{\lambda_0}$, and the potential matrix V^λ appearing in the right hand side of Eq. (3.12) becomes diagonal:

$$V^\lambda(r_\lambda, R_\lambda \geq R_{\lambda_0}) = v^\lambda(r_\lambda)\mathbf{I} , \qquad (3.20)$$

where $\mathbf{I}$ is the identity matrix. This leads to a total decoupling of Eqs. (3.6) and (3.10). For a given J and j_λ, we obtain

$$\left[-\frac{\hbar^2}{2\mu}\left(\frac{\partial^2}{\partial r_\lambda^2} + \frac{\partial^2}{\partial R_\lambda^2} - \frac{(j_\lambda^2 - \frac{1}{4})}{r_\lambda^2} + \frac{(J-j_\lambda)^2 - \frac{1}{4}}{R_\lambda^2} \right) + v^\lambda \right] F^{\lambda(a)}_{Jj_\lambda} = E F^{\lambda(a)}_{Jj_\lambda} , \qquad (3.21)$$

where the superscript (a) refers to the asymptotic region. This equation may be solved by separation of variables. The solution can be expanded as

$$F^{\lambda(a)}_{Jj_\lambda}(r_\lambda, R_\lambda) = \sum_{v_\lambda} g^{\lambda(a)}_{Jv_\lambda j_\lambda}(R_\lambda)\phi^{\lambda(a)}_{v_\lambda j_\lambda}(r_\lambda) , \qquad (3.22)$$

where $\phi^{\lambda(a)}_{v_\lambda j_\lambda}$ is a vibrational eigenfunction with vibrational energy $\epsilon^{\lambda(a)}_{v_\lambda j_\lambda}$ satisfying the equation

$$\left(-\frac{\hbar^2}{2\mu}\frac{d^2}{dr_\lambda^2} + v^\lambda(r_\lambda) + \frac{j_\lambda^2 - \frac{1}{4}}{r_\lambda^2} \right)\phi^{\lambda(a)}_{v_\lambda j_\lambda} = \epsilon^{\lambda(a)}_{v_\lambda j_\lambda}\phi^{\lambda(a)}_{v_\lambda j_\lambda} \qquad (3.23)$$

with boundary conditions $\phi^{\lambda(a)}_{v_\lambda j_\lambda}(0) = \phi^{\lambda(a)}_{v_\lambda j_\lambda}(r_{\lambda_0}) = 0$. $g^{\lambda(a)}_{Jv_\lambda j_\lambda}(R_\lambda)$ describes the translational motion associated with the propagation variable, R_λ, and satisfies the equation

$$\left(\frac{d^2}{dR_\lambda^2} - \frac{(J-j_\lambda)^2 - \frac{1}{4}}{R_\lambda^2} + k^{\lambda(a)}_{v_\lambda j_\lambda}{}^2 \right)g^{\lambda(a)}_{v_\lambda j_\lambda} = 0 , \qquad (3.24)$$

where

$$k^{\lambda(a)}_{v_\lambda j_\lambda}{}^2 = \frac{2\mu}{\hbar^2}(E - \epsilon^{\lambda(a)}_{v_\lambda j_\lambda}) \qquad (3.25)$$

is the square of the relative motion wave number when the diatom is in the vibration–rotation state labeled by the quantum numbers v_λ, j_λ. Equation (3.24) is closely related to the Bessel equation, and its general solution can be written as

$$g^{\lambda(a)}_{Jv_\lambda j_\lambda}(R_\lambda) = (|k^{\lambda(a)}_{v_\lambda j_\lambda}|R_\lambda)^{1/2}\begin{cases} a^\lambda_{Jv_\lambda j_\lambda}J_{J-j_\lambda}(k^{\lambda(a)}_{v_\lambda j_\lambda}R_\lambda) + c^\lambda_{Jv_\lambda j_\lambda}Y_{J-j_\lambda}(k^{\lambda(a)}_{v_\lambda j_\lambda}R_\lambda) & \text{for } \epsilon^{\lambda(a)}_{v_\lambda j_\lambda} < E \text{ (open channels)} \\ a^\lambda_{Jv_\lambda j_\lambda}I_{J-j_\lambda}(|k^{\lambda(a)}_{v_\lambda j_\lambda}|R_\lambda) + c^\lambda_{Jv_\lambda j_\lambda}K_{J-j_\lambda}(|k^{\lambda(a)}_{v_\lambda j_\lambda}|R_\lambda) & \text{for } \epsilon^{\lambda(a)}_{v_\lambda j_\lambda} > E \text{ (closed channels)} . \end{cases} \qquad (3.26)$$

The functions J_l and Y_l are, respectively, the regular and irregular ordinary Bessel functions[33] of order l and have the asymptotic behavior

$$x^{1/2}J_l(x) \underset{x \to \infty}{\sim} (2/\pi)^{1/2}\cos(x - l\pi/2 - \pi/4) , \qquad (3.27a)$$

$$x^{1/2}Y_l(x) \underset{x \to \infty}{\sim} (2/\pi)^{1/2}\sin(x - l\pi/2 - \pi/4) , \qquad (3.27b)$$

whereas I_l and K_l are the modified Bessel functions[33] and have the asymptotic behavior

$$x^{1/2}I_l(x) \underset{x \to \infty}{\sim} (2\pi)^{-1/2}\exp(x) , \qquad (3.28a)$$

$$x^{1/2}K_l(x) \underset{x \to \infty}{\sim} (\pi/2)^{1/2}\exp(-x) . \qquad (3.28b)$$

In Sec. V we will consider scattering asymptotic conditions which will determine the constants $a^\lambda_{Jv_\lambda j_\lambda}$ and $c^\lambda_{Jv_\lambda j_\lambda}$.

Let us rewrite Eqs. 3.26 and 3.26 in matrix notation, which will appear more convenient for subsequent use as the elements of $g^{\lambda(a)}$ as the column vec-

tor whose elements, labeled by the $v_\lambda j_\lambda$ index pair, are given by Eq. (3.26). When replaced into Eqs. (3.22), (3.5), and (2.13), it furnishes a single $\chi^\lambda_J(R_\lambda, r_\lambda, \gamma_\lambda)$, corresponding to a single a^λ_J, c^λ_J column vector pair, the elements of which are the $a^\lambda_{Jv_\lambda j_\lambda}$ and $c^\lambda_{Jv_\lambda j_\lambda}$ of Eq. (3.25). In order to satisfy Condition (c) of Sec. II.A, we will need a complete set of linearly independent solutions of the Schrödinger equation. The number of solutions in such a set is twice the number of $v_\lambda j_\lambda$ channels included in the expansions of Eqs. (3.22) and (3.5), which should be infinite but for practical reasons are truncated at a finite number N. (The errors introduced by this truncation will be discussed subsequently.[30]) We can assemble the corresponding $g^{\lambda(a)}$ vectors to form two square matrices of dimension $N \times N$ which we shall label $g^{\lambda(a)}(R_\lambda)$ and $g^{\lambda(a)}(R_\lambda)$. In each of these two matrices, the rows will be labeled by the $v_\lambda j_\lambda$ pairs and the columns by the (j) index. In the course of our development, we will obtain the scattering amplitudes the a...

propagation from Region I to IV and those labeled (−) by a propagation in the opposite direction. If we similarly form the matrices $\mathbf{a}_J^s$ and $\mathbf{c}_J^s$ from the corresponding $\mathbf{a}_J^s$ and $\mathbf{c}_J^s$ vectors, we can rewrite Eqs. (3.24) and (3.26) as

$$\frac{d^2 \mathbf{g}_J^{\lambda(a)s}}{dR_\lambda^2} = \mathbf{U}_J^{\lambda(a)}(R_\lambda)\mathbf{g}_J^{\lambda(a)s} \tag{3.29}$$

and

$$\mathbf{g}_J^{\lambda(a)s}(R_\lambda) = \mathbf{J}_J^\lambda(R_\lambda)\mathbf{a}_J^{\lambda s} + \mathbf{Y}_J^\lambda(R_\lambda)\mathbf{c}_J^{\lambda s} , \tag{3.30}$$

where

$$\mathbf{U}_J^{\lambda(a)} = -\mathbf{K}^{\lambda(a)2} + \mathbf{U}_J^{c\lambda(a)} , \tag{3.31}$$

$$[\mathbf{K}^{\lambda(a)2}]_{v_\lambda j_\lambda}^{v_\lambda' j_\lambda'} = \delta_{v_\lambda j_\lambda}^{v_\lambda' j_\lambda'} k_{v_\lambda j_\lambda}^{\lambda(a)2} , \tag{3.32}$$

$$[\mathbf{U}_J^{c\lambda(a)}]_{v_\lambda j_\lambda}^{v_\lambda' j_\lambda'} = \delta_{v_\lambda j_\lambda}^{v_\lambda' j_\lambda'} \frac{(J-j_\lambda)^2 - \frac{1}{4}}{R_\lambda^2} , \tag{3.33}$$

$$[\mathbf{J}_J^\lambda]_{v_\lambda j_\lambda}^{v_\lambda' j_\lambda'} = (|k_{v_\lambda j_\lambda}^{\lambda(a)}|R_\lambda)^{1/2} \delta_{v_\lambda j_\lambda}^{v_\lambda' j_\lambda'} \begin{cases} J_{J-j_\lambda}(k_{v_\lambda j_\lambda}^{\lambda(a)}R_\lambda) & \text{for } \epsilon_{v_\lambda j_\lambda}^{\lambda(a)} < E \text{ (open channels)} \\ I_{J-j_\lambda}(|k_{v_\lambda j_\lambda}^{\lambda(a)}|R_\lambda) & \text{for } \epsilon_{v_\lambda j_\lambda}^{\lambda(a)} > E \text{ (closed channels)} , \end{cases} \tag{3.34}$$

$$[\mathbf{Y}_J^\lambda]_{v_\lambda j_\lambda}^{v_\lambda' j_\lambda'} = (|k_{v_\lambda j_\lambda}^{\lambda(a)}|R_\lambda)^{1/2} \delta_{v_\lambda j_\lambda}^{v_\lambda' j_\lambda'} \begin{cases} Y_{J-j_\lambda}(k_{v_\lambda j_\lambda}^{\lambda(a)}R_\lambda) & \text{for } \epsilon_{v_\lambda j_\lambda}^{\lambda(a)} < E \text{ (open channels)} \\ K_{J-j_\lambda}(|k_{v_\lambda j_\lambda}^{\lambda(a)}|R_\lambda) & \text{for } \epsilon_{v_\lambda j_\lambda}^{\lambda(a)} > E \text{ (closed channels)} . \end{cases} \tag{3.35}$$

In Eqs. (3.32) through (3.35) the subscripts in a matrix element represent its row label and the superscripts its column label. Equations analogous to Eq. (3.29) will be developed for each of the other three subregions. Equation (3.30) and similar equations will be used in the reactance matrix analysis (Sec. V).

2. The weak interaction region

In this region, we retain the vibration–propagation variables r_λ, R_λ. However, since $Y^\lambda(r_\lambda, R_\lambda, \gamma_\lambda)$ and $V^\lambda(r_\lambda, R_\lambda)$ do vary with R_λ, the asymptotic vibrational eigenfunctions $\phi_{v_\lambda j_\lambda}^{\lambda(a)}$ are not necessarily the best basis for expanding the $F_{j_\lambda}^\lambda(r_\lambda, R_\lambda)$. To optimize a choice of basis functions, we divide Region II into n_{II}^λ subregions II_i ($i = 1, 2, \ldots, n_{II}^\lambda$) by constant R_λ lines having $R_\lambda = (R_{\lambda_0}', R_{\lambda_1}', \ldots, R_{\lambda_i}' = R_{\lambda_0})$. The range of R_λ for the ith subregion is $R_{\lambda_{i-1}}' \leq R_\lambda \leq R_{\lambda_i}'$. Let $R_{\lambda_i}^0$ be a selected value of R_λ in this range, such as its midpoint. We choose as a basis set for expansion in this subregion the functions $\phi_{v_\lambda j_\lambda}^{\lambda(w)}(r_\lambda; R_{\lambda_i}^0)$ which satisfy the eigenvalue equation

$$\left(-\frac{\hbar^2}{2\mu} \frac{d^2}{dr_\lambda^2} + V_{ref}^\lambda(r_\lambda; R_{\lambda_i}^0) + \frac{(j_\lambda^2 - \frac{1}{4})\hbar^2}{2\mu r_\lambda^2} \right) \phi_{v_\lambda j_\lambda}^{\lambda(w)}$$
$$= \epsilon_{v_\lambda j_\lambda}^{\lambda(w)}(R_{\lambda_i}^0) \phi_{v_\lambda j_\lambda}^{\lambda(w)} \tag{3.36}$$

with boundary conditions $\phi_{v_\lambda j_\lambda}^{\lambda(w)}(0; R_{\lambda_i}^0) = \phi_{v_\lambda j_\lambda}^{\lambda(w)}(r_{\lambda_0}; R_{\lambda_i}^0) = 0$. The superscript ($w$) refers to the weak interaction region. $V_{ref}^\lambda(r_\lambda; R_{\lambda_i}^0)$ is the value of a reference potential $V_{ref}^\lambda(r_\lambda, R_\lambda)$ at $R_\lambda = R_{\lambda_i}^0$. It is, in principle, arbitrary, but in practice must be chosen so that the vibrational basis functions $\phi_{v_\lambda j_\lambda}^{\lambda(w)}$ serve as an efficient representation of the r_λ dependence of the functions $F_{j_\lambda}^\lambda(r_\lambda, R_\lambda)$. Examples of possible reference potentials are (a) the first coefficient in the Fourier expansion [Eq. (3.8)] $V_0^\lambda(r_\lambda, R_\lambda)$, and (b) the exact potential $V^\lambda(R_\lambda, r_\lambda, \bar\gamma_\lambda)$ for a fixed $\bar\gamma_\lambda$. One important test of vibrational convergence in our method is the invariance of the final re-

sults to the choice of V_{ref}^λ. Equation (3.35) is the radial Schrödinger equation of a pseudomolecule whose interatomic potential is $V_{ref}^\lambda(r_\lambda; R_{\lambda_i}^0)$, characteristic of Subregion II_i, rather than $v^\lambda(r_\lambda)$, which characterizes the asymptotic region. [Its centrifugal potential is, however, not the normal $j_\lambda(j_\lambda + 1)\hbar^2/2\mu r_\lambda^2$ one.] The $\phi_{v_\lambda j_\lambda}^{\lambda(w)}$ and $\epsilon_{v_\lambda j_\lambda}^{\lambda(w)}$ are obtained by numerically solving Eq. (3.36),[34] subject to the boundary conditions just mentioned.

We now expand $F_{j_\lambda}^\lambda(r_\lambda, R_\lambda)$ in terms of the above vibrational basis functions:

$$F_{j_\lambda}^{\lambda(w)s}(r_\lambda, R_\lambda) = \sum_{v_\lambda} g_{J v_\lambda j_\lambda}^{\lambda(w)s}(R_\lambda; R_{\lambda_i}^0) \phi_{v_\lambda j_\lambda}^{\lambda(w)}(r_\lambda; R_{\lambda_i}^0) . \tag{3.37}$$

Substituting this into Eq. (3.6), multiplying by $\phi_{v_\lambda' j_\lambda}^\lambda(r_\lambda; R_{\lambda_i}^0)$ and integrating over r_λ, then interchanging v_λ and v_λ' and expressing the resulting coupled equations in the matrix form of the previous section, we get

$$\frac{d^2 \mathbf{g}_J^{\lambda(w)s}}{dR_\lambda^2} = \mathbf{U}_J^{\lambda(w)}(R_\lambda; R_{\lambda_i}^0)\mathbf{g}_J^{\lambda(w)s} , \tag{3.38}$$

where

$$\mathbf{U}_J^{\lambda(w)} = -\mathbf{K}^{\lambda(w)2} + \mathbf{U}_J^{c\lambda(w)} + \mathbf{U}_P^{\lambda(w)} . \tag{3.39}$$

The diagonal matrices $\mathbf{K}^{\lambda(w)2}$ and $\mathbf{U}_J^{c\lambda(w)}$ are defined by Eqs. (3.32) and (3.33), respectively, with the superscript (a) replaced by (w), while the J-independent coupling "potential" matrix $\mathbf{U}_P^{\lambda(w)}(R_\lambda; R_{\lambda_i}^0)$ (whose physical dimension is that of the square of a wave number) is given by

$$[\mathbf{U}_P^{\lambda(w)}(R_\lambda; R_{\lambda_i}^0)]_{v_\lambda j_\lambda}^{v_\lambda' j_\lambda'} = \frac{2\mu}{\hbar^2} \langle \phi_{v_\lambda j_\lambda}^{\lambda(w)}(r_\lambda; R_{\lambda_i}^0) | V_{j_\lambda j}(r_\lambda, R_\lambda) - V_{ref}^\lambda(r_\lambda; R_{\lambda_i}^0) | \phi_{v_\lambda' j_\lambda'}^{\lambda(w)}(r_\lambda; R_{\lambda_i}^0) \rangle$$

$$= \frac{2\mu}{\hbar^2} \langle \phi_{j_\lambda}^\lambda(\gamma_\lambda) \phi_{v_\lambda j_\lambda}^\lambda(r_\lambda; R_{\lambda_i}^0) | V^\lambda(r_\lambda, R_\lambda, \gamma_\lambda) - V_{ref}^\lambda(r_\lambda; R_{\lambda_i}^0) | \phi_{v_\lambda' j_\lambda'}^{\lambda(w)}(r_\lambda; R_{\lambda_i}^0) \phi_{j_\lambda'}^\lambda(\gamma_\lambda) \rangle$$

As long as the anisotropy of the potential remains small and the reference potential provides an efficient vibrational basis set for expanding the functions $F^{\lambda}_{j_{\lambda}}(r_{\lambda};R_{\lambda})$ within each subregion, the matrix $U_J^{\lambda(w)}$ should be nearly diagonal, and Eqs. (3.38) are only weakly coupled. The number and size of the subregions into which Region II is divided depends on the steepness of the variation of the potential matrix $\langle v_{\lambda}j_{\lambda}|V^{\lambda}|v'_{\lambda}j'_{\lambda}\rangle$ with R_{λ}. This number is generally small (i.e., less than 3).

As we propagate the solutions of Eq. (3.38) through Region II towards Regions I or III, the wavefunctions $\chi^{\lambda}_{J}(r_{\lambda},R_{\lambda},\gamma_{\lambda})$ must remain continuous and smooth during the change of basis functions that occurs at the boundaries of neighboring subregions. This requirement leads to the following relations between the functions $g^{\lambda(w)}_{J v_{\lambda}j_{\lambda}}(R_{\lambda};R^0_{\lambda_i})$ and $g^{\lambda(w)}_{J v_{\lambda}j_{\lambda}}(R_{\lambda};R^0_{\lambda_{i+1}})$ and their derivatives at the boundary of Subregions II_i and II_{i+1}:

$$g^{\lambda(w)s}_J(R'_{\lambda_i};R^0_{\lambda_{i+1}}) = S_i^{\lambda(w)} g^{\lambda(w)s}_J(R'_{\lambda_i};R^0_{\lambda_i}) , \qquad (3.41a)$$

$$\frac{dg^{\lambda(w)s}_J}{dR_{\lambda}}(R'_{\lambda_i};R^0_{\lambda_{i+1}}) = S_i^{\lambda(w)} \frac{dg^{\lambda(w)s}_J(R'_{\lambda_i};R^0_{\lambda_i})}{dR_{\lambda}} , \qquad (3.41b)$$

where the overlap matrix $S_i^{\lambda(w)}$ is given by

$$[S_i^{\lambda(w)}]^{v'_{\lambda}j'_{\lambda}}_{v_{\lambda}j_{\lambda}} = \delta_{j_{\lambda}j'_{\lambda}}\langle\phi^{\lambda(w)}_{v_{\lambda}j_{\lambda}}(r_{\lambda};R^0_{\lambda_{i+1}})|\phi^{\lambda(w)}_{v'_{\lambda}j'_{\lambda}}(r_{\lambda};R^0_{\lambda_i})\rangle . \qquad (3.42)$$

An important criterion for the choice of the size of the subregions is that the $S_i^{\lambda(w)}$ should be nearly orthogonal matrices. Lack of orthogonality implies lack of completeness of the basis sets $\phi^{\lambda(w)}_{v_{\lambda}j_{\lambda}}$ and results in the loss of information about the wavefunction as a result of the transformation of Eqs. (3.41). The relations at the boundary separating Regions I and II are achieved by setting $i=0$ in Eqs. (3.41) and interpreting $R^0_{\lambda_0}$ to mean R'_{λ_0} and $\phi^{\lambda(w)}_{v_{\lambda}j_{\lambda}}(r_{\lambda};R^0_{\lambda_0})$ to mean $\phi^{\lambda(w)}_{v_{\lambda}j_{\lambda}}(r_{\lambda})$.

3. The strong interaction region

In this region we use the polar coordinates $\rho_{\lambda},\varphi_{\lambda}$ regarding φ_{λ} as the propagation variable. If we transform Eq. (3.10) to these polar coordinates with the aid of Eq. (3.16), we obtain the vector equation

$$T^{\lambda(s)} F^{\lambda(s)}_J(\rho_{\lambda},\varphi_{\lambda}) + V^{w(s)}_J F^{\lambda(s)}_J = E F^{\lambda(s)}_J , \qquad (3.43)$$

where the superscript (s) refers to "strong interaction region." $T^{\lambda(s)}$ is given by

$$T^{\lambda(s)} = -\frac{\hbar^2}{2\mu}\left(\frac{\partial^2}{\partial\rho^2_{\lambda}} + \frac{1}{\rho_{\lambda}}\frac{\partial}{\partial\rho_{\lambda}} + \frac{1}{\rho^2_{\lambda}}\frac{\partial^2}{\partial\varphi^2_{\lambda}}\right) , \qquad (3.44)$$

and the matrix $V^{w(s)}_J(\rho_{\lambda},\varphi_{\lambda})$ is simply $V^{w}_J(r_{\lambda},R_{\lambda})$ expressed in the coordinates $\rho_{\lambda},\varphi_{\lambda}$.

For a typical reference potential V^{λ}_{ref} such as the $V^{\lambda}_0(r_{\lambda},R_{\lambda})$ defined by Eq. (3.8b) and plotted in Fig. 3 for $H+H_2$, the shape of the potential as a function of ρ_{λ} for a fixed $\varphi_{\lambda}(0\le\varphi_{\lambda}\le\varphi_{\lambda_0})$ is very much like that for a diatomic molecule. The deep potential well character of these cuts at constant φ_{λ} permits one to use their bound state eigenfunctions to efficiently represent the ρ_{λ} dependence of the wavefunction in this region. Accordingly, we divide Region III into n_{III} subregions $III_i(i=1, 2,\ldots,n_{III})$ by lines of constant

$$\varphi_i, \varphi_1 = \varphi_b , \varphi_{\nu}, \varphi_{\nu_0}, \ldots, \varphi_{\nu_{III}} = \varphi_{\mu}$$

For each such subregion, we choose a cut at a specific value $\varphi^0_{\lambda_i}$ of φ_{λ} (where $\varphi_{\lambda_{i-1}}\le\varphi^0_{\lambda_i}\le\varphi_{\lambda_i}$) to define our vibrational basis functions $\phi^{\lambda(s)}_{v_{\lambda}}(\rho_{\lambda};\varphi^0_{\lambda_i})$ and energy eigenvalues $\epsilon^{\lambda(s)}_{v_{\lambda}}(\varphi^0_{\lambda_i})$ as the solutions of the Schrödinger equation:

$$\left(-\frac{\hbar^2}{2\mu}\frac{d^2}{d\rho^2_{\lambda}} + V^{\lambda}_{ref}(\rho_{\lambda};\varphi^0_{\lambda_i})\right)\phi^{\lambda(s)}_{v_{\lambda}}(\rho_{\lambda};\varphi^0_{\lambda_i}) = \epsilon^{\lambda(s)}_{v_{\lambda}}(\varphi^0_{\lambda_i})\phi^{\lambda(s)}_{v_{\lambda}} , \qquad (3.45)$$

satisfying the boundary conditions $\phi^{\lambda(s)}_{v_{\lambda}}(\rho_{\lambda}=0) = \phi^{\lambda(s)}_{v_{\lambda}}(\rho_{\lambda} = \rho'_{\lambda_i}) = 0$, where ρ'_{λ_i} is the value of ρ_{λ} at the intersection of the line $\varphi_{\lambda} = \varphi^0_{\lambda_i}$ with the R_{λ} axis (Fig. 3). The potential $V^{\lambda}_{ref}(\rho_{\lambda},\varphi_{\lambda})$ is one of the reference potentials $V^{\lambda}_{ref}(r_{\lambda},R_{\lambda})$ defined in Sec. III.D.2 expressed in $\rho_{\lambda},\varphi_{\lambda}$ coordinates. Note that we have not included any j_{λ}-dependent centrifugal terms in the Hamiltonian of Eq. (3.45) (all of these terms being included in the "propagation part" of the Hamiltonian), and hence our eigenvalues and eigenfunctions depend only on the vibrational quantum number v_{λ}. This is done for computational convenience and does not seriously decrease the rate of convergence of our coupled-channel expansion.

We now expand the solutions $F^{\lambda(s)}_J$ of Eq. (3.43) in terms of the pseudovibrational functions $\phi^{\lambda(s)}_{v_{\lambda}}$,

$$F^{\lambda(s)s}_{J j_{\lambda}}(\rho_{\lambda},\varphi_{\lambda}) = \rho^{-1/2}_{\lambda}\sum_{n}g^{\lambda(s)s}_{J v_{\lambda}j_{\lambda}}(\varphi_{\lambda};\varphi^0_{\lambda_i})\phi^{\lambda(s)}_{v_{\lambda}}(\rho_{\lambda};\varphi^0_{\lambda_i}) . \qquad (3.46)$$

The counterpart of Eq. (3.38) becomes

$$\frac{d^2 g^{\lambda(s)s}_J}{d\varphi^2_{\lambda}} = \bar{U}^{\lambda(s)}_J(\varphi_{\lambda};\varphi^0_{\lambda_i})g^{\lambda(s)s}_J , \qquad (3.47)$$

where the effective "potential" matrix $\bar{U}^{\lambda(s)}_J$ (whose elements are dimensionless) can be written as

$$\bar{U}^{\lambda(s)}_J = \rho^2_{\lambda}(\varphi^0_{\lambda_i})U^{\lambda(s)}_J(\varphi_{\lambda};\varphi^0_{\lambda_i}) , \qquad (3.48)$$

in which

$$U^{\lambda(s)}_J = -K^{\lambda(s)2} + U^{c\lambda(s)}_J + U^{\lambda(s)}_{\rho} .$$

The matrix ρ^2_{λ} is given by

$$[\rho^2_{\lambda}(\varphi^0_{\lambda_i})]^{v'_{\lambda}j'_{\lambda}}_{v_{\lambda}j_{\lambda}} = \langle v_{\lambda}|\rho^2_{\lambda}|v'_{\lambda}\rangle\delta_{j_{\lambda}j'_{\lambda}} . \qquad (3.49)$$

The matrix $K^{\lambda(s)2}$ and the "potential" coupling matrix $U^{\lambda(s)}_{\rho}$ are quite similar to those in Eqs. (3.32) and (3.40) and are given by

$$[K^{\lambda(s)}(\varphi^0_{\lambda_i})]^{v'_{\lambda}j'_{\lambda}}_{v_{\lambda}j_{\lambda}} = \delta^{v'_{\lambda}j'_{\lambda}}_{v_{\lambda}j_{\lambda}}\frac{2\mu}{\hbar^2}[E - \epsilon^{\lambda(s)}_{v_{\lambda}}(\varphi^0_{\lambda_i})] \qquad (3.50)$$

and

$$[U^{\lambda(s)}_{\rho}(\varphi_{\lambda};\varphi^0_{\lambda_i})]^{v'_{\lambda}j'_{\lambda}}_{v_{\lambda}j_{\lambda}} = \frac{2\mu}{\hbar^2}\langle\phi^{\lambda(s)}_{v_{\lambda}}(\rho_{\lambda};\varphi^0_{\lambda_i})|V^{\lambda}_{j_{\lambda}v'_{\lambda}}(\rho_{\lambda},\varphi_{\lambda})$$
$$- V^{\lambda}_{ref}(\rho_{\lambda};\varphi_{\lambda})|\phi^{\lambda(s)}_{v'_{\lambda}}(\rho_{\lambda};\varphi^0_{\lambda_i})\rangle , \qquad (3.51)$$

respectively, but the centrifugal potential matrix is now defined as

$$[U^{c\lambda(s)}_J(\varphi_{\lambda};\varphi^0_{\lambda_i})]^{v'_{\lambda}j'_{\lambda}}_{v_{\lambda}j_{\lambda}} = \langle v_{\lambda}|\frac{j^2_{\lambda} - \frac14}{(r_{\lambda_0} - \rho_{\lambda}\cos\varphi_{\lambda})^2}$$
$$- \frac{(J - j_{\lambda})^2 - \frac14}{(R_{\lambda_0} - \rho_{\lambda}\sin\varphi_{\lambda})^2} - \frac{1}{4\rho^2_{\lambda}}|v'_{\lambda}\rangle . \qquad (3.52)$$

arises from the rotation of the diatom, the second from rotation of the atom–diatom system, and the third is a pseudocentrifugal potential arising from the use of the ρ_λ, φ_λ coordinates and associated with the nonphysical swinging motion around the point P_0 of Fig. 3 as φ_λ is changed. The centrifugal coupling [Eq. (3.52)] is still diagonal in j_λ [as is its counterpart for the (a) and (w) regions] but no longer in v_λ. In addition to the usual potential coupling resulting from the off-diagonal terms of $U_\rho^{\lambda(a)}$, we also have coupling arising from the nondiagonal ρ_λ^2 matrix which appears in Eq. (3.48) as a result of the swinging motion around P_0. The neglect of this latter coupling could introduce serious errors since ρ_λ^2 has large off-diagonal elements. Such an approximation has nevertheless often been used, [14,15] since it is one of the consequences of the one-vibrational-basis-function approximation. Note also that the effective potential matrix $\overline{U}_\rho^{\lambda(a)}$ is not symmetric, but is the product of two symmetric matrices as can be seen from Eq. (3.48). In Sec. III. E we discuss the Gordon method[25] used to integrate Eq. (3.47) and the modifications of it which are required when dealing with matrices of this type.

The smooth matching across the boundary separating any two neighboring subregions III_i and III_{i+1} is achieved through expressions analogous to Eqs. (3.41) in which the overlap matrix S_i^λ is given by

$$[S_i^\lambda(\varphi_\lambda^0)]_{v_\lambda j_\lambda}^{v_\lambda' j_\lambda'} = \delta_{j_\lambda j_\lambda'} \langle \phi_{v_\lambda}^{\lambda(a)}(\rho_\lambda; \varphi_{\lambda_{i+1}}^0) | \phi_{v_\lambda'}^{\lambda(a)}(\rho_\lambda; \varphi_{\lambda_i}^0) \rangle \quad (3.53)$$

and has elements which are independent of j_λ, j_λ'. Since the general characteristics of the ρ_λ dependence of the reference potential $V_{\text{ref}}^\lambda(\rho_\lambda, \varphi_\lambda)$ usually change quite rapidly as φ_λ is changed, the number of subregions in Region III required to keep S_i^λ nearly orthogonal for a truncated vibrational basis set is generally large (on the order of 20–30).

The smooth matching of the wavefunction χ_J^λ across the boundary between Regions II and III is achieved by the relations

$$g_J^{\lambda(a)s}(\varphi_\lambda = 0, \varphi_{\lambda_i}^0) = \rho_\lambda^{1/2} g_J^{\lambda(w)s}(R_{\lambda_0}; R_{\lambda_{\pm}^{0}}) \quad (3.54a)$$

and

$$\frac{dg_J^{\lambda(a)s}}{d\varphi_\lambda}(\varphi_\lambda = 0; \varphi_{\lambda_i}^0) = -\rho_\lambda^{3/2} \frac{dg_J^{\lambda(w)s}}{dR_\lambda}(R_{\lambda_0}; R_{\lambda_{\pm}^{0}}) , \quad (3.54b)$$

where

$$(\rho_\lambda^b)_{v_\lambda j_\lambda}^{v_\lambda' j_\lambda'} = \langle \phi_{v_\lambda}^{\lambda(a)}(\rho_\lambda; \varphi_\lambda^0) | \rho_\lambda^b | \phi_{v_\lambda'}^{\lambda(w)}(r_{\lambda_0} - \rho_\lambda; R_{\lambda_{\pm}^{0}}) \rangle \delta_{j_\lambda j_\lambda'}$$

$$b = \tfrac{1}{2}, \tfrac{3}{2} . \quad (3.55)$$

4. The matching region

As described in Sec. III. C, the coordinates used in this region are the polar variables ζ, η_λ depicted in Fig. 4, with η_λ being the propagation variable. The Schrödinger equation in Region IV is very similar to that in Region III [see Eqs. (3.43)–(3.52) with ρ_λ, φ_λ replaced by ζ, η_λ. From Eqs. (3.17) and (3.18) we obtain the counterpart of Eq. (3.43):

where

$$T^{\lambda(m)} = -\frac{\hbar^2}{2\mu}\left(\frac{\partial^2}{\partial\zeta^2} + \frac{1}{\zeta}\frac{\partial}{\partial\zeta} + \frac{1}{\zeta^2}\frac{\partial^2}{\partial\eta_\lambda^2}\right) . \quad (3.57)$$

The superscript (m) denotes "matching region," and $V_J^{\lambda(m)}(\zeta, \eta_\lambda)$ is obtained from $V_J^\lambda(r_\lambda, R_\lambda)$ by using Eq. (3.17). The division of Region IV into subregions is analogous to that for Regions II and III, and the vibrational basis functions $\phi_{v_\lambda}^{\lambda(m)}(\zeta; \eta_{\lambda_i}^0)$ with eigenvalue $\epsilon_{v_\lambda}^{\lambda(m)}(\eta_{\lambda_i}^0)$ satisfy the equation

$$\left(-\frac{\hbar^2}{2\mu}\frac{d^2}{d\zeta^2} + V_{\text{ref}}^\lambda(\zeta, \eta_{\lambda_i}^0)\right)\phi_{v_\lambda}^{\lambda(m)} = \epsilon_{v_\lambda}^{\lambda(m)}(\eta_{\lambda_i}^0)\phi_{v_\lambda}^{\lambda(m)} \quad (3.58)$$

with boundary conditions $\phi_{v_\lambda}^{\lambda(m)}(0) = \phi_{v_\lambda}^{\lambda(m)}(\zeta = \zeta_0) = 0$. The potential $V_{\text{ref}}^\lambda(\zeta, \eta_\lambda)$ is one of the reference potentials V_{ref}^λ defined in Sec. III. D. 2 and III. D. 3 but expressed in ζ, η_λ coordinates. Writing

$$F_{J j_\lambda}^{\lambda(m)} = \zeta^{-1/2} \sum_{v_\lambda} g_{v_\lambda j_\lambda}^{J\lambda(m)}(\eta_\lambda; \eta_{\lambda_i}^0)\phi_{v_\lambda}^{\lambda(m)}(\zeta; \eta_{\lambda_i}^0) , \quad (3.59)$$

the counterpart of Eq. (3.47) becomes

$$\frac{d^2 g_J^{\lambda(m)s}}{d\eta_\lambda^2} = \overline{U}_J^{\lambda(m)}(\eta_\lambda; \eta_{\lambda_i}^0) g_J^{\lambda(m)s} , \quad (3.60)$$

where the effective potential matrix (again being physically dimensionless) is

$$\overline{U}_J^{\lambda(m)} = \zeta^2(\eta_{\lambda_i}^0) U_J^{\lambda(m)}(\eta_\lambda; \eta_{\lambda_i}^0) \quad (3.61)$$

with

$$U_J^{\lambda(m)}(\eta_\lambda; \eta_{\lambda_i}^0) = -K^{\lambda(m)2} + U_J^{c\lambda(m)} + U_J^{\lambda(m)} . \quad (3.62)$$

The matrix $\zeta^2(\eta_{\lambda_i}^0)$ is defined analogously to ρ_λ^2 of Eq. (3.49) with ρ_λ replaced by ζ and φ_λ by η_λ. The matrices $K^{\lambda(m)2}$ and $U_J^{\lambda(m)}$ are given by expressions similar to Eqs. (3.50) and (3.51), respectively, with the superscript (m) replacing (s) and appropriate coordinate changes made, while the centrifugal potential matrix is given by

$$[U_J^{c\lambda(m)}(\eta_\lambda; \eta_{\lambda_i}^0)]_{v_\lambda j_\lambda}^{v_\lambda' j_\lambda'}$$

$$= \langle v_\lambda | \frac{j_\lambda^2 - \tfrac{1}{4}}{\zeta^2 \sin^2\eta_\lambda} + \frac{(J - j_\lambda)^2 - \tfrac{1}{4}}{\zeta^2 \cos^2\eta_\lambda} - \frac{1}{4\zeta^2} | v_\lambda' \rangle \delta_{j_\lambda j_\lambda'} . \quad (3.63)$$

Smooth transformation between subregions in Region IV involves Eqs. (3.41) with the overlap matrix S_i^λ given by

$$[S_i^\lambda(\eta_{\lambda_i}^0)]_{v_\lambda j_\lambda}^{v_\lambda' j_\lambda'} = \delta_{j_\lambda j_\lambda'} \langle \phi_{v_\lambda}^{\lambda(m)}(\zeta, \eta_{\lambda_{i+1}}^0) | \phi_{v_\lambda'}^{\lambda(m)}(\zeta, \eta_{\lambda_i}^0) \rangle , \quad (3.64)$$

and the transformation between Regions III and IV is achieved with equations

$$g_J^{\lambda(m)s}(\eta_{\lambda_0}; \eta_{\lambda_i}^0) = \zeta^{1/2} g_J^{\lambda(a)s}(\varphi_{\lambda_0}; \varphi_{\lambda_{III}}^0) \quad (3.65a)$$

and

$$\frac{dg_J^{\lambda(m)s}}{d\eta_\lambda}(\eta_{\lambda_0}; \eta_{\lambda_i}^0) = \zeta^{3/2} \frac{dg_J^{\lambda(a)s}}{d\varphi_\lambda}(\varphi_{\lambda_0}; \varphi_{\lambda_{III}}^0) , \quad (3.65b)$$

where

E. Integration of the Schrödinger equation

We generate solutions g_j^{λ} and their derivatives with respect to the propagation variable by choosing at $R_\lambda = R_{\lambda_0}'$ arbitrary initial values for these two matrices and integrating numerically Eqs. (3.38), (3.47), and (3.60) from the beginning of Region II to the end of Region IV. Similarly, we generate the g_j^{λ} solutions and their derivatives by choosing arbitrary initial values for these two matrices at $\eta_\lambda = \eta_{\lambda_1}$ and numerically integrating these equations from the end of Region IV to the beginning of Region II.

Any appropriate numerical procedure may be employed to integrate the coupled equations. The one we used, which is well suited to equations of the type of Eqs. (3.38), (3.47), and (3.60), is the one developed by Gordon.[35] In Region II, it can be applied without modification,[36] but in Regions III and IV, the nonsymmetric nature of the effective interaction potential matrices [Eqs. (3.48) and (3.61)] requires a short modification of the method. As formulated by Gordon, in propagating a system of coupled equations, a transformation to a representation in which the effective potential matrix (say U) becomes diagonal is required. This necessitates finding the eigenvalues of U. In the special case where U is real and symmetric, these eigenvalues are real and the eigenvector matrix is orthogonal. This simplifies the calculation and allows for an efficient program. The effective potential matrices of Regions III and IV as given by Eqs. (3.48) and (3.61) are real but nonsymmetric and thus could have complex eigenvalues and eigenvectors. These potential matrices are, however, equal to the product of two symmetric matrices, one of which (ρ_λ^2 for Region III and ζ^2 for Region IV) is the matrix representation of a positive definite operator (ρ_λ^2 or ζ^2) and hence has positive definite eigenvalues. By using these special properties to define the "square root" of ρ_λ^2 and ζ^2, it is shown in Appendix B that both the eigenvalues and eigenvectors of the effective potential matrix are always real but the eigenvector matrix is not generally orthogonal. This allows us to use real variables throughout the integration, with the only major program changes from the usual Gordon method being in the routines needed to find the eigenvalues and eigenvectors of the effective potential matrix, and in the manipulation of the eigenvector matrices.

F. Restrictions and limitations

We should at this point summarize the possible limitations and restrictions on the method other than those inherent in the numerical procedures involved or those arising from computer limitations.

First, the choice of matching surfaces in Eqs. (3.2) is largely determined by the shape of the potential energy surface in Fig. 2, and for many reactions, an efficient choice will require somewhat different matching planes. A change in the exact mathematical form of the matching surfaces can significantly affect the details of the integration in Region IV and in the matching procedure although the basic concepts will be preserved. In choosing the matching surfaces for a given reaction, primary consideration should be given to obtaining an efficient representation of the wavefunction in the vicinity of the matching surfaces. This requires us to avoid too large a potential anisotropy in the matching region, for in that case, our coupled-channel solution will require many closed rotational channels for convergence. At the same time, too small a potential anisotropy (resulting in considerable flux "leakage" through $\gamma_\lambda = \pi/2$ configurations in the matching region) can result in poor convergence of the matching procedure (as will be discussed in Sec. IV). One therefore needs to be clever in choosing these surfaces, and it is possible that for certain reactions, no choice satisfies all of the above criteria and simultaneously leads to a mathematically tractable matching procedure.

One case where the choice of surfaces specified by Eqs. (3.2) leads to a set of coupled equations in the matching region [Eqs. (3.60)], which is not easily solved without including a large number of closed rotational channels, is when α_{ν_λ} (or $\alpha_{\lambda\lambda}$) $\geq 3\pi/4$. [See Eq. (A3) for the definition of these angles.] The reason for this is that when this inequality is satisfied, integration in the matching region will extend into those regions of configuration space for which r_ν (or r_λ) = 0, and hence will sample the very high potential energy in those configurations [for which $\gamma_\lambda = 0$ (or π)] while possibly sampling low potential energy for other configurations (near $\gamma_\lambda = \pi/2$). That this is the case can be verified by noting that during the integration in the matching region, η_λ must scan the range from $(\pi - \alpha_{\nu_\lambda})/2$ to $\pi/4$ [from Eqs. (3.14), (3.15), and (3.17)] and that Eq. (A5) yields $r_\nu = 0$ when $\gamma_\lambda = 0$ and $\alpha_{\nu_\lambda} = 3\pi/4$ at some η_λ within this range. From Eqs. (A3) we note that $\alpha_{\nu_\lambda} \geq 3\pi/4$ implies $m_\alpha(m_\lambda + m_\nu + m_\alpha) < m_\lambda m_\nu$, so that this restriction applies primarily to reactions with one atom of the triatomic system considerably lighter than the other two. We should also point out that this problem can be eliminated by the use of a different coordinate system in the matching region or by the use of "rotationally adiabatic" rotational basis functions [rather than $\varphi_{j_\lambda}(\gamma_\lambda)$].

When one of the three arrangement channels is closed, the method must be somewhat modified,[21] but this is not a complication. Other practical limitations to the method occur for reactions where break-up collisions are allowed or for which virtual excitations to closed dissociative channels influence the other reactive and nonreactive processes significantly. The present method is not capable of treating any dissociation process, but this is not a serious limitation for many reactions at energies of chemical interest. A more general method which utilizes generalized hyperspherical functions is currently being developed in these laboratories for the purpose of treating both break-up and rearrangement collisions.

IV. THE MATCHING

A. Projection of the wavefunction onto the matching surface basis functions

At the completion of the integration in arrangement channel region λ, we have generated solutions which satisfy the Schrödinger equation in that region, but which do not, in general, match smoothly with the cor-

1·0

2·8

2·5

3·15

2·2

3·5

1·1

2·0

1·8

1·25

1·4

1·6

NATIONAL BUREAU OF STANDARDS
MICROCOPY RESOLUTION TEST CHART

responding wavefunctions obtained from the integrations in the other arrangement channel regions ν and κ. In this section we describe the procedure for accomplishing this smooth matching. This procedure may conveniently be broken up into two parts. First, we consider the projection of the full wavefunction and its derivative normal to the matching surface onto a set of orthonormal basis functions which span the matching surfaces. Second, we take linear combinations of the wavefunctions in each arrangement channel region and match them smoothly, on these surfaces, to linear combinations of the corresponding wavefunctions in the other arrangement channel regions. The resulting matrix equations can be solved to yield a set of solutions which satisfy Condition (a) of Sec. II. A and can subsequently (see Sec. V. A) be used to form the scattering solutions satisfying Condition (c) of that section.

Let us consider the projection procedure for the matching surface $\pi_{\nu\lambda}$ [Fig. 2(a)]. The analogous equations for $\pi_{\kappa\nu}$ and $\pi_{\lambda\kappa}$ are obtained from those derived below by cyclic permutation of the indices $\lambda\nu\kappa$. We first consider the wavefunction on $\pi_{\nu\lambda}$ obtained from the integration in arrangement channel λ. Using Eqs. (3.59), (3.5), (2.13), and (2.10), we get the following expression for the wavefunction in Region IV (Subregion i):

$$\Psi_J^{\lambda v_\lambda' j_\lambda' i}(\theta_\lambda, \zeta, \eta_\lambda, \gamma_\lambda)$$

$$= \frac{\sqrt{2}\varphi_J(\theta_\lambda)}{\zeta^{3/2}(\sin 2\eta_\lambda)^{1/2}} \left(\sum_{v_\lambda j_\lambda} \varphi_{j_\lambda}(\gamma_\lambda) \phi_{v_\lambda}^\lambda(\zeta; \eta_{\lambda_i}^0) g_{J v_\lambda j_\lambda}^{\lambda v_\lambda' j_\lambda' i}(\eta_\lambda; \eta_{\lambda_i}^0) \right). \tag{4.1}$$

Throughout Sec. IV we will consider superscript (m) of Sec. III. D. 4 to be present implicitly and will omit writing it explicitly. We have, however, added the indices $v_\lambda' j_\lambda'$ to denote different linearly independent solutions obtained by using different initial conditions in the numerical solution of the Schrödinger equation. As explained in Sec. III. D. 1, if we truncate the close coupling expansion after N vibration–rotation basis functions, there will be N sets of indices $v_\lambda' j_\lambda'$ in Eq. (4.1).

The expression in large parentheses in Eq. (4.1) is expanded in terms of a different set of vibrational functions $\phi_{v_\lambda}^\lambda(\zeta; \eta_{\lambda_i}^0)$ for each subregion i of Region IV. We now transform to a representation in terms of a single set of vibration–rotation basis functions $\varphi_{j_\lambda}(\gamma_\lambda)\phi_{v_\lambda}^\lambda(\zeta)$ for all of Region IV. The actual functions $\phi_{v_\lambda}^\lambda(\zeta)$ to be used are arbitrary, but for reactions such as $H + H_2$ which favor reaction through collinear geometries, the most efficient set for this purpose (as will be explained in more detail below) are the functions $\phi_{v_\lambda}^\lambda(\zeta; \eta_{\lambda_0})$ defined along the cut $\eta_\lambda = \eta_{\lambda_0}$ and which will be denoted by $\phi_{v_\lambda}^\lambda(\zeta)$ simply. The transformation equations associated with the change in the vibrational basis set are given by equations similar to Eqs. (3.41) and (3.53), where a different overlap matrix will be generated for each subregion i. We will denote the new "g" function thus obtained by $g_{J v_\lambda j_\lambda}^{\lambda v_\lambda' j_\lambda' i}(\eta_\lambda)$ (we will omit the parameter η_{λ_0}). With this change of vibrational basis, we can write a single expression for $\Psi_J^{\lambda v_\lambda' j_\lambda' i}$ valid throughout all of Region IV:

$$\Psi_J^{\lambda v_\lambda' j_\lambda' i}(\theta_\lambda, \zeta, \eta_\lambda, \gamma_\lambda) = \frac{\sqrt{2}\varphi_J(\theta_\lambda)}{\zeta^{3/2}(\sin 2\eta_\lambda)^{1/2}} \Phi_J^{\lambda v_\lambda' j_\lambda' i}(\zeta, \eta_\lambda, \gamma_\lambda), \tag{4.2}$$

where

$$\Phi_J^{\lambda v_\lambda' j_\lambda' i} = \sum_{v_\lambda j_\lambda} \varphi_{j_\lambda}(\gamma_\lambda)\phi_{v_\lambda}^\lambda(\zeta) g_{J v_\lambda j_\lambda}^{\lambda v_\lambda' j_\lambda' i}(\eta_\lambda). \tag{4.3}$$

On the matching surface $\pi_{\nu\lambda}$, η_λ and γ_λ are related to each other by the equation [from Eqs. (A14) and (3.18)]

$$\cot 2\eta_\lambda = -\cot\alpha_{\nu\lambda}\cos\gamma_\lambda, \quad 0 \le \gamma_\lambda \le \frac{\pi}{2} \text{ and } \frac{3\pi}{2} \le \gamma_\lambda < 2\pi. \tag{4.4}$$

Hence, if we substitute $\eta_\lambda(\gamma_\lambda)$ as obtained from Eq. (4.4) into Eqs. (4.2) and (4.3), we obtain the desired wavefunction on $\pi_{\nu\lambda}$.

In order to insure a smooth matching of the wavefunctions, we need also to match the derivative of the wavefunction of Eqs. (4.2) and (4.3) at the matching surfaces. Although many types of derivatives are possible, the normal derivative $\partial/\partial n_{\nu\lambda}$ to the matching half-plane possesses many useful mathematical properties (some of which are seen below), and for this reason we will consider it in the following discussion. Expressions for $\partial/\partial n_{\nu\lambda}$ in terms of ζ, η_λ, and γ_λ are derived in Appendix A [Eq. (A18)]. Since these are internal configuration coordinates (i. e., those on which V^λ depends) we are free to choose any one external variable (such as θ_λ or θ_ν) to hold constant during the differentiation process. We must, however, use this same variable in deriving all equations concerning the derivative matching on $\pi_{\nu\lambda}$. Choosing this external variable to be θ_λ and introducing Eq. (A18) into Eqs. (4.2) and (4.3), and then using Eq. (4.4) to express everything on the matching surface, we obtain

$$\frac{\partial \Psi_J^{\lambda v_\lambda' j_\lambda' i}}{\partial n_{\nu\lambda}} = \frac{\sqrt{2}\varphi_J(\theta_\lambda)\sin\alpha_{\nu\lambda}}{\zeta^{5/2}(\sin 2\eta_\lambda)^{3/2}} \Phi_J'^{\lambda v_\lambda' j_\lambda' i}(\zeta, \gamma_\lambda), \tag{4.5}$$

where

$$\Phi_J'^{\lambda v_\lambda' j_\lambda' i}(\zeta, \gamma_\lambda)$$
$$= \sum_{v_\lambda j_\lambda} \phi_{v_\lambda}^\lambda(\zeta)\varphi_{j_\lambda}(\gamma_\lambda)\left(\frac{1}{2}\frac{dg_{J v_\lambda j_\lambda}^{\lambda v_\lambda' j_\lambda' i}}{d\eta_\lambda} + \cot\alpha_{\nu\lambda}(\tfrac{1}{2}\cos\gamma_\lambda \right.$$
$$\left. + i j_\lambda \sin\gamma_\lambda)g_{J v_\lambda j_\lambda}^{\lambda v_\lambda' j_\lambda' i}[\eta_\lambda(\gamma_\lambda)] \right). \tag{4.6}$$

The derivative $dg/d\eta_\lambda$ must be evaluated by allowing η_λ to be independent of γ_λ before the expression $\eta_\lambda = \eta_\lambda(\gamma_\lambda)$ given by Eq. (4.4) is used.

We now wish to expand the functions $\Phi_J^{\lambda v_\lambda' j_\lambda' i}$ and $\Phi_J'^{\lambda v_\lambda' j_\lambda' i}$ on the matching surface $\pi_{\nu\lambda}$ in terms of a set of basis functions $B_{v_\lambda j_\lambda}^{\nu\lambda}$ which span that surface, ζ and γ_λ being the independent variables. We choose the $B_{v_\lambda j_\lambda}^{\nu\lambda}$ to be

$$B_{v_\lambda j_\lambda}^{\nu\lambda}(\zeta, \gamma_\lambda) = \phi_{v_\lambda}^\lambda(\zeta) A_{j_\lambda}^{\nu\lambda}(\gamma_\lambda), \tag{4.7}$$

where the $\phi_{v_\lambda}^\lambda$'s were defined above [in the paragraph preceding Eq. (4.2)], and the $A_{j_\lambda}^{\nu\lambda}(\gamma_\lambda)$ are a set of rotational functions which we shall require to be orthonormal and complete on the domain $0 \le \gamma_\lambda \le \tfrac{1}{2}\pi$, $\tfrac{1}{3}3\pi \le \gamma_\lambda < 2\pi$. For convenience, we will also impose the condition that $A_{j_\lambda}^{\nu\lambda}(\gamma_\lambda)$ be real and that

$$A_{j_\lambda}^{\nu_\lambda}(\gamma_\lambda) = (-1)^{j_\lambda} A_{j_\lambda}^{\nu_\lambda}(2\pi - \gamma_\lambda) . \qquad (4.8)$$

This is not a significantly restrictive assumption, and will lead to matching equations involving only real quantities.

The crucial characteristic in our choice of the rotational basis functions A is that they be complete for the domain $0 \leq \gamma_\lambda \leq \frac{1}{2}\pi$, $\frac{1}{2}3\pi \leq \gamma_\lambda < 2\pi$. This contrasts with the 0 to 2π interval over which the asymptotic rotational functions $\varphi_{j_\lambda}(\gamma_\lambda)$ are complete. What we have actually done is to divide the domain of γ_λ into two equal subdomains: (a) 0 to $\frac{1}{2}\pi$ and $\frac{1}{2}3\pi$ to 2π, on which we choose the $\pi_{\nu\lambda}$ rotational functions $A_{j_\lambda}^{\nu_\lambda}(\gamma_\lambda)$, and (b) $\frac{1}{2}\pi$ to $\frac{1}{2}3\pi$, where we use the analogous functions $A_{j_\lambda}^{\kappa_\lambda}(\gamma_\lambda)$ which span $\pi_{\lambda\kappa}$. The union $A_{j_\lambda}^\lambda(\gamma_\lambda)$ of the two sets of functions $\{A_{j_\lambda}^{\nu_\lambda}, A_{j_\lambda}^{\kappa_\lambda}\}$ forms a set of rotational functions which spans $(0, 2\pi)$ and this allows us to establish a one-to-one correspondence between the rotational functions $A_{j_\lambda}^\lambda$ which span the pair of matching surfaces $\pi_{\nu\lambda}$ and $\pi_{\lambda\kappa}$, and the asymptotic functions $\varphi_{j_\lambda}^\lambda(\gamma_\lambda)$. More specifically, if we have N vibration–rotation basis functions asymptotically in arrangement channel λ, the sum of the number of $B^{\nu\lambda}$ and $B^{\lambda\kappa}$ functions must be N. For a symmetric reaction (i.e., one in which channels ν and κ are equivalent), we must use $N/2$ functions in each of these two sets. In this case, the rotational quantum numbers j_λ spanned by the $B_{\nu_\lambda j_\lambda}^{\nu\lambda}$ (for each vibrational quantum number v_λ) include only one-half of those spanned by the asymptotic functions φ_{j_λ}. The number of the latter should in such cases be even, which is not a severe constraint.

We now discuss possible choices for the functions $A_{j_\lambda}^{\nu\lambda}$. Two sets of functions which are both orthonormal and complete over the range $0 \leq \gamma_\lambda \leq \frac{1}{2}\pi$ and $\frac{1}{2}3\pi \leq \gamma_\lambda < 2\pi$ are $(\pi)^{-1/2}\exp(2ij_\lambda\gamma_\lambda)$ and $(\pi)^{-1/2}\exp[(2j_\lambda + 1)i\gamma_\lambda]$ for $j_\lambda = 0, \pm1, \pm2, \ldots$ These do not satisfy the condition of Eq. (4.8), but certain linear combinations of them do such as (a) $(\pi)^{-1/2}$, $(2/\pi)^{1/2}\cos2\gamma_\lambda$, $(2/\pi)^{1/2}\sin2\gamma_\lambda$, $(2/\pi)^{1/2}\cos4\gamma_\lambda$, $(2/\pi)^{1/2}\sin4\gamma_\lambda$, ..., and (b) $(2/\pi)^{1/2}\sin\gamma_\lambda$, $(2/\pi)^{1/2}\cos\gamma_\lambda$, $(2/\pi)^{1/2}\sin3\gamma_\lambda$, $(2/\pi)^{1/2}\cos3\gamma_\lambda$, ... We can also choose mixtures of (a) and (b) above such as (c) $(2/\pi)^{1/2}\cos\gamma_\lambda$, $(2/\pi)^{1/2}\sin2\gamma_\lambda$, $(2/\pi)^{1/2}\cos3\gamma_\lambda$, ... This last set of functions (corresponding to $j_\lambda = 0, 1, 2, \ldots$, respectively) has the property that all its members vanish at $\gamma_\lambda = \pi/2$ and $3\pi/2$. This makes these functions very efficient for expanding the wavefunctions for certain reactions, as described below. An alternative to analytical functions would be a numerically determined set such as the rotational eigenfunctions for some approximate potential on the matching surface. To see what these functions might look like for H + H$_2$, in Fig. 6 we plot contours of the Porter–Karplus potential[31] on the two-dimensional matching half-plane $\pi_{\nu\lambda}$. The lines converging at the origin are intersections of $\pi_{\nu\lambda}$ with $\gamma_\lambda =$ constant planes and correspond therefore to constant values of η_λ. The figure indicates that only the region of the matching surface for which γ_λ is in the range 0–60° and 300°–360° (and η_λ in the range $\eta_{\lambda_0} = 30°$–36.9°) has a low enough potential energy to contribute significantly to the reaction at energies less than 1 eV. This implies that we should choose a basis set $B^{\nu\lambda}$ which describes the wavefunction best near
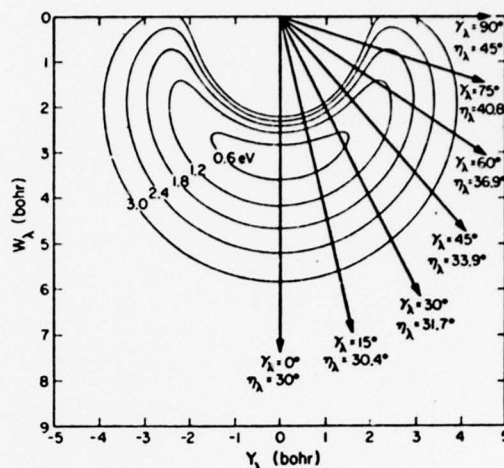
FIG. 6. Plot of equipotential contours on the matching surface $\pi_{\nu\lambda}$ for the H + H$_2$ reaction in the Cartesian coordinate system W_λ, Y_λ, where $W_\lambda = (X_\lambda^2 \sin^2\alpha_{\nu\lambda} + Z_\lambda^2 \cos^2\alpha_{\nu\lambda})^{1/2}$ and the system X_λ, Y_λ, Z_λ is the one described in Sec. III.A. Because of the symmetry of the H$_3$ system, Fig. 6 is equivalent to the lower half of Fig. 2(c) since the $Z_\lambda < 0$ half-plane of the $OY_\lambda Z_\lambda$ plane is for this system the same as the $\pi_{\kappa\nu}$ matching plane. The half-lines emanating from the origin correspond to constant values of γ_λ and η_λ, as indicated. To each such half-line, for which $\gamma_\lambda = \bar\gamma_\lambda$, there corresponds a symmetric one with respect to the vertical axis, having the same value of η_λ and a value of $\gamma_\lambda = 360° - \bar\gamma_\lambda$ in the 270° to 360° range.

$\gamma_\lambda = 0$, i.e., near $\eta_\lambda = \eta_{\lambda_0}$. For this reason, we previously chose the vibrational eigenfunctions $\phi_{\nu_\lambda}^\lambda(\zeta)$ to be solutions to Eq. (3.5) for $\eta_\lambda = \eta_{\lambda_0}$. [See paragraph preceding Eq. (4.2)]. Although there is no single γ_λ-dependent rotational potential which describes the rotational motion on the matching surface correctly for all ζ, it should be clear from Fig. 6 that rotational functions which are numerically determined from the potential on the matching surface for a fixed ζ (such as the ζ for which this potential, at $\gamma_\lambda = 0$, has a minimum) will be localized near $\gamma_\lambda = 0$ and must be close to zero near $\gamma_\lambda = \pi/2$ and $3\pi/2$. For this reason, the analytical set (c) should be efficient for expanding the wavefunction on $\pi_{\nu\lambda}$. Finally, we should mention that an important test of the correctness of the method is to demonstrate the invariance of the final converged results with respect to the choice of $A_{j_\lambda}^\lambda$.

We now expand the functions $\Phi_j^{\lambda v_\lambda' j_\lambda' \zeta_\lambda}$ and $\phi_j^{\prime \lambda v_\lambda' j_\lambda' \zeta_\lambda}$ [defined by Eqs. (4.3) and (4.6)] in terms of the matching surface functions $B_{\nu_\lambda j_\lambda}^{\nu\lambda}$ as follows:

$$\Phi_j^{\lambda v_\lambda' j_\lambda' \zeta_\lambda} = \sum_{v_\lambda j_\lambda} \bar{h}_{j v_\lambda j_\lambda}^{\lambda v_\lambda' j_\lambda' \zeta_\lambda} B_{v_\lambda j_\lambda}^{\nu\lambda}(\zeta, \gamma_\lambda) , \qquad (4.9)$$

$$\phi_j^{\prime \lambda v_\lambda' j_\lambda' \zeta_\lambda} = \sum_{v_\lambda j_\lambda} \bar{h}_{j v_\lambda j_\lambda}^{\prime \lambda v_\lambda' j_\lambda' \zeta_\lambda} B_{v_\lambda j_\lambda}^{\nu\lambda}(\zeta, \gamma_\lambda) . \qquad (4.10)$$

Whereas the indices $v_\lambda' j_\lambda'$ assume N values, $v_\lambda j_\lambda$ assume fewer values than that. In view of our previous discussion, $N/2$ is a convenient choice for this number for

the highly symmetric H_3 system. The coefficients $\bar{h}_{j_\nu \lambda j_\lambda}^{\lambda \nu v_\lambda'' j_\lambda''}$ and $\bar{h}_{j_\nu \lambda j_\lambda}^{'\lambda \nu v_\lambda'' j_\lambda''}$ may be found by equating Eq. (4.3) on $\pi_{\nu\lambda}$ with Eq. (4.9), and Eq. (4.6) with Eq. (4.10), multiplying the resulting expressions by $B_{v_\lambda' j_\lambda'}^{v_\lambda}$ and integrating them over ζ and γ_λ. Using the orthonormality of the $B_{v_\lambda j_\lambda}^{v_\lambda}$ functions on the matching surface and Eq. (4.8), and interchanging in the end the $v_\lambda'' j_\lambda''$ indices with the $v_\lambda j_\lambda$ ones, we get

$$\bar{h}_{j_\nu \lambda j_\lambda}^{\lambda v v_\lambda'' j_\lambda''} = \sqrt{\frac{2}{\pi}} \sum_{j_\lambda''} \int_0^{\pi/2} d\gamma_\lambda A_{j_\lambda}^{v\lambda}(\gamma_\lambda) g_{j_\nu v_\lambda j_\lambda''}^{\lambda v_\lambda'' j_\lambda''}[\eta_\lambda(\gamma_\lambda)] \begin{Bmatrix} \cos j_\lambda'' \gamma_\lambda \\ i \sin j_\lambda'' \gamma_\lambda \end{Bmatrix},$$

(4.11)

$$\bar{h}_{j_\nu \lambda j_\lambda}^{'\lambda v v_\lambda'' j_\lambda''} = \frac{1}{\sqrt{2\pi}} \sum_{j_\lambda''} \int_0^{\pi/2} d\gamma_\lambda A_{j_\lambda}^{v\lambda}(\gamma_\lambda) \Big\{ dg_{j_\nu v_\lambda j_\lambda''}^{\lambda v_\lambda'' j_\lambda''}[\eta_\lambda(\gamma_\lambda)]/d\eta_\lambda$$

$$\times \begin{pmatrix} \cos j_\lambda'' \gamma_\lambda \\ i \sin j_\lambda'' \gamma_\lambda \end{pmatrix} + \cot\alpha_{\nu\lambda} \Big[(j_\lambda'' + \tfrac{1}{2}) \begin{pmatrix} \cos(j_\lambda'' + 1)\gamma_\lambda \\ i \sin(j_\lambda'' + 1)\gamma_\lambda \end{pmatrix}$$

$$- (j_\lambda'' - \tfrac{1}{2}) \begin{pmatrix} \cos(j_\lambda'' - 1)\gamma_\lambda \\ i \sin(j_\lambda'' - 1)\gamma_\lambda \end{pmatrix} \Big] g_{j_\nu v_\lambda j_\lambda''}^{\lambda v_\lambda'' j_\lambda''}[\eta_\lambda(\gamma_\lambda)] \Big\},$$

(4.12)

where the upper term in the large parentheses is to be used for even j_λ, and the lower for odd j_λ, and use was made of Eq. (4.8).

We now must consider the expansion of the wavefunction obtained from the iteration in channel ν, in the same matching surface basis functions $B_{v_\lambda j_\lambda}^{v\lambda}$ of Eq. (4.7). To do this we first express the wavefunction and its normal derivative in a form analogous to Eqs. (4.2), (4.3), (4.5), and (4.6). For the wavefunction we get

$$\Psi_j^{v v_\nu j_\nu'} = \frac{\sqrt{2}\,\varphi_j(\theta_\nu)}{\zeta^{3/2}(\sin 2\eta_\nu)^{1/2}} \Phi_j^{v v_\nu j_\nu'}(\zeta, \eta_\nu, \gamma_\nu),$$

(4.13)

where

$$\Phi_j^{v v_\nu j_\nu'} = \sum_{v_\nu j_\nu} \varphi_{j_\nu}(\gamma_\nu) \phi_{v_\nu}^v(\zeta) g_{j_\nu v_\nu j_\nu}^{v v_\nu j_\nu'}(\eta_\nu).$$

(4.14)

The vibrational basis function $\phi_{v_\nu}^v(\zeta)$ is defined in a manner similar to $\phi_{v_\lambda}^\lambda(\zeta)$ and, in fact, may be identical to it (for $v_\nu = v_\lambda$) if the reference potentials are defined appropriately. In terms of the ν arrangement channel coordinates, the relation between η_ν and γ_ν on the matching surface $\pi_{\nu\lambda}$ is given by

$$\cot 2\eta_\nu = \cot\alpha_{\nu\lambda} \cos\gamma_\nu, \quad \tfrac{1}{2}\pi \le \gamma_\nu \le \tfrac{1}{2} 3\pi.$$

(4.15)

This is easily derived from Eq. (4.4), using the relations (A12) and (A15) of the Appendix and Eq. (3.18).

In calculating the normal derivative of the wavefunc-

tion of Eq. (4.13) on the matching surface $\pi_{\nu\lambda}$, we must remember that θ_λ must be held constant during the differentiation. It is therefore desirable to express θ_ν in terms of θ_λ,

$$\theta_\nu = \theta_\lambda + \Delta_{\nu\lambda},$$

(4.16)

where $\Delta_{\nu\lambda}$ is a function of the internal variables R_λ, r_λ, γ_λ only as seen in Eqs. (A9) of the Appendix. If we express those two equations in terms of the variables ζ, η_λ, and γ_λ, then find the normal derivative of $\Delta_{\nu\lambda}$ using Eq. (A18) and finally use Eq. (4.4) to express all quantities on the matching surface $\pi_{\nu\lambda}$, we obtain the very useful equation valid only on this surface:

$$\frac{\partial \Delta_{\nu\lambda}}{\partial n_{\nu\lambda}}(\zeta, \eta_\lambda, \gamma_\lambda) = 0.$$

(4.17)

As a consequence of this simplification, we can express the normal derivative of the wavefunction in arrangement channel ν on $\pi_{\nu\lambda}$ by

$$\frac{\partial \Psi_j^{v v_\nu j_\nu'}}{\partial n_{\nu\lambda}} = \frac{\sqrt{2}\,\varphi_j(\theta_\lambda) e^{i j \Delta_\nu}}{\zeta^{3/2}(\sin 2\eta_\nu)^{3/2}} \Phi_j^{'v v_\nu j_\nu'}(\zeta, \gamma_\nu),$$

(4.18)

where

$$\Phi_j^{'v v_\nu j_\nu'}(\zeta, \gamma_\nu) = \sum_{j_\nu v_\nu} \varphi_{j_\nu}(\gamma_\nu) \phi_{v_\nu}^v(\zeta) \Big[\frac{1}{2} \Big(\frac{dg_{j_\nu v_\nu j_\nu}^{v v_\nu j_\nu'}}{d\eta_\nu} \Big)_{\eta_\nu = \eta_\nu(r_\nu)}$$

$$- \cot\alpha_{\nu\lambda}(\tfrac{1}{2}\cos\gamma_\nu + i j_\nu \sin\gamma_\nu) g_{j_\nu v_\nu j_\nu}^{v v_\nu j_\nu'}[\eta_\nu(\gamma_\nu)] \Big].$$

(4.19)

We now expand the functions $\Phi_j^{v v_\nu j_\nu'}$ and $\Phi_j^{'v v_\nu j_\nu'}$ in terms of the matching surface functions $B_{v_\nu j_\nu}^{v\lambda}(\zeta, \gamma_\lambda)$. Note that we use the λ arrangement channel variables to express the ν arrangement channel wavefunction, using the transformation equations (A12), (A14), and (3.18) to relate the λ and ν sets of variables. The resulting expansions are

$$\Phi_j^{v v_\nu j_\nu'}(\zeta, \gamma_\lambda) = \sum_{v_\nu j_\nu} \bar{f}_{j_\nu v_\nu j_\nu}^{v v_\nu j_\nu'} B_{v_\nu j_\nu}^{v\lambda}(\zeta, \gamma_\lambda),$$

(4.20)

$$\Phi_j^{'v v_\nu j_\nu'}(\zeta, \gamma_\lambda) = \sum_{v_\nu j_\nu} \bar{f}_{j_\nu v_\nu j_\nu}^{'v v_\nu j_\nu'} B_{v_\nu j_\nu}^{v\lambda}(\zeta, \gamma_\lambda),$$

(4.21)

where the expansion coefficients are given by

$$\bar{f}_{j_\nu v_\nu j_\nu}^{v v_\nu j_\nu'} = \sqrt{\frac{2}{\pi}} \int_0^{\pi/2} d\gamma_\lambda \sum_{v_\nu' j_\nu'} (-1)^{j_\nu'} S_{v_\nu v_\nu'}^{v\lambda} A_{j_\nu}^{v\lambda}(\gamma_\lambda)$$

$$\times g_{j_\nu v_\nu' j_\nu'}^{v v_\nu j_\nu'}\{\eta_\nu[\gamma_\nu(\gamma_\lambda)]\} \begin{Bmatrix} \cos j_\nu'' \gamma_\lambda \\ i \sin j_\nu'' \gamma_\lambda \end{Bmatrix},$$

(4.22)

$$\bar{f}_{j_\nu v_\nu j_\nu}^{'v v_\nu j_\nu'} = -\frac{1}{\sqrt{2\pi}} \int_0^{\pi/2} d\gamma_\lambda \sum_{v_\nu' j_\nu'} (-1)^{j_\nu'} S_{v_\nu v_\nu'}^{v\lambda} A_{j_\nu}^{v\lambda}(\gamma_\lambda) \Big\{ \Big(\frac{dg_{j_\nu v_\nu' j_\nu'}^{v v_\nu j_\nu'}}{d\eta_\nu} \Big)_{\eta_\nu = \eta_\nu[\gamma_\nu(\gamma_\lambda)]} \begin{pmatrix} \cos j_\nu'' \gamma_\lambda \\ -i \sin j_\nu'' \gamma_\lambda \end{pmatrix}$$

$$+ \cot\alpha_{\nu\lambda} \Big[(j_\nu'' - \tfrac{1}{2}) \begin{pmatrix} \cos(j_\nu'' + 1)\gamma_\lambda \\ -i \sin(j_\nu'' + 1)\gamma_\lambda \end{pmatrix} - (j_\nu'' - \tfrac{1}{2}) \begin{pmatrix} \cos(j_\nu'' - 1)\gamma_\lambda \\ -i \sin(j_\nu'' - 1)\gamma_\lambda \end{pmatrix} \Big] g_{j_\nu v_\nu' j_\nu'}^{v v_\nu j_\nu'}\{\eta_\nu[\gamma_\nu(\gamma_\lambda)]\} \Big\},$$

(4.23)

where

$$S_{v_\nu v_{\nu'}}^{v\lambda} = \int_0^\infty \phi_{b_\nu}^\lambda(\zeta) \phi_{v_{\nu'}}^\nu(\zeta) \, d\zeta \ . \tag{4.24}$$

As before, the upper term in the large parentheses is used for even j_ν and the lower for odd j_ν.

B. The matching equations

With the wavefunctions from the integrations in both channels ν and λ expressed in terms of the basis set $B_{v_\lambda j_\lambda}^{r\lambda}(\zeta, \gamma_\lambda)$ on $\pi_{\nu\lambda}$, we can now take the appropriate linear combinations of these solutions to yield solutions to the full Schrödinger equation which are continuous and smooth throughout all of configuration space. Let us denote the fully matched solutions thus obtained by $\Psi_J^{(i)\nu j}$. There are N sets of indices νj, and the superscript (i) can have the values 1, 2, or 3. The full set of indices $(i)\nu j$ thus scans $3N$ values, and we will therefore obtain $3N$ linearly independent solutions to the Schrödinger equation.[37]

We now write $\Psi_J^{(i)\nu j}$ in terms of the solutions $\Psi_J^{\lambda v_\lambda j_\lambda \bullet}$ and also in terms of the $\Psi_J^{\nu v_\nu j_\nu \bullet}$:

$$\Psi_J^{(i)\nu j} = \sum_{v_\lambda' j_\lambda'} \left(\Psi_J^{\lambda v_\lambda' j_\lambda' \bullet} C_{J\lambda v_\lambda' j_\lambda'}^{(i)\nu j \bullet} + \Psi_J^{\lambda v_\lambda' j_\lambda' -} C_{J\lambda v_\lambda' j_\lambda'}^{(i)\nu j -} \right)$$

$$= \sum_{v_\nu' j_\nu'} \left(\Psi_J^{\nu v_\nu' j_\nu' \bullet} C_{J\nu v_\nu' j_\nu'}^{(i)\nu j \bullet} + \Psi_J^{\nu v_\nu' j_\nu' -} C_{J\nu v_\nu' j_\nu'}^{(i)\nu j -} \right) \tag{4.25}$$

and

$$\frac{\partial \Psi_J^{(i)\nu j}}{\partial n_{\nu\lambda}} = \sum_{v_\lambda' j_\lambda'} \left(\frac{\partial \Psi_J^{\lambda v_\lambda' j_\lambda' \bullet}}{\partial n_{\nu\lambda}} C_{J\lambda v_\lambda' j_\lambda'}^{(i)\nu j \bullet} + \frac{\partial \Psi_J^{\lambda v_\lambda' j_\lambda' -}}{\partial n_{\nu\lambda}} C_{J\nu v_\lambda' j_\lambda'}^{(i)\nu j -} \right)$$

$$= \sum_{v_\nu' j_\nu'} \left(\frac{\partial \Psi_J^{\nu v_\nu' j_\nu' \bullet}}{\partial n_{\nu\lambda}} C_{J\nu v_\nu' j_\nu'}^{(i)\nu j \bullet} + \frac{\partial \Psi_J^{\nu v_\nu' j_\nu' -}}{\partial n_{\nu\lambda}} C_{J\nu v_\nu' j_\nu'}^{(i)\nu j -} \right) \ . \tag{4.26}$$

The coefficients $C_{J\lambda v_\lambda' j_\lambda'}^{(i)\nu j \bullet}$ and $C_{J\nu v_\nu' j_\nu'}^{(i)\nu j \bullet}$ are to be determined by applying these two sets of equations on $\pi_{\nu\lambda}$ (and similar equations on $\pi_{\kappa\nu}$ and $\pi_{\lambda\kappa}$), and by imposing the scattering solution boundary conditions as explained in Sec. V.A. Equations (4.25) and (4.26), when evaluated on $\pi_{\nu\lambda}$, comprise the smooth matching conditions.

By substituting Eqs. (4.2), (4.13), and (4.16) into Eqs. (4.25), we obtain the following expression:

$$\sum_{v_\lambda' j_\lambda'} \left(\Phi_J^{\lambda v_\lambda' j_\lambda' \bullet} C_{J\lambda v_\lambda' j_\lambda'}^{(i)\nu j \bullet} + \Phi_J^{\lambda v_\lambda' j_\lambda' -} C_{J\lambda v_\lambda' j_\lambda'}^{(i)\nu j -} \right)$$

$$= e^{iJ\Delta_{\nu\lambda}} \sum_{v_\nu' j_\nu'} \left(\Phi_J^{\nu v_\nu' j_\nu' \bullet} C_{J\nu v_\nu' j_\nu'}^{(i)\nu j \bullet} + \Phi_J^{\nu v_\nu' j_\nu' -} C_{J\nu v_\nu' j_\nu'}^{(i)\nu j -} \right) \ . \tag{4.27}$$

The analogous expression for the normal derivatives is obtained from Eq. (4.27) by replacing the Φ by the Φ' in that equation. If we now substitute the expansions given by Eqs. (4.9), (4.10), (4.20), and (4.21) into Eq. (4.27) and into its equivalent for the normal derivatives, then multiply through by $B_{v_\lambda j_\lambda}^{v\lambda}(\zeta, \gamma_\lambda)$, and integrate over ζ and γ_λ, we obtain the following system of linear algebraic equations:

$$\sum_{v_\lambda' j_\lambda'} \left(\bar{h}_{J v_\lambda j_\lambda}^{\lambda v_\lambda' j_\lambda' \bullet} C_{J\lambda v_\lambda' j_\lambda'}^{(i)\nu j \bullet} + \bar{h}_{J v_\lambda j_\lambda}^{\lambda v_\lambda' j_\lambda' -} C_{J\lambda v_\lambda' j_\lambda'}^{(i)\nu j -} \right)$$

$$= \sum_{v_\nu' j_\nu'} (\bar{s}_{\nu\lambda}^J)_{v_\lambda j_\lambda}^{v_\nu j_\nu} \sum_{v_\nu' j_\nu'} \left(\bar{f}_{J v_\nu j_\nu}^{\nu v_\nu' j_\nu' \bullet} C_{J\nu v_\nu' j_\nu'}^{(i)\nu j \bullet} + \bar{f}_{J v_\nu j_\nu}^{\nu v_\nu' j_\nu' -} C_{J\nu v_\nu' j_\nu'}^{(i)\nu j -} \right) , \tag{4.28}$$

with the analogous equation for derivatives obtained by using $\bar{h}'$ and $\bar{f}'$ instead of $\bar{h}$ and $\bar{f}$ above. The matrix $\bar{s}_{\nu\lambda}^J$ is defined by

$$(\bar{s}_{\nu\lambda}^J)_{v_\lambda j_\lambda}^{v_\nu j_\nu} = \delta_{v_\lambda v_\nu} \begin{cases} 2 \int_0^{\pi/2} A_{j_\lambda}^{v\lambda} A_{j_\nu}^{v\lambda} \cos J\Delta_{\nu\lambda} \, d\gamma_\lambda \ \text{for} \ j_\lambda + j_\nu = \text{even} \\ 2i \int_0^{\pi/2} A_{j_\lambda}^{v\lambda} A_{j_\nu}^{v\lambda} \sin J \Delta_{\nu\lambda} \, d\gamma_\lambda \ \text{for} \ j_\lambda + j_\nu = \text{odd} , \end{cases} \tag{4.29}$$

or, by the expression (which is only equivalent to it for a *complete* set of functions $B^{v\lambda}$)

$$\bar{s}_{\nu\lambda}^J = \exp(iJ \Delta^{r\lambda}) , \tag{4.30}$$

where

$$(\Delta^{r\lambda})_{v_\lambda j_\lambda}^{v_\nu j_\nu} = \langle B_{v_\lambda j_\lambda}^{r\lambda} | \Delta_{\nu\lambda} | B_{v_\nu j_\nu}^{r\lambda} \rangle \ . \tag{4.31}$$

As should be evident from Eqs. (4.30) and (4.31), the matrix $\bar{s}_{\nu\lambda}^J$ is unitary since $\Delta_{\nu\lambda}$ is real, and therefore $\Delta^{r\lambda}$ is Hermitian.

By examining the definitions given in Eqs. (4.11), (4.12), (4.22), (4.23), and (4.29) for the various symbols used in Eq. (4.28) and its equivalent for the derivatives, we find that the latter set of equations involve either purely real terms or purely imaginary terms. Let us omit the factor i appearing in Eqs. (4.11), (4.12), (4.22), and (4.23) and replace it in Eq. (4.29) by $(-1)^{j_\nu}$. We denote all of the real coefficients thus obtained by removing the bars which previously appeared above their symbols. Equation (4.28) and its normal derivative counterpart continue to be valid for the unbarred quantities, which permits all of the calculations associated with the matching to be performed using real number arithmetic, a considerable computational simplification. Regarding the real coefficients appearing in these equations as elements of matrices, we can rewrite them as

$$h_J^{\lambda \bullet} C_{J\lambda}^{(i) \bullet} + h_J^{\lambda -} C_{J\lambda}^{(i) -} = s_{\nu\lambda}^J \{ f_J^{\nu \bullet} C_{J\nu}^{(i) \bullet} + f_J^{\nu -} C_{J\nu}^{(i) -} \} \tag{4.32}$$

and

$$h_J^{'\lambda \bullet} C_{J\lambda}^{(i) \bullet} + h_J^{'\lambda -} C_{J\lambda}^{(i) -} = s_{\nu\lambda}^J (f_J^{'\nu \bullet} C_{J\nu}^{(i) \bullet} + f_J^{'\nu -} C_{J\nu}^{(i) -}) \ . \tag{4.33}$$

The matrix $s_{\nu\lambda}^J$ is related to $\bar{s}_{\nu\lambda}^J$ by the unitary transformation $\bar{I}^\dagger \bar{s}_\nu^J \bar{I}$, where $\bar{I}$ is the unitary diagonal matrix whose diagonal elements alternate between 1 and i. Therefore, if the $B^{r\lambda}$ form a complete set, $s_{\nu\lambda}^J$ is unitary, and since it is real it is also orthogonal. As shown in the previous section, the number of basis functions $B_{v_\lambda j_\lambda}^{r\lambda}$ used to expand the wavefunction on $\pi_{\nu\lambda}$ is $N/2$, where N is the total number of vibration–rotation functions used in the coupled-channel expansion. This implies that there should only be $N/2$ rows in the matrices $h_J^{\lambda\pm}$. There are, however, N columns because the different columns denote the N linearly independent solutions propagated in either the forward (+) or backwards (−) integrations. Summarizing, the dimensions of the various matrices in Eqs. (4.32) or (4.33) are symbolically represented as follows:

$(N/2 \times N)(N \times N) + (N/2 \times N)(N \times N)$

$$= (N/2 \times N/2)\left[(N/2 \times N)(N \times N) + (N/2 \times N)(N \times N)\right] . \tag{4.34}$$

We can combine Eqs. (4.32) and (4.33) into a single expression which contains only square $N \times N$ matrices by defining the argumented $N \times N$ matrices $\hat{h}_j^{\lambda \bullet}$, $\hat{f}_j^{\prime \bullet}$, and $\hat{s}_\mu^{\prime}$ as

$$\hat{h}_j^{\lambda \bullet} = \begin{pmatrix} h_j^{\lambda \bullet} \\ h_j^{\lambda \bullet} \end{pmatrix} , \tag{4.35}$$

$$\hat{f}_j^{\prime \bullet} = \begin{pmatrix} f_j^{\prime \bullet} \\ f_j^{\prime \bullet} \end{pmatrix} , \tag{4.36}$$

$$\hat{s}_\mu^{\prime} = \begin{pmatrix} s_\mu^{\prime} & 0 \\ 0 & s_\mu^{\prime} \end{pmatrix} . \tag{4.37}$$

where 0 denotes an $(N/2 \times N/2)$ matrix of zeros. The resulting matching equation on $\pi_{\mu\lambda}$ becomes

$$\hat{h}_j^{\lambda \bullet} C_{j\lambda}^{(1)\bullet} + \hat{h}_j^{\lambda -} C_{j\lambda}^{(1)-} = \hat{s}_\mu^{\prime} \left(\hat{f}_j^{\prime \bullet} C_{j\nu}^{(1)\bullet} + \hat{f}_j^{\prime -} C_{j\nu}^{(1)-} \right) . \tag{4.38}$$

In order to solve for the unknown coefficient matrices $C_{j\lambda}^{(1)\bullet}$, $C_{j\nu}^{(1)\bullet}$ (and $C_{j\lambda}^{(1)\bullet}$), we must couple Eq. (4.38) with the corresponding equations obtained from the matching on $\pi_{\mu\nu}$ and $\pi_{\lambda\kappa}$. Using the same notation as in Eq. (4.38), the matching equations on these two additional surfaces are

$$\hat{h}_j^{\nu \bullet} C_{j\nu}^{(1)\bullet} + \hat{h}_j^{\nu -} C_{j\nu}^{(1)-} = \hat{s}_\nu^{\prime} \left(\hat{f}_j^{\nu \bullet} C_{j\kappa}^{(1)\bullet} + \hat{f}_j^{\nu -} C_{j\kappa}^{(1)-} \right) \tag{4.39}$$

and

$$\hat{h}_j^{\kappa \bullet} C_{j\kappa}^{(1)\bullet} + \hat{h}_j^{\kappa -} C_{j\kappa}^{(1)-} = \hat{s}_{\lambda\kappa}^{\prime} \left(\hat{f}_j^{\kappa \bullet} C_{j\lambda}^{(1)\bullet} + \hat{f}_j^{\kappa -} C_{j\lambda}^{(1)-} \right) . \tag{4.40}$$

We can now combine Eqs. (4.38), (4.39), and (4.40) into the following single matrix equation which involves square matrices of dimension $3N \times 3N$:

$$N_j^{\star} C_j^{\star} + N_j^{-} C_j^{-} = 0 , \tag{4.41}$$

where

$$N_j^{\star} = \begin{pmatrix} \hat{h}_j^{\lambda \bullet} & -\hat{s}_\mu^{\prime} \hat{f}_j^{\prime \bullet} & 0 \\ 0 & \hat{h}_j^{\nu \bullet} & -\hat{s}_\nu^{\prime} \hat{f}_j^{\nu \bullet} \\ -\hat{s}_{\lambda\kappa}^{\prime} \hat{f}_j^{\kappa \bullet} & 0 & \hat{h}_j^{\kappa \bullet} \end{pmatrix} , \tag{4.42}$$

$$C_j^{\star} = \begin{pmatrix} C_{j\lambda}^{(1)\bullet} & C_{j\lambda}^{(2)\bullet} & C_{j\lambda}^{(3)\bullet} \\ C_{j\nu}^{(1)\bullet} & C_{j\nu}^{(2)\bullet} & C_{j\nu}^{(3)\bullet} \\ C_{j\kappa}^{(1)\bullet} & C_{j\kappa}^{(2)\bullet} & C_{j\kappa}^{(3)\bullet} \end{pmatrix} , \tag{4.43}$$

and the 0 stands for a matrix of zeros of the appropriate dimensionality. Let us rearrange Eq. (4.41) to the form

$$C_j^{\star} (C_j^{-})^{-1} = - (N_j^{\star})^{-1} N_j^{-} . \tag{4.44}$$

Equation (4.44) is the essential result of the smooth matching procedure. It expresses the unknown coefficients $C_j^{\star}$ in terms of the known $N_j^{\star}$ and thus determines which linear combination of the solutions obtained from the integrations in each arrangement channel region will produce smoothly matched wavefunctions. Of course, Eq. (4.44) supplies only one $3N \times 3N$ matrix

equation for the two $3N \times 3N$ unknown matrices $C_j^{\star}$. This tells us that our matched solutions are not completely unique, which is not unexpected since we have not yet specified the asymptotic conditions which our matched wavefunctions must satisfy. We will do so in the next section, and when these additional conditions are combined with Eq. (4.44), we will obtain unique expressions for the coefficient matrices $C_j^{\star}$.

V. ASYMPTOTIC ANALYSIS

A. The reactance and scattering matrices

We will now describe how to obtain the reactance (R_j) and scattering (S_j) matrices from the asymptotic values of the primitive (but smoothly matched) solutions $\Psi_j^{(1)\nu j}$ described in the previous section. These functions are defined in the entire configuration space. Their asymptotic behavior in each of the three arrangement channels $\lambda = \alpha, \beta, \gamma$ can be obtained from Eqs. (3.22), (3.5), (2.13), (2.10), and (4.25) and is

$$\Psi_j^{(1)\nu j} \underset{R_\lambda \to \infty}{\sim} \varphi_j(\theta_\lambda) \sum_{v_\lambda j_\lambda} \frac{\varphi_{j_\lambda}(\gamma_\lambda) \phi_{v_\lambda j_\lambda}^\lambda(r_\lambda)}{\sqrt{r_\lambda R_\lambda}}$$

$$\times \sum_{v_\lambda^{\prime} j_\lambda^{\prime}} \left(g_{j v_\lambda j_\lambda}^{\lambda v_\lambda^{\prime} j_\lambda^{\prime} +}(R_\lambda) C_{j\lambda v_\lambda^{\prime} j_\lambda^{\prime}}^{(1)\nu j +} + g_{j v_\lambda j_\lambda}^{\lambda v_\lambda^{\prime} j_\lambda^{\prime} -}(R_\lambda) C_{j\lambda v_\lambda^{\prime} j_\lambda^{\prime}}^{(1)\nu j -} \right)$$

$$\lambda = \alpha, \beta, \gamma , \tag{5.1}$$

where we have dropped the superscript (a) as it will be implicit throughout Sec. V. The product functions $r_\lambda^{-1/2} \varphi_{j_\lambda}(\gamma_\lambda) \phi_{v_\lambda j_\lambda}^\lambda(r_\lambda)$ are the asymptotic vibration–rotation wavefunctions of the diatomic molecule corresponding to the λ arrangement channel. We note that $\phi_{v_\lambda j_\lambda}^\lambda(r_\lambda)$ vanishes in the asymptotic regions of arrangement channels ν and κ because $r_\lambda \to \infty$ in these regions. As a result, Eq. (5.1) can be rewritten as

$$\Psi_j^{(1)\nu j} \sim \sum_\lambda \varphi_j(\theta_\lambda) \sum_{v_\lambda j_\lambda} \frac{\varphi_{j_\lambda}(\gamma_\lambda) \phi_{v_\lambda j_\lambda}^\lambda(r_\lambda)}{\sqrt{r_\lambda R_\lambda}} e_{j\lambda v_\lambda j_\lambda}^{(1)\nu j}(R_\lambda) , \tag{5.2}$$

where

$$e_{j\lambda v_\lambda j_\lambda}^{(1)\nu j} = \sum_{v_\lambda^{\prime} j_\lambda^{\prime}} \left(g_{j v_\lambda j_\lambda}^{\lambda v_\lambda^{\prime} j_\lambda^{\prime} +} C_{j\lambda v_\lambda^{\prime} j_\lambda^{\prime}}^{(1)\nu j +} + g_{j v_\lambda j_\lambda}^{\lambda v_\lambda^{\prime} j_\lambda^{\prime} -} C_{j\lambda v_\lambda^{\prime} j_\lambda^{\prime}}^{(1)\nu j -} \right) , \tag{5.3}$$

and the λ summation extends over arrangement channels α, β, and γ. The analogous expression for the function $R_\lambda^{-1/2}(\partial/\partial R_\lambda)(R_\lambda^{1/2} \Psi_j^{(1)\nu j})$ is obtained from Eqs. (5.2) and (5.3) by replacing $g_{j v_\lambda j_\lambda}^{\lambda v_\lambda^{\prime} j_\lambda^{\prime}}$ by $dg_{j v_\lambda j_\lambda}^{\lambda v_\lambda^{\prime} j_\lambda^{\prime}}/dR_\lambda$ in the latter.

We now define the reactance and scattering matrix solutions for each partial wave J. In analogy with their corresponding three-dimensional multichannel definitions,[38,39] and using the asymptotic behavior of the coplanar solutions given in Eqs. (3.26), we define the reactance and scattering solutions and the corresponding matrices as follows:

$$\Psi_j^{v_\lambda j_\lambda}[R \text{ or } S] \sim \sum_\lambda \varphi_j(\theta_\lambda)$$

$$\sum_{v_\lambda j_\lambda} \frac{\varphi_{j_\lambda}(\gamma_\lambda) \phi_{v_\lambda j_\lambda}^\lambda(r_\lambda)}{\sqrt{r_\lambda R_\lambda}} b_{j\lambda v_\lambda j_\lambda}^{v_\lambda j_\lambda}[R \text{ or } S] , \tag{5.4}$$

where, for the R_j matrix solution,

$$b_{J\lambda v_\lambda j_\lambda}^{\lambda' v_\lambda' j_\lambda'}[R] = \left(\frac{\mu R_\lambda}{\hbar}\right)^{1/2} \begin{cases} J_{J-j_\lambda}(k_{v_\lambda j_\lambda}^\lambda R_\lambda)\,\delta_{\lambda' v_\lambda' j_\lambda'}^{\lambda v_\lambda j_\lambda} + Y_{J-j_\lambda}(k_{v_\lambda j_\lambda} R_\lambda)\,R_{J\lambda' v_\lambda' j_\lambda'}^{\lambda v_\lambda j_\lambda}, & \text{(for the open channels)} \\[12pt] I_{J-j_\lambda}(|k_{v_\lambda j_\lambda}^\lambda|R_\lambda)\,\delta_{\lambda' v_\lambda' j_\lambda'}^{\lambda v_\lambda j_\lambda} + K_{J-j_\lambda}(|k_{v_\lambda j_\lambda}|R_\lambda)\,R_{J\lambda' v_\lambda' j_\lambda'}^{\lambda v_\lambda j_\lambda}, & \text{(for the closed channels)}, \end{cases} \quad (5.5)$$

and for the $\mathbf{S}_J$ matrix solution

$$b_{J v_\lambda j_\lambda}^{\lambda' v_\lambda' j_\lambda'}[S] = \left(\frac{\mu R_\lambda}{\hbar}\right)^{1/2} \begin{cases} H_{J-j_\lambda}^{(2)}(k_{v_\lambda j_\lambda}^\lambda R_\lambda)\,\delta_{\lambda' v_\lambda' j_\lambda'}^{\lambda v_\lambda j_\lambda} + H_{J-j_\lambda}^{(1)}(k_{v_\lambda j_\lambda}^\lambda R_\lambda)\,S_{J\lambda' v_\lambda' j_\lambda'}^{\lambda v_\lambda j_\lambda}, & \text{(for the open channels)} \\[12pt] I_{J-j_\lambda}(|k_{v_\lambda j_\lambda}^\lambda|R_\lambda)\,\delta_{\lambda' v_\lambda' j_\lambda'}^{\lambda v_\lambda j_\lambda} + K_{J-j_\lambda}(|k_{v_\lambda j_\lambda}^\lambda|R_\lambda)\,S_{J\lambda' v_\lambda' j_\lambda'}^{\lambda v_\lambda j_\lambda}, & \text{(for the closed channels)}, \end{cases} \quad (5.6)$$

and the Hankel functions H_l are related to the Bessel functions J_l, Y_l by

$$H_l^{(1,2)} = J_l \pm iY_l \ . \tag{5.7}$$

The asymptotic sign in Eq. (5.4) signifies that for each λ in the summation the corresponding R_λ goes to infinity. The $\mathbf{R}_J$ and $\mathbf{S}_J$ matrices defined in Eqs. (5.5) and (5.6) have dimension $3N \times 3N$ and include both open and closed channel initial and final states. Only the open → open transitions have direct physical significance, and we will label the submatrices formed by the corresponding matrix elements by the symbols $\mathbf{R}_J^0$ and $\mathbf{S}_J^0$. It is these open channel matrices $\mathbf{R}_J^0$ and $\mathbf{S}_J^0$ which obey the usual properties that $\mathbf{R}_J^0$ is real and symmetric and $\mathbf{S}_J^0$ is unitary and symmetric,[24] as a result of the time reversal invariance and conservation of flux properties of the Schrödinger equation. Actually, Eqs. (5.4)–(5.7) are expressed in terms of the mass-scaled variables r_λ, R_λ of Eqs. (2.2a) and (2.2b), whereas the reactive and scattering matrices we are interested in are defined in terms of equivalent expressions involving the unscaled $\bar{r}_\lambda$, $\bar{R}_\lambda$. However, Eq. (5.4) and its unscaled variable counterpart are proportional to one another, and as a result $\mathbf{R}_J$ and $\mathbf{S}_J$ are invariant under the r_λ, $R_\lambda \to \bar{r}_\lambda$, $\bar{R}_\lambda$ transformation; this permits us to use directly the unbarred variable results to calculate these matrices. From Eqs. (5.7), Eqs. (5.5) and (5.6), we can obtain the following relation between the open channel subblocks of the reactance and scattering matrices, analogous to the one valid for three dimensions[38,39]:

$$\mathbf{S}_J^0 = (\mathbf{I} - i\mathbf{R}_J^0)(\mathbf{I} + i\mathbf{R}_J^0)^{-1} \ . \tag{5.8}$$

where $\mathbf{I}$ is the identity matrix. We will discuss the physical significance of the scattering matrix at the end of this section.

Let us indicate how $\mathbf{R}_J$ can be obtained from the numerically determined solutions $\psi_J^{(i)v j}$. We rewrite Eqs. (5.3) and (5.5) in $3N \times 3N$ matrix form as

$$\mathbf{e}_J = \mathbf{g}_J^+ \mathbf{C}_J^+ + \mathbf{g}_J^- \mathbf{C}_J^- \tag{5.9}$$

and

$$\mathbf{b}_J = \mathbf{V}^{-1/2}(\mathbf{J}_J + \mathbf{Y}_J \tilde{\mathbf{R}}_J) \ , \tag{5.10}$$

where

$$(\mathbf{g}_J^\pm)_{\lambda v_\lambda j_\lambda}^{\lambda' v_\lambda' j_\lambda'} = \delta_{\lambda\lambda'}\, g_{J v_\lambda j_\lambda}^{\lambda' v_\lambda' j_\lambda'} \ , \tag{5.11}$$

$$(\mathbf{V}^{-1/2})_{\lambda v_\lambda j_\lambda}^{\lambda' v_\lambda' j_\lambda'} = \delta_{\lambda\lambda'}\,\delta_{v_\lambda j_\lambda}^{v_\lambda' j_\lambda'}\,(V_{v_\lambda j_\lambda}^\lambda)^{-1/2} \ , \tag{5.12a}$$

$$V_{v_\lambda j_\lambda}^\lambda = \hbar k_{v_\lambda j_\lambda}^\lambda / \mu \ , \tag{5.12b}$$

$$(\mathbf{J}_J)_{\lambda v_\lambda j_\lambda}^{\lambda' v_\lambda' j_\lambda'} = \delta_{\lambda\lambda'}\,\delta_{v_\lambda j_\lambda}^{v_\lambda' j_\lambda'}\,(|k_{v_\lambda j_\lambda}|R_\lambda)^{1/2} \\ \times \begin{cases} J_{J-j_\lambda}(k_{v_\lambda j_\lambda}^\lambda R_\lambda) & \text{(open channels)} \\ I_{J-j_\lambda}(|k_{v_\lambda j_\lambda}^\lambda|R_\lambda) & \text{(closed channels)}, \end{cases} \tag{5.13}$$

$$(\mathbf{Y}_J)_{\lambda v_\lambda j_\lambda}^{\lambda' v_\lambda' j_\lambda'} = \delta_{\lambda\lambda'}\,\delta_{v_\lambda j_\lambda}^{v_\lambda' j_\lambda'}\,(|k_{v_\lambda j_\lambda}^\lambda|R_\lambda)^{1/2} \\ \times \begin{cases} Y_{J-j_\lambda}(k_{v_\lambda j_\lambda}^\lambda R_\lambda) & \text{(open channels)} \\ K_{J-j_\lambda}(|k_{v_\lambda j_\lambda}^\lambda|R_\lambda) & \text{(closed channels)}, \end{cases} \tag{5.14}$$

and $\tilde{\mathbf{R}}_J$ is the transpose of $\mathbf{R}_J$. The elements of the $\mathbf{e}_J$ and $\mathbf{b}_J$ matrices are the $c_{J\lambda v_\lambda j_\lambda}^{(i)v j}$ and $b_{J\lambda v_\lambda j_\lambda}^{(i)v j}[R]$, respectively. In all these matrix elements, the subscripts other than J denote the row and the superscripts the column to which they belong. The reactance matrix solution $\psi_J^{\lambda' v_\lambda' j_\lambda'}[R]$ can be obtained from our numerically determined solutions $\psi_J^{(i)v j}$ by taking linear combinations of the latter:

$$\psi_J^{\lambda' v_\lambda' j_\lambda'}[R] = \sum_{i=1}^3 \sum_{v j} \psi_J^{(i)v j}\, Q_{(i)v j}^{J\lambda' v_\lambda' j_\lambda'} \ . \tag{5.15}$$

As was mentioned at the end of Sec. IV, the matching equation [Eq. (4.44)] determines $\mathbf{C}_J^+ (\mathbf{C}_J^-)^{-1}$ but not $\mathbf{C}_J^+$ or $\mathbf{C}_J^-$ individually. To complete their evaluation we choose $Q_{(i)v j}^{i\lambda' v_\lambda' j_\lambda'} = \delta_{(i)v j}^{\lambda' v_\lambda' j_\lambda'}$ in Eq. (5.15), which is equivalent to requiring that the $\mathbf{C}_J^\pm$ produce solutions which are not only smoothly matched, but satisfy the reactance asymptotic conditions as well. (It will soon become apparent that there are enough degrees of freedom left over to permit this condition to be imposed.) We then substitute Eqs. (5.2) and (5.4) into Eq. (5.15) and equate coefficients of terms having the same arrangement channel λ and vibration–rotation basis functions $r_\lambda^{-1/2}\varphi_{j_\lambda}(\gamma_\lambda)\phi_{v_\lambda j_\lambda}^\lambda(r_\lambda)$. Expressing the resulting equations in matrix form and using Eqs. (5.9) and (5.10), we obtain

$$(\mathbf{g}_J^+ \mathbf{C}_J^+ + \mathbf{g}_J^- \mathbf{C}_J^-) = \mathbf{V}^{-1/2}(\mathbf{J}_J + \mathbf{Y}_J \tilde{\mathbf{R}}_J) \ . \tag{5.16}$$

The analogous equation for the derivative $(R_\lambda)^{-1/2}(\partial/\partial R_\lambda)[(R_\lambda)^{1/2}\psi_J[R]]$ is

$$(\mathbf{g}_J'^+ \mathbf{C}_J^+ + \mathbf{g}_J'^- \mathbf{C}_J^-) = \mathbf{V}^{-1/2}(\mathbf{J}_J' + \mathbf{Y}_J' \tilde{\mathbf{R}}_J) \ , \tag{5.17}$$

where prime denotes differentiation with respect to R_λ, with $\lambda = \alpha$, β, γ as appropriate. These last two equa-

tions and Eq. (4.44) can then be simultaneously solved to yield the following expression for $\bar{R}_J$:

$$\bar{R}_J = - V^{1/2} W_J^{-1} [(J_J' \, \theta_J') (N_J')^{-1} N_J - (J_J' \theta_J' - J_J \theta_J')]$$
$$\times [(Y_J' \theta_J' - Y_J \theta_J')(N_J')^{-1} N_J - (Y_J' \theta_J - Y_J \theta_J')]^{-1} W_J V^{-1/2} \quad (5.18)$$

where

$$W_J = Y_J' J_J - J_J' Y_J \quad (5.19)$$

is the diagonal matrix whose diagonal elements are the Wronskians of the regular and irregular ordinary or modified Bessel functions.[33] None of the matrices whose inverses appear in Eq. (5.18) are in general singular. Transposition of Eq. (5.18) gives R_J, and Eqs. (5.18) and (4.44) when substituted into Eqs. (5.16) or (5.17) permit an explicit and unique determination of C_J^+ and C_J^-.

The procedure just described furnished the full R_J matrix. Its closed channel parts may now be discarded and the open channel part of the scattering matrix S_J^0 may then be used to calculate $P_{J \lambda v_\lambda j_\lambda}^{\lambda' v_\lambda' j_\lambda'}$, the probability of transition from a given initial arrangement channel λ' and internal state $v_{\lambda'} j_{\lambda'}$ (for a given total angular momentum quantum number J) through the relation

$$P_{J \lambda v_\lambda j_\lambda}^{\lambda' v_\lambda' j_\lambda'} = |S_{J \lambda v_\lambda j_\lambda}^{0 \lambda' v_\lambda' j_\lambda'}|^2 . \quad (5.20)$$

Note that this is a distinguishable-atom transition probability. Effects of indistinguishability of particles will

be considered in Sec. VI. B. As mentioned in Sec. II. C, the total angular momentum is simply equal to the algebraic sum of the rotational and orbital angular momenta, i.e., $J = j_\lambda + l_\lambda$, which allows us to re-express $P_{J \lambda v_\lambda j_\lambda}^{\lambda' v_\lambda' j_\lambda'}$ in terms of initial and final orbital angular momenta l_λ and $l_{\lambda'}$. This has a useful semiclassical interpretation since the initial orbital angular momentum quantum number l_λ is related to the classical impact parameter b_λ through the relation

$$l_\lambda = \bar{k}_{v_\lambda j_\lambda}^\lambda b_\lambda , \quad (5.21)$$

where $\bar{k}_{v_\lambda j_\lambda}^\lambda$ is the wave number in the $\bar{R}_\lambda$, $\bar{r}_\lambda$ coordinate system (defined in Sec. II. B)

$$\bar{k}_{v_\lambda j_\lambda}^\lambda = \left(\frac{2\mu_\lambda v_\pi}{\hbar^2} (E - \epsilon_{v_\lambda j_\lambda}^\lambda) \right)^{1/2}$$
$$= a_\lambda k_{v_\lambda j_\lambda}^\lambda . \quad (5.22)$$

B. Distinguishable-atom scattering amplitudes and cross sections

In this section we define a coplanar dimensionless distinguishable-atom scattering amplitude and give its relation to the coplanar scattering matrix and differential and integral cross sections.

Let $\Psi^{\lambda v_\lambda j_\lambda}[P]$ be a "physical" solution to the Schrödinger equation (2.4), involving the mass-scaled coordinates r_λ, R_λ, which behaves asymptotically at large R_λ, R_ν, and R_π as

$$\Psi^{\lambda v_\lambda j_\lambda}[P] \sim \sum_{\lambda' v_{\lambda'} j_{\lambda'}} \left[\delta_{\lambda v_\lambda j_\lambda}^{\lambda' v_{\lambda'} j_{\lambda'}} e^{i k_{v_{\lambda'} j_{\lambda'}}^\lambda R_{\lambda'} \cos \theta_{\lambda'}} \right.$$
$$\left. + \left(\frac{\hbar}{\mu | V_{v_\lambda j_\lambda}^{\lambda'}|} \right)^{1/2} \hat{f}_{\lambda v_\lambda j_\lambda}^{\lambda' v_{\lambda'} j_{\lambda'}}(\theta_{\lambda'}) R_{\lambda'}^{-1/2} e^{i k_{v_{\lambda'} j_{\lambda'}}^{\lambda'} R_{\lambda'}} \right] \varphi_{j_{\lambda'}}(\theta_{r_{\lambda'}}) r_{\lambda'}^{-1/2} \phi_{v_{\lambda'} j_{\lambda'}}^{\lambda'}(r_{\lambda'}) . \quad (5.23)$$

This solution describes a collision between atom A_λ and molecule $A_\nu A_\pi$ in internal vibrational–rotational state $v_\lambda j_\lambda$, with the relative initial velocity of colliding partners, in scaled coordinates, being $V_{v_\lambda j_\lambda}^\lambda$. The direction of relative approach of the colliding partners is the x axis of Fig. 1. The scaled coordinate relative motion wave number $k_{v_\lambda' j_{\lambda'}}^{\lambda'}$ is real positive for open channels and imaginary positive for closed ones. The first and second $R_{\lambda'}$-dependent terms in Eq. (5.23) represent, respectively, the incident relative motion line wave and the scattered circular wave, which can be nonreactive ($\lambda' = \lambda$) or reactive ($\lambda' \neq \lambda$). These are the 2D analogues of the 3D incident plane wave and scattered spherical waves. The factor outside the square brackets is the planar-motion vibrational–rotational wavefunction of the isolated $A_\nu A_\pi$ molecule in state $v_{\lambda'}$, $j_{\lambda'}$, in scaled coordinates.

Equation (5.23) defines a set of dimensionless distinguishable atom scattering amplitudes $\hat{f}(\theta_{\lambda'})$. The differential cross section for the $\lambda v_\lambda j_\lambda \rightarrow \lambda' v_{\lambda'} j_{\lambda'}$ process (assuming that both these states are open at the total energy E being considered) is related to the corresponding $\hat{f}$ by

$$\sigma_{\lambda v_\lambda j_\lambda}^{\lambda' v_\lambda' j_{\lambda'}}(\theta_{\lambda'}) = (1/\bar{k}_{v_\lambda j_\lambda}^\lambda)|\hat{f}_{\lambda v_\lambda j_\lambda}^{\lambda' v_\lambda' j_{\lambda'}}|^2 , \quad (5.24)$$

where $\bar{k}_{v_\lambda j_\lambda}^\lambda$ is the unscaled initial relative motion wave number of the colliding particles. For either reactive or nonreactive collisions, $\theta_{\lambda'}$ is the angle between the initial and final velocity vectors of the atom with respect to the diatom in the center of mass system Oxy of Fig. 1. The integral cross section for the same process is

$$Q_{\lambda v_\lambda j_\lambda}^{\lambda' v_\lambda' j_{\lambda'}} = \int_0^{2\pi} \sigma_{\lambda v_\lambda j_\lambda}^{\lambda' v_\lambda' j_\lambda}(\theta_{\lambda'}) d\theta_{\lambda'} . \quad (5.25)$$

σ and Q have dimensions of a length per unit angle and of a length, respectively.

We now relate the scattering amplitudes to the scattering matrix. To do this, we expand the physical solution Eq. (5.23) in terms of the scattering matrix solution [Eqs. (5.4) and (5.6)] using an equation analogous to (2.12):

$$\Psi^{\lambda v_\lambda j_\lambda}[P] = \sum_{J = -\infty}^{\infty} C_J^{\lambda v_\lambda j_\lambda} \Psi_J^{\lambda v_\lambda j_\lambda}[S] . \quad (5.26)$$

To find expressions for the coefficients $C_J^{\lambda v_\lambda j_\lambda}$ and the scattering amplitudes $\hat{f}_{\lambda v_\lambda j_\lambda}^{\lambda' v_\lambda' j_{\lambda'}}$, we first expand the $\theta_{\lambda'}$-dependent portions of Eq. (5.23) in terms of the eigenfunctions $\varphi_J(\theta_{\lambda'})$, then express the $R_{\lambda'}$-dependent portions of Eqs. (5.23) and (5.6) in their asymptotic forms

[Eq. (3.27)] involving exponentials. We finally equate the coefficients of the corresponding R_λ exponentials, $\varphi_J(\theta_\lambda)$ and rotation–vibration basis functions in both sides of Eq. (5.26) and solve the resulting equations for $C_J^{\lambda v_\lambda j_\lambda}$ and for the coefficients of the expansion of $\hat{f}_{\lambda v_\lambda j_\lambda}^{\lambda' v_\lambda' j_\lambda'}(\theta_{\lambda'})$ in the $\varphi_J(\theta_{\lambda'})$.

The expansion for the line wave is[10]

$$e^{ik_{v_\lambda,j_\lambda}^{\lambda'}R_\lambda \cos\theta_\lambda} = \sum_{j=-\infty}^{\infty} i^J e^{iJ\theta_\lambda} J_J(k_{v_\lambda,j_\lambda,R_\lambda}^{\lambda'}) \;,$$

$$\underset{t_\lambda\to\infty}{\sim} \frac{1}{k_{v_\lambda,j_\lambda}^{\lambda'}R_\lambda} \sum_{j=-\infty}^{\infty} \left[e^{ik_{v_\lambda,j_\lambda}^{\lambda'}R_\lambda} e^{-i(\pi/4)} \right.$$
$$\left. + (-1)^J e^{-ik_{v_\lambda,j_\lambda}^{\lambda'}R_\lambda} e^{i(\pi/4)} \right] \varphi_J(\theta_\lambda)$$

$$(5.27)$$

As a result of the relation between γ_λ, θ_λ, and θ_{r_λ} given after Eq. (2.1), and of Eq. (2.9), we have

$$\varphi_{j_\lambda'}(\theta_{r_\lambda}) = (2\pi)^{1/2} \varphi_{j_\lambda}(\theta_\lambda) \varphi_{j_\lambda}(\gamma_{\lambda'}) \;. \tag{5.28}$$

Using Eqs. (5.26)–(5.28) and following the procedure outlined above, we get

$$C_J^{\lambda v_\lambda j_\lambda} = \left(\frac{\hbar\pi}{2\mu}\right)^{1/2} \exp[i(J-j_\lambda)\tfrac{1}{2}\pi] \tag{5.29}$$

and, for the dimensionless scattering amplitudes to open channels,

$$\hat{f}_{\lambda v_\lambda j_\lambda}^{\lambda' v_\lambda' j_\lambda'}(\theta_{\lambda'}) = \exp(-ij_\lambda,\theta_\lambda) \exp[i(j_{\lambda'} - j_\lambda - \tfrac{1}{2})\tfrac{1}{2}\pi]$$
$$\times \sum_{j=-\infty}^{\infty} \left(S_{J\lambda v_\lambda j_\lambda}^{0\lambda' v_\lambda' j_\lambda'} - \delta_{\lambda v_\lambda j_\lambda}^{\lambda' v_\lambda' j_\lambda'} \right) \varphi_J(\theta_{\lambda'}) \;. \tag{5.30}$$

Equation (5.30) differs from that obtained by Walker and Wyatt[41] only by the phase factor $\exp(-ij_\lambda,\theta_\lambda)$. Substitution of Eq. (5.30) into (5.24) and of the result into Eq. (5.25) leads to the following rather simple expression for the integral cross section:

$$Q_{\lambda v_\lambda j_\lambda}^{\lambda' v_\lambda' j_\lambda'} = \frac{1}{k_{v_\lambda j_\lambda}^{\lambda}} \sum_{j=-\infty}^{\infty} | S_{J\lambda v_\lambda j_\lambda}^{0\lambda v_\lambda' j_\lambda'} - \delta_{\lambda v_\lambda j_\lambda}^{\lambda' v_\lambda' j_\lambda'} |^2 \;. \tag{5.31}$$

Equations (5.35) and (5.36) may be written in terms of a sum over J from 0 to ∞ by using the relation

$$S_{J\lambda v_\lambda j_\lambda}^{0\lambda' v_\lambda' j_\lambda'} = S_{-J\lambda v_\lambda - j_\lambda}^{0\lambda' v_\lambda' - j_\lambda'} \;. \tag{5.32}$$

This expression is a consequence of the symmetry of the Hamiltonian with respect to reflection through the plane of motion. Additional symmetry relations which follow from Eq. (5.32) are

$$\hat{f}_{\lambda v_\lambda - j_\lambda}^{\lambda' v_\lambda' - j_\lambda'}(2\pi - \theta_{\lambda'}) = \hat{f}_{\lambda v_\lambda j_\lambda}^{\lambda' v_\lambda' j_\lambda'}(\theta_{\lambda'}) \tag{5.33}$$

and

$$Q_{\lambda v_\lambda - j_\lambda}^{\lambda' v_\lambda' - j_\lambda'} = Q_{\lambda v_\lambda j_\lambda}^{\lambda' v_\lambda' j_\lambda'} \;. \tag{5.34}$$

Equations (5.32), through (5.34) are valid for any planar atom plus diatomic molecule collision process. For reactions of higher symmetry such as $H + H_2$, there exist additional relationships, some of which will be discussed in the next section.

VI. APPLICATION TO PLANAR H + H₂

A. The integration, matching, and distinguishable-atom asymptotic analysis

In the application of the methods described in Sec. III and IV to the $H + H_2$ exchange reaction, a considerable reduction in computation time can be realized by utilizing two important symmetry properties of this collision system. The first is the invariance of the collision system and associated coordinate systems with respect to a cyclic permutation of the three atoms. Mathematically this means that all equations derived in Secs. III–V are invariant to a cyclic permutation of the indices $\lambda v \kappa$, which implies (1) that we need to integrate the Schrödinger equation in only one of the three arrangement channel regions depicted in Fig. 2, (2) that we need only calculate the projection coefficients $\bar{h}$, $\bar{h}'$, $\bar{f}$, and $\bar{f}'$ defined in Eqs. (4.11), (4.12), (4.22), and (4.23) on one of the three matching surfaces (such as $\pi_{v\lambda}$), and (3) that the $\lambda \to \nu$, $\nu \to \kappa$, and $\kappa \to \lambda$ distinguishable-atom scattering amplitudes are all identical, as are $\nu \to \lambda$, $\lambda \to \kappa$, $\kappa \to \nu$, and $\lambda \to \lambda$, $\nu \to \nu$, $\kappa \to \kappa$, so we may restrict ourselves to a calculation of the $\lambda \to \lambda$, $\lambda \to \nu$, and $\lambda \to \kappa$ scattering amplitudes only. The second symmetry property is related to the invariance of the collision system (but *not* the associated coordinate systems) with respect to an interchange of any two of the three atoms. This results in a potential function $V^\lambda(r_\lambda, R_\lambda, \gamma_\lambda)$ which is symmetric about $\gamma_\lambda = \pi/2$ and $3\pi/2$:

$$V^\lambda(r_\lambda, R_\lambda, \pi - \gamma_\lambda) = V^\lambda(r_\lambda, R_\lambda, \gamma_\lambda) \quad \text{for } 0 \leq \gamma_\lambda \leq \pi, \tag{6.1}$$
$$V^\lambda(r_\lambda, R_\lambda, 3\pi - \gamma_\lambda) = V^\kappa(r_\lambda, R_\lambda, \gamma_\lambda) \quad \text{for } \pi < \gamma_\lambda < 2\pi \;.$$

To a large extent, the consequences of this property depend on the coordinate system being used, for while Eq. (6.1) is valid in all regions of configuration space, the λ arrangement channel coordinates r_λ, R_λ, γ_λ are not the most convenient coordinates to use in all three arrangement channel regions. In arrangement channel region λ, Eq. (6.1) has the immediate effect of decoupling rotational states of even and odd quantum numbers j_λ. This means that the integration in arrangement channel region λ can be done in two separate steps, one for even j_λ and one for odd j_λ. In each of these steps the total number of basis functions required is only about half of that needed in the absence of this decoupling. Since the computation time varies as N^a, where N is the number of states being integrated and a is 2 for $N < 10$ and 3 for $N > 20$,[20] we see that a saving of factors of 2 to 4 in computation time may be realized by this decoupling. In a similar manner, the calculation of the matching surface coefficients of Eqs. (4.11), (4.12), (4.22), and (4.23) may be done in two separate steps, one for even j_λ and one for odd j_λ, and the coefficient matrices f''^λ and f''^λ may be obtained from $h_J^{\lambda\mu}$ and $h_J'^{\lambda\mu}$ by using the simple relations

$$(f_J''^\lambda)_{v_\lambda j_\lambda}^{v_\lambda' j_\lambda'} = (-1)^{j_\lambda + j_\lambda'} (h_J^{\lambda\mu})_{v_\lambda j_\lambda}^{v_\lambda' j_\lambda'} \;, \tag{6.2a}$$

$$(f_J''^\lambda)_{v_\lambda j_\lambda}^{v_\lambda' j_\lambda'} = -(-1)^{j_\lambda + j_\lambda'} (h_J'^{\lambda\mu})_{v_\lambda j_\lambda}^{v_\lambda' j_\lambda'} \;. \tag{6.2b}$$

We must note, however, that the number of matching surface functions $B_{v_\lambda j_\lambda}^\lambda$ is still $N/2$, where N is the total

number of even plus odd j_λ states. The matching procedure ultimately couples the even and odd rotational states j_λ [through Eq. (4.44)] so that decoupling beyond that point is lost. However, symmetry of the system about $\gamma_\lambda = \pi/2$ and $3\pi/2$ [Eq. (6.1)] may be used to relate the $\lambda \rightarrow \nu$ and $\lambda \rightarrow \kappa$ scattering amplitudes according to

$$\hat{f}_{\lambda \nu j}^{\nu \nu' j'} = (-1)^{j+j'} \hat{f}_{\lambda \nu j}^{\kappa \nu' j'} \, , \tag{6.3}$$

as is shown in Appendix C. Equation (6.3) may be used to reduce the work involved in the asymptotic analysis to the calculation of only the $\lambda \rightarrow \lambda$ and $\lambda \rightarrow \nu$ scattering amplitudes. An additional consequence of Eq. (6.1) valid only for the $\lambda \rightarrow \lambda$ scattering amplitudes (i.e., the nonreactive transitions) is the familiar relation (also derived in Appendix C)

$$\hat{f}_{\lambda \nu j}^{\lambda \nu' j'} = 0 \quad \text{for } j - j' = \text{odd} \, , \tag{6.4}$$

and the incorporation of this relation into the asymptotic analysis can also result in a reduction of computational effort. We should note, however, that the two symmetries given by Eqs. (6.3) and (6.4) depend on our use of a complete basis set $B_{v_\lambda j_\lambda}^{n\lambda}$ for expanding the wavefunction on the matching surface and therefore may be used as a test of the convergence of the method provided these symmetries are not built into the calculations.

B. Postantisymmetrization

Up to this point, we have considered the three atoms to be distinguishable. However, to calculate physically measurable quantities such as cross sections for reactions like $H + H_2$, we must include for effects due to indistinguishability of the three atoms and the Pauli principle. This means that the physically meaningful solutions to the Schrödinger equation must be antisymmetric with respect to interchange of hydrogen nuclei (which have spin $\frac{1}{2}$). Some conceptual difficulties are occasionally encountered when using time-independent solutions, since antisymmetrization seems to imply incoming waves in all three arrangement channels asymptotically. A consideration of the time-dependent wavepacket generated from the time-independent solutions resolves this, however. As Taylor has shown, [42] the asymptotic indistinguishable-atom wave packet is identical to its distinguishable-atom counterpart, so that at any given time before the collision, the incoming wave is localized in a single distinguishable-atom arrangement channel. Once the collision begins, such localization is lost and the concept of distinguishable-atom arrangement channels becomes meaningless.

There is actually a number of ways by which indistinguishable-atom scattering amplitudes may be obtained from time-independent wavefunctions:

1. We can preantisymmetrize the wavefunction, and solve the coupled integrodifferential equations generated when this wavefunction is substituted into the Schrödinger equation. Such a procedure was used by Wolken and Karplus[16] and the resulting solutions yield directly the indistinguishable-atom scattering amplitudes.

2. We can solve the Schrödinger equation using the method outlined in this paper for distinguishable particles, antisymmetrize the resultant primitive wavefunctions, and use the asymptotic form of these antisymmetrized wavefunctions to obtain the indistinguishable-atom scattering amplitudes. A related procedure was considered by Truhlar and Abdallah[43] in their method for studying rearrangement collisions.

3. We may use the distinguishable-atom primitive wavefunctions generated in (2) to determine the distinguishable-atom scattering amplitudes. These amplitudes may then be linearly combined to yield the corresponding indistinguishable-atom amplitudes. This is the usual procedure of postantisymmetrization[23] which we have used and which is described for the case of hydrogen atom exchange in Appendix D.

If exact solutions to the Schrödinger equation are used, then all three methods should give the same results, but the use of approximate solutions can lead to different results even when comparing methods (2) and (3) where the same distinguishable-atom primitive wavefunctions are used. An example of this arises when distinguishable-atom solutions that do not obey microscopic reversibility are considered. In this case the process of antisymmetrization of the wavefunction is not interchangeable with that of extracting the asymptotic form of the wavefunction, thus leading to different results when methods (2) and (3) are applied. Since the numerical method described in this paper is designed to provide accurate solutions to the Schrödinger equation for distinguishable atoms, the differences between methods (2) and (3) are of secondary importance and we shall restrict ourselves to considering method (3) for the remainder of this paper. The resulting expressions for the indistinguishable-particle transition amplitudes in terms of their distinguishable-atom counterparts, as described in Appendix D and also by Doll, George, and Miller, [44] are summarized below (where the direct and exchange amplitudes $\hat{f}_1^1$ and $\hat{f}_2^2$ of that Appendix are relabeled as $\hat{f}_\lambda^\lambda$ and $\hat{f}_\lambda^\nu$, respectively):

(a) para $\rightarrow$ para:

$$\sigma_{pp j}^{pp' j'}(\theta) = \frac{1}{k_{v j}^\lambda} \left| \hat{f}_{\lambda v j}^{\lambda v' j'}(\theta) - \hat{f}_{\lambda v j}^{\nu v' j'}(\theta) \right|^2 \, , \tag{6.5a}$$

(b) para $\rightarrow$ ortho:

$$\sigma_{pp j}^{oo' j'}(\theta) = \frac{3}{k_{v j}^\lambda} \left| \hat{f}_{\lambda v j}^{\nu v' j'}(\theta) \right|^2 \, , \tag{6.5b}$$

(c) ortho $\rightarrow$ para:

$$\sigma_{oo j}^{pp' j'}(\theta) = \frac{1}{k_{v j}^\lambda} \left| \hat{f}_{\lambda v j}^{pp' j'}(\theta) \right|^2 \, , \tag{6.5c}$$

(d) ortho $\rightarrow$ ortho:

$$\sigma_{oo j}^{oo' j'}(\theta) = \frac{1}{k_{v j}^\lambda} \left[\left| \hat{f}_{\lambda v j}^{\lambda v' j'}(\theta) + \hat{f}_{\lambda v j}^{\nu v' j'}(\theta) \right|^2 \right. $$
$$\left. + 2 \left| \hat{f}_{\lambda v j}^{\nu v' j'}(\theta) \right|^2 \right] \, . \tag{6.5d}$$

Note that there is no reference to arrangement channel on the left sides of Eqs. (6.5) since this distinction has no meaning after the effect of the Pauli principle is

included. The corresponding integral cross sections are

(a) para → para:

$$Q_{po j}^{v' j'} = \frac{1}{\overline{k}_{vj}^{\lambda}} \sum_{J=-\infty}^{\infty} |S_{J\lambda vj}^{0\lambda v' j'} - \delta_{vj}^{v' j'} - S_{J\lambda vj}^{0\nu v' j'}|^2 , \tag{6.6a}$$

(b) para → ortho:

$$Q_{oo j}^{v' j'} = \frac{3}{\overline{k}_{vj}^{\lambda}} \sum_{J=-\infty}^{\infty} |S_{J\lambda vj}^{0\lambda v' j'}|^2 , \tag{6.6b}$$

(c) ortho → para:

$$Q_{oo j}^{v' j'} = \frac{1}{\overline{k}_{vj}^{\lambda}} \sum_{J=-\infty}^{\infty} |S_{J\lambda vj}^{0\nu v' j'}|^2 , \tag{6.6c}$$

(d) ortho → ortho:

$$Q_{oo j}^{v' j'} = \frac{1}{\overline{k}_{vj}^{\lambda}} \sum_{J=-\infty}^{\infty} (|S_{J\lambda vj}^{0\lambda v' j'} - \delta_{vj}^{v' j'} + S_{J\lambda vj}^{0\nu v' j'}|^2 + 2|S_{J\lambda vj}^{0\nu v' j'}|^2) . \tag{6.6d}$$

As expected, the para → ortho and ortho → para cross sections are simply proportional to the distinguishable-atom reactive cross sections since only exchange scattering amplitudes contribute to them. These cross sections furnish direct information on the reactive process alone. The para → para and ortho → ortho cross sections will show effects due to the interference between the reactive and nonreactive (i.e., direct and exchange) scattering amplitudes. The interference effects should be most important when these two amplitudes have comparable magnitudes. We will discuss this interference phenomenon in more detail when presenting our results for planar H + H₂.[20] As pointed out in Appendix D, Eqs. (6.5) above are also valid for the three-dimensional H + H₂ reaction once the quantum numbers m_j are added to the v and j ones and $\overline{k}_{vj}^{\lambda}$ is replaced by $(\overline{k}_{vj}^{\lambda})^2$.

ACKNOWLEDGMENTS

APPENDIX A: THE λ → ν TRANSFORMATION EQUATIONS AND RELATIONS ON THE MATCHING SURFACES

In this Appendix we derive the important relations between the mass-scaled coordinates R_λ, r_λ ($\lambda = \alpha$, β, γ) defined by Eqs. (2.2). They permit us to change from coordinates appropriate for one arrangement channel to those appropriate for another one. We also examine the simplifications that occur when these relationships are evaluated on the matching surfaces defined by Eq. (3.2). This will allow us to prove that these surfaces are half-planes whose edge is the OY_λ axis in the $OX_\lambda Y_\lambda Z_\lambda$ space introduced in Sec. III. A. We will consider only the relationships between the arrangement

channel coordinates R_λ, r_λ and R_ν, r_ν explicitly. The corresponding relationships between R_ν, r_ν and R_κ, r_κ, and between R_κ, r_κ and R_λ, r_λ may be obtained by cyclic permutation of the indices λνκ.

The following relations between the vectors $\overline{R}_\lambda$, $\overline{r}_\lambda$ and $\overline{R}_\nu$, $\overline{r}_\nu$, valid for *any* configuration of the three atoms, follows from Fig. 1:

$$\overline{R}_\nu = -\overline{r}_\lambda - \frac{m_\lambda}{m_\lambda + m_\kappa} \overline{r}_\nu$$

$$\overline{r}_\nu = \overline{R}_\lambda - \frac{m_\nu}{m_\nu + m_\kappa} \overline{r}_\lambda .$$

From these and Eqs. (2.2) we get

$$\begin{pmatrix} R_\nu \\ r_\nu \end{pmatrix} = M \begin{pmatrix} R_\lambda \\ r_\lambda \end{pmatrix} , \tag{A1}$$

where M is the 2×2 orthogonal matrix

$$M = \begin{pmatrix} \cos\alpha_{\nu\lambda} & -\sin\alpha_{\nu\lambda} \\ \sin\alpha_{\nu\lambda} & \cos\alpha_{\nu\lambda} \end{pmatrix} , \tag{A2}$$

$\alpha_{\nu\lambda}$ being the angle between $\pi/2$ and π determined by

$$\cos\alpha_{\nu\lambda} = -\left(\frac{m_\lambda m_\nu}{(m_\lambda + m_\kappa)(m_\nu + m_\kappa)}\right)^{1/2} \tag{A3a}$$

and

$$\sin\alpha_{\nu\lambda} = \left(\frac{m_\kappa M}{(m_\lambda + m_\kappa)(m_\kappa + m_\nu)}\right)^{1/2} . \tag{A3b}$$

From these expressions we can get the equations for the θ_λ, R_λ, r_λ, $\gamma_\lambda \to \theta_\nu$, R_ν, r_ν, γ_ν transformation. Indeed, from Eqs. (A1) and (A2) and the definition of γ_λ following Eq. (2.1) we get

$$R_\nu^2 = R_\nu \cdot R_\nu = \cos^2\alpha_{\nu\lambda} R_\lambda^2 + \sin^2\alpha_{\nu\lambda} r_\lambda^2 - \sin2\alpha_{\nu\lambda} r_\lambda R_\lambda \cos\gamma_\lambda , \tag{A4}$$

$$r_\nu^2 = r_\nu \cdot r_\nu = \sin^2\alpha_{\nu\lambda} R_\lambda^2 + \cos^2\alpha_{\nu\lambda} r_\lambda^2 + \sin2\alpha_{\nu\lambda} r_\lambda R_\lambda \cos\gamma_\lambda , \tag{A5}$$

and therefore

$$R_\nu^2 + r_\nu^2 = R_\lambda^2 + r_\lambda^2 , \tag{A6}$$

which is a manifestation of the orthogonality of M. In addition, it follows from Eqs. (A1) and (A2) that the cross products $R_\lambda \times r_\lambda$ and $R_\nu \times r_\nu$ are equal and therefore that

$$R_\nu r_\nu \sin\gamma_\nu = R_\lambda r_\lambda \sin\gamma_\lambda . \tag{A7a}$$

Since γ_ν is in the range $0-2\pi$, in order to have it completely specified we should obtain its cosine. Also from Eqs. (A4) and (A5) we get

$$\cos\gamma_\nu = \frac{R_\nu \cdot r_\nu}{R_\nu r_\nu}$$

$$= \frac{1}{R_\nu r_\nu} [\tfrac{1}{2}\sin2\alpha_{\nu\lambda}(R_\lambda^2 - r_\lambda^2) + \cos2\alpha_{\nu\lambda}\cos\gamma_\lambda R_\lambda r_\lambda] . \tag{A7b}$$

Equations (A4), (A5), and (A7) completely describe the R_λ, r_λ, $\gamma_\lambda \to R_\nu$, r_ν, γ_ν transformation. To complete the λ → ν transformation we define the angle $\Delta_{\nu\lambda}$,

$$\Delta_{\nu\lambda} = \theta_\nu - \theta_\lambda , \tag{A8}$$

and express it in terms of the λ coordinates. We can write

$$R_\lambda = R_\lambda(\cos\theta_\lambda \hat{x} + \sin\theta_\lambda \hat{y}),$$

$$r_\lambda = r_\lambda[\cos(\theta_\lambda + \gamma_\lambda)\hat{x} + \sin(\theta_\lambda + \gamma_\lambda)\hat{y}],$$

where $\hat{x}$ and $\hat{y}$ are the unit vectors along the laboratory-fixed axis depicted in Fig. 1. From these expressions, their ν counterpart and Eqs. (A1) and (A2) we can easily obtain the following expressions which determine $\Delta_{\nu\lambda}$ modulo 2π:

$$R_\nu \cos\Delta_{\nu\lambda} = R_\lambda \cos\alpha_{\nu\lambda} - r_\lambda \sin\alpha_{\nu\lambda}\cos\gamma_\lambda, \tag{A9a}$$

$$R_\nu \sin\Delta_{\nu\lambda} = - r_\lambda \sin\alpha_{\nu\lambda}\sin\gamma_\lambda. \tag{A9b}$$

We see that $\Delta_{\nu\lambda}$ is independent of θ_λ and a function of R_λ, r_λ, and γ_λ only. This is due to the fact that these three variables uniquely determine the internal configuration of the triatomic system and hence the angle $\Delta_{\nu\lambda}$ between R_ν and R_λ (see Fig. 1).

Equations (A4), (A5), and (A7)–(A9) completely describe the $\lambda \rightarrow \nu$ transformation. It is useful to obtain the expressions they reduce to on the $\pi_{\nu\lambda}$ surface defined by Eq. (3.2a). In view of this definition and of Eq. (A6) we have, on this surface,

$$r_\nu = r_\lambda, \tag{A10a}$$

$$R_\nu = R_\lambda. \tag{A10b}$$

From these and Eq. (A4) we get the very useful relation

$$R_\lambda/r_\lambda = - \cot\alpha_{\nu\lambda}\cos\gamma_\lambda + (1 + \cot^2\alpha_{\nu\lambda}\cos^2\gamma_\lambda)^{1/2} \tag{A11}$$

between R_λ/r_λ and γ_λ on this surface. Other important relations among the internal variables are obtained by substituting Eqs. (A10) and (A11) into (A7). We find

$$\sin\gamma_\nu = \sin\gamma_\lambda$$

and, after some algebraic effort,

$$\cos\gamma_\nu = - \cos\gamma_\lambda,$$

which imply that

$$\gamma_\nu = \pi - \gamma_\lambda \quad \mathrm{mod}\,2\pi. \tag{A12}$$

Since $0 \le \gamma_\lambda \le \pi/2$ or $3\pi/2 \le \gamma_\lambda < 2\pi$, we see that $\pi/2 \le \gamma_\nu \le 3\pi/2$ on $\pi_{\nu\lambda}$.

From Eqs. (A10)–(A12) plus the expressions resulting from replacing those equations in (A9), the $\lambda \rightarrow \nu$ transformation equations on the $\pi_{\nu\lambda}$ matching surface are completely specified. In addition, since from Eqs. (A9) and (A10)

$$\cos\Delta_{\nu\lambda} = \cos\alpha_{\nu\lambda} - \sin\alpha_{\nu\lambda}\cos\gamma_\lambda(r_\lambda/R_\lambda) \tag{A13a}$$

and

$$\sin\Delta_{\nu\lambda} = - (r_\lambda/R_\lambda)\sin\alpha_{\nu\lambda}\sin\gamma_\lambda, \tag{A13b}$$

and since from Eq. (A11), r_λ/R_λ is a function of γ_λ only (on $\pi_{\nu\lambda}$), so is $\Delta_{\nu\lambda}$.

We shall now show that Eq. (A11) when evaluated over the range $0 \le \gamma_\lambda \le \pi/2$ and $3\pi/2 \le \gamma_\lambda < 2\pi$ represents a half-plane whose edge is the OY_λ axis in the $OX_\lambda Y_\lambda Z_\lambda$ space defined in Sec. III. A and illustrated in Fig. 2. From Eqs. (3.1) and (A11), we obtain the simple expression

$$\cot\omega_\lambda = - \cot\alpha_{\nu\lambda}\cos\gamma_\lambda \quad 0 \le \gamma_\lambda \le \pi/2 \text{ and } 3\pi/2 \le \gamma_\lambda < 2\pi \tag{A14}$$

for the equation of $\pi_{\nu\lambda}$ in spherical polar coordinates. In addition, from Eqs. (3.1b) and (A10) we have, on $\pi_{\nu\lambda}$,

$$\omega_\lambda = \omega_\nu. \tag{A15}$$

To display the geometrical character of $\pi_{\nu\lambda}$ we switch from polar coordinates ζ, ω_λ, γ_λ to Cartesian ones X_λ, Y_λ, Z_λ. Equation (A14) then becomes

$$Z_\lambda = - \cot\alpha_{\nu\lambda} X_\lambda \quad 0 \le \gamma_\lambda \le \pi/2 \text{ and } 3\pi/2 \le \gamma_\lambda < 2\pi. \tag{A16}$$

This is the equation of a half-plane whose edge is the Y_λ axis and which makes an angle $\pi - \alpha_{\nu\lambda}$ with the OZ_λ axis (measured counter clockwise from OZ_λ to $\pi_{\nu\lambda}$ as viewed from OY_λ).

Another quantity of considerable importance in the matching procedure is the derivative operator $\partial/\partial n_{\nu\lambda}$ normal to the surface $\pi_{\nu\lambda}$ in the direction of increasing ω_λ (Sec. IV. A). Since this surface is a half-plane, this operator is easily found by using the standard expression

$$\partial/\partial n_{\nu\lambda} = \hat{n}_{\nu\lambda} \cdot \nabla, \tag{A17}$$

where $\hat{n}_{\nu\lambda}$ is a unit vector normal to $\pi_{\nu\lambda}$ in the direction of increasing ω_λ, and ∇ is the gradient operator in $X_\lambda Y_\lambda Z_\lambda$ coordinates. Expressing Eq. (A17) in the spherical polar coordinates ζ, ω_λ, and γ_λ we find

$$
\begin{aligned}
\frac{\partial}{\partial n_{\nu\lambda}} &= \frac{1}{\zeta}\frac{\sin\alpha_{\nu\lambda}}{\sin\omega_\lambda}\left[\left(\frac{\partial}{\partial\omega_\lambda}\right)_{\gamma_\lambda,\zeta} + \cot\alpha_{\nu\lambda}\sin\gamma_\lambda\left(\frac{\partial}{\partial\gamma_\lambda}\right)_{\omega_\lambda,\zeta}\right] \\
&= \frac{1}{\zeta}(\sin^2\alpha_{\nu\lambda} + \cos^2\alpha_{\nu\lambda}\cos^2\gamma_\lambda)^{1/2}\left[\left(\frac{\partial}{\partial\omega_\lambda}\right)_{\gamma_\lambda,\zeta}\right. \\
&\quad\left. + \cot\alpha_{\nu\lambda}\sin\gamma_\lambda\left(\frac{\partial}{\partial\gamma_\lambda}\right)_{\omega_\lambda,\zeta}\right] \\
&= \frac{1}{\zeta}\frac{\sin\alpha_{\nu\lambda}}{\sin 2\eta_\lambda}\left[\frac{1}{2}\left(\frac{\partial}{\partial\eta_\lambda}\right)_{\gamma_\lambda,\zeta} + \cot\alpha_{\nu\lambda}\sin\gamma_\lambda\left(\frac{\partial}{\partial\gamma_\lambda}\right)_{\eta_\lambda,\zeta}\right],
\end{aligned}
\tag{A18}
$$

and the indicated differentiations must be done on the full wavefunction with ζ, ω_λ (or η_λ) and γ_λ considered as independent variables before the relation between ω_λ (or η_λ) and γ_λ describing $\pi_{\nu\lambda}$ is used. The third line of Eq. (A18) results from the use of η_λ rather than ω_λ as discussed in Sec. III. B. Equation (A17) can also be evaluated in terms of ν arrangement channel coordinates, in which case we find

$$
\begin{aligned}
\frac{\partial}{\partial n_{\nu\lambda}} &= -\frac{1}{\zeta}\frac{\sin\alpha_{\nu\lambda}}{\sin\omega_\nu}\left[\left(\frac{\partial}{\partial\omega_\nu}\right)_{\gamma_\nu,\zeta} - \cot\alpha_{\nu\lambda}\sin\gamma_\lambda\left(\frac{\partial}{\partial\gamma_\nu}\right)_{\omega_\nu,\zeta}\right] \\
&= -\frac{1}{\zeta_\lambda}(\sin^2\alpha_{\nu\lambda} + \cos^2\alpha_{\nu\lambda}\cos^2\gamma_\lambda)^{1/2}\left[\left(\frac{\partial}{\partial\omega_\nu}\right)_{\gamma_\nu,\zeta}\right. \\
&\quad\left. - \cot\alpha_{\nu\lambda}\sin\gamma_\lambda\left(\frac{\partial}{\partial\gamma_\nu}\right)_{\omega_\nu,\zeta}\right] \\
&= -\frac{1}{\zeta}\frac{\sin\alpha_{\nu\lambda}}{\sin 2\eta_\lambda}\left[\frac{1}{2}\left(\frac{\partial}{\partial\eta_\nu}\right)_{\gamma_\nu,\zeta} - \cot\alpha_{\nu\lambda}\sin\gamma_\lambda\left(\frac{\partial}{\partial\gamma_\nu}\right)_{\eta_\nu,\zeta}\right].
\end{aligned}
\tag{A19}
$$

APPENDIX B: EIGENVALUES OF A MATRIX OF THE FORM $U = \rho^2 V$

In this Appendix we show that the potential matrices in the strong interaction and matching regions [Eqs.

(3.48) and (3.61)] always have real eigenvalues even though they are not symmetric. These matrices have the general form

$$U = \rho^2 V ,\tag{B1}$$

where the real matrix ρ^2 is the matrix representation of a positive definitive operator [Eq. (3.49)] and therefore has positive real eigenvalues. V is a real symmetric matrix whose eigenvalues may be positive, negative, or zero.

The first step in finding the eigenvalues of U involves a diagonalization of ρ^2,

$$\tilde{K}\rho^2 K = \Lambda ,\tag{B2}$$

where Λ is a diagonal matrix whose elements are the (positive) eigenvalues of ρ^2, and K is the real orthogonal matrix of eigenvectors of ρ^2. We now form the real symmetric matrix ρ by

$$\rho = \tilde{K}\Lambda^{1/2} K ,\tag{B3}$$

where the diagonal matrix $\Lambda^{1/2}$ has diagonal elements which are the square roots of those of Λ. ρ behaves as if it were the "square root" of ρ^2 in many applications, since, from Eqs. (B2) and (B3),

$$\rho\rho = \rho^2 .\tag{B4}$$

Next, we define the real matrix W as

$$W = \rho^{-1}U\rho = \rho V\rho ,\tag{B5}$$

where the second equality in Eq. (B5) follows from Eq. (B1). From Eq. (B5), it is obvious that W is real symmetric, and it may therefore be diagonalized by a real orthogonal matrix which we denote by T:

$$\tilde{T}WT = E .\tag{B6}$$

The diagonal matrix E contains the real eigenvalues of W.

Finally, if we define the nonorthogonal, nonsymmetric, but real matrix S by

$$S = \rho T ,\tag{B7}$$

we obtain, from Eqs. (B5) and (B6),

$$S^{-1}US = E ,\tag{B8}$$

which proves that the matrix S diagonalizes U with the resulting real eigenvalues contained in E.

APPENDIX C: RELATIONS BETWEEN DISTINGUISHABLE ATOM SCATTERING AMPLITUDES FOR ATOM-DIATOM REACTIONS INVOLVING HOMONUCLEAR DIATOMIC MOLECULES

In this Appendix we investigate the consequences of two-atom permutational symmetry (as discussed in Sec. VI. A) on the distinguishable-atom scattering amplitudes. We show that in collisions for which Eq. (6.1) is valid (i.e., collisions of an atom with a homonuclear diatomic molecule), the resultant scattering amplitudes $f_{\nu\nu'j'}^{\lambda\nu'j'}$ and $f_{\kappa\nu'j'}^{\lambda\nu'j'}$ are related by Eq. (6.3) and that $f_{\lambda\nu'j'}^{\lambda\nu'j'}$ obeys Eq. (6.4). [The circumflex on $\hat{f}$ of Eq. (5.28) will be omitted in this Appendix.]

We first rewrite the asymptotic behavior of the scattering solution Eq. (5.23) as

$$\Psi^{\lambda v_\lambda j_\lambda}[P] \underset{R_\lambda \to \infty}{\sim} e^{i k_{v_\lambda j_\lambda}^\lambda R_\lambda \cos\theta_\lambda}\varphi_{j_\lambda}(\theta_{r_\lambda})\frac{\phi_{v_\lambda j_\lambda}^\lambda(r_\lambda)}{r_\lambda^{1/2}} + \sum_{v_\lambda' j_\lambda'}\frac{e^{i k_{v_\lambda' j_\lambda'}^\lambda R_\lambda}}{R_\lambda^{1/2}}f_{\lambda v_\lambda j_\lambda}^{\lambda v_\lambda' j_\lambda'}(\theta_\lambda)\varphi_{j_\lambda'}(\theta_{r_\lambda})\frac{\phi_{v_\lambda' j_\lambda'}^\lambda(r_\lambda)}{r_\lambda^{1/2}}\left(\frac{\hbar}{\mu|V_{v_\lambda' j_\lambda'}^\lambda|}\right)^{1/2}$$

$$\underset{R_\nu \to \infty}{\sim} \sum_{v_\nu j_\nu}\frac{e^{i k_{v_\nu j_\nu}^\nu R_\nu}}{R_\nu^{1/2}}f_{\lambda v_\lambda j_\lambda}^{\nu v_\nu j_\nu}(\theta_\nu)\varphi_{j_\nu}(\theta_{r_\nu})\frac{\phi_{v_\nu j_\nu}^\nu(r_\nu)}{r_\nu^{1/2}}\left(\frac{\hbar}{\mu|V_{v_\nu j_\nu}^\nu|}\right)^{1/2}$$

$$\underset{R_\kappa \to \infty}{\sim} \sum_{v_\kappa j_\kappa}\frac{e^{i k_{v_\kappa j_\kappa}^\kappa R_\kappa}}{R_\kappa^{1/2}}f_{\lambda v_\lambda j_\lambda}^{\kappa v_\kappa j_\kappa}(\theta_\kappa)\varphi_{j_\kappa}(\theta_{r_\kappa})\frac{\phi_{v_\kappa j_\kappa}^\kappa(r_\kappa)}{r_\kappa^{1/2}}\left(\frac{\hbar}{\mu|V_{v_\kappa j_\kappa}^\kappa|}\right)^{1/2} .\tag{C1}$$

If the diatomic target in the incident channel is homonuclear, the physical system should be invariant to the operator $P_{\nu\kappa}$ which interchanges the two identical atoms A_ν and A_κ involved. If we perform this interchange, the coordinates which define the system in each arrangement channel become (by inspection of Fig. 1)

$$(R_\lambda, r_\lambda) \to (R_\lambda, -r_\lambda), \quad (R_\nu, r_\nu) \to (R_\kappa, -r_\kappa), \quad (R_\kappa, r_\kappa) \to (R_\nu, -r_\nu) ,\tag{C2}$$

which is equivalent to

$$(R_\lambda, \theta_\lambda) \to (R_\lambda, \theta_\lambda), \quad (r_\lambda, \theta_{r_\lambda}) \to (r_\lambda, \theta_{r_\lambda} + \pi), \quad (R_\nu, \theta_\nu) \to (R_\kappa, \theta_\kappa),$$
$$(r_\nu, \theta_{r_\nu}) \to (r_\kappa, \theta_{r_\kappa} + \pi), \quad (R_\kappa, \theta_\kappa) \to (R_\nu, \theta_\nu), \quad (r_\kappa, \theta_{r_\kappa}) \to (r_\nu, \theta_{r_\nu} + \pi) .$$

If we make these substitutions into Eq. (C1) realizing that $\varphi_{j_\lambda}(\theta_{r_\lambda} + \pi) = (-1)^{j_\lambda}\varphi_{j_\lambda}(\theta_{r_\lambda})$, and appropriately relabel the quantum numbers which serve as summation indices, we obtain

$$P_{\nu\kappa}\Psi^{\lambda v_\lambda j_\lambda}[P] \underset{R_\lambda \to \infty}{\sim} (-1)^{j_\lambda}e^{i k_{j_\lambda v_\lambda}^\lambda R_\lambda \cos\theta_\lambda}\varphi_{j_\lambda}(\theta_{r_\lambda})\frac{\phi_{v_\lambda j_\lambda}^\lambda(r_\lambda)}{r_\lambda^{1/2}} + \sum_{v_\lambda' j_\lambda'}(-1)^{j_\lambda'}\frac{e^{i k_{v_\lambda' j_\lambda'}^\lambda R_\lambda}}{R_\lambda^{1/2}}f_{\lambda v_\lambda j_\lambda}^{\lambda v_\lambda' j_\lambda'}(\theta_\lambda)\varphi_{j_\lambda'}(\theta_{r_\lambda})\frac{\phi_{v_\lambda' j_\lambda'}^\lambda(r_\lambda)}{r_\lambda^{1/2}}\left(\frac{\hbar}{\mu|V_{v_\lambda' j_\lambda'}^\lambda|}\right)^{1/2}$$

$$\underset{R_\kappa \to \infty}{\sim} \sum_{v_\kappa j_\kappa}(-1)^{j_\kappa}\frac{e^{i k_{v_\kappa j_\kappa}^\kappa R_\kappa}}{R_\kappa^{1/2}}f_{\lambda v_\lambda j_\lambda}^{\kappa v_\kappa j_\kappa}(\theta_\kappa)\varphi_{j_\kappa}(\theta_{r_\kappa})\frac{\phi_{v_\kappa j_\kappa}^\kappa(r_\kappa)}{r_\kappa^{1/2}}\left(\frac{\hbar}{\mu|V_{v_\kappa j_\kappa}^\kappa|}\right)^{1/2}$$

$$\underset{R_\nu \to \infty}{\sim} \sum_{v_\nu j_\nu}(-1)^{j_\nu}\frac{e^{i k_{v_\nu j_\nu}^\nu R_\nu}}{R_\nu^{1/2}}f_{\lambda v_\lambda j_\lambda}^{\nu v_\nu j_\nu}(\theta_\nu)\varphi_{j_\nu}(\theta_{r_\nu})\frac{\phi_{v_\nu j_\nu}^\nu(r_\nu)}{r_\nu^{1/2}}\left(\frac{\hbar}{\mu|V_{v_\nu j_\nu}^\nu|}\right)^{1/2} .\tag{C3}$$

The line-wave part of (C3) differs only by a factor of $(-1)^{j_\lambda}$ from the corresponding part of (C1). Since the scattering solutions are unique (except for a normalization constant), this implies that this proportionality relation must hold over the entire configuration space, i.e., that

$$P_{\nu\kappa}\psi^{\lambda\nu_\lambda j_\lambda}[P] = (-1)^{j_\lambda}\psi^{\lambda\nu_\lambda j_\lambda}[P] \tag{C4}$$

everywhere. Replacement of Eqs. (C1) and (C3) into (C4) and identification of the corresponding outgoing wave parts in channel λ immediately yields

$$f_{\lambda\nu_\lambda j_\lambda}^{\lambda\nu'_\lambda j'_\lambda} = (-1)^{j_\lambda + j'_\lambda} f_{\lambda\nu_\lambda j_\lambda}^{\lambda\nu'_\lambda j'_\lambda} \tag{C5}$$

which is equivalent to Eq. (6.4). In order to compare the outgoing wave solutions in channels ν and κ, we first must realize that the $\phi^\nu_{\nu_\kappa j_\kappa}(r_\kappa)$ (and $k^\nu_{\nu_\kappa j_\kappa}$) of Eq. (C3), and the $\phi^\kappa_{\nu_\kappa j_\kappa}(r_\kappa)$ (and $k^\kappa_{\nu_\kappa j_\kappa}$) of Eq. (C1) are identical since these represent vibrational wavefunctions in the two product arrangement channels $A_\kappa A_\lambda$ and $A_\lambda A_\nu$, both of which are the same for a homonuclear target $A_\nu A_\kappa$. This allows us to compare the outgoing wave solutions in channels ν and κ in Eq. (C4), obtaining

$$f_{\lambda\nu_\lambda j_\lambda}^{\nu\nu_\kappa j_\kappa} = (-1)^{j_\lambda + j_\kappa} f_{\lambda\nu_\lambda j_\lambda}^{\kappa\nu_\kappa j_\kappa} \tag{C6}$$

in both cases. Equation (C6) is identical to Eq. (6.3).

If atoms A_λ and A_ν are identical, a derivation similar to that of (C4) leads to

$$P_{\lambda\nu}\psi^{\lambda\nu_\lambda j_\lambda}[P] = (-1)^{j_\lambda}\psi^{\nu\nu_\lambda j_\lambda}[P] \tag{C7}$$

and if A_λ and A_κ are identical we get

$$P_{\lambda\kappa}\psi^{\lambda\nu_\lambda j_\lambda}[P] = (-1)^{j_\lambda}\psi^{\kappa\nu_\lambda j_\lambda}[P] \tag{C8}$$

From Eq. (C7) results

$$f_{\nu\nu_\lambda j_\lambda}^{\nu\nu'_\lambda j'_\lambda} = (-1)^{j_\lambda + j'_\lambda} f_{\lambda\nu_\lambda j_\lambda}^{\lambda\nu'_\lambda j'_\nu} \tag{C9}$$

$$f_{\nu\nu_\lambda j_\lambda}^{\lambda\nu'_\lambda j'_\nu} = (-1)^{j_\lambda + j'_\nu} f_{\lambda\nu_\lambda j_\lambda}^{\nu\nu'_\lambda j'_\nu} \tag{C10}$$

$$f_{\nu\nu_\lambda j_\lambda}^{\kappa\nu_\kappa j_\kappa} = (-1)^{j_\lambda + j_\kappa} f_{\lambda\nu_\lambda j_\lambda}^{\kappa\nu_\kappa j_\kappa} \tag{C11}$$

and analogous expressions stem from Eq. (C8):

$$f_{\kappa\nu_\lambda j_\lambda}^{\kappa\nu_\kappa j_\kappa} = (-1)^{j_\lambda + j_\kappa} f_{\lambda\nu_\lambda j_\lambda}^{\lambda\nu_\lambda j_\lambda} \tag{C12}$$

$$f_{\kappa\nu_\lambda j_\lambda}^{\lambda\nu_\kappa j_\kappa} = (-1)^{j_\lambda + j_\kappa} f_{\lambda\nu_\lambda j_\lambda}^{\kappa\nu_\lambda j_\kappa} \tag{C13}$$

$$f_{\kappa\nu_\lambda j_\lambda}^{\nu\nu'_\lambda j'_\nu} = (-1)^{j_\lambda + j'_\nu} f_{\lambda\nu_\lambda j_\lambda}^{\kappa\nu'_\lambda j'_\nu} \tag{C14}$$

If all three atoms are identical, Eqs. (C4)–(C14) are all valid, as well as expressions resulting from cyclic permutations of indices λ, ν, κ.

For reactions in three dimensions, Eqs. (C2) are still valid. The rotational diatomic wavefunctions $\varphi_{j_\lambda}(\theta_{r_\lambda})$ are replaced by the spherical harmonics $Y_{j_\lambda = j_\lambda}(\theta_{r_\lambda}, \phi_{r_\lambda})$, where $\theta_{r_\lambda}, \phi_{r_\lambda}$ are the spherical polar angles of r_λ, and j_λ, m_{j_λ} are the diatom's angular momentum quantum numbers. Replacement of r_λ by $-r_\lambda$ is equivalent to replacing those polar angles by $\pi - \theta_{r_\lambda}$ and $\phi_{r_\lambda} + \pi$, respectively. The relation $Y_{j_\lambda m_\lambda}(\pi - \theta_{r_\lambda}, \phi_{r_\lambda} + \pi) = (-1)^{j_\lambda} \times Y_{j_\lambda m_\lambda}(\theta_{r_\lambda}, \phi_{r_\lambda})$, which is analogous to the relation $\varphi_{j_\lambda}(\theta_{r_\lambda} + \pi) = (-1)^{j_\lambda}\varphi_{j_\lambda}(\theta_{r_\lambda})$ used to derive Eq. (C4). As a result, that equation, as well as Eqs. (C5)–(C14) are also valid in three dimensions, as long as the quantum numbers $\nu_\lambda j_\lambda$ (and their ν and κ counterparts) are augmented by the diatomic rotational angular momentum projection quantum number m_{j_λ}.

APPENDIX D: POSTANTISYMMETRIZATION FOR THE H + H₂ EXCHANGE REACTION

Although correct expressions for the indistinguishable (antisymmetrized) cross sections in terms of the distinguishable atom reactive and nonreactive amplitudes have been listed by Doll, George, and Miller,[44] who have obtained their results using the integrodifferential equation approach described by Miller,[45] there seems to be confusion in the use of these expressions so we shall derive them here in order to clarify their meanings. We will follow the postantisymmetrization procedure outlined by Schiff[23] which is somewhat more transparent than Miller's. In all of our treatment below we assume that the interaction potential is not spin dependent and that there are no external magnetic fields present.

We start by rewriting the asymptotic physical solution [Eq. (5.23)] for distinguishable-atom scattering (in the mass-scaled coordinate system). To simplify the notation we omit the symbol $[P]$ (which will be implied throughout this Appendix) and replace the labels (α, β, γ) by $(1, 2, 3)$. Therefore, $(\lambda\nu\kappa)$ will stand for one of the cyclic permutations $(1, 2, 3)$, $(2, 3, 1)$, and $(3, 1, 2)$. Choosing the first of these we get

$$\psi^{1\nu_1 j_1}(1, 2, 3) \underset{R_1 \to \infty}{\sim} e^{i k_{v_1 j_1}^1 \cdot R_1} W_{v_1 j_1}^1(2, 3)$$
$$+ \sum_{v'_1 j'_1} \frac{e^{i k_{v'_1 j'_1}^1 R_1}}{R_1^{1/2}} W_{v'_1 j'_1}^1(2, 3) C_1^{v'_1 j'_1} f_{1v_1 j_1}^{1v'_1 j'_1}(\theta_1)$$
$$\underset{R_2 \to \infty}{\sim} \sum_{v_2 j_2} \frac{e^{i k_{v_2 j_2}^2 R_2}}{R_2^{1/2}} W_{v_2 j_2}^2(3, 1) C_2^{v_2 j_2} \hat{f}_{1v_1 j_1}^{2v_2 j_2}(\theta_2)$$
$$\underset{R_3 \to \infty}{\sim} \sum_{v_3 j_3} \frac{e^{i k_{v_3 j_3}^3 R_3}}{R_3^{1/2}} W_{v_3 j_3}^3(1, 2) C_3^{v_3 j_3} \hat{f}_{1v_1 j_1}^{3v_3 j_3}(\theta_3) , \tag{D1}$$

where

$$W_{v_\lambda j_\lambda}^\lambda(\nu, \kappa) = \frac{\varphi_{j_\lambda}(\theta_{r_\lambda})\phi_{v_\lambda j_\lambda}^\lambda(r_\lambda)}{r_\lambda^{1/2}} \tag{D2}$$

$$C_\lambda^{v_\lambda j_\lambda} = \left(\frac{\hbar}{\mu |V_{v_\lambda j_\lambda}^\lambda|}\right)^{1/2} \tag{D3}$$

Note that we have used the numbers 1, 2, and 3 as both an arrangement channel label and a particle label. Provided that we always permute particles in a cyclic way in our arrangement channel labeling, the two designations are identical and we will consider this to be the case here. This means that the coordinate r_1 is the internuclear vector from particle 2 to particle 3 (in the R_1, r_1 coordinate system), and therefore the 2, 3 diatomic molecule wavefunction is a function of r_1. For H + H₂, the separated arrangement channel quantum states are all identical, so the labels $v_1 j_1$, $v_2 j_2$, and $v_3 j_3$ are essentially dummy indices and do not imply, for example, that $W_{v_1 j_1}^1$ differs in its functional form from $W_{v_2 j_2}^2$ or $W_{v_3 j_3}^3$ when $j_1 = j_2 = j_3$ and $r_1 = r_2 = r_3$. As a result, we may drop the subscripts λ of the quantum numbers $v_\lambda j_\lambda$ and the constants C_λ as well as the superscript in the W, k, and V. Using Eq. (C4) for the cyclic permutation $(\lambda, \nu, \kappa) = (1, 2, 3)$, we get

$$P_{23}\psi^{1vj}(1, 3, 2) = \psi^{1vj}(1, 2, 3) = (-1)^j\psi^{1vj}(1, 3, 2) , \tag{D4a}$$

TABLE I. Antisymmetrized scattering amplitudes $\hat{f}^{\{i\}v'j'}_{\{i\}vj}$ and their relation to the distinguishable atom amplitudes $\hat{f}^{1v'j'}_{1vj}$ and $\hat{f}^{1v'j'}_{2vj}$.[a]

$\hat{f}^{\{i\}v'j'}_{\{i\}vj}$ Initial state		final state k j'	1 Odd ortho	2 Odd ortho	3 Odd ortho	4 Odd ortho	5 Odd ortho	6 Odd ortho	7 Even para	8 Even para
i	j									
1	Odd	ortho	$\hat{f}^1_1+\hat{f}^1_2$	0	0	0	0	0	0	0
2	Odd	ortho	0	$\hat{f}^1_1$	$\sqrt{2}\,\hat{f}^1_2$	0	0	0	$\sqrt{2}\,\hat{f}^1_2$	0
3	Odd	ortho	0	$\sqrt{2}\,\hat{f}^1_2$	$\hat{f}^1_1+\hat{f}^1_2$	0	0	0	$-\hat{f}^1_2$	0
4	Odd	ortho	0	0	0	$\hat{f}^1_1+\hat{f}^1_2$	$\sqrt{2}\,\hat{f}^1_2$	0	0	$\hat{f}^1_2$
5	Odd	ortho	0	0	0	$\sqrt{2}\,\hat{f}^1_2$	$\hat{f}^1_1$	0	0	$-\sqrt{2}\,\hat{f}^1_2$
6	Odd	ortho	0	0	0	0	0	$\hat{f}^1_1+2\hat{f}^1_2$	0	0
7	Even	para	0	$-\sqrt{2}\,\hat{f}^1_2$	$\hat{f}^1_2$	0	0	0	$\hat{f}^1_1-\hat{f}^1_2$	0
8	Even	para	0	0	0	$-\hat{f}^1_2$	$\sqrt{2}\,\hat{f}^1_2$	0	0	$\hat{f}^1_1-\hat{f}^1_2$

[a]The indices vj and $v'j'$ on the $\hat{f}^{1v'j'}_{1vj}$ and $\hat{f}^{1v'j'}_{2vj}$ are omitted.

which is valid in all of configuration space. In addition, using the cyclic permutation $(\lambda, \nu, \kappa) = (2, 3, 1)$, Eq. (C7) furnishes

$$P_{23}\Psi^{2vj}(2, 3, 1) = (-1)^j \Psi^{3vj}(3, 1, 2) \ . \tag{D4b}$$

Let us now consider the spin wavefunctions of the separated atom plus diatom system in arrangement channel 1. *Since the three hydrogen atoms have spin $\frac{1}{2}$,* there are eight such wavefunctions which can be chosen to be

$$v_1(1, 2, 3) = \alpha(1)\alpha(2)\alpha(3) \ , \tag{D5a}$$

$$v_2(1, 2, 3) = \beta(1)\alpha(2)\alpha(3) \ , \tag{D5b}$$

$$v_3(1, 2, 3) = \frac{1}{\sqrt{2}}\,\alpha(1)[\alpha(2)\beta(3) + \beta(2)\alpha(3)] \ , \tag{D5c}$$

$$v_4(1, 2, 3) = \frac{1}{\sqrt{2}}\,\beta(1)[\alpha(2)\beta(3) + \beta(2)\alpha(3)] \ , \tag{D5d}$$

$$v_5(1, 2, 3) = \alpha(1)\beta(2)\beta(3) \ , \tag{D5e}$$

$$v_6(1, 2, 3) = \beta(1)\beta(2)\beta(3) \ , \tag{D5f}$$

$$v_7(1, 2, 3) = \frac{1}{\sqrt{2}}\,\alpha(1)[\alpha(2)\beta(3) - \beta(2)\alpha(3)] \ , \tag{D5g}$$

$$v_8(1, 2, 3) = \frac{1}{\sqrt{2}}\,\beta(1)[\alpha(2)\beta(3) - \beta(2)\alpha(3)] \ . \tag{D5h}$$

They are orthonormal eigenfunctions of S_z but not of S^2 and have the symmetry property

$$v_i(1, 3, 2) = \begin{cases} v_i(1, 2, 3) & i = 1\text{--}6 \\ -v_i(1, 2, 3) & i = 7, 8 \ . \end{cases} \tag{D6}$$

The total separated atom plus diatom wavefunctions (including space and spin coordinates) are then

$$\Phi^{1vj(i)}(1, 2, 3) = \Psi^{1vj}(1, 2, 3)v_i(1, 2, 3) \quad i = 1\text{--}8 \ , \tag{D7}$$

where (i) designates the spin state of the system. Since $\Phi^{1vj}(1, 2, 3)$ must be antisymmetric with respect to permutation of particles 2 and 3, we have the requirements [in view of Eqs. (D4) and (D6)] that

$$j = \begin{cases} \text{odd for } i = 1\text{--}6 \ (\text{ortho states}) \\ \text{even for } i = 7, 8 \ (\text{para states}) \ . \end{cases} \tag{D8}$$

We now form the completely antisymmetric wavefunction $\Psi^{Avj(i)}(1, 2, 3)$ by taking the symmetric linear combination of the partly antisymmetric wavefunctions $\Phi^{1vj}(\lambda\nu\kappa)$ for the three cyclic permutations of $(1, 2, 3)$ having the same initial vj:

$$\Psi^{Avj(i)} = \Phi^{1vj(i)}(1, 2, 3) + \Phi^{2vj(i)}(2, 3, 1) + \Phi^{3vj(i)}(3, 1, 2)$$

$$i = 1\text{--}8. \tag{D9}$$

Equations (D4), (D6), and (D8) can be used to prove that $\Psi^{Avj(i)}$ is antisymmetric under a permutation of any two of the three particles in the system. This then is the correct scattering solution, and its asymptotic behavior can be used to determine the correct antisymmetrized scattering amplitudes. This asymptotic behavior can be determined by evaluating $\Psi^{Avj(i)}$ at large values of R_1 (or R_2 or R_3), which yields

$$\Psi^{Avj(i)}(1, 2, 3) \underset{R_1 \to \infty}{\sim} e^{i\mathbf{k}_{vj}\cdot\mathbf{R}_1}W_{vj}(2, 3)v_i(1, 2, 3)$$

$$+ \sum_{v'j'} \frac{e^{ik_{v'j'}\cdot R_1}}{R_1^{1/2}} W^1_{v'j'}(2, 3)C^{v'j'}\left(\hat{f}^{1v'j'}_{1vj}v_i(1, 2, 3) + \hat{f}^{1v'j'}_{2vj}v_i(2, 3, 1) + \hat{f}^{1v'j'}_{3vj}v_i(3, 1, 2)\right) \ . \tag{D10}$$

This has the form of a physical scattering solution, but the expression in large parentheses must be re-expressed in terms of the $v_k(1,2,3)$ spin functions of the final separated atom-diatom ($k = 1-8$). Accordingly, we write

$$\hat{f}_{1vj}^{1v'j'} v_l(1,2,3) + \hat{f}_{2vj}^{1v'j'} v_l(2,3,1) + \hat{f}_{3vj}^{1v'j'} v_l(3,1,2)$$

$$= \sum_{k=1}^{8} f_{(l)vj}^{A(k)v'j'} v_k(1,2,3) , \tag{D11}$$

where $f_{(l)vj}^{A(k)v'j'}$ is the antisymmetrized scattering amplitude for scattering from initial state $(i)vj$ (spin state i) to final state $(k)v'j'$ (where Eq. (D8) must be satisfied for both of these states). We can solve for the $f_{(l)vj}^{A(k)v'j'}$ by multiplying Eq. (D11) by $v_l(1,2,3)$, integrating over all spin variables and then replacing the index l by k in the result. The resulting expressions for $f_{(l)vj'i'}^{A(k)vj'i}$ in terms of the distinguishable-atom scattering amplitudes are given in Table I. The expressions in that table have been simplified by the use of the relation [see Eqs. (6.3)]:

$$\hat{f}_{2vj}^{1v'j'} = (-1)^{v-j} f_{3vj}^{1v'j'} . \tag{D12}$$

In the notation of Doll, George, and Miller, [4] $\hat{f}_{1vj}^{1v'j'}$ is the direct while $\hat{f}_{2vj}^{1v'j'}$ is the exchange scattering amplitude.

The state-to-state cross sections are [from Eq. (5.24)]

$$\sigma_{(l)vj}^{(l)v'j'} = \frac{1}{k_{vj}} |\hat{f}_{(l)vj}^{(l)v'j'}|^2 , \tag{D13}$$

and the cross sections of Eq. (6.5) are obtained by summing Eq. (D13) over final spin states and averaging over initial ones. As an example, the para-to-ortho cross section [Eq. (6.5b)] is given by (dropping the vj, $v'j'$ indices but retaining the spin labels)

$$\sigma_p^0 = \frac{1}{2}(\sigma_7^1 + \sigma_7^2 + \sigma_7^3 + \sigma_7^4 + \sigma_7^5 + \sigma_7^6 + \sigma_8^1 + \sigma_8^2 + \sigma_8^3 + \sigma_8^4 + \sigma_8^5 + \sigma_8^6)$$

$$= \frac{3}{k} |\hat{f}_2^1|^2 . \tag{D14}$$

The derivation of the antisymmetrized scattering amplitudes of Table I was based on the validity of Eqs. (D4) and (D6). The latter comes from the properties of the spin states of Eq. (D5) which are the correct ones for the three-dimensional world. Equations (D4a) and (D4b) came from Eqs. (C4) and (C7), respectively, which as pointed out at the end of Appendix C, are also valid in three dimensions after including the projection quantum numbers m_j. The other characteristics of Eq. (D1) which change in going from 2D to 3D are irrelevant for the derivation of the antisymmetrized scattering amplitudes. As a result, the formulas of Table I are also valid in three dimensions when augmented by the quantum numbers m_j. A similar statement is valid for Eqs. (6.5) if $\bar{k}_{vj}^2$ is replaced by $(\bar{k}_{vj})^2$.

Department of Chemical Physics, The Weizmann Institute of Science, P. O. Box 26, Rehovot, Israel.
§Contribution No. 5248.
[1] E. M. Mortenson and K. S. Pitzer, Chem. Soc. (London) Spec. Publ. 16, 57 (1962); E. M. Mortenson, J. Chem. Phys. 48, 4029 (1968).
[2] D. J. Diestler and V. McKoy, J. Chem. Phys. 48, 2951 (1968).
[3] C. C. Rankin and J. C. Light, J. Chem. Phys. 51, 1701 (1971); G. Miller and J. C. Light, J. Chem. Phys. 54, 1635 (1971); ibid. 54, 1643 (1971).
[4] D. J. Truhlar and A. Kuppermann, J. Chem. Phys. 52, 3841 (1970); ibid. 56, 2232 (1972).
[5] A. Kuppermann, Proc. Conf. Potential Energy Surf. Chem. U. C. Santa Cruz, August 1970 (1971), p. 121; Electronic and Atomic Collisions, Proceedings of VII ICPEAC (North-Holland, Amsterdam, 1971), p. 3.
[6] D. J. Diestler, J. Chem. Phys. 54, 4547 (1971).
[7] B. R. Johnson, Chem. Phys. Lett. 13, 172 (1972).
[8] S. F. Wu and R. D. Levine, Mol. Phys. 22, 881 (1971).
[9] E. Shipsey, J. Chem. Phys. 58, 232 (1973).
[10] G. C. Schatz, J. Bowman, and A. Kuppermann, J. Chem. Phys. 58, 4023 (1973); G. C. Schatz and A. Kuppermann, J. Chem. Phys. 59, 964 (1973); J. M. Bowman, G. C. Schatz, and A. Kuppermann, Chem. Phys. Lett. 24, 378 (1974); G. C. Schatz, J. M. Bowman, and A. Kuppermann, J. Chem. Phys. 63, 674, 685 (1975).
[11] J. T. Adams, R. L. Smith, and E. F. Hayes, J. Chem. Phys. 61, 2193 (1974).
[12] M. Baer and D. J. Kouri, Chem. Phys. Lett. 24, 37 (1974); M. Baer, J. Chem. Phys. 60, 1057 (1974); A. Persky and M. Baer, J. Chem. Phys. 60, 133 (1974); M. Baer, U. Halavee, and A. Persky, J. Chem. Phys. 61, 5122 (1974).
[13] P. B. Middleton and R. E. Wyatt, J. Chem. Phys. 56, 2702 (1972); E. A. McCollough and R. E. Wyatt, J. Chem. Phys. 54, 3578, 3592 (1971).
[14] R. P. Saxon and J. C. Light, J. Chem. Phys. 56, 3874, 3885 (1972).
[15] A. Altenberger-Siczek and J. C. Light, J. Chem. Phys. 61, 4373 (1974).
[16] G. Wolken and M. Karplus, J. Chem. Phys. 60, 351 (1974).
[17] (a) A. B. Elkowitz and R. E. Wyatt, J. Chem. Phys. 62, 2504, 3683 (1975); (b) S. A. Harms and R. E. Wyatt, J. Chem. Phys. 57, 2722 (1972); ibid. 62, 3162, 3173 (1975).
[18] M. Baer and D. J. Kouri, Chem. Phys. Lett. 11, 238 (1971); J. Chem. Phys. 56, 1758 (1972); ibid. 57, 3991 (1972).
[19] A. Kuppermann, G. C. Schatz, and M. Baer, J. Chem. Phys. 61, 4362 (1974).
[20] G. C. Schatz and A. Kuppermann, J. Chem. Phys. 65, 4624 (1976), following paper.
[21] For reactions for which one of the three arrangement channels is energetically inaccessible, the integration needs to be done usually in only the two remaining open arrangement channels and a somewhat different and simpler matching procedure is required. This situation is not described in this paper although it can be handled by a straightforward modification of the theory here presented.
[22] A. Kuppermann and G. C. Schatz, J. Chem. Phys. 62, 2502 (1975); see also the second (p. 4642) and third (p. 4668) paper following this one.
[23] L. I. Schiff, Quantum Mechanics (McGraw-Hill, New York, 1968), 3rd ed., p. 384—395.
[24] A. M. Lane and R. G. Thomas, Rev. Mod. Phys. 30, 257 (1958); these authors use the term "collision matrix" in lieu of "scattering matrix."
[25] L. M. Delves, Nucl. Phys. 9, 391 (1959); 20, 275 (1960).
[26] D. Jepsen and J. O. Hirschfelder, Proc. Natl. Acad. Sci. 45, 249 (1959).
[27] F. T. Smith, J. Math. Phys. 3, 735 (1962). Different sets of mass-scaled coordinates have been used by R. A. Marcus, J. Chem. Phys. 41, 603 (1964), by K. T. Tang, B. Kleinman, and M. Karplus, J. Chem. Phys. 50, 1119 (1969), and by

many others, but they do not display all of the convenient properties of the coordinates of Eq. (2.2).

[28]This is true because the incident plane-(i.e., line-) wave solution discussed in Sec. V.B contains a whole spectrum of total angular momenta (corresponding classically to a range of impact parameters), many of which contribute to the reaction.

[29]The angles θ_ν and θ_λ differ by an angle $\Delta_{\nu\lambda}$ which is a function of r_λ, R_λ, and γ_λ only as seen in Eqs. (A8) and (A9). In addition, Eqs. (A7) show that γ_ν also depends on those three variables only. Therefore, $\varphi_J(\theta_\lambda)$ is also an eigenfunction of $\hbar/i(\partial/\partial\theta_\lambda)_{r_\nu}$ with the same eigenvalue $J\hbar$. The quantum number J is, as a result, independent of the arrangement channel λ used to obtain it.

[30](a) A. Kuppermann, Chem. Phys. Lett. 32, 374 (1975); (b) ibid. J. Chem. Phys. (to be published).

[31]R. N. Porter and M. Karplus, J. Chem. Phys. 40, 1105 (1964).

[32]Actually, values of ω_{λ_0} smaller than $\pi - \alpha_{\nu\lambda}$ and of ω_{λ_1} greater than $\pi/2$ are also permissible but are not needed to determine the wavefunction on the matching half-plane $\pi_{\nu\lambda}$.

[33]Handbook of Mathematical Functions, edited by M. Abramowitz and I. A. Stegun (National Bureau of Standards, Washington, D.C., 1964), Chap. 9.

[34]D. G. Truhlar, dissertation, California Institute of Technology, 1970, Appendix 4.

[35]R. Gordon, J. Chem. Phys. 51, 14 (1969).

[36]We used a version of Gordon's method developed by A. Wagner for inelastic atom–diatom collisions. See A. Wagner and V. McKoy, J. Chem. Phys. 58, 5561 (1973).

[37]To clarify this concept, let us consider a scattering solution consisting of an incoming wave in arrangement channel λ and outgoing waves in all three arrangement channels, λ, ν, κ.

There will, in general, be N of these kinds of scattering solutions which are linearly independent (for a coupled-channel expansion truncated at N terms in each arrangement channel), along with N having incoming waves in channel ν and N with incoming waves in channel κ for a total of $3N$ solutions. The latter two sets of solutions will have only outgoing waves in channel λ and, in the absence of the inclusion of dissociated states, it will be impossible to linearly combine these latter $2N$ solutions to generate the N sets of solutions which have incoming waves in channel λ. Therefore we have $3N$ scattering solutions which are linearly independent when the entire configuration space is considered, although only $2N$ of them are independent in any one asymptotic arrangement channel.

[38]N. S. F. Mott and H. S. W. Massey, The Theory of Atomic Collisions (Clarendon, Oxford, 1956), 3rd ed., Chaps, 14 and 15.

[39]Note that there are a few differences in phases and signs between the formulas which describe coplanar scattering and those for 3D.[38] These changes result from the differences between the phases of the cylindrical and spherical Bessel functions[33] and, of course, have no physical significance.

[40]This expression is obtained from Ref. 33, p. 351, Eq. 9.1.41 by setting $t = i\exp(i\theta_\lambda)$.

[41]R. B. Walker and R. E. Wyatt, J. Chem. Phys. 61, 4839 (1974).

[42]J. R. Taylor, Scattering Theory (Wiley, New York, 1972), Chap. 22.

[43]D. G. Truhlar and J. Abdallah, Phys. Rev. A 9, 297 (1974).

[44]J. D. Doll, T. F. George, and W. H. Miller, J. Chem. Phys. 58, 1343 (1973).

[45]W. H. Miller, J. Chem. Phys. 50, 407 (1969).

Quantum mechanical reactive scattering for planar atom plus diatom systems. II. Accurate cross sections for H+H₂*

George C. Schatz[†] and Aron Kuppermann

Arthur Amos Noyes Laboratory of Chemical Physics, Division of Chemistry and Chemical Engineering,[‡]
California Institute of Technology, Pasadena, California 91125
(Received 22 December 1975)

The results of an accurate quantum mechanical treatment of the planar $H + H_2$ exchange reaction on a realistic potential energy surface are presented. Full vibration-rotation convergence was achieved in the calculations, and this, together with a large number of auxiliary convergence and invariance tests, indicates that the cross sections are accurate to 5% or better. The reactive differential cross sections are always backward peaked over the range of total energies from 0.3 to 0.65 eV. Nonreactive $j = 0$ to $j' = 2$ cross sections are backward peaked at low energy (0.4 eV) shifting to sidewards peaking for $E > 0.5$ eV. Quantum symmetry interference oscillations are very significant in the $j = 0$ to $j' = 2$ para-to-para cross sections for $E \geq 0.6$ eV. Reactive integral cross sections show two distinct kinds of energy dependence. At low energy (< 0.5 eV), barrier tunneling gives them a largely exponential energy dependence while above 0.5 eV (the effective threshold energy) the cross sections vary nearly linearly. Comparison of collinear and coplanar transition probabilities indicates similar 1D and 2D energy dependence but with a shift in energy from 1D to 2D due to bending motions in the transition state. An analysis of rotational distributions indicates surprisingly good correspondence with temperaturelike distributions. The results of a one-vibration-approximation calculation are examined, and errors of as much as three orders of magnitude are found at some energies. Shapes of angular distributions are, however, accurately predicted by this approximate method. Additional analyses include comparisons with previous distorted wave and coupled-channel results, and calculations of thermal rate constants.

I. INTRODUCTION

A reaction of fundamental interest in the field of chemical dynamics is the $H + H_2$ hydrogen atom exchange reaction. This simplest of chemical reactions has been the subject of numerous dynamical studies by quasiclassical,[1,2] semiclassical,[3-5] and quantum mechanical[6-16] methods and has been the focal point for the development of many approximate reaction rate theories.[17] In addition, this system provides the fundamental example for characterizing quantum effects in chemical reactions and determining their importance on experimental observables. For these reasons, the calculation of accurate quantum mechanical cross sections for $H + H_2$ is of great importance. Unfortunately, until recently there existed neither the proper methods for efficiently solving the Schrödinger equation for this system nor adequately powerful computers to handle the computations involved without the introduction of approximations of unknown accuracy.

In the preceding paper[18] (hereafter referred to as I) we presented a method for accurately and efficiently solving the Schrödinger equation for reactive collisions of an atom with a diatomic molecule moving on a fixed plane. The planar motion restriction was introduced for computational simplicity only, with no fundamental limitations involved in applying a similar procedure to three-dimensional collisions as well. In this paper, we present the results of an application of this method to planar $H + H_2$ on a realistic potential energy surface.[19] The results to be discussed include reactive and nonreactive transition probabilities, differential cross sections and integral cross sections, product rotational state distributions, and rate constants. In a

preliminary communication,[11] we examined the importance of closed vibrational channels in a vibration-rotation coupled-channel (i.e., close-coupling)[20] expansion and found that the errors associated with an early truncation of the vibrational basis set expansion could be very serious in many cases although qualitative trends obtained with the truncated basis were often properly described. We will examine the one vibrational basis function approximation in somewhat greater detail in this paper, and will, in addition, compare our results with the approximate results of others in which different methods, types of approximations, and potential surfaces were used.

As pointed out in Paper I, the method we have developed for solving the Schrödinger equation for planar atom plus diatomic molecule collisions can be extended to 3D systems without significant conceptual changes, so an additional reason for undertaking the current calculations was to test the feasibility of the method in preparation for its application to 3D reactive systems. The calculations for the 3D $H + H_2$ system have now been completed and are presented in detail in the following two papers.[21] A preliminary communication of the results of this 3D work and its relationship with some of the coplanar results presented here has already been published.[18]

In Sec. II we describe the reactive scattering calculations, including convergence tests and computational considerations, and the representation of the potential energy surface. The results of the calculations are presented and discussed in Sec. III. Section IV contains a general summary and discussion.

II. QUANTUM MECHANICAL CALCULATIONS FOR PLANAR REACTIVE H + H₂

A. General description of the method

The method used to solve the Schrödinger equation for planar reactive and nonreactive $H + H_2$ collisions has been extensively described in Paper I. As outlined there, the procedure for obtaining the full set of primitive solutions to the partial-wave Schrödinger equation is divided into two stages. In the first one, a coupled-channel[20] method is used to generate solutions to the Schrödinger equation in each of the three arrangement channel regions of internal configuration space. These solutions are then smoothly matched to one another in the second stage, and the resulting primitive solutions, which are everywhere smoothly continuous, are then linearly combined to yield the appropriate reactance and scattering matrix solutions. This procedure is then repeated for a sufficient number of partial waves to obtain converged reactive, inelastic, and (if desired) elastic cross sections. The potential energy surface used in all the calculations was the semi-empirical ground electronic state H_3 surface of Porter and Karplus[19] (all coupling to excited electronic surfaces being neglected). In solving the Schrödinger equation for these reactive collision systems, great care must be exercised to insure adequate invariance of the results with respect to a change in (a) the number of vibration–rotation basis functions used, (b) the refer-

ence potential V_{ref} used to generate these functions, (c) the representation of the potential surface (see Sec. II. B), and (d) the nature of the functions used to represent the wavefunction on the matching surface (i.e., the "matching surface basis functions" of Paper I).

As discussed in Paper I, a number of symmetry properties inherent in $H + H_2$ and similar systems may be utilized to reduce the computation time involved in doing these calculations. Most significant in this respect are (a) cyclic permutational symmetry of the three-atom system which allows one to consider only one arrangement channel region in doing all calculations, and (b) two-atom permutational symmetry, which allows one to decouple the even and odd rotational states throughout most of the calculation. These same symmetry properties allow us to reduce the number of different distinguishable atom scattering amplitudes between a given initial vibration–rotation state of the reagent H_2 and a given final state of the product H_2 to just two: one reactive and one nonreactive amplitude. We shall denote the reagent diatomic states by the vibration–rotation quantum numbers vj and the product ones by $v'j'$. Distinguishable-atom reactive transitions will be designated by the superscript R, nonreactive ones by N, and (indistinguishable) antisymmetrized ones by A. In this notation, the relation between the antisymmetrized differential cross sections and the distinguishable-atom dimensionless scattering amplitudes [Eqs. (6.5) of Paper I] is

$$\sigma^A_{vj-v'j'} = \begin{cases} \frac{1}{k_{vj}} \left| f^N_{vj-v'j'} - f^R_{vj-v'j'} \right|^2 & (j, j' \text{ even, para}-\text{para}) \\[2mm] \frac{3}{k_{vj}} \left| f^R_{vj-v'j'} \right|^2 = 3\sigma^R_{vj-v'j'} & (j \text{ even, } j' \text{ odd, para}-\text{ortho}) \\[2mm] \frac{1}{k_{vj}} \left| f^R_{vj-v'j'} \right|^2 = \sigma^R_{vj-v'j'} & (j \text{ odd, } j' \text{ even, ortho}-\text{para}) \\[2mm] \frac{1}{k_{vj}} \left(\left| f^N_{vj-v'j'} + f^R_{vj-v'j'} \right|^2 + 2 \left| f^R_{vj-v'j'} \right|^2 \right) & (j, j' \text{ odd, ortho}-\text{ortho}), \end{cases} \tag{2.1}$$

where k_{vj} is the (unscaled) wave number ($\bar{k}_{vj}$ of Paper I), and $f^N_{vj-v'j'}$ and $f^R_{vj-v'j'}$ were denoted by $\hat{f}^{v'j'}_{vj}$ and $\hat{f}^{v v'j'}_{vj}$, respectively, in Paper I. For planar systems, the diatom rotational quantum number j is an algebraic integer and may be either positive, negative, or zero. For $j \neq 0$, the two states j and $-j$ are degenerate and said to have different polarizations. Differential cross sections which have been summed over final rotational polarizations and averaged over initial ones will be indicated by the symbol $\sigma_{vj-v'j'}$ and the corresponding integral cross sections by $\bar{Q}_{vj-v'j'}$. For example, the integral cross section $\bar{Q}^R_{01-\infty}$ is given by

$$\bar{Q}^R_{01-\infty} = \tfrac{1}{2}(Q^R_{01-\infty} + Q^R_{01-0,-2} + Q^R_{0,-1-\infty} + Q^R_{0,-1-0,-2}) . \tag{2.2}$$

In Sec. V. B of Paper I we found that the symmetry of the Hamiltonian with respect to reflection through the triatom plane leads to the following relations between cross sections within the same rotational manifolds

(valid for R, N, or A transitions):

$$\sigma_{vj-v'j'}(\theta) = \sigma_{v,-j-v',-j'}(2\pi - \theta) \tag{2.3}$$

and

$$Q_{vj-v'j'} = Q_{v,-j-v',-j'} . \tag{2.4}$$

As defined in Paper I, the scattering angle θ is the angle between the directions of motion of the final and initial H atoms in the center of mass system and spans the range $0 \leq \theta \leq 2\pi$. For *reactive* differential cross sections, the more customary angle to use is the angle θ_R of the direction of the product H_2 with respect to the direction of the incident H, and is related to θ by

$$\theta_R = \theta + \pi \pmod{2\pi} . \tag{2.5}$$

Therefore, the backward reactive scattering direction corresponds to $\theta_R = \pi$ and $\theta = 0$.

B. Representation of the potential energy surface

In setting up the coupled differential equations which must be solved in each arrangement channel region $\lambda = \alpha,\ \beta,\ \gamma$, the potential energy surface $V^\lambda(r_\lambda, R_\lambda, \gamma_\lambda)$ is expanded (see definitions in Paper I) in a cosine Fourier series of the angle γ_λ [Eq. (3.8a) of Paper I]:

$$V^\lambda(r_\lambda, R_\lambda, \gamma_\lambda) = \sum_{k=0}^{\infty} V_k^\lambda(r_\lambda, R_\lambda) \cos k\gamma_\lambda .\qquad (2.6)$$

In the case of the $H + H_2$ reaction, $V^\lambda(r_\lambda, R_\lambda, \gamma_\lambda)$ is symmetric about $\gamma_\lambda = \pi/2$ and $3\pi/2$ [Eq. (6.1) of Paper I], so only even k terms need be included in Eq. (2.6). Once the coefficients $V_k^\lambda(r_\lambda, R_\lambda)$ are determined, the rotational coupling in the Schrödinger equation can be analytically evaluated [as in Eq. (3.9) of Paper I]; this greatly facilitates the determination of the potential matrix elements needed in the integration procedure. Unfortunately, in general, the $V_k^\lambda(r_\lambda, R_\lambda)$ must be calculated numerically from the relation

$$V_k^\lambda(r_\lambda, R_\lambda) = \frac{2}{(1 + \delta_{k0})\pi} \int_0^\pi \cos k\gamma_\lambda \, V^\lambda(r_\lambda, R_\lambda, \gamma_\lambda) d\gamma_\lambda ,$$

$$(2.7)$$

and the effort involved in computing this integral negates the advantage of using an expression which is analytical in γ_λ such as Eq. (2.6). However, for the Porter–Karplus potential surface[19] (and for many others as well), in the regions of internal configuration space sampled in the calculation, the expansion Eq. (2.6) converges very rapidly (after only three or four terms). We can then redefine the V_k^λ by requiring that, instead of satisfying Eq. (2.7), they force Eq. (2.6), with a finite number n of even terms, to be satisfied exactly at n values of γ_λ. For example, if three terms are included, then we can find V_0^λ, V_2^λ, and V_4^λ by solving the three algebraic equations obtained when Eq. (2.6), truncated after three even terms, is evaluated at $\gamma = 0$, $\pi/4$, and $\pi/2$. The result is

$$\begin{pmatrix} V_0^\lambda(r_\lambda, R_\lambda) \\ V_2^\lambda(r_\lambda, R_\lambda) \\ V_4^\lambda(r_\lambda, R_\lambda) \end{pmatrix} = \begin{pmatrix} \tfrac{1}{4} & \tfrac{1}{2} & \tfrac{1}{4} \\ \tfrac{1}{2} & 0 & -\tfrac{1}{2} \\ \tfrac{1}{4} & -\tfrac{1}{2} & \tfrac{1}{4} \end{pmatrix} \begin{pmatrix} V^\lambda(r_\lambda, R_\lambda, \gamma_\lambda = 0) \\ V^\lambda(r_\lambda, R_\lambda, \gamma_\lambda = \pi/4) \\ V^\lambda(r_\lambda, R_\lambda, \gamma_\lambda = \pi/2) \end{pmatrix} .\qquad (2.8)$$

For a small number of terms in the potential function expansion, the above interpolative procedure yields a representation of the full potential function $V^\lambda(r_\lambda, R_\lambda, \gamma_\lambda)$ which is computationally more efficient but has about the same accuracy as the one generated using Eq. (2.7). Of course, the goodness of this procedure depends very significantly on the nature of the potential energy surface being considered, but for the Porter–Karplus H_3 surface, it allows an adequate representation of the potential while requiring an exact evaluation of V^λ at only three or four values of γ_λ [and the use of Eq. (2.6) for all others]. In Fig. 2, of Paper I[18] we depicted equipotential contours of the potential energy surface at $\gamma_\lambda = 0$, $\pi/4$, and $\pi/2$, the values required in the evaluation of Eq. (2.8).

C. Convergence and accuracy tests

It is of crucial importance in coupled-channel calculations to establish that the resulting reaction probabilities and cross sections have converged adequately. Indeed, we shall see later that premature truncation of the vibration–rotation basis set expansion can result in errors in the final integral cross sections by several orders of magnitude, even though other tests, such as conservation of flux, may be approximately satisfied. Furthermore, many approximation quantum methods involve various kinds of truncations and/or other approximations, and it is highly desirable to obtain fully converged results which are of sufficient accuracy to assess the validity of those methods.

The most obvious criteria which must be satisfied by the results of an accurate quantum calculation are conservation of flux and time reversal invariance. These two principles require that the scattering matrix S_J be unitary and symmetric for each total angular momentum quantum number J and therefore that the corresponding probability matrix P_J [defined by Eq. (5.20) of Paper I] be symmetric and that the sum of the elements of each of its rows (or columns) should equal unity. These criteria are necessary but not sufficient to insure accurate results.

In the results to be discussed in detail in Sec. III, we consider a range of total energies E from 0.30 to 0.75 eV (translational energies relative to the $v = 0$, $j = 0$ reagent H_2 state of 0.03–0.48 eV). Flux conservation and microscopic reversibility were checked in each calculation, and for $E \leq 0.60$ eV, deviations from flux conservation were never worse than 1% and from symmetry less than about 5% (for nonnegligible transition probabilities). For 0.60 eV $< E \leq 0.75$ eV, deviations from flux conservation were less than 3% and from symmetry less than 10%. In order to insure satisfactory convergence (better than 5%) in the calculation, vibration–rotation basis sets including 40–60 terms (channels) were required. For energies less than 0.50 eV, a 40 channel basis consisting of 5 vibrational wavefunctions combined with 10, 10, 8, 6, and 6 rotational wavefunctions for $v = 0$, 1, 2, 3, and 4, respectively, were used in general. In the 0.50–0.60 eV range, a 48 channel basis set of 4 vibrations and 12 rotations per vibration was adequate, while for energies above 0.60 eV, a 60 channel basis of 5 vibrations and 12 rotations per vibration was used. Typical probability matrices from these calculations (for a 48 channel calculation at 0.55 eV) are given in Table I. Both the reactive and nonreactive transition probability matrices are highly symmetric, and the sums of the probabilities in each row or column differs from unity by a

TABLE I. Nonreactive (N) and reactive (R) probability matrices for $E = 0.55$ eV, $J = 2$.[a]

(vj)	$(v'j') = (00)$	(01)	$(0, -1)$	(02)	$(0, -2)$	(03)	$(0, -3)$
				N			
(00)	0.0186	0.263(−8)	0.113(−6)	0.404	0.276	0.370(−7)	0.248(−7)
(01)	0.287(−7)	0.0134	0.477	0.689(−7)	0.104(−7)	0.199	0.0629
(0, −1)	0.337(−7)	0.477	0.0899	0.897(−7)	0.112(−7)	0.129	0.140
(02)	0.406	0.204(−7)	0.228(−7)	0.240	0.172	0.289(−7)	0.108(−7)
(0, −2)	0.277	0.530(−8)	0.298(−7)	0.171	0.474	0.287(−8)	0.496(−8)
(03)	0.633(−8)	0.199	0.129	0.126(−8)	0.343(−8)	0.636	0.651(−2)
(0, −3)	0.527(−8)	0.0624	0.140	0.327(−8)	0.468(−8)	0.653(−2)	0.785
				R			
(00)	0.0436	0.0380	0.0265	0.0167	0.0803(−1)	0.0347(−1)	0.911(−3)
(01)	0.0380	0.0357	0.0219	0.0178	0.0567(−1)	0.0378(−1)	0.621(−3)
(0, −1)	0.0261	0.0220	0.0167	0.0980(−1)	0.0502(−1)	0.0181(−1)	0.664(−3)
(02)	0.0174	0.0175	0.0961(−1)	0.0857(−1)	0.0246(−1)	0.0211(−1)	0.232(−3)
(0, −2)	0.0774(−1)	0.0588(−1)	0.0518(−1)	0.0232(−2)	0.0180(−1)	0.412(−3)	0.243(−3)
(03)	0.0356(−1)	0.0373(−1)	0.0184(−1)	0.0206(−1)	0.412(−3)	0.500(−3)	0.407(−4)
(0, −3)	0.879(−3)	0.619(−3)	0.655(−3)	0.237(−3)	0.234(−3)	0.398(−4)	0.386(−4)
Sums[b]	1.0014	0.9997	1.0003	0.9980	1.0001	0.9999	1.0005

[a]Not all allowed transitions are shown. Numbers in parentheses indicate powers of 10 by which numbers preceding them should be multiplied.
[b]Sum of probabilities from a given initial state over all possible final states and arrangement channels.

very small amount in every case. In Table II we examine the convergence behavior of the transition probabilities both as the number of vibrations per rotation is increased and as the number of rotations per vibration is increased (all at 0.6 eV). In Part A of that table we see that the results change by less than 5% in going from 12 to 14 rotations per vibration and by somewhat larger amounts in going from 10 to 14. With fewer than 10 rotations, errors of 10% to nearly 100% are observed in certain transition probabilities. When vibrational convergence is examined (Part B of Table II), we find that 2% convergence is attained with 4 vibrations and that the use of fewer than that number can lead to errors as large as 50% along with poor flux conservation.

Another important accuracy test in these calculations is the invariance of the results to changes in the character of the vibration–rotation basis set. There are two important ways to test this. First, one should be able to change the number of rotations per vibration or the number of vibrations per rotation without changing the results as long as convergence has been attained. Second, the results should be independent of the reference potential $V_{ref}(r_1, R_1)$ [Eq. (3. 36) of Paper I] which serves to define the vibrational basis functions as long as V_{ref} becomes equal to the correct diatomic potential $v(r_1)$ in the limit $R_1 \to \infty$. In Table III we present the results of these two kinds of tests. The first column tabulates representative nonreactive and reactive transition probabilities for $E = 0.50$ eV, $J = 0$ calculations with a 48 channel basis (4 vibrations, 12 rotations/vibration) and a reference potential $V_{ref} = V(r_1, R_1, \gamma_1 = 0)$ (the one actually used in most of the calculations). In the second column we give the corresponding probabilities obtained when the reference potential $V_{ref} = V_0^\lambda(r_1, R_1)$ is used [Eqs. (2. 6) and (2. 8)]. Finally, in the last column we give the transition prob-

abilities obtained with the $V_0^\lambda(r_1, R_1)$ reference potential and a 50 channel basis (5 vibrations, 12, 12, 10, 8, and 8 rotations in $v = 0$, 1, 2, 3, and 4, respectively). The deviations between the corresponding probabilities is less than 5%. This result is typical of the accuracy for energies $E \leq 0.60$ eV. Somewhat larger changes are found for 0.6 eV $< E \leq 0.75$ eV, but usually less than 10%.

Two additional accuracy tests are (a) convergence of the results with respect to the number of terms in the expansion of the potential [Eq. (2.6)], and (b) invariance

TABLE II. Rotational and vibrational convergence of coplanar transition probabilities at $E = 0.60$ eV, $J = 1$.

N	U[a]	$P_{00 \to 02}^N$	$P_{01 \to 01}^N$	$P_{00 \to 00}^R$	$P_{00 \to 01}^R$	$P_{01 \to 0-1}^R$
A.	Rotational convergence (with 4 vibrations and N rotations per vibration)					
6	1.035	0.293	0.435	0.0738	0.0667	0.0356
8	1.020	0.276	0.339	0.0743	0.0525	0.0380
10	1.010	0.202	0.257	0.0840	0.0706	0.0416
12	1.004	0.194	0.230	0.0829	0.0645	0.0396
14	1.002	0.189	0.221	0.0821	0.0673	0.0397
B.	Vibrational convergence (with M vibrations and 12 rotations per vibration)					
1[b]	1.003	0.259	0.260	0.0404	0.0372	0.0295
2	1.063	0.161	0.204	0.0895	0.0738	0.0477
3	1.063	0.238	0.315	0.0749	0.0578	0.0329
4	1.004	0.194	0.230	0.0829	0.0645	0.0396
5	1.007	0.195	0.233	0.0832	0.0646	0.0396

[a]U indicates the sum of all transition probabilities from a specific vj state which differs by the largest amount from unity and hence is a conservative measure of deviations from flux conservation.
[b]The one vibration results were calculated according to the procedure outlined in Sec. II. D.

TABLE III. Nonreactive and reactive transition probabilities for $E = 0.50$ eV, $J = 0$.

	$N=48$, V_{coll} [a]	$N=48$, V_0 [b]	$N=50$, V_0 [c]
$P_{00\to00}^{N}$	0.180	0.180	0.183
$P_{00\to02}^{N}$	0.383	0.383	0.383
$P_{0\star1\to0\star1}^{N}$	0.207	0.207	0.211
$P_{0\star1\to0\star1}^{N}$	0.583	0.582	0.580
$P_{00\to00}^{R}$	0.787×10^{-2}	0.787×10^{-2}	0.755×10^{-2}
$P_{00\to0\star1}^{R}$	0.580×10^{-2}	0.578×10^{-2}	0.557×10^{-2}
$P_{0\star1\to0\star1}^{R}$	0.422×10^{-2}	0.419×10^{-2}	0.404×10^{-2}
$P_{0\star1\to0\star1}^{R}$	0.413×10^{-2}	0.410×10^{-2}	0.395×10^{-2}

[a] 48 channels ($v = 0-3$; 12 rotations/vibration), $V_{ref} = V_{coll}$ $= V(r_\lambda, R_\lambda, \gamma_\lambda = 0)$.
[b] 48 channels ($v = 0-3$; 12 rotations/vibration), $V_{ref} = V_0^\lambda(r_\lambda, R_\lambda)$.
[c] 50 channels ($v = 0-4$; 12, 12, 10, 8, 8 vibrations for $v = 0, 1, 2, 3, 4$, respectively), $V_{ref} = V_0^\lambda(r_\lambda, R_\lambda)$.

of the results with respect to a change in the matching surface basis functions $B^{v\lambda}$ [Eq. (4.7) of Paper I]. We find that the reaction probabilities change by less than 5% in going from three to four terms in Eq. (2.6) [with the coefficients calculated as described before Eq. (2.8)] and virtually not at all in going from four to five terms. All calculations reported in this paper were done with three terms in Eq. (2.6) and using Eq. (2.8) to calculate V_0, V_2, and V_4. The effects of completeness of the expansion of the wavefunction on the matching surface were studied in two ways. First, several different choices of matching surface basis functions $B^{v\lambda}$ were used [different sine and cosine combinations (see Paper I) and Legendre polynomials] and invariance of the results to within 2% was found. Best unitarity of S_J was obtained with the basis set (c) of Sec. IV. A of Paper I, and this choice was used in all further calculations. Second, the degree of completeness of the matching surface basis functions $B^{v\lambda}$ determines the degree of orthogonality of the matrix $s_{\nu\lambda}^J$ of Eq. (4.32) of Paper I which transforms the solution in ν coordinates to that in coordinates λ. This property of $s_{\nu\lambda}^J$ determines the unitarity property of the scattering matrix S_J to a certain extent but it is also necessary if the nonreactive transition probabilities between even and odd rotational states are to vanish as required by the symmetry of the H_3 system [see Eq. (6.4) of Paper I]. Examples of the effects of a nonorthogonal $s_{\nu\lambda}^J$ are seen in Table I, where the nonreactive ortho to para transition probabilities typically have magnitudes of $10^{-\,}$ rather than 10^{-25}, which is more typically the case[22] when the orthogonality is built in through the use of Eq. (4.30) of Paper I. In that equation, the matrix $\bar{s}_{\nu\lambda}^J$ (the complex counterpart of $s_{\nu\lambda}^J$) is related to a real symmetric matrix $\Delta^{v\lambda}$ via

$$\bar{s}_{\nu\lambda}^J = \exp(iJ\Delta^{v\lambda}) . \qquad (2.9)$$

This expression is inherently unitary even when a truncated basis is used to calculate $\Delta^{v\lambda}$. It should be apparent that this error is of negligible importance for the example given in Table I, but as J increases, the deviations from orthogonality of $s_{\nu\lambda}^J$ also increase. Fortunately, the reaction probabilities decrease rapidly

as this happens and since a nonorthogonal matching procedure has no effect on inelastic transition probabilities in the absence of reaction,[23] the problem with completeness of the matching surface functions disappears at higher J. No artificial orthogonalization procedures were introduced in the calculation (such as were used by Saxon and Light[8]), and therefore unitarity of S_J and zeroness of the even-to-odd reactive transition probabilities are tests of the completeness of $B^{v\lambda}$.

We conclude this section by quoting some computation times for these calculations. Both the integration and matching times vary roughly as N^3 for $N > 20$, where N is the number of channels. For 48 channel calculations using an IBM 370-158 computer, about 22 min of computation time per partial wave J was required, of which 17 min was spent in the integration of the coupled equations and the rest in the matching and asymptotic analysis. About 13 partial waves ($J = 0-12$) were required for convergence of the reactive cross sections and 30 partial waves ($J = 0-29$) for convergence of the inelastic nonreactive cross sections at energies near $E = 0.50$ eV.

D. The one-vibrational-basis-function approximation (OVA)

An often used[8-10] (but seldom justified) approximation in quantum calculations has been the neglect of closed vibrational channels in the vibration–rotation coupled-channel expansion. For $H + H_2$ at low energies, only the ground vibrational level is open, so this approximation involves the use of only one vibrational basis function plus a complete set of rotational functions for that vibration. The main reason for using this approximation is the large reduction in computation time (by 1–2 orders of magnitude for $H + H_2$) compared to a vibrationally converged calculation. One of the objectives of this paper is to examine the accuracy of this approximation by comparing the results of its application with the fully converged ones.

The procedure that we have used to perform these one-vibration-approximation (OVA) calculations is almost identical to the fully converged one outlined in Paper I. The following modifications are, however, needed:

(a) The overlap matrix S_i^λ between the vibration–rotation basis sets in subregions i and $i+1$ [Eq. (3.42) of Paper I] is orthogonalized according to the Schmidt procedure.[24] This is required because otherwise the strongly nonorthogonal overlap matrix associated with this severe truncation of the vibrational expansion results in an excessive lack of flux conservation.

(b) The effective potential matrix in the strong interaction region (and analogously in the matching region) is modified to [see Eq. (3.48) of Paper I]

$$(\bar{U}_J^{\lambda(s)})_{v_\lambda j_\lambda}^{v_\lambda' j_\lambda'} = \langle v_\lambda | \rho_\lambda^2 \left[\frac{2\mu}{\hbar^2} \left[V_{j_\lambda j_\lambda'}^\lambda - \delta_{j_\lambda j_\lambda'} (V_{ref}^\lambda + E - \epsilon_{v_\lambda}^{\lambda(s)}) \right] \right.$$
$$\left. + \left(\frac{j_\lambda^2 - \frac{1}{4}}{(r_{\lambda_0} - \rho_\lambda \cos\varphi_\lambda)^2} + \frac{(J - j_\lambda)^2 - \frac{1}{4}}{(R_{\lambda_0} - \rho_\lambda \sin\varphi_\lambda)^2} - \frac{1}{4\rho_\lambda^2} \right) \right] | v_\lambda' \rangle ,$$
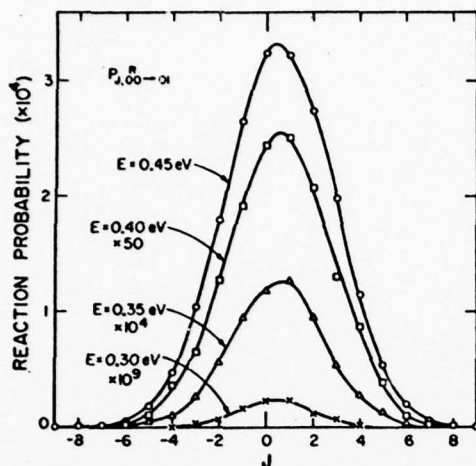$$(2.10)$$

FIG. 1. Converged coplanar reaction probability $P^R_{J,00-01}$ (for the $v=0$, $j=0 \to v'=0$, $j'=1$ transition) as a function of the total angular momentum quantum number J for $E=0.30$ eV (crosses), 0.35 eV (triangles), 0.40 eV (squares), and 0.45 eV (circles). Smooth curves have been drawn through the points.

where the only allowed values of v'_λ and v_λ are zero. For a complete vibration–rotation basis set expansion, this expression is identical to that in Eq. (3.48) of Paper I, but in the OVA they differ, the above expression being the more consistent one.[25]

Even with these modifications, there are still many ambiguities in the application of this procedure. The most serious of these is the lack of invariance of the results to our choice of $V_{ref}(r_\lambda, R_\lambda)$. In Sec. III we shall examine results for $V_{ref} = V(r_\lambda, R_\lambda, \gamma_\lambda = 0)$ and $V_{ref} = V^\lambda_0(r_\lambda, R_\lambda)$, with the hope that the range of results provided by these two calculations is representative of what can generally be obtained in this approximation.
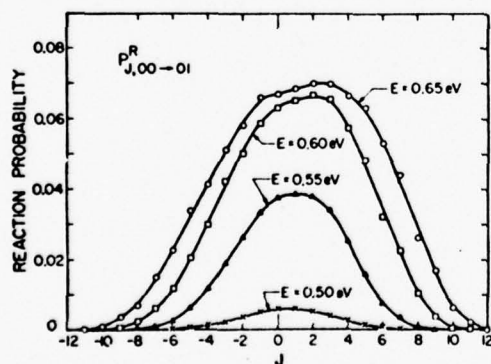

FIG. 2. Reaction probability $P^R_{J,00-01}$ as a function of the total angular momentum quantum number J analogous to Fig. 1 but at total energies of 0.50 eV (crosses), 0.55 eV (triangles), 0.60 eV (squares), and 0.65 eV (circles).
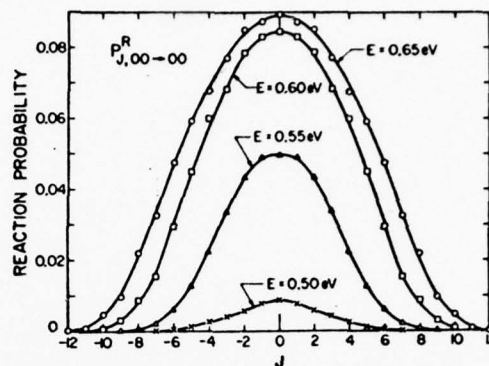

FIG. 3. Converged coplanar reaction probability $P^R_{J,00-00}$ as a function of the total angular momentum quantum number J. Symbols correspond to same values of energy E as in Fig. 2.

III. RESULTS FOR COPLANAR H + H₂

A. Transition probabilities

In this section we shall examine the J dependence of the distinguishable-atom reactive and inelastic non-reactive transition probabilities. The reactive probabilities $P^R_{J,00-01}$ (for the $v=0$, $j=0 \to v'=0$, $j'=1$ transition) are plotted in Figs. 1 and 2 for several energies as a function of J. The probabilities for negative J are obtained from those for positive J through the use of the relation [resulting from Eqs. (5.20) and (5.32) of Paper I and valid for R and N probabilities]

$$P_{J,vj-v'j'} = {}_cP_{-J,v-j-v'-j'} \, . \tag{3.1}$$

Figures 1 and 2 indicate that $P^R_{J,00-01}$ has a maximum near $J=0$ for small E with the peak gradually shifting to small positive J as E is increased. Furthermore, the number of values of J which must be included, in order that the differential reaction cross sections [see Eq. (5.30) of Paper I] should have converged to within approximately 2%, increases with E from about 9 at $E=0.30$ eV (i.e., $|J| \le 4$) to about 23 at $E=0.65$ eV ($|J| \le 11$). The maximum in the reaction probabilities at small J indicates that only small impact parameter collisions contribute significantly to the reaction cross section. The semiclassical relation between the impact parameter b and the orbital angular momentum l [as given by Eq. (5.21) of I] is

$$b = l/k_{vj} \, , \tag{3.2}$$

where we define the sign of b to be the same as that of l, and k_{vj} is the wave number associated with the incident state. Since $l = J - j$, and $j = 0$ for the transitions considered in Figs. 1 and 2, we see that b is proportional to J, and thus the range of impact parameters which contribute significantly to the reaction cross section increases with E in those figures (from $|b| \le 1.74$ bohr at 0.45 eV to $|b| \le 2.22$ bohr at 0.65 eV). In Fig. 3 we plot the reaction probabilities vs J at several energies for the transition $v=0$, $j=0 \to v'=0$, $j'=0$. Equation (3.1) indicates that this transition probability should be symmetric about $J=0$, but aside from that
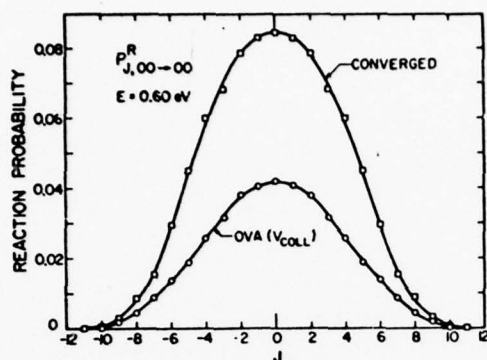
FIG. 4. Coplanar reaction probability $P^R_{J,00\to00}$ for $E = 0.60$ eV (translational energy $E_0 \approx 0.33$ eV) vs the total angular momentum quantum number J. Squares indicate the converged result while circles indicate the OVA probability for the collinear reference potential $[V_{coll} = V(r_\lambda, R_\lambda, \gamma_\lambda = 0)]$.

restriction, we find that the curves in that figure are otherwise very similar in appearance to those in Fig. 2. This conclusion applies quite generally to the reaction probability vs J plots obtained for most other reactive transitions. A discussion of the energy dependence of the reaction probabilities will be given in Sec. III. D.

In Fig. 4 we compare the converged reaction probabilities $P^R_{J,00\to00}$ with the corresponding OVA results for a collinear reference potential $V_{coll} = V^\lambda(r_\lambda, R_\lambda, \gamma_\lambda = 0)$ at an energy of 0.60 eV. We see that the OVA result has the correct functional dependence on J but that the magnitudes of the probabilities at each J are nearly a factor of 2 too small. OVA calculations using V_{ref}

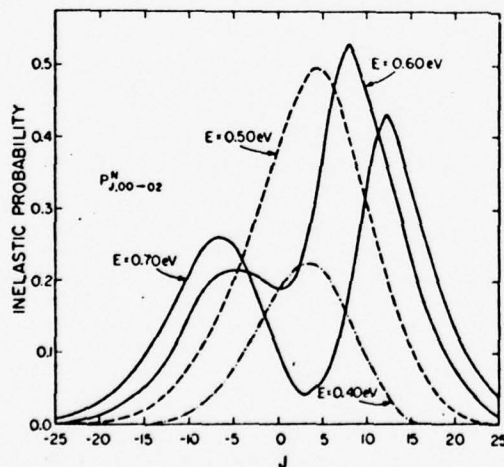FIG. 5. Coplanar converged inelastic probability $P^N_{J,00\to02}$ as a function of J for total energies $E = 0.40$ eV (dash–dot), 0.50 eV (dashed), 0.60 eV (solid), and 0.70 eV (solid).
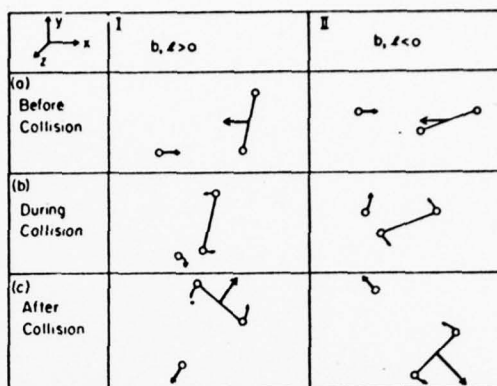
FIG. 6. Schematic representation of dominant collisions contributing to the $j = 0 \to j' > 0$ collisional (nonreactive) excitation process. Shown are (a) the initial approach of the collision partners in the center of mass coordinate system, (b) the collision itself with the direction of the rotational polarization indicated by curved arrows, and (c) the receding scattered particles. Collision I considers l (and hence b) initially positive (relative to the coordinate system shown). Collision II considers negative initial l and b. Note that the diatomic rotor with $j = 0$ is classically motionless with equal probability for any rotational phase. The particular phase chosen was that believed to give significant rotational excitation for each situation pictured.

$= V^\lambda_0(r_\lambda, R_\lambda)$ yield probabilities which are only slightly different from the OVA results in Fig. 4. (For example, the $V_{ref} = V^\lambda_0$ OVA reaction probability for $J = 0$ is 0.0397 compared to 0.0420 in Fig. 4). The analogous comparison at other energies between 0.3 and 0.6 eV indicates that the OVA probabilities for the two choices of V_{ref} always have values within 30% of one another. More important, the OVA probabilities and converged results are generally in good agreement in their J dependence, but in very poor agreement in energy dependence, differing by several orders of magnitude at low energies. This difference in energy dependence has a dominant influence on the behavior of the reaction cross sections, as will be discussed in Sec. III. C.

In Fig. 5 we plot the inelastic nonreactive probabilities for the transition $v = 0$, $j = 0 \to v' = 0$, $j' = 2$ vs J for several energies E. The inelastic probabilities are seen to span a much larger range of J's than the reactive ones, indicating that larger impact parameter collisions can contribute significantly to the inelastic processes. At all energies in Fig. 6, the maximum rotational excitation probability occurs for J positive (although a smaller magnitude negative J peak does appear at the higher energies). The increased likelihood of exciting a positive rotational sublevel in a nonreactive collision with J initially positive is in agreement with the classical picture of the collision shown in Fig. 6 (Collision I) in which the incident atom having a positive impact parameter [see Eq. (3.2)] impulsively strikes the "bottom" atom of the diatomic molecule in Fig. 6, I(a), thus exerting positive torque on that

FIG. 7. Converged coplanar reactive differential cross section $\sigma_{00 \to 01}^R$ vs the scattering angle θ_R for total energies $E = 0.30$, 0.35, 0.40, and 0.45 eV.

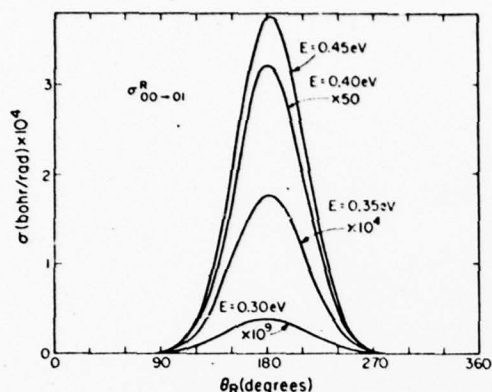FIG. 9. Converged coplanar reactive differential cross section $\sigma_{00 \to 00}^R$ vs scattering angle θ_R at same energies as in Fig. 8. These curves are symmetric about $\theta_R = 180°$.

molecule and exciting it into a rotational state with positive j'. For this collision, one would expect the dominant scattering angle θ to lie between 180° and 360° relative to the y axis of Fig. 6. In the next section we shall see that this is precisely what the differential cross sections indicate. Still unexplained, however, are the double-peaked distributions at the higher energies in Fig. 5. Intuitively, one would expect that the positive J peak results from the mechanism described above (Collision I in Fig. 6). The negative J peak must arise from a different collision mechanism, quite possibly that pictured in Collision II of Fig. 6, in which the incident atom, having small negative impact parameter, still strikes the bottom atom of the diatom in Fig. 6, IIa, but rebounds into the $0° \le \theta \le 180°$ hemisphere.

B. Differential cross sections

Figures 7, 8, and 9 depict the differential reactive cross sections corresponding to the same transitions and energy ranges as were used for the reaction prob-

FIG. 8. Converged coplanar reactive differential cross section $\sigma_{00 \to 01}^R$ as a function of the scattering angle θ_R analogous to Fig. 7 but at total energies $E = 0.50$, 0.55, 0.60, and 0.65 eV.

abilities in Figs. 1, 2, and 3, respectively. The $v = 0$, $j = 0 \to v' = 0$, $j' = 1$ distinguishable-atom reactive cross sections of Figs. 7 and 8 can be trivially converted to the corresponding antisymmetrized para - ortho quantities by multiplication by 3 [see (Eq. 2.1)]. Because of Eq. (2.3), the curves in Fig. 9 are exactly symmetric about $\theta_K = 180°$. We see that all reactive differential cross sections are strongly backward peaked. This is in agreement with the results of three- and two-dimensional quasiclassical calculations[1,2] and with the results of experiments on $D + H_2$[26] and $H + T_2$,[27] and is consistent with a rebound-type collision mechanism. The magnitudes of the differential cross sections near $\theta_R = 0°$ are all sufficiently small to allow us to conclude that forward scattering contributions to the reactive angular distributions are negligible. The small-amplitude oscillations in some of the higher energy differential cross sections in Figs. 8 and 9 are very likely spurious since they typically result from incomplete interference between different partial waves. This type of oscillatory behavior can be caused by as little as a 5% relative error in the matrix elements of S_J for a single partial wave, thus pointing out that equally accurate calculations for each partial wave (even those contributing relatively little to the integral cross sections) are necessary if spurious effects of this type are to be avoided. Of course, if there were rotational resonances in certain partial waves, then we would properly expect to see some form of oscillatory behavior in the angular distributions. Rotational resonances have indeed been observed in calculations on nonreactive atom diatom scattering, but these resonances have always been associated with attractive wells in the potential surfaces used.[28] In the case of the purely repulsive Porter–Karplus[19] potential, such wells do not exist, and thus purely rotational resonances are unlikely.[29] The full-width at half-maximum (FWHM) of the backward-scattered peak in the differential cross section remains relatively constant over the energy range studied and roughly equal to 70° (i.e., $145° \le \theta_R \le 215°$)

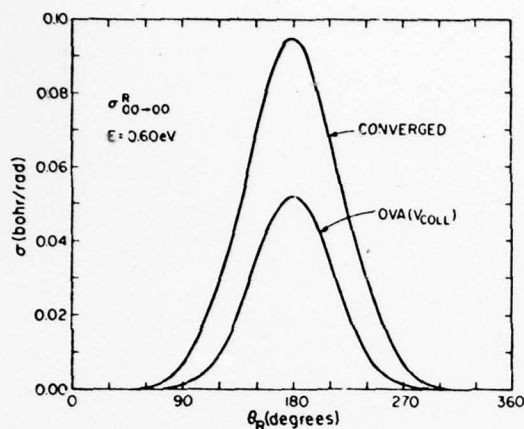FIG. 10. Vibrationally converged and OVA differential cross section σ^R_{00-00} as a function of scattering angle θ_R at $E = 0.60$ eV ($E_0 = 0.36$ eV). The OVA cross section was computed with a collinear reference potential $[V_{coll} = V(r_\lambda, R_\lambda, \gamma_\lambda = 0)]$. The cross section for this transition is symmetric about $\theta_R = 180°$.

in Fig. 9. Some broadening does, however, occur at the higher energies.

The angular distributions for the OVA results previously considered in Fig. 4 are plotted in Fig. 10. As in Fig. 4, we see that the shape of the converged curve is qualitatively well approximated by that of the OVA one, but there is about a factor of 2 difference in the magnitudes of the cross sections. This similarity in shape continues to exist at other energies as well, but the differences in magnitude can become much larger, as discussed in Sec. III. C.

In Fig. 11 we plot the distinguishable atom nonreactive inelastic differential cross sections σ^N_{00-02} at $E = 0.40$, 0.50, 0.60, and 0.70 eV. These angular dis-
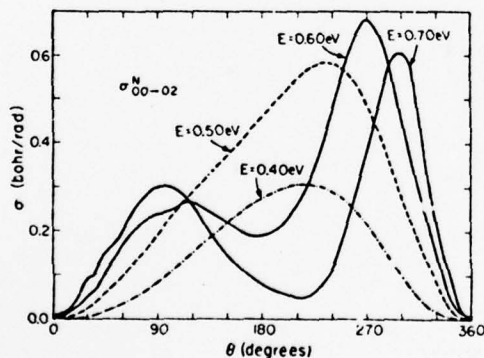
FIG. 11. Inelastic nonreactive (converged) differential cross section σ^N_{00-02} for the coplanar $v = 0$, $j = 0 \to v' = 0$, $j' = 2$ transition as a function of scattering angle at total energies $E = 0.40$ eV (dash–dot), 0.50 eV (dashed), 0.60 eV (solid), and 0.70 eV (solid).
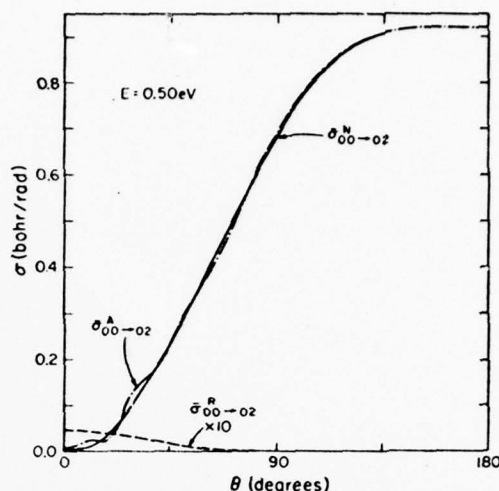
FIG. 12. Nonreactive (solid), reactive (dashed), and antisymmetrized (dash–dot) differential cross sections as a function of scattering angle for the coplanar $v = 0$, $j = 0 \to v' = 0$, $|j'| = 2$ transition (summed over final rotational polarizations) at $E = 0.50$ eV ($E_0 = 0.23$ eV). Note that the scattering angle used is θ and $\theta = 0$ corresponds, for reactive scattering, to $\theta_R = 180°$ [see Eq. (2.5)].

tributions clearly reflect the one- or two-peaked nature of the nonreactive probability plots of Fig. 5 and show predominantly backward to sidewards peaking with the position of the maximum shifting gradually to a more forward direction with increasing energy. The maximum value of σ^N_{00-02} always occurs for $180° \le \theta \le 360°$, in agreement with our qualitative classical ideas of Sec. III. A. At higher energies we see double-peaked distributions, possibly corresponding to the two mechanisms pictured in Fig. 6. There is little evidence of any high frequency oscillations in any of the cross sections plotted in Fig. 11, which indicates that the collision process is predominantly direct (nonresonant). The small-amplitude oscillations occurring at $\theta < 100°$ for $E = 0.60$ and 0.70 eV are probably spurious and of same origin as those for the reactive cross sections in Figs. 8 and 9.

Since the $v = 0$, $j = 0 \to v' = 0$, $j' = 2$ transition considered in Fig. 11 corresponds to a para-to-para transition which can occur by both nonreactive and reactive mechanisms, the correct physically measurable quantity (in a 2D world) to consider is the antisymmetrized para-to-para cross sections which can be obtained through the use of Eq. (2.1). In Figs. 12, 13, and 14 we plot the resulting antisymmetrized angular distributions $\bar{\sigma}^A_{00-02}$ (summed over degenerate product rotational polarizations) for total energies of 0.5, 0.6, and 0.7 eV, respectively. Also plotted for comparison are the corresponding distinguishable-atom nonreactive and reactive cross sections where, for consistency, the angle θ rather than θ_R [see Eq. (2.5)] is used for plotting the reactive differential cross sections. In terms of θ, the reactive cross section is forward peaked (i.e., back-
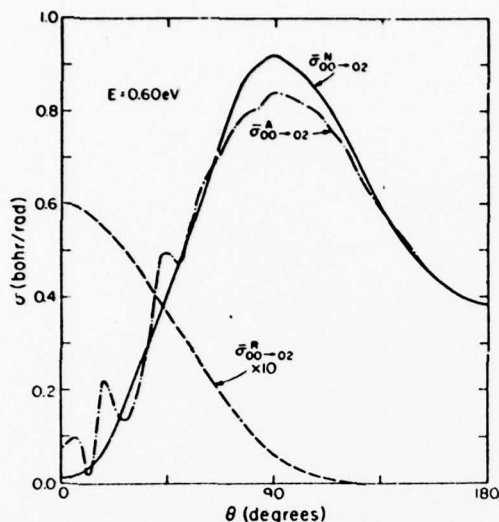
FIG. 13. Nonreactive, reactive, and antisymmetrized differential cross sections analogous to Fig. 12 at $E = 0.60$ eV (E_0 = 0.33 eV). See remark about θ in the caption for that figure.

ward peaked in terms of θ_R), while the nonreactive one is backward peaked at 0.5 eV shifting to sidewards peaking at the higher energies. At 0.50 eV (Fig. 12), the reactive cross section has a maximum value of 0.0045 bohr/rad, which is over 200 times smaller than the maximum value of the nonreactive one, 0.92 bohr/rad. This implies that $f^N_{vj-v'j'}$ in Eq. (2.1) has a much larger absolute value than $f^R_{vj-v'j'}$, so that the antisymmetrized and nonreactive differential cross sections are
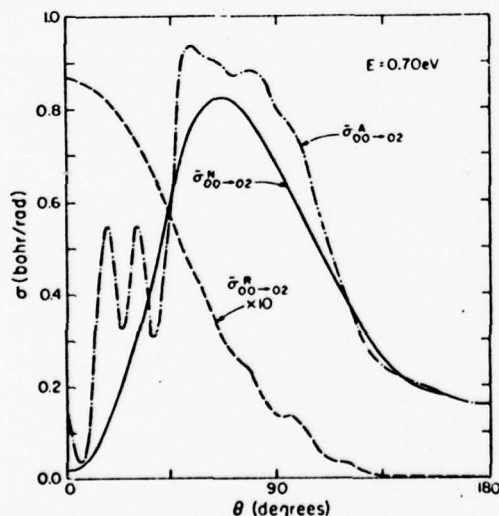
FIG. 14. Nonreactive, reactive, and antisymmetrized differential cross sections analogous to Fig. 12 at $E = 0.70$ eV (E_0 = 0.43 eV). See remark about θ in the caption of that figure.
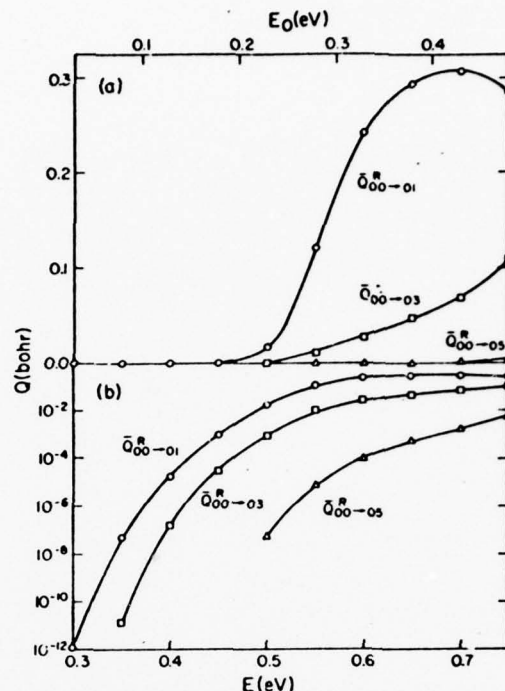
FIG. 15. Converged integral reactive cross sections $\bar{Q}^R_{00-01}$, $\bar{Q}^R_{00-03}$, and $\bar{Q}^R_{00-05}$ (summed over final rotational polarizations) vs total energy E and translational energy E_0: (a) linear scale, (b) semilogarithmic scale.

nearly identical. Some small amplitude oscillations are seen in σ^A_{00-02} at small θ in the neighborhood of the region where the reactive cross section has a maximum. These oscillations are real and result from interference between the direct and exchange contributions to the antisymmetrized cross section. They are similar in origin to the quantum symmetry oscillations which have been observed in atom–atom elastic and inelastic scattering.[30] As the energy is increased, the reactive cross sections increase much more rapidly than do the nonreactive ones (at all scattering angles), and (as is indicated in Figs. 13 and 14) the oscillations in the antisymmetrized differential cross sections for $\theta < 60°$ become quite pronounced in the forward θ (backward θ_R) direction. (The oscillations in the antisymmetrized curve of Fig. 14 at $\theta > 80°$ correlate with those in the reactive curve. As for Figs. 8 and 9, the latter are probably spurious, and therefore the former should not be considered to be real either.) A small increase in the oscillation frequency with increasing energy is also apparent from the figures.

C. Integral cross sections

In Fig. 15 we plot the reactive integral cross sections $\bar{Q}^R_{00-01}$, $\bar{Q}^R_{00-03}$, and $\bar{Q}^R_{00-05}$ (summed over final rotational polarizations) as a function of the total energy E and initial translational energy E_0. Both linear and
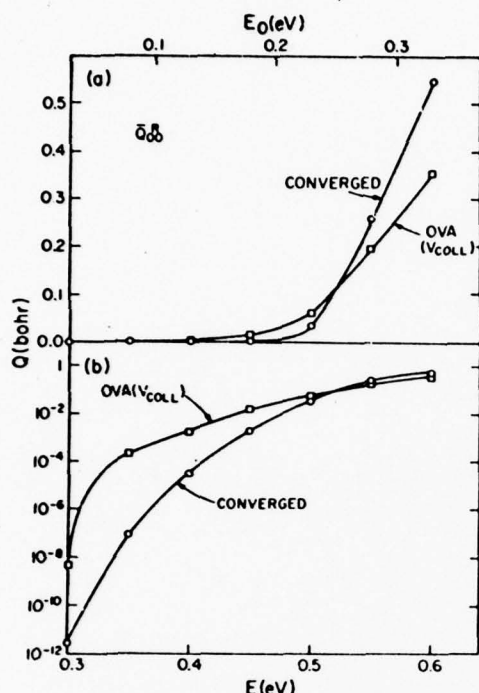
FIG. 16. Integral reactive cross section $\bar{Q}_{0\,0}^{R}$ (summed over all accessible final states) vs total energy E and relative energy E_0. Circles represent vibrationally converged results and squares the OVA ones using a collinear reference potential: (a) linear scale, (b) semilogarithmic scale.

semilogarithmic scales are used to show the functional dependence of these cross sections over a wide range of energies. If we define the effective threshold energy for a process as being that value of E for which the corresponding integral cross section is 0.01 bohr, then the threshold energies for $\bar{Q}_{00-01}^{R}$, $\bar{Q}_{00-03}^{R}$, and $\bar{Q}_{00-05}^{R}$ are 0.49 eV, 0.55 eV, and >0.75 eV, respectively. A discussion of the significance of the effective threshold energies will be deferred to Sec. III. D, where we also compare the coplanar results with those of collinear calculations on the same potential energy surface. Above threshold, $\bar{Q}_{00-01}^{R}$ rises in a nearly linear manner with E up to about 0.65 eV and achieves a maximum value of 0.31 bohr at about $E = 0.70$ eV. $\bar{Q}_{00-03}^{R}$ and $\bar{Q}_{00-05}^{R}$ increase monotonically in the energy range spanned by this figure but may level off at higher energies. At very low energies, the integral cross sections exhibit approximate exponential dependence on E. A characterization of the product rotational state distribution implicit in Fig. 15 is given in Sec. III. E. We should finally note that the reactive cross sections in Fig. 15 can be converted to the corresponding para –ortho quantities by multiplication by 3.

In Fig. 16 we compare the reactive cross section $\bar{Q}_{00}^{R}$ (summed over all product states) with the OVA re-

sult [using $V_{ref} = V(r_\lambda, R_\lambda, \gamma_\lambda = 0)$]. As mentioned in Sec. III. A, the results obtained using $V_{ref} = V_0^\lambda(r_\lambda, R_\lambda)$ have almost the same energy dependence. It is apparent from the figure that the vibrationally converged integral cross section differs quite significantly from the OVA result over much of the energy range considered, the difference being about 3 orders of magnitude for total energies below 0.30 eV. The two curves do cross near $E = 0.52$ eV, which is quite interesting, since a previous analysis of the collinear $H + H_2$ system (on a slightly different potential surface) indicated that this reaction is very nearly vibrationally adiabatic at this energy.[31] Since, as we shall see in the next section, collinear and coplanar calculations can be related in a reasonably accurate manner, one might be able to assess the accuracy of OVA calculations in two and three dimensions by analyzing the extent of vibrational adiabaticity in the corresponding collinear systems.

In Fig. 17 we compare the nonreactive and antisymmetrized integral cross sections $\bar{Q}_{00-02}^{N}$ and $\bar{Q}_{00-02}^{A}$ as a function of E and E_0. The rotationally inelastic cross sections have much larger magnitudes than the reactive ones of Figs. 15 and 16 with a peak value of 3.76 bohr near $E = 0.54$ eV. Since the $v' = 0$, $j' = 2$ state of H_2 becomes energetically accessible at $E = 0.30$ eV, we see that there is essentially zero threshold energy for the nonreactive process so that $\bar{Q}_{00-02}^{A}$ coincides almost exactly with its distinguishable-atom counterpart $\bar{Q}_{00-02}^{N}$ at all energies below 0.50 eV. Thereafter, $\bar{Q}_{00-02}^{A}$ becomes progressively larger than $\bar{Q}_{00-02}^{N}$ with no apparent oscillatory behavior as a function of energy resulting, in contrast to the angular distributions of Figs. 12–14.
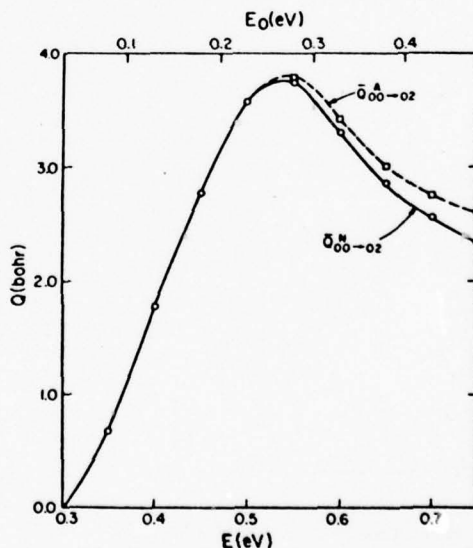
FIG. 17. Inelastic nonreactive integral cross sections $\bar{Q}_{00-02}^{N}$ and $\bar{Q}_{00-02}^{A}$ (summed over final polarizations) vs the total energy E and relative translational energy E_0.

D. Comparison of planar and collinear results

Because planar cross sections have the dimensions of length while collinear ones are dimensionless (i.e., the collinear cross section is equal to the collinear reaction probability), a direct comparison of these quantities is not possible. One could devise models for converting collinear results into planar ones by assigning a model impact parameter dependence to the collinear reaction probabilities. A more straightforward comparison can be effected instead by examining the behavior of the corresponding collinear[32,33] and planar reaction probabilities (the latter for $J = 0$) as are plotted in Fig. 18. Probabilities for other J's or different initial vj states could have been used, but those for $J = 0$ and $v = j = 0$ were chosen for this comparison because they correspond more closely to the collinear conditions. This choice is furthermore justified by the fact that the form of the energy dependence of the planar probabilities for different J or j (for reasonably small values of these quantum numbers) is essentially the same as that of P_{00}^R ($J=0$), as is demonstrated in Fig. 19 [where P_{00}^R ($J=0$), P_{00}^R ($J=4$), and P_{01}^R ($J=0$) are plotted]. The $P_{00}^R(J)$ curves, for $J = 1$, 2, 3, would all lie between the corresponding curves for $J = 0$ and $J = 4$. Figure 18 indicates that the collinear and coplanar results have nearly the same energy dependence, the en-

FIG. 19. Coplanar total reaction probabilities $P_{00}^R(J=0)$ (circles, solid curve), $P_{00}^R(J=4)$ (triangles, dash–dotted curve), and $P_{01}^R(J=0)$ (squares, dotted curve) summed over all final states vs total energy E and translational energy E_0: (a) linear scale, (b) logarithmic scale.

FIG. 18. Total reaction probabilities P_0^R(1D) (collinear) and P_{00}^R(2D, $J=0$) (coplanar, $J=0$, $v=0$, $j=0$ and summed over all final states) vs the total energy E and translational energy E_0: (a) linear scale, with the collinear results multiplied by 0.6; (b) semilogarithmic scale.

ergy scale being shifted upwards by about 0.055 eV in going from the collinear to the coplanar curves. In addition, the maximum value of the collinear reaction probability is 1.0, whereas that of the coplanar one is about 0.6. Both the energy shift and the difference in the maximum probability are explainable in terms of relatively simple concepts. To understand the energy shift, we examine the nature of the triatomic H_3 system in its transition state. In the linear case, this triatomic pseudomolecule has two vibrational degrees of freedom: an asymmetric stretch mode, which is unstable and leads to motion along the reaction coordinate, and a stable symmetric stretch mode. When the reaction occurs and the system passes through the transition state region, the total energy partitions itself between these two vibrational modes. Energy in the symmetric stretch mode is not easily converted into the asymmetric stretch mode making it unavailable to overcome the potential surface barrier. This is a partial physical interpretation of the fact that the collinear threshold energy (the value of E at which the reaction probability is 0.01) is 0.42 eV, which is somewhat larger than the 0.396 eV Porter–Karplus surface barrier height. Collinear threshold phenomena such as this have been analyzed in detail elsewhere.[4,31] In going from a linear to a planar transition state we add one bending degree of freedom to the internal motion of the
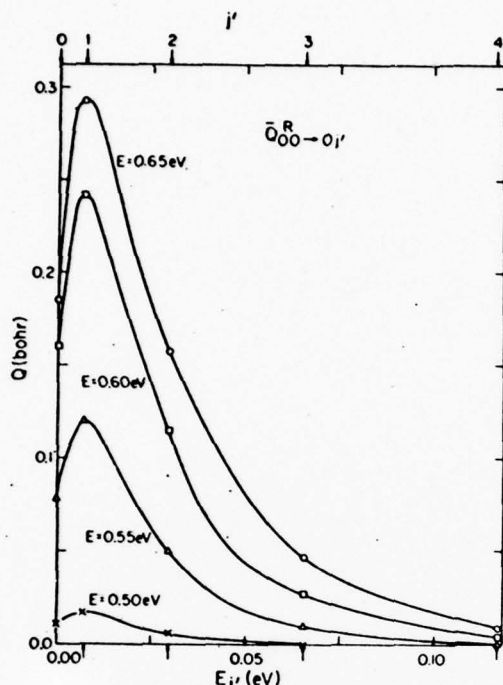
FIG. 20. Converged coplanar integral reaction cross sections $\bar{Q}^R_{00-0j'}$ vs the final rotational energy at total energies $E = 0.50$ eV (triangles), 0.55 eV (triangles), 0.60 eV (squares), and 0.65 eV (circles). The arrows in lower and upper abcissa indicate the $E_{j'}$ rotational energies. The curves are drawn smoothly through the points.

transition state which also does not contribute effectively to motion along the reaction coordinate and which will also tie up some of the energy needed to overcome the activation barrier. This additional energy in the bending motion is a plausible explanation for the 0.055 eV upward energy shift observed in Fig. 18 and is approximately equal to the zero point bending energy of about 0.06 eV for the surface used.[34] Much of the above explanation has its basis on an approximate statistical theory proposed by Marcus.[35] The difference in the maximum probabilities attained by the collinear and coplanar results can be understood by examining the orientation dependence of the reaction probability. In the planar case with $j = 0$ initially, the diatomic molecule does not rotate and has equal probability of being in any orientation with respect to the direction of approach of the incident atom. Since the barrier height of the potential energy surface is 0.396 eV for collinear collisions and increases to 2.8 eV for perpendicular ones, we would expect that in the energy range being considered, the reaction probability should be greater for linear collisions and decrease to zero for perpendicular ones. The coplanar probability should represent an average over all initial orientations and if we assume unit reaction probability for $0 \le \gamma_\lambda \le 54°$ and $306° \le \gamma_\lambda \le 360°$ and, by symmetry, for $|180° - \gamma_\lambda| \le 54°$ and zero

probability elsewhere, we obtain a coplanar reaction probability of 0.60 in agreement with Fig. 18. The 54° cut-off angle is in reasonable agreement with previous estimates of the orientation dependence of the reaction probability obtained from distorted wave results[15] and from classical trajectory results.[1]

E. Product state rotational distributions

In Fig. 20 we plot the integral cross sections $\bar{Q}^R_{00-0j'}$ (summed over final rotational polarizations) as a function of the production rotational energy and quantum number for several total energies E. We see from the figure that only small j' rotational states are appreciably excited in these reactive collisions. The relative population of final rotational states is not strongly dependent on total energy although some broadening of the distribution does occur at higher E. Not shown in the figure are the final rotational state distributions from initial states $j \ne 0$. The qualitative *shapes* of these distributions are not strongly dependent on j and look very much like those for $j = 0$ in Fig. 20. However, the *magnitudes* of the $\bar{Q}^R_{0j-0j'}$ decrease monotonically with increasing j for a given j'.[36]

To a large extent, the distributions in Fig. 20 resemble rotational Boltzman-like distributions with a single temperature parameter. Distributions of this type, for a planar system, may be expected to have the form[37]

$$f_{j'}(\bar{E}) = A(E)(2 - \delta_{j'0}) e^{-E_{j'}/kT(E)} , \qquad (3.3)$$

where $A(E)$ and $T(E)$ are energy dependent constants and $2 - \delta_{j'0}$ is a degeneracy factor. In Fig. 21 we plot $[2/(2 - \delta_{j'0})]\bar{Q}^R_{00-0j'}$ as a function of the product rotational energy on a logarithmic ordinate scale. The resulting curves for different E are approximately linear (most nearly so at the higher energies) in agreement with the predictions of Eq. (3.3), with temperature parameters $T(E)$ in the neighborhood of 250–400 K. We should point out that although the rotational distributions are temperaturelike, we find no evidence of long lived compound state (i.e., complex) formation in this reaction at the energies being considered.[38] The rotational distributions seem to be determined to a large extent by the shape of the potential energy surface in the transition state region of configuration space [see lower half of Fig. 2(c) of Paper I]. In this transition state, the asymptotic free rotational motion has become a seriously restricted bending motion. This bending motion becomes again a free rotational motion after the reaction, and, at least qualitatively, the distribution of different product rotational states appears to be determined by the overlap of this bending wavefunction and the asymptotic free rotor wavefunction. If this reasoning is correct, the resemblance of the rotational distribution in Figs. 20 and 21 to thermal distributions is at least partially coincidental. This phenomenon should, however, be quite common since restricted bending motion in the transition state region is a common feature of the potential energy surfaces for many reactions.

In Fig. 22 we plot the OVA cross sections in a man-
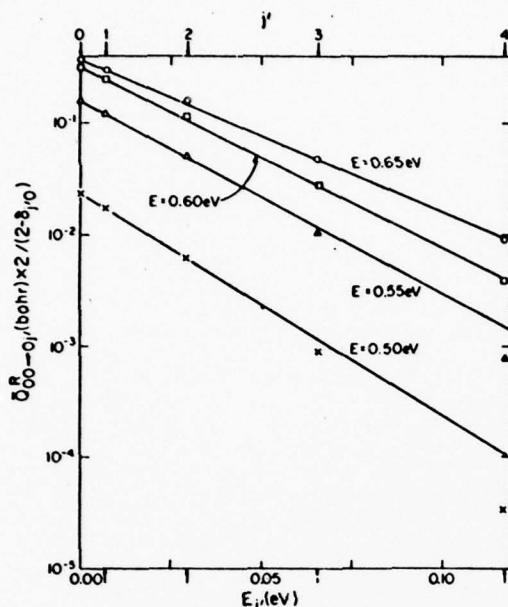
FIG. 21. Semilogarithmic plot of the integral reactive cross section $\bar{Q}^R_{00\rightarrow 0j'}$ $[\times 2/(2-\delta_{j'0})]$ vs the final rotational energy at total energies $E = 0.50$, 0.55, 0.60, and 0.65 eV (symbols analogous to those of Fig. 20). Straight lines are drawn connecting the low j' points. The arrows are as in Fig. 20.
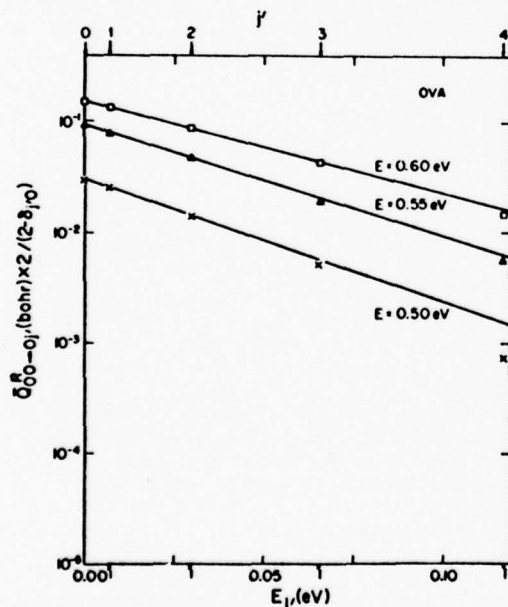
FIG. 22. Semilogarithmic plot of the OVA reactive cross section $\bar{Q}^R_{00\rightarrow 0j'}$ $[\times 2/(2-\delta_{j'0})]$ as a function of the final rotational energy at energies $E = 0.50$, 0.55, and 0.60 eV. The straight lines drawn connect the low j' points. The arrows are as in Fig. 20.
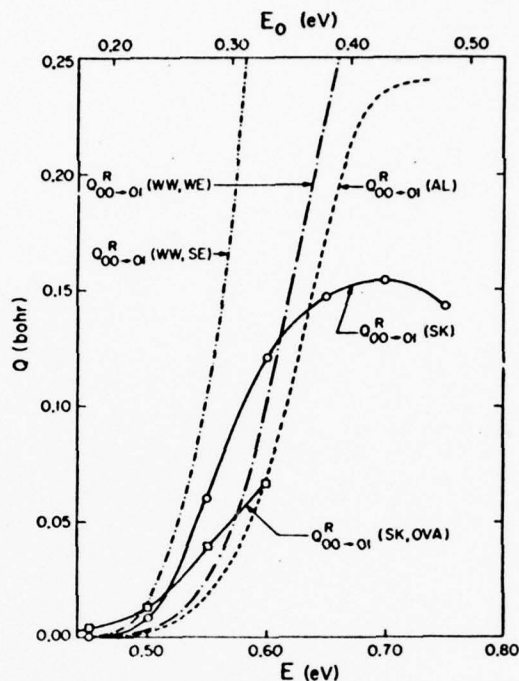
FIG. 23. Integral cross section $Q^R_{00\rightarrow 01}$ vs total energy E and translational energy E_0 for several exact and approximate coplanar calculations. $Q^R_{00\rightarrow 01}$(SK) refers to the present converged results, $Q^R_{00\rightarrow 01}$ (SK, OVA) are the present one-vibration-approximation results, for a collinear V_{ref}, obtained as described in Sec. II.D, $Q^R_{00\rightarrow 01}$(WW, WE) and $Q^R_{00\rightarrow 01}$(WW, SE) are the results of distorted wave calculations of Ref. 15, and $Q^R_{00\rightarrow 01}$ (AL) is the OVA result (on a different potential surface and using a method somewhat different from ours) of Ref. 10.

ner analogous to that done for the converged cross sections in Fig. 21. Figure 22 indicates that the OVA rotational distributions fit the temperaturelike distribution given in Eq. (3.3) to about the same accuracy as the converged results. However, the OVA temperature parameters are somewhat higher (450–620 K), indicating that this approximate procedure predicts rotational distributions which are much broader than the converged ones.

F. Comparisons with other coplanar calculations

In Fig. 23 we plot our converged $Q^R_{00\rightarrow 01}$ (SK) and the corresponding one-vibration-approximation results $Q^R_{00\rightarrow 01}$ (SK, OVA) using a collinear reference function (see Sec. II. D), along with the results of two other studies on coplanar $H + H_2$. $Q^R_{00\rightarrow 01}$ (WW, SE) and $Q^R_{00\rightarrow 01}$ (WW, WE) come from two different applications of the distorted wave approximation by Walker and Wyatt[15] on the Porter–Karplus surface. SE and WE refer, respectively, to the strong and weak expansion path choices of the nonreactive reference potential used to generate the distorted wavefunctions. $Q^R_{00\rightarrow 01}$ (AL) is the coupled-channel result (using one variation of the OVA)
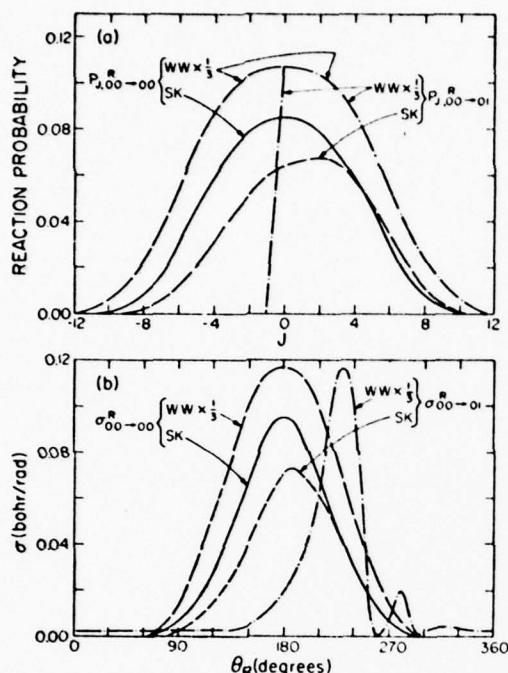
FIG. 24. Reaction probabilities $P_{J,00-00}^R$ and $P_{J,00-01}^R$ and differential cross sections σ_{00-00}^R and σ_{00-01}^R as a function of reactive scattering angle θ_R. WW refers to the SE results of Ref. 15 with long dashed curves referring to 00 → 00 transitions and dash–dot curves to 00 → 01 ones. SK refers to the results of this paper (Figs. 2, 3, 8, and 9) with solid curves for 00 → 00 and short dashed for 00 → 01 transitions. WW results are at $E_0 = 0.34$ eV ($E = 0.61$ eV), while SK results are at $E_0 = 0.33$ eV ($E = 0.60$ eV).

of Altenberger-Siczek and Light,[10] in which an earlier calculation of Saxon and Light[8] is corrected. These calculations were done for an analytical surface fitted to the *ab initio* SSMK[38] surface. The two approximate calculations of Walker and Wyatt seem to bracket our result at low energies, but for $E > 0.60$ eV, the absence of conservation of flux in the distorted wave calculation results in a gross overestimation of the integral cross sections. Thus, the distorted wave method remains accurate only when the reaction probabilities or cross sections are small. A similar conclusion was also drawn from an analogous collinear comparison.[39] The shapes of the distorted wave differential cross section σ_{00-00}^R vs reactive scattering angle θ_R (Fig. 24) are in good agreement with the corresponding results of our converged calculations, but not the magnitude of those cross sections. A similar comparison of the cross sections σ_{00-01}^R in that figure indicates serious disagreement in both shape and magnitude, apparently due to a much more rapid falloff in the distorted wave reaction probabilities with decreasing $J (J < 0)$ than is the case with our results [as seen in Fig. 24(a)].

The results of Altenberger-Siczek and Light[10] of Fig.

23 cannot be quantitatively compared with ours because of the difference in potential energy surfaces used in the two calculations, but some qualitative observations are nevertheless appropriate. First, the effective threshold energies (defined in Sec. III. C) of the integral cross sections are about 0.50 eV for the converged Q_{00-01}^R(SK), 0.49 eV for the Q_{00-01}^R(SK, OVA), and 0.53 eV for Q_{00-01}^R(AL). The difference of 0.04 eV between these last two numbers is approximately equal to the 0.03 eV difference between the heights of the respective potential barriers (0.396 eV and 0.425 eV) in the surfaces used in the calculations. Since the properties of the saddle point regions of these surfaces are similar, one might expect that a small change in barrier height should indeed result in a correspondingly small change in effective threshold energy as observed. Second, even if the AL curve is shifted to lower energies by 0.03 eV to correct for this difference in barrier heights, it agrees neither with our converged nor with our OVA results; above the phenomenological threshold, it increases more rapidly with energy and to larger values than either of the latter. This may be due to differences in the characteristics of the two surfaces other than the barrier heights. Third, except for some possibly spurious oscillations, the Altenberger-Siczek and Light angular distributions (Figs. 8–10 of Ref. 10) have shapes which are generally similar to ours (Figs. 8, 9 of this paper) for all transitions considered. The dominant peak near 180° in their angular distributions is somewhat narrower than ours and their reaction probabilities fall off more rapidly with increasing $|J|$ than do ours in Figs. 1–3. Both of these differences could be a result of the different potential surfaces used, since as seen in Figs. 4 and 10 the OVA does not strongly affect the shapes of σ^R vs θ_R and P^R vs J curves.

G. Rate constants

In this section we examine the behavior of the para-to-ortho thermal rate constant $k_{p-o}(T)$. The ortho-to-para rate constant can, of course, be obtained from k_{p-o} by using the easily calculable equilibrium constant for this reaction,[10] computed for the coplanar world of this paper. To obtain $k_{p-o}(T)$ we first require the para-to-ortho cross sections $\bar{Q}_{vj}^A$ [summed over all final ortho states and averaged over initial (para) rotational polarizations]. These are listed in Table IV for both the converged and OVA calculations.

The planar para-to-ortho rate constant is given by

$$k_{p-o}(T) = \frac{1}{Z} \sum_{v=0}^{\infty} \sum_{\substack{j=0 \\ (j=even)}}^{\infty} (2 - \delta_{j0}) e^{-E_{vj}/kT} k_{vj}^A(T), \quad (3.4)$$

where Z is the planar partition function

$$Z = \sum_{v=0}^{\infty} \sum_{\substack{j=0 \\ (j=even)}}^{\infty} (2 - \delta_{j0}) e^{-E_{vj}/kT} \quad (3.5)$$

and

$$k_{vj}^A(T) = \left(\frac{2}{\mu}\right)^{1/2} \frac{1}{kT} \int_0^{\infty} e^{-E_{vj}'/kT} \bar{Q}_{vj}^A(E_{vj}') E_{vj}'^{1/2} dE_{vj}'. \quad (3.6)$$

TABLE IV. Para-to-ortho integral cross sections (in bohr) for $H + H_2$.[a]

E		Converged			OVA	
	$\bar{Q}_{00}^A$	$\bar{Q}_{02}^A$	$\bar{Q}_{04}^A$	$\bar{Q}_{00}^A$	$\bar{Q}_{02}^A$	$\bar{Q}_{04}^A$
0.30	0.356(−11)	⋯	⋯	0.543(−8)	⋯	⋯
0.35	0.144(−6)	0.137(−7)	⋯	0.343(−3)	0.221(−4)	⋯
0.40	0.499(−4)	0.868(−5)	0.400(−4)	0.280(−2)	0.976(−3)	0.228(−7)
0.45	0.299(−2)	0.721(−3)	0.104(−5)	0.0249	0.958(−2)	0.288(−3)
0.50	0.0543	0.0319	0.127(−3)	0.0918	0.0476	0.336(−2)
0.55	0.391	0.140	0.309(−2)	0.294	0.166	0.0250
0.60	0.841	0.361	0.0233	0.533	0.339	0.0727
0.65	1.025	0.619	0.0724	b	b	b
0.70	1.134	0.877	0.194	b	b	b
0.75	1.204	1.088	0.344	b	b	b

[a]All cross sections have been summed over final ortho (odd j') states and averaged over initial rotational polarizations. The numbers in parentheses indicate powers of 10 by which the numbers preceding them are multiplied.
[b]These cross sections were not calculated, but estimates of their values (through various extrapolation procedures) were used in the rate constant calculations. Because they involve higher energy results, their contributions to the rate constants are small, and the errors in these rate constants resulting from the extrapolations are usually less than 10%.

E_{vj} is the vibration–rotation energy of the initial state with quantum numbers vj, and E'_{vj} is the translational energy relative to that state ($E'_{vj} = E - E_{vj}$). μ is the reduced mass associated with the relative motion of the reagents and the factor $2 - \delta_{j0}$ is introduced to account explicitly for rotational degeneracy. The initial spin degeneracy is 1 for all para states. The rate constant thus defined has the units cm²/molecule · sec, which is appropriate for a planar world in which concentrations are measured in molecule/cm².

Using Eqs. (3.4)–(3.6) along with the data in Table IV, $k_{p\rightarrow o}(T)$ has been calculated, and the resulting Arrhenius plots for the vibrationally converged and OVA $[V_{ref} = V(r_\lambda, R_\lambda, \gamma_\lambda = 0)]$ results are presented in Fig. 25. As might be expected from the appearance of the integral cross sections in Fig. 16, the OVA rate constant is considerably larger than the converged one at low temperatures, with the ratio of the two being 12.4 and 2.83 at 200 K and 300 K, respectively. At high temperatures, the two rate constants approach each other quite closely, a reflection of the similar effective threshold energies of the converged and OVA cross sections. The high temperature portions of the Arrhenius plots in Fig. 25 are nearly linear with resulting Arrhenius activation energies of 5.2 and 5.0 kcal/mole for the converged and OVA results, respectively. The high temperature Arrhenius straight line corresponding to the converged results is represented by the dashed line of Fig. 25. We will defer a detailed comparison of these rate constants with those of accurate one- and three-dimensional calculations and with approximate theoretical and experimental ones to a separate paper.

IV. CONCLUSION

It should be apparent from the wealth of dynamical information presented in Sec. III that these calculations can be extremely useful to our understanding of chemical dynamics. We would like to stress that these calculations are not overly time consuming, but it is un-

likely that similar ones will be done on more than the very simplest of chemical systems. Rather, the primary emphasis is to use these results as benchmarks against which approximate theories may be compared, with the hope that these theories may be in turn applied
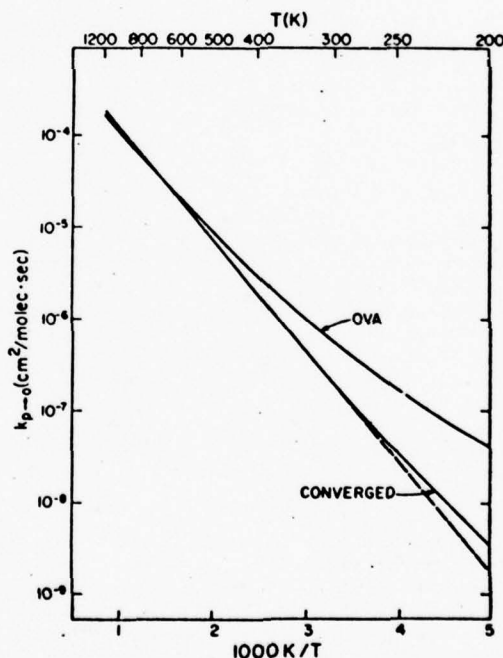

FIG. 25. Arrhenius plot of the converged and OVA para-to-ortho coplanar thermal rate constants for $H + H_2$ for the converged and OVA (collinear reference potential) results. The dashed straight line is tangent to the converged one at high temperatures.

to more complicated systems. The comparisons with approximate calculations presented in Sec. III. F were incomplete in that the results of quasiclassical and semiclassical coplanar calculations on the Porter-Karplus H_3 surface are needed to assess the quantitative accuracy of these important approximate theories. Also requiring further consideration is the use of collinear-type theories to provide approximate coplanar results, and similarly of coplanar theories to describe the three-dimensional world.[41] This was discussed briefly in Sec. III. D and will be further investigated in a separate paper.

The coplanar calculations are also important in elucidating what kinds of phenomena are significant in chemical reactions. The magnitude of the quantum symmetry oscillations in the para-to-para angular distributions (Sec. III. B) as a function of energy (Sec. III. C) and their absence in the corresponding integral cross sections are a good example. Such quantum symmetry effects may eventually be a useful experimental tool for characterizing reactive potential surfaces. Also of great importance is the characterization of the reaction in terms of direct and resonant mechanisms. This was briefly mentioned in Sec. II. B, where we remarked that the reaction appeared to be completely dominated by the direct mechanism. A more detailed analysis at energies higher than were considered in this work indicates that in the neighborhood of certain energies (such as $E \sim 0.92$ eV) this no longer seems to be correct as very significant resonantlike effects are observed. The importance of these resonant processes is discussed elsewhere.[32]

Finally, as was mentioned in the introduction, these calculations are significant in that they demonstrate the feasibility of the method outlined in Paper I for doing quantum 2D scattering calculations. Extension of this method to the 3D problem has recently been accomplished,[12,21] and the results of these 3D calculations and their comparison with 2D and 1D ones should be extremely useful to our understanding of chemical dynamics.

ACKNOWLEDGMENT

[1]M. Karplus, R. N. Porter, and R. D. Sharma, J. Chem. Phys. 43, 3259 (1965); the classical angular distribution is reported in Ref. 9.
[2]R. P. Saxon and J. C. Light, J. Chem. Phys. 57, 2758 (1972).
[3]J. M. Bowman and A. Kuppermann, J. Chem. Phys. 59, 6524 (1973).
[4]J. D. Doll, T. F. George, and W. H. Miller, J. Chem. Phys. 58, 1343 (1973).
[5]J. J. Tyson, R. P. Saxon, and J. C. Light, J. Chem. Phys. 59, 363 (1973).
[6]D. G. Truhlar and A. Kuppermann, J. Chem. Phys. 56, 2232 (1972).
[7]G. C. Schatz and A. Kuppermann, J. Chem. Phys. 59, 964 (1973).
[8]R. P. Saxon and J. C. Light, J. Chem. Phys. 56, 3874 (1972); 56, 3885 (1972).
[9]G. Wolken and M. Karplus, J. Chem. Phys. 60, 351 (1974).
[10]A. Altenberger-Siczek and J. C. Light, J. Chem. Phys. 61, 4373 (1974).
[11]A. Kuppermann, G. C. Schatz, and M. Baer, J. Chem. Phys. 61, 4362 (1974).
[12]A. Kuppermann and G. C. Schatz, J. Chem. Phys. 62, 2502 (1975).
[13]K. T. Tang and M. Karplus, Phys. Rev. A 4, 1844 (1971).
[14]K. T. Tang and B. H. Choi, J. Chem. Phys. 62, 3642 (1975).
[15]R. B. Walker and R. E. Wyatt, J. Chem. Phys. 61, 4839 (1974).
[16]Reference 2 contains an extensive list of collinear studies of this reaction.
[17]H. S. Johnston, Gas-Phase Reaction Rate Theory (Ronald, New York, 1966), Chap. 10 and references therein.
[18]A. Kuppermann, G. C. Schatz, and M. Baer, J. Chem. Phys. 65, 4596 (1976), preceding paper, referred to as Paper I in the present paper.
[19]R. N. Porter and M. Karplus, J. Chem. Phys. 40, 1105 (1964).
[20]We prefer the terms "coupled channel" or "coupled equation" rather than "close coupling" because we have found that many channels are needed to achieve convergence, including those which are not "close" to either the initial or final states considered.
[21]G. C. Schatz and A. Kuppermann, J. Chem. Phys. 65, 4642 (1976); 65, 4668 (1976), following two papers.
[22]Double precision (64 bit) arithmetic was used for all calculations.
[23]As J increases, the repulsive centrifugal potential increases, effectively raising the potential in the interaction region and decreasing the reaction probability. The "physical" scattering wavefunction becomes small in the interaction region as this happens. On the other hand, when integrating the coupled-channel equations, the closed-channel wavefunctions always increase exponentially in the direction of integration because of the dominance of the increasing exponential solution over the decreasing one. For large J, all channels are closed in the strong interaction region. As a result, the solutions generated by propagation into that region (the plus solutions) become exponentially large, whereas those generated by integrating in the outward direction (the minus solutions) are small in the strong interaction region when compared with the values they attain outside of it. These minus solutions, which decrease exponentially as one penetrates the potential barrier, are the only physically meaningful ones and therefore the only ones which will contribute significantly to the physical solution. This implies that the matching procedure will attach a very small weight to the plus solutions [i.e., $c_j^+(c_j^-)^{-1} \approx 0$ in Eq. (5.44) of Paper I]. From Eqs. (5.9)–(5.14) and especially (5.18) of Paper I, we see that $c_j^+(c_j^-)^{-1} = 0$ leads to a reactance matrix which is independent of any information about the matching, and hence the resulting nonreactive transition probabilities will not be

sensitive to the lack of orthogonality of $S_{\nu\lambda}^j$.

[24] For example, see R. Courant and D. Hilbert, *Methods of Mathematical Physics* (Interscience, New York, 1970), Vol. 1, p. 4.

[25] We have tested both expressions in doing the OVA calculations, and have found that Eq. (3.48) of Paper I leads to a much poorer approximation to the converged results than does Eq. (2.10) of the present paper, and that use of the former expression can actually lead to spurious resonantlike behavior in some transition probabilities. This could presumably result from the fact that in Eq. (2.10), we have analytically assumed completeness in carrying out the matrix multiplication present in Eq. (3.48) of Paper I, so the effects of a severe basis set truncation might be less important than in Eq. (3.48) of I, where this completeness is neither assumed nor explicitly included.

[26] J. Geddes, H. F. Krause, and W. L. Fite, J. Chem. Phys. 56, 3298 (1972).

[27] G. H. Kwei, V. W. S. Lo, and E. A. Entemann, J. Chem. Phys. 59, 3421 (1973).

[28] D. A. Micha, Phys. Rev. 162, 88 (1967); D. A. Micha, Chem. Phys. Lett. 1, 139 (1967); R. D. Levine, B. R. Johnson, J. T. Muckerman, and R. B. Bernstein, J. Chem. Phys. 49, 56 (1968); R. D. Levine and R. B. Bernstein, J. Chem. Phys. 53, 686 (1970).

[29] This argument does not rule out vibrational internal excitation resonances. These resonances have actually been observed in planar and 3D $H + H_2$[32] (at higher energies than are considered in this paper). As one might expect, however, they affect more than one partial wave[32] and are probably not responsible for the oscillations observed here.

[30] For examples, see J. M. Farrer and Y. T. Lee, J. Chem. Phys. 56, 5801 (1972); P. E. Siska, J. M. Parson, T. P. Schafer, and Y. T. Lee, J. Chem. Phys. 55, 5762 (1971),

J. M. Farrar and Y. T. Lee, J. Chem. Phys. 57, 5492 (1972); H. Haberland, C. H. Chen, and Y. T. Lee, At. Phys. 3, 339 (1973); B. Andresen and A. Kuppermann, Mol. Phys. 30, 997 (1975).

[31] J. M. Bowman, A. Kuppermann, J. T. Adams, and D. G. Truhlar, Chem. Phys. Lett. 20, 229 (1973).

[32] G. C. Schatz and A. Kuppermann, Phys. Rev. Lett. 35, 1266 (1975).

[33] (a) D. J. Diestler, J. Chem. Phys. 54, 4547 (1971); (b) J. W. Duff and D. G. Truhlar, Chem. Phys. Lett. 23, 327 (1973).

[34] A. B. Elkowitz and R. E. Wyatt, J. Chem. Phys. 63, 702 (1975).

[35] R. A. Marcus, J. Chem. Phys. 46, 959 (1967).

[36] Using microscopic reversibility the dependence of $\bar{Q}_{0j \to 00}^R$ on j can be extracted from the $\bar{Q}_{00 \to 0j}^R$ in Fig. 21 by multiplying the latter by the ratio $2k_{00}/[k_{02}(1+\delta_{j0})]$, where the wave numbers k_{00} and k_{02} refer to the $v=0$, $j=0$ and $v=0$, $j=2$ states of H_2, respectively, and $(1+\delta_{j0})/2$ is a degeneracy factor.

[37] The distribution may be derived from an information theoretic formalism [see, for example, A. Ben-Shaul, R. D. Levine, and R. B. Bernstein, J. Chem. Phys. 57, 5427 (1972)] by assuming that the surprisal function is linear in the product rotational energy. Note that the 2D translational density of states is independent of $E_{j'}$ and is therefore omitted from Eq. (3.3).

[38] I. Shavitt, R. M. Stevens, F. L. Minn, and M. Karplus, J. Chem. Phys. 48, 2700 (1968).

[39] R. B. Walker and R. E. Wyatt, Chem. Phys. Lett. 16, 52 (1972).

[40] A. Farkas, *Orthohydrogen, Parahydrogen and Heavy Hydrogen*, (Cambridge U.P., London, 1935), p. 13.

[41] For a recent paper on this subject, see R. B. Walker and R. E. Wyatt, Mol. Phys. 28, 101 (1974).

Quantum mechanical reactive scattering for three-dimensional atom plus diatom systems. I. Theory*

George C. Schatz† and Aron Kuppermann

Arthur. Amos Noyes Laboratory of Chemical Physics,‡ California Institute of Technology. Pasadena. California 91125
(Received 22 December 1975)

A method is presented for accurately solving the Schrödinger equation for the reactive collision of an atom with a diatomic molecule in three dimensions on a single Born-Oppenheimer potential energy surface. The Schrödinger equation is first expressed in body-fixed coordinates. The wavefunction is then expanded in a set of vibration-rotation functions, and the resulting coupled equations are integrated in each of the three arrangement channel regions to generate primitive solutions. Next, these are smoothly matched to each other on three matching surfaces which appropriately separate the arrangement channel regions. The resulting matched solutions are linearly combined to generate wavefunctions which satisfy the reactance and scattering matrix boundary conditions, from which the corresponding R and S matrices are obtained. The scattering amplitudes in the helicity representation are easily calculated from the body fixed S matrices, and from these scattering amplitudes several types of differential and integral cross sections are obtained. Simplifications arising from the use of parity symmetry to decouple the coupled-channel equations, the matching procedures and the asymptotic analysis are discussed in detail. Relations between certain important angular momentum operators in body-fixed coordinate systems are derived and the asymptotic solutions to the body-fixed Schrödinger equation are analyzed extensively. Application of this formalism to the three-dimensional $H + H_2$ reaction is considered including the use of arrangement channel permutation symmetry, even–odd rotational decoupling and postantisymmetrization. The range of applicability and limitations of the method are discussed.

I. INTRODUCTION

One of the most important goals of chemical dynamics is the accurate calculation of cross sections for reactive bimolecular collisions. Such calculations can be used to develop and test approximate reaction dynamic theories and statistical theories, to advance our understanding of dynamical processes governing reactive collisions, and to interpret, analyze, and make predictions concerning the results of experiments.

In recent years, a number of attempts have been made to solve this problem accurately (i.e., quantum mechanically) for the simplest possible such chemical reaction, the collision of an atom with a diatomic molecule on a single electronically adiabatic potential energy surface. One of the major difficulties in achieving this goal in the past has been the absence of computationally efficient procedures for obtaining accurate solutions to the Schrödinger equation for reactive collisions. For the simple case in which the three atoms are confined to move on a space-fixed straight line, adequately accurate and efficient methods have been developed within the last several years and applied to a variety of systems. [1-13] However, when the collinearity restriction is eliminated, the problem becomes more difficult, especially when the atom is permitted to react with either end of the diatom. To tackle such noncollinear problems, several different techniques have been proposed and to a certain extent tested. Baer and Kouri[14] have developed an integral equation method and have applied it to a simple three-dimensional model atom plus diatom system in which reaction with only one end is permitted. Saxon and Light, and Altenberger-Siczek and Light,[15] have investigated the coplanar $H + H_2$ reaction using a coupled-equation (i.e., close-coupling) procedure which ignored closed vibrational channels, while Wyatt and co-workers[16] have developed a some-

what different coupled-equation procedure in which closed channels are included and for which the use of hindered rotor basis functions leads to simple bifurcation properties. Quite recently, Elkowitz and Wyatt[16a] have applied this procedure to the three-dimensional $H + H_2$ reaction. Wolken and Karplus[17] have applied an integrodifferential equation method proposed by Miller[18] to 3D $H + H_2$ using a one-vibrational-basis-function approximation.

In a previous paper[19] (hereafter referred to as Paper I) we described a method for accurately solving the Schrödinger equation for reactions of the type $A + BC \rightarrow AB + C$ or $AC + B$ on a single electronic potential energy surface with the restriction that the motions of the three atoms be constrained to lie in a single space-fixed plane. An extensive application of this method to the planar $H + H_2$ exchange reaction has now been made.[20,21] The present paper describes an extension of this method to three-dimensional atom–diatom collisions. It yields a computationally practical procedure for accurately calculating reaction cross sections for many atom–diatom chemical reactions. A number of additional concepts not present in the planar problem are introduced, and the simplifications occurring in an application to three-dimensional $H + H_2$ are discussed. Preliminary results of an application of this method to the $H + H_2$ reaction on a realistic potential surface have recently been published,[22] providing the first fully converged quantum mechanical cross sections for a chemical reaction. The extension of these calculations to energies above the threshold for vibrational excitation has lead to the discovery of an internal excitation resonance[23] for that reaction, a phenomenon whose experimental detection may be an important tool in the characterization of reactive potential energy surfaces. A more complete description of these results for $H + H_2$ follows.[24]

The method utilizes a coupled-channel (i.e., close-coupling) propagation technique to generate complete sets of solutions in each of the three arrangement channel regions of configuration space, followed by a "matching procedure" in which the solutions are smoothly matched to one another on a set of three appropriately chosen surfaces which separate these three regions. The scattering matrices, amplitudes, and cross sections are then determined by analyzing the asymptotic behavior of these matched solutions. As thus formulated, the method is similar in spirit to the corresponding planar theory described in Paper I and, for this reason, many of the concepts presented in that paper and which carry into the three-dimensional world without modification will only be summarized briefly. There are, however, some aspects which are different, most notably in the matching procedure, and these will be discussed in detail. In addition, the concepts of angular momentum coupling, of body- and space-fixed coordinate systems, and of parity symmetry decoupling will be developed thoroughly as their utilization is of great importance to the three-dimensional method.

In Sec. II we discuss the body-fixed partial wave Schrödinger equation along with angular momentum coupling and the division of configuration space into arrangement channel regions. The fully coupled Schrödinger equation for the four different internal configuration space regions of each arrangement channel region is discussed in Sec. III and the matching procedure is described in Sec. IV. In Sec. V. the body-fixed R and S matrices are defined and their relationships to the helicity representation scattering amplitudes and cross sections are derived. In Sec. VI we discuss the limitations of the method and its possible generalizations. In each section, where appropriate, the simplifications pertinent to the H + H$_2$ exchange reaction are indicated. Appendix A outlines the derivation of the body-fixed Schrödinger equation and indicates relationships between several important angular momentum operators. Appendix B includes a discussion of parity symmetry and the simplifications in the method which may be gained by explicitly including it.

II. THE BODY-FIXED ROTATIONALLY COUPLED SCHRÖDINGER EQUATION

A. Separation of internal configuration space into arrangement channel regions

We consider the three-dimensional collision of an atom A with a diatomic molecule BC and, in parallel, the B plus CA and C plus AB collisions. A convenient procedure for specifying the locations of A ($\equiv A_\alpha$), B ($\equiv A_\beta$), and C ($\equiv A_\gamma$) in the center of mass system is depicted in Fig. 1. $\bar{R}_\alpha$ is the vector from the center of mass of BC to A, and $\bar{r}_\alpha$ is the B to C internuclear vector. As $|\bar{R}_\alpha| \to \infty$, with $|\bar{r}_\alpha|$ remaining finite, we obtain the separated A + BC arrangement channel (denoted by the symbol α). The vectors $\bar{R}_\beta$, $\bar{r}_\beta$ and $\bar{R}_\gamma$, $\bar{r}_\gamma$ are defined analogously for the arrangement channels β (B + AC) and γ (C + AB), respectively. Note that the arrangement of the vectors in Fig. 1 is cyclic in the indices $\alpha\beta\gamma$. We let $\lambda\nu\kappa$ represent any one of the cyclic permutations
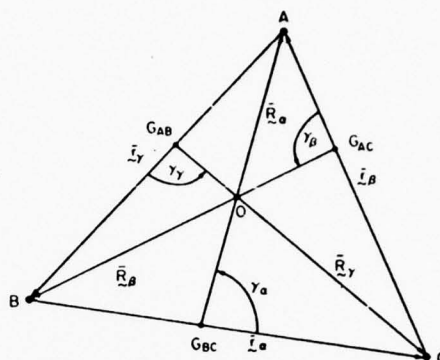
FIG. 1. Vectors used to specify the location of the three atoms A, B, and C relative to the center of mass O. G_{BC}, G_{AC}, and G_{AB} denote the locations of the centers of mass of the diatoms BC, AC, and AB, respectively. The vectors $\bar{R}_\alpha$, $\mathbf{r}_\alpha$, $\bar{R}_\beta$, $\mathbf{r}_\beta$, $\bar{R}_\gamma$, $\mathbf{r}_\gamma$ are defined in text.

$\alpha\beta\gamma$, $\beta\gamma\alpha$, and $\gamma\alpha\beta$, and define the vectors $\bar{R}_\lambda$, $\bar{r}_\lambda$, $\bar{R}_\nu$, $\bar{r}_\nu$, and $\bar{R}_\kappa$, $\bar{r}_\kappa$ accordingly. We also introduce the scaled variables R_λ, r_λ which are related to $\bar{R}_\lambda$, $\bar{r}_\lambda$ by

$$r_\lambda = a_\lambda^{-1} \bar{r}_\lambda , \qquad (2.1a)$$

$$R_\lambda = a_\lambda \bar{R}_\lambda , \qquad (2.1b)$$

where

$$a_\lambda = (\mu_{\lambda,\nu\kappa}/\mu_{\nu\kappa})^{1/4} , \qquad (2.2a)$$

and $\mu_{\lambda,\nu\kappa}$ and $\mu_{\nu\kappa}$ are the reduced masses corresponding to $\bar{R}_\lambda$ and $\bar{r}_\lambda$ motion, respectively:

$$\mu_{\lambda,\nu\kappa} = m_\lambda(m_\nu + m_\kappa)/(m_\lambda + m_\nu + m_\kappa) , \qquad (2.2b)$$

$$\mu_{\nu\kappa} = m_\nu m_\kappa/(m_\nu + m_\kappa) . \qquad (2.2c)$$

This notation is identical to that used in Paper I and is dictated by the considerable mathematical convenience associated with using scaled variables.[25-27]

We are interested in solving the six-dimensional Schrödinger equation for the motion of the three nuclei, on a single electronically adiabatic potential energy surface, obtained after the motion of the center of mass of the system is removed. The surface (in the absence of external fields) is a function of only three appropriately chosen variables which specify the internal configuration of the system. A convenient representation of this potential V is afforded by the use of the variables R_λ, r_λ, and γ_λ ($\lambda = \alpha, \beta,$ or γ), where γ_λ is the angle between R_λ and r_λ defined by

$$\gamma_\lambda = \cos^{-1} \frac{R_\lambda \cdot r_\lambda}{|R_\lambda||r_\lambda|} \qquad 0 \le \gamma_\lambda \le \pi \qquad (2.3)$$

in terms of which $V = V^\lambda(r_\lambda, R_\lambda, \gamma_\lambda)$. As was discussed in Paper I (Sec. III. A), the variables R_λ, r_λ are useful for describing the triatomic motions only for configurations in which R_λ is significantly larger than, say, R_ν or R_κ. This is most easily understood by representing V^λ in terms of variables $\zeta = (r_\lambda^2 + R_\lambda^2)^{1/2}$ [which, as shown in Eq. (A6) of Paper I is independent of λ], $\omega_\lambda = 2\tan^{-1}(r_\lambda/R_\lambda)$ (in the 0 to π range), and γ_λ. The properties of such

a representation have been discussed elsewhere,[26] the most important one being that a change from polar coordinates ζ, ω_λ, γ_λ to ζ, ω_ν, γ_ν rotates the map of V without distorting it. For the Porter–Karplus H_3 surface, this representation of V is given in Fig. 2 of Paper I and discussed in Sec. III. A of that paper. However, the range of γ_ν in the 3D case if 0 to π rather than the 0 to 2π of the 2D case. From that figure one can see that the three-dimensional internal configuration space is naturally divided into arrangement channel region subspaces, labeled by the indices $\lambda = \alpha, \beta, \gamma$. In region λ, for large ζ, R_λ is approximately equal to Z_λ and r_λ is approximately half of the distance of the point $P(\zeta, \omega_\lambda, \gamma_\lambda)$ to the Z_λ axis. Therefore, in that region, R_λ, r_λ, γ_λ are the "natural" variables for describing the translational, vibrational, and rotational motions, respectively, of the three atoms, but these same variables are both awkward and inefficient for representing the corresponding motions in arrangement channels ν and κ. As a result, we will use R_λ, r_λ, γ_λ in region λ only. Associated to these, we will pick a set of three additional external variables (which specify the orientation of the instantaneous three-atom triangle with respect to a laboratory system) which will also be different for different arrangement channel regions. Accordingly, our procedure for solving the Schrödinger equation involves first the generation of solutions in each of the three arrangement channel regions $\lambda = \alpha, \beta, \gamma$ in separate calculations using variables appropriate to each region. This is followed by a matching procedure which yields a set of smooth and continuous solutions throughout all of configuration space. To complete the problem, we need to linearly combine these "primitive" solutions to generate ones which satisfy the desired asymptotic boundary conditions.

The procedure thus outlined is general and can be applied to any nondissociative reactive system, but in any specific application, we must specify the boundaries (in internal configuration space) of the three arrangement channel regions. As was discussed in Sec. III. A of Paper I, the choice of boundary surfaces is primarily determined by the nature of the potential surface, but for $H + H_2$ and many other reactive systems, a very useful separation is obtained by the use of the three half-planes $\pi_{\nu\lambda}$, $\pi_{\kappa\nu}$, and $\pi_{\lambda\kappa}$ of Fig. 2 of I and defined by Eq. (3.2) of that paper. They are limited by and intersect on the OY_λ axis. $\pi_{\nu\lambda}$ makes an angle $\beta_{\nu\lambda}$ (in the 0 to $\pi/2$ range) with the $OY_\lambda Z_\lambda$ plane given by

$$\cos\beta_{\nu\lambda} = \left(\frac{m_\nu m_\lambda}{(m_\lambda + m_\kappa)(m_\nu + m_\kappa)}\right)^{1/2}, \quad (2.4a)$$

$$\sin\beta_{\nu\lambda} = \left(\frac{m_\kappa M}{(m_\lambda + m_\kappa)(m_\nu + m_\kappa)}\right)^{1/2}, \quad (2.4b)$$

where

$$M = m_\lambda + m_\nu + m_\kappa. \quad (2.5)$$

Analogous expressions are valid for the angles between $\pi_{\kappa\nu}$ and $OY_\lambda Z_\nu$ and between $\pi_{\lambda\kappa}$ and $OY_\lambda Z_\kappa$. These $\pi_{\nu\lambda}$ surfaces ($\nu\lambda = \alpha\beta, \beta\gamma, \gamma\alpha$), hereafter called the matching surfaces, are analogous to those used in Paper I, and their properties are described in great detail in Appen-

dix A of that paper. They are of great importance in the matching procedure of Sec. IV, and the method of solution of the Schrödinger equation in each arrangement channel region must include a procedure for determining the wavefunction of these surfaces. The remainder of this section will be concerned with the rotationally coupled Schrödinger equations for each arrangement channel region.

B. Partial wave analysis

In the system of coordinates specified by the index λ, the Schrödinger equation for the motions of the three nuclei is

$$\left(-\frac{\hbar^2}{2\mu_{\lambda,\nu\kappa}}\nabla_{\bar{R}_\lambda}^2 - \frac{\hbar^2}{2\mu_{\nu\kappa}}\nabla_{\bar{r}_\lambda}^2 + V^\lambda(\bar{r}_\lambda, \bar{R}_\lambda, \gamma_\lambda) - E\right)\Psi^\lambda(\bar{r}_\lambda, \bar{R}_\lambda) = 0, \quad (2.6)$$

where $\nabla_{\bar{R}_\lambda}^2$ and $\nabla_{\bar{r}_\lambda}^2$ are the appropriate Laplacian operators, and E is the total energy excluding that associated with the motion of the center of mass. Upon introduction of the scaled coordinates of Eq. (2.1), Eq. (2.6) is converted to

$$\left(-\frac{\hbar^2}{2\mu}(\nabla_{R_\lambda}^2 + \nabla_{r_\lambda}^2) + V^\lambda(r_\lambda, R_\lambda, \gamma_\lambda) - E\right)\Psi^\lambda(r_\lambda, R_\lambda) = 0, \quad (2.7)$$

where the reduced mass μ is given by

$$\mu = (\mu_{\lambda,\nu\kappa}\mu_{\nu\kappa})^{1/2} = [m_\lambda m_\nu m_\kappa/(m_\lambda + m_\nu + m_\kappa)]^{1/2} \quad (2.8)$$

and is independent of the choice of arrangement channel.

We now introduce the space fixed coordinate system $Oxyz$ (Fig. 2) centered on the center of mass O of the triatom system and whose axes are constantly parallel to the axes of a laboratory-fixed system of coordinates. In $Oxyz$ the polar and azimuthal angles of R_λ and r_λ are θ_λ, ϕ_λ and θ_{r_λ}, ϕ_{r_λ}, respectively. By expressing the Laplacian operators in Eq. (2.7) in terms of R_λ, r_λ and these angles, the Schrödinger equation can be rewritten
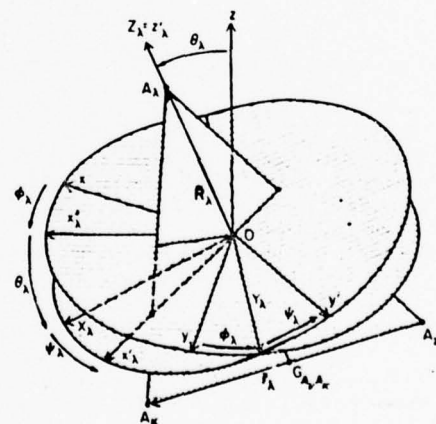

FIG. 2. Space-fixed coordinate system $Oxyz$ and body-fixed systems $OX_\lambda Y_\lambda Z_\lambda$ and $Ox'_\lambda y' z'_\lambda$ (Sec. IIB). The origin O of this figure is the same as that of Fig. 1.

as

$$\left[-\frac{\hbar^2}{2\mu} \left(\frac{1}{R_\lambda} \frac{\partial^2}{\partial R_\lambda^2} R_\lambda + \frac{1}{r_\lambda} \frac{\partial^2}{\partial r_\lambda^2} r_\lambda \right) \right.$$

$$\left. + \frac{j_\lambda^2}{2\mu r_\lambda^2} + \frac{l_\lambda^2}{2\mu R_\lambda^2} + V^\lambda(r_\lambda, R_\lambda, \gamma_\lambda) - E \right] \Psi^\lambda(r_\lambda, R_\lambda) = 0 , \quad (2.9)$$

where l_λ and j_λ are the usual orbital and rotational angular momentum operators expressed in the spherical coordinates $\theta_\lambda, \phi_\lambda$ and $\theta_{r_\lambda}, \phi_{r_\lambda}$ and are given in Appendix A. The total angular momentum operator J is the vector sum of l_λ and j_λ,

$$J = l_\lambda + j_\lambda , \quad (2.10)$$

and is independent of arrangement channel.

The operators J^2 and J_z (the z component of J) commute with each other and with the Hamiltonian H. In the partial wave analysis procedure, we expand $\Psi^\lambda(r_\lambda, R_\lambda)$ in terms of simultaneous eigenfunctions $\Psi^\lambda_{JM}(r_\lambda, R_\lambda)$ of J^2, J_z, and H with eigenvalues $\hbar^2 J(J+1)$, $\hbar M$, and E, respectively:

$$\Psi^\lambda(r_\lambda, R_\lambda) = \sum_{J=0}^{\infty} \sum_{M=-J}^{J} C_{JM}^\lambda \Psi^\lambda_{JM}(r_\lambda, R_\lambda) . \quad (2.11)$$

The Ψ^λ_{JM} still satisfy Eq. (2.9).

C. The body-fixed Schrödinger equation

In the standard space-fixed theory (as formulated, for example, by Arthurs and Dalgarno[29]), one now expands Ψ^λ_{JM} in terms of a set of simultaneous eigenfunctions of J^2, J_z, l_λ^2, and j_λ^2, thereby obtaining a set of coupled equations in the quantum numbers j_λ and l_λ. This derivation is summarized in Appendix A. A more convenient and computationally efficient procedure for our purposes is to transform to a system of body-fixed coordinates. These coordinate systems were applied to quantum mechanical problems long ago by Hirschfelder and Wigner[30] and have been discussed extensively by Curtiss, Hirschfelder, and Adler[31] and more recently by Pack,[32] and much of the present development will follow that of Pack. In a fully converged calculation, both the body-fixed and space-fixed formalisms lead to the same number of coupled equations and, for fully converged nonreactive atom diatom calculations, they may be implemented with comparable ease. However, body-fixed coordinate systems lead to an approximate decoupling of certain degrees of freedom which is not naturally present in the space-fixed analysis and which is useful in the development of approximate theories. More important, the body-fixed analysis leads to both computational and conceptual simplifications in the matching procedure, thus providing a considerable advantage in reactive scattering calculations over the corresponding space-fixed theory.

We now introduce the two different body fixed coordinate systems $OX_\lambda Y_\lambda Z_\lambda$ and $Ox'_\lambda y'_\lambda z'_\lambda$ (see Fig. 2) as follows: (1) $OX_\lambda Y_\lambda Z_\lambda$ (not to be confused with the internal configuration space coordinate system $OX_\lambda Y_\lambda Z_\lambda$ of Fig. 2 of Paper I) is obtained from $Oxyz$ by rotating through the Euler angles[33] $\alpha = \phi_\lambda$, $\beta = \theta_\lambda$, $\gamma = 0$ so that the resulting Z_λ axis points along the R_λ direction and the Y_λ axis lies in the xy plane; (2) $Ox'_\lambda y'_\lambda z'_\lambda$ is obtained from $OX_\lambda Y_\lambda Z_\lambda$

by rotating it counterclockwise about OZ_λ ($\equiv Oz'_\lambda$) by an angle ψ_λ (in the 0 to 2π range) so as to bring Ox'_λ into the R_λ, r_λ plane and Oy' (which is independent of λ) perpendicular to it and oriented in the direction of $R_\lambda \times r_\lambda$:

$$\hat{y}' = \frac{R_\lambda \times r_\lambda}{|R_\lambda \times r_\lambda|} . \quad (2.12)$$

The Euler angles which rotate $Oxyz$ into $Ox'_\lambda y'_\lambda z'_\lambda$ are therefore $\alpha = \phi_\lambda$, $\beta = \theta_\lambda$, $\gamma = \psi_\lambda$. In either of the body-fixed coordinate systems $OX_\lambda Y_\lambda Z_\lambda$ or $Ox'_\lambda y'_\lambda z'_\lambda$ the variables used to describe the system are $r_\lambda, R_\lambda, \phi_\lambda, \theta_\lambda, \psi_\lambda, \gamma_\lambda$. As seen from Fig. 2, ψ_λ is the counterclockwise angle from OY_λ to Oy' or from OX_λ to Ox'_λ as viewed from the positive OZ_λ axis. Since OY_λ is perpendicular to the $OX_\lambda Z_\lambda$ plane and therefore the R_λ, Oz plane, and Oy' is perpendicular to the R_λ, r_λ plane, we conclude that ψ_λ is the angle between these last two planes. This can also be seen by noticing that the plane containing the three axes OX_λ, Ox'_λ, and OY_λ is perpendicular to the R_λ vector and intersects the R_λ, Oz and R_λ, r_λ planes along the OX_λ and Ox'_λ axes, respectively. Therefore, the angle ψ_λ between these two axes is equal to the angle between those two planes. A motion in which R_λ, ϕ_λ, $\theta_\lambda, r_\lambda$, and γ_λ are kept constant but ψ_λ varies is a "tumbling" (i.e., rigid rotation) of the triatomic system around the R_λ vector, and for this reason the ψ_λ angle will be called the tumbling angle. In what follows we will find it most convenient to use the coordinate system $OX_\lambda Y_\lambda Z_\lambda$ for deriving the coupled form of the Schrödinger equation and $Ox'_\lambda y'_\lambda z'_\lambda$ in developing the matching procedure. The procedure for expressing the operators j_λ^2 and l_λ^2 of Eq. (2.9) in variables $\phi_\lambda, \theta_\lambda, \psi_\lambda, \gamma_\lambda$ is described in Appendix A.

We now expand Ψ^λ_{JM} in terms of the elements of the Wigner rotation matrix $D (\alpha, \beta, \gamma)$ as follows[32]:

$$\Psi^\lambda_{JM}(r_\lambda, R_\lambda) = \sum_{\Omega_\lambda=-J}^{J} D^J_{M\Omega_\lambda}(\phi_\lambda, \theta_\lambda, 0) \Psi^\lambda_{J\Omega_\lambda}(r_\lambda, R_\lambda, \gamma_\lambda, \psi_\lambda) . \quad (2.13)$$

The notation used for the matrix elements is that of Davydov.[33] $\Psi^\lambda_{J m_\lambda}$ is called a body-fixed wavefunction. The quantum number Ω_λ in Eq. (2.13) specifies the component of the total angular momentum J around R_λ or, equivalently, OZ_λ. The component of l_λ (the angular momentum conjugate to R_λ) around this axis vanishes and therefore Ω_λ also specifies the Z_λ component of the rotational angular momentum j_λ in the body-fixed frame. The equality of J_{Z_λ} and $j_{\lambda Z_\lambda}$ is verified independently in Table I (which is described in Appendix A). We will refer to either J_{Z_λ} or $j_{\lambda Z_\lambda}$ as the tumbling angular momentum (since it describes the tumbling of the triatom around R_λ) and Ω_λ as the tumbling quantum number in arrangement channel λ.

As outlined in Appendix A, substitution of Eq. (2.13) into Eq. (2.9) yields the following set of Ω_λ-coupled equations for the $\Psi^\lambda_{J\Omega_\lambda}(r_\lambda, R_\lambda, \gamma_\lambda, \psi_\lambda)$:

$$H^{J\lambda}_{\Omega_\lambda, \Omega_\lambda} \Psi^\lambda_{J, \Omega_\lambda} + H^{J\lambda}_{\Omega_\lambda, \Omega_\lambda+1} \Psi^\lambda_{J, \Omega_\lambda+1} + H^{J\lambda}_{\Omega_\lambda, \Omega_\lambda-1} \Psi^\lambda_{J, \Omega_\lambda-1} = E\Psi^\lambda_{J\Omega_\lambda} . \quad (2.14)$$

The $H^{J\lambda}_{\Omega_\lambda, \Omega_\lambda'}$ can be considered as the elements of a tridiagonal Hamiltonian operator matrix $H^{J\lambda}(r_\lambda, R_\lambda, \gamma_\lambda, \psi_\lambda)$ whose diagonal and off-diagonal elements are defined, respectively, by

TABLE I. Angular momentum operators in space-fixed and body-fixed coordinate systems. [a]

$Oxyz$	$OX_\lambda Y_\lambda Z_\lambda$	$Ox'_\lambda y' z'_\lambda$
$J_x = -i\hbar\left(-\cos\phi\cot\theta\dfrac{\partial}{\partial\phi} -\sin\phi\dfrac{\partial}{\partial\theta} +\dfrac{\cos\phi}{\sin\theta}\dfrac{\partial}{\partial\chi}\right)$	$J_{X_\lambda} = -i\hbar\left(-\dfrac{1}{\sin\theta}\dfrac{\partial}{\partial\phi}+\cos\theta\dfrac{\partial}{\partial\chi}\right)$	$J_{x'_\lambda} = -i\hbar\left(-\dfrac{\cos\psi}{\sin\theta}\dfrac{\partial}{\partial\phi}+\sin\psi\dfrac{\partial}{\partial\theta}+\cot\theta\cos\psi\dfrac{\partial}{\partial\psi}\right)$
$J_y = -i\hbar\left(-\sin\phi\cot\theta\dfrac{\partial}{\partial\phi}+\cos\phi\dfrac{\partial}{\partial\theta}+\dfrac{\cos\phi}{\sin\theta}\dfrac{\partial}{\partial\chi}\right)$	$J_{Y_\lambda} = -i\hbar\dfrac{\partial}{\partial\theta}$	$J_{y'} = -i\hbar\left(\dfrac{\sin\psi}{\sin\theta}\dfrac{\partial}{\partial\phi}+\cos\psi\dfrac{\partial}{\partial\theta}-\cot\theta\sin\psi\dfrac{\partial}{\partial\psi}\right)$
$J_z = -i\hbar\dfrac{\partial}{\partial\phi}$	$J_{Z_\lambda} = -i\hbar\dfrac{\partial}{\partial\psi}$	$J_{z'_\lambda} = -i\hbar\dfrac{\partial}{\partial\psi}$
$j_{\lambda x} = -i\hbar\left[\cos\phi\sin\theta+\sin\phi\sin\psi\cot\gamma -\cos\phi\cos\theta\cos\psi\cot\gamma)\dfrac{\partial}{\partial\chi} -(\sin\phi\cos\psi+\cos\phi\cos\theta\sin\psi)\dfrac{\partial}{\partial\gamma}\right]$	$j_{\lambda X_\lambda} = -i\hbar\left(-\cos\psi\cot\gamma\dfrac{\partial}{\partial\psi}-\sin\psi\dfrac{\partial}{\partial\gamma}\right)$	$j_{\lambda x'_\lambda} = -i\hbar\left(-\cot\gamma\dfrac{\partial}{\partial\psi}\right)$
$j_{\lambda y} = -i\hbar\left[(\sin\phi\sin\theta-\cos\phi\sin\psi\cot\gamma -\sin\phi\cos\theta\cos\psi\cot\gamma)\dfrac{\partial}{\partial\chi} +(\cos\phi\cos\psi-\sin\phi\cos\theta\sin\psi)\dfrac{\partial}{\partial\gamma}\right]$	$j_{\lambda Y_\lambda} = -i\hbar\left(-\sin\psi\cot\gamma\dfrac{\partial}{\partial\psi}+\cos\psi\dfrac{\partial}{\partial\gamma}\right)$	$j_{\lambda y'} = -i\hbar\dfrac{\partial}{\partial\gamma}$
$j_{\lambda z} = -i\hbar\left[(\cos\theta+\sin\theta\cos\psi\cot\gamma)\dfrac{\partial}{\partial\chi}+\sin\theta\sin\psi\dfrac{\partial}{\partial\gamma}\right]$	$j_{\lambda Z_\lambda} = -i\hbar\dfrac{\partial}{\partial\psi}$	$j_{\lambda z'_\lambda} = -i\hbar\dfrac{\partial}{\partial\psi}$
$J^2 = J_x^2+J_y^2+J_z^2$ $= -\hbar^2\left[\dfrac{\partial^2}{\partial\theta^2}+\cot\theta\dfrac{\partial}{\partial\theta}+\dfrac{1}{\sin^2\theta}\left(\dfrac{\partial^2}{\partial\phi^2}+\dfrac{\partial^2}{\partial\chi^2}\right)-\dfrac{2\cos\theta}{\sin^2\theta}\dfrac{\partial^2}{\partial\phi\partial\chi}\right]$	$J^2 = J_{X_\lambda}^2+J_{Y_\lambda}^2+J_{Z_\lambda}^2$ $-i\hbar\cot\theta J_{Y_\lambda}$	$J^2 = J_{x'_\lambda}^2+J_{y'}^2+J_{z'_\lambda}^2$
$j_\lambda^2 = j_{\lambda x}^2+j_{\lambda y}^2+j_{\lambda z}^2$ $= -\hbar^2\left(\dfrac{\partial^2}{\partial\gamma^2}+\cot\gamma\dfrac{\partial}{\partial\gamma}+\dfrac{1}{\sin^2\gamma}\dfrac{\partial^2}{\partial\chi^2}\right)$	$j_\lambda^2 = j_{\lambda X_\lambda}^2+j_{\lambda Y_\lambda}^2+j_{\lambda Z_\lambda}^2$	$j_\lambda^2 = j_{\lambda x'_\lambda}^2+j_{\lambda y'}^2+j_{\lambda z'_\lambda}^2$ $-i\hbar\cot\gamma\, j_{\lambda y'}$
$j_\lambda\cdot J = j_{\lambda z}J_z+j_{\lambda x}J_x+j_{\lambda y}J_y$ $= -\hbar^2\left[\dfrac{\cos\psi\cot\gamma}{\sin\theta}\dfrac{\partial^2}{\partial\chi\partial\phi}+\dfrac{\sin\psi}{\sin\theta}\dfrac{\partial^2}{\partial\gamma\partial\phi}-\sin\psi\cot\theta\dfrac{\partial^2}{\partial\psi\partial\gamma}-\sin\psi\cot\gamma\dfrac{\partial^2}{\partial\chi\partial\theta}+\cos\psi\dfrac{\partial^2}{\partial\gamma\partial\theta}+(1-\cos\psi\cot\gamma\cot\theta)\dfrac{\partial^2}{\partial\chi^2}\right]$	$j_\lambda\cdot J = j_{\lambda Z_\lambda}J_{Z_\lambda}+j_{\lambda X_\lambda}J_{X_\lambda}+j_{\lambda Y_\lambda}J_{Y_\lambda}$	$j_\lambda\cdot J = j_{\lambda z'_\lambda}J_{z'_\lambda}+j_{\lambda x'_\lambda}J_{x'_\lambda}+j_{\lambda y'}J_{y'}-i\hbar\cot\gamma J_{y'}$

[a] The subscript λ has been omitted from the symbols θ, ϕ, γ, ψ. The expressions for J^2, j_λ^2, and $j_\lambda\cdot J$ in terms of θ, ϕ, γ, ψ are independent of coordinate system.

$$H^{J\lambda}_{\Omega_\lambda,\Omega_\lambda} = -\frac{\hbar^2}{2\mu}\left(\frac{1}{r_\lambda}\frac{\partial^2}{\partial r_\lambda^2}r_\lambda+\frac{1}{R_\lambda}\frac{\partial^2}{\partial R_\lambda^2}R_\lambda\right)+\frac{j_\lambda^2}{2\mu r_\lambda^2}$$
$$+\frac{1}{2\mu R_\lambda^2}[J(J+1)\hbar^2-2\Omega_\lambda\hbar j_{\lambda z_\lambda}+j_\lambda^2]+V^\lambda(r_\lambda,R_\lambda,\gamma_\lambda) \tag{2.15}$$

and

$$H^{J\lambda}_{\Omega_\lambda,\Omega_\lambda\pm1} = -\frac{\hbar}{2\mu R_\lambda^2}\sqrt{J(J+1)-\Omega_\lambda(\Omega_\lambda\pm1)}\; j_\lambda^\mp. \tag{2.16}$$

The $j_\lambda^\mp$ are the lowering (−) and raising (+) operators of the rotational angular momentum j_λ in the body-fixed $OX_\lambda Y_\lambda Z_\lambda$ coordinate system. The $1/2\mu R_\lambda^2$ term in Eq.

(2.15) results directly from the $l_\lambda^2/2\mu R_\lambda^2$ term in Eq. (2.9). Defining Ψ_J^λ as the $(2\Omega_\lambda+1)$-dimensional column vector whose elements are the $\Psi_{J\Omega_\lambda}^\lambda$, Eq. (2.14) can be put in the matrix form

$$\mathbf{H}^{J\lambda}\Psi_J^\lambda = E\Psi_J^\lambda. \tag{2.17}$$

Equations (2.14) or (2.17) are the body-fixed partial wave Schrödinger equation. Equation (2.14) is identical to the corresponding result of Pack[32] and indicates that the kinetic energy operator is no longer diagonal in the body-fixed representation and is the sole mechanism which couples different tumbling quantum numbers Ω_λ.

The potential coupling is diagonal in Ω_λ and is responsible for coupling between states of different vibration–rotation quantum numbers $v_\lambda j_\lambda$, as indicated later in Eq. (3.16) and its counterparts for the strong interac-

tion and matching regions. This separation of kinematic and potential coupling is of prime importance in the development of approximate decoupling procedures, as will be discussed in the next section.

D. The rotationally coupled Schrödinger equation; tumbling-decoupling approximations

We now expand the body-fixed wavefunctions $\Psi^\lambda_{J\Omega_\lambda}$ in terms of the spherical harmonics $Y_{j_\lambda\Omega_\lambda}(\gamma_\lambda,\psi_\lambda)$ which, as discussed in Appendix A, are the simultaneous eigenfunctions of j_λ^2 and $j_{\lambda z_\lambda}$:

$$\Psi^\lambda_{J\Omega_\lambda}(r_\lambda,R_\lambda,\gamma_\lambda,\psi_\lambda)=\sum_{j_\lambda=|\Omega_\lambda|}^{\infty} Y_{j_\lambda\Omega_\lambda}(\gamma_\lambda,\psi_\lambda)w^\lambda_{Jj_\lambda\Omega_\lambda}(r_\lambda,R_\lambda) \quad \Omega_\lambda=-J,-J+1,\ldots,J; \quad J=0,1,2,\ldots \tag{2.18}$$

If we substitute this into Eq. (2.14), multiply throughout by $Y^*_{j'_\lambda\Omega'_\lambda}(\gamma_\lambda,\psi_\lambda)$ and integrate over γ_λ and ψ_λ (using the solid angle volume element $\sin\gamma_\lambda\, d\gamma_\lambda d\psi_\lambda$), and finally interchange the primed and unprimed quantum numbers, it becomes a Schrödinger equation in the two scaled distances r_λ,R_λ:

$$(t^{J\lambda j_\lambda}_{\Omega_\lambda\Omega_\lambda}-E)w^\lambda_{Jj_\lambda\Omega_\lambda}(r_\lambda,R_\lambda)+\sum_{j'_\lambda=|\Omega_\lambda|}^{\infty}V^{\lambda\Omega_\lambda}_{j_\lambda j'_\lambda}w^\lambda_{Jj'_\lambda\Omega_\lambda}(r_\lambda,R_\lambda)+t^{J\lambda j_\lambda}_{\Omega_\lambda,\Omega_\lambda+1}w^\lambda_{Jj_\lambda,\Omega_\lambda+1}(r_\lambda,R_\lambda)+t^{J\lambda j_\lambda}_{\Omega_\lambda,\Omega_\lambda-1}w^\lambda_{Jj_\lambda,\Omega_\lambda-1}(r_\lambda,R_\lambda)=0$$

$$J=0,1,2,\ldots; \quad \Omega_\lambda=-J,-J+1,\ldots,J; \quad j_\lambda=|\Omega_\lambda|,\ |\Omega_\lambda|+1,\ldots, \tag{2.19}$$

where

$$t^{J\lambda j_\lambda}_{\Omega_\lambda\Omega_\lambda}=-\frac{\hbar^2}{2\mu}\left(\frac{1}{R_\lambda}\frac{\partial^2}{\partial R^2_\lambda}R_\lambda+\frac{1}{r_\lambda}\frac{\partial^2}{\partial r^2_\lambda}r_\lambda\right)+\frac{j_\lambda(j_\lambda+1)\hbar^2}{2\mu r^2_\lambda}+\frac{\hbar^2}{2\mu R^2_\lambda}[J(J+1)-2\Omega^2_\lambda+j_\lambda(j_\lambda+1)], \tag{2.20}$$

$$t^{J\lambda j_\lambda}_{\Omega_\lambda,\Omega_\lambda\pm1}=-\frac{\hbar^2}{2\mu R^2_\lambda}\xi_\pm(J,\Omega_\lambda)\xi_\pm(j_\lambda,\Omega_\lambda), \tag{2.21}$$

$$\xi_\pm(J,\Omega_\lambda)=[J(J+1)-\Omega_\lambda(\Omega_\lambda\pm1)]^{1/2} \quad |\Omega_\lambda|\le J, \tag{2.22}$$

and

$$V^{\lambda\Omega_\lambda}_{j_\lambda j'_\lambda}(r_\lambda,R_\lambda)=\langle j_\lambda\Omega_\lambda|V^\lambda(r_\lambda,R_\lambda,\gamma_\lambda)|j'_\lambda\Omega_\lambda\rangle, \tag{2.23}$$

Equation (2.19) is the three-dimensional generalization of an analogous equation for collinear and coplanar[19] reactions. None of the four angular coordinates θ_λ, ϕ_λ, γ_λ, ψ_λ appear in it, with only the two scaled distances r_λ,R_λ remaining. In the collinear case, none of the angular momentum quantum numbers J, Ω_λ, or j_λ appear, and we have only one such equation. For systems confined to a space-fixed plane, Ω_λ does not appear (or it can be considered to have the fixed value zero) since the system does not tumble, and there is therefore no Ω_λ coupling. In that case, j_λ assumes all integer values, including negative ones, and there is one set of j_λ-coupled equations for each J. In the present three-dimensional case, there is both j_λ and Ω_λ coupling, but still no J coupling. Let us consider a kinetic energy matrix $t^\lambda(r_\lambda,R_\lambda)$ (which includes the centrifugal potential terms) and a potential energy matrix $V^\lambda(r_\lambda,R_\lambda)$ whose rows and columns are scanned by the indices j_λ,Ω_λ and $j'_\lambda,\Omega'_\lambda$, respectively. They are defined by

$$(t^{J\lambda})^{j'_\lambda\Omega'_\lambda}_{j_\lambda\Omega_\lambda}=\delta_{j_\lambda j'_\lambda}\sum_{i=-1}^{1}\delta_{\Omega_\lambda,\Omega'_\lambda+i}\,t^{J\lambda j_\lambda}_{\Omega_\lambda,\Omega_\lambda+i} \tag{2.24}$$

and

$$(V^\lambda)^{j'_\lambda\Omega'_\lambda}_{j_\lambda\Omega_\lambda}=\delta_{\Omega_\lambda\Omega'_\lambda}V^{\lambda\Omega_\lambda}_{j_\lambda j'_\lambda}, \tag{2.25}$$

respectively, where the several t and V were defined by Eqs. (2.20)–(2.23). It can be seen that $t^{J\lambda}$ is diagonal in j_λ (and tridiagonal in Ω_λ) whereas V^λ is diagonal in Ω_λ. Defining $w^\lambda_J(r_\lambda,R_\lambda)$ as the column vector whose

elements, scanned by $j_\lambda\Omega_\lambda$, are the functions $w^\lambda_{Jj_\lambda\Omega_\lambda}(r_\lambda,R_\lambda)$ Eq. (2.19) can be rewritten as

$$(t^{J\lambda}+V^\lambda)w^\lambda_J=Ew^\lambda_J. \tag{2.26}$$

Equation (2.26) shows clearly that the potential coupling is diagonal in Ω_λ. This, along with the weakness of the centrifugal coupling (due to the terms in $t^{J\lambda}$ of angular origin) for small J and j_λ has lead to the development of fairly accurate tumbling-decoupling approximations by several workers[32,34] in studies of nonreactive atom–diatom scattering. In such procedures, the $t^{J\lambda j_\lambda}_{\Omega_\lambda,\Omega_\lambda\pm1}$ terms in Eqs. (2.19) and (2.24) are neglected, thereby making Eq. (2.26) be diagonal in Ω_λ. In addition, the $\hbar^2/2\mu R^2_\lambda$ term in Eq. (2.20) [which arises from the l^2_λ term in Eq. (2.9)] is usually replaced by an approximate expression. Pack[32] replaces it by $\hbar^2 J(J+1)/2\mu R^2_\lambda$, and McGuire and Kouri[34] b, $\hbar^2 l_\lambda(l_\lambda+1)/2\mu R^2_\lambda$, where l_λ is the orbital angular momentum quantum number in the space-fixed system of coordinates.[36] Such additional approximations are unnecessary to produce Ω_λ decoupling and may furthermore introduce additional errors without significant computational simplification; we suggest that they should be omitted. For the case of reactive scattering, an Ω_λ decoupling requires neglect of the $t^{J\lambda j_\lambda}_{\Omega_\lambda,\Omega_\lambda+1}$ in Eq. (2.19) for each arrangement channel region $\lambda=\alpha,\beta,\gamma$. The exact matching procedure described in Sec. III may be retained, or be replaced by approximate ones which retain the spirit of Ω_λ decoupling. In a separate paper

we will present some results of an application of some of these possible procedures to 3D reactive scattering.

The elements of the potential coupling matrix of Eqs. (2.23) and (2.26) may be conveniently calculated by expanding the potential $V^\lambda(r_\lambda, R_\lambda, \gamma_\lambda)$ in a series of Legendre polynomials

$$V^\lambda(r_\lambda, R_\lambda, \gamma_\lambda) = \sum_{k=0}^{\infty} V_k^\lambda(r_\lambda, R_\lambda) P_k(\cos\gamma_\lambda) \qquad (2.27)$$

which, when substituted into Eq. (2.23), leads to[32]

$$V_{j_\lambda j_\lambda'}^{\lambda \Omega_\lambda}(r_\lambda, R_\lambda) = \sum_{k=0}^{\infty} \left(\frac{2j_\lambda + 1}{2j_\lambda' + 1}\right)^{1/2} C(j_\lambda k j_\lambda'; \Omega_\lambda 0 \Omega_\lambda)$$

$$C(j_\lambda k j_\lambda'; 000) V_k^\lambda(r_\lambda, R_\lambda) , \qquad (2.28)$$

where the Clebsch–Gordan coefficients C are expressed in the notation of Rose.[37] For collisions of an atom with a homonuclear diatomic molecule (as in $H + H_2$), the only nonzero terms in Eq. (2.27) occur for even k [since $V^\lambda(r_\lambda, R_\lambda, \gamma_\lambda)$ is symmetric about $\gamma_\lambda = \pi/2$]. Since[38]

$$C(j_\lambda k j_\lambda'; 000) = 0 \quad \text{for } j_\lambda + k + j_\lambda' = \text{odd}, \qquad (2.29)$$

we see that V^λ does not couple even with odd rotational states. Use of this decoupling in reducing the necessary calculations for reactions like $H + H_2$ was discussed in Paper I for the planar case, and most of the simplifications described there are valid for 3D collisions as well. Note that Eq. (2.28) involves a single sum over products of Clebsch–Gordan coefficients, a substantial simplification over the corresponding space-fixed expansion which requires $6-j$ symbols[32]

Let us now define a new function $F_{j_\lambda \Omega_\lambda}^\lambda(r_\lambda, R_\lambda)$ by

$$F_{j_\lambda \Omega_\lambda}^\lambda(r_\lambda, R_\lambda) = R_\lambda r_\lambda u_{j_\lambda \Omega_\lambda}^\lambda(r_\lambda, R_\lambda) . \qquad (2.30)$$

Substitution of this into Eq. (2.19) leads to

$$(\bar{t}_{\Omega_\lambda \Omega_\lambda}^{j_\lambda j_\lambda} - E) F_{j_\lambda \Omega_\lambda}^\lambda$$

$$+ \sum_{j_\lambda'} V_{j_\lambda j_\lambda'}^{\lambda \Omega_\lambda} F_{j_\lambda' \Omega_\lambda}^\lambda + t_{\Omega_\lambda, \Omega_\lambda+1}^{j_\lambda j_\lambda} F_{j_\lambda, \Omega_\lambda+1}^\lambda + t_{\Omega_\lambda, \Omega_\lambda-1}^{j_\lambda j_\lambda} F_{j_\lambda, \Omega_\lambda-1}^\lambda = 0$$

$$\qquad (2.31)$$

where

$$\bar{t}_{\Omega_\lambda \Omega_\lambda}^{j_\lambda j_\lambda} = -\frac{\hbar^2}{2\mu}\left(\frac{\partial^2}{\partial R_\lambda^2} + \frac{\partial^2}{\partial r_\lambda^2}\right) + \frac{j_\lambda(j_\lambda + 1)\hbar^2}{2\mu r_\lambda^2}$$

$$+ \frac{\hbar^2}{2\mu R_\lambda^2}[J(J+1) - 2\Omega_\lambda^2 + j_\lambda(j_\lambda + 1)] , \qquad (2.32)$$

and the remaining quantities are defined by Eqs. (2.21)–(2.23). In matrix form, Eq. (2.31) can be written as

$$(\bar{t}^{j\lambda} + V^\lambda) F_J^\lambda = E F_J^\lambda , \qquad (2.33)$$

where $\bar{t}^{j\lambda}$ is defined similarly to $t^{j\lambda}$ and F_J^λ similarly to w_J^λ. Equations (2.31) and (2.33) are called the body-fixed rotationally coupled Schrödinger equation.

III. THE INTEGRATION IN ARRANGEMENT CHANNEL REGION λ

A. Division of r_λ, R_λ configuration space into regions

To solve Eq. (2.31) or (2.33) we expand the wavefunction $F_{j_\lambda \Omega_\lambda}^\lambda(r_\lambda, R_\lambda)$ in terms of a set of one-variable
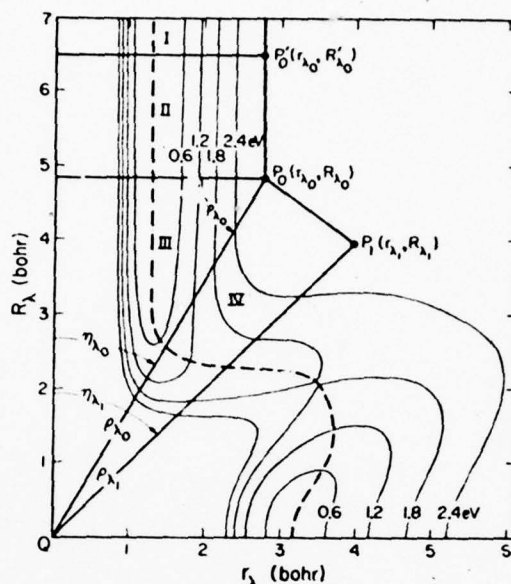
FIG. 3. Division of the R_λ, r_λ space into four regions, I, II, III, and IV. The contours are equipotentials of the matrix element $V_0^\lambda(r_\lambda, R_\lambda)$ [see Eq. (2.27)] in eV for the Porter–Karplus $H \cdot H_2$ potential energy function. The dashed line is the line of steepest ascents for V_0^λ. The locations of the points P_0', P_0, and P_1 are discussed in Sec. III.A of the text. Q is the origin of this space.

pseudovibrational functions which locally span the r_λ, R_λ configuration space along cuts which are approximately perpendicular to a conveniently defined reaction coordinate. The resulting expansion coefficients satisfy ordinary coupled differential equations which must be numerically integrated through the arrangement channel region λ to generate a set of solutions to the Schrödinger equation in that region. In order to obtain an efficient representation of the pseudovibrational motion everywhere, we must change both coordinate systems and basis sets frequently during this propagation. This may be done in many different ways depending on the boundaries of the arrangement channel regions and the shape of the potential energy surface in these regions. For the $H + H_2$ reaction, and most others for which the choice of matching surfaces is given by Eq. (3.2) of Paper I, a convenient procedure consists of dividing the r_λ, R_λ configuration space into four areas called regions, as depicted in Fig. 3. For reference contours of the potential matrix element $V_0(r_\lambda, R_\lambda)$ of Eq. (2.27) for the H_3 Porter–Karplus surface[39] are plotted on the same figure. The regions are denoted as follows: I—asymptotic region; II—weak interaction region; III—strong interaction region; and IV—matching region. The boundary points P_0', P_0, and P_1 are required to lie in the high-energy plateau region corresponding to dissociation of the triatomic system into A + B + C (i.e., large r_λ and R_λ), in positions which are primarily determined by certain geometrical criteria. These are

described in detail in Sec. III.C of Paper I and are un-
changed in the present application. Within each region,
we choose a set of orthogonal coordinates which effi-
ciently describe the local vibrational and translational
motion. The choice of these coordinates is also the
same as in Sec. III.C of Paper I.

B. The coupled Schrödinger equation in the propagation variable

We now consider the solution of Eq. (2.31) in each of
the four regions in arrangement channel region λ. Much
of this treatment is completely analogous to the corre-
sponding coplanar theory (Sec. III. D of Paper I), and
that paper should be consulted for a more detailed ex-
planation of the concepts involved.

1. The asymptotic region

The coordinates for this region are r_λ, R_λ. In terms
of these, the potential function $V^\lambda(r_\lambda, R_\lambda, \gamma_\lambda)$ becomes
the isolated diatomic potential $v^\lambda(r_\lambda)$ since the bound-
aries of the asymptotic region are chosen[19] so that in it
the potential has assumed its asymptotic form. We now
expand the wavefunction $F^\lambda_{J_{j_\lambda}\Omega_\lambda}(r_\lambda, R_\lambda)$ of Eq. (2.31) in
terms of the eigenfunctions $\phi^{\lambda(a)}_{v_\lambda j_\lambda}(r_\lambda)$ of the vibrational
Hamiltonian:

$$F^{\lambda(a)}_{J_{j_\lambda}\Omega}(r_\lambda, R_\lambda) = \sum_{v_\lambda} g^{\lambda(a)}_{J v_\lambda j_\lambda \Omega_\lambda}(R_\lambda) \phi^{\lambda(a)}_{v_\lambda j_\lambda}(r_\lambda), \qquad (3.1)$$

where the (a) refers to asymptotic region, and the $\phi^{\lambda(a)}_{v_\lambda j_\lambda}$
are vibrational basis functions which satisfy

$$\left(-\frac{\hbar^2}{2\mu}\frac{d^2}{dr_\lambda^2} + \frac{j_\lambda(j_\lambda+1)\hbar^2}{2\mu r_\lambda^2} + v^\lambda(r_\lambda)\right)\phi^{\lambda(a)}_{v_\lambda j_\lambda}(r_\lambda) = \epsilon^{\lambda(a)}_{v_\lambda j_\lambda}\phi^{\lambda(a)}_{v_\lambda j_\lambda}(r_\lambda) \qquad (3.2)$$

with boundary conditions

$$\phi^{\lambda(a)}_{v_\lambda j_\lambda}(r_{\lambda_0}) = \phi^{\lambda(a)}_{v_\lambda j_\lambda}(0) = 0. \qquad (3.3)$$

$\epsilon^{\lambda(a)}_{v_\lambda j_\lambda}$ is the asymptotic diatomic vibration–rotation ener-
gy, and $r_\lambda^{-1}\phi^{\lambda(a)}_{v_\lambda j_\lambda}(r_\lambda)$, except for a normalization con-
stant, is the radial part of the corresponding diatomic
eigenfunction. Substituting Eq. (3.1) into Eq. (2.31),
using Eq. (3.2), multiplying by $\phi^{\lambda(a)}_{v_\lambda j_\lambda}(r_\lambda)$, integrating
over r_λ, and replacing r'_λ by v_λ, we obtain the Schrö-
dinger equation for translational R_λ motion in the
asymptotic region:

$$\left(\frac{d^2}{dR_\lambda^2} - \frac{1}{R_\lambda^2}[J(J+1) - 2\Omega_\lambda^2 + j_\lambda(j_\lambda+1)] + k^{\lambda(a)2}_{v_\lambda j_\lambda}\right)g^{\lambda(a)}_{J v_\lambda j_\lambda \Omega_\lambda}(R_\lambda)$$

$$+ \frac{1}{R_\lambda^2}[\xi_+(J, \Omega_\lambda)\xi_+(j_\lambda, \Omega_\lambda)g^{\lambda(a)}_{J v_\lambda j_\lambda, \Omega_\lambda+1}(R_\lambda)$$

$$+ \xi_-(J, \Omega_\lambda)\xi_-(j_\lambda, \Omega_\lambda)g^{\lambda(a)}_{J v_\lambda j_\lambda, \Omega_\lambda-1}] = 0, \qquad (3.4)$$

where

$$k^{\lambda(a)2}_{v_\lambda j_\lambda} = \frac{2\mu}{\hbar^2}(E - \epsilon^{\lambda(a)}_{v_\lambda j_\lambda}). \qquad (3.5)$$

Note that while no vibrational or rotational coupling
exists in Eq. (3.4), the kinetic energy coupling be-
tween g's of different Ω_λ persists in this asymptotic re-
gion, decreasing only as R_λ^{-2} (rather than exponential-
ly or as R_λ^{-4} as is often the case with potential coupling).

Of course, as $R_\lambda \to \infty$ (the "far" asymptotic region),
Eqs. (3.4) completely uncouple and the $g^{\lambda(a)}_{J v_\lambda j_\lambda \Omega_\lambda}$ become
solutions to

$$\left(\frac{d^2}{dR_\lambda^2} + k^{\lambda(a)2}_{v_\lambda j_\lambda}\right)g^{\lambda(a)}_{J v_\lambda j_\lambda \Omega_\lambda}(R_\lambda) = 0, \qquad (3.6)$$

which are simply linear combinations of $\exp(\pm ik^{\lambda(a)}_{v_\lambda j_\lambda}R_\lambda)$
for open channels $(E > \epsilon^{\lambda(a)}_{v_\lambda j_\lambda})$ and $\exp(\pm|k^{\lambda(a)}_{v_\lambda j_\lambda}|R_\lambda)$ for
closed ones $(E < \epsilon^{\lambda(a)}_{v_\lambda j_\lambda})$. Equation (3.4) may be solved
analytically either by diagonalizing the Hamiltonian in
that equation or by realizing that the corresponding
space-fixed Schrödinger equation is already diagonal,[29]
and thus its solutions may be linearly combined to sat-
isfy Eq. (3.4).[35] The solutions of the space-fixed
Schrödinger equation for open channels are related to
the regular and irregular spherical Bessel functions
$j_{l_\lambda}(k^{\lambda(a)}_{v_\lambda j_\lambda}R_\lambda)$ and $y_{l_\lambda}(k^{\lambda(a)}_{v_\lambda j_\lambda}R_\lambda)$,[29] where l_λ is the orbital
angular momentum quantum number. The correspond-
ing body-fixed solutions are found by equating Eqs. (A5)
and (A13) of Appendix A and using Eq. (A14) to solve
for the body-fixed coefficients $w^\lambda_{j_\lambda \Omega_\lambda}$. Since Eqs. (2.30)
and (3.1) apply equally to space-fixed and body-fixed
solutions, we can immediately write the asymptotic
body-fixed solutions for open channels as linear com-
binations of the regular and irregular solutions

$$g^{\lambda(a)}_{J v_\lambda j_\lambda \Omega_\lambda}(R_\lambda) = k^{\lambda(a)}_{v_\lambda j_\lambda}R_\lambda\left(\frac{2J+1}{4\pi}\right)^{1/2}(-1)^{j_\lambda-\Omega_\lambda}$$

$$\times \sum_{l_\lambda} C(Jj_\lambda l_\lambda; \Omega_\lambda - \Omega_\lambda 0)\begin{pmatrix}j_{l_\lambda}(k^{\lambda(a)}_{v_\lambda j_\lambda}R_\lambda)\\y_{l_\lambda}(k^{\lambda(a)}_{v_\lambda j_\lambda}R_\lambda)\end{pmatrix}$$

$$(E > \epsilon^{\lambda(a)}_{v_\lambda j_\lambda}), \qquad (3.7)$$

where the upper (lower) term in the large parentheses
refers to the regular (irregular) solution. The use of
Eq. (3.6) in formulating the asymptotic R and S matrix
boundary conditions will be discussed in Sec. V. A.
For closed channels, the body-fixed solution is still of
the form in Eq. (3.7) but with the spherical Bessel
functions j_{l_λ} and y_{l_λ} replaced by the modified spherical
Bessel functions $i_{l_\lambda}(|k^{\lambda(a)}_{v_\lambda j_\lambda}|R_\lambda)$ and $k_{l_\lambda}(|k^{\lambda(a)}_{v_\lambda j_\lambda}|R_\lambda)$.[40]

Let us now introduce a matrix notation for the Schrö-
dinger equation [Eq. (3.4)]. We consider the $g^{\lambda(a)}_{J v_\lambda j_\lambda \Omega_\lambda}$
as elements of a column vector $\mathbf{g}^{\lambda(a)}_J$ whose elements
are labeled by the indices $v_\lambda j_\lambda \Omega_\lambda$, which are assumed
to scan a total of N values (in a truncated coupled-chan-
nel expansion). This vector represents one of $2N$ pos-
sible linearly independent solutions of Eq. (3.4). These
$2N$ solutions which form $2N$ column vectors can be as-
sembled into two matrices of dimension $N \times N$ which we
label as $\mathbf{g}^{\lambda(a)+}_J$ and $\mathbf{g}^{\lambda(a)-}_J$, where a set of indices $v'_\lambda j'_\lambda \Omega'_\lambda$
analogous to the row indices explained above is asso-
ciated with each column.[41] The labels $\pm$ are in general
arbitrary, but may be chosen to distinguish the solu-
tions generated in the propagation from Region I–IV
(labeled plus) and from IV–I (labeled minus). Both
propagations are necessary to generate all $2N$ solutions
(we get N from the propagation in each direction). Us-
ing this notation, Eq. (3.4) may be written as

$$\frac{d^2 \mathbf{g}^{\lambda(a)\pm}_J}{dR_\lambda^2} = \mathbf{U}^{\lambda(a)}_J(R_\lambda)\mathbf{g}^{\lambda(a)\pm}_J, \qquad (3.8)$$

where

$$U_J^{\lambda(a)} = -K^{\lambda(a)2} + U_J^{c\lambda(a)} , \qquad (3.9)$$

$$(K^{\lambda(a)2})_{l_\lambda'}^{l_\lambda'} = \delta_{l_\lambda'l_\lambda'} k_{v_\lambda j_\lambda}^{\lambda(a)2} , \qquad (3.10)$$

$$(U_J^{c\lambda(a)})_{l_\lambda}^{l_\lambda'} = \frac{\delta_{v_\lambda j_\lambda}^{v_\lambda' j_\lambda'}}{R_\lambda^2} \{ \delta_{\Omega_\lambda, \Omega_\lambda'} [J(J+1) - 2\Omega_\lambda^2 + j_\lambda(j_\lambda+1)] $$
$$- \delta_{\Omega_\lambda+1, \Omega_\lambda'} \xi_+(J, \Omega_\lambda) \xi_+(j_\lambda, \Omega_\lambda) $$
$$- \delta_{\Omega_\lambda-1, \Omega_\lambda'} \xi_-(J, \Omega_\lambda) \xi_-(j_\lambda, \Omega_\lambda) \} . \qquad (3.11)$$

The symbol l_λ stands for the set of indices $v_\lambda j_\lambda \Omega_\lambda$ and the subscripts and superscripts on a matrix element designate its row and column, respectively. The $U_J^{c\lambda(a)}$ matrix arises from the $1/R_\lambda^2$ centrifugal terms. Equation (3.8) is the full coupled propagation equation for the asymptotic region I.

2. The weak interaction region

In this region we still use the variables r_λ and R_λ to represent vibrational and translational motion, but the potential $V^\lambda(r_\lambda, R_\lambda, \gamma_\lambda)$ is now dependent on R_λ and γ_λ as well as r_λ, so we no longer use the asymptotic vibrational eigenfunctions of Eqs. (3.1) and (3.2) to expand the wavefunction. Since it may be desirable to change vibrational basis functions several times within Region II, we subdivide that region into n_{II}^λ subregions separated by lines of constant R_λ at

$$R_\lambda = R_{\lambda_0}', \quad R_{\lambda_1}', \quad \dots, \quad R_{\lambda_{n_{II}}}' = R_{\lambda_0} .$$

The range of R_λ for the ith subregion is $R_{\lambda_{i-1}}' \le R_\lambda \le R_{\lambda_i}'$ and we choose the expansion basis functions for that subregion to be the eigenfunctions of a reference potential $V_{rot}^\lambda(r_\lambda; R_{\lambda_i}^0)$ at a point $R_{\lambda_i}^0$ belonging to the subregion (such as the midpoint). The reference potential $V_{rot}^\lambda(r_\lambda; R_\lambda)$ is in general arbitrary provided that a complete vibration–rotation expansion is used, but an efficient representation of the vibrational motions can greatly reduce the number of closed channels required for such completeness. Examples of reference potentials are the $V_0^\lambda(r_\lambda, R_\lambda)$ of Eq. (2.27) and the exact potential $V^\lambda(r_\lambda, R_\infty, \bar\gamma_\lambda)$ at fixed $\bar\gamma_\lambda$. Once a reference potential is chosen, the vibrational basis functions for subregion i may be determined by solving

$$\left(-\frac{\hbar^2}{2\mu} \frac{d^2}{dr_\lambda^2} + \frac{j_\lambda(j_\lambda+1)\hbar^2}{2\mu r_\lambda^2} + V_{rot}(r_\lambda; R_{\lambda_i}^0) \right) \phi_{v_\lambda j_\lambda}^{\lambda(w)}(r_\lambda; R_{\lambda_i}^0) $$
$$= \epsilon_{v_\lambda j_\lambda}^{\lambda(w)}(R_{\lambda_i}^0) \phi_{v_\lambda j_\lambda}^{\lambda(w)}(r_\lambda; R_{\lambda_i}^0) \qquad (3.12)$$

subject to boundary conditions analogous to Eq. (3.3) where the superscript (w) indicates weak interaction region. We now expand the wavefunction $F_{J j_\lambda \Omega_\lambda}^\lambda$ in terms of these basis functions,

$$F_{J j_\lambda \Omega_\lambda}^{\lambda(w)a}(r_\lambda, R_\lambda) = \sum_{v_\lambda} g_{J v_\lambda j_\lambda \Omega_\lambda}^{\lambda(w)a}(R_\lambda; R_{\lambda_i}^0) \phi_{v_\lambda j_\lambda}^{\lambda(w)}(r_\lambda; R_{\lambda_i}^0) . \qquad (3.13)$$

Substituting this into Eq. (2.31), using Eq. (3.12) to simplify, then multiplying by $\phi_{v_\lambda j_\lambda}^{\lambda(w)}(r_\lambda; R_{\lambda_i}^0)$ and integrating over r_λ, we obtain the following coupled differential equations (in the matrix notation of Sec. III.B.1):

$$\frac{d^2 g_J^{\lambda(w)a}}{dR_\lambda^2} = U_J^{\lambda(w)}(R_\lambda; R_{\lambda_i}^0) g_J^{\lambda(w)a} , \qquad (3.14)$$

where

$$U_J^{\lambda(w)} = -K^{\lambda(w)2} + U_J^{c\lambda(w)} + U_p^{\lambda(w)} . \qquad (3.15)$$

The matrices $K^{\lambda(w)2}$ and $U_J^{c\lambda(w)}$ are given by Eqs. (3.10) and (3.11) with the superscript (w) substituted for (a), while the J-independent potential coupling potential matrix $U_p^{\lambda(w)}$ is given by

$$(U_p^{\lambda(w)})_{l_\lambda}^{l_\lambda'} = \frac{2\mu}{\hbar^2} \delta_{\Omega_\lambda \Omega_\lambda'} \int \phi_{v_\lambda j_\lambda}^{\lambda(w)}(r_\lambda; R_{\lambda_i}^0) $$
$$\times [V_{j_\lambda \Omega_\lambda}^{\lambda \Omega_\lambda}(r_\lambda, R_\lambda) - V_{rot}(r_\lambda; R_{\lambda_i}^0)] \phi_{v_\lambda' j_\lambda'}^{\lambda(w)}(r_\lambda; R_{\lambda_i}^0) dr_\lambda \qquad (3.16)$$
$$= \langle l_\lambda | V^\lambda(r_\lambda, R_\lambda, \gamma_\lambda) - V_{rot}^\lambda(r_\lambda; R_{\lambda_i}^0) | l_\lambda' \rangle ,$$

where l_λ was defined after Eq. (3.11) and the γ_λ integral is performed as indicated in Eq. (2.23). Equation (3.16) clearly shows that this potential energy matrix is diagonal in Ω_λ but couples states of different vibration–rotation quantum numbers $v_\lambda j_\lambda$, as stated at the end of Sec. II.B. Equation (3.14) must now be integrated (as described in Sec. III.C) through each subregion i of Region II. At the boundary between two subregions (say, i and $i+1$), a vibrational basis set change is performed. If one makes both $\Psi_{J\Omega_\lambda}^\lambda$ and its derivative with respect to R_λ continuous at this boundary $R_\lambda = R_{\lambda_i}'$, the following relations between the "g" coefficients in two adjacent subregions are obtained:

$$g_J^{\lambda(w)a}(R_{\lambda_i}'; R_{\lambda_{i+1}}^0) = S_i^{\lambda(w)} g_J^{\lambda(w)a}(R_{\lambda_i}'; R_{\lambda_i}^0) , \qquad (3.17a)$$

$$\frac{dg_J^{\lambda(w)a}(R_{\lambda_i}'; R_{\lambda_{i+1}}^0)}{dR_\lambda} = S_i^{\lambda(w)} \frac{dg_J^{\lambda(w)a}(R_{\lambda_i}'; R_{\lambda_i}^0)}{dR_\lambda} \qquad (3.17b)$$

where the overlap matrix $S_i^{\lambda(w)}$ is given by

$$[S_i^{\lambda(w)}]_{l_\lambda}^{l_\lambda'} = \delta_{j_\lambda \Omega_\lambda}^{j_\lambda' \Omega_\lambda'} \langle \phi_{v_\lambda j_\lambda}^{\lambda(w)}(r_\lambda; R_{\lambda_{i+1}}^0) | \phi_{v_\lambda' j_\lambda'}^{\lambda(w)}(r_\lambda; R_{\lambda_i}^0) \rangle . \qquad (3.18)$$

As discussed in Paper I (Sec. III.D), $S_i^{\lambda(w)}$ should be orthogonal for a complete vibrational expansion. For a truncated expansion, as required by practical considerations, $S_i^{\lambda(w)}$ must be nearly orthogonal in order for us to obtain scattering matrices which satisfy conservation of flux (see Sec. V) to an acceptable degree of accuracy. The transformation between Regions I and II is accomplished by setting $i = 0$ in Eqs. (3.17) and interpreting $R_{\lambda_0}^0$ to mean R_{λ_0}' (Fig. 3) and $\phi_{v_\lambda j_\lambda}^{\lambda(a)}(r_\lambda; R_{\lambda_0}^0)$ to mean $\phi_{v_\lambda j_\lambda}^{\lambda(a)}(r_\lambda)$.

3. The strong interaction region

In this region we use the polar coordinates ρ_λ, ψ_λ of Eq. (3.16) of I and regard ψ_λ as the propagation variable. Before we can expand the wavefunction in terms of a set of pseudovibrational eigenfunctions in the variable ρ_λ, we must first transform Eq. (2.31) to these polar coordinates. The only important change in this transformation occurs in $\hat{l}_{\Omega_\lambda \Omega_\lambda'}^{J \lambda j_\lambda}$ [of Eq. (2.32)], which becomes

$$\hat{l}_{\Omega_\lambda \Omega_\lambda'}^{J \lambda j_\lambda} = -\frac{\hbar^2}{2\mu} \left(\frac{1}{\rho_\lambda} \frac{\partial}{\partial \rho_\lambda} \rho_\lambda \frac{\partial}{\partial \rho_\lambda} + \frac{1}{\rho_\lambda^2} \frac{\partial^2}{\partial \psi_\lambda^2} \right) + \frac{j_\lambda(j_\lambda+1)\hbar^2}{2\mu(r_\infty - \rho_\lambda \cos\psi_\lambda)^2}$$

$$+ \frac{\hbar^2[J(J+1) - 2\Omega_\lambda^2 + j_\lambda(j_\lambda+1)]}{2\mu(R_{\lambda_0} - \rho_\lambda \sin\varphi_\lambda)^2} . \qquad (3.19)$$

As for Region II, we divide Region III into n_{III}^λ subregions bounded by lines of constant

$$\varphi_\lambda (= \varphi_{\lambda_1}', \varphi_{\lambda_2}', \ldots, \varphi_{\lambda_{n_{III}}}' = \varphi_{\lambda_0}) .$$

We choose our vibrational basis set to satisfy

$$\left(-\frac{\hbar^2}{2\mu}\frac{d^2}{d\rho_\lambda^2} + V_{ref}^\lambda(\rho_\lambda; \varphi_{\lambda_i}^0)\right)\phi_{v_\lambda}^{\lambda(s)}(\rho_\lambda; \varphi_{\lambda_i}^0) = \epsilon_{v_\lambda}^{\lambda(s)}(\varphi_{\lambda_i}^0)\phi_{v_\lambda}^{\lambda(s)} \qquad (3.20)$$

with boundary conditions analogous to Eq. (3.3). $\varphi_{\lambda_i}^0$ is generally a point within the ith subregion and the reference potential has been re-expressed in the polar coordinates ρ_λ, φ_λ so that it has the shape of a diatomic potential as a function of ρ_λ for a given $\varphi_{\lambda_i}^0$ within Region III (see Fig. 3). The superscript (s) in Eq. (3.20) refers to strong interaction region. Note that the centrifugal term appearing in Eqs. (3.2) and (3.12) has been omitted. [It has been transferred to Eq. (3.26) below.] This results in a vibrational function

$\phi_{v_\lambda}^{\lambda(s)}$ independent of j_λ, which simplifies the matching procedure (Sec. IV) and should not seriously slow down the rate of convergence of the vibrational expansion. If we now expand $F_{j_\lambda\Omega_\lambda}^{\lambda(s)}$ in terms of these $\phi_{v_\lambda}^{\lambda(s)}$,

$$F_{j_\lambda\Omega_\lambda}^{\lambda(s)s}(\rho_\lambda, \varphi_\lambda) = \rho_\lambda^{-1/2} \sum_{v_\lambda} g_{v_\lambda j_\lambda\Omega_\lambda}^{\lambda(s)s}(\varphi_\lambda, \varphi_{\lambda_i}^0)\phi_{v_\lambda}^{\lambda(s)}(\rho_\lambda; \varphi_{\lambda_i}^0) , \qquad (3.21)$$

we obtain the following matrix equation:

$$\frac{d^2 g_J^{\lambda(s)s}}{d\varphi_\lambda^2} = \bar{U}_J^{\lambda(s)}(\varphi_\lambda; \varphi_{\lambda_i}^0)g_J^{\lambda(s)s} , \qquad (3.22)$$

where

$$\bar{U}_J^{\lambda(s)} = \rho_\lambda^2(\varphi_{\lambda_i}^0)U_J^{\lambda(s)}(\varphi_\lambda; \varphi_{\lambda_i}^0) \qquad (3.23)$$

and

$$U_J^{\lambda(s)}(\varphi_\lambda; \varphi_{\lambda_i}^0) = -K^{\lambda(s)2} + U_J^{c\lambda(s)} + U_p^{\lambda(s)} . \qquad (3.24)$$

The matrix ρ_λ^2 (whose elements have the physical dimension of the square of a length) is given by

$$[\rho_\lambda^2(\varphi_{\lambda_i}^0)]_{v_\lambda'}^{v_\lambda} = \delta_{j_\lambda\Omega_\lambda}^{j_\lambda'\Omega_\lambda'}\langle v_\lambda|\rho_\lambda^2|v_\lambda'\rangle , \qquad (3.25)$$

while the centrifugal coupling matrix $U_J^{c\lambda(s)}$ is

$$[U_J^{c\lambda(s)}(\varphi_\lambda; \varphi_{\lambda_i}^0)]_{v_\lambda'}^{v_\lambda} = \delta_{j_\lambda\Omega_\lambda}^{j_\lambda'\Omega_\lambda'}\left[\langle v_\lambda|\left(-\frac{1}{4\rho_\lambda^2} + \frac{J(J+1) - 2\Omega_\lambda^2 + j_\lambda(j_\lambda+1)}{(R_{\lambda_0} - \rho_\lambda \sin\varphi_\lambda)^2} + \frac{j_\lambda(j_\lambda+1)}{(r_{\lambda_0} - \rho_\lambda\cos\varphi_\lambda)^2}\right)|v_\lambda'\rangle\right.$$
$$\left. - \delta_{j_\lambda j_\lambda'}\langle v_\lambda|\frac{1}{(R_{\lambda_0} - \rho_\lambda\sin\varphi_\lambda)^2}|v_\lambda'\rangle[\delta_{\Omega_\lambda+1,\Omega_\lambda'}\xi_+(J,\Omega_\lambda)\xi_+(j_\lambda,\Omega_\lambda) + \delta_{\Omega_\lambda-1,\Omega_\lambda'}\xi_-(J,\Omega_\lambda)\xi_-(j_\lambda,\Omega_\lambda)]\right] . \qquad (3.26)$$

The matrices $K^{\lambda(s)2}$ and $U_p^{\lambda(s)}$ are given by equations analogous to Eqs. (3.10) and (3.16) with superscripts and coordinates appropriate to the strong interaction region substituted where necessary. Note that the centrifugal coupling [Eq. (3.26)] is no longer diagonal in v_λ. The effective potential matrix $\bar{U}_J^{\lambda(s)}$ is not symmetric in this region but rather is equal to the product of two symmetric matrices [Eq. (3.23)], one of which (ρ_λ^2) is the matrix representation of a positive definite operator. The nonsymmetric nature of $\bar{U}_J^{\lambda(s)}$ complicates the integration of Eq. (3.22), and a way of handling this problem was described in Paper I (Sec. III.E and Appendix B).

To solve the Schrödinger equation in Region III, we need to propagate the solution of Eq. (3.22) through each subregion of that region, relating solutions in adjacent subregions by equations analogous to Eqs. (3.17) and (3.18). To relate the solutions at the boundary of Regions II and III, we use the following formula [which is derived in a manner analogous to Eq. (3.17)]:

$$g_J^{\lambda(s)s}(\varphi_\lambda = 0; \varphi_{\lambda_1}^0) = \rho_\lambda^{1/2} g_J^{\lambda(w)s}(R_{\lambda_0}; R_{\lambda_{n_{II}}}^0) , \qquad (3.27a)$$

$$dg_J^{\lambda(s)s}(\varphi_\lambda = 0; \varphi_{\lambda_1}^0)/d\varphi_\lambda = -\rho_\lambda^{3/2}[dg_J^{\lambda(w)s}(R_{\lambda_0}; R_{\lambda_{n_{II}}}^0)/dR_\lambda] , \qquad (3.27b)$$

where

$$[\rho_\lambda^b]_{v_\lambda}^{v_\lambda'} = \delta_{j_\lambda\Omega_\lambda}^{j_\lambda'\Omega_\lambda'}\langle\phi_{v_\lambda}^{\lambda(s)}(\rho_\lambda; \varphi_{\lambda_1}^0)|\rho_\lambda^b|\phi_{v_\lambda'}^{\lambda(w)}(r_{\lambda_0} - \rho_\lambda; R_{\lambda_{n_{II}}}^0)\rangle \quad b = \tfrac{1}{2}, \tfrac{3}{2} . \qquad (3.28)$$

4. The matching region

The polar coordinates ζ, η_λ of Eq. (3.17) of I are used in Region IV with η_λ acting as the propagation variable. Upon transformation of Eq. (2.31) to these coordinates, the operator $\bar{T}_{\Omega_\lambda\Omega_\lambda'}^{J\lambda J}$ of Eq. (2.32) becomes

$$T_{\Omega_\lambda\Omega_\lambda'}^{J\lambda J} = -\frac{\hbar^2}{2\mu}\left(\frac{1}{\zeta}\frac{\partial}{\partial\zeta}\zeta\frac{\partial}{\partial\zeta} + \frac{1}{\zeta^2}\frac{\partial^2}{\partial\eta_\lambda^2}\right) + \frac{\hbar^2 j_\lambda(j_\lambda+1)}{2\mu\zeta^2\sin^2\eta_\lambda} + \frac{\hbar^2[J(J+1) - 2\Omega_\lambda^2 + j_\lambda(j_\lambda+1)]}{2\mu\zeta^2\cos^2\eta_\lambda} . \qquad (3.29)$$

In analogy with Region III, Region IV is divided into n_{IV}^λ subregions by lines of constant η_λ, with the vibrational eigenfunctions of each subregion satisfying an equation analogous to (3.20):

$$\left(-\frac{\hbar^2}{2\mu}\frac{d^2}{d\zeta^2} + V_{ref}(\zeta; \eta_{\lambda_i}^0)\right)\phi_{v_\lambda}^{\lambda(m)}(\zeta; \eta_{\lambda_i}^0) = \epsilon_{v_\lambda}^{\lambda(m)}(\eta_{\lambda_i}^0)\phi_{v_\lambda}^{\lambda(m)} , \qquad (3.30)$$

where the superscript (m) denotes matching region. Writing

$$F_{J J_\lambda \Omega_\lambda}^{\lambda(m)}(\zeta, \eta_\lambda) = \zeta^{-1/2} \sum_{v_\lambda'} \kappa_{J v_\lambda j_\lambda \Omega_\lambda}^{\lambda(m)}(\eta_\lambda; \eta_{\lambda_i}^0) \phi_{v_\lambda}^{\lambda(m)}(\zeta; \eta_{\lambda_i}^0) , \tag{3.31}$$

the counterpart of Eq. (3.22) becomes

$$\frac{d^2}{d\eta_\lambda^2} \mathbf{g}_J^{\lambda(m)} = \bar{\mathbf{U}}_J^{\lambda(m)}(\eta_\lambda; \eta_{\lambda_i}^0) \mathbf{g}_J^{\lambda(m)} , \tag{3.32}$$

where

$$\bar{\mathbf{U}}_J^{\lambda(m)} = \zeta^2(\eta_{\lambda_i}^0) \mathbf{U}_J^{\lambda(m)}(\eta_\lambda; \eta_{\lambda_i}^0) \tag{3.33}$$

and

$$\mathbf{U}_J^{\lambda(m)}(\eta_\lambda; \eta_{\lambda_i}^0) = -\mathbf{K}^{\lambda(m)^2} + \mathbf{U}_J^{c\lambda(m)} + \mathbf{U}_p^{\lambda(m)} . \tag{3.34}$$

The matrix $\zeta^2(\eta_{\lambda_i}^0)$ is defined analogously to ρ_λ^2 of Eq. (3.25) with ζ substituted for ρ_λ. The matrices $\mathbf{K}^{\lambda(m)^2}$ and $\mathbf{U}_p^{\lambda(m)}$ are given by equations similar to Eqs. (3.10) and (3.16), respectively, with the superscript (m) inserted and the appropriate coordinate changes made. The centrifugal coupling matrix $\mathbf{U}_J^{c\lambda(m)}$ is given by

$$[\mathbf{U}_J^{c\lambda(m)}(\eta_\lambda; \eta_{\lambda_i}^0)]_{i_\lambda'}^{i_\lambda} = \langle v_\lambda | \zeta^{-2} | v_\lambda' \rangle (\{\delta_{j_\lambda \Omega_\lambda}^{j_\lambda' \Omega_\lambda'} \{-\tfrac{1}{4} + [J(J+1) - 2\Omega_\lambda^2 + j_\lambda(j_\lambda+1)] / \cos^2\eta_\lambda + j_\lambda(j_\lambda+1) / \sin^2\eta_\lambda\} \tag{3.35}$$

$$- \delta_{j_\lambda, j_\lambda'} [\delta_{\Omega_\lambda+1, \Omega_\lambda'} \xi_+(J, \Omega_\lambda) \xi_+(j_\lambda, \Omega_\lambda)$$

$$+ \delta_{\Omega_\lambda-1, \Omega_\lambda'} \xi_-(J, \Omega_\lambda) \xi_-(j_\lambda, \Omega_\lambda)] / \cos^2\eta_\lambda) .$$

To solve the Schrödinger equation in Region IV, one must integrate Eq. (3.32) through each subregion, relating solutions in adjacent subregions by equations analogous to Eqs. (3.17) and (3.18). The transformation between Regions III and IV is accomplished by equations analogous to Eqs. (3.27a) and (3.27b) (with a plus rather than a minus sign in the right hand side of the latter) and the matrix ζ^b substituted for ρ_λ^b, where

$$[\zeta^b]_{i_\lambda}^{i_\lambda'} = \delta_{j_\lambda \Omega_\lambda}^{j_\lambda' \Omega_\lambda'} \langle \phi_{v_\lambda}^{\lambda(m)}(\zeta, \eta_{\lambda_1}^0) \left| \left(\frac{\cdot \zeta}{\rho_{\lambda_0} - \zeta} \right)^b \right| \phi_{v_\lambda}^{\lambda(s)}\left(\rho_{\lambda_0} - \zeta; \varphi_{\lambda_{III}}^0 \right) \rangle \qquad b = \tfrac{1}{2}, \tfrac{3}{2} . \tag{3.36}$$

with ρ_{λ_0} defined in Fig. 3.

C. Integration of the Schrödinger equation

We generate the solution $\mathbf{g}_J^\lambda$ and its derivative with respect to the propagation variable by choosing at $R_\lambda = R_{\lambda 0}'$ (Fig. 3) arbitrary initial values for these two matrices and integrating numerically Eqs. (3.8), (3.14), (3.22), and (3.32) from the beginning of Region II to the end of Region IV. The solution $\mathbf{g}_J^\lambda$ and its derivative are determined by integrating the same equations from the end of Region IV to the beginning of Region II. Any appropriate numerical procedure may be used to solve these coupled ordinary second order differential equations. A particular one which is well suited to such equations and which we used is the Gordon method.[42] More particulars of this procedure are described in Paper I (Sec. III.E).

For the $H + H_2$ reaction, the coupled equations need only be solved in one of the three equivalent arrangement channels. Reactions of the type $A + B_2$ involving two identical atoms will require two such integrations, and reactions with three different atoms will require three. For arrangement channels for which the target is homonuclear, Eq. (2.29) implies zero potential coupling between odd and even rotational states. Since all kinetic energy coupling is diagonal in j_λ in all four regions, our matrix differential equations may be decoupled into two separate ones for the even and odd rotational states with a consequent savings in computation time. Both must be integrated before the matching, which mixes these two sets of solutions, is performed.

Any chemical reaction displays in addition parity

(i.e., inversion through the center of mass) symmetry, as shown for triatomic systems in Appendix B. Although the body-fixed wavefunctions obtained from Eqs. (2.13), (2.18), (2.30), and either (3.1), (3.13), (3.21), or (3.31) are not eigenfunctions of the parity operator, they may be linearly combined to yield solutions which are, and this transformation to the "parity representation" results in a partial decoupling of Eqs. (3.8), (3.14), (3.22), and (3.32) into two sets, one for even and one for odd parity. A description of this transformation and other consequences of the parity operation are given in Appendix B. By using parity eigenfunctions, the integration in each arrangement channel is done in two separate steps (four for homonuclear targets). Since the transformation between arrangement channels preserves parity (as shown in Appendix B), the matching procedure also can be done separately for solutions of each parity, as can the calculation of the reactance and scattering matrices. The final plane wave solution is not, however, an eigenfunction of the parity operator, and as a result the calculation of scattering amplitudes requires a transformation back to the body-fixed representation of the previous two sections. The enormous reduction in computation time more than outweighs the additional work involved in this transformation. Appendix B describes this in more detail.

IV. THE MATCHING

A. The λ to ν transformation

At the completion of the integrations in each of the three arrangement channel regions, one has solutions

to the Schrödinger equation which span all of configuration space but which are neither smooth nor continuous at the internal configuration space boundaries of these regions. In this section we describe the procedure for linearly combining these solutions so as to produce a smooth matching at those boundaries. This procedure will also include the transformation from λ to ν coordinates (appropriate for arrangement channels λ and ν, respectively), a transformation which is both conceptually and numerically facilitated by the use of body-fixed coordinates. Our analysis will focus primarily on the behavior of the wavefunction in the vicinity of the half-plane matching surfaces defined in Eq. (3.2) of I.

Equations describing the λ to ν transformation have been derived for coplanar reactions in Appendix A of Paper I, and most of these expressions are still valid in 3D. However, some angles which span a range of 2π in 2D become polar angles in 3D (with a range of π), so some care is required in making the analogy. The basic equations which govern the transformation are given by[19]

$$\begin{pmatrix} R_\nu \\ r_\nu \end{pmatrix} = \begin{pmatrix} \cos\alpha_{\nu\lambda} & -\sin\alpha_{\nu\lambda} \\ \sin\alpha_{\nu\lambda} & \cos\alpha_{\nu\lambda} \end{pmatrix}\begin{pmatrix} R_\lambda \\ r_\lambda \end{pmatrix} , \quad (4.1)$$

where $\alpha_{\nu\lambda}$ is the angle between $\pi/2$ and π defined by

$$\alpha_{\nu\lambda} = \pi - \beta_{\nu\lambda} , \quad (4.2)$$

$\beta_{\nu\lambda}$ having been given by Eqs. (2.4). Equation (4.1) may be easily derived from Fig. 1 and Eq. (2.1). By taking the scalar products $R_\nu \cdot R_\nu$, $r_\nu \cdot r_\nu$, and $R_\nu \cdot r_\nu$ and using Eqs. (4.1) and (2.3), we find the following expressions for the R_λ, r_λ, $\gamma_\lambda - R_\nu$, r_ν, γ_ν transformation:

$$R_\nu^2 = \cos^2\alpha_{\nu\lambda} R_\lambda^2 + \sin^2\alpha_{\nu\lambda} r_\lambda^2 - \sin 2\alpha_{\nu\lambda}\cos\gamma_\lambda r_\lambda R_\lambda , \quad (4.3)$$

$$r_\nu^2 = \sin^2\alpha_{\nu\lambda} R_\lambda^2 + \cos^2\alpha_{\nu\lambda} r_\lambda^2 + \sin 2\alpha_{\nu\lambda}\cos\gamma_\lambda r_\lambda R_\lambda , \quad (4.4)$$

$$\cos\gamma_\nu = (R_\nu r_\nu)^{-1}[\tfrac{1}{2}(R_\lambda^2 - r_\lambda^2)\sin 2\alpha_{\nu\lambda}$$
$$+ R_\lambda r_\lambda \cos 2\alpha_{\nu\lambda}\cos\gamma_\lambda] . \quad (4.5)$$

Equations (4.3) and (4.4) may be combined to yield

$$R_\nu^2 + r_\nu^2 = R_\lambda^2 + r_\lambda^2 \quad (4.6)$$

which, together with Eq. (3.17) of I proves the invariance of ζ to arrangement channel. Also of use in our analysis below is the polar angle $\Delta_{\nu\lambda}$ (in the 0 to π range) between R_λ and R_ν which is determined by

$$\cos\Delta_{\nu\lambda} = \frac{R_\nu \cdot R_\lambda}{R_\nu R_\lambda} = \cos\alpha_{\nu\lambda}\frac{R_\lambda}{R_\nu} - \sin\alpha_{\nu\lambda}\cos\gamma_\lambda\frac{r_\lambda}{R_\nu} . \quad (4.7)$$

We now examine the consequences of Eqs. (4.3)–(4.7) on the matching surface $\pi_{\nu\lambda}$. Combining Eq. (3.2a) of I with Eq. (4.6) gives

$$R_\lambda = R_\nu , \quad (4.8)$$

and this equation together with Eqs. (3.2a) of I and (4.3) leads to

$$R_\lambda/r_\lambda = -\cot\alpha_{\nu\lambda}\cos\gamma_\lambda + (1 + \cot^2\alpha_{\nu\lambda}\cos^2\gamma_\lambda)^{1/2} , \quad (4.9)$$

which is the equation of the matching surface $\pi_{\nu\lambda}$ in R_λ,

r_λ, γ_λ coordinates. If Eqs. (4.8) and (4.9) and Eq. (3.2) of I are now substituted into Eq. (4.5), we find

$$\cos\gamma_\nu = -\cos\gamma_\lambda ,$$

and since γ_λ and γ_ν are in the range 0 to π we conclude that on $\pi_{\nu\lambda}$

$$\gamma_\nu = \pi - \gamma_\lambda . \quad (4.10)$$

Equations (4.7)–(4.9) and Eq. (3.2) of I may be combined to yield

$$\cos\Delta_{\nu\lambda} = \cos\alpha_{\nu\lambda} - \sin\alpha_{\nu\lambda}\cos\gamma_\lambda[\cot\alpha_{\nu\lambda}\cos\gamma_\lambda$$
$$+ (1 + \cot^2\alpha_{\nu\lambda}\cos^2\gamma_\lambda)^{1/2}] , \quad (4.11)$$

which implies that on $\pi_{\nu\lambda}$ the angle $\Delta_{\nu\lambda}$ is a function of γ_λ only.

It will also be useful to convert from R_λ, r_λ to the polar coordinates ζ, η_λ [of Eqs. (3.17) of Paper I]. First, from Eqs. (3.17) of Paper I and (4.8), we have

$$\eta_\lambda = \eta_\nu \quad \text{on } \pi_{\nu\lambda} \quad (4.12)$$

and, after some manipulation, Eq. (4.9) becomes

$$\cot 2\eta_\lambda = -\cot\alpha_{\nu\lambda}\cos\gamma_\lambda \quad \text{on } \pi_{\nu\lambda} , \quad (4.13)$$

which is the equation of $\pi_{\nu\lambda}$ in ζ, η_λ, γ_λ coordinates. Since $\eta_\lambda = \tan^{-1}(r_\lambda/R_\lambda)$ and is in the 0 to $\pi/2$ range, we conclude that

$$\eta_\lambda = \tfrac{1}{2}\omega_\lambda , \quad (4.14)$$

where ω_λ was defined after Eq. (2.3). Therefore, Eq. (4.13) is equivalent to

$$\cot\omega_\lambda = -\cot\alpha_{\nu\lambda}\cos\gamma_\lambda , \quad (4.15)$$

which is the equation of the $\pi_{\nu\lambda}$ half-plane of Fig. 2 of I in the polar coordinates ζ, ω_λ, γ_λ. Finally, Eq. (4.11) may be re-expressed in η_λ, γ_λ coordinates as

$$\cos\Delta_{\nu\lambda} = \cos\alpha_{\nu\lambda} - \sin\alpha_{\nu\lambda}\cos\gamma_\lambda\tan\eta_\lambda . \quad (4.16)$$

We now consider the transformation from the body-fixed coordinate system $Ox'_\lambda y'z'_\lambda$ (Fig. 2) to $Ox'_\nu y'z'_\nu$. Both systems have the same y' axis (which is perpendicular to the three-atom plane), and from Eq. (4.7) and Fig. 2 it can easily be shown that this coordinate transformation is a clockwise rotation about Oy' by $\Delta_{\nu\lambda}$.

Let us determine the effect of the $(R_\lambda, r_\lambda) \to (R_\nu, r_\nu)$ transformation on the wavefunctions. The complete body-fixed wavefunction, as obtained from Eqs. (2.13), (2.18), and (2.30) is

$$\Psi_{JM} = \sum_{f_\lambda\Omega_\lambda} D_{M\Omega_\lambda}^J(\phi_\lambda, \theta_\lambda, 0) Y_{f_\lambda\Omega_\lambda}(\gamma_\lambda, \psi_\lambda)\frac{F_{Jf_\lambda\Omega_\lambda}^\lambda(r_\lambda, R_\lambda)}{r_\lambda R_\lambda}$$
$$= \frac{1}{\sqrt{2\pi}}\sum_{\Omega_\lambda} D_{M\Omega_\lambda}^J(\phi_\lambda, \theta_\lambda, \psi_\lambda)\chi_{J\Omega_\lambda}^\lambda(r_\lambda, R_\lambda, \gamma_\lambda) , \quad (4.17)$$

where, from Eq. (A3),

$$\chi_{J\Omega_\lambda}^\lambda = \sum_{f_\lambda=|\Omega_\lambda|}\frac{\Theta_{f_\lambda}^{\Omega_\lambda}(\cos\gamma_\lambda)F_{Jf_\lambda\Omega_\lambda}^\lambda(r_\lambda, R_\lambda)}{r_\lambda R_\lambda} . \quad (4.18)$$

In the second line of Eq. (4.17), the $\exp i\Omega_\lambda\psi_\lambda$ part of $Y_{f_\lambda\Omega_\lambda}(\gamma_\lambda, \psi_\lambda)$ has been incorporated into the rotation matrix $D_{M\Omega_\lambda}^J$ which trivially converts Ψ_{JM} from the

$OX_\lambda Y_\lambda Z_\lambda$ to the $Ox'_\lambda y' z'_\lambda$ coordinate system. If Ψ_{JM} is fully matched (i.e., a smoothly continuous solution of the Schrödinger equation), it may be expressed in the $Ox'_\nu y' z'_\nu$ coordinate system in an analogous way:

$$\Psi_{JM} = \frac{1}{\sqrt{2\pi}} \sum_{\Omega_\nu} D^J_{M\Omega_\nu}(\phi_\nu, \theta_\nu, \psi_\nu) \chi^\nu_{J\Omega_\nu}(r_\nu, R_\nu, \gamma_\nu) . \tag{4.19}$$

We now define Ψ_J, $\chi^\lambda_J(r_\lambda, R_\lambda, \gamma_\lambda)$, and $\chi^\nu_J(r_\nu, R_\nu, \gamma_\nu)$ as the $(2J+1)$-dimensional column vectors whose components are, respectively, the Ψ_{JM}, $\chi^\lambda_{J\Omega_\lambda}$, and $\chi^\nu_{J\Omega_\nu}$, where each one of the indices M, Ω_λ, and Ω_ν assumes the values (top to bottom) $J, J-1, \ldots, -J$. In matrix notation, Eqs. (4.17) and (4.19) can be written as

$$\Psi_J = \frac{1}{\sqrt{2\pi}} \mathbf{D}^J(\phi_\lambda, \theta_\lambda, \psi_\lambda) \chi^\lambda_J(r_\lambda, R_\lambda, \gamma_\lambda)$$

$$= \frac{1}{\sqrt{2\pi}} \mathbf{D}^J(\phi_\nu, \theta_\nu, \psi_\nu) \chi^\nu_J(r_\nu, R_\nu, \gamma_\nu) ,$$

from which one gets

$$\chi^\lambda_J = \mathbf{D}^{J^{-1}}(\phi_\lambda, \theta_\lambda, \psi_\lambda) \mathbf{D}^J(\phi_\nu, \theta_\nu, \psi_\nu) \chi^\nu_J . \tag{4.20}$$

The $Oxyz \to Ox'_\lambda y' z'_\lambda$ transformation, which is a rotation defined by the Euler angles $\phi_\lambda, \theta_\lambda, \psi_\lambda$, can be accomplished through a sequence of two rotations, the $Oxyz \to Ox'_\nu y' z'_\nu$ one (Euler angles $\phi_\nu, \theta_\nu, \psi_\nu$) followed by $Ox'_\nu y' z'_\nu \to Ox'_\lambda y' z'_\lambda$ (Euler angles $0, \Delta_{\nu\lambda}, 0$). From this results the relation $\mathbf{D}^J(\phi_\nu, \theta_\nu, \psi_\nu) = \mathbf{D}^J(\phi_\lambda, \theta_\lambda, \psi_\lambda) \mathbf{d}^J(\Delta_{\nu\lambda})$, where $\mathbf{d}^J(\Delta_{\nu\lambda}) = \mathbf{D}^J(0, \Delta_{\nu\lambda}, 0)$. Since the $\mathbf{D}^J$ are unitary and $\mathbf{d}^J$ is in addition real, we get from Eq. (4.20)

$$\chi^\lambda_J = [\mathbf{d}^J(\Delta_{\nu\lambda})]^{-1} \chi^\nu_J = \tilde{\mathbf{d}}^J(\Delta_{\nu\lambda}) \chi^\nu_J ,$$

and therefore, in the notation of Davydov,[33]

$$\chi^\lambda_{J\Omega_\lambda} = \sum_{\Omega_\nu} d^J_{\Omega_\nu \Omega_\lambda}(\Delta_{\nu\lambda}) \chi^\nu_{J\Omega_\nu} . \tag{4.21}$$

This equation relating the matched solutions χ^λ and χ^ν is valid for any internal configuration of the triatom (i.e., is not restricted to those configurations corresponding to the $\pi_{\nu\lambda}$ matching surface).

B. Projection of the wavefunction onto the matching surface basis functions

In this section we consider the evaluation of the unmatched wavefunctions and normal derivatives obtained from the integrations in both channels λ and ν on the matching surface $\pi_{\nu\lambda}$, and their expansion in a set of functions $B^\lambda_{\nu\lambda j_\lambda \Omega_\lambda}(\zeta, \gamma_\lambda)$ which span that surface. The complete, unmatched wavefunction in the $Ox'_\lambda y' z'_\lambda$ coordinate system in Region IV of internal configuration space (subregion i) is [from Eqs. (4.17), (4.18), and (3.31)]

$$\psi^{Mi'_\lambda \bullet}_{JM} = \frac{1}{\sqrt{2\pi}} \sum_{\Omega_\lambda} D^J_{M\Omega_\lambda}(\phi_\lambda, \theta_\lambda, \psi_\lambda) \bar{\chi}^{Mi'_\lambda \bullet}_{J\Omega_\lambda}(\zeta, \eta_\lambda, \gamma_\lambda) , \tag{4.22}$$

where

$$\bar{\chi}^{Mi'_\lambda \bullet}_{J\Omega_\lambda} = \sum_{v_\lambda j_\lambda} \frac{2 \vartheta^{\Omega_\lambda}_{j_\lambda}(\cos\gamma_\lambda) \phi^\lambda_{v_\lambda}(\zeta; \eta^0_{\lambda i}) g^{Mi'_\lambda \bullet}_{Jv_\lambda j_\lambda \Omega_\lambda}(\eta_\lambda; \eta^0_{\lambda i})}{\zeta^{5/2} \sin 2\eta_\lambda} . \tag{4.23}$$

Here we have dropped the superscript (m), as it will be

implicit throughout this section, but we have included the labels $l'_\lambda \pm \equiv (v'_\lambda j'_\lambda \Omega'_\lambda \pm)$ to denote the $2N$ linearly independent solutions obtained (from an N coupled-channel calculation). Equation (4.23) may be evaluated on $\pi_{\nu\lambda}$ by using Eq. (4.13) to relate η_λ and γ_λ. Since $0 \le \gamma_\lambda \le \pi/2$ on $\pi_{\nu\lambda}$, we find that η_λ must lie between $\eta_{\lambda 0} = (\pi - \alpha_{\nu\lambda})/2$ and $\eta_{\lambda 1} = \pi/4$ to satisfy Eq. (4.13). In order to evaluate Eq. (4.23) over this range of η_λ, it is convenient to change to a common set of vibrational basis functions $\phi^\lambda_{v_\lambda}(\zeta)$ for all subregions i. This is accomplished by transformations analogous to Eq. (3.17) and (3.18), with the result that

$$\bar{\chi}^{Mi'_\lambda \bullet}_{J\Omega_\lambda} = 2\zeta^{-5/2}(\sin 2\eta_\lambda)^{-1} \Phi^{Mi'_\lambda \bullet}_{J\Omega_\lambda} , \tag{4.24}$$

where

$$\Phi^{Mi'_\lambda \bullet}_{J\Omega_\lambda} = \sum_{v_\lambda j_\lambda} \vartheta^{\Omega_\lambda}_{j_\lambda}(\cos\gamma_\lambda) \phi^\lambda_{v_\lambda}(\zeta) g^{Mi'_\lambda \bullet}_{Jv_\lambda j_\lambda \Omega_\lambda}(\eta_\lambda) . \tag{4.25}$$

To insure a smooth matching, we must also consider the derivative of $\bar{\chi}$ normal to $\pi_{\nu\lambda}$ (other derivatives are possible) for points on this plane. Expressions for this normal derivative operator were derived in Paper I (Appendix A), where it was found that

$$\frac{\partial}{\partial n_{\nu\lambda}} = \frac{1}{\zeta} \frac{\sin\alpha_{\nu\lambda}}{\sin\omega_\lambda} \left(\frac{\partial}{\partial\omega_\lambda} + \cot\alpha_{\nu\lambda}\sin\gamma_\lambda \frac{\partial}{\partial\gamma_\lambda} \right)$$

$$= \frac{1}{\zeta} \frac{\sin\alpha_{\nu\lambda}}{\sin 2\eta_\lambda} \left(\frac{1}{2} \frac{\partial}{\partial\eta_\lambda} + \cot\alpha_{\nu\lambda}\sin\gamma_\lambda \frac{\partial}{\partial\gamma_\lambda} \right)$$

$$= -\frac{1}{\zeta} \frac{\sin\alpha_{\nu\lambda}}{\sin 2\eta_\lambda} \left(\frac{1}{2} \frac{\partial}{\partial\eta_\nu} - \cot\alpha_{\nu\lambda}\sin\gamma_\lambda \frac{\partial}{\partial\gamma_\nu} \right) . \tag{4.26}$$

Applying this operator to Eq. (4.23), and evaluating the result on $\pi_{\nu\lambda}$, we find

$$\frac{\partial \bar{\chi}^{Mi'_\lambda \bullet}_{J\Omega_\lambda}}{\partial n_{\nu\lambda}} = \frac{2\sin\alpha_{\nu\lambda}}{\zeta^{7/2}\sin^2 2\eta_\lambda} \Phi'^{Mi'_\lambda \bullet}_{J\Omega_\lambda} , \tag{4.27}$$

where

$$\Phi'^{Mi'_\lambda \bullet}_{J\Omega_\lambda} = \sum_{v_\lambda j_\lambda} \phi^\lambda_{v_\lambda}(\zeta) G'^{Mi'_\lambda \bullet}_{Jv_\lambda j_\lambda \Omega_\lambda} \tag{4.28}$$

and

$$G'^{Mi'_\lambda \bullet}_{Jv_\lambda j_\lambda \Omega_\lambda} = \frac{1}{2} \vartheta^{\Omega_\lambda}_{j_\lambda}(\cos\gamma_\lambda) \frac{dg^{Mi'_\lambda \bullet}_{Jv_\lambda j_\lambda \Omega_\lambda}[\eta_\lambda(\gamma_\lambda)]}{d\eta_\lambda} - \cot\alpha_{\nu\lambda}$$

$$\times g^{Mi'_\lambda \bullet}_{Jv_\lambda j_\lambda \Omega_\lambda}(\eta_\lambda(\gamma_\lambda)) \left[j_\lambda \cos\gamma_\lambda \vartheta^{\Omega_\lambda}_{j_\lambda}(\cos\gamma_\lambda) \right.$$

$$\left. - \left(\frac{2j_\lambda + 1}{2j_\lambda + 3} \right)^{1/2} [(j_\lambda + 1)^2 - \Omega^2_\lambda]^{1/2} \vartheta^{\Omega_\lambda}_{j_\lambda + 1}(\cos\gamma_\lambda) \right] . \tag{4.29}$$

In deriving Eq. (4.29), the use has been made of Eq. (A2) and certain recursion relations between the associated Legendre polynomials.[34]

We now wish to expand Eqs. (4.25) and (4.28) on the matching surface in terms of a set of functions $B^{\nu\lambda}_{v_\lambda j_\lambda \Omega_\lambda}(\zeta, \gamma_\lambda)$ which are orthonormal and complete on it. (We choose ζ and γ_λ to be the independent variables which scan $\pi_{\nu\lambda}$.) The $B^{\nu\lambda}_{v_\lambda j_\lambda \Omega_\lambda}$ are given by

$$B^{\nu\lambda}_{v_\lambda j_\lambda \Omega_\lambda}(\zeta, \gamma_\lambda) = \phi^\lambda_{v_\lambda}(\zeta) A^{\nu\lambda}_{j_\lambda \Omega_\lambda}(\gamma_\lambda) , \tag{4.30}$$

where the $\phi_{v_\lambda}^\lambda$'s are those of Eq. (4.25) and the $A_{j_\lambda\Omega_\lambda}^{v\lambda}$ are a set of rotational functions which must be orthonormal (with weight function $\sin\gamma_\lambda$) and complete on the domain $0 \leq \gamma_\lambda \leq \pi/2$. The reason for this choice of the domain of γ_λ is analogous to that used for the coplanar matching in Paper I (Sec. IV A). An important consequence of this procedure is that the number of functions $B_{v_\lambda j_\lambda\Omega_\lambda}^{v\lambda}$ used to expand the wavefunction of Eq. (4.25) for each v_λ, Ω_λ must be less than the number of vibration-rotation basis functions $\phi_{v_\lambda}(\zeta)\mathcal{P}_{j_\lambda}^{\Omega_\lambda}(\cos\gamma_\lambda)$ in that equation. For many reactions, including $H + H_2$, the number of $B_{v_\lambda j_\lambda\Omega_\lambda}^{v\lambda}$'s should be half the number of vibration-rotation basis functions, and we shall use this number in the discussion below. This would imply that the number of j_λ's for each v_λ, Ω_λ used in the close coupling expansion must be even. An example of how this might be done would be to use a complete set of Ω_λ's for each j_λ within a given vibrational manifold, except for the case $j_\lambda = j_{\lambda_{max}}$. For this case (as long as $J \geq j_{\lambda_{max}}$) one uses $\Omega_\lambda = j_{\lambda_{max}} - 1$, $j_{\lambda_{max}} - 3, \ldots, -j_{\lambda_{max}} + 1$. For $J < j_{\lambda_{max}}$, we use the same procedure and then eliminate those Ω_λ for which $|\Omega_\lambda| > J$. Other choices are possible, but this particular set of quantum numbers is useful because it leads, for $j_\lambda = j_{\lambda_{max}}$, to an asymptotic uncoupling of those terms in Eq. (2.31) which are not diagonal in Ω_λ, and this allows us to solve for the asymptotic behavior of these partially truncated solutions in a simple way.[43] Whatever the choice, this restriction on the method is seldom a serious limitation because it only affects the highest rotational state j_λ for each v_λ, Ω_λ, and this channel is usually closed in a converged treatment. An example of a choice of $A_{j_\lambda\Omega_\lambda}^{v\lambda}$ which is real and orthonormal over the 0 to $\pi/2$ range (weighted by $\sin\gamma_\lambda$) is

$$A_{j_\lambda\Omega_\lambda}^{v\lambda}(\gamma_\lambda) = \begin{cases} \sqrt{2}\,\mathcal{P}_{j_\lambda}^{\Omega_\lambda}(\cos\gamma_\lambda) & \text{for } j_\lambda + \Omega_\lambda = \text{odd} \\ 0 & \text{for } j_\lambda + \Omega_\lambda = \text{even}. \end{cases} \quad (4.31)$$

This choice is very appropriate for expanding the γ_λ-dependent part of Eq. (4.25) for a collinearly dominated reaction such as $H + H_2$ because these $A_{j_\lambda\Omega_\lambda}^{v\lambda}$ vanish at $\gamma_\lambda = \pi/2$ (where the interaction potential on the matching surface is high and the wavefunction very small) and are most effective in representing the wavefunction near $\gamma_\lambda = 0$ (where the potential is low). Other choices for the $A_{j_\lambda\Omega_\lambda}^{v\lambda}$ may be made in analogy with those discussed for the planar problem in Paper I.

We now expand Eqs. (4.25) and (4.28) in terms of the $B_{v_\lambda j_\lambda\Omega_\lambda}^{v\lambda}$, obtaining

$$\Phi_{J\Omega_\lambda}^{\lambda v'_\lambda \bar{\lambda}} = \sum_{v_\lambda j_\lambda} h_{Jv_\lambda j_\lambda\Omega_\lambda}^{\lambda v'_\lambda \bar{\lambda}} B_{v_\lambda j_\lambda\Omega_\lambda}^{v\lambda}(\zeta, \gamma_\lambda), \quad (4.32)$$

$$\Phi_{J\Omega_\lambda}^{\prime \lambda v'_\lambda \bar{\lambda}} = \sum_{v_\lambda j_\lambda} h_{Jv_\lambda j_\lambda\Omega_\lambda}^{\prime \lambda v'_\lambda \bar{\lambda}} B_{v_\lambda j_\lambda\Omega_\lambda}^{v\lambda}(\zeta, \gamma_\lambda), \quad (4.33)$$

$$h_{Jv_\lambda j_\lambda\Omega_\lambda}^{\lambda v'_\lambda \bar{\lambda}} = \sum_{j'_\lambda} \int_0^{\pi/2} A_{j_\lambda\Omega_\lambda}^{v\lambda}(\gamma_\lambda)\mathcal{P}_{j'_\lambda}^{\Omega_\lambda}(\cos\gamma_\lambda)$$
$$\times g_{Jv_\lambda j'_\lambda\Omega_\lambda}^{\lambda v'_\lambda \bar{\lambda}}[\eta_\lambda(\gamma_\lambda)]\sin\gamma_\lambda\,d\gamma_\lambda, \quad (4.34)$$

and

$$h_{Jv_\lambda j_\lambda\Omega_\lambda}^{\prime \lambda v'_\lambda \bar{\lambda}} = \sum_{j'_\lambda} \int_0^{\pi/2} A_{j_\lambda\Omega_\lambda}^{v\lambda}(\gamma_\lambda) G_{Jv_\lambda j'_\lambda\Omega_\lambda}^{\prime \lambda v'_\lambda \bar{\lambda}}(\gamma_\lambda)\sin\gamma_\lambda\,d\gamma_\lambda, \quad (4.35)$$

where Eq. (4.29) is to be used in evaluating Eq. (4.35). Note that the row (lower) indices $v_\lambda j_\lambda\Omega_\lambda$ in Eqs. (4.32)–(4.35) can assume only $N/2$ values (from the discussion above), whereas the column (upper) indices $v'_\lambda j'_\lambda\Omega'_\lambda$ (implied in t'_λ) scan N values. This means that the matrices h_J^v and $h_J^{\prime\lambda}$ have dimensions $N/2 \times N$.

We now consider the expansion of the wavefunction $\bar{\chi}_{J\Omega_\nu}^{v t'_\nu \bar{\lambda}}$ obtained from the integration in arrangement channel region ν on $\pi_{\nu\lambda}$ in a manner analogous to that for $\bar{\chi}_{J\Omega_\lambda}^{\lambda t'_\lambda \bar{\lambda}}$. The expressions for the wavefunctions are given by Eqs. (4.24) and (4.25) with ν replacing λ everywhere. To find the normal derivatives, the rightmost side of Eq. (4.26) is used. The resulting expression is given by Eqs. (4.27) and (4.28) with ν replaced by λ and with the function $G_{Jv_\nu j_\nu\Omega_\nu}^{\prime \nu t'_\nu \bar{\lambda}}$ given by

$$G_{Jv_\nu j_\nu\Omega_\nu}^{\prime \nu t'_\nu \bar{\lambda}} = -(-1)^{j_\nu-\Omega_\nu}\left\{\frac{1}{2}\mathcal{P}_{j_\nu}^{\Omega_\nu}(\cos\gamma_\lambda)\frac{dg_{Jv_\nu j_\nu\Omega_\nu}^{\nu t'_\nu \bar{\lambda}}[\eta_\nu(\gamma_\lambda)]}{d\eta_\nu}\right.$$
$$- \cot\alpha_{\nu\lambda}g_{Jv_\nu j_\nu\Omega_\nu}^{\nu t'_\nu \bar{\lambda}}[\eta_\nu(\gamma_\lambda)]\left[j_\nu\cos\gamma_\lambda\mathcal{P}_{j_\nu}^{\Omega_\nu}(\cos\gamma_\lambda)\right.$$
$$\left.\left. - \left(\frac{2j_\nu+1}{2j_\nu+3}\right)^{1/2}[(j_\nu+1)^2-\Omega_\nu^2]^{1/2}\mathcal{P}_{j_\nu+1}^{\Omega_\nu}(\cos\gamma_\lambda)\right]\right\}. \quad (4.36)$$

Note that Eq. (4.10) has been used in Eq. (4.36) [along with the property $\mathcal{P}_j^m(-x) = (-1)^{j+m}\mathcal{P}_j^m(x)$] to express all quantities in terms of γ_λ. The relation between η_ν and γ_λ on $\pi_{\nu\lambda}$ is obtained from Eqs. (4.12) and (4.13).

The expansions analogous to Eqs. (4.32) and (4.33) are given by

$$\Phi_{J\Omega_\nu}^{\nu t'_\nu \bar{\lambda}} = \sum_{v_\nu j_\nu} f_{Jv_\nu j_\nu\Omega_\nu}^{\nu t'_\nu \bar{\lambda}} B_{v_\nu j_\nu\Omega_\nu}^{\lambda\nu}(\zeta, \gamma_\lambda), \quad (4.37)$$

$$\Phi_{J\Omega_\nu}^{\prime \nu t'_\nu \bar{\lambda}} = \sum_{v_\nu j_\nu} f_{Jv_\nu j_\nu\Omega_\nu}^{\prime \nu t'_\nu \bar{\lambda}} B_{v_\nu j_\nu\Omega_\nu}^{\lambda\nu}(\zeta, \gamma_\lambda), \quad (4.38)$$

where $B^{\lambda\nu}$ differs from $B^{\nu\lambda}$ by the use, in Eq. (4.30), of ϕ^ν instead of ϕ^λ. This approach is slightly different from the one followed previously,[19] in which the basis functions used to expand the Φ_J^λ and Φ_ν^ν were the same. For homonuclear targets, this difference disappears. The f and f' are given by

$$f_{Jv_\nu j_\nu\Omega_\nu}^{\nu t'_\nu \bar{\lambda}} = \sum_{j'_\nu}(-1)^{j'_\nu-\Omega_\nu}\int_0^{\pi/2} A_{j_\nu\Omega_\nu}^{\nu\lambda}(\gamma_\lambda)\mathcal{P}_{j'_\nu}^{\Omega_\nu}(\cos\gamma_\lambda)$$
$$\times g_{Jv_\nu j'_\nu\Omega_\nu}^{\nu t'_\nu \bar{\lambda}}[\eta_\nu(\gamma_\lambda)]\sin\gamma_\lambda\,d\gamma_\lambda, \quad (4.39)$$

$$f_{Jv_\nu j_\nu\Omega_\nu}^{\prime \nu t'_\nu \bar{\lambda}} = \sum_{j'_\nu}\int_0^{\pi/2} A_{j_\nu\Omega_\nu}^{\nu\lambda}(\gamma_\lambda) G_{Jv_\nu j'_\nu\Omega_\nu}^{\prime \nu t'_\nu \bar{\lambda}}(\gamma_\lambda)\sin\gamma_\lambda\,d\gamma_\lambda, \quad (4.40)$$

with Eq. (4.36) being used to evaluate Eq. (4.40). All expansions are made in terms of the coordinate γ_λ to facilitate later manipulations.

For atom plus homonuclear diatom collisions, the coefficients $f_{Jv_\nu j_\nu\Omega_\lambda}^{\nu t'_\lambda \bar{\lambda}}$ obtained by matching on the $\pi_{\nu\lambda}$ plane can be related to the $h_{Jv_\nu j_\nu\Omega_\lambda}^{\lambda t'_\lambda \bar{\lambda}}$ of the $\pi_{\nu\lambda}$ plane matching by noting in Eq. (4.39) (with λ substituted for ν and κ for λ) that $g_{Jv_\lambda j'_\lambda \cdots \Omega_\lambda}^{\lambda t'_\lambda \cdots} = 0^{44}$ for $j''_\lambda - j'_\lambda = $ odd and therefore that $(-1)^{j'_\lambda} = (-1)^{j''_\lambda}$ for the nonvanishing terms. For

collisions with a homonuclear diatom, $m_\gamma = m_\alpha$ so $\beta_{\lambda\kappa} = \beta_{\nu\lambda}$ [from Eq. (2.4)], and the mathematical expressions analogous to Eqs. (4.12)–(4.16) for $\pi_{\lambda\kappa}$ are identical to those equations. Therefore, from Eqs. (4.34) and (4.39) (transformed to $\pi_{\lambda\kappa}$), we have

$$f^{\lambda t'_\lambda s}_{J\nu_\lambda j_\lambda \Omega_\lambda} = (-1)^{j'_\lambda - \Omega_\lambda} h^{\lambda t'_\lambda s}_{J\nu_\lambda j_\lambda \Omega_\lambda} \; . \qquad (4.41)$$

By similar arguments for the derivative equations, Eqs. (4.35) and (4.4), using Eqs. (4.29) and (4.36), we find

$$f'^{\lambda t'_\lambda s}_{J\nu_\lambda j_\lambda \Omega_\lambda} = -(-1)^{j'_\lambda - \Omega_\lambda} h'^{\lambda t'_\lambda s}_{J\nu_\lambda j_\lambda \Omega_\lambda} \; . \qquad (4.42)$$

C. The matching equations

We now wish to find the appropriate linear combinations of the $\bar{\chi}$'s and $\partial \bar{\chi}/\partial n_{\nu\lambda}$'s of Eqs. (4.24) and (4.27) in channels λ and ν which give smoothly matched solutions χ and $\partial\chi/\partial n_{\nu\lambda}$ satisfying Eq. (4.20) and its normal derivative counterpart, both evaluated on $\pi_{\nu\lambda}$. Accordingly, we write

$$\chi^{(i)t}_{\lambda J \Omega_\lambda} = \sum_{t'_\lambda} (\bar{\chi}^{\lambda t'_\lambda s}_{J \Omega_\lambda} C^{(i)t s}_{J \lambda t'_\lambda} + \bar{\chi}^{\lambda t'_\lambda c}_{J \Omega_\lambda} C^{(i)t c}_{J \lambda t'_\lambda}) \; , \qquad (4.43)$$

where the coefficients $C_{J\lambda}$ in Eq. (4.43) are to be determined by evaluating Eq. (4.20) and its normal derivative on $\pi_{\nu\lambda}$, and analogous equations on $\pi_{\kappa\nu}$ and $\pi_{\lambda\kappa}$. The indices $(i)t \equiv (i)tj\Omega$ denote different linearly independent matched solutions, with t assuming N values and $i = 1, 2,$ or 3 for a total of $3N$ solutions. This is equal to the number of linearly independent scattering solutions possible, as was discussed in Paper I (Sec. IV B). The normal derivative of Eq. (4.43) is

$$\frac{\partial\chi^{(i)t}_{\lambda J \Omega_\lambda}}{\partial n_{\nu\lambda}} = \sum_{t'_\lambda}\left(\frac{\partial\bar{\chi}^{\lambda t'_\lambda s}_{J \Omega_\lambda}}{\partial n_{\nu\lambda}} C^{(i)t s}_{J \lambda t'_\lambda} + \frac{\partial\bar{\chi}^{\lambda t'_\lambda c}_{J \Omega_\lambda}}{\partial n_{\nu\lambda}} C^{(i)t c}_{J \lambda t'_\lambda}\right) \; . \qquad (4.44)$$

The normal derivative of Eq. (4.20) is in general a complicated quantity, but for the particular choice of matching surface specified by Eq. (2.5a), we have the important relation[19]

$$\left(\frac{\partial\Delta_{\nu\lambda}}{\partial n_{\nu\lambda}}\right)_{\text{on }\sigma_{\nu\lambda}} = 0 \; , \qquad (4.45)$$

which implies

$$\frac{\partial\chi^{(i)t}_{\lambda J \Omega_\lambda}}{\partial n_{\nu\lambda}} = \sum_{\Omega_\nu} d^J_{\Omega_\nu \Omega_\lambda}(\Delta_{\nu\lambda}) \frac{\partial\chi^{(i)t}_{\nu J \Omega_\nu}}{\partial n_{\nu\lambda}} \; . \qquad (4.46)$$

Let us now substitute Eq. (4.43) and its counterpart for channel ν into Eq. (4.20), as well as (4.44) and its ν counterpart into (4.46), utilizing Eqs. (4.24) and (4.27) (and their ν counterparts) along with Eq. (4.12). We obtain

$$\sum_{t'_\lambda}(\Phi^{\lambda t'_\lambda s}_{J \Omega_\lambda} C^{(i)t s}_{J \lambda t'_\lambda} + \Phi^{\lambda t'_\lambda c}_{J \Omega_\lambda} C^{(i)t c}_{J \lambda t'_\lambda})$$

$$= \sum_{\Omega_\nu} d^J_{\Omega_\nu \Omega_\lambda}(\Delta_{\nu\lambda}) \sum_{t'_\nu}(\Phi^{\nu t'_\nu s}_{J \Omega_\nu} C^{(i)t s}_{J \nu t'_\nu} + \Phi^{\nu t'_\nu c}_{J \Omega_\nu} C^{(i)t c}_{J \nu t'_\nu}) \; , \qquad (4.47)$$

with a similar equation involving Φ' resulting from the matching of the normal derivatives. If we now substitute Eqs. (4.32) and (4.37) into Eq. (4.47), multiply the

resulting expression by the $B^{\nu\lambda}_{\nu_\lambda j_\lambda \Omega_\lambda}$ [defined by Eq. (4.30)], and integrate it using the orthonormality properties of these $B^{\nu\lambda}$, we obtain

$$\sum_{t_\lambda}(h^{\lambda t'_\lambda s}_{J\nu_\lambda j_\lambda \Omega_\lambda} C^{(i)t s}_{J \lambda t'_\lambda} + h^{\lambda t'_\lambda c}_{J\nu_\lambda j_\lambda \Omega_\lambda} C^{(i)t c}_{J \lambda t'_\lambda})$$

$$= \sum_{\nu_\nu j_\nu \Omega_\nu} (s^J_{\nu\lambda})^{\nu_\nu j_\nu \Omega_\nu}_{\nu_\lambda j_\lambda \Omega_\lambda} \sum_{t_\nu} (f^{\nu t'_\nu s}_{J\nu_\nu j_\nu \Omega_\nu} C^{(i)t s}_{J \nu t'_\nu} + f^{\nu t'_\nu c}_{J\nu_\nu j_\nu \Omega_\nu} C^{(i)t c}_{J \nu t'_\nu}) \; . \qquad (4.48)$$

An analogous equation results for the derivatives with h' and f' substituted for h and f. The $(s^J_{\nu\lambda})^{\nu_\nu j_\nu \Omega_\nu}_{\nu_\lambda j_\lambda \Omega_\lambda}$ are the elements of an "arrangement channel transformation" matrix $s^J_{\nu\lambda}$ and are defined by

$$(s^J_{\nu\lambda})^{\nu_\nu j_\nu \Omega_\nu}_{\nu_\lambda j_\lambda \Omega_\lambda} = S^{\lambda\nu}_{\nu_\lambda \nu_\nu} \int_0^{\pi/2} A^{\nu\lambda}_{j_\lambda \Omega_\lambda}(\gamma_\lambda) d^J_{\Omega_\nu \Omega_\lambda}[\Delta_{\nu\lambda}(\gamma_\lambda)]$$

$$\times A^{\nu\lambda}_{j_\nu \Omega_\nu}(\gamma_\lambda) \sin\gamma_\lambda \, d\gamma_\lambda \; , \qquad (4.49)$$

where

$$S^{\lambda\nu}_{\nu_\lambda \nu_\nu} = \int_0^\infty \phi^\lambda_{\nu_\lambda}(\zeta) \phi^\nu_{\nu_\nu}(\zeta) d\zeta \; . \qquad (4.50)$$

As shown in Appendix C, $s^J_{\nu\lambda}$ is a real orthogonal matrix as long as the $A^{\nu\lambda}_{j_\lambda \Omega_\lambda}(\gamma_\lambda)$ of Eq. (4.30) form a complete set of orthonormal functions which span the γ_λ space, and the $\phi^\lambda_{\nu_\lambda}(\zeta)$ and $\phi^\nu_{\nu_\nu}(\zeta)$ form two sets of orthonormal functions which span the ζ space and are related by a real orthogonal transformation. Let us now write Eq. (4.48) as a matrix equation by regarding the h, f, and C appearing there as the elements of matrices, obtaining

$$h^{\lambda s}_J C^{(i)s}_{J\lambda} + h^{\lambda c}_J C^{(i)c}_{J\lambda} = s^J_{\nu\lambda}(f^{\nu s}_J C^{(i)s}_{J\nu} + f^{\nu c}_J C^{(i)c}_{J\nu}) \; . \qquad (4.51)$$

According to the arguments of the previous section, the matrices $h^{\lambda s}_J$ and $f^{\nu s}_J$ have dimensions $N/2 \times N$, while the $s^J_{\nu\lambda}$ are $N/2 \times N/2$ and the C's are $N \times N$ matrices. The corresponding derivative equation is obtained from Eq. (4.51) by substituting h' and f' for h and f. We can combine function and derivative equations into a single matrix equation involving only $N \times N$ matrices by defining the augmented $N \times N$ matrices $\hat{h}^{\lambda s}_J$, $\hat{f}^{\nu s}_J$, and $\hat{s}^J_{\nu\lambda}$ as

$$\hat{h}^{\lambda s}_J = \begin{pmatrix} h^{\lambda s}_J \\ h'^{\lambda s}_J \end{pmatrix} \; , \qquad (4.52)$$

$$\hat{f}^{\nu s}_J = \begin{pmatrix} f^{\nu s}_J \\ f'^{\nu s}_J \end{pmatrix} \; , \qquad (4.53)$$

$$\hat{s}^J_{\nu\lambda} = \begin{pmatrix} s^J_{\nu\lambda} & 0 \\ 0 & s^J_{\nu\lambda} \end{pmatrix} \; . \qquad (4.54)$$

where 0 is an $N/2 \times N/2$ null matrix. The resulting smooth matching equation on $\pi_{\nu\lambda}$ is

$$\hat{h}^{\lambda s}_J C^{(i)s}_{J\lambda} + \hat{h}^{\lambda c}_J C^{(i)c}_{J\lambda} = \hat{s}^J_{\nu\lambda}(\hat{f}^{\nu s}_J C^{(i)s}_{J\nu} + \hat{f}^{\nu c}_J C^{(i)c}_{J\nu}) \; . \qquad (4.55)$$

Following the same arguments as were used in Paper I (Sec. IV. B), we now combine Eq. (4.55) and its counterparts on $\pi_{\kappa\nu}$ and $\pi_{\lambda\kappa}$ into a single $3N \times 3N$ equation which can then be solved for the coefficients C^i_J which determine the matched solutions. The final result is

$$C^s_J (C^c_J)^{-1} = -(N^s_J)^{-1} N^c_J \; , \qquad (4.56)$$

where

$$N_j^a = \begin{pmatrix} \hat{h}_j^{\lambda\nu} & -\hat{s}_{\nu\lambda}^j \hat{f}_j^{\nu\nu} & 0 \\ 0 & \hat{h}_j^{\nu\nu} & -\hat{s}_{\kappa\nu}^j \hat{f}_j^{\kappa\nu} \\ -\hat{s}_{\lambda\kappa}^j \hat{f}_j^{\lambda\nu} & 0 & \hat{h}_j^{\kappa\nu} \end{pmatrix} \qquad (4.57)$$

and

$$C_j^a = \begin{pmatrix} C_{j\lambda}^{(1)a} & C_{j\lambda}^{(2)a} & C_{j\lambda}^{(3)a} \\ C_{j\nu}^{(1)a} & C_{j\nu}^{(2)a} & C_{j\nu}^{(3)a} \\ C_{j\kappa}^{(1)a} & C_{j\kappa}^{(2)a} & C_{j\kappa}^{(3)a} \end{pmatrix} . \qquad (4.58)$$

0 here represents an $N \times N$ matrix of zeros.

Equation (4.56) can now be used in conjunction with the asymptotic analysis of the next section to determine the $3N \times 3N$ coefficient matrices C_j^a which will provide wavefunctions which are both smooth and continuous everywhere and which also satisfy the proper scattering boundary conditions. Note that our procedure for matching simultaneously combines the primitive solutions in channels λ, ν, and κ to yield solutions which are smoothly continuous throughout all of configuration space. This contrasts with the analogous procedures of Wyatt and co-workers[16] and of Light and co-workers,[15] which seem not to include the coupling between channels ν and κ (here represented by the $\pi_{\kappa\nu}$ matching equation) explicitly when dealing with collisions originating in channel λ. They may have included such coupling implicitly by utilizing the symmetry of the H_3 system. However, if A_ν and A_κ are different atoms, we believe that the $\nu-\kappa$ coupling must be included explicitly.

V. ASYMPTOTIC ANALYSIS

A. The reactance and scattering matrices

In this section we define the reactance and scattering solutions and relate these to the matched solutions of the previous section so as to complete the determination of the coefficient matrices C_j^a and also the reactance and scattering matrices R_J and S_J. In Paper I we proved that the R and S matrices (which are physically dimensionless) can be equivalently defined in the scaled variables r_λ, R_λ or in the "physical" ones $\bar{r}_\lambda$, $\bar{R}_\lambda$. Here, for simplicity, we use the scaled coordinates in all definitions except that of the scattering amplitudes of Sec. V.B.

If we use Eqs. (2.13), (2.18), (2.30), and (3.1) to express the matched wavefunction [of Eqs. (4.17), (4.18), and (4.43)] in the asymptotic region of each arrangement channel, we find

$$\Psi_{JM}^{(1)t} \sim \sum_\lambda \sum_{\bar{t}_\lambda} D_{M\Omega_\lambda}^J(\phi_\lambda, \theta_\lambda, 0) \, Y_{j_\lambda\Omega_\lambda}(\gamma_\lambda, \psi_\lambda)$$

$$\times \frac{\phi_{v_\lambda j_\lambda}^\lambda(r_\lambda)}{r_\lambda R_\lambda} \, c_{\lambda J \bar{t}_\lambda}^{(1)t}(R_\lambda) \ , \qquad (5.1)$$

where

$$c_{\lambda J \bar{t}_\lambda}^{(1)t} = \sum_{\bar{t}_\lambda} \left(g_{J \bar{t}_\lambda}^{\lambda \bar{t}_\lambda +} C_{J\lambda \bar{t}_\lambda}^{(1)t+} + g_{J \bar{t}_\lambda}^{\lambda \bar{t}_\lambda -} C_{J\lambda \bar{t}_\lambda}^{(1)t-} \right) \ . \qquad (5.2)$$

Here we have dropped the superscript (a) which denotes the asymptotic region as it will be implicit throughout Sec. V. The sum over arrangement channels serves as a convenient notation for expressing the asymptotic wavefunction in all three arrangement channels simultaneously and is made possible by the fact that asymptotically there is no overlap between the separated atom plus diatom wavefunctions in different arrangement channels. An equation analogous to Eq. (5.1) for the derivative $(1/R_\lambda)(\partial/\partial R_\lambda) R_\lambda \Psi_{JM}^{(1)t}$ can be obtained by replacing $g_{J \bar{t}_\lambda}^{\lambda \bar{t}_\lambda \pm}$ by $dg_{J \bar{t}_\lambda}^{\lambda \bar{t}_\lambda \pm}/dR_\lambda$ in Eq. (5.2).

The reactance and scattering body-fixed solutions are defined to have the asymptotic form

$$\Psi_{J \bar{t}_0}^{M \bar{t}_0}[R \text{ or } S] \xrightarrow[R_\infty, R_\theta, R_\nu \to \infty]{} \sum_\lambda \sum_{\bar{t}_\lambda} D_{M\Omega_\lambda}^J(\phi_\lambda, \theta_\lambda, 0) \, Y_{j_\lambda\Omega_\lambda}(\gamma_\lambda, \psi_\lambda) \frac{\phi_{v_\lambda j_\lambda}^\lambda(r_\lambda)}{r_\lambda R_\lambda} \, b_{\lambda J \bar{t}_\lambda}^{M \bar{t}_0}[R \text{ or } S] \ , \qquad (5.3)$$

where, in the far asymptotic region [in which both potential coupling and the centrifugal coupling of Eq. (3.4) have become negligible], we have, for the R solution,

$$b_{\lambda J \bar{t}_\lambda}^{\lambda' \bar{t}_\lambda'}[R] = (|V_{v_\lambda j_\lambda}^\lambda|)^{-1/2} \begin{cases} \sin[k_{v_\lambda j_\lambda}^\lambda R_\lambda - (J + j_\lambda)\frac{1}{2}\pi] \, \delta_{\lambda \bar{t}_\lambda}^{\lambda' \bar{t}_\lambda'} \\ + \cos[k_{v_\lambda j_\lambda}^\lambda R_\lambda - (J + j_\lambda)\frac{1}{2}\pi] R_{J\lambda' v_\lambda' j_\lambda' \Omega_\lambda'}^{\lambda v_\lambda j_\lambda \Omega_\lambda} & \text{(open channels)} \\ \exp(|k_{v_\lambda j_\lambda}^\lambda|R_\lambda) \, \delta_{\lambda \bar{t}_\lambda}^{\lambda' \bar{t}_\lambda'} - \exp(-|k_{v_\lambda j_\lambda}^\lambda|R_\lambda) R_{J\lambda' v_\lambda' j_\lambda' \Omega_\lambda'}^{\lambda v_\lambda j_\lambda \Omega_\lambda} & \text{(closed channels)} , \end{cases} \qquad (5.4)$$

and, for the S solution,[32]

$$b_{\lambda J \bar{t}_\lambda}^{\lambda' \bar{t}_\lambda'}[S] = (|V_{v_\lambda j_\lambda}^\lambda|)^{-1/2} \begin{cases} \exp\{-i[k_{v_\lambda j_\lambda}^\lambda R_\lambda - (J + j_\lambda)\frac{1}{2}\pi]\} \, \delta_{\lambda \bar{t}_\lambda}^{\lambda' \bar{t}_\lambda'} \\ - \exp\{i[k_{v_\lambda j_\lambda}^\lambda R_\lambda - (J + j_\lambda)\frac{1}{2}\pi]\} S_{J\lambda' v_\lambda' j_\lambda' \Omega_\lambda'}^{\lambda v_\lambda j_\lambda \Omega_\lambda} & \text{(open channels)} \\ \exp(|k_{v_\lambda j_\lambda}^\lambda|R_\lambda) \, \delta_{\lambda \bar{t}_\lambda}^{\lambda' \bar{t}_\lambda'} - \exp(-|k_{v_\lambda j_\lambda}^\lambda|R_\lambda) S_{J\lambda' v_\lambda' j_\lambda' \Omega_\lambda'}^{\lambda v_\lambda j_\lambda \Omega_\lambda} & \text{(closed channels)} . \end{cases} \qquad (5.5)$$

$V^\lambda_{v_\lambda j_\lambda}$ is the velocity (in scaled variables) and is related to the wave number of Eq. (3.5) by

$$V^\lambda_{v_\lambda j_\lambda} = \hbar k^\lambda_{v_\lambda j_\lambda}/\mu \ . \tag{5.6}$$

The primed variables $v'_\lambda j'_\lambda \Omega'_\lambda$ in Eqs. (5.4) and (5.5) define the reagent state in the λ' arrangement channel. (Note our use of the abbreviation $\lambda' l'_\lambda \equiv \lambda' l'_{\lambda'}$.) R_J and S_J are the partial wave reactance and scattering matrices and, for exact solutions of the Schrödinger equation, they are symmetric.[45] Note that $-\Omega'_\lambda$ rather than Ω'_λ appears in the definition of R_J and S_J. This choice allows the open channel part of the scattering matrix to become the identity matrix in the limit of zero interaction potential (as will be evident from the partial wave expression for the scattering amplitude in Sec. V. B). The phase factors $i^{\pm(J+j_\lambda)}$ appearing in Eqs. (5.4) and (5.5) are arbitrary but will prove convenient later on. The open-channel subblocks of R_J and S_J are labeled R^0_J and S^0_J, and from Eqs. (5.4) and (5.5), one can easily show[46]

that

$$S^0_J = (I + iR^0_J)(I - iR^0_J)^{-1} \ , \tag{5.7}$$

where I is the identity matrix, and that the closed channel parts of R_J and S_J are identical. In addition to being symmetric, R^0_J is real and S^0_J is unitary. From the unitarity of S^0_J one can prove flux conservation, and microscopic reversibility results from its symmetry.[45]

In an actual calculation, we wish to use the R and S solutions of the Schrödinger equation at a finite R_λ for which the potential coupling has become negligible but the centrifugal coupling in Eq. (3.4) has not. These solutions can be obtained by taking the appropriate linear combinations of space-fixed Bessel functions as was done in Eq. (3.7) so that the far asymptotic behavior in Eqs. (5.3) and (5.4) is obtained in that limit. In other words, as soon as potential coupling has become negligible (but not the centrifugal one), the b in Eq. (5.3) can be written according to Eq. (3.7) as

$$b^{\lambda' l'_\lambda}_{\lambda j_\lambda l_\lambda}[R] = (|V^\lambda_{v_\lambda j_\lambda}|)^{-1/2} \sum_{\lambda'' l''_\lambda} \{I^{\lambda'' l''_\lambda}_{J\lambda l_\lambda}[R]\delta^{\lambda' l'_\lambda}_{\lambda'' l''_{\lambda'}} + O^{\lambda'' l''_\lambda}_{J\lambda l_\lambda}[R]R^{\lambda'' l''_\lambda}_{J\lambda' v'_\lambda j'_\lambda - \Omega'_\lambda}\} \ , \tag{5.8}$$

$$b^{\lambda' l'_\lambda}_{\lambda j_\lambda l_\lambda}[S] = (|V^\lambda_{v_\lambda j_\lambda}|)^{-1/2} \sum_{\lambda'' l''_\lambda} \{I^{\lambda'' l''_\lambda}_{J\lambda l_\lambda}[S]\delta^{\lambda' l'_\lambda}_{\lambda'' l''_{\lambda'}} - O^{\lambda'' l''_\lambda}_{J\lambda l_\lambda}[S]S^{\lambda'' l''_\lambda}_{J\lambda' v'_\lambda j'_\lambda - \Omega'_\lambda}\} \ , \tag{5.9}$$

where, for both R and S matrix solutions,

$$\binom{I_J}{O_J}^{\lambda' l'_\lambda}_{J\lambda l_\lambda} = \delta^{\lambda'' v'_\lambda j'_\lambda}_{\lambda v_\lambda j_\lambda}(-1)^{\Omega'_\lambda - \Omega_\lambda}\sum_{l_\lambda}C(Jj_\lambda l_\lambda; \Omega'_\lambda, -\Omega'_\lambda, 0) C(Jj_\lambda l_\lambda; \Omega_\lambda, -\Omega_\lambda, 0)\binom{s_{Jv_\lambda j_\lambda l_\lambda}}{O_{Jv_\lambda j_\lambda l_\lambda}} \ . \tag{5.10}$$

For the R solution,

$$s_{Jv_\lambda j_\lambda l_\lambda}[R] = |k^\lambda_{v_\lambda j_\lambda}|R_\lambda \begin{cases} y_{l_\lambda}(k^\lambda_{v_\lambda j_\lambda}R_\lambda)\sin[(J+j_\lambda-l_\lambda)\tfrac{1}{2}\pi] + j_{l_\lambda}(k^\lambda_{v_\lambda j_\lambda}R_\lambda)\cos[(J+j_\lambda-l_\lambda)\tfrac{1}{2}\pi] & \text{(open channels)} \\ 2i_{l_\lambda}(|k^\lambda_{v_\lambda j_\lambda}|R_\lambda) & \text{(closed channels)} , \end{cases} \tag{5.11a}$$

$$O_{Jv_\lambda j_\lambda l_\lambda}[R] = |k^\lambda_{v_\lambda j_\lambda}|R_\lambda \begin{cases} -y_{l_\lambda}(k^\lambda_{v_\lambda j_\lambda}R_\lambda)\cos[(J+j_\lambda-l_\lambda)\tfrac{1}{2}\pi] + j_{l_\lambda}(k^\lambda_{v_\lambda j_\lambda}R_\lambda)\sin[(J+j_\lambda-l_\lambda)\tfrac{1}{2}\pi] & \text{(open channels)} \\ k_{l_\lambda}(|k^\lambda_{v_\lambda j_\lambda}|R_\lambda) & \text{(closed channels)} , \end{cases} \tag{5.11b}$$

while, for the S solution,

$$s_{Jv_\lambda j_\lambda l_\lambda}[S] = |k^\lambda_{v_\lambda j_\lambda}|R_\lambda \begin{cases} \exp[i(J+j_\lambda-l_\lambda)\tfrac{1}{2}\pi]h^{(-)}_{l_\lambda}(k^\lambda_{v_\lambda j_\lambda}R_\lambda) & \text{(open channels)} \\ 2i_{l_\lambda}(|k^\lambda_{v_\lambda j_\lambda}|R_\lambda) & \text{(closed channels)} , \end{cases} \tag{5.12a}$$

$$O_{Jv_\lambda j_\lambda l_\lambda}[S] = |k^\lambda_{v_\lambda j_\lambda}|R_\lambda \begin{cases} \exp[-i(J+j_\lambda-l_\lambda)\tfrac{1}{2}\pi]h^{(+)}_{l_\lambda}(k^\lambda_{v_\lambda j_\lambda}R_\lambda) & \text{(open channels)} \\ k_{l_\lambda}(|k^\lambda_{v_\lambda j_\lambda}|R_\lambda) & \text{(closed channels)} , \end{cases} \tag{5.12b}$$

where

$$h^{(\pm)}_{l_\lambda} = -y_{l_\lambda} \pm ij_{l_\lambda} \ , \tag{5.13}$$

and y_{l_λ}, j_{l_λ}, i_{l_λ}, and k_{l_λ} are the spherical Bessel functions of Sec. III. B. 1. To show that Eqs. (5.8) and (5.9) do indeed reduce, respectively, to Eqs. (5.4) and (5.5) in the far asymptotic limit, one simply uses the asymptotic form of these Bessel functions at large values of the argument $|k^{\lambda(\pm)}_{v_\lambda j_\lambda}|R_\lambda$.[38,40] We may use Eq.

(A14) to relate the usual space-fixed S matrix $\hat{S}_J$ to the body-fixed S_J. We obtain the R_λ-independent unitary transformation

$$\hat{S}_J = \mathcal{J}^\dagger S_J \mathcal{J} \ , \tag{5.14}$$

where

$$(\mathscr{J})_{\lambda v_\lambda j_\lambda \Omega_\lambda}^{\lambda' v'_\lambda j'_\lambda \Omega'_\lambda} = \delta_{\lambda v_\lambda j_\lambda}^{\lambda' v'_\lambda j'_\lambda} C(Jj_\lambda l'_\lambda ; \Omega_\lambda, -\Omega_\lambda, 0) i^{l'_\lambda - l_\lambda}(-1)^{\Omega_\lambda} . \tag{5.15}$$

In order to obtain R_J, we generate an R solution of the Schrödinger equation satisfying the asymptotic conditions of Eqs. (5.3) or (5.8) by taking linear combinations of the matched solutions $\Psi_{JM}^{(i)t}$ of Eq. (5.1):

$$\Psi_{JM}^{\lambda' v'_\lambda}[R] = \sum_{(i)t} \Psi_{JM}^{(i)t} Q_{(i)t}^{\lambda' v'_\lambda} . \tag{5.16}$$

As in Paper I, we are free to choose $Q_{(i)t}^{\lambda' v'_\lambda} = \delta_{(i)t}^{\lambda' v'_\lambda}$ and require the $C_J^\cdot$ matrices to provide for us those linear combinations of the primitive solutions satisfying both the matching condition [Eq. (4.56)] and the asymptotic conditions. If we substitute Eqs. (5.1)–(5.3) and (5.8) into Eq. (5.16) and express everything in matrix notation (involving matrices of dimension $3N \times 3N$), we get

$$V^{-1/2}(I_J[R] + O_J[R]\bar{R}_J)(C_J^\cdot)^{-1} = g_J^\cdot C_J^\cdot (C_J^\cdot)^{-1} + g_J^\cdot , \tag{5.17}$$

where $\bar{R}_J$ is related to R_J of Eq. (5.8) by

$$(\bar{R}_J)_{\lambda v_\lambda j_\lambda \Omega_\lambda}^{\lambda' v'_\lambda j'_\lambda \Omega'_\lambda} = (R_J)_{\lambda' v'_\lambda j'_\lambda - \Omega'_\lambda}^{\lambda v_\lambda j_\lambda \Omega_\lambda} \tag{5.18}$$

and

$$(V)_{\lambda l_\lambda}^{\lambda' l'_\lambda} = |V_{v_\lambda j_\lambda}^\lambda| \delta_{\lambda l_\lambda}^{\lambda' l'_\lambda} . \tag{5.19}$$

Note that the $(g_J)_{\lambda l_\lambda}^{\lambda' l'_\lambda}$ in Eq. (5.17) is identical to $\delta_{\lambda \lambda'}$ times the $g^{\lambda \lambda'}$ of Eq. (5.2). An equation analogous to Eq. (5.17) for the derivative $R_\lambda^{-1}(\partial/\partial R_\lambda)R_\lambda \Psi_{JM}^{\lambda' v'_\lambda}$ is easily shown to be

$$V^{-1/2}(I'_J[R] + O'_J[R]\bar{R}_J)(C_J^\cdot)^{-1} = g_J^{'\cdot} C_J^\cdot (C_J^\cdot)^{-1} + g_J^{'\cdot} . \tag{5.20}$$

where prime denotes differentiation with respect to R_λ. The quantity $C_J^\cdot (C_J^\cdot)^{-1}$ is given by Eq. (4.56). Equations (5.17) and (5.20) therefore provide two simultaneous linear matrix equations in the two unknown matrices $(C_J^\cdot)^{-1}$ and $\bar{R}_J$. Eliminating the former from these two equations and using Eq. (4.56), we get

$$\bar{R}_J = -V^{1/2}W^{-1}\{(I'_J[R]g_J^\cdot - I_J[R]g_J^{'\cdot})(N_J^\cdot)^{-1}N_J^\cdot - (I'_J[R]g_J^\cdot$$
$$- I_J[R]g_J^{'\cdot})\}\{(O'_J[R]g_J^\cdot - O_J[R]g_J^{'\cdot})$$
$$\times (N_J^\cdot)^{-1}N_J^\cdot - (O'_J[R]g_J^\cdot - O_J[R]g_J^{'\cdot})\}^{-1}WV^{-1/2} . \tag{5.21}$$

Here

$$W = O'[R]I[R] - I'_J[R]O_J[R] \tag{5.22}$$

is a Wronskian matrix which, as can be seen by inspection of Eqs. (5.10) and (5.11), is diagonal and constant, i.e., independent of R_λ. The right-hand side of Eq. (5.21) involves real matrices which are obtained directly from the integration and matching steps of the calculation. Therefore, $\bar{R}_J$ and R_J are real, as expected.

With $\bar{R}_J$, and hence R_J determined, we use Eq. (5.7) to calculate S_J^0, which in turn can be related to the scattering amplitude by the formulas of the next section. In addition, the scattering matrix is related to the probability of transition from initial arrangement channel λ and quantum state $v_\lambda j_\lambda \Omega_\lambda$ to final channel λ' and state $v'_\lambda j'_\lambda \Omega'_\lambda$ by[47]

$$P_{J\lambda v_\lambda j_\lambda \Omega_\lambda}^{\lambda' v'_\lambda j'_\lambda \Omega'_\lambda} = |S_{J\lambda v_\lambda j_\lambda \Omega_\lambda}^{\lambda' v'_\lambda j'_\lambda \Omega'_\lambda}|^2 . \tag{5.23}$$

[In the rest of this paper, lower (upper) indices, which refer to the initial (final) state, will be unprimed (primed).] The scattering matrix may also be related to the opacity function as discussed in the next section.

B. Scattering amplitudes and cross sections

We now define the scattered plane wave solution and relate it to the scattering solution of the previous section so as to express the scattering amplitude in terms of the open parts of the partial wave scattering matrices. Our analysis will be done using the helicity representation[48] in which the axis of quantization of the incoming and outgoing rotational states is chosen to coincide with the direction of the incident and final wave vectors respectively. The helicity formalism is very closely related to the use of body-fixed coordinate systems of the type described in Sec. II.B and leads to a particularly simple relation between the helicity scattering amplitudes and body-fixed S matrices.

We define the helicity representation scattered plane wave solution by

$$\bar{\Psi}^{\lambda l_\lambda}[P] \sim \exp[i\bar{k}_{v_\lambda j_\lambda}^\lambda (\bar{R}_\lambda)_e] \frac{\bar{\phi}_{v_\lambda j_\lambda}^\lambda(\bar{r}_\lambda)}{\bar{r}_\lambda} Y_{j_\lambda = \Omega_\lambda}(\theta_{r_\lambda}\phi_{r_\lambda})$$
$$+ \sum_{\lambda' l'_\lambda} \frac{\exp(i\bar{k}_{v'_\lambda j'_\lambda}^{\lambda'}\bar{R}_{\lambda'})}{\bar{R}'_\lambda} \frac{\bar{\phi}_{v'_\lambda j'_\lambda}^{\lambda'}(\bar{r}'_\lambda)}{\bar{r}'_\lambda}$$
$$\times Y_{j'_\lambda = \Omega'_\lambda}(\gamma_{\lambda'}, \psi_{\lambda'})\bar{f}_{\lambda l_\lambda}^{\lambda' l'_\lambda}(\theta_{\lambda'}, \phi_{\lambda'}), \tag{5.24}$$

where the sum over final states includes both open and closed channels. For closed-channel solutions (which we shall ignore below), $\bar{k}_{v_\lambda j_\lambda}^\lambda$ is pure imaginary, so $\exp(i\bar{k}_{v_\lambda j_\lambda}^\lambda \bar{R}_\lambda)$ decreases exponentially. Note that the physical coordinates $\bar{R}_\lambda$, $\bar{r}_\lambda$ and wave numbers $\bar{k}_{v_\lambda j_\lambda}^\lambda = a_\lambda k_{v_\lambda j_\lambda}^\lambda$ have been used in Eq. (5.24). In addition, we have introduced the global index $\hat{l}$ to denote the quantum numbers vjm_j. (We will relate m_j to Ω and hence $\hat{l}$ to l below.) For simplicity, the space-fixed z axis has been chosen to be in the direction of the incident wave vector. It then follows (by inspection of Fig. 2) that the space-fixed and body-fixed z axes will point in opposite directions initially (i.e., for $(\bar{R}_\lambda)_e \to -\infty$). The outgoing body-fixed z'_λ axis points in the same direction as the outgoing wave vector, thus allowing us to use $Y_{j'_\lambda = -\Omega'_\lambda}(\gamma'_\lambda, \psi'_\lambda)$ instead of $Y_{j'_\lambda = \Omega'_\lambda}(\theta_{r'_\lambda}, \phi_{r'_\lambda})$ in the summation appearing in Eq. (5.24).

The differential scattering cross section is defined as the ratio of the outgoing radial flux per unit solid angle to the incoming plane wave flux and, from Eq. (5.24), is related to the scattering amplitude $\bar{f}$ by

$$\sigma_{\lambda l_\lambda}^{\lambda' l'_\lambda} = \frac{\bar{V}_{v'_\lambda j'_\lambda}^{\lambda'}}{\bar{V}_{v_\lambda j_\lambda}^\lambda} |\bar{f}_{\lambda l_\lambda}^{\lambda' l'_\lambda}|^2 \tag{5.25}$$

for $\lambda v_\lambda j_\lambda m_{j_\lambda}$ and $\lambda' v'_\lambda j'_\lambda m'_{j_\lambda}$ representing open final and initial channels, respectively. Here $\bar{V}_{v_\lambda j_\lambda}^\lambda$ is the physical velocity

$$\bar{V}_{v_\lambda j_\lambda}^\lambda = \frac{1}{a_\lambda} V_{v_\lambda j_\lambda}^\lambda = \left(\frac{2(E - \epsilon_{v_\lambda j_\lambda}^\lambda)}{\mu_{\lambda, vR}}\right)^{1/2} . \tag{5.26}$$

In order to relate $\bar{f}$ to the scattering matrices, it is desirable to first define a scattering solution analogous to Eq. (5.24) in terms of the scaled coordinates of Eq. (2.1). This is easily done by removing the "bars" on all symbols containing them in Eq. (5.24). By comparing the plane wave parts, we see that the resulting $\Psi^{\lambda \hat{t}_\lambda}[\circ]$ is proportional to $\bar{\Psi}^{\lambda \hat{t}_\lambda}[P]$ with a proportionality constant $a_\lambda^{3/2}$. Comparison of the outgoing wave parts of Ψ and $\bar{\Psi}$ then yields

$$\bar{f}^{\lambda' \hat{t}_\lambda'}_{\lambda \hat{t}_\lambda} = a_{\lambda'}^{-1} f^{\lambda' \hat{t}_\lambda'}_{\lambda \hat{t}_\lambda} \left(\frac{a_{\lambda'}^2}{a_\lambda}\right)^{1/2} , \tag{5.27}$$

which will be useful below.

One now expands the plane wave part of $\Psi^{\lambda \hat{t}_\lambda}[P]$ in terms of a series of products of Legendre polynomials $P_{l_\lambda}(\cos\theta_\lambda)$ times spherical Bessel functions $j_{l_\lambda}(k^\lambda_{v_\lambda j_\lambda} R_\lambda)$, takes the asymptotic limit $(R_\lambda \to \infty)$, and converts the result to the body-fixed variables $r_\lambda \gamma_\lambda \psi_\lambda$ and $R_\lambda \theta_\lambda \phi_\lambda$, following the procedure outlined by Pack,[32] obtaining

$$\exp[i k^\lambda_{v_\lambda j_\lambda}(\mathbf{R}_\lambda)_z] \left(\frac{\phi^\lambda_{v_\lambda j_\lambda}(r_\lambda)}{r_\lambda}\right) Y_{j_\lambda m_{j_\lambda}}(\theta_{r_\lambda}, \phi_{r_\lambda}) \sim \frac{1}{2 k^\lambda_{v_\lambda j_\lambda} R_\lambda} \left(\frac{\phi^\lambda_{v_\lambda j_\lambda}(r_\lambda)}{r_\lambda}\right) \sum_{J M \Omega_\lambda} \delta_{M = j_\lambda} D^J_{M \Omega_\lambda}(\phi_\lambda, \theta_\lambda, 0)$$

$$\times Y_{j_\lambda \Omega_\lambda}(\gamma_\lambda, \psi_\lambda)(2J+1) i^{J+j_\lambda+1} \left(\exp\{-i[k^\lambda_{v_\lambda j_\lambda} R_\lambda - (J+j_\lambda)\tfrac{1}{2}\pi]\}\delta_{M, -\Omega_\lambda} - \exp\{i[k^\lambda_{v_\lambda j_\lambda} R_\lambda - (J+j_\lambda)\tfrac{1}{2}\pi]\}\delta_{M \Omega_\lambda}\right) . \tag{5.28}$$

In analogy to Eq. (2.11), the scattered plane wave solution $\Psi^{\lambda v_\lambda j_\lambda m_{j_\lambda}}[P]$ may be expanded in terms of the scattering solutions $\Psi^{\lambda v_\lambda j_\lambda \Omega_\lambda}[S]$ as

$$\Psi^{\lambda v_\lambda j_\lambda m_{j_\lambda}}[P] = \sum_{J M \Omega_\lambda} C^{\lambda v_\lambda j_\lambda m_{j_\lambda} \Omega_\lambda}_{JM} \Psi^{\lambda v_\lambda j_\lambda \Omega_\lambda}_{JM}[S] . \tag{5.29}$$

Using Eq. (5.28) to express $\Psi[P]$ in terms of body-fixed quantities, Eqs. (5.3) and (5.5) for the asymptotic form of $\Psi^{\lambda}_{JM}[S]$, and equating coefficients of the incoming spherical wave parts, one finds

$$C^{\lambda v_\lambda j_\lambda m_{j_\lambda} \Omega_\lambda}_{JM} = \delta_{M, -\Omega_\lambda} \delta_{M=j_\lambda} \left(\frac{\hbar}{\mu}\right)^{1/2} \frac{2J+1}{2} i^{J+j_\lambda+1} . \tag{5.30}$$

This shows that the only value of Ω_λ contributing to the right-hand side of Eq. (5.29) is $\Omega_\lambda = -m_{j_\lambda}$, which relates $\hat{t}_\lambda \equiv v_\lambda j_\lambda m_{j_\lambda}$ and $t_\lambda \equiv v_\lambda j_\lambda \Omega_\lambda$ for the reagent states. If we now equate coefficients of outgoing spherical wave parts and use Eq. (5.30) to simplify the result, we get

$$f^{\lambda' \hat{t}_\lambda'}_{\lambda \hat{t}_\lambda} = \left(\frac{V^\lambda_{v_\lambda j_\lambda}}{V^{\lambda'}_{v_\lambda' j_\lambda'}}\right)^{1/2} \frac{C^{i' m'_{j_\lambda} \phi_{\lambda'}}}{2 k^\lambda_{v_\lambda j_\lambda}} i^{j_\lambda - j_\lambda' + 1} \sum_{J=0}^\infty (2J+1) d^J_{m_{j_\lambda} m'_{j_\lambda}}(\theta_{\lambda'}) T^{\lambda' \hat{t}_\lambda'}_{J \lambda \hat{t}_\lambda} , \tag{5.31}$$

where

$$\mathbf{T}_J = \mathbf{I} - \mathbf{S}^0_J \tag{5.32}$$

is the transition matrix,[32] and $m'_{j_\lambda} = \Omega'_\lambda$ for the product states so that $\hat{t}_\lambda'$ and t_λ' are identical. Equation (5.31) shows that the helicity amplitude and body-fixed scattering matrix are related by a single sum reminiscent of the analogous result for potential scattering. This illustrates one of the primary advantages of the use of helicity amplitudes in conjunction with body-fixed coordinates such as those depicted in Fig. 2. Combining Eqs. (5.31) and (5.27), and using Eq. (5.26) and its counterpart for the wave numbers $\bar{k}^\lambda_{v_\lambda j_\lambda}$ and $k^\lambda_{v_\lambda j_\lambda}$, we find that the physical scattering amplitude $\bar{f}^{\lambda' \hat{t}_\lambda'}_{\lambda \hat{t}_\lambda}$ is given by an expression identical to Eq. (5.31) with all velocities and wave numbers "barred." Substituting this into Eq. (5.25), we find

$$\sigma^{\lambda' \hat{t}_\lambda'}_{\lambda \hat{t}_\lambda}(\theta_{\lambda'}) = \frac{1}{4 k^\lambda_{v_\lambda j_\lambda}} \left| \sum_{J=0}^\infty (2J+1) d^J_{m_{j_\lambda} m'_{j_\lambda}}(\theta_{\lambda'}) T^{\lambda' \hat{t}_\lambda'}_{J \lambda \hat{t}_\lambda} \right|^2 , \tag{5.33}$$

which demonstrates that the differential cross section

is independent of $\phi_{\lambda'}$.[49] Using the properties $d^J_{m' m}(0) = \delta_{m' m}$ and $d^J_{m' m}(\pi) = (-1)^{J+m} \delta_{m', -m}$ [derivable directly from the definition of $d^J_{m' m}(\beta)$], we get from Eq. (5.33)

$$\sigma^{\lambda' \hat{t}_\lambda'}_{\lambda \hat{t}_\lambda}(0) = \delta_{m'_{j_\lambda} = j_\lambda} \frac{1}{4 k^{\lambda 2}_{v_\lambda j_\lambda}} \left| \sum_{J=0}^\infty (2J+1) T^{\lambda' \hat{t}_\lambda'}_{J \lambda \hat{t}_\lambda} \right|^2$$

and

$$\sigma^{\lambda' \hat{t}_\lambda'}_{\lambda \hat{t}_\lambda}(\pi) = \delta_{m'_{j_\lambda} = -j_\lambda} \frac{1}{4 k^{\lambda 2}_{v_\lambda j_\lambda}} \left| \sum_{J=0}^\infty (-1)^J (2J+1) T^{\lambda' \hat{t}_\lambda'}_{J \lambda \hat{t}_\lambda} \right|^2 ,$$

which show that for $m'_{j_\lambda} \neq m_{j_\lambda}$, $\sigma^{\lambda' \hat{t}_\lambda'}_{\lambda \hat{t}_\lambda}(0)$ vanishes, and for $m'_{j_\lambda} \neq -m_{j_\lambda}$, $\sigma^{\lambda' \hat{t}_\lambda'}_{\lambda \hat{t}_\lambda}(\pi)$ vanishes. These are rigorous selection rules for forward and backward scattering related to the conservation of J_z.[24]

The integral cross section $Q^{\lambda' \hat{t}_\lambda'}_{\lambda \hat{t}_\lambda}$ is obtained by integrating Eq. (5.33) over $\theta_{\lambda'}$ and $\phi_{\lambda'}$ and using the orthonormality property of the d^J functions.[23] This yields the remarkably simple expression

$$Q^{\lambda' \hat{t}_\lambda'}_{\lambda \hat{t}_\lambda} = \frac{\pi}{k^{\lambda 2}_{v_\lambda j_\lambda}} \sum_{J=0}^\infty (2J+1) \left| T^{\lambda' \hat{t}_\lambda'}_{J \lambda \hat{t}_\lambda} \right|^2 . \tag{5.34}$$

Both $\sigma^{\lambda' \hat{t}_\lambda'}_{\lambda \hat{t}_\lambda}$ and $Q^{\lambda' \hat{t}_\lambda'}_{\lambda \hat{t}_\lambda}$ may be averaged over initial m_{j_λ} and summed over final m'_{j_λ} to give the degeneracy-averaged quantities $\sigma^{\lambda' v_\lambda' j_\lambda'}_{\lambda v_\lambda j_\lambda}$ and $Q^{\lambda' v_\lambda' j_\lambda'}_{\lambda v_\lambda j_\lambda}$, respectively. The latter of these two can be written as[32]

$$Q^{\lambda' v_\lambda' j_\lambda'}_{\lambda v_\lambda j_\lambda} = \frac{\pi}{k^{\lambda 2}_{v_\lambda j_\lambda}} \sum_{J=0}^\infty (2J+1) P^{v_\lambda' j_\lambda'}_{J v_\lambda j_\lambda} , \tag{5.35}$$

where the opacity function P_J is

$$P^{v_\lambda' j_\lambda'}_{J v_\lambda j_\lambda} = (2j_\lambda+1)^{-1} \sum_{m_{j_\lambda}} \sum_{m'_{j_\lambda}} P^{\lambda' \hat{t}_\lambda'}_{J \lambda \hat{t}_\lambda} , \tag{5.36}$$

and the ranges of the sums are $|m_{j_\lambda}| \leq \min(j_\lambda, J)$ and $|m'_{j_\lambda}| \leq \min(j_\lambda', J)$.

In an application to the $H + H_2$ reaction, the number of different distinguishable atom scattering amplitudes and cross sections may be greatly reduced by considering the symmetries involved. This was done in Paper I and the derivations are essentially unchanged in 3D. First, the scattering amplitudes are invariant to a cyclic permutation of arrangement channel indices so that (suppressing the $\hat{t}_\lambda, \hat{t}_\lambda'$) $f^\lambda_\lambda = f^\nu_\nu = f^\kappa_\kappa$, $f^\kappa_\lambda = f^\lambda_\nu = f^\nu_\kappa$, and $f^\lambda_\nu = f^\nu_\kappa = f^\kappa_\lambda$. Second, f^κ_λ and f^ν_λ are related by[10]

$$f_{\lambda v_j j_j m_j}^{v' j' m_j'} = (-1)^{j+j'} f_{\lambda v_j j_j m_j}^{v' j' m_j'} \qquad (5.37)$$

and the nonreactive f_λ^ν satisfy

$$f_{\lambda v_j j_j m_j}^{v' j' m_j'} = 0 \quad \text{if } j - j' = \text{odd.} \qquad (5.38)$$

These statements imply that f_λ^1 and f_λ^ν are the only distinct scattering amplitudes and that many components of f_λ^1 are zero. These symmetry relations also apply to the scattering matrix S, so that the entire distinguishable-atom cross section calculation can be considerably streamlined. It should be mentioned that although the cyclic permutational symmetry is built into the calculation if the integration is done in only one of the three equivalent arrangement channel regions, Eqs. (5.37) and (5.38) will only hold rigorously if $s_{\nu\lambda}^j$ defined by Eq. (4.49) is orthogonal, and this will only be the case if the matching surface basis functions given by Eq. (4.30) form a sufficiently complete set. This provides a test of convergence of the method as long as the symmetries of Eqs. (5.37) and (5.38) are not built in to the calculation.

To convert these distinguishable-atom scattering amplitudes into the corresponding indistinguishable ones when two or more of the atoms are identical, the standard technique of postantisymmetrization[50] may be used. Application to $H + H_2$ was given in Paper I and is unchanged in the three-dimensional treatment. In the notation of this paper we obtain the following expressions for the antisymmetrized differential cross sections:

(a) para – para ($j, j' = $ even):

$$\sigma_{oi}^{oi'} = \frac{\overline{V}_{v'j'}}{\overline{V}_{vj}} |\overline{f}_{\lambda i}^{\lambda i'} - \overline{f}_{\lambda i}^{\nu i'}|^2 , \qquad (5.39a)$$

(b) para – ortho ($j = $ even, $j' = $ odd):

$$\sigma_{oi}^{oi'} = 3 \frac{\overline{V}_{v'j'}}{\overline{V}_{vj}} |\overline{f}_{\lambda i}^{\nu i'}|^2 , \qquad (5.39b)$$

(c) ortho – para ($j = $ odd, $j' = $ even):

$$\sigma_{oi}^{oi'} = \frac{\overline{V}_{v'j'}}{\overline{V}_{vj}} |\overline{f}_{\lambda i}^{\nu i'}|^2 , \qquad (5.39c)$$

(d) ortho – ortho ($j, j' = $ odd):

$$\sigma_{oi}^{oi'} = \frac{\overline{V}_{v'j'}}{\overline{V}_{vj}} (|\overline{f}_{\lambda i}^{\lambda i'} + \overline{f}_{\lambda i}^{\nu i'}|^2 + 2|\overline{f}_{\lambda i}^{\nu i'}|^2), \qquad (5.39d)$$

where Eqs. (5.27) and (5.31) are to be used in evaluating Eqs. (5.39). The expressions for the antisymmetrized integral reaction cross sections are

(a) para – para:

$$Q_{\rho i}^{oi'} = \frac{\pi}{k_{vj}^2} \sum_J (2J+1) |\delta_i^{i'} - S_{\lambda i}^{o\lambda i'} + S_{\lambda i}^{\lambda \lambda i'}|^2 , \qquad (5.40a)$$

(b) para – ortho:

$$Q_{\rho i}^{oi'} = 3 \frac{1}{k_{vj}^2} \sum_J (2J+1) |S_{\lambda i}^{o\nu i'}|^2 , \qquad (5.40b)$$

(c) ortho – para:

$$Q_{oi}^{oi'} = \frac{\pi}{k_{vj}^2} \sum_J (2J+1) |S_{\lambda i}^{o\nu i'}|^2 , \qquad (5.40c)$$

(d) ortho – ortho:

$$Q_{oi}^{oi'} = \frac{\pi}{k_{vj}^2} \sum_J (2J+1) (|\delta_i^{i'} - S_{\lambda i}^{o\lambda i'} - S_{\lambda i}^{o\nu i'}|^2 + 2|S_{\lambda i}^{o\nu i'}|^2). \qquad (5.40d)$$

As was pointed out in Sec. III. C, parity symmetry may be used in both the integration and matching procedures for any chemical reaction to reduce the number of states coupled in these stages of the calculation. One may also define parity scattering matrices, but the plane wave solution Eq. (5.24) does not have parity symmetry so that these two decoupled parity S matrices must be recoupled before performing the calculation of the scattering amplitude in Eq. (5.31). This procedure is outlined in Appendix B.

VI. DISCUSSION

The method we have outlined in Secs. II–V has a number of limitations or restrictions which we shall now analyze. First, we have considered the reactive collision of an atom with a diatomic molecule on a single electronically adiabatic potential energy surface. The extension to multisurface reactions is straightforward and would follow the general format previously developed for collinear reactions.[51] All three reactive arrangement channels are assumed to be energetically accessible and the diatom in each arrangement channel is assumed to be in a $^1\Sigma$ electronic state. A straightforward modification of the matching procedure which simplifies it appropriately is required for single reaction path systems (for which one of the three arrangement channels is closed). This was discussed in Paper I. For diatoms having electronic states other than $^1\Sigma$ (such as $^1\Lambda$ with $\Lambda \neq 0$), the rotational states $Y_{j_\lambda m_{j_\lambda}}(\theta_{r_\lambda}, \phi_{r_\lambda})$ must be modified[33] to $D_{m_{j_\lambda}\Lambda}^{j_\lambda}(\theta_{r_\lambda}, \phi_{r_\lambda}, 0)$ and electronic–vibration–rotation coupling must be considered, but the basic integration and matching procedures are unchanged. One basic restriction of the method is its inability to treat dissociative or break-up channels. This is not a serious limitation for many important chemical reactions at thermal energies. A procedure for treating both dissociative and reactive collisions is currently being developed in this laboratory.

The integration procedure outlined in Sec. III may be applied to any reaction for which the criteria of the preceding paragraph apply, but the matching procedure (and hence the choice of coordinate system in the matching region) is strongly dependent on our choice of matching surfaces [Eq. (2.3) of I]. Other choices will require significant modifications in the details of Sec. IV, although the basic concepts involved in matching will still be applicable. The matching surfaces considered in Eqs. (2.3) of I should be useful for many chemical reactions but may not always be ideal for obtaining rapidly convergent coupled-channel expansions. In particular, if the reaction has a low barrier for $\gamma_\lambda = \pi/2$ configurations, the expansion of the wavefunction in terms of matching surface basis functions $T^{v\lambda}$ (Sec. IV. B) may be slowly convergent. Conversely, too strong an anisotropy favoring collinear reactions over perpendicular ones leads to an ill-conditioned coupled-equation problem. These and related restrictions on

the matching surfaces were outlined in Paper I.

The asymptotic analysis of Sec. V is quite general and should be applicable to those chemical reactions which fit the criteria of the first paragraph of this section. The antisymmetrized results presented in Sec. V are only applicable to a collision system of three identical spin $\frac{1}{2}$ particles. Other combinations of identical particles and spins may be treated by postantisymmetrization procedures analogous to that in Appendix D of Paper I.

The final criterion regarding the applicability of the method is computational efficiency. The large number of open rotational channels present in any 3D atom–diatom system makes the application of any coupled-channel method a large computational project. Much effort has, however, been spent in designing the method so that a minimum number of such channels are needed for convergence of the results. We therefore feel that this method should provide a computationally feasible procedure for studying simple chemical reactions. The first application of this procedure (to 3D H + H$_2$)[24] supports this statement.

ACKNOWLEDGMENT

APPENDIX A: ANGULAR MOMENTUM OPERATORS AND THE SCHRÖDINGER EQUATION IN SPACE-FIXED AND BODY-FIXED COORDINATE SYSTEMS

In this Appendix we will establish the relations between the rotational and total angular momentum operators in the space-fixed and body-fixed coordinate systems defined in Sec. II.B and Fig. 2.

We first consider the space-fixed coordinate system $Oxyz$. In terms of the variables ϕ_{r_λ}, θ_{r_λ}, ϕ_λ, and θ_λ (Sec. II.B), the various components of the rotational (j_λ) and orbital (l_λ) angular momentum operators are given by the usual spherical polar coordinate expressions

$$j_{\lambda z} = -i\hbar \frac{\partial}{\partial \phi_{r_\lambda}} \, , \tag{A1a}$$

$$j_{\lambda x} = -i\hbar \left(-\cos\phi_{r_\lambda} \cot\theta_{r_\lambda} \frac{\partial}{\partial \phi_{r_\lambda}} - \sin\phi_{r_\lambda} \frac{\partial}{\partial \theta_{r_\lambda}} \right) , \tag{A1b}$$

$$j_{\lambda y} = -i\hbar \left(-\sin\phi_{r_\lambda} \cot\theta_{r_\lambda} \frac{\partial}{\partial \phi_{r_\lambda}} + \cos\phi_{r_\lambda} \frac{\partial}{\partial \theta_{r_\lambda}} \right) , \tag{A1c}$$

and similar expressions for the components of l_λ with ϕ_λ, θ_λ substituted for ϕ_{r_λ}, θ_{r_λ}. Expressions for the components of J are trivially obtained by the addition $J = l_\lambda + j_\lambda$. The eigenfunctions of the operators j_λ^2 and l_λ^2 appearing in Eq. (2.9) (and also of $j_{\lambda z}$ and $l_{\lambda z}$) are the spherical harmonics $Y_{j_\lambda m_{j_\lambda}}(\theta_{r_\lambda}, \phi_{r_\lambda})$ and $Y_{l_\lambda m_{l_\lambda}}(\theta_\lambda, \phi_\lambda)$. For notational convenience we shall define the modified associated Legendre function $\mathcal{P}_j^{m_j}$ by

$$\mathcal{P}_j^{m_j}(\cos\theta) = P_j^{|m_j|}(\cos\theta) \left(\frac{(j - |m_j|)!}{(j + |m_j|)!} \frac{2j + 1}{2} \right)^{1/2}$$

$$\times \begin{cases} (-1)^{m_j} & m_j > 0 \\ 1 & m_j \leq 0 \end{cases} , \tag{A2}$$

where $P_j^{|m_j|}$ is the usual associated Legendre function. The spherical harmonic $Y_{j m_j}$ is expressed in terms of $\mathcal{P}_j^{m_j}$ by

$$Y_{j m_j}(\theta, \phi) = \frac{e^{im_j \phi}}{\sqrt{2\pi}} \mathcal{P}_j^{m_j}(\cos\theta). \tag{A3}$$

In the space-fixed formalism of Arthurs and Dalgarno,[29] the full wavefunction is expanded in terms of a set of functions $\mathcal{Y}_{l_\lambda j_\lambda}^{JM}(\theta_\lambda, \phi_\lambda; \theta_{r_\lambda}, \phi_{r_\lambda})$ which are simultaneous eigenfunctions of J^2, J_z, l_λ^2, and j_λ^2. These $\mathcal{Y}_{l_\lambda j_\lambda}^{JM}$ are related to the $Y_{j_\lambda m_{j_\lambda}}$ and $Y_{l_\lambda m_{l_\lambda}}$ via

$$\mathcal{Y}_{l_\lambda j_\lambda}^{JM}(\theta_\lambda, \phi_\lambda; \theta_{r_\lambda}, \phi_{r_\lambda}) = \sum_{m_{j_\lambda} m_{l_\lambda}} C(j_\lambda l_\lambda J; m_{j_\lambda} m_{l_\lambda} M)$$

$$\times Y_{j_\lambda m_{j_\lambda}}(\theta_{r_\lambda}, \phi_{r_\lambda}) Y_{l_\lambda m_{l_\lambda}}(\theta_\lambda, \phi_\lambda), \tag{A4}$$

where the notation of Rose[37] is used for the Clebsch–Gordan coefficients C. The full space-fixed wavefunction is then written as

$$\Psi_{JM}(r_\lambda, R_\lambda) = \sum_{l_\lambda j_\lambda} \mathcal{Y}_{l_\lambda j_\lambda}^{JM}(\theta_\lambda, \phi_\lambda; \theta_{r_\lambda}, \phi_{r_\lambda}) G_{j_\lambda l_\lambda}^{JM}(r_\lambda, R_\lambda), \tag{A5}$$

and the space-fixed coupled Schrödinger equation for $G_{j_\lambda l_\lambda}^{JM}$ is[29]

$$\left[-\frac{\hbar^2}{2\mu} \left(\frac{1}{R_\lambda} \frac{\partial^2}{\partial R_\lambda^2} R_\lambda + \frac{1}{r_\lambda} \frac{\partial^2}{\partial r_\lambda^2} r_\lambda \right) + \frac{j_\lambda(j_\lambda + 1)\hbar^2}{2\mu r_\lambda^2} \right.$$

$$\left. + \frac{l_\lambda(l_\lambda + 1)\hbar^2}{2\mu R_\lambda^2} - E \right] G_{j_\lambda l_\lambda}^{JM} + \sum_{j_\lambda' l_\lambda'} \langle l_\lambda j_\lambda | V | l_\lambda' j_\lambda' \rangle G_{j_\lambda' l_\lambda'}^{JM} = 0 . \tag{A6}$$

We now consider the transformation to the body-fixed coordinate systems $OX_\lambda Y_\lambda Z_\lambda$ and $Ox_\lambda' y' z_\lambda'$ of Sec. II.B. A convenient representation of angular momentum operators in these coordinate systems involves choosing the operators J and j_λ as independent and expressing the l_λ^2 of Eq. (2.9) by the expansion

$$l_\lambda^2 = |J - j_\lambda|^2 = J^2 + j_\lambda^2 - (J \cdot j_\lambda + j_\lambda \cdot J) . \tag{A7}$$

To convert the operators j_λ and J, and thus the Hamiltonian of Eq. (2.9), to the body-fixed systems requires first a change from the variables $\theta_\lambda \phi_\lambda \theta_{r_\lambda} \phi_{r_\lambda}$ to $\theta_\lambda \phi_\lambda \gamma_\lambda \psi_\lambda$ as defined in Sec. II.B, followed by successive rotations of the components of the operators. These rotational transformations may be accomplished by using the general expression[32]

$$J_{k'} = R(\alpha\beta\gamma)^{-1} J_k R(\alpha\beta\gamma) , \tag{A8}$$

where J_k refers to the kth component of any angular momentum operator J in an initial system and

$$R(\alpha\beta\gamma) = e^{i\gamma J_z/\hbar} e^{i\beta J_y/\hbar} e^{i\alpha J_z/\hbar}. \tag{A9}$$

$J_{k'}$ refers to the k'th component of J in a transformed coordinate system which is obtained through rotations by Euler angles $\alpha\beta\gamma$ from the initial system. One important point to note in the application of Eq. (A8) to the body-fixed coordinate systems $OX_\lambda Y_\lambda Z_\lambda$ or $Ox_\lambda' y' z_\lambda'$ is that the components J_k and $(j_\lambda)_k$ of the operators J

and j_λ will in general operate upon one or more of the Euler angles ϕ_λ, θ_λ, and ψ_λ of the transformations, and thus great care must be taken with the order of the operators. In Table I we express the resulting components of the operators J and j_λ as well as various combinations thereof in terms of the variables $\theta_\lambda \phi_\lambda \gamma_\lambda \psi_\lambda$ in the three coordinate systems $Oxyz$, $OX_\lambda Y_\lambda Z_\lambda$, and $Ox'_\lambda y'_\lambda z'_\lambda$. Some of the relations in that table have been given previously by Vezzetti and Rubinow, [33] Morse and Feshbach, [54] and Curtiss, Hirschfelder, and Adler. [31]

One very useful point to notice about $j_{\lambda X_\lambda}$, $j_{\lambda Y_\lambda}$, and $j_{\lambda Z_\lambda}$ is that their expressions in terms of γ_λ, ψ_λ in Table I have the same functional form as the corresponding $j_{\lambda x}$, $j_{\lambda y}$, and $j_{\lambda z}$ in Eqs. (A1). This implies that the rotational angular momentum eigenfunctions in the $X_\lambda Y_\lambda Z_\lambda$ coordinate system will simply be the spherical harmonics $Y_{j_\lambda \Omega_\lambda}(\gamma_\lambda, \psi_\lambda)$ where, as is explained in Sec. II. B, Ω_λ is the quantum number associated with $j_{\lambda Z_\lambda}$.

In terms of the coordinate system $OX_\lambda Y_\lambda Z_\lambda$, the Hamiltonian of Eq. (2.9) may be written as

$$H = -\frac{\hbar^2}{2\mu}\left(\frac{1}{R_\lambda}\frac{\partial^2}{\partial R_\lambda^2}R_\lambda + \frac{1}{r_\lambda}\frac{\partial^2}{\partial r_\lambda^2}r_\lambda\right) + \frac{j_\lambda^2}{2\mu r_\lambda^2} + \frac{1}{2\mu R_\lambda^2}\left[J^2 + j_\lambda^2 - 2j_{\lambda Z_\lambda}J_{Z_\lambda} - (j_\lambda^- J^+ + j_\lambda^+ J^-)\right] + V^\lambda(r_\lambda, R_\lambda, \gamma_\lambda), \tag{A10}$$

where the raising and lowering operators are defined in terms of the X_λ and Y_λ components of J and j_λ in the usual way. [37] In order to express the Schrödinger equation in $OX_\lambda Y_\lambda Z_\lambda$ coordinates, we rotate the wavefunction according to Eq. (2.13). Substituting this expression, along with Eq. (A10) into Eq. (2.9), and using the normal raising and lowering properties of the rotation matrix, [33] i.e.,

$$J^\pm D^J_{M\Omega_\lambda} = \hbar[J(J+1) - \Omega_\lambda(\Omega_\lambda \mp 1)]^{1/2} D^J_{M\Omega_\lambda \mp 1} \tag{A11}$$

(where the $\pm$ components refer to the body-fixed system), we obtain the following coupled equations for the $\psi^\lambda_{j\Omega_\lambda}$:

$$\left[-\frac{\hbar^2}{2\mu}\left(\frac{1}{R_\lambda}\frac{\partial^2}{\partial R_\lambda^2}R_\lambda + \frac{1}{r_\lambda}\frac{\partial^2}{\partial r_\lambda^2}r_\lambda\right) + \frac{j_\lambda^2}{2\mu r_\lambda^2} + \frac{1}{2\mu R_\lambda^2}\left[J(J+1)\hbar^2 + j_\lambda^2 - 2\hbar\Omega_\lambda j_{\lambda Z_\lambda}\right] + V^\lambda(r_\lambda, R_\lambda, \gamma_\lambda) - E\right]$$

$$\times \psi^\lambda_{j\Omega_\lambda} - \frac{\hbar}{2\mu R_\lambda^2}[J(J+1) - \Omega_\lambda(\Omega_\lambda+1)]^{1/2} j_\lambda^- \psi^\lambda_{j,\Omega_\lambda+1} - \frac{\hbar}{2\mu R_\lambda^2}[J(J+1) - \Omega_\lambda(\Omega_\lambda-1)]^{1/2} j_\lambda^+ \psi^\lambda_{j,\Omega_\lambda-1} = 0. \tag{A12}$$

Since the rotational eigenfunctions in the $OX_\lambda Y_\lambda Z_\lambda$ coordinate system are the $Y_{j_\lambda \Omega_\lambda}(\gamma_\lambda, \psi_\lambda)$, the rotationally coupled body-fixed solutions analogous to Eq. (A5) are given by

$$\Psi_{JM}(r_\lambda, R_\lambda) = \sum_{j_\lambda \Omega_\lambda} D^J_{M\Omega_\lambda}(\phi_\lambda, \theta_\lambda, 0) Y_{j_\lambda \Omega_\lambda}(\gamma_\lambda, \psi_\lambda) w^\lambda_{j_\lambda \Omega_\lambda}(r_\lambda, R_\lambda), \tag{A13}$$

which is a combination of Eqs. (2.18) and (2.13). The body-fixed and space-fixed representations may be related by using the equality

$$D^J_{M\Omega_\lambda}(\phi_\lambda, \theta_\lambda, 0) Y_{j_\lambda \Omega_\lambda}(\gamma_\lambda, \psi_\lambda) = \left(\frac{4\pi}{2J+1}\right)^{1/2}\sum_{l_\lambda}(-1)^{j_\lambda - \Omega_\lambda} C(Jj_\lambda l_\lambda; \Omega_\lambda - \Omega_\lambda, 0) \mathcal{Y}^{JM}_{j_\lambda l_\lambda}(\theta_\lambda \phi_\lambda; \theta_{r_\lambda}\phi_{r_\lambda}). \tag{A14}$$

Equation (A14) is of great utility in the asymptotic analysis of Sec. V. A.

APPENDIX B: PARITY DECOUPLING

In this Appendix we consider the decoupling that occurs when eigenfunctions of the parity (or inversion) operator $\hat{\mathscr{I}}$ are used in the coupled-channel expansion. This operator inverts all atoms through the system's center of mass. For the three-particle system we are considering,

$$\hat{\mathscr{I}}\Psi(r_\lambda, R_\lambda) = \Psi(-r_\lambda, -R_\lambda), \tag{B1}$$

where Ψ is any wavefunction describing the system. $\hat{\mathscr{I}}$ commutes with $\nabla^2_{R_\lambda}$ and $\nabla^2_{r_\lambda}$. In addition, the internal configuration of the system before and after inversion is the same and consequently the potential energy is not changed by the parity operation. We conclude that $\hat{\mathscr{I}}$ commutes with the Hamiltonian in Eq. (2.7) for any triatomic system.

If we express R_λ and r_λ in body-fixed variables, we find that

$$\hat{\mathscr{I}}\Psi(r_\lambda, \gamma_\lambda, \psi_\lambda, R_\lambda, \theta_\lambda, \phi_\lambda)$$

$$= \Psi(r_\lambda, \gamma_\lambda, \pi - \psi_\lambda, R_\lambda, \pi - \theta_\lambda, \pi + \phi_\lambda). \tag{B2}$$

The body-fixed wavefunction we are considering is given, from Eqs. (2.13), (2.18), (2.30), and (3.1), by

$$\Psi_{JM}(r_\lambda, R_\lambda) = \sum_{v_\lambda j_\lambda \Omega_\lambda} D^J_{M\Omega_\lambda}(\phi_\lambda, \theta_\lambda, 0) Y_{j_\lambda \Omega_\lambda}(\gamma_\lambda, \psi_\lambda)$$

$$\times \frac{\phi^\lambda_{v_\lambda j_\lambda}(r_\lambda)}{r_\lambda R_\lambda} g^\lambda_{J v_\lambda j_\lambda \Omega_\lambda}(R_\lambda). \tag{B3}$$

Since $\hat{\mathscr{I}}$ leaves γ_λ and the scalars R_λ and r_λ unchanged, all derivations of this Appendix are independent of which of the four regions of each arrangement channel region we are concerned with, so we shall omit any explicit reference to them, using the general form for Ψ_{JM} in Region I or II and dropping the superscript (a) or (w) in the ϕ^λ vibrational basis functions. Let us now apply $\hat{\mathscr{I}}$

to Eq. (B3), using the relations[33] $D^J_{M\Omega_\lambda}(\phi_\lambda + \pi, \pi - \theta_\lambda, 0)$ $= (-1)^J \times D^J_{M, -\Omega_\lambda}(\phi_\lambda, \theta_\lambda, 0)$ and $Y_{j_\lambda\Omega_\lambda}(\gamma_\lambda, \pi - \psi_\lambda) = Y_{j_\lambda, -\Omega_\lambda}$ $\times (\gamma_\lambda, \psi_\lambda)$. By changing the sign of Ω_λ in Eq. (B3) and remembering that its summation limits in that equation are invariant with respect to a sign change, we find

$$\hat{\mathcal{I}}\Psi_{JM}(\mathbf{r}_\lambda, \mathbf{R}_\lambda) = (-1)^J \sum_{v_\lambda j_\lambda \Omega_\lambda} D^J_{M\Omega_\lambda}(\phi_\lambda, \theta_\lambda, 0)\, Y_{j_\lambda\Omega_\lambda}(\gamma_\lambda, \psi_\lambda)$$

$$\times \frac{\phi^\lambda_{v_\lambda j_\lambda}(r_\lambda)}{r_\lambda R_\lambda}\, g^\lambda_{Jv_\lambda j_\lambda, -\Omega_\lambda}(R_\lambda). \tag{B4}$$

The $-\Omega_\lambda$ index of g^λ in the right-hand side of this equation indicates that Ψ^λ_{JM} is not an eigenfunction of the parity operator $\hat{\mathcal{I}}$ unless $J = 0$ (since Ω must equal zero as well in that case). Since $\hat{\mathcal{I}}$ commutes with the Hamiltonian, we should be able to linearly combine the Ψ_{JM}'s so as to produce simultaneous eigenfunctions of $\hat{\mathcal{I}}$ and H. Let us consider the linear combinations

$$\bar{\Psi}^\pm_{JM}(\mathbf{r}_\lambda, \mathbf{R}_\lambda) = \frac{1}{\sqrt{2}}\{\Psi_{JM}(\mathbf{r}_\lambda, \mathbf{R}_\lambda) \pm (-1)^J \Psi_{JM}(-\mathbf{r}_\lambda, -\mathbf{R}_\lambda)\}. \tag{B5}$$

By substituting Eqs. (B3) and (B4) in Eq. (B5) and re-arranging the result, we find that

$$\bar{\Psi}^\pm_{JM}(\mathbf{r}_\lambda, \mathbf{R}_\lambda) = \sum_{v_\lambda j_\lambda \Omega_\lambda} D^J_{M\Omega_\lambda}(\phi_\lambda, \theta_\lambda, 0)\, Y_{j_\lambda\Omega_\lambda}(\gamma_\lambda, \psi_\lambda) \frac{\phi^\lambda_{v_\lambda j_\lambda}(r_\lambda)}{r_\lambda R_\lambda}$$

$$\times \begin{pmatrix} \frac{1}{\sqrt{2}}\left(g^\lambda_{Jv_\lambda j_\lambda \Omega_\lambda} + g_{Jv_\lambda j_\lambda, -\Omega_\lambda}\right) \\ \frac{1}{\sqrt{2}}\left(g_{Jv_\lambda j_\lambda \Omega_\lambda} - g_{Jv_\lambda j_\lambda, -\Omega_\lambda}\right) \end{pmatrix}, \tag{B6}$$

where the upper term in the large parentheses refers to the plus solution and the lower to the minus solution. From Eq. (B4), it should be apparent that

$$\hat{\mathcal{I}}\bar{\Psi}^\pm_{JM}(\mathbf{r}_\lambda, \mathbf{R}_\lambda) = \pm(-1)^J \bar{\Psi}^\pm_{JM}(\mathbf{r}_\lambda, \mathbf{R}_\lambda). \tag{B7}$$

Since the basis functions $D^J_{M\Omega_\lambda} Y_{j_\lambda\Omega_\lambda} \phi^\lambda_{v_\lambda j_\lambda}$ in Eq. (B6) are the same as those in Eq. (B3), the equations of Secs. II–IV may be converted to the corresponding ones involving parity solutions by simply linearly combining the g's according to the expression in braces in Eq. (B6). To facilitate this, we define a new function $\bar{g}$ via[55]

$$\bar{g}^\lambda_{Jv_\lambda j_\lambda \Omega_\lambda}(R_\lambda) = \begin{cases} \frac{1}{\sqrt{2}}\left(g^\lambda_{Jv_\lambda j_\lambda \Omega_\lambda} + g^\lambda_{Jv_\lambda j_\lambda, -\Omega_\lambda}\right) & \text{for } \Omega_\lambda > 0 \\ g^\lambda_{Jv_\lambda j_\lambda \Omega_\lambda} & \text{for } \Omega_\lambda = 0 \\ \frac{1}{\sqrt{2}}\left(-g^\lambda_{Jv_\lambda j_\lambda \Omega_\lambda} + g^\lambda_{Jv_\lambda j_\lambda, -\Omega_\lambda}\right) & \text{for } \Omega_\lambda < 0, \end{cases} \tag{B8}$$

or in the matrix notation of Sec. III.A,

$$\bar{\mathbf{g}}^\lambda_J(R_\lambda) = \mathcal{A}_\lambda\, \mathbf{g}^\lambda_J(R_\lambda), \tag{B9}$$

where the orthogonal matrix $\mathcal{A}_\lambda$ is given by

$$(\mathcal{A}_\lambda)^{v'_\lambda j'_\lambda \Omega'_\lambda}_{v_\lambda j_\lambda \Omega_\lambda} = \delta^{v'_\lambda j'_\lambda}_{v_\lambda j_\lambda}\begin{cases} \frac{1}{\sqrt{2}}\left(\delta_{\Omega_\lambda\Omega'_\lambda} + \delta_{\Omega_\lambda, -\Omega'_\lambda}\right) & \text{for } \Omega_\lambda > 0 \\ \delta_{\Omega_\lambda\Omega'_\lambda} & \text{for } \Omega_\lambda = 0 \\ \frac{1}{\sqrt{2}}\left(-\delta_{\Omega_\lambda\Omega'_\lambda} + \delta_{\Omega_\lambda, -\Omega'_\lambda}\right) & \text{for } \Omega_\lambda < 0. \end{cases} \tag{B10}$$

If we include initial conditions of the proper symmetry to form the matrix $\mathbf{g}^\lambda_J$, we find that

$$\bar{\mathbf{g}}^\lambda_J(R_\lambda) = \mathcal{A}_\lambda \mathbf{g}^\lambda_J(R_\lambda) \tilde{\mathcal{A}}_\lambda. \tag{B11}$$

To convert the equations of Sec. III to the corresponding expressions involving parity solutions, we need only to use Eq. (B11) to transform them into expressions for $\bar{\mathbf{g}}^\lambda_J$ rather than $\mathbf{g}^\lambda_J$. For example, the fully coupled Schrödinger equation [Eq. (3.14)] becomes

$$\frac{d^2\bar{\mathbf{g}}^\lambda_J}{dR_\lambda^2} = \bar{\mathbf{U}}^\lambda_J\, \bar{\mathbf{g}}^\lambda_J, \tag{B12}$$

where

$$\bar{\mathbf{U}}^\lambda_J = \mathcal{A}_\lambda \mathbf{U}^\lambda_J \tilde{\mathcal{A}}_\lambda. \tag{B13}$$

$\bar{\mathbf{U}}^\lambda_J$ is identical to $\mathbf{U}^\lambda_J$ in all terms of Eq. (3.15) except those off-diagonal in Ω_λ (i.e., in $\mathbf{U}^{c\lambda}_J$). From Eqs. (3.11) and (B10), we find that

$$(\bar{\mathbf{U}}^{c\lambda}_J)^{v'_\lambda j'_\lambda}_{v_\lambda j_\lambda} = \delta^{v'_\lambda j'_\lambda}_{v_\lambda j_\lambda}/R_\lambda^2\{\delta_{\Omega_\lambda\Omega'_\lambda}[J(J+1) - 2\Omega_\lambda^2 + j_\lambda(j_\lambda+1)]$$

$$- a_{\Omega_\lambda}\delta_{\Omega_\lambda+1,\Omega'_\lambda}\xi_+(J, \Omega_\lambda)\xi_+(j_\lambda, \Omega_\lambda)$$

$$- b_{\Omega_\lambda}\delta_{\Omega_\lambda-1,\Omega'_\lambda}\xi_-(J, \Omega_\lambda)\xi_-(j_\lambda, \Omega_\lambda)\}, \tag{B14}$$

where

$$a_{\Omega_\lambda} = \begin{cases} 1 & \text{for } \Omega_\lambda > 1 \text{ and } \Omega_\lambda < -1 \\ \sqrt{2} & \text{for } \Omega_\lambda = 0 \\ 0 & \text{for } \Omega_\lambda = -1 \end{cases} \tag{B15}$$

and

$$b_{\Omega_\lambda} = \begin{cases} 1 & \text{for } \Omega_\lambda > 1 \text{ and } \Omega_\lambda \le -1 \\ \sqrt{2} & \text{for } \Omega_\lambda = 1 \\ 0 & \text{for } \Omega_\lambda = 0. \end{cases} \tag{B16}$$

An examination of the structure of $\bar{\mathbf{U}}^{c\lambda}_J$ indicates that it contains no elements which couple states whose Ω_λ is positive or zero to those whose Ω_λ is negative. Since only $\bar{\mathbf{U}}^{c\lambda}_J$ provides off-diagonal Ω_λ coupling in Eq. (B12), we see that our coupled Schrödinger equations have been separated into two uncoupled sets—those with $\Omega_\lambda \ge 0$ [of parity $(-1)^J$] and those with $\Omega_\lambda < 0$ [parity $-(-1)^J$]. This uncoupling is preserved throughout the integration in a given arrangement channel region since the only Ω_λ-dependent coupling appearing anywhere in this process occurs in centrifugal terms analogous to those of Eq. (B14). Thus by constructing parity eigenfunctions, we can separate our integration problem into two smaller ones [each of which can be further separated into two parts for homonuclear targets (Sec. III.C)].

Parity is also preserved in the matching procedure because, as can be seen by inspection of Fig. 1, the parity operation is invariant to which arrangement channel coordinate system one is considering. This means that solutions of the same parity symmetry but expressed in different arrangement channel coordinates should be related to each other by a transformation which does not mix in solutions of the opposite parity. To prove this, we must first transform the coefficient matrices $\mathbf{h}^\lambda_J$, $\mathbf{h}'^\lambda_J$, $\mathbf{f}^\lambda_J$, and $\mathbf{f}'^\lambda_J$ of Sec. IV.B to the representation involving parity eigenfunctions. This requires a transformation similar to Eq. (B11),

$$\mathbf{f}'_\lambda = \mathbf{s}'_{v\lambda} \mathbf{h}'_\lambda \mathbf{j}_\lambda . \tag{B17}$$

where $\mathbf{s}'_{v\lambda}$ is an $N/2 \times N/2$ matrix (N = total number of solutions of both parities) whose precise mathematical form is identical to $\mathbf{s}_\lambda$ in Eq. (B10), but whose actual structure is different because the set of indices $v_\lambda j_\lambda$ involving the matching surface basis functions of Eq. (4.30) will assume only half the number of values that the asymptotic solutions do (as discussed in Sec. IV. C). Note that we still right multiply $\mathbf{h}'_\lambda$ by $\mathbf{j}_\lambda$ in Eq. (B17) because right multiplication corresponds to linearly combining different initial conditions, and the number of these is always N. By writing equations analogous to Eq. (B17) for $\mathbf{h}'_\lambda$, $\mathbf{f}'_\lambda$, and $\mathbf{f}'_\lambda$, substituting these into Eq. (4.55) [using Eqs. (4.52)–(4.54) and simplifying, we obtain

$$\hat{\mathbf{h}}'_{\lambda J} \mathbf{C}^{(1)}_{\lambda J} + \hat{\mathbf{h}}'_{\lambda J} \mathbf{C}^{(1)}_{\lambda J} = \hat{\mathbf{s}}'_{v\lambda} \{ \hat{\mathbf{i}}'_{\lambda J} \mathbf{C}^{(1)}_{\lambda J} + \hat{\mathbf{i}}'_{\nu J} \mathbf{C}^{(1)}_{\nu J} \} , \tag{B18}$$

where the circumflex symbol implies definitions analogous to Eqs. (4.52)–(4.54) for barred (i.e., parity) quantities, and

$$\hat{\mathbf{s}}'_{v\lambda} = \mathbf{s}'_{v\lambda} \mathbf{s}'_{v\lambda} \mathbf{j}'_{v\lambda} . \tag{B19}$$

From Eq. (4.49) we can rewrite $\hat{\mathbf{s}}'_{v\lambda}$ as

$$(\hat{\mathbf{s}}'_{v\lambda})^{v_\nu j_\nu \Omega_\nu}_{v_\lambda j_\lambda \Omega_\lambda} = S^{w}_{v_\lambda v_\nu} \int A^{v_\lambda}_{j_\lambda \Omega_\lambda}(\gamma_\lambda)$$

$$\times A^{v_\lambda}_{j_\nu \Omega_\nu}(\gamma_\lambda) \frac{| (d^J_{\Omega_\nu,\Omega_\lambda} + d^J_{\Omega_\nu,-\Omega_\lambda}) |}{| (d^J_{\Omega_\nu,\Omega_\lambda} - d^J_{\Omega_\nu,-\Omega_\lambda}) |} f_{\Omega_\lambda \Omega_\nu} \sin\gamma_\lambda d\gamma_\lambda , \tag{B20}$$

where

$$f_{\Omega_\lambda \Omega_\nu} = \begin{cases} 1/\sqrt{2} & \text{for } \Omega_\lambda = 0 \text{ or } \Omega_\nu = 0 \\ 1/2 & \text{for } \Omega_\lambda = \Omega_\nu = 0 \\ 1 & \text{for } \Omega_\lambda \times \Omega_\nu > 0 \\ 0 & \text{for } \Omega_\lambda \times \Omega_\nu < 0 , \end{cases} \tag{B21}$$

and the upper term in the braces is used for $\Omega_\lambda, \Omega_\nu \geq 0$ and the lower term for $\Omega_\lambda, \Omega_\nu < 0$. It should be evident from Eq. (B21) that $\hat{\mathbf{s}}'_{v\lambda}$ does not couple terms of different parity nor does any part of Eq. (B18); this implies that the matching procedure can be done separately for solutions of each parity. It should also be noted that for a complete set of matching surface functions, the two subblocks of $\hat{\mathbf{s}}'_{v\lambda}$ corresponding to solutions of different parity are separately orthogonal.

A convenient procedure for extracting the asymptotic information from the matched solutions involves first a calculation of reactance and scattering matrices which are defined in terms of parity eigenfunctions. This is followed by a coupling transformation in which the positive and negative parity $\mathbf{S}_J$ matrices are combined to yield the body-fixed $\mathbf{S}_J$ matrix of Eq. (5.5). From that point onward the formulas of Sec. V. B must be used, since the plane wave scattering solution is not an eigenfunction of $\hat{\mathbf{s}}$ [as seen by inspection of Eq. (5.24)]. The parity scattering and reactance matrix solutions are defined by equations identical in form to Eqs. (5.4) and (5.5), or to Eqs. (5.8) and (5.9), but the incoming and outgoing solutions $\mathbf{I}_J$ and $\mathbf{O}_J$ of Eq. (5.10) must be parity eigenfunctions and hence satisfy Eq. (B12) asymptotical-

ly. One can find these solutions by actually diagonalizing the asymptotic Hamiltonian obtained from Eq. (B12), or by performing transformations analogous to Eq. (B11) on $\mathbf{I}_J$ and $\mathbf{O}_J$. Both procedures lead to expressions for $\mathbf{I}_J$ and $\mathbf{O}_J$ identical to Eq. (5.10) except for the following two changes:

(a) the sum over l_λ in that equation includes only those l_λ of the same parity as is specified by the signs of Ω_λ and Ω'_λ appearing in that equation. (The only nonzero terms will always involve Ω_λ and Ω'_λ of the same signs.) In other words, when $\Omega_\lambda, \Omega'_\lambda \geq 0$, $l_\lambda = J + j_\lambda, J + j_\lambda - 2, \cdots, |J - j_\lambda|$ and when $\Omega_\lambda, \Omega'_\lambda < 0$, $l_\lambda = J + j_\lambda - 1, \cdots, |J - j_\lambda| + 1$.

(b) Equation (5.10) is to be multiplied by $\bar{f}_{\Omega_\lambda \Omega'_\lambda}$, where

$$\bar{f}_{\Omega_\lambda \Omega_\nu} = \begin{cases} \sqrt{2} & \text{for } \Omega_\lambda = 0 \text{ or } \Omega_\nu = 0 \\ 1 & \text{for } \Omega_\lambda = \Omega_\nu = 0 \\ 2 & \text{for } \Omega_\lambda \times \Omega_\nu > 0 \\ 0 & \text{for } \Omega_\lambda \times \Omega_\nu < 0 . \end{cases} \tag{B22}$$

This form of $\bar{f}_{\Omega_\lambda \Omega_\nu}$ leads to block diagonal $\mathbf{I}_J$ and $\mathbf{O}_J$ matrices, thus decoupling the reactance and scattering matrix analysis for solutions of different parities.

When these expressions for $\mathbf{I}_J$ and $\mathbf{O}_J$ are substituted into Eq. (5.21) along with the parity expressions for $\mathbf{g}'_J$, $\mathbf{g}'_J$, and $\mathbf{C}'_J$, the correct parity reactance matrix $\bar{\mathbf{R}}'_J$ [analogous to $\bar{\mathbf{R}}'_J$ of Eq. (5.18)] is obtained (where we consider $\bar{\mathbf{R}}'_J$ to contain the even and odd parity reactance matrices as separate subblocks). This may be subsequently converted to $\bar{\mathbf{S}}'_J$ via an equation analogous to Eq. (5.7) and the remark which follows it. The rows and columns of the parity scattering matrix may then be rearranged to form the body-fixed scattering matrix $\bar{\mathbf{S}}_J$ via

$$\bar{\mathbf{S}}_J = \mathbf{T} \bar{\mathbf{S}}'_J \mathbf{T} , \tag{B23}$$

where the $3N \times 3N$ matrix $\mathbf{T}$ is obtained from the $N \times N$ matrices $\mathbf{T}_\lambda, \mathbf{T}_\nu, \mathbf{T}_\kappa$ [whose definitions are analogous to Eq. (B10)], by

$$\mathbf{T} = \begin{pmatrix} \mathbf{T}_\lambda & \mathbf{0} & \mathbf{0} \\ \mathbf{0} & \mathbf{T}_\nu & \mathbf{0} \\ \mathbf{0} & \mathbf{0} & \mathbf{T}_\kappa \end{pmatrix} \tag{B24}$$

in which $\mathbf{0}$ is an $N \times N$ matrix of zeros. Finally, the body-fixed scattering matrix $\mathbf{S}_J$ used to calculate the scattering amplitudes according to Eqs. (5.31) and (5.32) is obtained from $\bar{\mathbf{S}}_J$ by

$$(\mathbf{S}_J)^{v'_\lambda j'_\lambda \Omega_\lambda}_{v_\lambda j_\lambda \Omega_\lambda} = (\bar{\mathbf{S}}_J)^{w_\lambda j_\lambda \Omega_\lambda}_{v'_\lambda j'_\lambda,-\Omega_\lambda} . \tag{B25}$$

It should be noted that the decoupling of the integration and matching procedures described above to generate parity eigenfunctions is completely general, not depending on an identicity between any of the three atoms A, B, C comprising the system. This results in an appreciable saving of computer time when implementing this calculational procedure.

APPENDIX C: ORTHOGONAL NATURE OF THE ARRANGEMENT CHANNEL TRANSFORMATION MATRIX $\mathbf{s}_{\nu\lambda}^{J}$

In this Appendix we show that the arrangement channel transformation matrix $\mathbf{s}_{\nu\lambda}^{J}$ defined by Eq. (4.49) is real orthogonal under certain conditions which are easily satisfied.

The definition of $d_{\Omega_{\nu}\Omega_{\lambda}}^{J}$ appearing in Eq. (4.49) is

$$d_{\Omega_{\nu}\Omega_{\lambda}}^{J}(\Delta_{\nu\lambda}) = \langle J\Omega_{\lambda} \, | \exp\left(\frac{i}{\hbar}\Delta_{\nu\lambda}J_{y'}\right) | J\Omega_{\nu} \rangle , \qquad (C1)$$

where $|J\Omega_{\nu}\rangle$ and $|J\Omega_{\lambda}\rangle$ are simultaneous orthonormal eigenfunctions of J^{z} and $J_{z'_{\lambda}}$ in coordinate system $Ox'_{\lambda}y'z'_{\lambda}$, having eigenvalues J, Ω_{ν} and J, Ω_{λ}, respectively; they are functions of θ_{λ}, ϕ_{λ}, and ψ_{λ} and the integration implied by the angular brackets is performed over these three angles with weighing function $\sin\theta_{\lambda}$. Replacing Eqs. (C1), (4.30), and (4.50) into Eq. (4.49) furnishes

$$(s_{\nu\lambda}^{J})_{n_{\nu}J_{\lambda}\Omega_{\lambda}}^{n_{\nu}J_{\nu}\Omega_{\nu}} = \langle n_{\lambda} \, | \, n_{\nu} \rangle \langle Jj_{\lambda}\Omega_{\lambda}| \, \exp\left(\frac{i}{\hbar}\Delta_{\nu\lambda}J_{y'}\right) | Jj_{\nu}\Omega_{\nu} \rangle , \qquad (C2)$$

where

$$|Jj_{\nu}\Omega_{\nu}\rangle = A_{j_{\nu}\Omega_{\nu}}^{\nu\lambda}(\gamma_{\lambda}) \, |J\Omega_{\nu}\rangle , \qquad (C3)$$

$$\langle Jj_{\lambda}\Omega_{\lambda}| = A_{j_{\lambda}\Omega_{\lambda}}^{\nu\lambda}(\gamma_{\lambda}) \langle J\Omega_{\lambda}| ,$$

$$| \, n_{\nu} \rangle = \phi_{n_{\nu}}^{\nu}(\zeta) , \qquad (C4)$$

$$\langle n_{\lambda} | = \phi_{n_{\lambda}}^{\lambda*}(\zeta) .$$

The integration implied in $\langle n_{\lambda} \, | \, n_{\nu} \rangle$ is over ζ, and the other integration in Eq. (C2) is over the independent variables γ_{λ}, θ_{λ}, ϕ_{λ}, ψ_{λ} with weighing function $\sin\gamma_{\lambda}\sin\theta_{\lambda}$. As long as they form a complete orthonormal set of functions in γ_{λ} space, the $|Jj_{\nu}\Omega_{\nu}\rangle$ form a complete orthonormal set in γ_{λ}, θ_{λ}, ϕ_{λ}, ψ_{λ} space, and Eq. (C2) can be written as

$$\mathbf{s}_{\nu\lambda}^{J} = \mathbf{S}^{\lambda\nu} \otimes \exp\left(\frac{i}{\hbar}\Delta_{\nu\lambda}^{J}\right) , \qquad (C5)$$

where

$$(\Delta_{\nu\lambda}^{J})_{j_{\lambda}\Omega_{\lambda}}^{j_{\nu}\Omega_{\nu}} = \langle Jj_{\lambda}\Omega_{\lambda} \, | \, \Delta_{\nu\lambda}J_{y'} \, | \, Jj_{\nu}\Omega_{\nu} \rangle \qquad (C6)$$

and

$$(S^{\lambda\nu})_{n_{\lambda}}^{n_{\nu}} = \langle n_{\lambda} \, | \, n_{\nu} \rangle = S_{n_{\lambda}n_{\nu}}^{\lambda\nu} , \qquad (C7)$$

the $S_{n_{\lambda}n_{\nu}}^{\lambda\nu}$ being given by Eq. (4.50) and the $\otimes$ in Eq. (C5) representing a direct product of the two matrices appearing in its right-hand side. The elements of $\exp[(i/\hbar)\Delta_{\nu\lambda}^{J}]$ are equal to the integral over γ_{λ} in the right-hand side of Eq. (4.49) and are therefore real if the functions $A_{j_{\lambda}\Omega_{\lambda}}^{\nu\lambda}(\gamma_{\lambda})$ are real. It is convenient to use the notation $|j_{\nu}\Omega_{\nu}\rangle = A_{j_{\nu}\Omega_{\nu}}^{\nu\lambda}(\gamma_{\lambda})$ and $\langle j_{\lambda}\Omega_{\lambda}| = A_{j_{\lambda}\Omega_{\lambda}}^{\nu\lambda*}(\gamma_{\lambda})$, in terms of which we can write

$$|Jj_{\nu}\Omega_{\nu}\rangle = |j_{\nu}\Omega_{\nu}\rangle |J\Omega_{\nu}\rangle$$

and

$$\langle Jj_{\lambda}\Omega_{\lambda}| = \langle J\Omega_{\lambda}| \langle j_{\lambda}\Omega_{\lambda}| .$$

Since on the matching surface $\pi_{\nu\lambda}$, $\Delta_{\nu\lambda}$ is a function of γ_{λ} only [see Eq. (4.11)] and $J_{y'}$ operates on variables θ_{λ}, ϕ_{λ}, ψ_{λ} only, Eq. (C6) can be written as

$$(\Delta_{\nu\lambda}^{J})_{j_{\lambda}\Omega_{\lambda}}^{j_{\nu}\Omega_{\nu}} = \langle j_{\lambda}\Omega_{\lambda} \, | \, \Delta_{\nu\lambda}(\gamma_{\lambda}) \, | j_{\nu}\Omega_{\nu} \rangle \langle J\Omega_{\lambda} \, | J_{y'} \, | J\Omega_{\nu} \rangle . \qquad (C8)$$

Each of the two matrices represented by the factors in the right-hand side of this equation is Hermitian and therefore

$$\left[(\Delta_{\nu\lambda}^{J})_{j_{\nu}\Omega_{\nu}}^{j_{\lambda}\Omega_{\lambda}}\right]^{*} = (\Delta_{\nu\lambda}^{J})_{j_{\lambda}\Omega_{\lambda}}^{j_{\nu}\Omega_{\nu}} ,$$

from which we conclude that $\Delta_{\nu\lambda}^{J}$ is Hermitian and that $\exp[(i/\hbar)\Delta_{\nu\lambda}^{J}]$ is unitary. If the $\phi_{n_{\lambda}}^{\lambda}(\zeta)$ and $\phi_{n_{\nu}}^{\nu}(\zeta)$ are separately complete sets of orthonormal functions which span the ζ space, their overlap matrix $\mathbf{S}^{\nu\lambda}$ is also unitary. $\mathbf{s}_{\nu\lambda}^{J}$ then is the direct product of two unitary matrices and therefore is unitary. Furthermore, if $\mathbf{S}^{\nu\lambda}$ is in addition real [as will be the case if, for example, the $\phi_{n_{\lambda}}^{\lambda}(\zeta)$ and $\phi_{n_{\nu}}^{\nu}(\zeta)$ are real], and the $A_{j_{\lambda}\Omega_{\lambda}}^{\nu\lambda}$ are also real, so is $\mathbf{s}_{\nu\lambda}^{J}$, as can be seen by inspection of the right-hand side of Eq. (4.49). We conclude that if $\phi_{n_{\lambda}}^{\lambda}(\zeta)$ and $\phi_{n_{\nu}}^{\nu}(\zeta)$ are two complete sets of orthonormal functions which span the ζ space and are related by a real orthogonal transformation, and if $A_{j_{\lambda}\Omega_{\lambda}}^{\nu\lambda}(\gamma_{\lambda})$ is a complete set of real orthonormal functions which span the γ_{λ} space, then the arrangement channel transformation matrix $\mathbf{s}_{\nu\lambda}^{J}$ is real and orthogonal. These conditions are satisfied by the $A_{j_{\lambda}\Omega_{\lambda}}^{\nu\lambda}(\gamma_{\lambda})$ of Eq. (4.31), the $\phi_{n_{\lambda}}^{\lambda}(\zeta)$ vibrational basis functions appearing in Eqs. (4.25) and (4.28), and the analogous functions $\phi_{n_{\nu}}^{\nu}(\zeta)$ for arrangement channel ν.

If Eq. (C5) is used to evaluate $\mathbf{s}_{\nu\lambda}^{J}$, the second factor in the right-hand side of Eq. (C8) can be calculated using the explicit expression[33]

$$\langle J\Omega_{\lambda} \, | J_{y'} \, | J\Omega_{\nu} \rangle = \frac{1}{2}\frac{\hbar}{i}\{[(J-\Omega_{\lambda})(J+\Omega_{\lambda}+1)]^{1/2}\delta_{\Omega_{\lambda},\Omega_{\nu}-1} $$
$$- [(J+\Omega_{\lambda})(J-\Omega_{\lambda}+1)]^{1/2}\delta_{\Omega_{\lambda},\Omega_{\nu}+1}\} . \qquad (C9)$$

*Research supported in part by the United States Air Force Office of Scientific Research (Grant No. AFOSR-73-2539).

†Work performed in partial fulfillment of the requirements for the Ph. D. in Chemistry at the California Institute of Technology.

‡Contribution No. 5250.

[1] D. J. Diestler and V. McKoy, J. Chem. Phys. 48, 2951 (1968).

[2] D. J. Diestler, J. Chem. Phys. 54, 4547 (1971).

[3] E. M. Mortenson and K. S. Pitzer, Chem. Soc. (London) Spec. Publ. 16, 57 (1962); J. Chem. Phys. 48, 4029 (1968).

[4] D. J. Truhlar and A. Kuppermann, J. Chem. Phys. 52, 3841 (1970); ibid. 56, 2232 (1972).

[5] A. Kuppermann, Proc. Conf. Potential Energy Surf. Chem. U. C. Santa Cruz, August, 1970 (UCRL), p. 121; Electronic and Atomic Collisions, Proceedings of VII ICPEAC (North-Holland, Amsterdam, 1971), p. 3.

[6] G. C. Schatz, J. Bowman, and A. Kuppermann, J. Chem. Phys. 58, 4023 (1973); J. M. Bowman, G. C. Schatz, and A. Kuppermann, Chem. Phys. Lett. 24, 378 (1974); G. C. Schatz, J. M. Bowman, and A. Kuppermann, J. Chem. Phys. 63, 674, 685 (1975).

[7] C. C. Rankin and J. Light, J. Chem. Phys. 51, 1701 (1969); G. Miller and J. C. Light, J. Chem. Phys. 54, 1635 (1971); ibid. 54, 1643 (1971).

[8] B. R. Johnson, Chem. Phys. Lett. 13, 172 (1972).

[9] S. F. Wu and R. D. Levine, Mol. Phys. 22, 881 (1971).

[10]E. Shipsey, J. Chem. Phys. 58, 232 (1973).

[11]J. T. Adams, R. L. Smith, and E. F. Hayes, J. Chem. Phys. 61, 2193 (1974).

[12]M. Baer and D. J. Kouri, Chem. Phys. Lett. 24, 37 (1974); M. Baer, J. Chem. Phys. 60, 1057 (1974); A. Persky and M. Baer, J. Chem. Phys. 60, 133 (1974); M. Baer, U. Halavee, and A. Persky, J. Chem. Phys. 61, 5122 (1974).

[13]P. B. Middleton and R. E. Wyatt, J. Chem. Phys. 56, 2720 (1972); E. A. McCollough and R. E. Wyatt, J. Chem. Phys. 54, 3578 (1971); ibid. 54, 3592 (1971).

[14]M. Baer and D. J. Kouri, Chem. Phys. Lett. 11, 238 (1971); J. Chem. Phys. 56, 1758 (1972); ibid. 57, 3991 (1972).

[15]R. P. Saxon and J. C. Light, J. Chem. Phys. 56, 3874 (1972); 56, 3835 (1972); A. Altenberger-Siczek and J. C. Light, J. Chem. Phys. 61, 4373 (1974).

[16](a) A. B. Elkowitz and R. E. Wyatt, J. Chem. Phys. 62, 2504 (1975); 62, 3683 (1975); (b) S. A. Harms and R. E. Wyatt, J. Chem. Phys. 62, 3162 (1975); 62, 3173 (1975).

[17]G. Wolken and M. Karplus, J. Chem. Phys. 60, 351 (1974).

[18]W. H. Miller, J. Chem. Phys. 50, 407 (1969).

[19]A. Kuppermann, G. C. Schatz, and M. Baer, J. Chem. Phys. 65, 4596 (1976), first paper of this series.

[20]A. Kuppermann, G. C. Schatz, and M. Baer, J. Chem. Phys. 61, 4362 (1974).

[21]G. C. Schatz and A. Kuppermann, J. Chem. Phys. 65, 4624 (1976), preceding paper.

[22]A. Kuppermann and G. C. Schatz, J. Chem. Phys. 52, 2502 (1975).

[23]G. C. Schatz and A. Kuppermann, Phys. Rev. Lett. 35, 1266 (1975).

[24]G. C. Schatz and A. Kuppermann, J. Chem. Phys. 65, 4668 (1976), following paper.

[25]L. M. Delves, Nucl. Phys. 9, 391 (1959); 20, 275 (1960).

[26]D. Jepsen and J. O. Hirschfelder, Proc. Natl. Acad. Sci. 45, 249 (1959).

[27]F. Smith, J. Math. Phys. 3, 735 (1962).

[28]A. Kuppermann, Chem. Phys. Lett. 33, 374 (1975); J. Chem. Phys. (to be published).

[29]A. M. Arthurs and A. Dalgarno, Proc. R. Soc. London Ser. A 256, 540 (1960).

[30]J. O. Hirschfelder and E. P. Wigner, Proc. Natl. Acad. Sci. 21, 113 (1935).

[31]C. F. Curtiss, J. O. Hirschfelder, and F. T. Adler, J. Chem. Phys. 18, 1638 (1950).

[32]R. T. Pack, J. Chem. Phys. 60, 633 (1974).

[33]A. S. Davydov, Quantum Mechanics, translated by D. ter Haar (Addison-Wesley, Reading, MA, 1965), Chap. VI.

[34]P. McGuire and D. J. Kouri, J. Chem. Phys. 60, 2488 (1974).

[35]R. B. Walker and J. C. Light, Chem. Phys. 7, 84 (1975).

[36]It can be shown that the McGuire-Kouri approximation is equivalent to replacing l_λ^2 in body-fixed coordinates (involving the four angles θ_λ, ϕ_λ, γ_λ, ψ_λ) by its expression in space-fixed coordinates (involving only the angles θ_λ, ϕ_λ). This approximate body-fixed l_λ^2 commutes with the approximate body-fixed Hamiltonian resulting from its use. Simultaneous eigenfunctions of these two approximate operators can be written as $Y_{l_\lambda m_{l_\lambda}} (\theta_\lambda, \phi_\lambda) \times \psi_\lambda^j (R_\lambda, r_\lambda, \gamma_\lambda, \psi_\lambda)$, in terms of which any eigenfunction of the approximate Hamiltonian may be expanded. An expansion of the ψ_λ^j in terms of the $Y_{j_\lambda \Omega_\lambda}(\gamma_\lambda, \psi_\lambda)$ leads to coefficients $u_{n_\lambda \Omega_\lambda}^{j_\lambda}(r, R_\lambda)$ which satisfy an equation similar to Eq. (2.19) with the off-diagonal Ω_λ terms missing and the factor multiplying $\hbar^2/2\mu R_\lambda^2$ in Eq. (2.20) replaced by $l_\lambda(l_\lambda \cdot 1)$.

[31]M. E. Rose, Elementary Theory of Angular Momentum, (Wiley, New York, 1957), Chap. 3.

[38]Handbook of Mathematical Functions, edited by M. Abramowitz and I. A. Stegun (National Bureau of Standards, Washington, D.C., 1964).

[39]R. N. Porter and M. Karplus, J. Chem. Phys. 40, 1105 (1964).

[40]$i_n(x) = (\pi/2x)^{1/2} I_{n+1/2}(x)$ and $k_n(x) = (\pi/2x)^{1/2} K_{n+1/2}(x)$, where I_m and K_m are the modified cylindrical Bessel functions described by Abramowitz and Stegun,[38] p. 374.

[41]The row indices designate the different tumbling and vibration rotation basis functions and the column indices the different linearly independent solutions.

[42]R. Gordon, J. Chem. Phys. 51, 14 (1969).

[43]These asymptotic solutions are simply the noninteger order spherical Bessel functions which solve Eq. (3.4) when the l_a terms are set equal to zero. Note that in the R and S matrix determination outlined in Sec. V, the complications arising from these truncated basis expansions are ignored. In actual calculations[44] these effects have, however, been correctly included.

[44]As noted in Sec. III. C, the even and odd j_λ solutions are not coupled for atom plus homonuclear diatomic arrangement channels. We are accordingly allowed (but not required) to set the components of g_J connecting even and odd rotational quantum numbers equal to zero. This results in scattering solutions of the correct homonuclear symmetry and allows us to considerably decouple the problem as described in Sec. III. C.

[45]A. M. Lane and R. G. Thomas, Rev. Mod. Phys. 30, 257 (1958).

[46]N. S. F. Mott and H. S. W. Massey, The Theory of Atomic Collisions (Clarendon, Oxford, 1965), 3rd ed., Chaps. 14 and 15.

[47]The transition probability is defined as the ratio of the outgoing radial flux in a specified product channel to the incoming radial flux in a specified reagent channel. Equation (5.23) easily follows from application of this definition to Eqs. (5.3) and (5.5).

[48]M. Jacob and G. C. Wick, Ann. Phys. 7, 404 (1959).

[49]This lack of dependence of σ on ϕ is a simple consequence of our choice of incident quantization axis as being the direction of the incident wave vector. This results in an "initial" probability density which is cylindrically symmetric about that axis [from Eq. (5.24)] which implies that the "final" probability density must be symmetric as well in the absence of external fields.

[50]L. I. Schiff, Quantum Mechanics (McGraw-Hill, New York, 1968), 3rd ed., pp. 384-395.

[51]J. M. Bowman, Ph. D. Thesis, California Institute of Technology, 1974.

[52]A. Messiah, Quantum Mechanics, (North-Holland, Amsterdam, 1966), Vol. II, Eq. XIII.54, p. 530. Note that Messiah's $R(\alpha\beta\gamma)$ (Eq. XIII.60, p. 534) is Davydov's[33] $R(\alpha\beta\gamma)^{-1}$.

[53]D. J. Vezzetti and S. I. Rubinow, Ann. Phys. 35, 373 (1965).

[54]P. M. Morse and H. Feshbach, Methods of Theoretical Physics (McGraw-Hill, New York, 1953), Vol. II, p. 1721.

[55]A factor of $\sqrt{2}$ has been omitted in the $\Omega_\lambda = 0$ solution. This is always permitted because the integrated solutions are undetermined to within an overall constant multiplicative factor. This choice has the advantage of making the s_λ defined by Eq. (B10) orthogonal.

Quantum mechanical reactive scattering for three-dimensional atom plus diatom systems. II. Accurate cross sections for H+H₂*

George C. Schatz† and Aron Kuppermann

Arthur Amos Noyes Laboratory of Chemical Physics,‡ California Institute of Technology, Pasadena, California 91125
(Received 22 December 1975)

Accurate three-dimensional reactive and nonreactive quantum mechanical cross sections for the H + H₂ exchange reaction on the Porter–Karplus potential energy surface are presented. Tests of convergence in the calculations indicate an accuracy of better than 5% for most of the results in the energy range considered (0.3 to 0.7 eV total energy). The reactive differential cross sections are exclusively backward peaked, with peak widths increasing monotonically from about 32° at 0.4 eV to 51° at 0.7 eV. Nonreactive inelastic differential cross sections show backwards to sidewards peaking, while elastic ones are strongly forward peaked with a nearly monotonic decrease with increasing scattering angle. Some oscillations due to interferences between the direct and exchange amplitudes are obtained in the para-to-para and ortho-to-ortho antisymmetrized cross sections above the effective threshold for reaction. Nonreactive collisions do not show a tendency to satisfy a "j_z-conserving" selection rule. The reactive cross sections show significant rotational angular momentum polarization with the $m_j = m'_j = 0$ transition dominating for low reagent rotational quantum number j. In contrast, the degeneracy averaged rotational distributions can be fitted to statistical temperaturelike expressions to a high degree of accuracy. The integral cross sections have an effective threshold total energy of about 0.55 eV, and differences between this quantity and the corresponding 1D and 2D results can largely be interpreted as resulting from bending motions in the transition state. In comparing these results with those of previous approximate dynamical calculations, we find best overall agreement between our reactive integral and differential cross sections and the quasiclassical ones of Karplus, Porter, and Sharma [J. Chem. Phys. 43, 3259 (1965)], at energies above the quasiclassical effective thresholds. This results in the near equality of the quantum and quasiclassical thermal rate constants at 600 K. At lower temperatures, however, the effects of tunneling become very important with the quantum rate constant achieving a value larger than the quasiclassical one by a factor of 3.2 at 300 K and 18 at 200 K.

I. INTRODUCTION

"The underlying physical laws necessary for the mathematical theory of a large part of physics and the whole of chemistry are thus completely known, and the difficulty is only that the exact application of these laws leads to equations much too complicated to be soluble." This legendary statement made by Dirac in 1929[1a] has been valid for the 50 years of existence of Schrödinger's wave mechanics,[1b] at least insofar as the dynamics of chemical reactions are concerned. Since the advent of electronic digital computers some 25 years ago, very large strides have been made in the accurate *ab initio* calculation of electronic wavefunctions of atoms and molecules, of electronic, vibrational, and rotational energy levels and of molecular equilibrium geometries. However, until very recently, the problem of accurately solving the Schrödinger equation describing the dynamics of even a very simple chemical reaction occurring on a given potential energy surface remained intractable, owing to both conceptual and computational difficulties. These difficulties have now been overcome, and the present paper describes accurate results obtained for the H + H₂ hydrogen atom exchange reaction.

This simplest of chemical reactions has been of fundamental theoretical interest in the field of chemical dynamics ever since the beginning of quantum mechanics. Great progress in understanding it has been made both in the accurate determination of it's ground state electronically adiabatic potential energy surface,[2] and in the approximate calculation of the corresponding cross sections and other dynamical quantities.[3–14] A long sought objective of these dynamical studies has been the accurate quantum mechanical treatment of the three-dimensional collision dynamics. Such an accurate *ab initio* calculation for H + H₂ is important, for this system has served as a prime example in the development and testing of approximate reaction dynamic theories such as quasiclassical methods,[3,11a] semiclassical methods,[6,11d] and approximate quantum methods.[4,5,7,8,11,12] In addition, H + H₂ has been valuable in the development of transition state theory,[15] in the characterization of tunnelling[16a,16] and of the concept of vibrational adiabaticity,[17] and in analyzing the effects of changes in the potential energy surface on the reaction dynamics.[18] Much of our understanding of the influence of initial rotational[3] and vibrational[14a] state on chemical dynamics comes from studies on this system as does our knowledge concerning the influence of varying impact parameter[3,11c] or total angular momentum,[5,7,11a,b] of resonance and direct reaction mechanisms,[3,19–21] and other dynamical effects. Nonreactive elastic and inelastic H + H₂ collisions have also been of theoretical interest in the analysis of rotational excitation and deactivation processes,[11,12,22–25] and in examining the nature of the competition and interference between reactive and nonreactive processes.[11a,19] A number of reactive and nonreactive experimental studies of H + H₂ and its isotopic counterparts have been done ranging from kinetic rate constant determinations[26] to hot atom[27] and molecular beam[28] experiments. The in-

teraction of theory and experiment has been of mutual benefit throughout their respective evolutionary developments.

In a previous paper[29] we presented a method for accurately solving the Schrödinger equation for the dynamics of the three-dimensional collision of an atom with a diatomic molecule on a single electronically adiabatic potential energy surface. This method was an extension of an earlier coplanar method[30] which has since been used extensively to study the 2DH + H$_2$ system.[13] In the present paper we describe the results of an application of this 3D procedure to H + H$_2$. These results include reactive and nonreactive transition probabilities, integral and differential cross sections, and reagent and product rotational state distributions. These results are extensively compared with those of earlier 3D approximate reactive and nonreactive calculations, and with 1D and 2D accurate ones. Some of the comparisons between the accurate 2D and 3D calculations were considered in preliminary communications,[9,21] and we shall elaborate upon them here by developing simple dynamical models for relating results of different dimensionality. Additional topics considered include the effects of indistinguishability of particles, angular momentum decoupling approximations, and thermal rate constants. In the present calculations, we use the semiempirical Porter–Karplus[2c] potential surface. This surface has been the subject of several earlier studies, thus enabling comparisons of those results and ours without ambiguity being introduced by the use of different potentials. Results for the more accurate surface of Liu[2f] (as parameterized by us) will be deferred to a later publication.

Section II provides a brief outline of the procedure used, and of the computational considerations governing convergence and accuracy. The results for the Porter–Karplus potential energy surface are given in Sec. III, and Sec. IV includes a summary of the more significant conclusions.

II. THE CALCULATION

A. Summarized description of the method

The method used to solve the Schrödinger equation for three-dimensional reactive and nonreactive H + H$_2$ collisions has been extensively described in the preceding paper.[29] The space-fixed and body-fixed coordinates and systems of reference considered are described in Sec. II C and Fig. 2 of that paper. The calculation is done in body-fixed coordinates. Rotational motion is described by quantum numbers j_λ and Ω_λ, where the tumbling quantum number Ω_λ is associated with the tumbling angle ψ_λ and the component of rotational angular momentum along the Oz'_λ (body-fixed) axis which passes through atom A_λ and the center of mass of the $A_\nu A_\kappa$ diatom. As shown previously,[29] the component of the orbital angular momentum about Oz'_λ is zero, so Ω_λ is also associated with the projection of the *total* angular momentum along that axis. In order to simultaneously satisfy both criteria, Ω_λ must obey the inequality

$$\Omega_\lambda \leq \min(J, j_\lambda), \qquad (2.1)$$

where J is the total angular momentum quantum number.

Of crucial significance in the body-fixed coordinate system of Fig. 2 of the preceding paper is the fact[29] that the kinetic energy operator couples vibration–rotation states with different Ω_λ tumbling quantum numbers but the same vibrational and rotational ones $(v_\lambda j_\lambda)$, while the potential energy coupling is diagonal in Ω_λ but not in $v_\lambda j_\lambda$. This allows for the approximate separation of effects due to tumbling of the three atom plane about Oz'_λ from those due to the interaction potential energy, and we shall examine this separation in Sec. III. In addition, it provides for the natural development of centrifugal decoupling schemes, which will be discussed in future publication. Once the body-fixed fully coupled Schrödinger equations are set up, they are solved in two steps. The first one involves a numerical integration of these coupled equations through each arrangement channel region in coordinates appropriate to that region. This is followed by a second step in which the solutions thus generated in each of the three arrangement channel regions are smoothly matched to one another on a set of three surfaces which separate these regions in a symmetrized coordinate space in which all three arrangement channel coordinates are treated equivalently.[31] The resulting solutions, which are smooth and continuous everywhere, are then linearly combined to yield the appropriate reactance and scattering partial wave matrix solutions which are then combined to form the full scattering solutions. By using helicity representation scattering amplitudes, we obtain a very simple relationship between these amplitudes and the body-fixed partial wave scattering matrices S_J, namely [from Eq. (5.31) of the preceding paper],

$$f^{\lambda' v'_\lambda, j'_\lambda, =_{j'_{\lambda'}}}_{\lambda v_\lambda j_\lambda =_{j_\lambda}} = \left(\frac{\overline{V}^\lambda_{v_\lambda j_\lambda}}{\overline{V}^{\lambda'}_{v'_{\lambda'} j'_{\lambda'}}}\right)^{1/2} \frac{1}{2\overline{k}^\lambda_{v_\lambda j_\lambda}} i^{j_\lambda - j'_\lambda +1}$$

$$\times \sum_{J=0}^{\infty} d^J_{=_{j_\lambda}=_{j'_{\lambda'}}}(\theta_{\lambda'}) (\delta^{\lambda' v'_\lambda, j'_\lambda, =_{j'_{\lambda'}}}_{\lambda v_\lambda j_\lambda =_{j_\lambda}} - S^{\lambda' v'_\lambda, j'_\lambda, =_{j'_{\lambda'}}}_{J \lambda v_\lambda j_\lambda =_{j_\lambda}}), \qquad (2.2)$$

where the reagent state has $m_{j_\lambda} = M = -\Omega_\lambda$ and the product state has $m'_{j'_\lambda} = \Omega'_{\lambda'}$, for all J. $\overline{V}^\lambda_{v_\lambda j_\lambda}$ and $\overline{k}^\lambda_{v_\lambda j_\lambda}$ represent the appropriate (unscaled) velocities and wave numbers and

$$d^J_{=_{j_\lambda}=_{j'_{\lambda'}}}(\theta_{\lambda'})$$

is a Wigner rotation function (in the notation of Davydov)[32] of the scattering angle $\theta_{\lambda'}$.

For H + H$_2$, the problem can be simplified considerably because of arrangement channel symmetry and even–odd decoupling within each arrangement channel (as described in the preceding paper). A major consequence of these symmetry properties is that only two scattering amplitudes between a given initial state

vjm_j and final state $v'j'm_j'$ (where m_j' is an abbreviation for $m_{j'}'$) need be considered: the nonreactive (or direct) one (labeled N) and the reactive (or exchange) one (labeled R). Thus all the arrangement channel indices λ and λ' in Eq. (2.2) may be dropped as long as the symbols N or R are included as appropriate. As an additional consequence, nonreactive transitions between even and odd rotational states are forbidden. From the reactive and nonreactive scattering amplitudes f^N and f^R, one may then calculate differential (distinguishable atom) cross sections via

$$\sigma^{N,R}_{vjm_j \to v'j'm_j'}(\theta) = \frac{\overline{V}_{v'j'}}{\overline{V}_{vj}} \left| f^{N,R}_{vjm_j \to v'j'm_j'} \right|^2 , \tag{2.3}$$

so that the integral cross section is given by

$$Q^{N,R}_{vjm_j \to v'j'm_j'} = \frac{\pi}{k_{vj}^2} \sum_{J=0}^{\infty} (2J+1) \left| T^{N,R}_{J,vjm_j \to v'j'm_j'} \right|^2 , \tag{2.4}$$

where

$$T^N_{J,vjm_j \to v'j'm_j'} = \delta^{v'j'm_j'}_{vjm_j} - S^N_{J,vjm_j \to v'j'm_j'} \tag{2.5a}$$

and

$$T^R_{J,vjm_j \to v'j'm_j'} = - S^R_{J,vjm_j \to v'j'm_j'} . \tag{2.5b}$$

The transition probability $P^{N,R}_{J,vjm_j \to v'j'm_j'}$ is given by

$$P^{N,R}_{J,vjm_j \to v'j'm_j'} = \left| S^{N,R}_{J,vjm_j \to v'j'm_j'} \right|^2 . \tag{2.6}$$

If we consider the effects of parity symmetry on the cross sections, we find[33]

$$\sigma^{N,R}_{vjm_j \to v'j'm_j'} = \sigma^{N,R}_{vj-m_j \to v'j'-m_j'} \tag{2.7}$$

with analogous expressions valid for Q and P_j. The angle θ of Eq. (2.3) refers to the direction of the scattered H atom with respect to the reagent H atom beam. For reactive collisions, a more customary angle to use is θ_R, which is the angle of the product H_2 with respect to the incident H, and is the supplement of θ (i. e., $\theta_R = \pi - \theta$).

For $H + H_2$, the physically measurable cross sections must be obtained from wavefunctions which have been properly antisymmetrized with respect to interchange of any two nuclei. This can be done by the technique of postantisymmetrization as was detailed in the preceding paper, and leads to the following indistinguishable-atom differential cross sections (labeled by the symbol A):

$$\sigma^A_{vjm_j \to v'j'm_j'} = \frac{\overline{V}_{v'j'}}{\overline{V}_{vj}} \begin{cases} \left| f^N_{vjm_j \to v'j'm_j'} - f^R_{vjm_j \to v'j'm_j'} \right|^2 & (j,j' \text{ even, para–para}) \\ 3 \left| f^R_{vjm_j \to v'j'm_j'} \right|^2 & (j \text{ even, } j' \text{ odd, para–ortho}) \\ \left| f^R_{vjm_j \to v'j'm_j'} \right|^2 & (j \text{ odd, } j' \text{ even, ortho–para}) \\ \left\{ \left| f^N_{vjm_j \to v'j'm_j'} + f^R_{vjm_j \to v'j'm_j'} \right|^2 + 2 \left| f^R_{vjm_j \to v'j'm_j'} \right|^2 \right\} & (j,j' \text{ odd, ortho–ortho}). \end{cases} \tag{2.8}$$

For para-to-ortho (ortho-to-para) transitions, the antisymmetrized cross sections are proportional to the reactive ones, with a proportionality constant of 3(1), so either quantity gives equivalent information. For other transitions, there will be interference between direct and exchange amplitudes as is implied in Eq. (2.8).

Since the rotational sublevels for a given vibration-rotation state are degenerate, we may define both integral and differential degeneracy-averaged cross sections by (valid for R, N, or A transitions):

$$\sigma_{vj \to v'j'} = \frac{1}{2j+1} \sum_{m_j=-j}^{j} \sum_{m_j'=-j'}^{j'} \sigma_{vjm_j \to v'j'm_j'} \tag{2.9}$$

and

$$Q_{vj \to v'j'} = \frac{1}{2j+1} \sum_{m_j=-j}^{j} \sum_{m_j'=-j'}^{j'} Q_{vjm_j \to v'j'm_j'} . \tag{2.10}$$

We may also sum these cross sections over all final states, obtaining

$$\sigma^N_{vj} = \sum_{v'j'} \sigma^N_{vj \to v'j'} , \tag{2.11}$$

$$\sigma^R_{vj} = 2 \sum_{v'j'} \sigma^R_{vj \to v'j'} , \tag{2.12}$$

$$\sigma^A_{vj} = \sum_{v'j'} \sigma^A_{vj \to v'j'} , \tag{2.13}$$

with analogous expressions holding for the integral cross sections with Q substituted for σ. The factor of 2 in Eq. (2.12) arises from a sum over the two equivalent reactive arrangement channels (in a distinguishable-atom sense). Finally, we may wish to define the cross sections $\sigma^A_{vj \text{-para(ortho)}}$ in which the final state is restricted to being para (ortho). The corresponding expression is analogous to Eq. (2.13) with the sum over j' in the right-hand side restricted to even (odd) values, and a similar equation defines the integral cross section $Q^A_{vj \text{-para(ortho)}}$.

B. Convergence and accuracy tests and calculational details

In order to establish the reliability of the results of these calculations, a number of convergence and accuracy tests were performed, including (a) tests of flux conservation and microscopic reversibility, (b) tests of invariance of the results with respect to the inclusion of additional vibrational or rotational basis functions in the close coupling expansion, (c) tests of invariance of the results with respect to a change in the number of

TABLE I. Nonreactive (N) and reactive (R) transition probability matrices for $E = 0.60$ eV, $J = 0$.[a]

$(v'j')$ (vj)	(00)	(01)	(02)	(03)	(04)	(05)	(06)
				N				
(00)	0.0538	0	0.739	0	0.0195	0	0.398(-8)
(01)	0	0.460	0	0.226	0	0.215(-3)	0
(02)	0.741	0	0.0690	0	0.0303	0	0.761(-8)
(03)	0	0.226	0	0.742	0	0.219(-2)	0
(04)	0.0196	0	0.0304	0	0.948	0	0.822(-7)
(05)	0	0.222(-3)	0	0.219(-2)	0	0.998	0
(06)	0.328(-8)	0	0.642(-8)	0	0.867(-7)	0	1.000
				R				
(00)	0.0249	0.0422	0.0219	0.425(-2)	0.251(-3)	0.249(-5)	0.334(-9)
(01)	0.0415	0.0713	0.0361	0.694(-2)	0.410(-3)	0.393(-5)	0.558(-9)
(02)	0.0220	0.0368	0.0183	0.331(-2)	0.177(-3)	0.172(-5)	0.279(-9)
(03)	0.421(-2)	0.699(-2)	0.327(-2)	0.537(-3)	0.273(-4)	0.338(-6)	0.544(-10)
(04)	0.257(-3)	0.411(-3)	0.183(-3)	0.280(-4)	0.177(-5)	0.462(-7)	0.431(-11)
(05)	0.280(-5)	0.451(-5)	0.202(-5)	0.406(-6)	0.601(-7)	0.215(-8)	0.116(-12)
(06)	0.197(-9)	0.318(-9)	0.147(-9)	0.285(-10)	0.337(-11)	0.113(-12)	0.767(-17)
Sums[b]	1.0005	1.0018	0.9981	0.9997	1.0000	1.0000	1.0000

[a]All projection quantum numbers m_j and m'_j are zero. Numbers in parentheses indicate the power 10 by which the number preceding it should be multiplied.
[b]Sum of probabilities from a given initial state over all possible final states and arrangement channels.

terms used to expand the potential [see Eq. (2.14) below], and (d) tests of invariance of the results with respect to a change in the nature of the reference potential $V_{ref}(r_1, R_1)$[20] used to generate vibrational basis functions for the integration. Two additional tests are (e) the invariance of the results with respect to a change in the matching surface basis functions, and (f) the effects of lack of completeness of these matching surface functions on the ortho to para nonreactive transition probabilities. These latter two tests were not performed, but the analogous planar tests[13b] indicated that both effects were not important in that calculation. Since comparable planar and 3D vibration–rotation basis sets and matching surface functions were used in the two sets of calculations, we have assumed that the matching surface basis functions of Eq. (4.28) of the preceding paper will produce adequate (5% or better) convergence of the 3D results.

Conservation of flux and microscopic reversibility may be tested by examining the probability matrices for each partial wave, an example of which is given in Table I for total energy $E = 0.6$ eV and $J = 0$. Flux conservation requires that the sum of each row or column of P_J should equal unity, while microscopic reversibility requires that P_J be symmetric. In the table we see that both of these properties are well satisfied (0.18% maximum deviation from flux conservation and 3% from symmetry for probabilities greater than 10^{-4}). In the results presented in this paper, we consider the energy range 0.3–0.7 eV. For energies E in the range 0.3–0.6 eV (including all J), we find maximum deviations from flux conservation of 1% and from symmetry 10% (for nonnegligible probabilities). Between 0.6 and 0.7 eV we find 4% maximum deviations from flux conservation and 15% from symmetry. In order to obtain re-

sults of this quality, we used the vibration–rotation basis sets specified in Table II. For $J = 0$, Eq. (2.1) greatly reduces the number of channels coupled, thus reducing computation time, allowing us to use more complete basis sets. This leads to excellent results for the $J = 0$ probabilities (with accuracies similar to or better than those in Table I at all energies considered). However, for larger J, the number of projections Ω increases greatly. This leads to prohibitively large computation times if basis sets analogous to those for $J = 0$ are used. The ones actually used are those described in Table II. The above mentioned accuracy limits were obtained with them.

Convergence with respect to the inclusion of additional vibrational or rotational channels is examined in Table III. In Part A of that table, we examine several important transition probabilities at $E = 0.65$ eV, $J = 1$ for three different rotational basis sets (all with four vibrations). Upon changing from a $j_{max} = 5$ to a $j_{max} = 6$ basis set, we find changes of less than 1% in all probabilities. In Part B we examine several 0.65 eV, $J = 0$ probabilities with four and five vibrations (all with $j_{max} = 7$). Here we find 4% maximum change. An examination of the nature of the convergence properties with respect to the inclusion of additional basis functions was examined in greater detail in the planar calculation[13b] where we found that typically four vibrations and $j_{max} = 5$ were required for 5% convergence. A less extensive study of the three-dimensional results indicates similar convergence properties and the results of Table III are in agreement with this statement.

The two criteria (c) and (d) mentioned at the beginning of this section refer to changes in the representation of the potential $V^\lambda(r_\lambda, R_\lambda, \gamma_\lambda)$ [where γ_λ is the angle

TABLE II. Basis sets used and associated computation times for each partial wave.

					Computation times (IBM 370/158)[c]		
J	No. of vibrations	j_{MAX}[a]	Total No. of rotational states	N[b]	Number of channels	Integration time (min)	Total time (min)
0	4–6	7–11	8–12	32–60	40	11	14
1	4 or 5	5 or 6	14 or 18	56–90	90	42	54
2	4	5	22	88	88	37	48
3	4	4 or 5	20 or 26	92[d]	92	36	47
≥ 4	4	4 or 5	20 or 30	100[e]	100	47	61

[a]j_{MAX} is the largest value of j within each rotational manifold.
[b]Total number of channels included in each arrangement channel.
[c]Computation times are for double precision arithmetic and the number of channels indicated and apply to computations for which both ortho–para and parity decoupling are used. The difference between the total time and the integration time is the time used in the matching procedure and asymptotic analysis.
[d]Refers to a basis with 26 rotational states for $v = 0$, 1, and 20 for $v = 2, 3$.
[e]Refers to a basis with 30 rotational states for $v = 0$, 1, and 20 for $v = 2, 3$.

between R_λ and r_λ (Fig. 1 of preceding paper)], and in the character of the reference potential $V^\lambda_{ref}(r_\lambda, R_\lambda)$ used to generate the vibrational eigenfunctions. As detailed in the preceding paper, the potential is expanded in a series of Legendre polynomials

$$V^\lambda(r_\lambda, R_\lambda, \gamma_\lambda) = \sum_{k=0}^{\infty} V^\lambda_k(r_\lambda, R_\lambda) P_k(\cos\gamma_\lambda), \quad (2.14)$$

where, for an atom plus homonuclear diatomic molecule system like $H + H_2$, the sum over k includes only even terms. In an actual calculation, Eq. (2.14) is truncated after n terms (such as $n = 3$). This procedure is justified if the resulting probabilities are not significantly changed when an additional term is added. To evaluate the effects of changing n, we compare in Table IV the results of calculations with $n = 2, 3, 4,$ and 5[34] for selected transition probabilities at two different energies. Although the $n = 2$ results are often significantly in error (by as much as 30%), we find less than 7% changes in going from $n = 3$ to $n = 4$ and virtually no change at all in going from $n = 4$ to $n = 5$. All calculations of this paper other than those whose results are presented in Table IV used $n = 3$. The reference potential V^λ_{ref} which is used to numerically generate the vibrational basis functions according to the procedure of Ref. 29 still allows for some freedom of choice in the interaction region due to nonseparability of vibrational motions from translational or rotational ones. In the coplanar calculations, two different choices of the reference potential $[V^\lambda_{ref} = V(r_\lambda, R_\lambda, \gamma_\lambda = 0)$ and $V^\lambda_{ref} = V^\lambda_0(r_\lambda, R_\lambda)]$ were used. A comparison of these calculations indicated that for basis sets with four or more vibrations, the results from the two reference potentials differed by less than 5%. A limited number of three-dimensional calculations indicates a behavior comparable to the planar case.

III. RESULTS FOR THREE-DIMENSIONAL H + H₂

A. Transition probabilities

In this section we examine the J dependence of the reactive and inelastic transition probabilities in the energy range 0.3–0.7 eV. Figures 1(a) and 2(a) present the

reactive probabilities $P^R_{J,00-01}$ (summed over final m'_j). These figures indicate that the probability is a rapidly decreasing function of J with a peak near $J = 0$ for all but the highest energy considered. If we define J_{MAX} as the lowest value of J for which $P^R_{J,vj-v'j'}$ has decreased to less than 1% of its maximum value, then J_{MAX} is 4 at 0.3 eV and increases monotonically to about 10 at 0.7 eV. The contributions of these transition probabilities to the integral reaction cross sections are weighted by the factor $2J + 1$ [see Eqs. (2.4)–(2.6)]. Figures 1(b) and 2(b) depict the product $(2J + 1)$

TABLE III. Nonreactive and reactive transition probabilities for $E = 0.65$ eV.

Transition $(vj \to v'j')$	Reactive or nonreactive	Basis set		
		$a(N = 56)$	$b(N = 72)$	$c(N = 64)$
A. $J = 1$, $m_j = m'_j = 0$				
00 → 02	N	0.531	0.527	0.531
01 → 03	N	0.193	0.186	0.186
00 → 00	R	0.0404	0.0408	0.0402
00 → 01	R	0.0740	0.0741	0.0739
01 → 01	R	0.134	0.135	0.134
		$d(N = 32)$	$e(N = 40)$	
B. $J = 0$, $m_j = m'_j = 0$				
00 → 02	N	0.517	0.512	
01 → 03	N	0.223	0.216	
00 → 00	R	0.0432	0.0434	
00 → 01	R	0.0780	0.0802	
01 → 01	R	0.145	0.150	

Basis sets[a]

a. 4 vibrations, 14 rotations/vibration ($j_{MAX} = 5$)
b. 4 vibrations, 18 rotations/vibration ($j_{MAX} = 6$)
c. 4 vibrations, 18 rotations for $v = 0, 1$; 14 for $v = 3, 4$
d. 4 vibrations, 8 rotations/vibration ($j_{MAX} = 7$)
e. 5 vibrations, 8 rotations/vibration ($j_{MAX} = 7$)

[a]In each basis set, all values of the projection quantum numbers compatible with angular momentum restrictions and with matching restrictions were included (see Sec. II A and preceding paper).
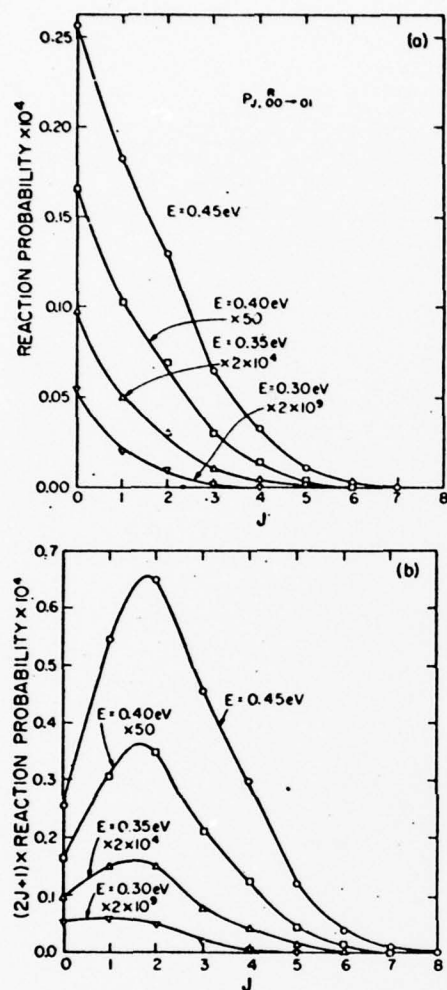
FIG. 1. (a) Reaction probability $P_{J,00\to01}^{R}$ (summed over final m_j') as a function of J for total energies $E = 0.30$, 0.35, 0.40, and 0.45 eV. (b) The same reaction probabilities multiplied by $2J+1$. The scale factors indicated for the last three energies are the numbers by which the probabilities were multiplied before being plotted.

$\times P_{J,00\to01}^{R}$, and we see that the partial wave which gives the largest contribution to $Q_{00\to01}^{R}$ varies from $J=1$ at 0.3 eV to $J=4$ at 0.7 eV. To examine the contributions of the different projection quantum numbers to the curves in Figs. 1(a) and 2(a), we plot in Fig. 3 the reaction probabilities $P_{J,000\to01m_j'}^{R}$ for $m_j' = 0$, ± 1 (and their sum) at $E = 0.3$ eV. It is apparent from the figure that $m_j' = 0$ makes the dominant contribution to $P_{J,00\to01}^{R}$ for this transition at all J for which the transition probability is nonnegligible. The $m_j' = \pm 1$ probability [which, from the P_J analog of Eq. (2.7), is independent of the sign of m_j'] shows a peak near $J = 4$ followed by a somewhat slower de-

crease with increasing J than is exhibited by the $m_j' = 0$ probability. An examination of other transition probabilities at 0.6 eV indicates that in general, the $m_j = 0$ to $m_j' = 0$ reaction probability is the dominant one for a given vj and $v'j'$. This effect becomes less important as either J, j, or j' increase, as is illustrated in Fig. 4 for the probability $P_{J,000\to03m_j'}^{R}$, but it remains a general fact that the $m_j = m_j' = 0$ transition probability is the largest one for $J < J_{MAX}$ and $j \leq 4$. This statement is also true for other energies considered. Its effect on the integral cross sections will be discussed in Sec. IIIC.

Let us now consider the meaning of this rotational
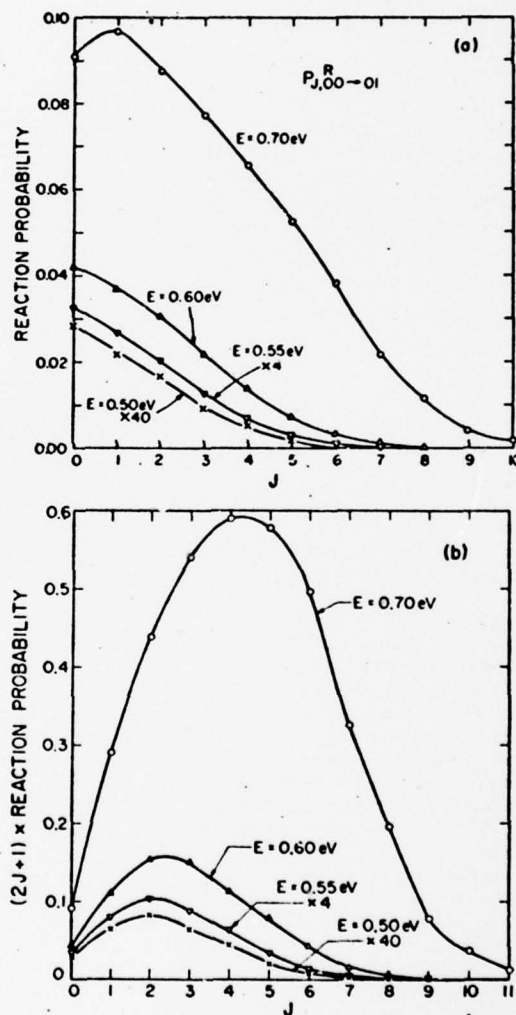
FIG. 2. (a) Reaction probability $P_{J,00\to01}^{R}$ analogous to Fig. 1 as a function of J at $E = 0.50$, 0.55, 0.60, 0.65, and 0.70 eV. (b) $2J+1$ times these reaction probabilities. Scale factors have the same meaning as in Fig. 1.

TABLE IV. Convergence of selected[a] nonreactive and reactive transition probabilities with respect to number of terms included in expansion of $V(r_\lambda, R_\lambda, \gamma_\lambda)$.[b]

Energy	$(vj) \rightarrow (v'j')$	Reactive or nonreactive	Number of terms			
			2	3	4	5
0.55 eV	00→02	N	0.737	0.707	0.706	0.706
	01→03	N	0.153	0.161	0.161	0.161
	00→00	R	0.720(-2)	0.483(-2)	0.511(-2)	0.511(-2)
	00→01	R	0.0119	0.811(-2)	0.838(-2)	0.847(-2)
	01→01	R	0.0206	0.0130	0.0135	0.0135
0.625 eV	00→02	N	0.605	0.642	0.629	0.624
	01→02	N	0.206	0.225	0.224	0.220
	00→00	R	0.0400	0.0353	0.0372	0.0377
	00→01	R	0.0726	0.0641	0.0655	0.0673
	01→01	R	0.128	0.115	0.117	0.120

[a]Only $J = m_j = m'_j = 0$ transition probabilities are considered in this comparison. Notation is analogous to Table I. Numbers in parentheses indicate the power of 10 by which the numbers preceding them should be multiplied.
[b]The expansion is given in Eq. (2.14).

projection quantum number "quasi selection rule." In the helicity representation being used, the rotational wavefunction of the diatom at large distances from the atom is $Y_{j_\lambda m_\lambda}(\gamma_\lambda, \psi_\lambda)$ before the collision (except for a phase factor) and

$$Y_{j'_\lambda m'_{j_\lambda}}(\gamma_{\lambda'}, \psi_{\lambda'})$$

after the collision. For the Porter–Karplus potential used,[2c] linear orientations, corresponding to γ_λ and $\gamma_{\lambda'}$ equal to 0 or π, greatly favor reaction over other orientations. (The linear barrier height is 0.396 eV, while the perpendicular one is about 2.8 eV.) Since those spherical harmonics have nodal lines along these directions unless the polar component of the angular momentum vanishes, we conclude that the $m_j = m'_j = 0$ reaction probabilities should be larger than all others, in agreement with our results. This can be visualized classi-

cally by recalling that initially $\Omega = -m_j$ so that $m_j = 0$ implies (for nonzero j) that the axis of rotation is perpendicular to the direction of approach, as schematically indicated in Fig. 5. In this situation, twice during each diatom rotation the three atoms go through a collinear configuration (for zero impact parameter collisions). For $m_j \neq 0$ no collinear configurations are sampled. After the collision, $m'_j = \Omega'$ so that again only for $m'_j = 0$ can we have a postcollision linear orientation (regardless of the scattering angle). We should also note that the isolated diatom rotational period $\{2.7 \times 10^{-13} / [j(j+1)]^{1/2} \text{ sec}\}^3$ is generally larger than the interaction time (which is less than 3×10^{-14} sec [35] for the energies considered here) so that the rotational motions are generally slow compared to collision times at these energies and the collision orientation does not change rapidly during the approach and departure steps. This
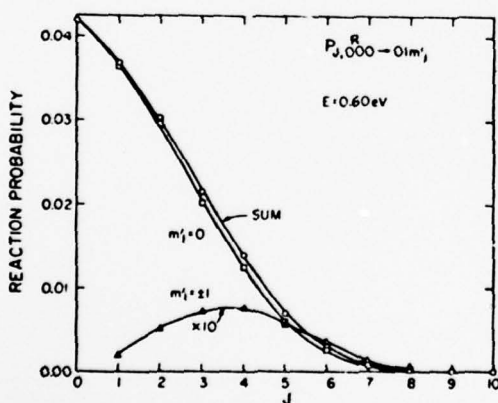
FIG. 3. Reaction probability $P^R_{J,000 \rightarrow 01m'_j}$ vs J for $m'_j = 0, \pm 1$ at 0.60 eV total energy ($E_0 = 0.328$ eV). Curve labeled sum is the sum of the probabilities over m'_j. Scale factor has the same meaning as in Fig. 1.
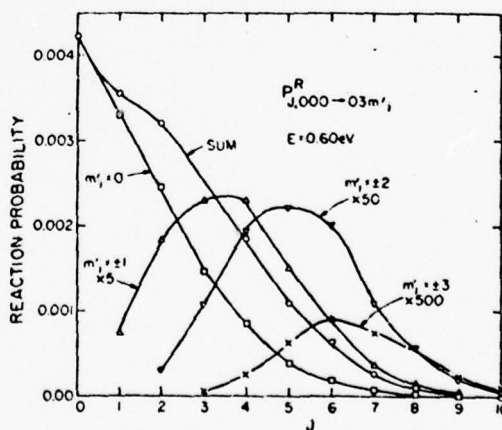
FIG. 4. Reaction probability $P^R_{J,000 \rightarrow 03m'_j}$ vs J for $m'_j = 0, \pm 1, \pm 2, \pm 3$ at 0.60 eV total energy, analogous to Fig. 3.
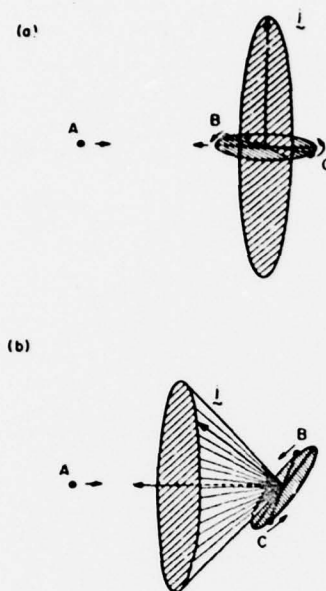
FIG. 5. Influence of projection quantum number m_j (for $j > 0$) on the allowed relative orientations of atom (A) with respect to diatom (BC) for zero impact parameter collisions: (a) $m_j = 0$ initially so that the rotational angular momentum vector is perpendicular to direction of relative motion; (b) $m_j \neq 0$ initially so that the j vector lies on a cone about the relative motion vector and makes an acute angle with it. In both (a) and (b) the rotation plane of the diatom is indicated by the smaller ellipse.

analysis indicates not only that the $m_j = m'_j = 0$ reaction probability should be larger than all others, as pointed out above, but also explains why this rule becomes less rigid for large J (in which case nonzero impact parameter collisions can lead to linear orientations for m_j, $m'_j \neq 0$) and for large j (where the diatom rotates fast enough to change the orientation rapidly during the collision, thus reducing the advantage of a linear orientation at any one point during the collision). As a second prediction of this model, we would expect that those transition probabilities for which $m_j = 0$ or $m'_j = 0$ (but not both) and the corresponding integral reaction cross sections should dominate over those for which neither m_j nor m'_j are zero. We shall see in Sec. IIIC that this prediction is correct. We emphasize that this projection quantum number selection rule presupposes (a) a potential surface which favors linear orientations, and (b) that the projection quantum numbers are referenced to the body fixed coordinate system of Fig. 2 of the preceding paper. The latter condition is important because it singles out the m_j or $m'_j = 0$ collisions as leading to a linear collision orientation with a greater probability than m_j or $m'_j \neq 0$. By rotating the quantization axis to another direction (such as one perpendicular to the three-atom plane as is done for the coplanar reaction, or along a space-fixed direction), the body-fixed projections would become mixed and we would not be able to unscramble the information as easily.

Figure 6 shows the J dependence of the phases of the scattering matrix elements $S^R_{J,000-01m'_j}$ for $m'_j = 0, \pm 1$ at 0.6 eV (the same transitions considered in Fig. 3). It is important to note that the phase is most slowly varying near $J = 0$. Semiclassically this implies that the deflection angle should be small for small impact parameter collisions. [36] This implies that a small scattering angle θ will result from these low J collisions, or, equivalently, a reactive scattering angle θ_R near 180°.

In Fig. 7(a) we examine the nonreactive transition probability $P_{J,000-02m'_j}$, and its sum over final m'_j at 0.6 eV as a function of J. Here we find $J_{MAX} = 30$, so that a much larger number of partial waves contribute to the nonreactive cross section than is the case for the reactive transitions in Figs. 1-4. Note that the $m'_j = 0$ transition probability is dominant only for very small J (< 3) indicating that the linear orientation rule is probably not significant here (as might be expected for a nonreactive collision where the nature of the potential in the transition state is of lesser significance than it is for reactive collisions). An examination of other nonreactive transition probabilities indicates no strong tendency for a $m_j = -m'_j$ ($\Omega = \Omega'$) "j_z-conserving" selection rule as has been assumed in rotationally inelastic scattering, [37] thus indicating that the strong coupling or sudden limit does not apply to $H + H_2$ inelastic collisions for the potential used. We shall examine this subject in a separate publication. The transition probabilities of Fig. 7(a) may also be expressed in terms of the orbital angular momentum quantum number l (as might be used in a space-fixed analysis) by performing a unitary transformation on the body-fixed scattering matrix [see Eqs. (5.14) and (5.15) of Ref 29]. Figure 7(b) indicates the resulting transition probabilities for $E = 0.60$ eV (the sum over projections
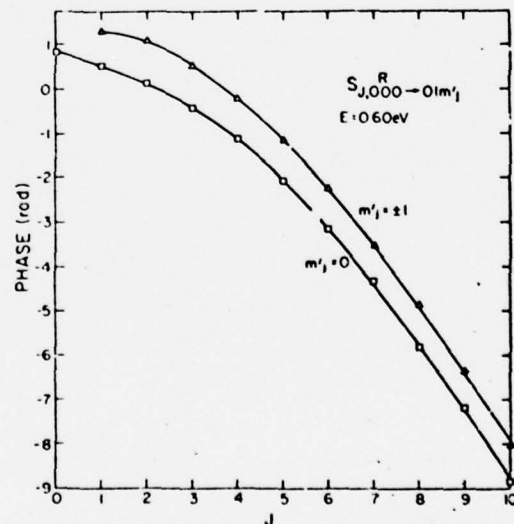
FIG. 6. Phases of $S^R_{J,000-01m'_j}$ for $m'_j = 0, \pm 1$ as a function of J at $E = 0.60$ eV.

being an invariant). Here we again see no particular
selection rule governing the transition probabilities.

B. Differential cross sections

In Figs. 8 and 9 we plot the antisymmetrized para-
to-ortho differential cross sections σ_{00-01}^A as a function
of the reactive scattering angle θ_R. From Eqs. (2.3)
and (2.8) it should be apparent that these cross sections
are just 3 times the distinguishable atom σ_{00-01}^R. We
see in both figures that the reactive cross section is
strongly backward peaked at all energies considered in
the calculation. The width of the backward peak at
half-maximum is 48°, 32°, 33°, 41°, and 51° at $E = 0.3$,
0.4, 0.5, 0.6, and 0.7 eV, respectively. At the thresh-
old energy of the process considered, one would nor-
mally expect isotropic scattering since only the $J = 0$
partial wave would contribute to the cross section. At
0.3 eV, Fig. 1 indicates that partial waves other than
$J = 0$ still contribute significantly ($J_{MAX} = 4$), so that the
differential cross section is backward peaked, but
rather broad. The width of this peak decreases with
increasing energy above 0.3 eV to a minimum near
0.4 eV. As E increases further, the width begins to
increase, presumably as a result of increased con-
tributions of larger impact parameter collisions (from
Figs. 1, 2) to the reaction cross section.

As was the case in the coplanar reaction,[13b] the shape
of the differential cross section is a sensitive test of
the accuracy of the calculation. Small inaccuracies in

FIG. 8. Differential cross sections σ_{00-01}^A as a function of the
reactive scattering angle $\theta_R = 180° - \theta$ at the same energies as
were considered in Fig. 1. Scale factors have the same mean-
ing as in that figure.

FIG. 7. (a) Nonreactive body-fixed transition probability
$P_{J,000-02m_j'}^N$ as a function of J at 0.60 eV total energy for $m_j' = 0$,
± 1, ± 2. Curve labeled sum is the sum of these five prbabili-
ties. (b) Analogous space-fixed probabilities for the three or-
bital angular momenta $l' = J$, $J + 2$, $J - 2$. The sum is invariant
to the use of body-fixed or space-fixed representations.
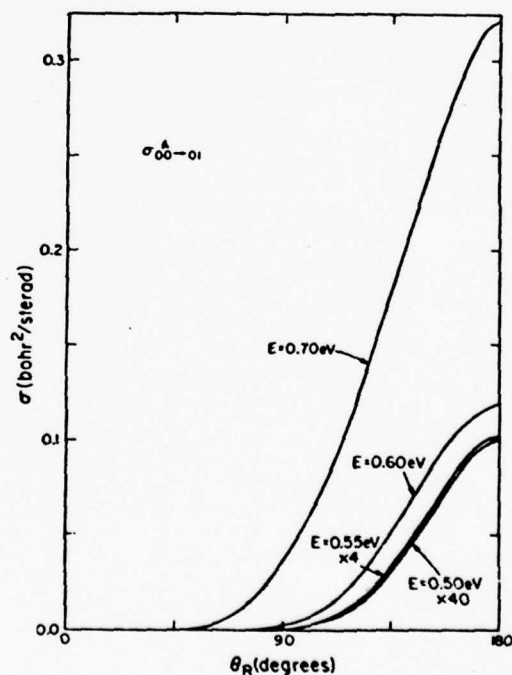
FIG. 9. Differential cross sections σ_{00-01}^A, as in Fig. 8 for the
same energies considered in Fig. 2. Scale factors have the
same meaning as in Fig. 1.
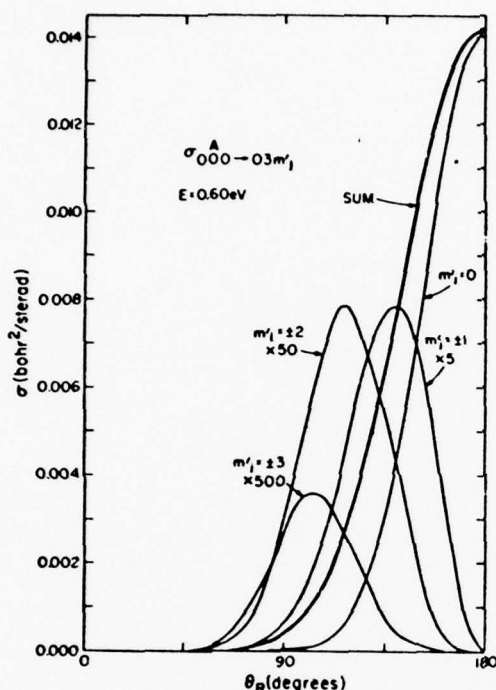
FIG. 10. Differential cross section $\sigma^A_{000-03m'_j}$ as a function of reactive scattering angle $\theta_R = 180° - \theta$ for $m'_j = 0, \pm 1, \pm 2, \pm 3$ at $E = 0.60$ eV. Curve labeled sum is the sum of all seven cross sections and is equal to the degeneracy-averaged σ^A_{00-03}. Scale factors have the same meaning as in Fig. 1.

either the magnitudes or phases of the scattering matrix elements for any partial wave can result in spurious oscillations in the differential cross sections. In addition, premature truncation of the partial wave sum [Eq. (2.2)] can lead to a spurious forward peaking. In order to avoid such spurious oscillations in the cross sections, we checked convergence at several values of J (by the criteria of Sec. II B) and found that equivalent convergence had been attained at all J. [Recall from Table II that the nature of the vibration–rotation basis set has to be changed for each $J(J \leq 4)$.] Premature truncation of the partial wave sum was avoided by requiring that the reactive probabilities at the cutoff value J_c be no larger than 10^{-4} times those at $J = 0$. In general, we found $J_c \sim J_{MAX} + 5$. Both Figs. 8 and 9 show essentially no indication of spurious oscillations or forward peaking (typically the $\theta_R = 0$ cross section is 200 to 1000 times smaller than the $\theta = 180°$ result). We should also note that the appearance of Figs. 8 and 9 is quite typical of all degeneracy-averaged para-to-ortho and ortho-to-para cross sections.

To examine the m_j dependence of the differential cross sections, we plot in Fig. 10 $\sigma^A_{000-03m'_j}$ for $m'_j = 0, \pm 1, \pm 2, \pm 3$, and their sum. (The corresponding probabilities were considered in Fig. 4.) We see that only the $m'_j = 0$ projection gives scattering peaked in the back-

ward $\theta_R = 180°$ direction. As $|m'_j|$ increases from zero, we find a shift towards more forward scattering with the cross sections peaking at $\theta_R = 139°$, $117°$, and $102°$ for $|m'_j| = 1, 2, 3$, respectively. Much of the structure of the angular distributions in Fig. 10 can be understood by examining Eq. (2.2). The Wigner rotation function[32] $d^j_{0m'_j}(\theta)$ is proportional to the associated Legendre function $P^{m'_j}_j(\cos\theta)$ and is therefore proportional to $(\sin\theta)^{|m'_j|}$ times a polynomial in $\cos\theta$. Since $\theta_R = \pi - \theta$, the $\sigma^A_{000-03m'_j}$ should have a $(\sin\theta_R)^{2|m'_j|}$ envelope and, for $m'_j \neq 0$, vanish at $\theta_R = 0$ and $180°$. Indeed, one can qualitatively obtain the $m'_j = \pm 1$ curve by multiplying the $m'_j = 0$ one by $\sin^2\theta_R$ and similar prescriptions can be used for the higher m'_j curves. The vanishing of the $m'_j \neq 0$ cross sections at $\theta_R = 0°$ and $180°$ is also a consequence of angular momentum conservation. To see this, we recall that the incident plane wave solution is an eigenfunction of J_z, the operator corresponding to the projection of the total angular momentum along the space-fixed z axis, with eigenvalue $M = m_i$ (since m_i, the z component of the orbital angular momentum, is initially zero for the plane wave solution). Since J_z commutes with the Hamiltonian,[38] M will be a good quantum number, i.e., $J_z \Psi^{Mλ}[P] = M\hbar\Psi^{Mλ}$ everywhere in configuration space. In particular, for $\theta_R = 0°$ (180°), the final Oz'_i axis[39] will be antiparallel (parallel) to the initial Oz axis, so that conservation of J_z requires that the outgoing projection quantum number m'_j must equal $-M(+M)$, unless the corresponding scattering amplitude vanishes in that direction. Therefore, if the corresponding scattering amplitudes do not vanish, we must have $m_j = M = -m'_j$ for $\theta_R = 0°$ and $m_j = M = m'_j$ for $\theta_R = 180°$. Applying this reasoning to the $\sigma^A_{000-03m'_j}$ cross section, we conclude that for $m'_j \neq 0$, J_z cannot be conserved for $\theta_R = 0°$ or $\theta_R = 180°$ unless that cross section vanishes in both of those directions, in agreement with the conclusion reached above. Finally we should point out that the dominance of the $m'_j = 0$ component of $\sigma^A_{000-03m'_j}$ in Fig. 10 is again a consequence of the favored linear transition state geometry, discussed in Sec. III A. The $m'_j = 0$ collisions for small impact parameters have a significant reaction probability only for linear or nearly linear configurations which leads to the observed dominant backward scattering for this transition. For $m'_j \neq 0$, the collision configurations are nonlinear (at least in the product arrangement channel) and we would expect to see the sidewards scattering exhibited in Fig. 10.

In Fig. 11 we plot the nonreactive differential cross sections $\sigma^v_{000-02m'_j}$ ($m'_j = 0, \pm 2$, and summed) at $E = 0.6$ eV as a function of θ. Here the predominant scattering direction is approximately $90°$ although significant cross sections are obtained at all angles. The structure in these curves in the forward direction ($\theta < 15°$) may be a spurious artifact introduced by small errors in the phases of certain large J elements of S_J (see related discussion of Ref. 22). Our previous analysis regarding the individual m'_j cross sections in the $\theta = 0°$ and $180°$ directions applies to Fig. 11 as well. We note, however, that the absence of a linear or near linear orientation restriction in nonreactive collisions leads to significant cross sections at all m'_j and at all
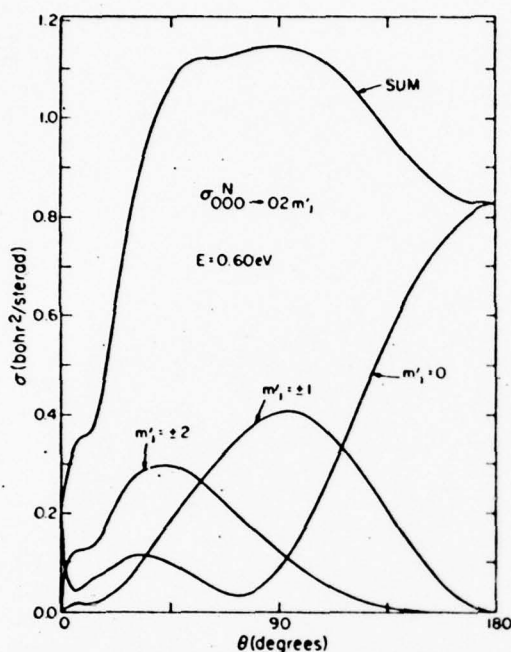
FIG. 11. Differential nonreactive cross section $\sigma_{000-02m_j'}^N$ as a function of scattering angle θ for $m_j' = 0, \pm 1, \pm 2$ at $E = 0.60$ eV. Curve labeled sum is the sum of all five cross sections and is equal to the degeneracy-averaged σ_{00-02}^N.
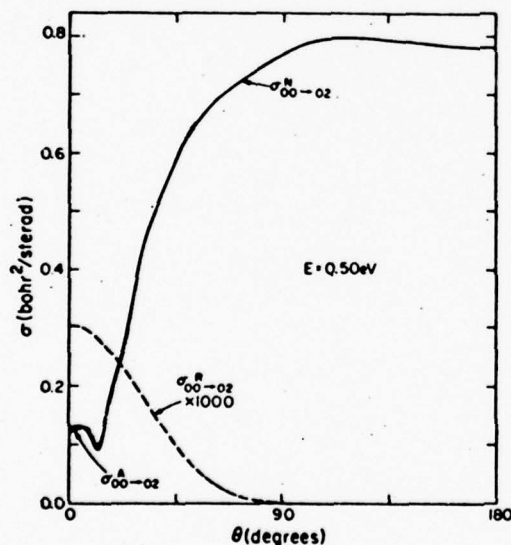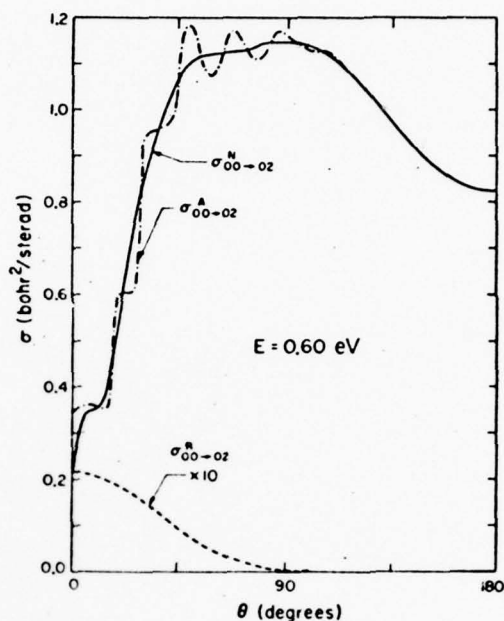

FIG. 13. Degeneracy-averaged σ_{00-02}^N, σ_{00-02}^R, and σ_{00-02}^A analogous to Fig. 11 but at $E = 0.60$ eV ($E_0 = 0.328$ eV).

FIG. 12. Degeneracy-averaged differential cross sections σ_{00-02}^N, σ_{00-02}^R, and σ_{00-02}^A as a function of scattering angle θ at $E = 0.50$ eV ($E_0 = 0.228$ eV). The nonreactive and antisymmetrized curves are essentially identical for $\theta > 20°$. Note the use of θ rather than θ_R for plotting the reactive differential cross section. The scale factor has the same meaning as in Fig. 1.

scattering angles not too close to these directions. Since the $j = 0$ to $j' = 2$ transition can occur by both nonreactive and reactive mechanisms, the more meaningful quantity to consider is the antisymmetrized cross section of Eq. (2.8). In Figs. 12, 13, and 14 we plot this para-to-para cross section σ_{00-02}^A (summed over m_j') along with the nonreactive and reactive counterparts at $E = 0.5$, 0.6, and 0.7 eV. At the lowest energy, the reactive cross section is typically 3 orders of magnitude smaller than the nonreactive one, so the resulting para-to-para cross section is dominated by the direct amplitude and differs very little from its nonreactive counterpart. As the energy is increased, the reactive amplitude increases rapidly and begins to interfere significantly with the nonreactive one. This results in the oscillations observed in σ_{00-02}^A in Figs. 13 and 14. The period of these quantum symmetry oscillations seems to be roughly 10°–15° in both Figs. 13 and 14 for $\theta < 90°$ with a gradual increase in period with increasing θ until the oscillations wash out completely at large θ. Figures 12–14 also indicate that the peak in σ_{00-02}^N shifts gradually to forward scattering angles (corresponding to backward reactive scattering angles) as the energy is increased. The contributions of different m_j' to σ_{00-02}^A at 0.7 eV are shown in Fig. 15 (along with the distinguishable atom $\sigma_{000-02m_j'}^N$ for comparison). We see that the oscillations in the cross section are largest for $m_j' = 0$ followed by $m_j' = \pm 1$ and $m_j' = \pm 2$. This results from the dominant role of the $m_j' = 0$ reactive scattering amplitude (as evidenced in Fig. 10) followed in importance by the $m_j' = \pm 1$ and the $m_j' = \pm 2$ contributions. Note also that the phases of the oscillations in
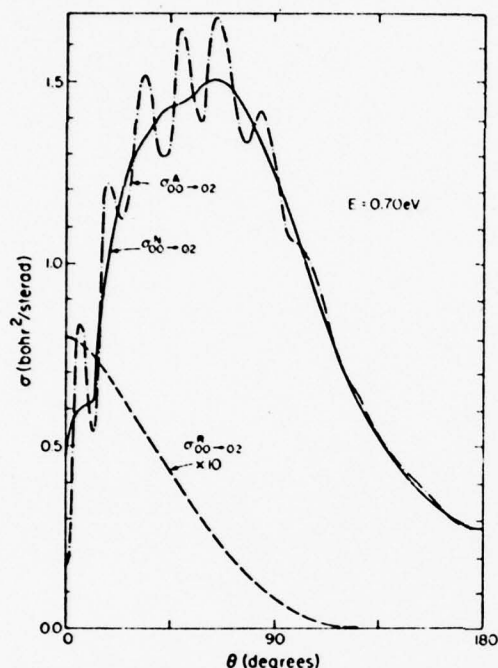
FIG. 14. Degeneracy-averaged σ_{00-02}^N, σ_{00-02}^R, and σ_{00-02}^A analogous to Fig. 11 but at 0.70 eV ($E_0 = 0.428$ eV).

Fig. 15(a), (b), and (c) are not particularly coherent, so that a certain amount of cancellation occurs in the sum over projections shown in Fig. 14.

C. Integral cross sections and product polarization

A number of reactive, nonreactive and antisymmetrized integral cross sections are listed in Table V. Some of the reactive and para-to-ortho cross sections of that table are plotted as a function of energy in Fig. 16. Both logarithmic and linear scales are used to exhibit the tunnelling and the threshold regions. If we define the effective threshold energy E_T as that energy for which the cross section is 0.05 bohr^2, then $E_T = 0.545$, 0.550, and 0.615 eV for Q_{000}^R, Q_{00-01}^A, and Q_{00-03}^A, respectively. Alternatively, since somewhat above the threshold region the energy dependence of the cross sections is linear, we could define an effective threshold energy E_T' as the energy at which a line fitted to the points in this linear region extrapolates to zero cross section. From this definition, we find $E_T' = 0.568$, 0.565, and 0.605 eV for these same cross sections, respectively. Either way we find that the threshold energies are considerably greater than the barrier height (0.396 eV), and this fact will be discussed in detail in Sec. III E. At energies below the effective threshold, the effects of tunnelling give the cross section an approximately exponential dependence on translational energy E_0.

To examine the m_j dependence of the cross sections,

we list in Table VI a portion of the "cross section matrix" $Q_{0jm_j-0j'm_j'}^R$ for j, $j' \le 2$ at 0.6 eV. (Note that these cross sections are distinguishable reactive ones.) The table indicates that the $m_j = m_j' = 0$ cross section is typically 10–20 times larger than any other one with the same vj and $v'j'$. In addition, for given vjm_j and $v'j'$, Q is a decreasing function of $|m_j'|$ (and, by microscopic reversibility, for given vj and $v'j'm_j'$, Q decreases with $|m_j|$). These observations are indicative of the very significant product rotational angular momentum polarization effect that can occur when only a restricted range of collision geometries can lead to reaction. This approximate selection effect breaks down eventually for large enough j or j'. Let us consider the cross sections $Q_{000-0j'm_j'}^R$ for varying j' and m_j' at 0.6 eV. The ratio of the $m_j' = 0$ to the $m_j' = \pm 1$ cross section is 22.3 for $j' = 1$ decreasing to 7.1 for $j' = 2$, 3.1 for $j' = 3$ and 1.1 for $j' = 4$. The $j' = 1$ ratio is 10.6, 24.7, 24.9, 22.3, and 14.7 at $E = 0.3$, 0.4, 0.5, 0.6, and 0.7 eV, respectively, indicating that this selection rule is most rigorously obeyed in the range of energies just below the effective threshold. We shall examine the dependence of the degeneracy-averaged reactive integral cross sections on j and j' in Sec. III F.

The nonreactive degeneracy-averaged cross sections Q_{00-02}^N are listed in Table V. At 0.6 eV, the $Q_{000-02m_j}^N$
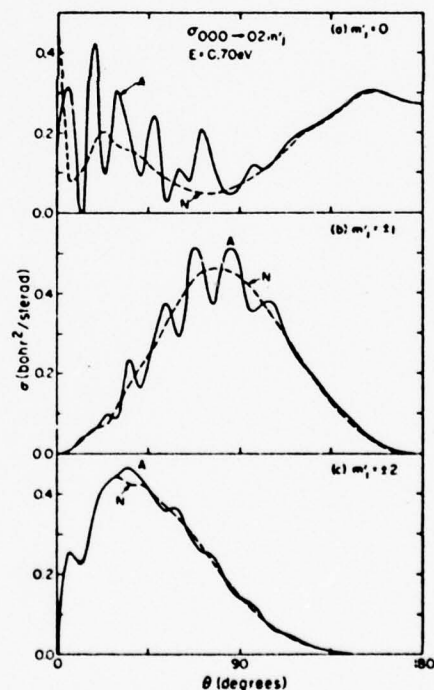
FIG. 15. Differential cross sections $\sigma_{000-02m_j}^A$ (solid lines labeled A) and $\sigma_{000-02m_j}^N$ (dashed lines labeled N) as a function of the scattering angle θ for (a) $m_j' = 0$, (b) $m_j' = \pm 1$, and (c) $m_j' = \pm 2$ at $E = 0.70$ eV. The degeneracy-averaged results corresponding to these curves are shown in Fig. 14.

TABLE V. Integral cross sections at selected total energies.

Cross section[a] (bohr²)	Total energy (eV)								
	0.30	0.35	0.40	0.45	0.50	0.55	0.60	0.65	0.70
Q^A_{00-01}	0.388(-13)	0.360(-8)	0.200(-5)	0.141(-3)	0.372(-2)	0.0400	0.234	0.571	0.905
Q^A_{00-03}	b	b	0.410(-8)	0.241(-5)	0.166(-3)	0.346(-2)	0.0295	0.104	0.222
Q^A_{00}-ortho	0.388(-13)	0.360(-8)	0.201(-5)	0.144(-3)	0.390(-2)	0.0435	0.264	0.676	1.13
Q^A_{02}-ortho	b	0.916(-10)	0.149(-6)	0.183(-4)	0.628(-3)	0.910(-2)	0.0632	0.209	0.423
Q^A_{04}-ortho	b	b	b	0.289(-8)	0.218(-5)	0.478(-3)	0.131(-2)	0.0155	0.0269
Q^R_{00}	0.156(-12)	0.480(-8)	0.252(-5)	0.184(-3)	0.501(-2)	0.0574	0.352	0.933	1.52
Q^R_{01}	0.232(-13)	0.205(-8)	0.130(-5)	0.106(-3)	0.306(-2)	0.0372	0.228	0.648	1.11
Q^R_{02}	b	0.120(-9)	0.186(-6)	0.234(-4)	0.806(-3)	0.0120	0.0843	0.291	0.575
Q^R_{03}	b	b	0.333(-8)	0.145(-5)	0.908(-4)	0.196(-2)	0.0166	0.0677	0.160
Q^R_{04}	b	b	b	0.371(-8)	0.289(-5)	0.700(-3)	0.179(-2)	0.0224	0.0484
Q^N_{00-02}	b	d	3.00	d	8.82	d	13.0	d	13.2
Q^R_{00-02}	b	0.595(-10)	0.114(-6)	0.142(-4)	0.473(-3)	0.643(-2)	0.0437	0.130	0.220
Q^A_{00-02}	b	d	3.00	d	8.82	d	13.0	d	13.5
Q^N_{00-00}	299[e]	d	260[e]	d	234[e]	d	217[e]	d	205[e]

[a]All cross sections have been degeneracy averaged. Those para-to-ortho cross sections which have been summed over final states are only summed over those final states of the correct spin symmetry. Numbers in parentheses indicate the power of 10 by which the numbers preceding them should be multiplied.
[b]Transition is energetically forbidden.
[c]Obtained by the extrapolation procedure of Sec. III D.
[d]Calculation not done.

have values of 3.01, 3.31, and 1.67 bohr³ for $m_{j'} = 0$, ±1, and ±2, respectively, which is indicative of the lack of strong rotational angular momentum polarization effects such as are observed for the reactive cross sections. The reason, as pointed out previously, is the lack of linear or near linear orientation restrictions for nonreactive rotationally inelastic collisions. Table V also indicates that Q^N_{00-02} and Q^A_{00-04} are equal (within the accuracy of the calculation) except at the highest energy considered. An additional discussion of the energy dependence of these nonreactive cross sections is given in Sec. IIIG.

D. Elastic and total cross sections

The calculation of converged elastic cross sections requires a large number of partial waves (up to 70 at 0.70 eV). Since the Porter–Karplus surface has a repulsive exponential long-range functionaltiy[2c] rather than the correct attractive R_1^{-6} dependence[40] a fully coupled calculation of the elastic cross sections for the purpose of comparison with experiments[40] on this and related systems would not be worthwhile without inclusion of this attractive tail in the potential. Nevertheless, an accurate calculation of the elastic differential

TABLE VI. Integral reactive cross sections $Q^R_{vfm_j-v'f'm'_j}$ (in bohr²) at $E = 0.60$ eV.[a]

vfm_j ╲ $v'f'm'_j$	000	011	010	01-1	022	021	020	02-1	02-2
000	0.0432	0.00322	0.0717	0.00322	0.227(-3)	0.00474	0.0338	0.00474	0.227(-3)
011	0.00337	0.549(-3)	0.00596	0.835(-3)	0.488(-4)	0.709(-3)	0.00261	0.00127	0.774(-4)
010	0.0751	0.00596	0.128	0.00596	0.380(-3)	0.00812	0.0578	0.00812	0.380(-3)
01-1	0.00337	0.835(-3)	0.00596	0.549(-3)	0.774(-4)	0.00127	0.00261	0.709(-3)	0.488(-4)
022	0.262(-3)	0.538(-4)	0.419(-3)	0.855(-4)	0.111(-4)	0.811(-4)	0.209(-3)	0.134(-3)	0.146(-4)
021	0.00549	0.783(-3)	0.0089	0.00140	0.811(-4)	0.00113	0.00407	0.00228	0.134(-3)
020	0.0391	0.00288	0.0638	0.00288	0.209(-3)	0.00407	0.0286	0.00407	0.209(-3)
02-1	0.00549	0.00140	0.00897	0.783(-3)	0.134(-3)	0.00228	0.00407	0.00113	0.811(-4)
02-2	0.262(-3)	0.855(-4)	0.419(-3)	0.538(-4)	0.146(-4)	0.134(-3)	0.209(-3)	0.811(-4)	0.111(-4)

[a]All reactance matrices have been symmetrized [see Ref. 14(a)] before the above cross sections were calculated. Numbers in parentheses indicate the power of 10 by which the numbers preceding them should be multiplied.
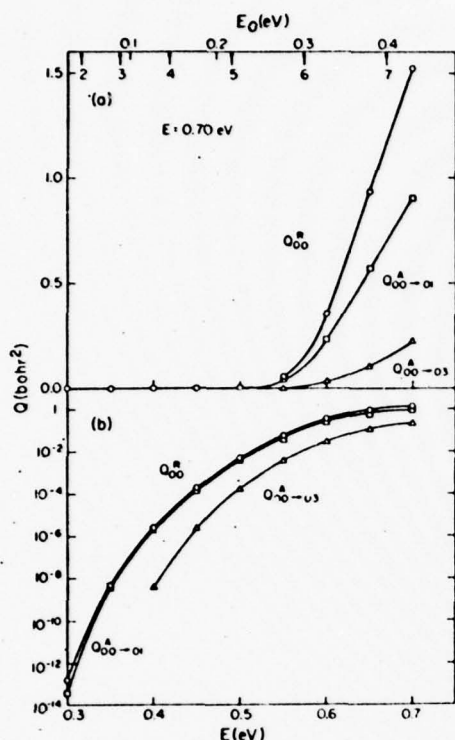
FIG. 16. Integral cross sections Q_{03}^R, Q_{00-01}^A, and Q_{00-03}^A (degeneracy averaged) as a function of the total energy E and translational energy E_0. Arrows in upper abscissa indicate the energies at which the rotational states $j = 2 - 7$ (for $v = 0$) of H_2 become energetically accessible: (a) linear scale, (b) logarithmic scale.

and integral cross sections for this Porter–Karplus surface is still worthwhile in order to provide a comparison standard for approximate techniques used in calculating these same cross sections, such as the central field approximation being invoked in the interpretation of molecular *beam* scattering experimental data.[41,42] This requires the calculation of the scattering matrix element phases for very large J. We found a very accurate extrapolation procedure which could be used to obtain these phase shifts. For J large enough so that both reactive and inelastic nonreactive transition probabilities are negligible, it is often the case that the elastic phase shifts have not yet decayed to zero. Since these large J collisions correspond to large impact parameters, we would expect that only the isotropic tail of the potential is important. In such circumstances, a central field, single channel model of the potential should suffice to predict these phase shifts. Using a standard central potential integration routine[43] with the spherically averaged potential $V_0(r_e, R)$ of Eq. (2.14), where r_e is the equilibrium internuclear distance, we have calculated the elastic $v = j = 0$ phase shifts at the energies considered in Table V. Typical results are

presented in Fig. 17, where we have also plotted the phase shift of the exact scattering matrix elements $[\frac{1}{2}\arg(S_{J,000-000}^N)]$. The figure indicates that the accurate phase shifts are essentially identical to their central field counterparts for $J > 10$. Indeed, between $J = 11$ and $J = 39$ (the highest J for which a fully coupled calculation was done), the difference between these two phase shifts is always less than 0.05 rad and usually less than 0.02 rad. This is rather interesting, since at $J = 11$ the modulus of $S_{J,000-000}^N$ (equal to $[P_{J,000-000}^N]^{1/2}$) is not even close to unity, as is illustrated in Fig. 17. This presumably indicates that the phases of the scattering matrix elements are much less sensitive to the presence of reactive and inelastic channels than are the moduli. By using these elastic central field phase shifts, we can now extrapolate the large J behavior of the converged results and thus calculate accurate elastic cross sections.[44] Typical results for $\sigma_{000-000}^N$ at $E = 0.7$ eV are plotted in Fig. 18. The elastic differential cross section shows strong forward ...king with a small oscillation near $\theta = 6°$ and otherw... decreases in a nearly monotonic manner to $\theta = 18...$ The indicated $\theta = 110°$ to 180° behavior of $\sigma_{000-000}^N$ ...robably not accurate since the small cross sectio... in this region must result from extensive cancella... n in the partial wave sum [Eq. (2.2)] and are easily affected by small errors in the scattering matrix elements. Also plotted on the same graph are the central field elastic cross section σ^E(CF) [obtained using $V_0(r_e, R)$ for all J] and the total cross section σ_{000}^T [which is the sum of the cross sections for all possible processes (N or R) starting from reagents $v = j = m_j = 0$]. We see that all three cross sections are essentially identical for $\theta < 30°$. This suggests that the central field approximation used to interpret total differential cross sections[41] out to scattering angles which are not too large is a good one. Even for very large scattering angles σ_{000}^T and σ^E(CF) agree to within better than a factor of 2. Moreover, the integral cross sections Q_{000}^T and Q^E (CF) are 221.0 bohr^2 and
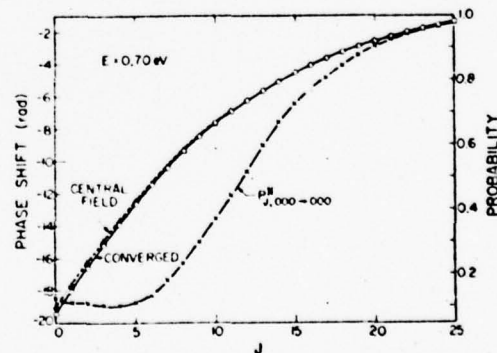
FIG. 17. Phase shift associated with the elastic scattering matrix element $S_{J,000-000}^N$ (i.e., $[\arg(S_J)]/2$) as a function of J for $E = 0.70$ eV. Curve labeled converged is the coupled-channel result, while the central field curve is the result of a single channel calculation described in text. Also plotted is the (converged) elastic transition probability $P_{J,000-000}^N$ at the same energy referenced to right hand ordinate scale.
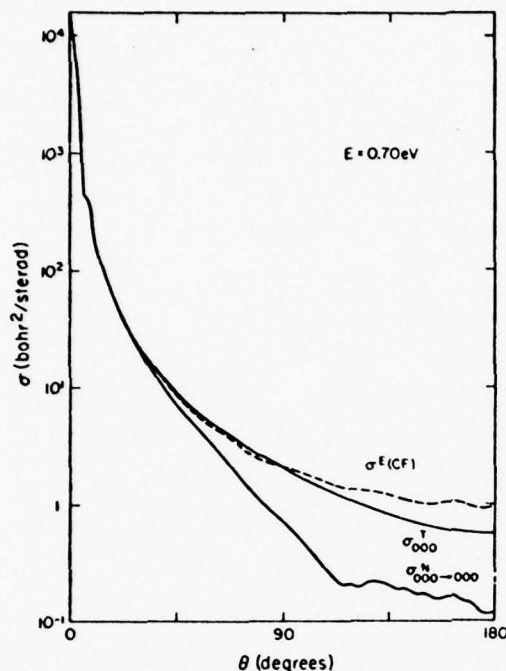
FIG. 18. Elastic differential cross section $\sigma^N_{000-000}$ and total cross section σ^T_{000} (both obtained from the coupled-channel calculation), along with the central field elastic cross section σ^E(CF) as a function of scattering angle at $E = 0.70$ eV.

220.8 bohr^2, respectively, indicating that Levine's conservation of total cross section rule[45] is obeyed quite accurately for this system and that the use of the central field approximation to interpret total cross section experiments[42] is valid. The $H + H_2$ total cross section just mentioned is considerably larger than the recently measured experimental one[40] (for $D + H_2$), which is about 151 bohr^2 at 0.75 eV. This is probably due to differences between the long-range parts of the Porter-Karplus and correct potential energy surfaces.

If the antisymmetrized cross section $\sigma^A_{000-000}$ is considered, we find that quantum symmetry effects due to interference between the elastic and reactive scattering amplitudes are much less significant than they were with the inelastic transitions in Fig. 14. Nevertheless, oscillations in this cross section can result in differences between σ^A and σ^N as big as 10% of σ^N for scattering angles between 30° and 90°.

E. Comparison of collinear, coplanar, and three dimensional results

In the analysis of the coplanar results,[13b] it was determined that a physically meaningful comparison of the 1D and 2D results could be obtained by examining the $J = 0$ total reaction probabilities. We extend this comparison in Figs. 19 and 20 by plotting the 1D,[21,46] 2D, and 3D total reaction probabilities $P^R_{00}(J = 0)$ [P^R_0 for 1D]

as a function of E. Both logarithmic and linear scales are used so as to enable examination over a wide energy range. The figures indicate a surprisingly similar energy dependence over several orders of magnitude of the probabilities. There are, however, two important differences both of which provide significant insight into the reactive collision dynamics. First, an energy shift of about 0.05 eV occurs in going from 1D to 2D and again in going from 2D to 3D. In the coplanar analysis,[13b] we explained the 1D to 2D shift as arising from an additional bending energy required in the coplanar transition state over the linear one. This bending energy is added to the symmetric stretch energy of the collinear transition state which, in turn, is primarily responsible for the shift in the collinear effective threshold energy over the barrier height energy[14] (0.396 eV). In the three-dimensional case, the bending mode of the transition state is doubly degenerate so that a second quantum of bending energy (approximately equal to the bending zero point energy of about 0.06 eV) will be required. Indeed, an examination of Fig. 19 indicates that the 1D to 2D and 2D to 3D energy shifts for $P^R = 0.01$ are identical to within the accuracy to which
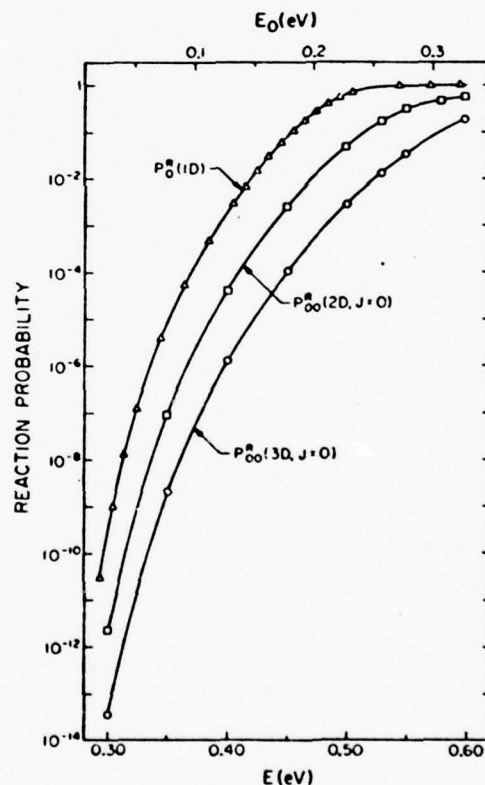
FIG. 19. One-, two-, and three-dimensional total reaction probabilities P^R_0(1D), P^R_{00}(2D, $J = 0$), and P^R_{00}(3D, $J = 0$), summed over all final states, as a function of the total energy E and translational energy E_0.
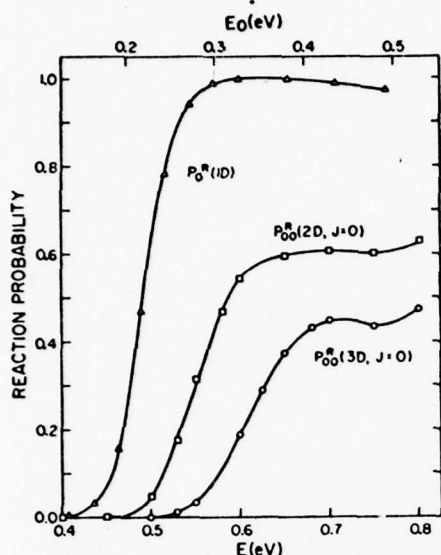
FIG. 20. One-, two-, and three-dimensional total reaction probabilities analogous to Fig. 19 but with a linear rather than logarithmic ordinate scale.

the probabilities can be interpolated. The second difference between 1D, 2D, and 3D results lies in the magnitudes of the maximum probabilities in Fig. 20. The collinear probability peaks near unity while the planar one levels off at about 0.6, and the 3D one roughly at 0.45. The difference between the 1D and 2D plateau values has been previously analyzed[13b] in terms of the orientation dependence of the 2D probability. Since the potential barrier varies from 0.396 eV at $\gamma_\lambda = 0$ to 2.8 eV at $\gamma_\lambda = 90°$,[2c] one would expect a decreasing probability of reaction with increasing γ_λ (assuming that we can consider the orientation of the atom with respect to the diatom as fixed throughout the reaction). If we consider that the total reaction probability is unity for $0 \leq \gamma_\lambda \leq \bar{\gamma}_\lambda$ and zero for $\bar{\gamma}_\lambda \leq \gamma_\lambda \leq 90°$, and use symmetry about 90° for $90° \leq \gamma_\lambda \leq 180°$, then we find that $P_{00}^R(2D) = 2\bar{\gamma}_\lambda/\pi$ and $P_{00}^R(3D) = 1 - \cos\bar{\gamma}_\lambda$. In the 2D case, we find that $\bar{\gamma}_\lambda = 54°$ is required to give a reaction probability of 0.6. This estimate of $\bar{\gamma}_\lambda$ is in approximate agreement with previous estimates of this angle from a classical analysis.[3] The same angle used in the 3D formula yields $P_{00}^R(3D) = 0.41$ which is not considerably different from the observed value of 0.45. This indicates that the 2D and 3D orientation dependence is probably quite similar with primarily dimensionality considerations responsible for the difference in reaction probabilities.

At least two procedures for converting 2D integral or differential cross sections into 3D ones have been proposed[11,47] both of which use semiclassical arguments in making the connection. We will leave for future publications a thorough analysis of these conversion procedures as well as an evaluation of approximate 3D procedures which require comparable or smaller amounts of com-

putation time than the 2D calculation while providing 3D information directly. We would like to point out, however, one rather remarkable comparison between 2D and 3D results which is obtained by examining the differential cross sections. In Fig. 21 we plot the 2D and 3D differential cross section σ_{00-01}^A (adjusting the respective ordinate scales to bring them into approximate agreement at $\theta_R = 180°$). The 2D result at 0.55 eV is compared to the 3D one at 0.60 eV so as to include the energy shift effect due to the bending energy.

These two cross sections show a remarkably similar angular dependence over the entire range of scattering angles. A similar comparison at other energies in the range considered in this paper usually leads to comparable agreement. This indicates that the dynamical processes involved are indeed quite similar. Such behavior is not unexpected, for the same potential is sampled in both cases and the primary difference between the two calculations is the additional centrifugal coupling resulting from tumbling of the three-atom plane, which is present in 3D but not in 2D. The existence of a strong rotational polarization selection effect as evidenced in Table VI indicates that such coupling is weak in comparison to the potential coupling since it is the potential which is responsible for the linear geometry requirement. Thus 2D and 3D dynamics should be quite similar and conversion of 2D to 3D results could prove to be an accurate approximate technique.
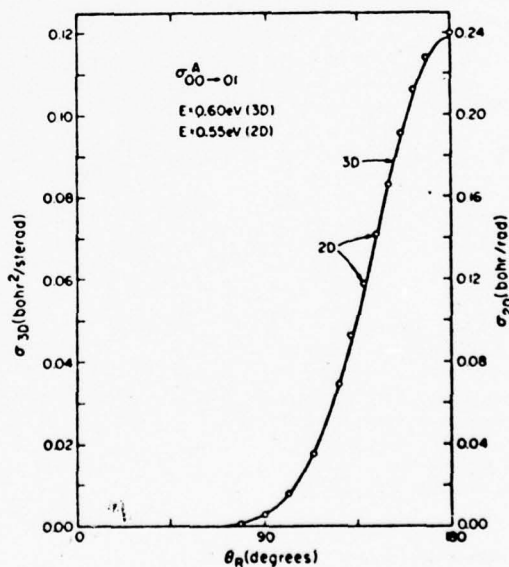
FIG. 21. Two- and three-dimensional differential cross sections σ_{00-01}^A (2D)[$\bar{\sigma}^A$ of Ref. 13(b)] and σ_{00-01}^A (3D) as a function of reactive scattering angle θ_R. The 3D cross section (solid curve), at 0.60 eV total energy, is referenced to the left side ordinate scale while the 2D result (circles) at 0.55 eV is referenced to the right side one.
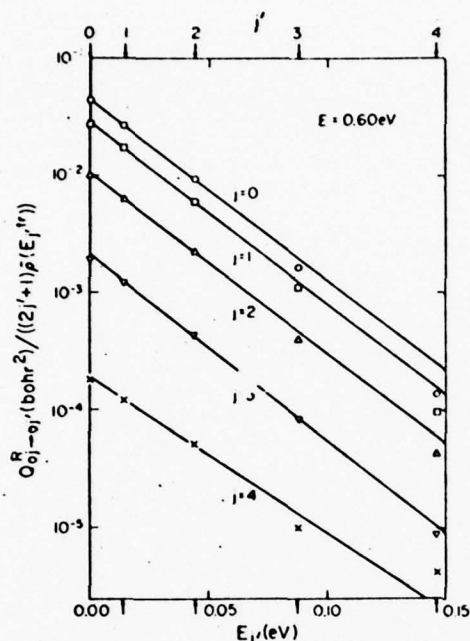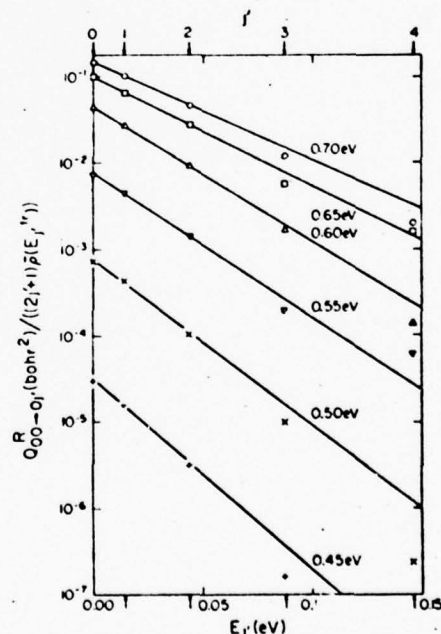
FIG. 22. Reactive degeneracy-averaged integral cross sections $Q_{0j-0j'}^R$, divided by $(2j'+1) \times \bar{\rho}(E_{j'}^{tr})$, as a function of the product rotational energy $E_{j'}$ and rotational quantum number j at 0.60 eV total energy for initial rotational quantum numbers $j=0-4$.

F. Reagent and product rotational state distributions

We now consider the rotational distributions of the degeneracy-averaged reactive distinguishable atom cross sections (all for $v=v'=0$). In the coplanar $H+H_2$ study,[13b] we found that a surprisingly accurate fit to this distribution could be obtained with a temperaturelike expression (for a 2D system). This type of distribution can be derived from an information theoretic formalism through the assumption that the surprisal function[48] is a linear function of the final state rotational energy. For 3D collisions, with only one open vibrational channel, the information theoretic expression for the degeneracy-averaged cross section between rotational states j and j' may be written as

$$Q_{j-j'}^R = A_j(E)\rho(E_{j'}^{tr})(2j'+1)e^{-E_{j'}/kT_j(E)}, \qquad (3.1)$$

where the pre-exponential factors comprise the reference or statistical distribution, and T_j and A_j are the two j'-independent parameters of the theory. $\rho(E_{j'}^{tr})$ is the product translational density of states and is a function of the translational energy $E_{j'}^{tr}$ relative to state j'. $E_{j'}$ is the product rotational energy, so that $E_{j'}^{tr}=E-E_{j'}-E^0$, where E^0 is the $v'=j'=0$ zero point energy. The $2j'+1$ in Eq. (3.1) is the product rotational degeneracy factor. To see how well our 3D cross sections obey Eq. (3.1), we have plotted in Fig. 22 the cross sections $Q_{0j-0j'}^R$ divided by $(2j'+1)\times\bar{\rho}(E_{j'}^{tr})$ on a logarithmic scale as a function of $E_{j'}$ for several initial states j at 0.6 eV,

where $\bar{\rho}(E_{j'}^{tr})=\rho(E_{j'}^{tr})/\rho(E-E^0)$ so that for $E_{j'}=0$, $\bar{\rho}=1$. If Eq. (3.1) is satisfied, then the resulting curves should be linear with slopes inversely proportional to $T_j(E)$. We see from the figure that the calculated points for low j' do indeed fall on nearly straight lines for each j, thus indicating that the temperaturelike distribution is quite accurate for describing the reactive cross sections. The temperature parameters obtained from these low j' straight lines are 3??, 326, 328, 318, and 376 K for $j=0$, 1, 2, 3, and 4, respectively. The first four values are identical to one another within the accuracy of the straight line fits. Actually, one can easily show by applying microscopic reversibility to Eq. (3.1) that if the rotational distribution is temperaturelike for all j then $T_j(E)$ must be independent of j, which can be written simply as $T(E)$. The above listed temperatures should therefore all be the same if the distributions are truly temperaturelike. Only for $j=4$ or $j'=4$ are deviations from temperaturelike behavior significant. If we now perform a similar analysis at several other total energies we obtain Fig. 23 which depicts the $j=0$ distributions between 0.45 and 0.70 eV. Temperaturelike behavior is evident to a comparable extent at all energies considered. The temperature parameters obtained from the slopes of the lines in Fig. 23 vary from 228 K to 446 K as E varies from 0.45 eV to 0.70 eV in steps of roughly 40 K/0.05 eV increase in energy.

As pointed out by Wyatt,[49] these temperaturelike pa-

FIG. 23. Reactive degeneracy-averaged integral cross sections $Q_{v0-0j'}^R$, divided by $(2j'+1)\times\bar{\rho}(E_{j'}^{tr})$, as a function of the product rotational energy $E_{j'}$ and rotational quantum number j' at 0.45, 0.50, 0.55, 0.60, 0.65, and 0.70 eV total energy.

rameters should *not* be interpreted as being equal to the temperature of a canonical ensemble describing a thermal equilibrium between a bath and the products of the reaction (which actually belong to a nonequilibrium microcanonical ensemble). Under conditions leading to product population inversions, Eq. (3.1), when satisfied, furnishes negative $T_r(E)$. We have expressed the present reaction product rotational population results in terms of temperaturelike parameters because the latter turned out to be positive and a quantitative feeling for the relative population of the product states is immediately conveyed by reporting their values. An alternative but equivalent procedure is to express the results in terms of the slopes $\theta(E)$ of the linear surprisal plots.[48,49] It is easy to show that $\theta(E)$ is related to $T(E)$ by $\theta(E) = (E - E^{v'})/[kT(E)]$, where $E^{v'}$ is the vibrational energy of the products whose rotational population is being considered. In the present instance $E^{v'}$ is the zero-point vibrational energy of H_2 and the surprisal slope parameters $\theta(E)$ corresponding to Fig. 23 vary from 9.1 at $E = 0.45$ eV to 11.1 at $E = 0.70$ eV in a nonlinear manner. The results obtained by Wyatt[49] for an approximate version of the Yates–Lester–Liu (YLL) potential energy surface[2f,50] furnish $\theta = 8.9$ for $E = 0.70$ eV and 0.80 eV. The difference between these results may be attributed in part to the difference between the YLL[50] and PK[2c] surfaces and in part to the difference between the methods used in the scattering calculations (see Sec. III G).

In the coplanar study[13b] we pointed out that the existence of temperaturelike rotational distributions could be a reflection of the shape of the potential energy surface near the transition state and the significant restriction in bending motions which the potential induces there. Since the transition state bending motions correlate adiabatically with asymptotic free rotor motions one might expect that the average rotational energy of the products should be related to the average energy in bending. This relation does not seem to be quantitative, however, for the average product state rotational energy corresponds roughly to the temperature parameter while the bending energy, as estimated in the previous section, seems to be somewhat higher (228–446 K for the former and 550 K for the latter). The model explains the similarity between the coplanar and three-dimensional temperature parameters (311 K for 2D[13b] vs 326 K for 3D, both at 0.6 eV) only if we further assume that only one of the two degenerate 3D bending modes becomes product rotational motion. This assumption disagrees with the interpretation given above for the energy shifts of Figs. 19 and 20. It therefore appears that some refinement in the model which relates product rotational energies to transition state bending energies is necessary in order to quantitatively explain the temperature parameters obtained from the distributions of Figs. 22 and 23.

G. Comparisons with the results of other three dimensional calculations

In Figs. 24 and 25 we compare our integral cross sections (labeled SK) with the corresponding ones obtained by several other methods, all applied to $H + H_2$ on

the Porter–Karplus potential surface. In Fig. 24 we plot the quasiclassical total reactive cross sections of Karplus, Porter, and Sharma[3] (KPS) and the quantum mechanical results of Elkowitz and Wyatt[10] (EW), while Fig. 25 contains the antisymmetrized distorted wave Q_{00-01}^A results of Tang and Karplus[5] (TK) and of Choi and Tang[8] (CT) and the one-vibration close-coupling results of Wolken and Karplus[7] (WK).

It is apparent that the best agreement in either figure is between our Q_{00}^R(SK) and Q_{01}^R(SK) and the corresponding quasiclassical quantities. Our converged quantum result and the quasiclassical cross sections are essentially identical between 0.6 and 0.7 eV to within the statistical accuracy of the quasiclassical calculation. Agreement between Q_{02}^R(SK) and Q_{02}^R(KPS) is much less quantitative but still reasonable if one considers the small cross sections involved and the inherent statistical uncertainty in the quasiclassical result. Below the classical thresholds, we observe characteristic tunneling behavior in our quantum cross sections which will have an important effect in the comparison of classical
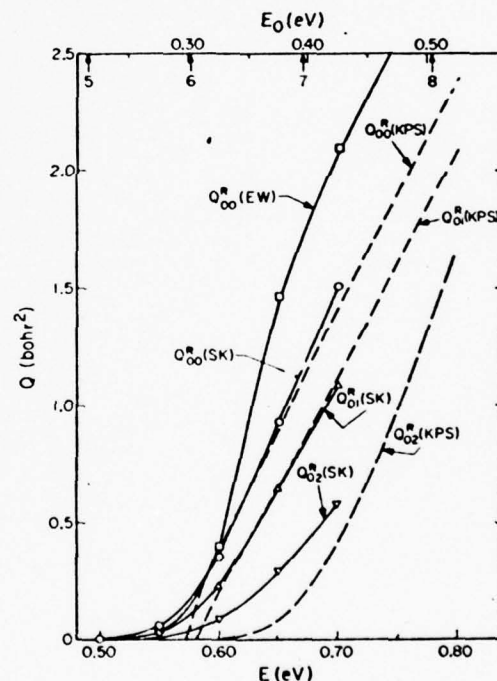

FIG. 24. Comparison of reactive integral cross sections as a function of the total energy E for several calculations. The Q_{0j}^R (KPS) for $j = 0$, 1, and 2 are the quasiclassical results of Karplus, Porter, and Sharma (indicated by dashed lines), while Q_{00}^R(EW) is the analogous total reaction cross section obtained by Elkowitz and Wyatt (indicated by squares). The present results are connected by solid lines and labeled Q_{0j}^R(SK) with $j = 0$, 1, 2. The arrows below the upper abscissa indicate the energies at which the ground vibrational state product rotational levels having the j values indicated become energetically accessible.
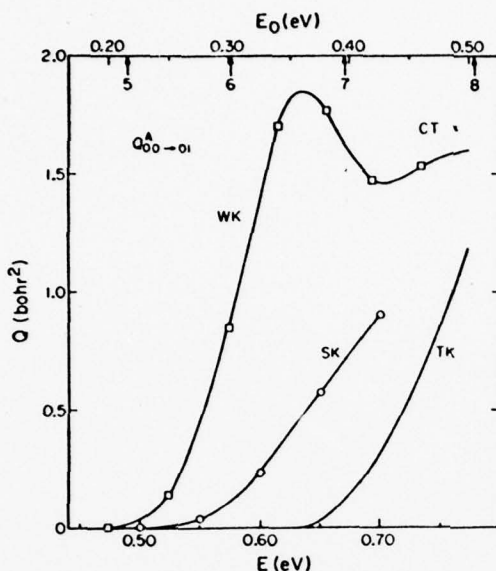
FIG. 25. Comparison of the integral cross sections $Q_{00 \to 01}^A$ as a function of E. The results labeled WK are those of Wolken and Karplus, TK denotes those of Tang and Karplus, CT the one point of Choi and Tang, and SK the present results. The TK results in Ref. 5 have been multiplied by the necessary factor of 3 to obtain the curve plotted. The arrows below the upper abscissa have the same meaning as in Fig. 24.

and quantum thermal rate constants (see Sec. III H).

Agreement between our results and the corresponding one of Elkowitz and Wyatt[10](EW) is not as good as one would have expected considering that both calculations were done on the same potential energy surface and they both employed extended vibration-rotation basis sets. Recently, EW have made some corrections in their calculations[51] which improve the agreement between their Q_{00}^R curve and ours. In addition, over the energy range 0.6–0.7 eV, the corrected EW values for Q_{00-01}^A agree with ours to within 20%. On the other hand, their Q_{00-00}^A are about 2.5 times greater than ours, and as a result, when we compare the cross section ratios Q_{00-00}^A/Q_{00-01}^A from Table V with the corresponding ones from Fig. 1(a) of Ref. 10 or with EW corrected values,[51] we find that the difference between them is quite large. For example, at $E = 0.70$ eV we get 0.24 for that ratio, whereas the EW value is 0.62. This implies that the distribution of energy among the rotational degrees of freedom of the products is very different in both calculations, and that the temperaturelike parameters which may result from their calculations will be significantly larger than the ones reported in the previous section. A search is presently going on for the reasons for this difference in the cross sections. In this context it should be noticed that EW simplified their calculation in three ways,[52] one or more of which could have an appreciable effect on the results, particularly at large energies: (a) They omitted certain Coriolis

coupling terms from the kinetic energy part of the Hamiltonian; (b) The potential was fitted to analytic expressions whose form was chosen so as to omit vibration–rotation coupling; and (c) Only the $v = 0, 1, 2$ vibrational states were included in the coupled-channel expansion and convergence with respect to the number of vibrational states was not tested. In our case, as pointed out in Sec. II B, Table III, and in Ref. 13, usually four vibrational basis functions were required for convergence of the reaction probabilities to a few percent.

The Tang and Karplus distorted wave curve in Fig. 25 has a much higher effective threshold energy than ours and consequently much smaller cross sections at the same energy. Part of the difficulty could be the "linear" assumption used[5] in evaluating the integrals for the transition amplitude. When this assumption was removed, as was done by Choi and Tang,[6] the cross section increased significantly at the one energy they considered. We should also note that Choi and Tang[6b] have also observed an m_j' dependence in their $P_{J,000-01=j'}^R$ reaction probabilities quite similar to that of Fig. 3. It would be interesting to obtain distorted wave results such as those of CT at lower energies so that a more direct comparison with our results may be made. The one vibrational basis function results of Wolken and Karplus[7] have an effective threshold energy much lower than ours for the same transition. This is probably a consequence of the severely truncated basis set used (only vibrational quantum state $v = 0$ and the $j = 0$–3 rotational states). Convergence properties of such severely truncated basis sets were examined in the coplanar $H + H_2$ study,[19b] and it was determined there that errors of several orders of magnitude in cross sections were possible in some cases if both vibrational and rotational convergence was not achieved.

The quasiclassical and quantum differential cross sections σ_{00}^R (at somewhat different energies) are examined in Fig. 26. Both angular distributions are backward peaked with very similar shapes. A very interesting comparison between classical and quantum dynamics would involve an examination of the classical rotational polarization effect analogous to the one found in the quantum results and displayed in Fig. 10. Such a detailed comparison of cross sections between individual quantum states (rather than summed over several as is the case in Figs. 24 and 26) would be highly desirable in establishing the general validity of the quasiclassical procedure. Figure 27 provides a comparison of the WK, CT, and SK σ_{00-01}^A angular distributions at similar energies. We find the shape of the distorted wave differential cross section curve of Choi and Tang to be very similar to ours, while that of the Wolken and Karplus cross section differs rather substantially from either. Part of the error in the WK result could be due to an ambiguity in the interpolation of amplitudes and phases of scattering matrix elements for those partial waves they did not explicitly calculate. (Only every third partial wave was calculated.)[7] Indeed, we have found interpolation procedures to be extremely dangerous (especially for the phases), and for this reason,
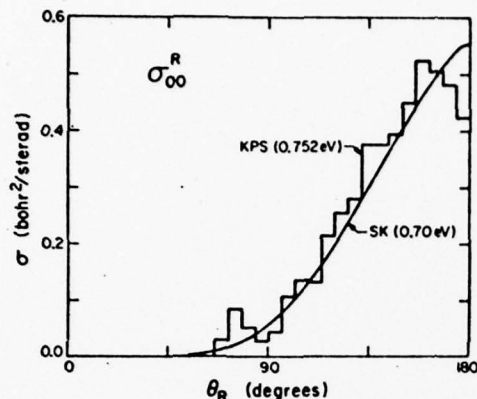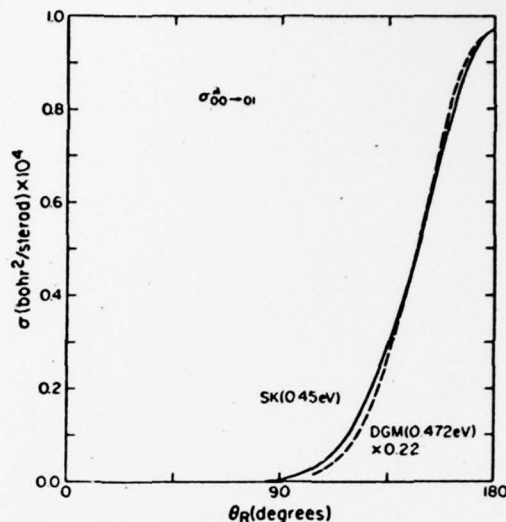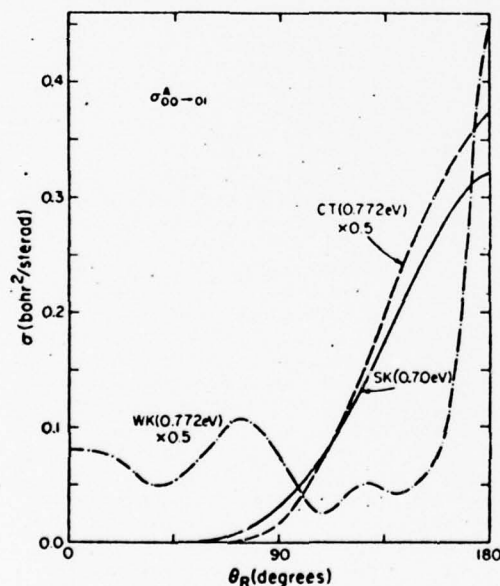
FIG. 26. Comparison of the differential reaction cross section σ_{00}^R as a function of the reactive scattering angle θ_R as obtained by (a) the quasiclassical trajectory method of Karplus, Porter, and Sharma (the histogram labeled KPS) at $E = 0.752$ eV, and (b) the present coupled channel method (labeled SK) at 0.70 eV.

we have always computed scattering matrices for every partial wave required for convergence of the cross section. Another comparison of angular distributions is indicated in Fig. 28, where we examine the semiclassi-

FIG. 27. Comparison of the differential cross section $\sigma_{00\text{-}01}^A$ as a function of the reactive scattering angle θ_R as calculated by (a) the distorted wave method of Choi and Tang (dashed curve labeled CT) at $E = 0.772$ eV, (b) the one vibration coupled channel method of Wolken and Karplus (dash-dotted curve labeled WK) at $E = 0.772$ eV, and (c) the present method (solid curve labeled SK at 0.70 eV.

FIG. 28. Comparison of the semiclassical differential cross section $\sigma_{00\text{-}01}^A$ as a function of the reactive scattering angle θ_R calculated by Doll, George, and Miller (dashed curve labeled DGM) at 0.472 eV total energy with the corresponding $\sigma_{00\text{-}01}^A$ of the present work (solid curve labeled SK) at 0.45 eV. The scaling factor of 0.22 was chosen so as to make the displayed curves coincide at $\theta_R = 180°$.

cal $\sigma_{00\text{-}01}^R$ of Doll, George, and Miller[8] (DGM) at a much lower energy than has been considered in the previous two figures. The DGM cross sections are about 5 times larger than the present quantum ones, but the agreement between the shapes of the curves in Fig. 28 is excellent. In Fig. 29, the results of two methods (primitive semiclassical and classical semiclassical in the terminology of Ref. 53) used by DGM to calculate reaction probabilities are displayed. They are a factor 6–18 greater than the present ones. Presumably a "uniform" type of expression for evaluating the semiclassical reaction probability is required to bring those results into an agreement comparable to what was obtained in the same energy range for collinear $H + H_2$.[53] The results of Wolken and Karplus shown in the same figure are a factor of 10–30 greater than the present ones.

We conclude this section with a comparison of our nonreactive integral and differential cross sections with those of Wolken, Miller, and Karplus.[22] The latter calculation considered the same potential surface[2c] as did we but ignored the possibility of reactive collisions. A comparison of the resulting integral cross sections $Q_{00\text{-}00}^N$ is given in Fig. 30. The two curves agree within the accuracy of the respective calculations, except perhaps at the highest energies considered. This is quite interesting, for WMK used a one-vibration-basis-function approximation (with, however, $j_{max} = 6$) in their calculation. This could indicate that the absence of closed vibrational channels is of much less significance for nonreactive collisions than it is for reactive ones.
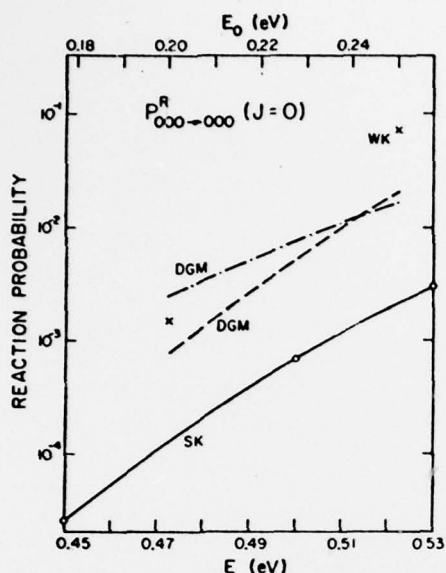
FIG. 29. Reaction probability $P^R_{J,000-000}$ for $J=0$ as a function of the total energy E and translational energy E_0. The two curves labeled DGM are the semiclassical results of Doll, George, and Miller using the primitive semiclassical expression (dashed) and classical semiclassical expression (dash-dotted) in the terminology of Ref. 53. The two crosses are points from the work of Wolken and Karplus (WK), and the present results (SK) are denoted by circles and the solid line. The DGM and WK probabilities have been divided by 3 as described in Ref. 6 to make the comparison with our distinguishable-atom probabilities meaningful.
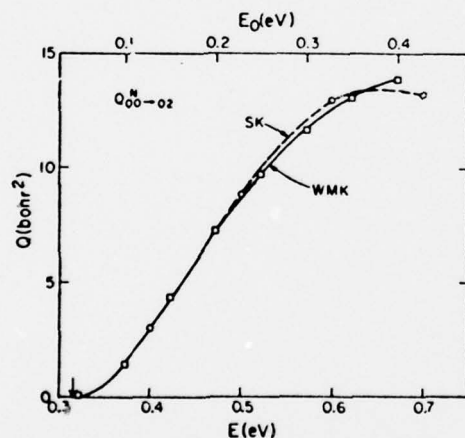
FIG. 30. Nonreactive integral cross section Q^N_{00-02} as a function of the total energy E and translational energy E_0. The solid curve labeled WMK is the coupled-channel result of Wolken, Miller, and Karplus. (The actual points calculated are denoted by squares.) The present results (SK), given by circles, are connected by a dashed line. Arrow in abscissa indicates the energy at which the $v=0$, $j=2$ state of H_2 becomes energetically accessible.
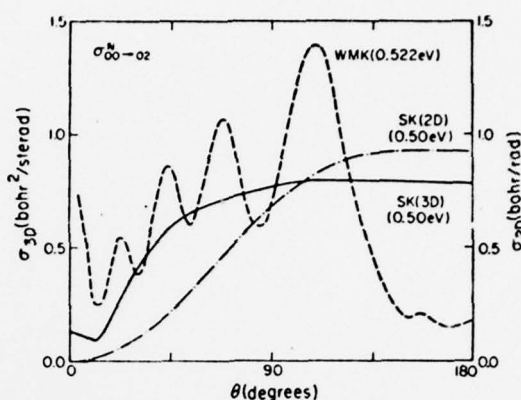
FIG. 31. Nonreactive differential cross section σ^N_{00-02}. The dashed curve indicates the results of Wolken, Miller, and Karplus (WMK) at 0.522 eV. The present result (SK) (at 0.50 eV) is denoted by a solid curve, and the dash-dotted curve denotes the coplanar result (at 0.50 eV) of Ref. 13(b) with ordinate scale given on the right side of the graph.

Unfortunately, a comparison between the WMK differential cross sections σ^N_{00-02} and ours (Fig. 31) shows a significant disagreement between them, with the WMK curve being highly oscillatory, in contrast with our very smooth one. We believe that the smooth behavior is more reasonable because (a) it is consistent with a direct mechanism being dominant in the collision process; (b) it agrees qualitatively with our coplanar result at the same energy (also plotted in Fig. 31) which is obtained from an entirely different calculation[13b]; and (c) it also qualitatively agrees with the corresponding nonreactive cross sections of Allison and Dalgarno[23] for the same system but a different interaction potential. Recently, Choi and Tang[24b] have used a coupled equations technique to recompute σ^N_{00-02} for the same problem considered by WMK. They obtained a smooth angular distribution in very good agreement with our result. Note that Fig. 31 also shows the absence of any forward peak in the planar cross section. This is additional evidence for the conclusion of Sec. III B that the forward peak in the 3D result may be spurious.

H. Rate constants

In this section we will examine the behavior of the para-to-ortho rate constant for $H + H_2$. The ortho-to-para rate constant can be easily obtained from $k_{p-0}(T)$ by using the readily available equilibrium constant.[54]

We first define the rate constant for the transition $vjm_j \rightarrow v'j'm'_j$ (valid for R, N, or A transitions):

$$k_{vjm_j - v'j'm_j} = \langle Q_{vjm_j - v'j'm_j}V_{vj}\rangle$$

$$= \int Q_{vjm_j - v'j'm_j}(V_{vj})V_{vj}P(V_{vj})d^3V_{vj}, \quad (3.2)$$

where the velocities V_{vj} were introduced in Sec. II A and $P(V_{vj})$ is the Boltzmann distribution function. Upon explicit substitution of this function into Eq. (3.2), we find

TABLE VII. Para-to-ortho thermal rate constants for $H + H_2$.[a]

$T(K)$	$k_{p-o}(SK)$	$k_{p-o}^{dist}(SK)$	$k_{p-o}(KPS)$[b]	$k_{p-o}(TST)$[b]
100	0.270(4)	0.341(4)	0.783(-2)	0.405(-5)
200	0.688(7)	0.722(7)	0.375(6)	0.161(5)
250	0.753(8)	0.773(8)	0.127(8)	0.125(7)
300	0.442(9)	0.449(9)	0.136(9)	0.225(8)
400	0.486(10)	0.490(10)	0.268(10)	0.835(9)
500	0.224(11)	0.224(11)	0.168(11)	0.737(10)
600	0.640(11)	0.640(11)	0.595(11)	0.322(11)

[a]All rate constants are in units of $cm^3/(mole \cdot sec)$. Quantum rate constants are believed accurate to 20%.
[b]Results of Ref. 3.

$$k_{vj=j \to v'j'=j'} = N_A \left(\frac{8}{\pi \mu_j}\right)^{1/2} \frac{1}{(kT)^{5/2}}$$
$$\times \int_0^\infty E_{vj}^{tr} Q_{vj=j \to v'j'=j'}(E_{vj}^{tr}) e^{-E_{vj}^{tr}/kT} dE_{vj}^{tr},$$
$$(3.3)$$

where μ is the reduced mass corresponding to the motion of the atom with respect to the diatom and E_{vj}^{tr} is the translational energy relative to state $vj(E_{vj}^{tr} = \frac{1}{2}\mu V_{vj}^2)$. N_A is Avogadro's number, so that k has units of $cm^3/(mole \cdot sec)$. Expressions for degeneracy-averaged rate constants $k_{vj \to v'j'}$ may be obtained by using the degeneracy averaged $\sigma_{vj \to v'j'}$ in Eq. (3.3) rather than $\sigma_{vj=j \to v'j'=j'}$. The para-to-ortho rate constant is then obtained from the $k_{vj \to v'j'}^A$ via

$$k_{p-o}(T) = \sum_{\substack{vj \\ (j \, even)}} \frac{f_j(2j+1)e^{-E_{vj}/kT}}{Q_p(T)} \sum_{\substack{v'j' \\ (j' \, odd)}} k_{vj \to v'j'}^A(T), \quad (3.4)$$

where

$$Q_p(T) = \sum_{\substack{vj \\ (j \, even)}} f_j(2j+1)e^{-E_{vj}/kT} \quad (3.5)$$

is the para-state reagent internal partition function and E_{vj} is the vibration rotation energy of state $vj(E = E_{vj} + E_{vj}^{tr})$. The nuclear spin degeneracy factor f_j has the value 1 for j even and 3 for j odd and thus is always unity for k_{p-o}. Calculation of this rate constant can be made using Eqs. (3.3)–(3.5) and the cross sections $Q_{vj-ortho}^A$ which were defined at the end of Sec. II A. Some values of these integral cross sections are given in Table V. By evaluating the integral in the degeneracy-averaged counterpart of Eq. (3.3) numerically, we have obtained the para-to-ortho rate constants given in the second column of Table VII. Both linear and logarithmic interpolation were used between the energies at which cross sections were calculated and the results from the two methods agree to 20% or better. (The linear results are given in Table VII.) Only temperatures below 600 K have been used in the calculation because of substantial errors which occur in truncating the integral in Eq. (3.3) at 0.7 eV total energy for temperatures above 600 K.

The quantum para-to-ortho rate constant may also be obtained (approximately) from distinguishable atom cross sections. It is desirable to do this in order to provide additional comparisons between quantum and quasiclassical rate constants. The total reaction rate

constant $k^R(T)$ for distinguishable atom collisions is[3]

$$k^R(T) = 2 \sum_{vj} \frac{f_j(2j+1)e^{-E_{vj}/kT}}{Q(T)} \sum_{v'j'} k_{vj \to v'j'}^R(T), \quad (3.6)$$

where

$$Q(T) = \sum_{vj} f_j(2j+1)e^{-E_{vj}/kT}. \quad (3.7)$$

The factor of 2 at the beginning of the right-hand side of Eq. (3.6) arises from an explicitly performed sum over the two equivalent product arrangement channels. In the limit in which a large number of quantum states contribute to the sums in Eqs. (3.4) and (3.6), we may assume that a sum of rate constants over just odd product states (or just even states) is approximately half the sum over all possible states, i.e.,

$$\sum_{\substack{v'j' \\ (j' \, odd) \\ or \\ (j' \, even)}} k_{vj \to v'j'}^R(T) \sim \frac{1}{2} \sum_{\substack{v'j' \\ (all \, j')}} k_{vj \to v'j'}^R(T). \quad (3.8)$$

In addition, for high enough temperatures,

$$Q_o = \sum_{\substack{vj \\ (j \, odd)}} f_j(2j+1)e^{-E_{vj}/kT} \sim 3 \sum_{\substack{v'j' \\ (j \, even)}} f_j(2j+1)e^{-E_{vj}/kT} = 3Q_p, \quad (3.9)$$

so that

$$Q = Q_o + Q_p \sim 4Q. \quad (3.10)$$

By realizing that k_{o-p} is given by an expression analogous to Eqs. (3.4) and (3.5) but with the even and odd sums interchanged, and by combining the expressions for k_{o-p} and k_{p-o}, using Eqs. (3.8)–(3.10) and the relations between antisymmetrized and distinguishable reactive rate constants implicit in the discussion following Eq. (2.8), we find

$$k^R(T) \sim k_{p-o}(T) + k_{o-p}(T) \quad (3.11)$$
$$\sim k_{p-o}(T)\left(1 + \frac{1}{K_{eq}}\right),$$

where K_{eq} is the equilibrium constant. To the same order of approximation, Eq. (3.9) implies that $K_{eq} \sim 3$, so Eq. (3.11) yields

$$k^R(T) \sim \frac{4}{3} k_{p-o}(T). \quad (3.12)$$

This implies that by computing $k^R(T)$ and using Eqs. (2.12) and (3.11) or (3.12), we can approximately compute $k_{p-o}(T)$ from distinguishable-atom reactive cross sections Q^R. In the third column of Table VII we list the k_{p-o}^{dist} so obtained. Equation (3.11) (in which K_{eq} is not assumed to have the value 3) was found to give slightly better agreement between k_{p-o}^{dist} and k_{p-o} for $T < 300$ K than Eq. (3.12) and was therefore used in calculating k_{p-o}^{dist} in the table. We see that for $T \geq 300$ K, $k_{p-o}^{dist}(T)$ and $k_{p-o}(T)$ are identical to at least two significant features indicating that the approximation is quite accurate even at fairly low temperatures. If we use Eq. (3.11) to convert the Karplus, Porter, and Sharma[3] rate constant $k^R(KPS)$ to $k_{p-o}(KPS)$, we obtain the results in the fourth column of Table VII. In the fifth column we have listed the analogous transition state theory result $k_{p-o}(TST)$ without tunneling corrections [which is obtained from Eq. (3.11) and the formula given in Ref. 3]. Note that transition state theory
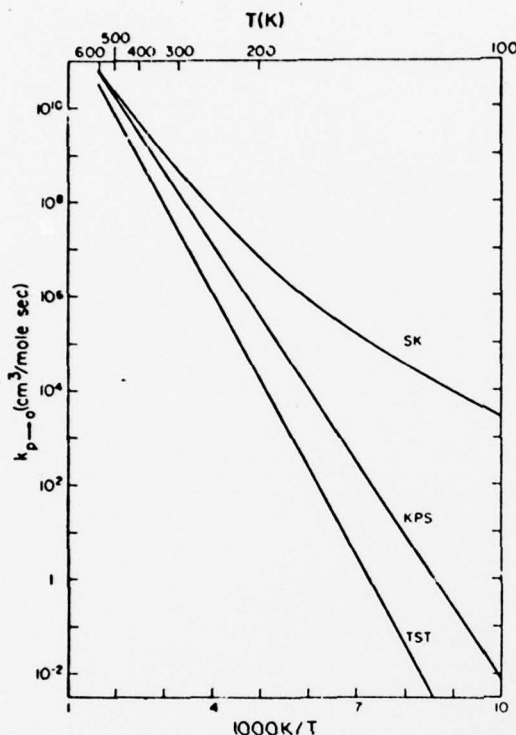
FIG. 32. Arrhenius plot of the para-to-ortho thermal rate constant. The present quantum result is denoted by SK, while the quasiclassical result of Karplus, Porter, and Sharma is labeled KPS and the transition state theory result is labeled TST.

ordinarily does not distinguish different possible product spin states, so that in order to define $k_{p \to o}(TST)$, we have to make the additional obvious assumption that the individual nuclear spins are good constants of the motion. It is worthwhile noting here that a number of rate constants in addition to those in Table VII may be calculated, but most of these additional rate constants provide no new information (see also Ref. 55). For example, any ortho-to-para rate constant is simply $k_{o \to p}$ $= k_{p \to o}/K_{eq}$, and any distinguishable-atom rate constant $k_{p \to o}^{dis}$ (which includes those in the last three columns of Table VII) may be related to the corresponding total rate constant using Eq. (3.11). One exception is the quasiclassical para-to-ortho rate constant $k_{p \to o}^{R}$ which is obtained by selecting only those trajectories which fall into bins connecting even and odd states. This quantity cannot be extracted from the results of Ref. 3, and is only approximated by $k_{p \to o}(KPS)$ as obtained using Eq. (3.11).

Arrhenius plots of the quantum, quasiclassical, and transition state theory rate constants are presented in Fig. 32. At 600 K, the quasiclassical $k_{p \to o}(KPS)$ differs from $k_{p \to o}(SK)$ by only 7%, while the TST result is in error by 79%. The close agreement of the quasiclassi-

cal and quantum results is an obvious consequence of the excellent agreement of the corresponding integral cross sections (above the classical thresholds) in Fig. 24 coupled with the excellent validity of Eqs. (3.11) and (3.12). Presumably, the quantum and quasiclassical rate constants will continue to be in very good agreement at temperatures above 600 K. At lower temperatures, however, tunneling effects become extremely important with $k_{p \to o}(SK)$ a factor of 3.3 larger than $k_{p \to o}(KPS)$ at 300 K and 18 times larger at 200 K. The significant nonlinearity in the quantum curve in Fig. 31 is also apparently related to tunneling, although we should note that previous studies on collinear $H + H_2$ have shown[56] that tunneling can make significant contributions to the rate constant even at 1000 K where the collinear reaction Arrhenius plot is quite linear. The transition state theory rate constant deviates from $k_{p \to o}(SK)$ even more severely than $k_{p \to o}(KPS)$, with $k_{p \to o}(SK)/k_{p \to o}(TST)$ being 20 at 300 K and 427 at 200 K. Part of the error in the TST result is probably due to the neglect of tunneling corrections in the expression used[3] (i.e., a transmission coefficient of unity has been assumed). For a scaled version[14a] of the SSMK surface,[2d] Truhlar and Kuppermann[14a] have calculated vibrationally adiabatic zero curvature (VAZC) transmission coefficients of 0.903 at 600 K, 0.98 at 300 K, and 1.72 at 200 K, thus indicating that inclusion of these factors is not apt to improve the situation significantly. In addition, the ratio $k_{p \to o}(KPS)/k_{p \to o}(TST)$ deviates substantially from unity in Table VII despite the fact that tunneling has been omitted from both calculations. Because of the strongly nonlinear behavior of $k_{p \to o}(SK)$ in Fig. 32, the attempt to characterize that rate constant by a single activation energy is probably not too meaningful. If one does, however, compute such a quantity by arbitrarily fitting a straight line between the 500 K and 600 K points, one finds activation energies of 6.3, 7.5, and 8.8 kcal/mole for $k_{p \to o}(SK)$, $k_{p \to o}(KPS)$, and $k_{p \to o}(TST)$, respectively. The quantum activation energy is 1.1 kcal/mole (0.048 eV) above the corresponding coplanar one (5.2 kcal/mole),[19b] and this difference is almost identical to the 0.05 eV 2D to 3D shift observed in Figs. 19 and 20 for the reaction probability curves.

Since the Porter–Karplus potential surface we used has an incorrect barrier height (0.396 eV[2c] vs 0.425 eV for the more accurate Liu surface[19]), a comparison with experimental results of thermal rate constant measurements will be deferred to a paper in which the results obtained with the full noncollinear Liu surface are described.

IV. SUMMARY

Let us now summarize the significant concepts developed in this paper. First, in the analysis of the reactive transition probabilities and cross sections we found a fairly accurate rotational projection quantum number (i.e., polarization) selection rule ($m_j = m_j' = 0$). Although one can find many factors which are at least partially responsible for this effect, the primary reason for this specificity and selectivity is the restriction to nearly linear geometries in the transition state as is

determined by the potential energy surface. No comparable selection effect was found for the nonreactive collisions (compare, for example, Figs. 10 and 11). At higher energies, quantum symmetry interference oscillations were observed in the $j = 0$ to $j' = 2$ para-to-para differential cross sections (see Fig. 15). Such oscillations might be capable of interpretation in terms of parameters which characterize the potential energy surface as has been done for the related atom–diatom and molecule–molecule elastic scattering situations.[57] The elastic cross sections revealed a lack of sensitivity of the $\theta < 30°$ angular distributions to the loss of flux into inelastic and reactive channels, and demonstrated the approximate validity of Levine's[45] conservation of total cross section rule and the validity of the central field approximation in this angular range. A comparison of the results of 1D, 2D, and 3D calculations revealed the importance of bending motions in the transition state and demonstrated their connection with threshold energies. In addition, the orientation dependence of the reaction probabilities was analyzed and found to be compatible with the observed maximum values of the total reaction probabilities. The results of 1D, 2D, and 3D comparisons afforded in this paper should be of great use in the improvement of 1D and 2D models so that they can be used to make quantitative predictions about 3D results. The degeneracy-averaged rotational distributions were found to obey Boltzmann-like expressions with a surprising degree of accuracy. A precise understanding of why this occurs remains unknown at present, but an analysis of the scattering wavefunction at the transition state in terms of vibrationally and rotationally adiabatic wavefunctions may help to clarify the relation of bending energy to product state rotational energy and hence to the temperature parameter. A comparison of our integral and differential cross sections with those of several other approximate calculations indicates best agreement with the quasiclassical results at energies for which tunneling effects are not important. On the other hand, the lack of tunneling in the classical cross sections produces important differences in the para-to-ortho thermal rate constant at temperatures below 300 K but the agreement is good at 600 K.

The wealth of dynamical information presented here makes clear the great usefulness of these calculations. At the same time, the large expenditure of computer time indicated in Table II implies that analogous calculations will be done for only a limited number of additional systems for which a very detailed understanding of the important dynamical processes involved is highly desirable. This places prime emphasis on the development of accurate but efficient approximate techniques, and the comparisons between accurate results and approximate ones such as those considered in Secs. III E and III G and in decoupling schemes presently being used by us indicate that such techiques may indeed exist.

ACKNOWLEDGMENT

[1](a) P. A. M. Dirac, Proc. R. Soc. London Ser. A 123, 714 (1929); (b) E. Schrödinger, Ann. Phys. 79, 361, 489 (1925); 80, 437 (1926); 81, 109 (1926).
[2](a) F. London, Z. Elektrochem. 35, 552 (1929); H. Eyring and M. Polanyi, Z. Phys. Chem. B 12, 279 (1931); (b) S. Sato, J. Chem. Phys. 23, 592 (1955); (c) R. N. Porter and M. Karplus, J. Chem. Phys. 40, 1105 (1964); (d) I. Shavitt, R. M. Stevens, F. L. Minn, and M. Karplus, J. Chem. Phys. 48, 2700 (1968); (e) H. Conroy and B. Bruner, J. Chem. Phys. 42, 4047 (1965); ibid. 47, 921 (1967); (f) B. Liu, J. Chem. Phys. 58, 1925 (1973); (g) see also C. Edmiston and M. Krauss, J. Chem. Phys. 49, 192 (1968) and references therein.
[3]M. Karplus, R. N. Porter, and R. D. Sharma, J. Chem. Phys. 43, 3259 (1965).
[4]D. Micha, Ark. Fys. 30, 427 (1965).
[5]M. Karplus and K. T. Tang, Discuss. Faraday Soc. 44, 56 (1967); K. T. Tang and M. Karplus, Phys. Rev. A. 4, 1844 (1971).
[6]J. D. Doll, T. F. George, and W. H. Miller, J. Chem. Phys. 58, 1343 (1973).
[7]G. Wolken and M. Karplus, J. Chem. Phys. 60, 351 (1974).
[8](a) B. H. Choi and K. T. Tang, J. Chem. Phys. 2462 (1974); (b) ibid. 61, 5147 (1974).
[9]A. Kuppermann and G. C. Schatz, J. Chem. Phys. 62, 2502 (1975).
[10]A. B. Elkowitz and R. E. Wyatt, J. Chem. Phys. 62, 2504 (1975).
[11](a) R. P. Saxon and J. C. Light, J. Chem. Phys. 56, 3874 (1972); ibid. 56, 3885 (1972); (b) A. Altenberger-Siczek and J. C. Light, J. Chem. Phys. 61, 4373 (1974); (c) R. P. Saxon and J. C. Light, J. Chem. Phys. 57, 2758 (1972); (d) J. J. Tyson, R. P. Saxon, and J. C. Light, J. Chem. Phys. 59, 363 (1973).
[12]R. B. Walker and R. E. Wyatt, J. Chem. Phys. 61, 4839 (1974).
[13](a) A. Kuppermann, G. C. Schatz, and M. Baer, J. Chem. Phys. 61, 4362 (1974); (b) G. C. Schatz and A. Kuppermann, J. Chem. Phys. 65, 4624 (1976), two papers back.
[14](a) D. G. Truhlar and A. Kuppermann, J. Chem. Phys. 56, 2232 (1972); (b) ibid., references therein.
[15](a) H. Eyring, J. Chem. Phys. 3, 107 (1935); H. Pelzer and E. Wigner, Z. Phys. Chem. B 15, 445 (1932); (b) H. S. Johnston, Gas Phase Reaction Rate Theory (Ronald, New York, 1966), Chap. 10.
[16]I. Shavitt, J. Chem. Phys. 49, 4048 (1969).
[17]J. M. Bowman, A. Kuppermann, J. T. Adams, and D. G. Truhlar, Chem. Phys. Lett. 20, 229 (1973); J. M. Bowman, Ph. D. thesis, California Institute of Technology, 1974.
[18]D. J. Diestler, J. Chem. Phys. 56, 2092 (1972).
[19](a) R. D. Levine and S. F. Wu, Chem. Phys. Lett. 11, 557 (1971); S. F. Wu and R. D. Levine, Mol. Phys. 22, 881 (1971).
[20]G. C. Schatz and A. Kuppermann, J. Chem. Phys. 59, 964 (1973).
[21]G. C. Schatz and A. Kuppermann, Phys. Rev. Lett. 35, 1266 (1975).
[22]G. Wolken, W. H. Miller, and M. Karplus, J. Chem. Phys. 56, 4930 (1972).
[23]A. C. Allison and A. Dalgarno, Proc. Phys. Soc. London 90, 609 (1967).

[24](a) K. T. Tang, Phys. Rev. 187, 122 (1969); (b) B. H. Choi and K. T. Tang, J. Chem. Phys. 63, 1783 (1975).

[25]E. F. Hayes, C. A. Wells, and D. J. Kouri, Phys. Rev. A 4, 1017 (1971).

[26]A. A. Westenberg and N. de Haas, J. Chem. Phys. 47, 1393 (1967); D. N. Mitchell and D. J. LeRoy, J. Chem. Phys. 58, 3449 (1973); see Ref. 15(b) for earlier references.

[27]A. Kuppermann and J. M. White, J. Chem. Phys. 44, 4352 (1966); A. Kuppermann, in *Proceedings of the Nobel Symposium 5 on Fast Reactions in Primary Processes in Chemical Kinetics*, edited by S. Claesson (Interscience, New York, 1967), pp. 131–140; Israel J. Chem. 7, 303 (1969).

[28]J. Geddes, H. F. Krause, and W. L. Fite, J. Chem. Phys. 52, 3296 (1970); *ibid.* 56, 3298 (1972); *ibid.* 59, 566 (1973); G. H. Kwei, V. W. S. Lo, and E. A. Entemann, J. Chem. Phys. 59, 3421 (1973); S. Datz and E. H. Taylor, J. Chem. Phys. 39, 1896 (1963).

[29]G. C. Schatz and A. Kuppermann, J. Chem. Phys. 65, 4642 (1976), preceding paper.

[30]A. Kuppermann, G. C. Schatz and M. Baer, J. Chem. Phys. 65, 4596 (1976), three papers back.

[31]A. Kuppermann, Chem. Phys. Lett. 32, 374 (1975).

[32]A. S. Davydov, *Quantum Mechanics* (Addison-Wesley, Reading, MA, 1965), Chap. 6.

[33]Equation (2.7) can be proven by considering the effect of the inversion operator ℓ of Appendix B of Ref. 29 on the scattering matrix solution $\psi_{J\mu}^{\lambda'v'j'\Omega'_\lambda}[S]$ of Eq. (5.3) of Ref. 29. By using Eqs. (B4) and (5.5) of that paper, one can easily show that the incident spherical wave parts of $(-1)^J \psi_{J\mu}^{\lambda'v'j'\Omega'_\lambda}$ and $\psi_{J\mu}^{\lambda'v'j'\Omega'_\lambda}$ are identical and as a result so are the corresponding outgoing parts, from which we conclude that $S_{J\lambda'v'_\lambda j'_\lambda\Omega'_\lambda}^{\lambda v j\Omega_\lambda}$ and $S_{J\lambda'v'_\lambda j'_\lambda-\Omega'_\lambda}^{\lambda v j-\Omega_\lambda}$ are equal. According to Eq. (5.30) of Ref. 29, we may replace $-\Omega'_\lambda$ by m'_λ, whereas Ω_λ may be replaced by m_{j_λ}. From this results $S_{J\lambda'v'_\lambda j'_\lambda m_{j_\lambda}}^{\lambda v j\Omega_\lambda} = S_{J\lambda'v'_\lambda j'_\lambda-m_{j_\lambda}}^{\lambda v j-\Omega_\lambda}$, which when substituted into Eq. (2.2) (of the present paper) together with the property[32]

$$d_{m_{j_\lambda}m'_{j_\lambda}}^J(\theta) = (-1)^{m_{j_\lambda}-m'_{j_\lambda}} d_{-m_{j_\lambda}-m'_{j_\lambda}}^J(\theta)$$

yields the relation

$$\begin{matrix} \lambda'v'_\lambda j'_\lambda - m'_{j_\lambda} \\ f\lambda v_\lambda j_\lambda - m_{j_\lambda} \end{matrix} = (-1)^{m'_{j_\lambda}-m_{j_\lambda}} \begin{matrix} \lambda'v'_\lambda j'_\lambda m_{j_\lambda} \\ f\lambda v_\lambda j_\lambda m_{j_\lambda} \end{matrix}$$

from which Eq. (2.7) follows.

[34]The various expansion coefficients V_n^λ of Eq. (2.14) were evaluated using a procedure outlined in Ref. 13(b) in which the n-term truncated expansion in Eq. (2.14) is required to be exactly satisfied at n values of γ_λ and the V_n^λ are obtained algebraically from this condition.

[35]This number can be obtained from a time delay analysis of the scattering matrix, similar to the one described previously.[29]

[36]R. G. Newton, *Scattering Theory of Waves and Particles* (McGraw-Hill, New York, 1966), pp. 572–575.

[37]R. T. Pack, J. Chem. Phys. 60, 633 (1974); P. McGuire and D. J. Kouri, J. Chem. Phys. 60, 2488 (1974).

[38]This can be verified by examining the expressions for J_z and H given in Ref. 29.

[39]This follows from (a) the assumption of Ref. 29 [which is implicit in Eq. (2.3)] that the initial relative velocity vector is parallel to the space fixed z axis, (b) the definition of the angle θ (or θ_λ of Fig. 1), which is the angle between the outgoing z'_λ axis and the space-fixed z axis, and (c) the relation $\theta_R = 180 - \theta$ of Sec. II.A.

[40]For example, R. Gengenbach, C. Hahn, and J. P. Toennies, J. Chem. Phys. 62, 3620 (1975); M. A. Fluendy, R. M. Martin, E. E. Muschlitz, and D. R. Herschbach, J. Chem. Phys. 46, 2172 (1967); W. C. Stwalley, A. Niehaus, and D. R. Herschbach, J. Chem. Phys. 51, 2287 (1969).

[41]A. Kuppermann, R. J. Gordon, and M. J. Coggiola, J. Chem. Soc. Faraday Discuss. 55, 145 (1973).

[42]H. P. Butz, R. Feltgen, H. Pauly, and H. v. Vehmeyer, Z. Phys. 247, 70 (1971).

[43]R. Gordon, J. Chem. Phys. 51, 14 (1969).

[44]Some ambiguity still exists because of the small difference (< 0.05 rad between the single channel and converged phase shifts.

[45]R. D. Levine, Chem. Phys. Lett. 4, 309 (1969); J. Chem. Phys. 57, 1015 (1972).

[46](a) D. J. Diestler, J. Chem. Phys. 54, 4547 (1971); (b) J. W. Duff and D. G. Truhlar, Chem. Phys. Lett. 23, 327 (1973).

[47]R. B. Walker and R. E. Wyatt, Mol. Phys. 28, 101 (1974).

[48]A. Ben-Shaul, R. D. Levine, and R. B. Bernstein, Chem. Phys. Lett. 15, 160 (1972); J. Chem. Phys. 57, 5427 (1972).

[49]R. E. Wyatt, Chem. Phys. Lett. 34, 167 (1975).

[50]A. C. Yates and W. A. Lester, Chem. Phys. Lett. 24, 305 (1974).

[51]R. E. Waytt (private communication).

[52]A. B. Elkowitz and R. E. Wyatt, J. Chem. Phys. 63, 702 (1975).

[53]J. M. Bowman and A. Kuppermann, J. Chem. Phys. 59, 6524 (1973); W. H. Miller and T. F. George, J. Chem. Phys. 57, 2458 (1972).

[54]A. Farkas, *Orthohydrogen, Parahydrogen and Heavy Hydrogen* (Cambridge U. P., Cambridge, 1935), p. 13.

[55]D. G. Truhlar, J. Chem. Phys. 65, 1008 (1976).

[56]A. Kuppermann, J. T. Adams, and D. G. Truhlar, (to be published).

[57]For examples, see J. M. Farrar and J. T. Lee, J. Chem. Phys. 56, 5801 (1972); P. E. Siska, J. M. Parson, T. P. Schaefer, and Y. T. Lee, J. Chem. Phys. 55, 5762 (1971); J. M. Farrar and Y. T. Lee, J. Chem. Phys. 57, 5492 (1972).

LARGE QUANTUM EFFECTS IN A MODEL ELECTRONICALLY NONADIABATIC REACTION: Ba + $N_2O \rightarrow BaO^* + N_2$ [*]
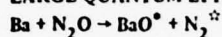
Joel M. BOWMAN [‡], Steven C. LEASURE [‡]
Department of Chemistry, Illinois Institute of Technology,
Chicago, Illinois 60616, USA

and

Aron KUPPERMANN
Arthur Amos Noyes Laboratory of Chemical Physics [†], *California Institute of Technology,*
Pasadena, California 91125, USA

Received 7 June 1976

Calculations of reaction probabilities have previously been performed for a collinear model of the electronically nonadiabatic reaction Ba + $N_2O \rightarrow BaO(X^1\Sigma)$, $BaO(a^3\Pi) + N_2$, treating N_2 as a mass point and using accurate quantum mechanical as well as quasi-classical trajectory surface-hopping techniques. In the present paper we compare these two sets of results and conclude that large quantum effects exist and that the Landau–Zener surface-hopping model for the description of this system is inadequate.

The chemiluminescent Ba + N_2O reaction has recently been the object of intensive experimental investigations [1–9]. The observed chemiluminescence has been assigned to the $A^1\Sigma \rightarrow X^1\Sigma$ transition of BaO [1–9], but the pressure dependence of the emission intensity has led to the suggestion that the $a^3\Pi$ state of BaO is the dominant reaction product and that the radiating $A^1\Sigma$ state is populated by subsequent nonreactive bimolecular collisions of $BaO(a^3\Pi)$ with the pressurizing gas [4,10].

We have modeled the Ba + N_2O reaction as a col-

linear two-electronic-state process in order to investigate the properties of such a model with N_2 treated as a mass point [11–13]. Intersecting model ground (singlet) state and excited (triplet) state LEPS surfaces, V_s and V_t, respectively, were chosen as was an interaction potential surface, V_i. V_s has a 0.05 eV barrier located in the near-asymptotic region of the product channel and an exothermicity of 9.. eV [13]. This was made substantially lower than the experimentally determined 4 eV [2] exothermicity in order to keep the number of open exit channels down to a manageable amount while preserving the characteristics of the surface crossing. For the total energies considered, V_t is energetically inaccessible except in the near-asymptotic and asymptotic regions of the product channel. V_i has a maximum value of 0.05 eV and is localized along the seam of intersection of V_s and V_t. The quantum calculations were done by an extension [12] of the coupled-channel propagation method developed previously [14–16]. The initial relative kinetic energies E_0 ranged between 0.0 and

0.12 eV. In this energy interval the number of open vibrational states of the model $BaO(X\,^1\Sigma)$ lies between four and six and that for the model $BaO(a\,^3\Pi)$ between one and three. A total of up to twenty eight channels were required in the quantum calculations to ensure unitarity and symmetry of the scattering matrix (conservation of flux to within 2% and symmetry to within 5%). The trajectory surface hopping method (in the simple Landau–Zener version) of Tully and Preston [17] was used to obtain the quasiclassical trajectory results [18].

In fig. 1 the results of some of these calculations are presented. $P^R_{n\upsilon \to n'\upsilon'}$ is the reaction probability from state n, υ of N_2O to state n', υ' of BaO where υ and υ' are vibrational quantum numbers, n or $n' = 1$ refer to the ground electronic states and $n' = 2$ to the triplet state. We observe that for E_0 less than 0.05 eV $P^R_{10 \to 10}$ is the dominant reaction probability (confirming the repulsive nature [19] of the model V_1) and that the quantal and quasiclassical results agree "in average" for this electronically adiabatic transition. The quasiclassical $P^R_{10 \to 10}$ effective threshold energy is approximately 0.01 eV greater than the quantal one, however. All of the quantal reaction probabilities show pronounced oscillations which appear to be "averaged" out in the corresponding quasiclassical results. This behavior had been observed in a previous comparison of quantal and quasiclassical studies of the collinear H + H_2 reaction [20]. The existence of quantum oscillations is compatible with an analysis of the system's de Broglie wavelength λ. Using mass-scaled coordinates [21,22], the value of λ for the Ba + $N_2O(\upsilon = 0) \to BaO$ $(a\,^3\Pi; \upsilon' = 0) + N_2$ process varies from 0.56 bohr for the reagents at $E_0 = 0.05$ eV to 0.36 bohr for the products formed from reagents at $E_0 = 0.10$ eV. For E_0 in this range, the smallest distance Δs along the reaction coordinate of the singlet surface over which the local wavenumber changes by 20% lies between 0.2 and 0.5 bohr. Therefore, the condition $\Delta s \gg \lambda$ for validity of the WKB approximation [23] is not satisfied, and large quantum effects are possible.

The comparison of the quantal and quasiclassical electronically nonadiabatic reaction probability $P^R_{10 \to 20}$ of fig. 1d shows fairly good average agreement for E_0 between 0.05 eV and 0.07 eV, but at somewhat higher energies the quasiclassical result differs significantly from the accurate quantal one, in contrast with the good average agreement found for the electronically
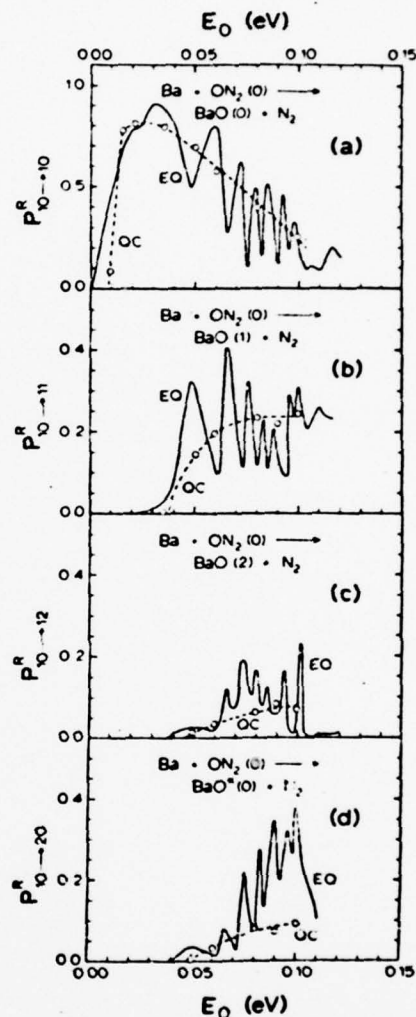

Fig. 1. Reaction probabilities for collinear Ba + $ON_2 \to BaO(\upsilon)$, $BaO^*(\ )$ N_2 as a function of initial relative kinetic energy E_0 (BaO and BaO* represent the ground and electronically excited products, respectively). (a)–(c) Reaction probabilities to form BaO in $\upsilon = 0, 1$, and 2, respectively from ground vibrational state reagent ON_2. (d) Reaction probabilities to form BaO* in $\upsilon' = 0$ from ground vibrational state reagent. The exact quantum (EQ) and quasiclassical (QC) results are represented by solid and dashed curves, respectively.

adiabatic processes of figs. 1a, 1b and 1c. This disagreement should be due at least in part to a shortcoming of the simple Landau–Zener surface-hopping model used in these calculations. The usual conditions for the validity of the Landau–Zener approximation [24] are met by the Ba + N_2O model system. However, the seam between the singlet and triplet surfaces which we used is located in the product channel and is displaced from the equilibrium internuclear position of BaO towards greater internuclear distances. This displacement means that the ground electronic state of the BaO product must have about one quantum of vibrational energy before the seam can be reached classically. This should result in a significant decrease of the amount of quasiclassical surface-hopping in comparison with the quantum situation since in the latter case the seam is felt over a wider range of internuclear distances. Such analysis is consistent with the fact that the quantal and quasi-classical $P_{10 \to 20}^R$ effective thresholds are approximately equal to the corresponding values for the electronically adiabatic $10 \to 11$ and $10 \to 12$ processes which produce vibrationally excited ground electronic state products. This suggests a correlation between vibrational excitation of BaO($X\,^1\Sigma$) and formation of BaO($a\,^3\Pi$).

One may improve the surface-hopping model by permitting hopping to occur from a band around the seam rather than at the seam only. Even then, this first-order perturbation model may not work too well for systems for which the electronically nonadiabatic transition probabilities are large, as in the present case. These results indicate that caution should be exercised in using the quasiclassical surface-hopping method for performing calculations of reactive electronically nonadiabatic transition probabilities even for systems as heavy as the present one. The large quantum effects observed will not necessarily disappear in going to a three-dimensional world [25,26].

References

[1] Ch. Ottinger and R.N. Zare, Chem. Phys. Letters 5 (1970) 243.

[2] C.D. Jonah, R.N. Zare and Ch. Ottinger, J. Chem. Phys. 56 (1972) 263.

[3] R.H. Obenauf, C.J. Hsu and H.B. Palmer, J. Chem. Phys. 57 (1972) 5607; 58 (1973) 2674.

[4] C.J. Hsu, W.D. Krugh and H.B. Palmer, J. Chem. Phys. 60 (1974) 5118.

[5] A. Schultz and R.N. Zare, J. Chem. Phys. 60 (1974) 5120.

[6] C.R. Jones and H.P. Broida, J. Chem. Phys. 59 (1973) 6677; 60 (1974) 4369.

[7] D.J. Eckstrom, S.A. Edelstein and S.W. Benson, J. Chem. Phys. 60 (1974) 2930.

[8] D.J. Eckstrom, S.A. Edelstein, D.L. Huestis, B.E. Perry and S.W. Benson, J. Chem. Phys. 63 (1975) 3828.

[9] D.J. Wren and M. Menzinger, J. Chem. Phys. 63 (1975) 4557.

[10] R.W. Field, C.R. Jones and H.P. Broida, J. Chem. Phys. 60 (1974) 4377.

[11] J.M. Bowman and A. Kuppermann, IXth International Conference on the Physics of Electronic and Atomic Collisions Abstracts of Papers, University of Washington, Seattle (1975) p. 351.

[12] J.M. Bowman and A. Kuppermann, to be published.

[13] J.M. Bowman, Ph.D. Thesis, Part III, California Institute of Technology (1974), unpublished.

[14] A. Kuppermann, VIIth International Conference on the Physics of Electronic and Atomic Collisions, Abstracts of Papers (North-Holland, Amsterdam, 1971) p. 1.

[15] G.C. Schatz, J.M. Bowman and A. Kuppermann, J. Chem. Phys. 58 (1973) 4023; 61 (1974) 674, 685.

[16] G.C. Schatz and A. Kuppermann, J. Chem. Phys. 59 (1973) 964.

[17] J.C. Tully and R.K. Preston, J. Chem. Phys. 55 (1971) 562.

[18] S.C. Leasure and J.M. Bowman, to be published.

[19] J.C. Polanyi and J.L. Schreiber, in : Physical chemistry - an advanced treatise, Vol. 6, Kinetics of gas reactions, eds. H. Eyring, W. Jost and D. Henderson (Academic Press, New York, 1974) ch. 9.

[20] J.M. Bowman and A. Kuppermann, Chem. Phys. Letters 12 (1971) 1.

[21] L.M. Delves, Nucl. Phys. 9 (1959) 391.

[22] D. Jepsen and J.O. Hirschfelder, Proc. Natl. Acad. Sci. US 45 (1959) 249.

[23] L.I. Schiff, Quantum mechanics, 3rd Ed. (McGraw-Hill, New York, 1968) p. 271.

[24] E.E. Nikitin, in : Chemische Elementarprozesse, ed. H. Hartmann (Springer, Berlin, 1968) p. 51.

[25] G.C. Schatz and A. Kuppermann, Phys. Rev. Letters 35 (1975) 1266.

[26] G.C. Schatz and A. Kuppermann, Quantum Mechanical Reactive Scattering for Three-Dimensional Atom Plus Diatom Systems, II. Accurate Cross Sections for H + H_2, J. Chem. Phys., submitted for publication.

VALIDITY OF THE ADIABATIC APPROXIMATION FOR VIBRATIONAL ENERGY TRANSFER IN COLLISIONS BETWEEN DIATOMIC MOLECULES[†]

John P. DWYER * and Aron KUPPERMANN

Arthur Amos Noyes Laboratory of Chemical Physics‡, California Institute of Technology, Pasadena, California 91125, USA

Accurate quantum mechanical transition probabilities for vibrational to vibrational and vibrational to translational energy transfer in collinear collisions of two hydrogen molecules were calculated for a model potential by numerical integration of the Schrödinger equation. The accuracy of these calculations was checked by conservation of flux and convergence tests and by verifying that they satisfied a rigorous theorem proven by Clarke and Thiele. These accurate results were then used to determine the range of validity of the adiabatic approximation of Thiele and Katz as applied to this model system by Clarke and Thiele. This approximation yielded probabilities which agreed with the accurate ones to 10% or better for total energies E up to 6.1 (in units of diatom vibrational quanta). However, at $E = 7.9$ these approximate results could be off by a factor of 1.5 or higher.

1. Introduction

In a recent paper [1] (hereafter called I) Clarke and Thiele studied energy transfer in the collinear collision of two diatomic molecules. After reducing the problem to a pseudo atom–diatom collision (using a method developed by Zelechow et al. [2]), they used the adiabatic approximation of Thiele and Katz [3] and the first order distorted wave T and K matrix methods to calculate vibrational–vibrational (V–V) and translational–vibrational (T–V) transition probabilities. In a previous paper [4] (hereafter called II), Riley and Kuppermann calculated the exact quantum transition probabilities for the same system. Because of the special form of the interaction potential used (exponentially repulsive), part of the calculation can be done analytically. From this information, Clarke and Thiele were able to show that some of the probabilities calculated in II must be inaccurate. We have redone the

Riley and Kuppermann calculations and have found that the number of basis functions which had been used was insufficient for convergence. Using larger basis sets we have obtained converged results which also satisfy the conditions derived in I.

2. Theory

We will briefly examine the equations to be solved. A more complete treatment is given by Riley [5]. The diatomic molecules are assumed to be harmonic oscillators, confined to move on a space-fixed straight line while the intermolecular potential is exponentially repulsive and dependent only on the nearest end-atom separation. The Schrödinger equation to be solved is

$$[(-\partial^2/\partial y^2 + y^2) + \omega(-\partial^2/\partial x^2 + x^2) - \mu^{-1}\,\partial^2/\partial r^2$$

$$+ e^{-\alpha(r-y-\beta x)} - E]\,\psi(x,y,r) = 0, \tag{1}$$

where r describes the intermolecular separation, x and y are related to the intramolecular separations, μ is an effective mass of the system, E is the total energy, ω and β are measures of the relative frequencies of the oscillators, and α is a length which describes the near-

499

est end-atom repulsion. All of these parameters are in reduced units. Following I and II we treated the case of identical homonuclear diatomics, which results in $\mu = \frac{1}{2}$, $\beta = 1$, and $\omega = 1$. The value of α was taken to be 0.2973 as before, which is appropriate for describing a collision between two hydrogen molecules. We define the reference hamiltonian H_0 by

$$H_0(x,y) = (-\partial^2/\partial y^2 + y^2) + \omega(-\partial^2/\partial x^2 + x^2), \quad (2)$$

whose eigenfunctions and eigenvalues are denoted by $\Phi_{ij}(x,y)$ and W_{ij}, respectively, i and j being the vibrational quantum numbers of the isolated molecules. The separability of the x and y coordinates in eq. (2) permits us to write

$$\Phi_{ij}(x,y) = \phi_i(y)\phi_j(x) \quad (3)$$

and

$$W_{ij} = (2i+1) + \omega(2j+1). \quad (4)$$

The solutions $\psi^{n'm'}(x,y,r)$ of eq. (1) can be expanded in the $\Phi_{ij}(x,y)$ basis set to give

$$\psi^{n'm'}(x,y,r) = \sum_{n=0}^{N-1} \sum_{m=0}^{M-1} f_{nm}^{n'm'}(r)\Phi_{nm}(x,y), \quad (5)$$

$$n' = 0, ..., N-1, \qquad m' = 0, ..., M-1,$$

where N and M are the number of eigenstates in the expansion for coordinates y and x, respectively. For the present case $N = M$, and the transition probabilities are considered converged when increasing N produces in them an acceptably small change.

Substituting eq. (5) into eq. (1) gives the following set of coupled differential equations

$$[f_{nm}^{n'm'}(r)]'' = [V_{nm}^{n'm'}(r) - k_{nm}^2] f_{nm}^{n'm'}(r), \quad (6)$$

where

$$V_{nm}^{n'm'}(r) = \mu \langle \Phi_{nm}(x,y)|e^{-\alpha(r-y-\beta x)}|\Phi_{n'm'}(x,y)\rangle \quad (7)$$

and

$$k_{nm} = [\mu(E - W_{nm})]^{1/2}, \quad (8)$$

the integrations implied in eq. (7) being performed over the x and y coordinates. These equations are solved by a method described previously [5].

Table 1
Transition probabilities for the V–V energy transfer of 1 and 2 quanta

Transition	E [a]	Riley and Kuppermann [b] $M = N = 3$	Clarke and Thiele [c]	$M = N = 5$	$M = N = 6$
$01 \rightarrow 10$	4.1	0.4100×10^{-2}	0.4100×10^{-2}	0.4100×10^{-2}	0.4100×10^{-2}
	4.5	0.2109×10^{-1}	0.2094×10^{-1}	0.2109×10^{-1}	0.2109×10^{-1}
	5.0	0.4376×10^{-1}	0.4285×10^{-1}	0.4376×10^{-1}	0.4376×10^{-1}
	5.5	0.6805×10^{-1}	0.6545×10^{-1}	0.6808×10^{-1}	0.6808×10^{-1}
	6.1	0.9894×10^{-1}	0.9319×10^{-1}	0.9924×10^{-1}	0.9924×10^{-1}
	7.0	0.1459	0.1371	0.1483	0.1483
	7.9	0.1875	0.1780	0.1957	0.1957
$02 \rightarrow 11$	6.1	0.7821×10^{-2}	0.7843×10^{-2}	0.7850×10^{-2}	0.7850×10^{-2}
	7.0	0.7609×10^{-1}	0.7882×10^{-1}	0.8033×10^{-1}	0.8033×10^{-1}
	7.9	0.1317	0.1480	0.1544	0.1544
$02 \rightarrow 20$	6.1	0.1695×10^{-4}	0.1710×10^{-4}	0.1711×10^{-4}	0.1711×10^{-4}
	7.0	0.1571×10^{-2}	0.1707×10^{-2}	0.1780×10^{-2}	0.1780×10^{-2}
	7.9	0.5165×10^{-2}	0.6508×10^{-2}	0.7248×10^{-2}	0.7248×10^{-2}

[a] Total energy in units of diatom vibrational quanta.
[b] Refs. [4,5].
[c] Ref. [1], using the adiabatic method of Thiele and Katz [3].

3. Results and discussion

The results for $N = 5$ and $N = 6$ are presented in tables 1 and 2 for a variety of transitions and of total energies (in units of diatom vibrational quanta). Included are the values of Riley and Kuppermann ($N = 3$) and those of Clarke and Thiele. In I, Clarke and Thiele present a partial decoupling scheme which reduces the problem to a pseudo atom–diatom collision. Although they used approximate methods to calculate transition probabilities, they showed rigorously that

$$P_{00 \rightarrow 11}/P_{00 \rightarrow} = 2,$$

where $P_{ij \rightarrow kl}$ is the probability of going from the i, j states of the initial molecules to the corresponding k, l states of the final ones. On the basis of this result they were able to conclude that certain of the transition probabilities calculated in II are incorrect. Table 3 lists this ratio for various choices of N. First note that the results in tables 1 and 2 are nearly identical for $N = 5$ and $N = 6$. The largest discrepancy is 1 part in 2000. In addition, table 3 shows that the ratio $P_{00 \rightarrow 11}/P_{00 \rightarrow 02}$ has converged to 2 to within this accuracy, in agreement with Clarke and Thiele's predictions. From this and the fact that flux conservation is satisfied in these calculations to six significant digits, we conclude that our results have not only converged but are also accurate. At the lowest energies (4.1 and 4.5) the

Table 2
Transition probabilities for the T–V energy transfer of 1 and 2 quanta

Transition	E [a]	Riley and Kuppermann [b] $M = N = 3$	Clarke and Thiele [c]	$M = N = 5$	$M = N = 6$
$00 \rightarrow 01$	4.1	0.169×10^{-5}	0.167×10^{-5}	0.1665×10^{-5}	0.1665×10^{-5}
	4.5	0.784×10^{-4}	0.802×10^{-4}	0.7883×10^{-4}	0.7884×10^{-4}
	5.0	0.650×10^{-3}	0.672×10^{-3}	0.6503×10^{-3}	0.6503×10^{-3}
	5.5	0.231×10^{-2}	0.244×10^{-2}	0.2325×10^{-2}	0.2325×10^{-2}
	6.1	0.641×10^{-2}	0.701×10^{-2}	0.6568×10^{-2}	0.6568×10^{-2}
	7.0	0.174×10^{-1}	0.207×10^{-1}	0.1879×10^{-1}	0.1879×10^{-1}
	7.9	0.326×10^{-1}	0.439×10^{-1}	0.3854×10^{-1}	0.3854×10^{-1}
$01 \rightarrow 11$	6.1	0.195×10^{-5}	0.169×10^{-5}	0.1691×10^{-5}	0.1691×10^{-5}
	7.0	0.826×10^{-3}	0.675×10^{-3}	0.6513×10^{-3}	0.6512×10^{-3}
	7.9	0.653×10^{-2}	0.514×10^{-2}	0.4745×10^{-2}	0.4745×10^{-2}
$01 \rightarrow 02$	6.1	0.111×10^{-5}	0.324×10^{-5}	0.3238×10^{-5}	0.3237×10^{-5}
	7.0	0.152×10^{-3}	0.128×10^{-2}	0.1168×10^{-2}	0.1188×10^{-2}
	7.9	0.444×10^{-3}	0.122×10^{-1}	0.8269×10^{-2}	0.8270×10^{-2}
$01 \rightarrow 20$	6.1	0.560×10^{-7}	0.115×10^{-6}	0.1216×10^{-6}	0.1216×10^{-6}
	7.0	0.455×10^{-4}	0.629×10^{-4}	0.1139×10^{-3}	0.1139×10^{-3}
	7.9	0.413×10^{-3}	0.258×10^{-2}	0.1314×10^{-2}	0.1314×10^{-2}
$00 \rightarrow 11$	6.1	0.150×10^{-7}	0.998×10^{-8}	0.1128×10^{-7}	0.1128×10^{-7}
	7.0	0.224×10^{-4}	0.989×10^{-5}	0.1262×10^{-4}	0.1262×10^{-4}
	7.9	0.397×10^{-3}	0.120×10^{-3}	0.1945×10^{-3}	0.1944×10^{-3}
$00 \rightarrow 02$	6.1	0.350×10^{-8}	0.494×10^{-8}	0.5638×10^{-8}	0.5639×10^{-8}
	7.0	0.189×10^{-5}	0.494×10^{-5}	0.6308×10^{-5}	0.6309×10^{-5}
	7.9	0.181×10^{-4}	0.599×10^{-4}	0.9720×10^{-4}	0.9722×10^{-4}

[a] Total energy in units of diatom vibrational quanta.
[b] Refs. [4,5].
[c] Ref. [1], using the adiabatic method of Thiele and Katz [3] except for the $00 \rightarrow 11$ and $00 \rightarrow 02$ transitions, for which the "corrected" adiabatic results are given.

Table 3
Ratio of $P_{00 \to 11}$ and $P_{00 \to 02}$ probabilities

E [a]	Riley and Kuppermann [b] $M = N = 3$	$M = N = 4$	$M = N = 5$	$M = N = 6$
6.1	4.314	1.998	2.000	2.000
7.0	11.84	2.012	2.001	2.000
7.9	21.96	2.185	2.000	2.000

[a] Total energy in units of diatom vibrational quanta.
[b] From the data of refs. [4,5].

Clarke and Thiele approximate results agree with our accurate ones to better than 1%. In general, the inaccuracy is less than 10% for all transitions at $E \leqslant 6.1$. However, at $E = 7.9$, their result for the 01 → 20 transition is too large by a factor of about 2.

For V–V transitions, the results of Riley and Kuppermann are in good agreement with ours for the transition involving the lowest internal excitation (01 → 10). As expected, the agreement is somewhat worse for higher internal excitation transitions. For T–V transitions, the agreement is good only for the lowest four energies of the 00 → 01 transition.

We conclude that the adiabatic method of Thiele and Katz gives results for this model problem in good agreement with the exact quantum probabilities for all but the highest energies considered.

References

[1] J. Clarke and E. Thiele, Chem. Phys. 4 (1974) 447.
[2] A. Zelechow, D. Rapp and T. Sharp, J. Chem. Phys. 48 (1968) 286.
[3] E. Thiele and R. Katz, J. Chem. Phys. 55 (1971) 3195.
[4] M. Riley and A. Kuppermann, Chem. Phys. Letters 1 (1968) 537.
[5] M. Riley, Ph.D. Thesis, California Institute of Technology (1968).

ANGULAR MOMENTUM DECOUPLING APPROXIMATIONS
IN THE QUANTUM DYNAMICS OF REACTIVE SYSTEMS*

Aron KUPPERMANN, George C. SCHATZ** and John P. DWYER

*Arthur Amos Noyes Laboratory of Chemical Physics‡, California Institute of Technology,
Pasadena, California 91125, USA*

Two methods for implementing angular momentum decoupling approximations in quantum mechanical reactive scattering are examined. Applications to both reactive and nonreactive H + H₂ collisions indicate that for the most intense individual reactive transitions and for all degeneracy-averaged ones, these decoupling methods (especially the "proper" decoupling method) yield results in good agreement with those of fully-coupled calculations. However, for the less intense reactive transitions and all individual nonreactive transitions, very large errors can result from use of these approximate methods.

Accurate ab initio three-dimensional quantum-mechanical reactive scattering calculations have recently been performed for the first time [1–5]. However, the computation times required limit the feasibility of such calculations to very simple systems. This, as well as the pursuit of physical insight, makes it very important to develop approximate calculation techniques which are significantly more efficient while preserving an acceptable level of accuracy. One approach is to introduce angular momentum decoupling schemes which partially decouple the large number of channels involved. Several such schemes have been recently proposed and tested for non-reactive [6–13] and for reactive systems [14]. In this paper we describe two schemes developed for reactive systems and give some of the results of their applications to collisions of H with H₂ on the Porter–Karplus potential energy surface [15]. They show that for the most intense reactive transitions quite accurate integral cross sec-

tions are obtained, but for the less intense ones and for all individual non-reactive transitions very large errors can result.

Consider a triatomic system $A_\alpha A_\beta A_\gamma$ in which r_λ is the vector from A_ν to A_κ and R_λ that from the center of mass of $A_\nu A_\kappa$ to A_λ, $\lambda\nu\kappa$ being any cyclic permutation of $\alpha\beta\gamma$. Consider next a system of body-fixed coordinates in which the Z_λ axis lies along R_λ. Expansion of the system's wavefunction in products of Wigner rotation functions [16] and spherical harmonics of the angular coordinates leads to a set of Schrödinger equations [2,3,6] in the wavefunctions $W_{Jj_\lambda\Omega_\lambda}(r_\lambda, R_\lambda)$. The indices $Jj_\lambda\Omega_\lambda$ are the quantum numbers associated respectively with the total, the $A_\nu A_\kappa$ diatom, and its Z_λ-component angular momenta. These equations couple $W_{Jj_\lambda\Omega_\lambda}$ to $W_{Jj_\lambda\Omega_\lambda \pm 1}$ and to all $W_{Jj'_\lambda\Omega_\lambda}$ ($j'_\Omega > |\Omega_\lambda|$). The Ω_λ-coupling terms are

$$(-\hbar^2/2\mu R_\lambda^2)[J(J+1) - \Omega_\lambda(\Omega_\lambda \pm 1)]^{1/2}$$

$$\times [j_\lambda(j_\lambda+1) - \Omega_\lambda(\Omega_\lambda \pm 1)]^{1/2} W_{Jj_\lambda\Omega_\lambda \pm 1}$$

and stem entirely from the tumbling of the triatom plane around R_λ. Neglect of these Ω_λ-coupling terms in non-reactive systems along with additional approximations on the terms which are diagonal in Ω_λ has led to reasonably accurate results [6–13].

71

For reactive systems we neglect the Ω_λ-coupling terms in each of the three arrangement channels but retain without modification all other terms in the resulting Ω_λ-decoupled but j_λ-coupled equations. When linearly combining the solutions of these equations to generate wavefunctions which are everywhere smoothly continuous [1–3], we either exclude Ω-mixing in this arrangement channel matching procedure in the "simple" angular momentum decoupling scheme (SD), or do the matching correctly [1–3] in the "proper" angular momentum decoupling scheme (PD). Let $v_\lambda j_\lambda m_{j_\lambda}$ be the vibrotation quantum numbers of the isolated diatom in arrangement channel λ, in the helicity representation [17]. In the SD approximation the probabilities and cross sections for the $\lambda v_\lambda j_\lambda m_{j_\lambda} \rightarrow \lambda' v'_\lambda m'_{j'_\lambda}$ process vanish identically un-

less $m'_{j'_\lambda} = -m_{j_\lambda}$ (i.e. $\Omega'_{\lambda'} = \Omega_\lambda$ *), because of the complete Ω-decoupling in both the j_λ-coupled equations and the matching procedure. In the PD approximation this is not true, because of the Ω-coupling introduced by the matching process. This Ω-coupling physically results from the non-collinearity of the reagent and product z-axes.

For $m'_{j'} = m_j = 0$ reactive transitions for $H + H_2$, the PD approximation works very well and the SD one only moderately well. This is illustrated in figs. 1 and 2. The $000 \rightarrow 010$ and $000 \rightarrow 020$ PD integral reaction cross sections of fig. 1 differ from the accurate ones

---

* We have $\Omega'_{\lambda'} = m'_{j'_\lambda}$, but $\Omega_\lambda = -m_{j_\lambda}$ because of the final R_λ and final relative atom–diatom velocity vectors are the same but those of the corresponding initial quantities are opposite.
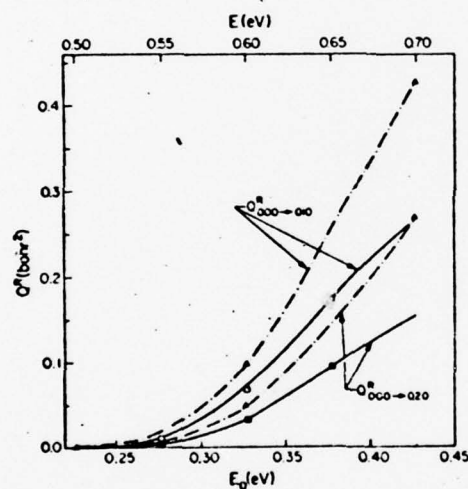

Fig. 1. Distinguishable-atom integral reaction cross sections for the $000 \rightarrow 010$ and $000 \rightarrow 020$ transitions as a function of initial relative translational energy E_0 and total energy E, for collisions of H with H_2 on the Porter–Karplus [15] potential energy surface. The full curves are the results of accurate three-dimensional quantum-mechanical calculations. The triangles (connected by dash-dotted curves) correspond to the simple angular momentum decoupling scheme and the squares to the proper angular momentum decoupling scheme (see text). The open symbols correspond to the $000 \rightarrow 010$ reactive transition and the full ones to the $000 \rightarrow 020$ reactive transition.
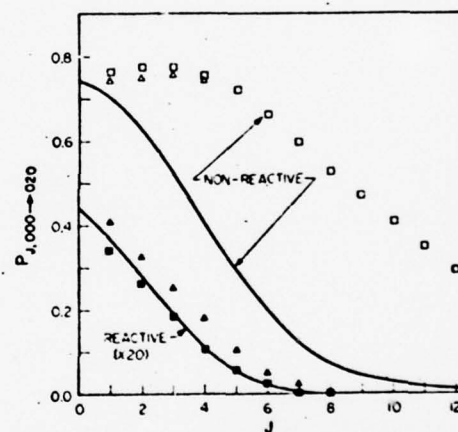

Fig. 2. Distinguishable-atom probabilities for the $000 \rightarrow 020$ transition as a function of total angular momentum quantum number for reactive and non-reactive collisions of H with H_2 on the Porter–Karplus [15] potential energy surface at a total energy $E = 0.6$ eV and initial relative translational energy $E_0 = 0.328$ eV. The curves are smooth lines drawn through the points (not indicated) corresponding to accurate three-dimensional quantum-mechanical calculations. The triangles correspond to the SD scheme and the squares to the PD scheme (see text). The open symbols represent probabilities for non-reactive transitions and the full ones probabilities for reactive transitions (after multiplication by 20). For $J > 4$ the SD non-reactive probabilities are indistinguishable from the PD ones, within plotting accuracy.

by less than 7.5% in the 0.45 to 0.65 eV range of total energy, over which the cross sections themselves increase by more than three orders of magnitude. This agreement is of the same order as the accuracy of the accurate calculations themselves [1,3] ! The corresponding error in the SD cross sections can be as high as 60% in the same energy range, indicating the importance of Ω-coupling between different arrangement channels.

For reactive collisions in which the condition $m'_{j'} = m_j = 0$ is *not* fulfilled, the PD and SD probabilities can be in error by one or more orders of magnitude. For example, for the Ω-conserving $01-1 \rightarrow 011$ reactive process at $E = 0.6$ eV and $J = 5$, the ratio of the SD and PD probabilities to the accurate one (0.13×10^{-3}) are 0.35 and 0.47×10^{-3}, respectively. For the non-Ω-conserving $000 \rightarrow 011$ process the SD results vanish identically and the analogous PD to accurate (0.57×10^{-3}) probability ratio is 0.041. However, the reactive $vjm_j \rightarrow v'j'm'_{j'}$ transitions for which $m'_{j'} = m_j = 0$ are an order of magnitude or more more intense than the other reactive ones [3]. Consequently the corresponding summed (over $m'_{j'}$) and averaged (over m_j) PD integral cross sections $Q^R_{vj \rightarrow v'j'}$ are still reasonably accurate for low j and j'.

Both the SD and PD approximations are very poor for all individual *non*-reactive transitions, as illustrated in fig. 2. The reason is related to the fact that a wider range of atom–molecule distances contribute to non-reactive rather than to reactive scattering, increasing the importance of kinematic angular momentum coupling terms.

In summary, for $H + H_2$ collisions, the PD integral cross sections for reactive (distinguishable-atom) $m'_{j'} = m_j = 0$ transitions – which are the dominant reactive processes in this collinearly-dominated system – agree with the accurate ones essentially to within the accuracy of the latter. This successful approximation results furthermore in a very substantial saving in computational time. It should permit extension of three-dimensional quantum-mechanical reactive scattering calculations to systems involving larger numbers of channels. For the other reactive and all individual $0jm_j \rightarrow 0j'm'_{j'}$ nonreactive processes in $H + H_2$, the

Ω-decoupling approximations considered give quite poor results, indicating a strong breakdown of "j_z-conservation" [6–11] for those transitions. However, it is interesting to note that both the simple and proper decoupling summed and averaged cross sections are in good ($\approx 5\%$) agreement with the fully coupled calculation. This seems to indicate that the nonreactive flux is transferred from different m_j to $m_j = 0$ for the *same* j.

References

[1] A. Kuppermann and G.C. Schatz, J. Chem. Phys. 62 (1975) 2503.

[2] G.C. Schatz and A. Kuppermann, Quantum Mechanical Reactive Scattering for Three Dimensional Atom Plus Diatom Systems: I. Theory, J. Chem. Phys., to be published.

[3] G.C. Schatz and A. Kuppermann, Quantum Mechanical Reactive Scattering for Three Dimensional Atom Plus Diatom Systems: II. Accurate Cross Sections for H + H$_2$, J. Chem. Phys., to be published.

[4] A.B. Elkowitz and R.E. Wyatt, J. Chem. Phys. 62 (1975) 2504.

[5] A.B. Elkowitz and R.E. Wyatt, J. Chem. Phys. 63 (1975) 702.

[6] R.T Pack, J. Chem. Phys. 60 (1974) 633.

[7] P. McGuire and D.J. Kouri, J. Chem. Phys. 60 (1974) 2488.

[8] D.J. Kouri and P. McGuire, Chem. Phys. Letters 29 (1974) 414.

[9] P. McGuire, J. Chem. Phys. 62 (1975) 525.

[10] P. McGuire and H. Krieger, J. Chem. Phys. 63 (1975) 1090.

[11] P. McGuire, Chem. Phys. 8 (1975) 231.

[12] R.B. Walker and J.C. Light, Chem. Phys. 7 (1975) 84.

[13] M. Tamir and M. Shapiro, Chem. Phys. Letters 31 (1975) 166.

[14] A.B. Elkowitz and R.E. Wyatt, Mol. Phys. 31 (1976) 189.

[15] R.N. Porter and M. Karplus, J. Chem. Phys. 40 (1964) 1105.

[16] A.S. Davydov, Quantum mechanics, transl. D. ter Haar (Addison-Wesley, Reading, 1965) ch. 6.

[17] M. Jacob and G.C. Wick, Ann. Phys. NY 7 (1959) 404.

END

DATE
FILMED

4-78

DDC